frontiers | Research Topics

Acute leukemias: Molecular characterization, leukemia-initiating cells, and influence of the microenvironment

Edited by
Spiros Vlahopoulos, Garrett Dancik, Ioannis Voutsas and Lokman Varisli

Published in
Frontiers in Oncology

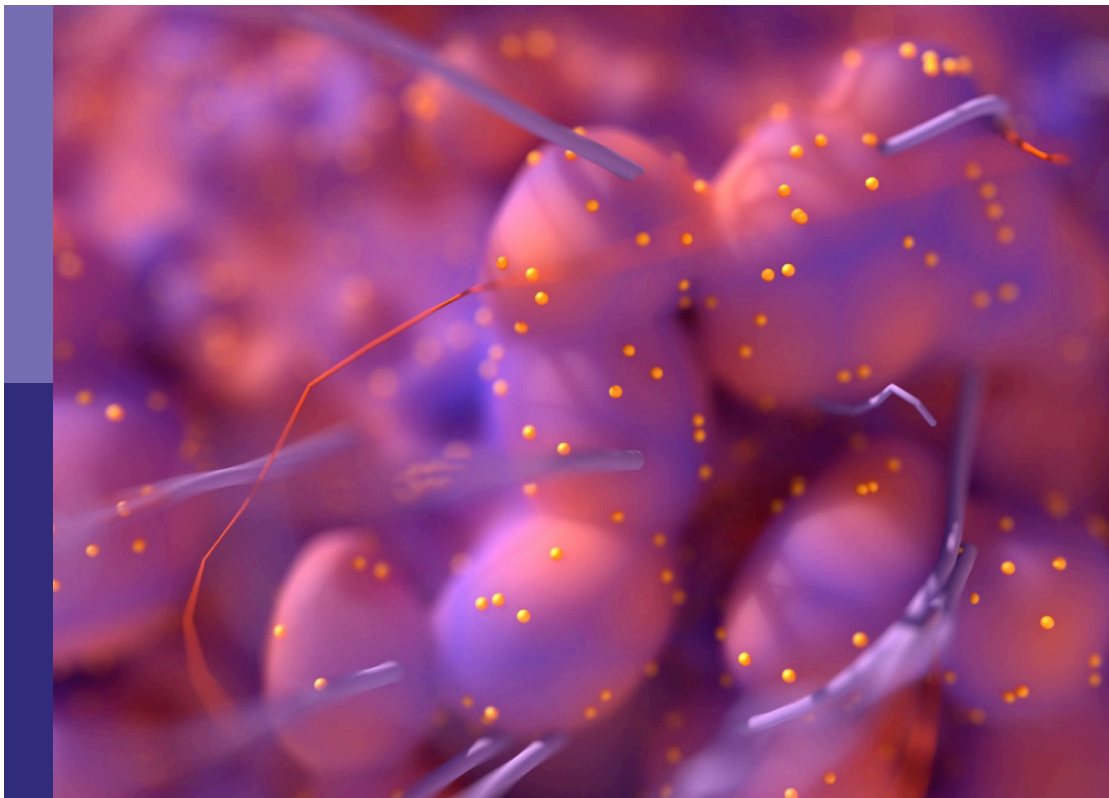

ISSN 1664-8714
ISBN 978-2-8325-2534-0
DOI 10.3389/978-2-8325-2534-0

About Frontiers

Frontiers is more than just an open access publisher of scholarly articles: it is a pioneering approach to the world of academia, radically improving the way scholarly research is managed. The grand vision of Frontiers is a world where all people have an equal opportunity to seek, share and generate knowledge. Frontiers provides immediate and permanent online open access to all its publications, but this alone is not enough to realize our grand goals.

Frontiers journal series

The Frontiers journal series is a multi-tier and interdisciplinary set of open-access, online journals, promising a paradigm shift from the current review, selection and dissemination processes in academic publishing. All Frontiers journals are driven by researchers for researchers; therefore, they constitute a service to the scholarly community. At the same time, the *Frontiers journal series* operates on a revolutionary invention, the tiered publishing system, initially addressing specific communities of scholars, and gradually climbing up to broader public understanding, thus serving the interests of the lay society, too.

Dedication to quality

Each Frontiers article is a landmark of the highest quality, thanks to genuinely collaborative interactions between authors and review editors, who include some of the world's best academicians. Research must be certified by peers before entering a stream of knowledge that may eventually reach the public - and shape society; therefore, Frontiers only applies the most rigorous and unbiased reviews. Frontiers revolutionizes research publishing by freely delivering the most outstanding research, evaluated with no bias from both the academic and social point of view. By applying the most advanced information technologies, Frontiers is catapulting scholarly publishing into a new generation.

What are Frontiers Research Topics?

Frontiers Research Topics are very popular trademarks of the *Frontiers journals series*: they are collections of at least ten articles, all centered on a particular subject. With their unique mix of varied contributions from Original Research to Review Articles, Frontiers Research Topics unify the most influential researchers, the latest key findings and historical advances in a hot research area.

Find out more on how to host your own Frontiers Research Topic or contribute to one as an author by contacting the Frontiers editorial office: frontiersin.org/about/contact

Acute leukemias: Molecular characterization, leukemia-initiating cells, and influence of the microenvironment

Topic editors

Spiros Vlahopoulos — University of Athens, Greece
Garrett Dancik — Eastern Connecticut State University, United States
Ioannis Voutsas — Hospital Agios Savvas, Greece
Lokman Varisli — Dicle University, Türkiye

Citation

Vlahopoulos, S., Dancik, G., Voutsas, I., Varisli, L., eds. (2023). *Acute leukemias: Molecular characterization, leukemia-initiating cells, and influence of the microenvironment*. Lausanne: Frontiers Media SA.
doi: 10.3389/978-2-8325-2534-0

Table of contents

frontiers | Frontiers in Oncology

TYPE Editorial
PUBLISHED 10 May 2023
DOI 10.3389/fonc.2023.1199354

OPEN ACCESS

EDITED AND REVIEWED BY
Alessandro Isidori,
AORMN Hospital, Italy

*CORRESPONDENCE
Spiros Vlahopoulos
v_spiros@hotmail.com

RECEIVED 03 April 2023
ACCEPTED 27 April 2023
PUBLISHED 10 May 2023

CITATION
Dancik GM, Varisli L, Voutsas IF and Vlahopoulos S (2023) Editorial: Acute leukemias: molecular characterization, leukemia-initiating cells, and influence of the microenvironment.
Front. Oncol. 13:1199354.
doi: 10.3389/fonc.2023.1199354

Editorial: Acute leukemias: molecular characterization, leukemia-initiating cells, and influence of the microenvironment

Garrett M. Dancik[1], Lokman Varisli[2,3], Ioannis F. Voutsas[4] and Spiros Vlahopoulos[5]*

[1]Department of Computer Science, Eastern Connecticut State University, Willimantic, CT, United States, [2]Cancer Research Center, Dicle University, Diyarbakir, Türkiye, [3]Department of Molecular Biology and Genetic, Faculty of Science, Dicle University, Diyarbakir, Türkiye, [4]Cancer Immunology and Immunotherapy Center, Cancer Research Center, Saint Savas Cancer Hospital, Athens, Greece, [5]First Pediatric Clinic, University of Athens, Athens, Greece

KEYWORDS

leukemia (acute myeloid), leukemia-initiating cells (LICs), microenvironment, cellular transition dynamics, cell death, drug resistance, biomarker

Editorial on the Research Topic
Acute leukemias: molecular characterization, leukemia-initiating cells, and influence of the microenvironment

Acute leukemias remain a challenge, in spite of improvements in diagnosis and treatment. Fully establishing the depth and extent of the relative impact of the molecular mechanisms of disease progression and the pathways to recurrent disease will require decades of research, until our comprehension enables the routine development of simple and effective cures. This special issue was aimed to address progress in the characterization of the molecular basis of acute leukemias and to explore potential links with disease course. The articles presented in this issue deal with the subject in general from two main perspectives.

The first perspective in this Research Topic is the identification of factors that associate with a negative disease course, and potentially affect drug efficacy. Wang et al., investigated the effect of Nrf level on chemotherapy success in adult B-ALL patients and demonstrated a direct negative relationship between Nrf level and vincristine therapy response, for the first time. Mechanistically, they have uncovered that vincristine treatment causes an increase in the Nrf2 mRNA and protein levels in adult B- ALL patients, elevated Nrf2 decreases pro-apoptotic BAD protein level in a PI3K/AKT dependent manner and consequently decreases vincristine chemotherapy sensitivity. We report a retrospective study of pediatric ALL patients performed by Feng et al., on the adverse effect of CDKN2A/B deletions on clinical outcomes in pediatric B-ALL patients. Since the reports about the clinical effect of CDKN2A/B deletions in pediatric ALL are controversial, Feng et al. have conducted a comprehensive analysis of CDKN2A/B deletions in 599 pediatric B-ALL patients and consequently demonstrated that CDKN2A/B deletions were associated with

older age at diagnosis, higher white blood cell counts, and prominent hepatosplenomegaly. Moreover, they also demonstrated that the patients with CDKN2A/B deletions had the worst clinical outcomes, especially in the TP53 deletion carriers. Zhang et al., establish a transcriptome-wide m7G methylome profile for AML and identified N7-methylguanosine modification of messenger RNA as a potential source of acute myeloid leukemia (AML) drug resistance. They showed that there were significant differences in the genes modified by m7G methylation in resistant AML cells, and the number of methylated genes and peaks in drug-resistant cells was greater than those in non-resistant cells. Zhang et al., explained why in moderate-to-severe lower respiratory tract infections, lung microbiome changes in children with hematological malignancies are a source of negative disease course. Hong et al., investigated for the probable correlations of TIM-3 expression between leukemic blasts and T lymphocytes since TIM-3 is thought to be involved both in the self-renewal of leukemic stem cells and the immune escape of AML cells. They demonstrated that TIM-3 expression levels of leukemic blasts and T lymphocytes in the bone marrow of *de novo* AML patients correlate with the presence of core binding factor (CBF) translocations, without having a detectable impact on the clinical outcome. Zhao et al. investigated the function of ECHDC3, which is upregulated in CD34+ progenitor cells of AML after chemotherapy, but whose prognostic significance and function are as yet unknown. They demonstrated that ECHDC3 alters the bone marrow microenvironment by inducing changes in the composition of infiltrating immune cells. Furthermore, they also showed that knocking down ECHDC3 in AML cells by RNAi promoted the death of leukemia cells with cytarabine and doxorubicin. Nilius-Eliliwi et al., demonstrate the power of optical genome mapping (OGM) to yield novel clinically significant results, including information helpful in disease monitoring and AML disease biology. They applied a "next-generation diagnostic workup" strategy with OGM and whole-exome sequencing (WES), and detected a DDX3X: MLLT10 gene fusion, which would otherwise be missed by routine diagnostics. They also discovered several aspects of lineage ambiguity, not shown by standard diagnostics: these included deletions of SUZ12 and ARPP21, as well as T-cell receptor recombination. Their findings could explain an aggressive disease course. Schwarz et al., characterized a method to inhibit the constitutive activity of oncogenic receptor FMS-like tyrosine kinase 3 internal tandem duplication (FLT3ITD) in AML cells, by disrupting oligomerization of receptor protein tyrosine phosphatase PTPRJ. They showed that interfering with PTPRJ self-association may be used as a tool to restrict oncogenic FLT3 activity, affecting FLT3-driven cell proliferation and clonal growth. Yuan et al., presented a hypothesis that germline mutation in RecQ-like helicase can be involved in hereditary predisposition to acute leukemias. They performed whole exome sequencing in peripheral blood mononuclear cells in a familial leukemia case, and for the first time to our knowledge, found a germline RECQL mutation potentially involved in hereditary predisposition to acute leukemia. The hypothetical biological process in which RECQL gene mutation (rs146924988) affects DSBs repair and mediates the generation of fusion genes provides a new understanding for the pathogenesis of leukemia, and highlights the necessity for next-generation sequencing-based screening of genes involved in this process in potential HPS patients. Xu et al., used weighted gene co-expression network analysis, extracting gene co-expression modules to relate them to clinical features, and identified TRIM32 as a potential driver of unfavorable AML disease course. Consequently, they demonstrated that TRIM32 is highly expressed in AML cells compared with cells from healthy donors and Knockdown of TRIM32 significantly inhibited the proliferation of AML cell lines, *in vitro*. Jiang et al., investigated the role of mitochondria-related metabolic reprogramming in the occurrence, development, drug resistance, and recurrence of acute myeloid leukemia. They analyzed immune infiltration and immunosuppressive genes and demonstrated that the mitochondria-related gene risk signature of AML patients was strikingly positively correlated with an immune cell infiltration and expression of critical immune checkpoints, indicating that poor prognosis might be attributed to an immunosuppressive tumor microenvironment. Takeda et al., presented a case of repeated lineage switches in acute leukemia and they reported that dynamic lineage conversion from ALL to AML occurred after clofarabine monotherapy was provided as a fourth induction regimen. They proposed that a monoallelic deletion and a frameshift mutation in TP53 gene accompanied by MLL gene amplification may have contributed to lineage plasticity and therapeutic resistance in this case, the first reported case of acute leukemia presenting with lineage ambiguity and MLL gene amplification.

The second perspective in this Research Topic concerns AML cell death, and generally, pathways to block the uncontrolled proliferation of acute leukemia disease clones. Zhong et al., investigated molecular patterns related to ferroptosis in AML cells. They integrated the genome information of 992 AML specimens, including expression profile chip data and high-throughput sequencing data, and analyzed the characteristics of immune cell infiltration, lipid metabolism, and inflammation development in the tumor microenvironment of AML patients. They used RSL3, a targeted inhibitor of GPX4, in AML cell lines HL-60 and THP1, to explore the biological effects of inducing ferroptosis. They demonstrated that RSL3 induced cell death in a dose-dependent fashion, indicating that GPX4 is a potential target for AML treatment. Li et al., constructed a cuproptosis-related lncRNA signature, to classify AML patients into high and low risk and revealed multiple signaling pathways, especially immune-related processes, were found to be significantly enriched in the high-risk group. In addition, their results indicated for AML patients in the high-risk group had a lower sensitivity to a range of anti-leukemia agents, including cytarabine, methotrexate, etoposide, and ABT-263 (a BCL-2 inhibitor, also called Navitoclax), while indicating a higher sensitivity to drugs like rapamycin, bortezomib, Erlotinib, even though some of them are currently not in clinical use for the treatment of AML. Tomaz et al., noted a significant induction of apoptotic AML cell death after treatment with the non-steroidal anti-inflammatory drug nimesulide, either alone or in combination with prednisolone. They also demonstrated that nimesulide potentiates the cytotoxic *in vitro* effect of several chemotherapy drugs used in AML, including cytarabine. They report the case of a patient with AML who presented a partial

response after utilization of nimesulide, characterized by complete clearance of peripheral blood blasts and an 82% decrease of bone marrow blasts associated with myeloblast differentiation. Weighted correlation network analysis of serial whole-transcriptome data of cell lines treated with nimesulide revealed that the sets of genes upregulated after treatment with nimesulide were enriched for genes associated with autophagy and apoptosis, and on the other hand, the sets of downregulated genes were associated with cell cycle and RNA splicing.

We also received 2 comprehensive review articles that discuss the established knowledge with current literature. Yin et al., presented a survey of novel biomarker candidates, and their critical comparison to representative existing biomarkers. They concluded that integrated analysis of AML biomarkers from cytogenetics, molecular biology, and pathophysiology is conducive to the correct evaluation of prognostic factors to achieve the precise implementation of individualized hierarchical treatment. Gu et al., discussed the roles of Cancer-associated fibroblasts (CAFs) in acute leukemia. Although, CAFs can originate from diverse cell types, leukemia transformation is rare in patients with non-fibrotic myeloproliferative neoplasms. However, it is common in patients with myelofibrosis, which is also associated with an unfavorable disease course. Consequently, they concluded that CAFs in bone marrow may correlate with myelofibrosis, promote leukemia progression, and induce chemoresistance.

As the guest editors for the Research Topic "*Acute Leukemias: Molecular Characterization, Leukemia-Initiating Cells, and Influence of the Microenvironment* " we thank all contributing authors and hope you enjoy these interesting papers.

Author contributions

All authors listed have made a substantial, direct, and intellectual contribution to the work and approved it for publication.

Acknowledgments

The authors would like to thank the reviewers and scientists who contributed to this Research Topic.

Conflict of interest

The authors declare that the research was conducted in the absence of any commercial or financial relationships that could be construed as a potential conflict of interest.

Publisher's note

frontiers in Oncology

ORIGINAL RESEARCH
published: 10 March 2022
doi: 10.3389/fonc.2022.823831

Identification of a Mitochondria-Related Gene Signature to Predict the Prognosis in AML

Nan Jiang[1,2,3†], Xinzhuo Zhang[2†], Qi Chen[4], Fahsai Kantawong[3], Shengli Wan[1,3,4], Jian Liu[1], Hua Li[1], Jie Zhou[1], Bin Lu[5] and Jianming Wu[1*]*

[1] School of Pharmacy, Southwest Medical University, Luzhou, China, [2] Foreign Language School, Southwest Medical University, Luzhou, China, [3] Faculty of Associated Medical Sciences, Chiang Mai University, Chiang Mai, Thailand, [4] The Affiliated Hospital of Southwest Medical University, Southwest Medical University, Luzhou, China, [5] The Second Affiliated Hospital, Hengyang Medical School, University of South China, Hengyang, China

OPEN ACCESS

Edited by:
Spiros Vlahopoulos, University of Athens, Greece

Reviewed by:
Garima Pandey, Moffitt Cancer Center, United States
Natalia Baran, University of Texas MD Anderson Cancer Center, United States

***Correspondence:**
Jianming Wu
jianmingwu@swmu.edu.cn
Bin Lu
lubinmito@usc.edu.cn

[†]These authors have contributed equally to this work

Specialty section:
This article was submitted to Hematologic Malignancies, a section of the journal Frontiers in Oncology

Received: *28 November 2021*
Accepted: *31 January 2022*
Published: *10 March 2022*

Citation:
Jiang N, Zhang X, Chen Q, Kantawong F, Wan S, Liu J, Li H, Zhou J, Lu B and Wu J (2022) Identification of a Mitochondria-Related Gene Signature to Predict the Prognosis in AML. Front. Oncol. 12:823831. doi: 10.3389/fonc.2022.823831

Mitochondria-related metabolic reprogramming plays a major role in the occurrence, development, drug resistance, and recurrence of acute myeloid leukemia (AML). However, the roles of mitochondria-related genes (MRGs) in the prognosis and immune microenvironment for AML patients remain largely unknown. In this study, by least absolute shrinkage and selection operator (LASSO) Cox regression analysis, 4 MRGs' (HPDL, CPT1A, IDH3A, and ETFB) signature was established that demonstrated good robustness in TARGET AML datasets. The univariate and multivariate Cox regression analyses both demonstrated that the MRG signature was a robust independent prognostic factor in overall survival prediction with high accuracy for AML patients. Based on the risk score calculated by the signature, samples were divided into high- and low-risk groups. Gene set enrichment analysis (GSEA) suggested that the MRG signature is involved in the immune-related pathways. *Via* immune infiltration analysis and immunosuppressive genes analysis, we found that MRG risk of AML patients was strikingly positively correlated with an immune cell infiltration and expression of critical immune checkpoints, indicating that the poor prognosis might be caused by immunosuppressive tumor microenvironment (TME). In summary, the signature based on MRGs could act as an independent risk factor for predicting the clinical prognosis of AML and could also reflect an association with the immunosuppressive microenvironment, providing a novel method for AML metabolic and immune therapy based on the regulation of mitochondrial function.

Keywords: acute myeloid leukemia, prognostic signature, mitochondria-related genes, The Cancer Genome Atlas, Therapeutically Applicable Research to Generate Effective Treatments, LASSOR

INTRODUCTION

Acute myeloid leukemia (AML) is a common hematological cancer, characterized by the accumulation of undifferentiated myeloid progenitor in the hematopoietic system, leading to normal blood component decrease, severe infections, anemia, and hemorrhage (1). AML patients' genomes carry the fewest mutations discovered in most other cancers, with about 13 coding mutations found per patient (2). Accumulating research reported potential driver mutation and epigenetic abnormalities related to AML pathogenesis; however, the therapeutic strategy for AML patients has remained chemotherapy with or without stem cell transplantation for many years (2–4). Despite advanced progress in early diagnosis, drug mining, and multidisciplinary tumor management, the long-term overall survival (OS) of AML patients remains poor (5–7). Therefore, it is urgent to identify novel and effective potential biomarkers and prognostic models to improve treatment allocation by identifying patients at high risk of a poor prognosis.

Mitochondria are at the center of energy production and are important for cell growth, proliferation, differentiation, and death (8). Therefore, mitochondria are fundamentally involved in cancer-related biological processes, including cancer initiation, development, invasion, recurrence, and drug resistance (9). Many studies reported that epigenetic modulation and mutation of mitochondria-related genes (MRGs) and bio-energetic reprogramming are important in cancer pathogenesis (9, 10). Moreover, studies have found that the mitochondria-related biology process is a potential cancer therapy (11, 12). Recent studies have reported that AML cells have a dependency on mitochondrial function, especially leukemia stem cells. Targeting mitochondrial respiration became a novel treatment of AML (13). Thus, exploration of underlying mitochondria-related alterations in AML patients may bring out some novel insights to promote the prognosis.

In this study, by differential expression analysis, univariate Cox regression, and 10-fold least absolute shrinkage and selection operator (LASSO) Cox regression analysis, an MRG signature was established to predict the prognosis of AML patients. Gene set enrichment analysis (GSEA) has been performed to explore the functional change in the high-risk group. Single-sample GSEA (ssGSEA) immune infiltration analysis and immunosuppressive genes analysis were applied to investigate immune cell infiltration and immunosuppressive condition of AML. In summary, our results demonstrate that the signature based on MRGs could act as a reliable independent biomarker for predicting the clinical prognosis of AML, and high MRG risk AML patients were closely associated with an immunosuppressive microenvironment. Therefore, our study may provide a novel method for AML metabolic and immune therapy based on the regulation of mitochondrial function.

MATERIALS AND METHODS

Data Acquisition

RNA-seq data and clinical data (149 AML samples) from TCGA-AML cohorts combined with whole blood cohorts (337 normal whole blood samples) from GTEx were downloaded from the UCSC Xena database (https://xenabrowser.net/datapages/). We also obtained clinical and expression data of AML patients from the Therapeutically Applicable Research to Generate Effective Treatments (TARGET) database (https://ocg.cancer.gov/programs/target) as the validation set to validate our prognostic model. All eligible samples from The Cancer Genome Atlas (TCGA) and validation sets were collected according to the following inclusive criteria: 1) diagnosed AML specimen; 2) availability of transcriptome data; and 3) availability of general survival information and related clinical data. The corresponding information of AML samples is shown in **Table 1**.

Identification of Differentially Expressed Mitochondria-Related Genes

MRGs in the present study were defined as the coding genes of mitochondria-located proteins, including all proteins located in the mitochondrial membrane, matrix, cristae, and mitochondria-associated endoplasmic reticulum membranes. Depending on subcellular localization, a total of 1,136 mitochondria-located genes were downloaded from MitoCarta3.0 (14) (https://www.broadinstitute.org/) (**Supplementary Table 1**). Then, we extracted the MRG expression data from TCGA-GTEx gene expression dataset (337 normal blood samples and 149 AML samples). All the RNA-seq data have been pre-normalized by GDC mRNA analysis pipeline. The differentially expressed MRGs (DE MRGs) between the AML samples and normal controls were identified using the combination of DESeq2, EdgeR, and Limma (voom). Log2 $|\text{Fold Change}| > 1$ and adjusted $p < 0.05$ were used as the cutoff to screen DE MRGs.

Bio-Functional Analysis of the Acute Myeloid Leukemia-Related Mitochondria-Related Genes

The bio-functional enrichment analysis of DE MRGs, including Gene Ontology (GO) analysis and Kyoto Encyclopedia of Genes and Genomes (KEGG) pathway enrichment analyses, was conducted using the clusterProfiler and enrichplot packages (15, 16), using MRGs as background genes and $p < 0.05$ as the cutoff. To find out whether bio-function differed between low- and high-risk patients, we also performed KEGG pathways and AML-related GSEA using the GSEA software (GSEA 4.0.3) (17, 18). For each analysis, the permutations of the gene set were all performed 1,000 times.

Establishment of Prognostic Classifiers

A univariate Cox regression was performed for all DE MRGs, and the genes with $p < 0.05$ were identified as prognostic MRGs. Then the 10-fold LASSO cross-validation Cox regression analysis was applied to all prognostic MRGs for selection of the most useful biomarkers and to build a survival predicting classifier. LASSO is a popular prognostic model-building method of compression estimation, which can automatically remove unnecessary features and only keep the most important

TABLE 1 | Clinical information of samples.

Clinical features	TCGA-AML dataset (n = 149)		p-Value	Clinical Features	TARGET-AML dataset (n = 187)		p-Value
	High-risk group	Low-risk group			High-risk group	Low-risk group	
Vital status			0.004	Vital status			0.002
Alive	19	37		Alive	35	56	
Dead	55	38		Dead	59	37	
Gender			0.363	Gender			0.943
female	31	38		Female	49	47	
male	43	37		Male	45	46	
BM blast			0.211	BM blast			0.136
<70%	63	55		<70%	30	40	
≥70%	12	19		≥70%	62	50	
Age class			0.036	Age class			0.947
<55	24	38		<10	53	51	
≥55	50	37		≥10	41	42	
FAB category			<0.001	FAB category			<0.001
M0	5	8		M0	12	11	
M1	16	17		M1	10	11	
M2	13	22		M2	15	30	
M3	1	12		M3	0	0	
M4	19	14		M4	23	29	
M5	16	1		M5	30	5	
M6	2	0		M6	2	1	
M7	2	1		M7	2	6	

BM, bone marrow.

variables in the final model (19). The predicting risk scores were calculated based on the following formula:

$$\text{Risk Score} = \Sigma(\text{Cox coefficient} \times \text{Genes expression levels})$$

The low- and high-risk groups of AML patients were divided by the median risk score. The predictive ability of the model for training and validation cohorts was evaluated using the receiver operating characteristic (ROC) curve analysis, Kaplan–Meier (KM) log-rank test, and univariate and multivariate Cox regression analyses.

Estimation of Immune Cell Type Proportion

In order to further study the relationship between model predicting risk and immune cell infiltration, the ssGSEA algorithm was used to estimate the abundances of 28 immune cell types obtained from Charoentong et al. (20). To avoid the blast cell signal from overwhelming the immune environment cell signals, we extract samples with <70% blast for the immune environment analysis. The abundance of immune cells was calculated according to the expression of the reference gene within the gene set from transcriptomic data, using the GSVA package *via* R software (21).

Statistical Analysis

All statistical analysis and figure construction were conducted by R version 4.1 (http://www.R-project.org) and GraphPad Prism 8.0 statistical software (GraphPad Software, Inc., La Jolla, CA, USA). The KM survival analysis was performed and analyzed using a log-rank test. The correlation between risk score and clinicopathological characteristics was analyzed by the chi-square test. The Wilcoxon test was used to compare the difference between groups. In all the statistical analyses, p-value <0.05 was considered statistically significant.

RESULTS

The Differential Expression of Mitochondria-Related Genes in Acute Myeloid Leukemia

It has been reported that mitochondrial alterations led to metabolic vulnerabilities in AML cells and participated in AML development in various ways (22, 23). To find out the DE MRGs in AML, 149 AML samples and 337 normal whole blood samples were extracted from TCGA-GTEx datasets. First, principal component analysis (PCA) was performed to check the quality of the expression data, showing good separation between normal and AML groups (**Figure 1A**). Then, 3 differential expression analyses were performed to identify DE MRGs (**Supplementary Figures 1A–F**). A total of 415 common DE MRGs were identified, while 184 of these were upregulated and 231 were downregulated (**Figures 1B–D**). Detailed information on DE MRGs is given in **Supplementary Table 2**. GO and KEGG were performed to explore the biology function change related to mitochondria. GO biological process analysis showed that the upregulated MRGs were associated with the DNA replication and DNA repair, which was closely related to AML cell proliferation (**Figure 1E**), and the downregulated MRGs were associated with the apoptotic process and apoptosis pathways, which showed an anti-apoptosis ability in AML cells (**Figure 1F**). Moreover, according to KEGG enrichment analysis, upregulated MRGs were enriched in organic molecule degradation and

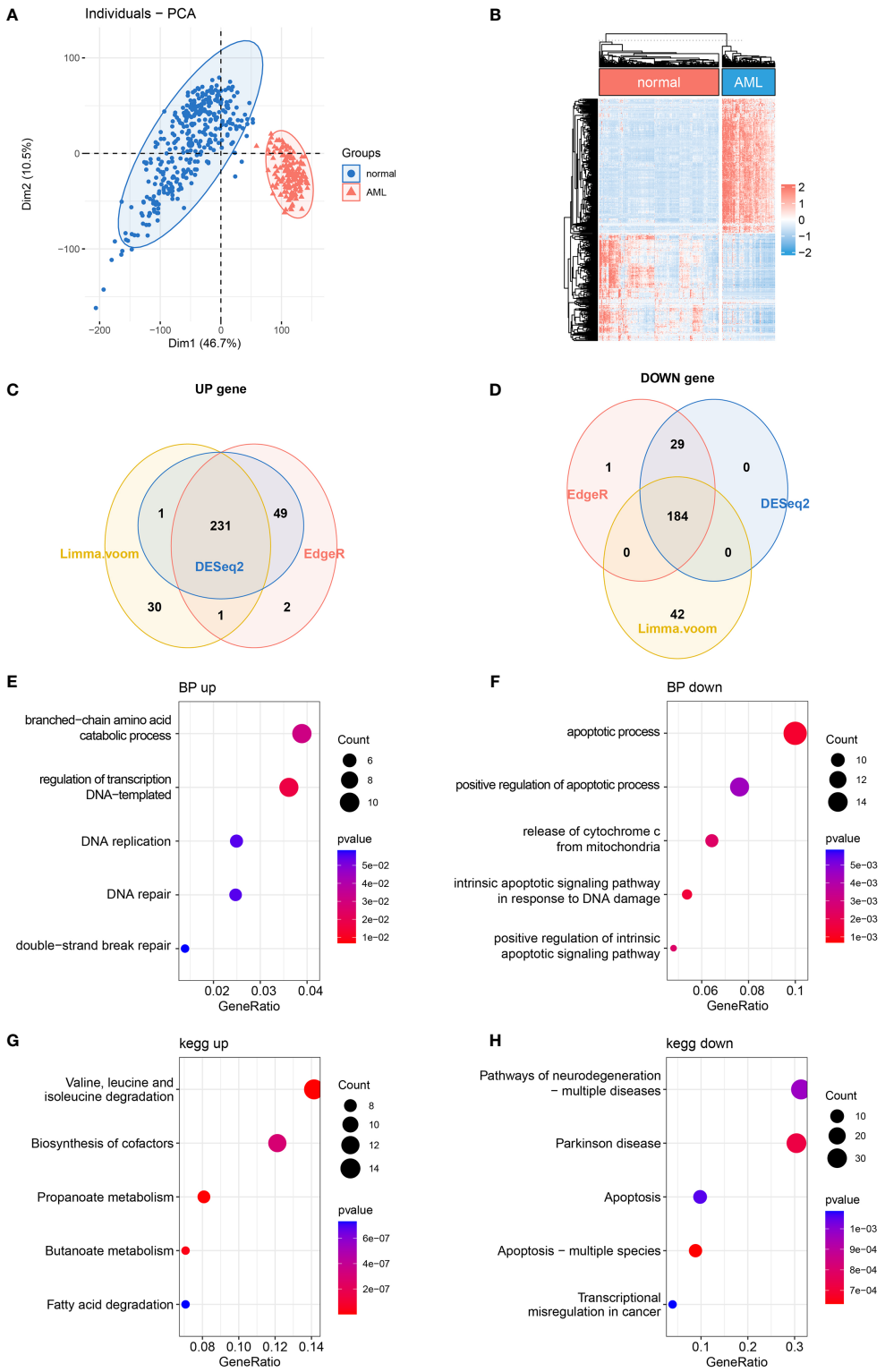

FIGURE 1 | Differentially expressed MRG analysis. **(A)** PCA and **(B)** DE MRG heatmap. **(C, D)** Venn plots of 3 different DE analyses. **(E, F)** Bubble plots of GO enrichment analysis of DE MRGs. BP, biological process. **(G, H)** Bubble plots of KEGG pathway enrichment analysis of DE MRGs. MRG, mitochondria-related gene; PCA, principal component analysis; DE MRGs, differentially expressed MRGs; GO, Gene Ontology; KEGG, Kyoto Encyclopedia of Genes and Genomes.

metabolism (**Figure 1G**), and downregulated MRGs were also connected with apoptosis (**Figure 1H**). The functional enrichment analysis above suggested that AML was associated with promoting proliferation and anti-apoptosis.

Construction of a Prognostic Models Composed of 4 Mitochondria-Related Genes' Signature

In order to further explore the prognostic value of MRG in AML, univariate Cox regression analysis was performed to identify the clinically relevant MRGs from 415 differentially expressed genes (DEGs), and 76 of them were significantly associated with OS (**Supplementary Table 3**). To minimize model over-fitting, LASSO regression was applied to construct the prognostic model. Thus, the independent variable's trajectory was explored in **Figure 2A**, and 10-fold cross-validation was used to analyze the CI under each lambda, as shown in **Figure 2B**. We finally established a mitochondria-related prognostic signature with 4 MRGs, including HPDL, CPT1A, IDH3A, and ETFB. The LASSO correlation coefficient of each MRG is shown in **Table 2**. Risk scores were calculated according to the expression level of the sample, and the risk score distribution is explored in **Figures 2C–E**, showing that the proportion of death with a high-risk score is significantly higher than that of samples with a low-risk score and expressions of 4 MRGs all upregulated as the risk score went up (**Supplementary Figure 2**). ROC was applied to evaluate the predictive classification efficiencies of the LASSO model, as shown in **Figure 2F**. The area under the curve (AUC) values of the model were 0.75, 0.71, and 0.79 at 1, 3, and 5 years. A KM plot was drawn using samples divided into the high- and low-risk groups by median risk score, showing the high-risk group had a poorer prognosis with significant difference ($p < 0.0001$) (**Figures 2G, H**). Finally, the KM plots of the 4 MRGs showed significantly predictive ability for the prognosis of patients in high- and low-expression groups (**Figures 2I–L**).

Robust Validation of Mitochondria-Related Gene Risk Signature in Different Cohorts

To determine the model's robustness, TARGET-AML datasets were introduced as an independent validation cohort. The risk score of each sample was calculated and explored according to the same LASSO coefficients and the expression level of 4 MRGs (**Figures 3A–C**). In accordance with TCGA training set, the samples with high-risk scores had a higher death proportion than those with low-risk scores. Moreover, in the TARGET-AML cohort, the ROC for 1, 3, and 5 years was 0.7, 0.64, and 0.63, respectively (**Figure 3D**). The KM plot also showed that the high-risk group had a poorer prognosis with significant difference ($p = 0.001$) (**Figures 3E, F**). The above results show that the MRG model had good robustness with prognostic predictive ability in different cohorts.

Relationship Between Mitochondria-Related Genes' Expression and Cytogenetic Risk in Acute Myeloid Leukemia

Clinically, AML patients are often divided into different groups according to their clinical characteristics and morphology, immunology, cytogenetics and molecular biology (MICM) feature, which is known as cytogenetic risk stratification (24, 25). The relationship between AML cytogenetic risk stratification and the expression level of 4 MRGs was analyzed. The heatmap demonstrated 4 MRGs' expression distribution along with AML cytogenetic risk stratification in TCGA cohort (**Figure 4A**), showing that the expression of 4 MRGs significantly went up in the higher cytogenetic risk group. Quantitative statistics further confirmed the significant difference of MRG expression levels in different risk stratification (**Figure 4B**), showing that the 4 MRGs' expression levels went up along with the increased risk stratification. The expression trend of the 4 MRGs was further confirmed by the TARGET-AML cohort, showing the same pattern of the AML patients in TCGA (**Figures 4C, D**).

Clinical Independence of Mitochondria-Related Gene Signature

To assess the independence of MRG signature in clinical application, we performed univariate and multivariate Cox regression analyses in TCGA-AML dataset. The risk scores and clinicopathological characteristics, including age, gender, bone marrow blast cell, peripheral leukocyte, peripheral monocyte, hemoglobin, and cytogenetics risk category, were used as covariates. The univariate and multivariate Cox regression analyses revealed that both age and risk score were independent prognostic factors of OS, and risk score is superior to age (**Figures 5A, B**). These results indicated that the prognostic signature could be an independent unfavorable prognostic model for AML patients. With the use of multivariable Cox regression analysis, a nomogram (1, 3, and 5 years) was established to visualize the MRG risk model (**Figure 5C**). The corresponding calibration line for the nomogram showed good precise prediction (**Figures 5D–F**).

Identification of Mitochondria-Related Gene–Related Signaling Pathways With Gene Set Enrichment Analysis

GSEA was applied to compare the two MRG risk groups to explore which signaling mechanisms were triggered in the high-risk group, showing that higher-risk groups were found enriched in signaling molecule interaction, immune system, and immune diseases, such as cytokine–cytokine receptor interaction, cell adhesion, intestinal immune network for IGA production, autoimmune thyroid disease, and systemic lupus erythematosus (**Figures 6A–F**). Besides, as shown in **Figures 6G–I**, several AML-related gene sets from C2 curated gene sets in MSigDB were also enriched in the high-risk groups, which included Verhaak's AML with NPM1 mutated upregulation, Valk's AML cluster 5, and Yagi's AML FAB markers. Therefore, the above results suggested that MRG–related classification is highly related to immune response and AML progress.

Immune Landscape Between High and Low Mitochondria-Related Gene-Related Risk Groups of Acute Myeloid Leukemia Patients

Accumulating studies have shown that the mitochondria-related biological process such as mitophagy could protect tumor cells

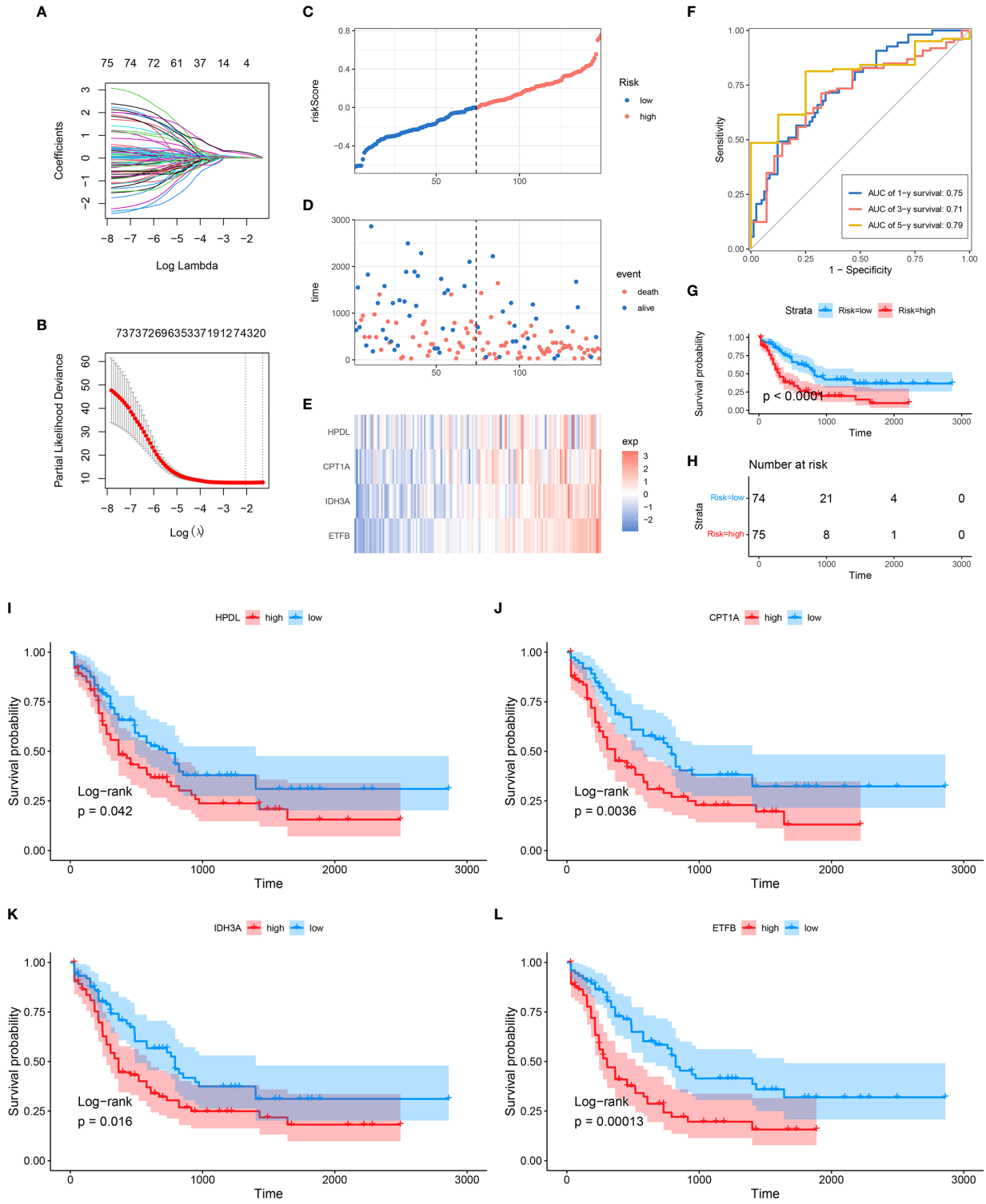

FIGURE 2 | Construction of MRG-based prognostic classifier. **(A)** Each gene's trajectory. The horizontal axis represents the log value of the gene lambda, and the vertical axis represents the independent gene's coefficient. **(B)** CIs with different values of lambda, **(C–E)** Distribution of risk score, survival status, and expression of 4 MRGs in TCGA-AML cohort. **(F)** ROC curve of 4 MRGs' signature prediction. **(G, H)** KM survival curves between two risk groups based on 8-gene signature classification. **(I–L)** The KM survival plots of 4 MRGs. MRG, mitochondria-related gene; ROC, receiver operating characteristic; KM, Kaplan–Meier.

TABLE 2 | The MRGs in the prognostic classifier.

Gene	Univariate Cox regression analysis			LASSO coefficient
	HR	95% CI	p-Value	
HPDL	1.43	1.11–1.83	0.0049	0.019734
CPT1A	1.69	1.26–2.26	5.00E−04	0.027628
IDH3A	1.79	1.35–2.38	1.00E−04	0.170339
ETFB	1.87	1.42–2.45	0	0.245829

MRGs, mitochondria-related genes; HR, hazard ratio; LASSO, least absolute shrinkage and selection operator.

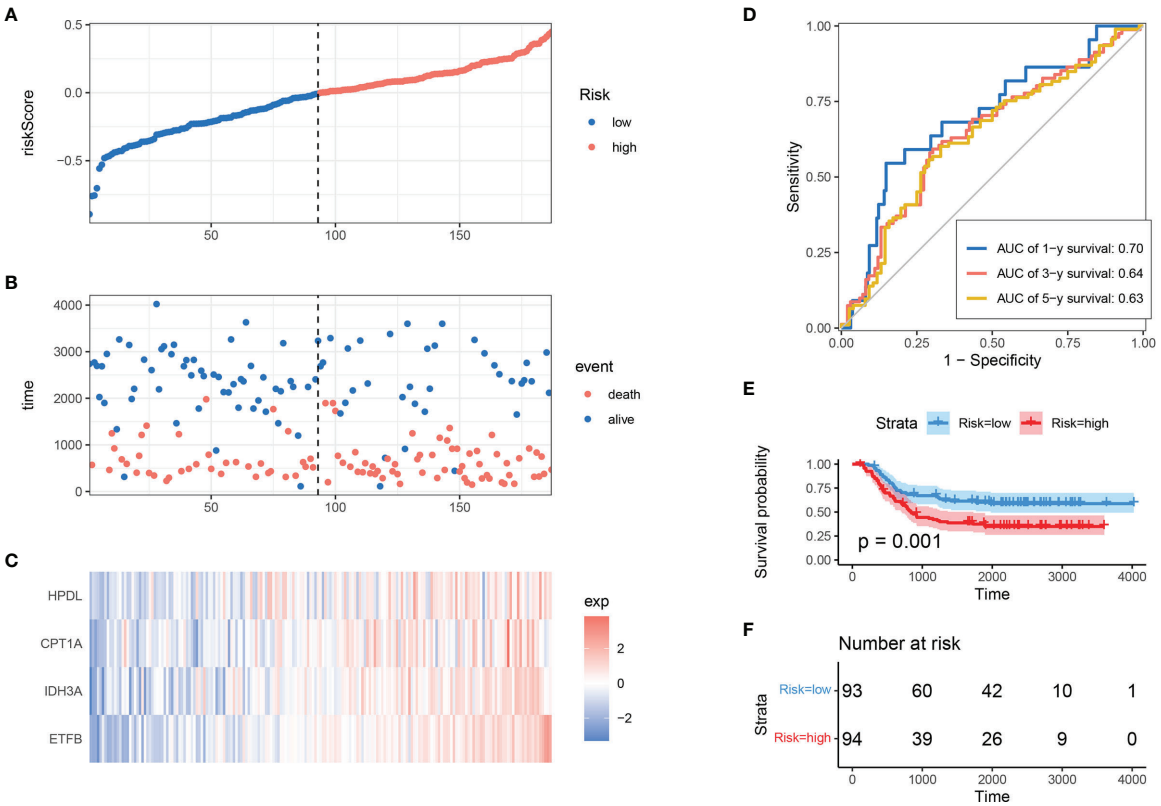

FIGURE 3 | Validation of MRG-based prognostic classifier. **(A–C)** Distribution of risk score, survival status, and expression of 4 MRGs along with risk score in TARGET-AML cohort. **(D)** ROC curve of 4 MRGs' signature classification in TARGET-AML cohort. **(E, F)** Survival curves between two risk groups based on 4 MRGs' signature classification in TARGET-AML cohort. MRG, mitochondria-related gene; ROC, receiver operating characteristic.

from antitumor immune responses, therefore promoting immune escape (26, 27). Also, the GSEA showed that many immune-related pathways were enriched in the high-risk group (**Figure 6A**). So the function of the MRG risk classification in the immune landscape was further explored. Thus, we estimated the differences in the 28 immune cell types' immune penetration between low- and high-risk AML patients using the ssGSEA algorithm. The results of the immune landscape of AML patients are summarized in **Figure 7A**, showing that AML patients with high MRG risk had significantly higher proportions in memory CD4+ T cell, neutrophils, macrophages, monocyte, dendritic cell, natural killer (NK) cells, myeloid-derived suppressor cell (MDSCs), regulatory T cells, and immature B cells. However, there was no significant difference between the 2 groups in the activated CD4+, CD8+ T cell, CD56 bright NK cell, and activated B cell (**Figure 7B**). Therefore, MRG classification might be highly related to an immunosuppressive microenvironment.

Immunosuppressive Microenvironment in High Mitochondria-Related Gene Risk Group

Cancer-Immunity Cycle manages the delicate balance between the recognition of cancer and the prevention of autoimmunity. Immune escape of cancer cells is largely achieved by disrupting certain steps in the tumor immune cycle (28, 29). This cycle is often suppressed by several genes, which could induce the immunosuppressive

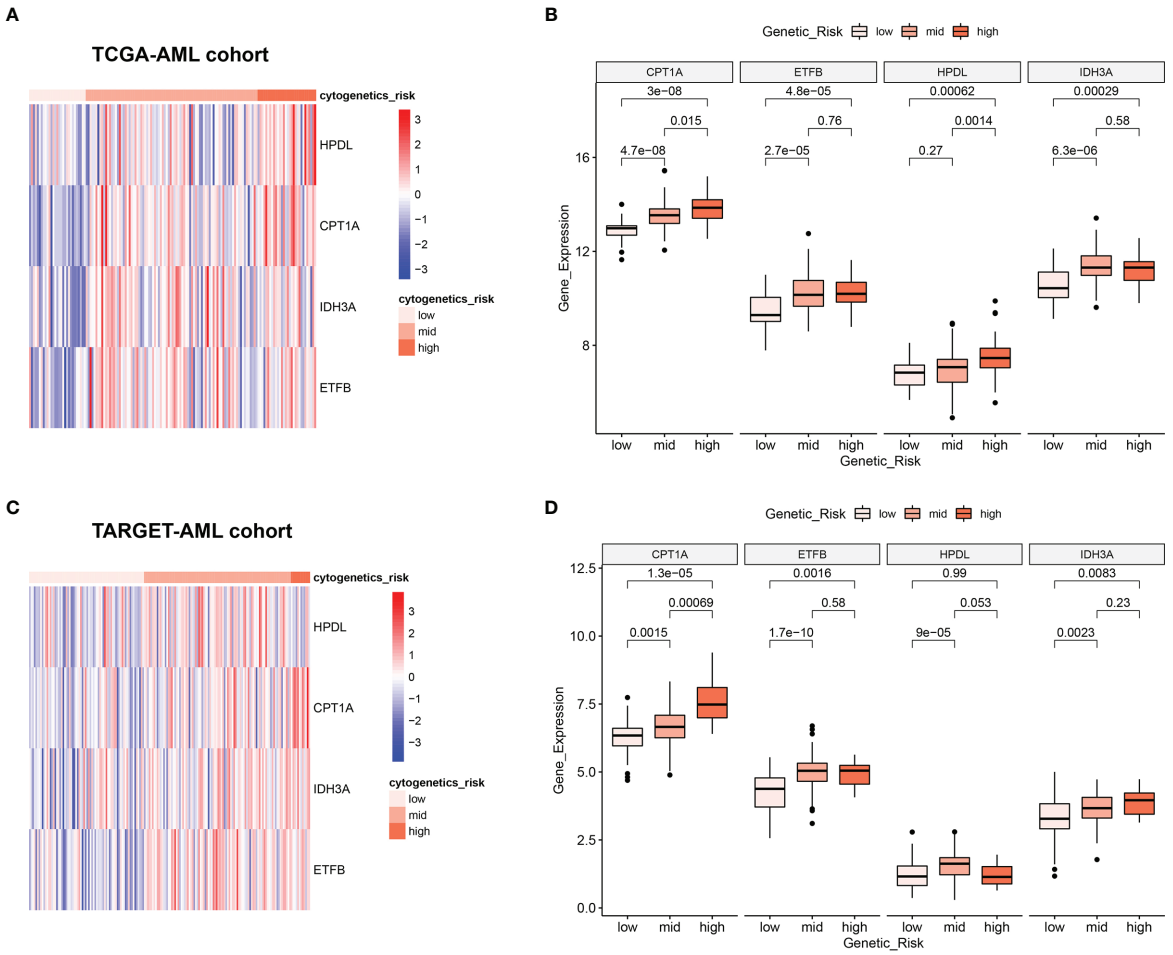

FIGURE 4 | Relationship between 4 MRGs' expression and cytogenetic risk in AML. **(A)** The heatmap of 4 MRGs in different risk stratification in TCGA-AML. **(B)** The boxplot of the 4 MRGs in different risk stratification in TCGA-AML. **(C)** The heatmap of 4 MRGs in different risk stratification in TARGET-AML. **(D)** The boxplot of the 4 MRGs in different risk stratification in TARGET-AML cohort. AML, acute myeloid leukemia.

microenvironment of cancer (30). Thus, in this study, 42 immunosuppressive genes involved in seven-step anticancer immunity were obtained from the Tracking Tumor Immunophenotype database (TIP; http://biocc.hrbmu.edu.cn/TIP/index.jsp) (31). Then the expression level of immunosuppressive genes in high and low MRG risk groups was explored. As shown in the heatmaps, most of these immunosuppressive genes were found significantly upregulated in the high MRG risk group in both TCGA and TARGET AML cohorts (**Figures 8A, B**). Immune checkpoint genes are essential for immune escape and immunotherapy of AML (32, 33). In this study, 5 common immune checkpoints genes, including PD1(PDCD1), PDL1(CD274), PDL2(PDCD1LG2), LAG3, and CTLA4, were found to be significantly upregulated in the high MRG risk group and positively associated with MRG risk score in both TCGA cohort and TARGET cohort (**Figures 8C–V**). Moreover, other than immune checkpoint genes, 12 immunosuppressive genes including VTCN1, CD160, TIGIT, NOS3, IDO2, SMC3, VSIR, EDNRB, LGALS9, LAIR1, DNMT1, and TGFB1 were found significantly higher in the high-risk groups in both TCGA cohort and TARGET cohort (**Supplementary Figure 3**).

DISCUSSION

More and more evidence suggests that a mitochondrion plays a key role in regulating cell energy level, apoptosis, and metabolism, which in turn could influence cell proliferation and differentiation, leading to the accumulation of immature myeloid progenitor in the hematopoietic system, which is the major manifestation of AML (34, 35). Studies have also demonstrated the clinical significance of mitochondrial targets for their effectiveness against relapsed or refractory AML (11, 23, 35). Thus, the identification of mitochondria-related prognostic biomarkers can be used to predict the prognosis of AML to improve patient management.

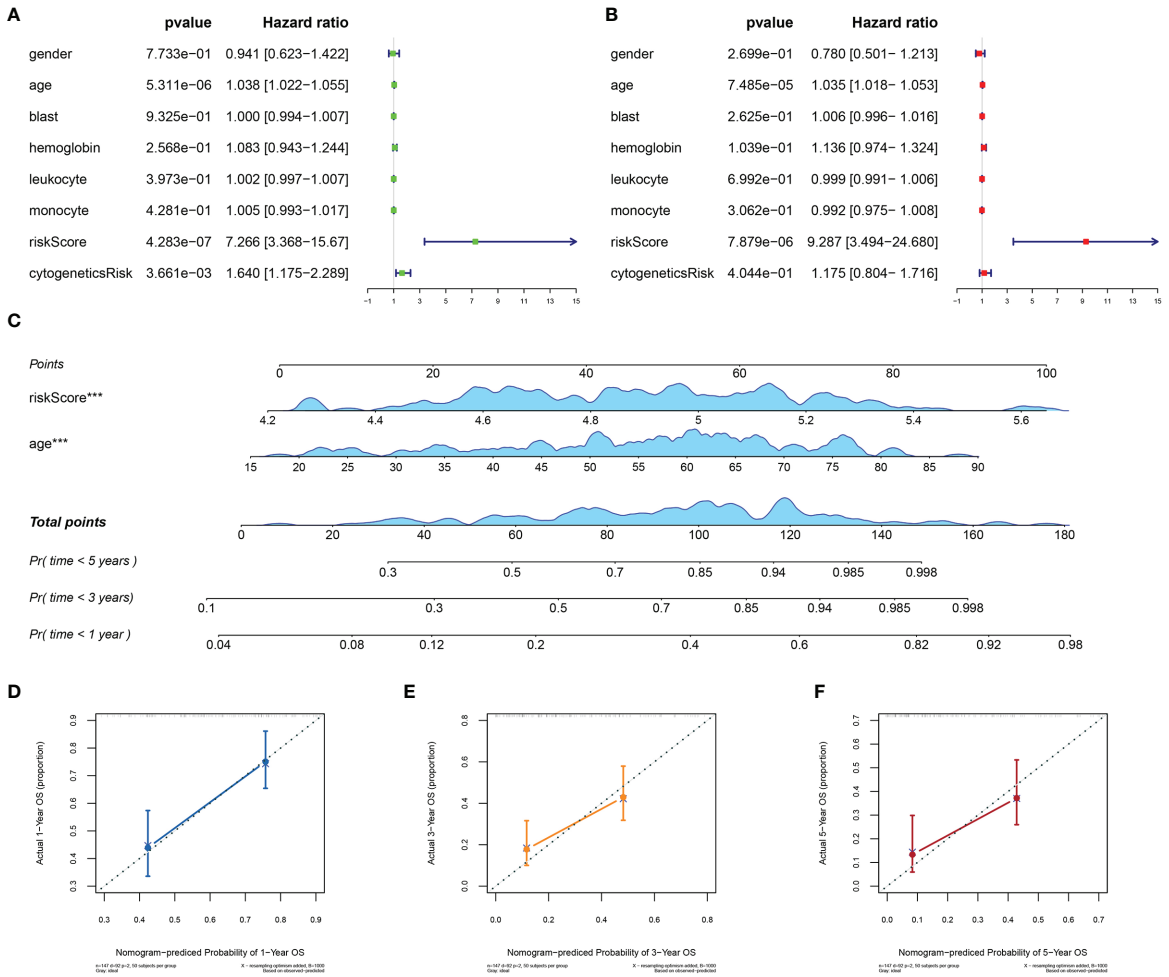

FIGURE 5 | Efficiency of the MRG risk signature in prognostic prediction in AML from TCGA database. **(A, B)** Univariate and multivariate Cox analyses, which evaluated the risk signature's independence in prognostic value in terms of overall survival in pediatric AML patients. **(C)** Nomograms for the probability of death at 1, 3, and 5 years. **(D–F)** The calibration curve of the nomograms. MRG, mitochondria-related gene; AML, acute myeloid leukemia; TCGA, The Cancer Genome Atlas. ***p < 0.001 in multivariate Cox analysis.

In this study, for the first time, a prognostic model based on 4 MRGs was constructed and validated for AML patients. The model performed well in predicting the OS state of AML patients in TCGA training and TARGET validation cohorts. Furthermore, the prediction efficacy of the risk model was superior to that of bone marrow blasts, leukocyte level, and cytogenetic risk, which are previously reported to be popular risk factors for AML development (24). Additionally, the correlation analysis has shown that the MRG-based risk score and expression level of 4 MRGs in the classifier were positively related to the cytogenetic risk of samples, showing a good prediction efficacy on AML prognosis. All 4 MRGs of the risk model, ETFB, CPT1A, HPDL, and IDH3A, were risk-associated and highly expressed in the high-risk group, indicating potential roles of these genes in the development of AML. Among them, HPDL, 4-hydroxyphenylpyruvate dioxygenase-like protein, a previously uncharacterized protein, localized in mitochondria, where it may function as 4-hydroxyphenylpyruvate dioxygenase, which was recently reported to be positively associated with the development of pancreatic ductal adenocarcinoma (PDAC) (36), AML (37), and breast cancer (38). Overexpression of HPDL promotes tumorigenesis and protects tumor cells from oxidative stress by reprogramming the metabolic profile of PDAC cells toward glutamine metabolism (36). ETFB, electron transfer flavoprotein subunit beta, is located in the inner membrane of the mitochondrial matrix in a complex with ETFA, FAD, and AMP, which together function as an electron acceptor in the fatty acid oxidation cascade and subsequent ATP production (39). However, recent studies have reported ETFB as a novel prognostic biomarker of many cancers, such as follicular carcinoma and breast cancer (40, 41). CPT1A catalyzes the rate-limiting step of the fatty acid oxidation (FAO) pathway, promoting cell proliferation and suppressing apoptosis (42). Abnormal CPT1A expression was associated with the poor OS

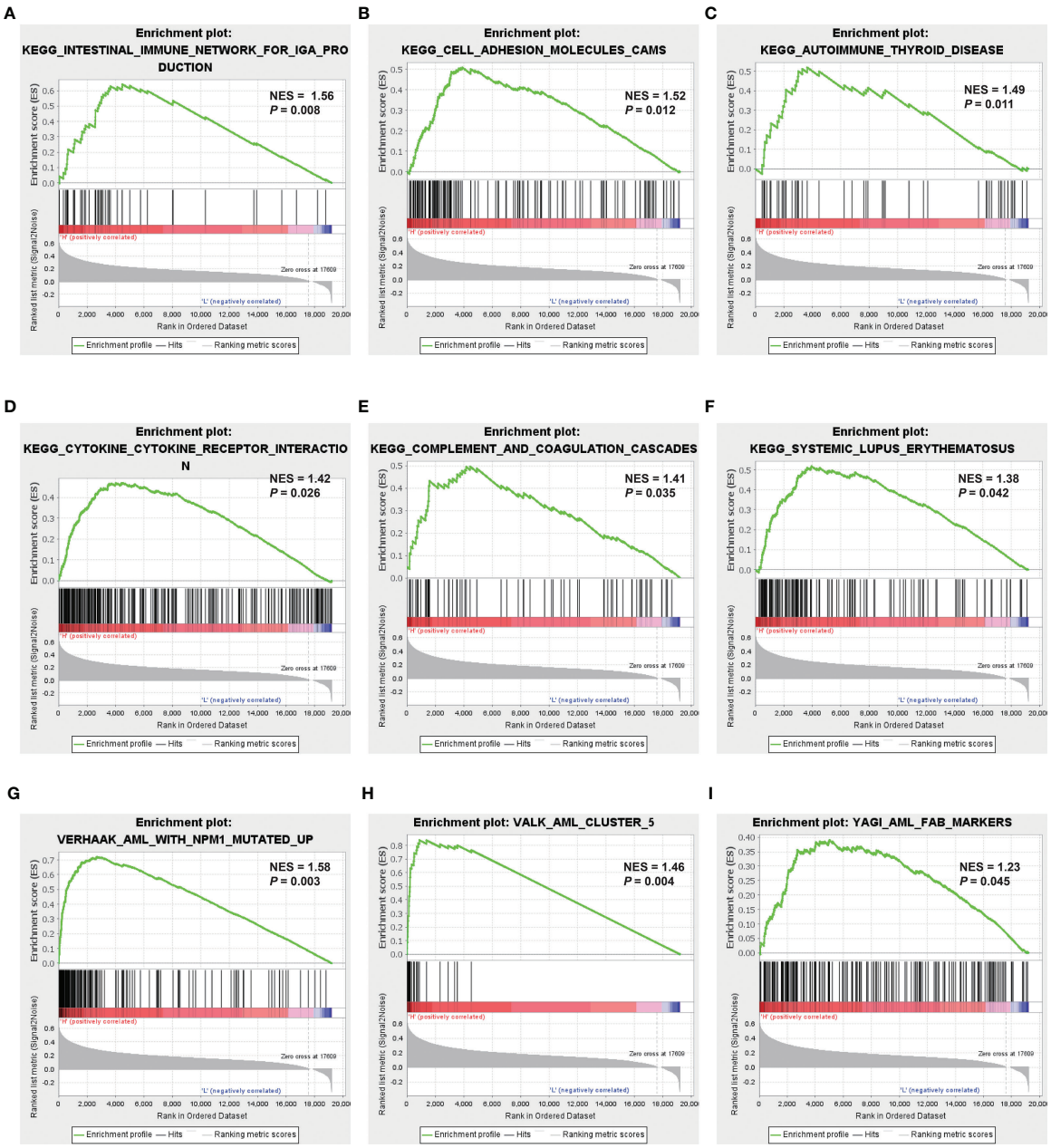

FIGURE 6 | Identification of MRG-related signaling pathways with GSEA. **(A–F)** GSEA results of the gene KEGG enrichment in the AML patients from TCGA. **(G–I)** GSEA results of AML-related gene sets enrichment by the AML-TCGA data. MRG, mitochondria-related gene; GSEA, gene set enrichment analysis; KEGG, Kyoto Encyclopedia of Genes and Genomes; AML, acute myeloid leukemia; TCGA, The Cancer Genome Atlas.

of AML (43), ovarian cancer (44), and glioblastoma stem cells (45). Leslimar et al. reported that CPT1A could regulate prostate cancer survival in hypoxic conditions and promote aggressiveness (46). IDH3A, isocitrate dehydrogenases 3 Catalytic Subunit Alpha, is the key part of isocitrate dehydrogenases, catalyzing the oxidative decarboxylation of isocitrate to α-ketoglutarate in citrate cycle (47). Recently, a study reported that IDH3A could regulate one-carbon metabolism in glioblastoma *via* the IDH3A-cSHMT signaling axis, promoting cancer progression through metabolic reprogramming (48). Abnormal IDH3A expression was associated with the poor OS of lung and breast cancer patients, promoting tumor growth by inducing HIF-1-mediated metabolic reprogramming and angiogenesis (49).

The GSEAs show that the enriched pathways in AML patients with higher MRG risk mainly related to signaling molecule

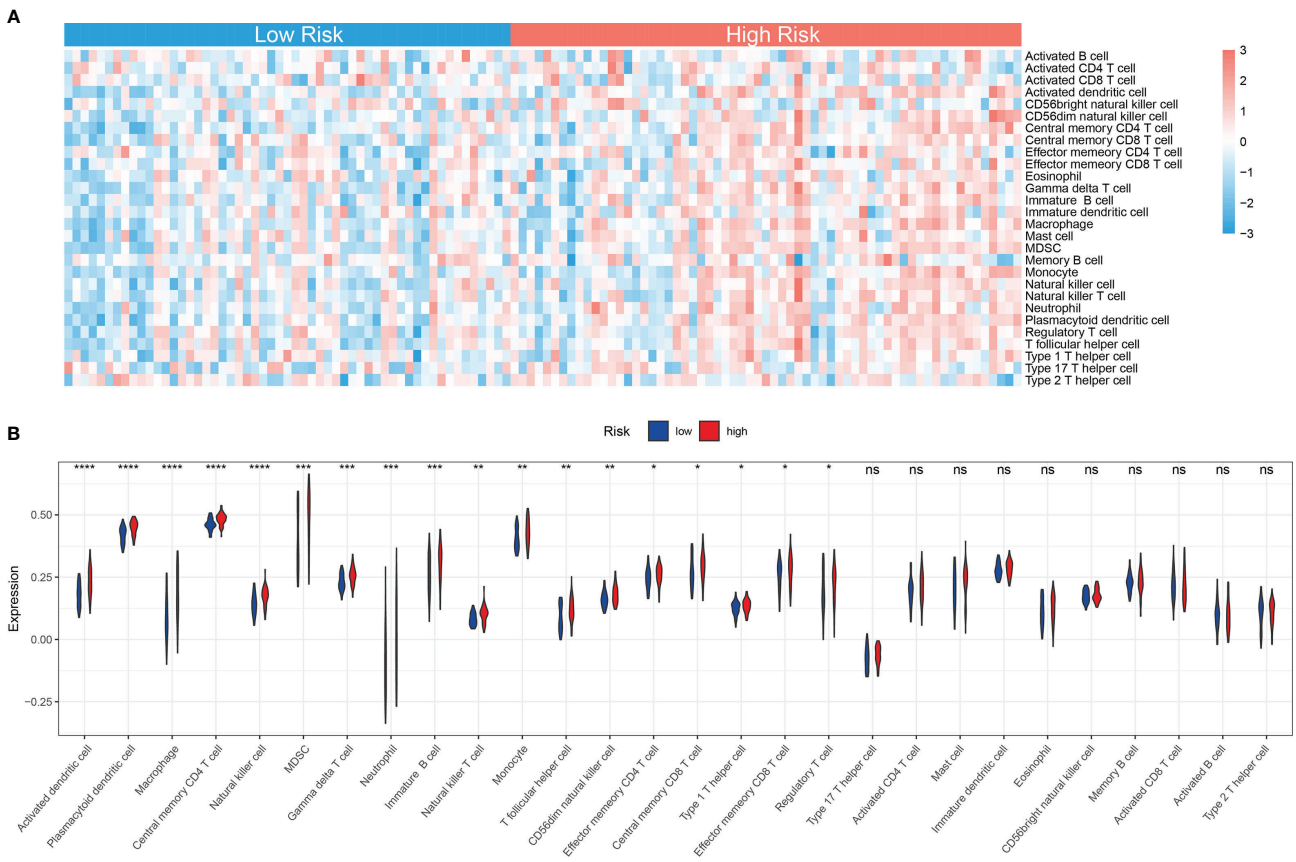

FIGURE 7 | Immune landscape between low and high MRG risk groups of AML patients. **(A)** Heatmap of immune infiltration of 28 immune cell types between two MRG risk groups in TCGA-AML cohort. **(B)** Box plots showing significant differences of immune cells between two MRG risk groups. MRG, mitochondria-related gene; AML, acute myeloid leukemia. *p < 0.05, **p < 0.01, ***p < 0.001 and ns, not significant, high risk group versus low risk group.

interaction, immune system, immune diseases, such as cytokine–cytokine receptor interaction, cell adhesion, intestinal immune network for IGA production, autoimmune thyroid disease, and systemic lupus erythematosus (**Figure 6**). Moreover, several AML-related gene sets from C2 curated gene sets in MSigDB were also enriched in the high-risk groups including AML with Verhaak's AML with NPM1 mutated upregulation, Valk's AML cluster 5, and Yagi's AML FAB markers, showing a close relationship with AML prognosis. Mitochondria deeply involved in energy generation, differentiation, and activation processes of immune cells play a key role in the immune system, regulating innate and adaptive immunity (50–52). Mitochondrial dysfunction is also involved in many immunological diseases, such as systemic lupus erythematosus (53), rheumatoid arthritis (54), and type 1 diabetes (55).

Accumulating evidence shows that immune cells are closely related to the tumor microenvironment (TME) (56–58). It was reported that the innate immune cells (macrophages, neutrophils, dendritic cells, innate lymphoid cells, MDSCs, and NK cells) as well as adaptive immune cells (T cells and B cells) could promote tumor progression in TME (58). Moreover, mitochondria-related metabolic reprogramming in cancer cells deeply affects gene expression, cellular differentiation, and the TME (59). In our research, we found that AML patients with high MRG risk had significantly higher proportions in memory CD4+ T cell, neutrophils, macrophages, monocyte, dendritic cell, NK cells, MDSCs, regulatory T cells, and immature B cells. However, there was no significant difference in the activated CD4+, CD8+ T cell, CD56 bright NK cell, and activated B cell, suggesting that MRG classification might be highly related to an immunosuppressive microenvironment. It was reported that tumor-associated macrophages can account for up to 50% of some tumor mass, supporting tumor progression and resistance to drugs by providing cancer cell nutritional support (60). Tumor-associated macrophages and neutrophils were reported to be protumoral, promoting tumor cell invasion and metastasis and angiogenesis, remodeling extracellular matrix, and suppressing immune surveillance (61). Dendritic cells have been reported to be tumor-promoting in TMEs and to correlate with a positive prognosis in endometrial carcinoma (62). NK cells are considered killers of tumor cells. However, their activity is often suppressed in the TME, due to nutrient and oxygen deprivation, tumor-derived metabolic

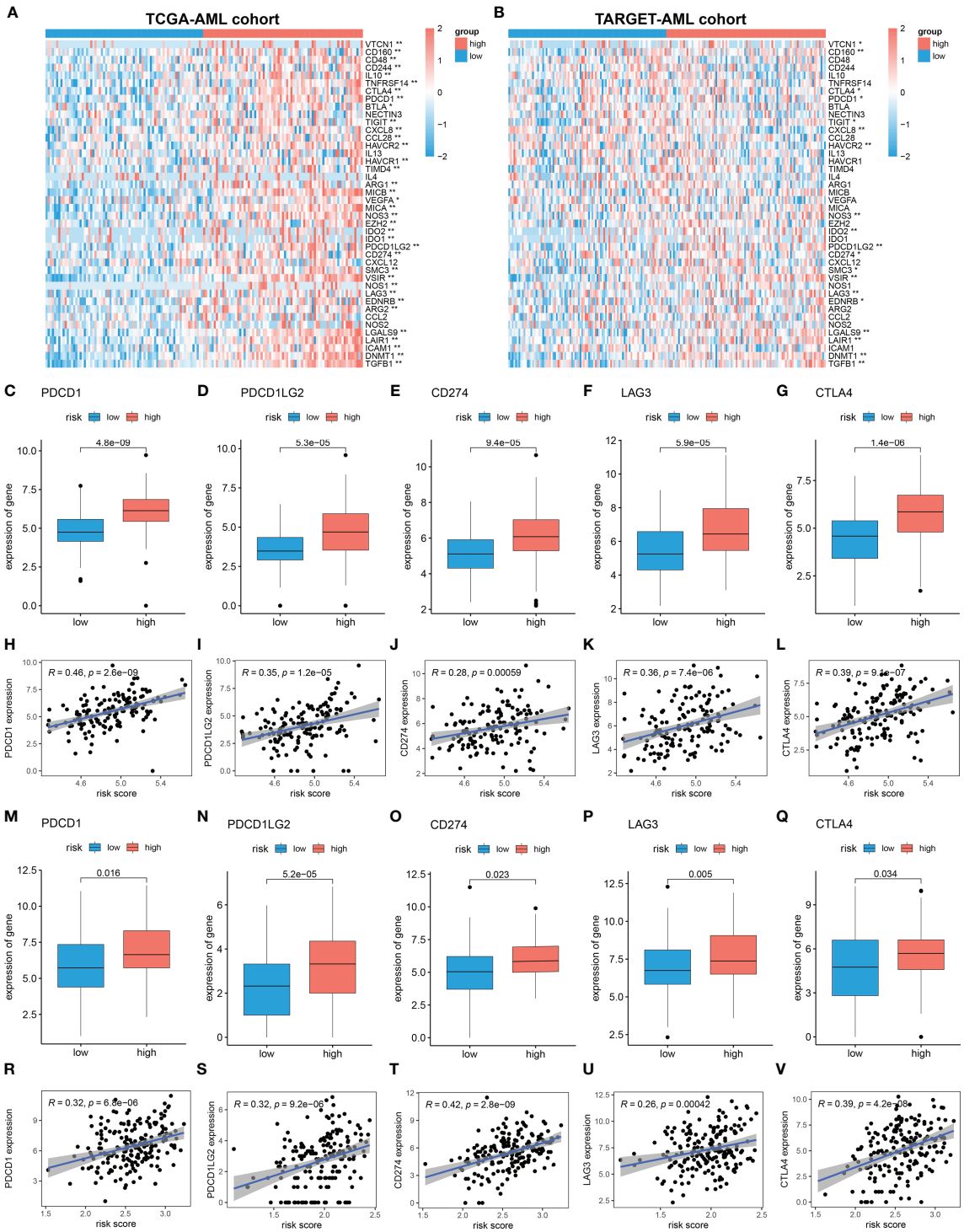

FIGURE 8 | Immunosuppressive microenvironment in high MRG risk group. **(A, B)** Heatmaps of the immunosuppressive genes in high and low MRG risk groups in TCGA **(A)** and TARGET **(B)**. **(C–L)** Expressions of 5 immune checkpoints (PD1(PDCD1), PDL1(CD274), PDL2(PDCD1LG2), LAG-3, and CTLA-4) in two MRG risk groups and their correlation with MRG risk score in AML-TCGA patients. **(M–V)** Expressions of 5 immune checkpoints (PD1(PDCD1), PDL1(CD274), PDL2 (PDCD1LG2), LAG-3, and CTLA-4) in two MRG risk groups and their correlation with MRG risk score in AML-TARGET patients. MRG, mitochondria-related gene; TCGA, The Cancer Genome Atlas. *p < 0.05 and **p < 0.01, high risk group versus low risk group.

end products, and impaired metabolism in the TME (63). MDSCs are one of the major players in the TME, exerting immune-suppressive activity (64). Regulatory T cells could also suppress anticancer immunity and inhibit effective antitumor immune responses in TME (65). Immune checkpoints play a crucial role in carcinogenesis and development for enhancing immunosuppression in cancer (66). Ok et al. pointed out that in hematological malignancies, the common targets of immune checkpoints mainly include PD1, PD-L1, PD-L2, CTLA-4, TIM-3, and LAG3 (67). In our study, 5 common immune checkpoints (PD1, PDL1/2, LAG3, and CTLA4) were significantly upregulated in the high MRG risk group and positively related to MRG risk scores, suggesting an immunosuppressive bone marrow microenvironment in the high MRG risk group (**Figure 8**). It was reported that there is resistance to immunotherapy in most leukemia patients, partially due to the immunosuppressive bone marrow microenvironment (68). Moreover, leukemia cells could create the immunosuppressive bone marrow microenvironment through reprogramming metabolism to generate enough energy and to escape antitumor immune surveillance (68). Additionally, leukemia cells escape immune recognition through expressing inhibitors or immune checkpoint molecules such as PD-L1 or CTLA-4 (69).

Inevitably, due to the limitations of data sources and research methods, the present study has some deficiencies. Firstly, it was a retrospective study based on public databases of TCGA, GTEx, and TARGET, consisting of only 673 samples included, and this still requires further verification *in vivo* and *in vitro*. Finally, the clinical application of the MRG-based model still requires large-scale, multicenter, and in-depth research.

In conclusion, this was the first research to establish a mitochondria-related prognostic model for AML, which could be used as an independent prognostic indicator for AML patients. Moreover, we also found that high MRG risk AML patients were closely associated with an immunosuppressive microenvironment, indicating that attenuating immunosuppression in the bone marrow microenvironment may be an important treatment for AML. Additionally, we identified several targeted therapy drugs for MRG risk signature. Our study may provide a reference for the clinical prognosis and treatment of AML based on the regulation of mitochondrial function.

DATA AVAILABILITY STATEMENT

The datasets presented in this study can be found in online repositories. The names of the repositories can be found in the data acquisition section.

AUTHOR CONTRIBUTIONS

NJ, XZ, JW and BL designed the research study. NJ, QC and SW carried out the data analysis. NJ and FK prepared the manuscript. JL, HL, and JZ revised the manuscript critically. BL and JW did the final approval of the version to be published. All authors contributed to the article and approved the submitted version.

FUNDING

This research was funded by grants from the National Natural Science Foundation of China [grant numbers 81774013, 82074129 and 31771534], the National Major Science and Technology Project of the Ministry of Science and Technology of China [grant number 2018ZX09721004-006-004], the Science and Technology Planning Project of Sichuan Province, China [grant numbers 2019JDPT0010, 2019YJ0473, and 19PTDJ0026], and Science and Technology Program of Luzhou, China [grant numbers 2019LZXNYDJ05, 2020LZXNYDJ30, 2018LZXNYD-PT02, 2020LZXNYDZ03, 2020LZXNYDP01, and 2018LZXNYD-YL05].

ACKNOWLEDGMENTS

We thank Dr. Jianming Zeng (University of Macau) and all the members of his bioinformatics team, biotrainee, for generously sharing their experience and codes.

SUPPLEMENTARY MATERIAL

The Supplementary Material for this article can be found online at: https://www.frontiersin.org/articles/10.3389/fonc.2022.823831/full#supplementary-material

Supplementary Figure 1 | MRGs differential expression analysis between TCGA-AML and GTEx are shown in the **(A–C)** Heatmap and **(D–F)** volcano plot.

Supplementary Figure 2 | High expression level of the 4 MRGs signature in high MRG risk group.

Supplementary Figure 3 | Immunosuppressive genes promoted in high MRG risk group in **(A–L)** TCGA-AML cohort and **(M–X)** TARGET cohort.

Supplementary Table 1 | MRGs list from MitoCarta3.0.

Supplementary Table 2 | Differential expression list of MRGs.

Supplementary Table 3 | Unicox analyisis of Differentially expressed MRGs ($p<0.05$).

REFERENCES

1. Khwaja A, Bjorkholm M, Gale RE, Levine RL, Jordan CT, Ehninger G, et al. Acute Myeloid Leukaemia. *Nat Rev Dis Primers* (2016) 2:16010. doi: 10.1038/nrdp.2016.10
2. Cancer Genome Atlas Research, N, Ley TJ, Miller C, Ding L, Raphael BJ, Mungall AJ, et al. Genomic and Epigenomic Landscapes of Adult De Novo Acute Myeloid Leukemia. *N Engl J Med* (2013) 368(22):2059–74. doi: 10.1056/NEJMoa1301689
3. Mazzarella L, Riva L, Luzi L, Ronchini C, Pelicci PG. The Genomic and Epigenomic Landscapes of AML. *Semin Hematol* (2014) 51(4):259–72.
4. Bose P, Vachhani P, Cortes JE. Treatment of Relapsed/Refractory Acute Myeloid Leukemia. *Curr Treat Options Oncol* (2017) 18(3):17. doi: 10.1007/s11864-017-0456-2

5. Shah A, Andersson TM-L, Rachet B, Björkholm M, Lambert PC. Survival and Cure of Acute Myeloid Leukaemia in E Nglan-2006: A Population-Based Study. *Br J Haematol* (2013) 162(4):509–16. doi: 10.1111/bjh.12425
6. Cooper SL, Brown PA. Treatment of Pediatric Acute Lymphoblastic Leukemia. *Pediatr Clinics* (2015) 62(1):61–73. doi: 10.1016/j.pcl.2014.09.006
7. Zeidan AM, Podoltsev NA, Wang X, Bewersdorf JP, Shallis RM, Huntington SF, et al. Temporal Patterns and Predictors of Receiving No Active Treatment Among Older Patients With Acute Myeloid Leukemia in the United States: A Population-Level Analysis. *Cancer* (2019) 125(23):4241–51. doi: 10.1002/cncr.32439
8. Abate M, Festa A, Falco M, Lombardi A, Luce A, Grimaldi A, et al. Mitochondria as Playmakers of Apoptosis, Autophagy and Senescence. *Semin Cell Dev Biol* (2020) 98:139–53.
9. Kim HK, Noh YH, Nilius B, Ko KS, Rhee BD, Kim N, et al. Current and Upcoming Mitochondrial Targets for Cancer Therapy. *Semin Cancer Biol* (2017) 47:154–67.
10. Shock LS, Thakkar PV, Peterson EJ, Moran RG, Taylor SM. DNA Methyltransferase 1, Cytosine Methylation, and Cytosine Hydroxymethylation in Mammalian Mitochondria. *Proc Natl Acad Sci* (2011) 108(9):3630–5. doi: 10.1073/pnas.1012311108
11. Caino MC, Altieri DC. Molecular Pathways: Mitochondrial Reprogramming in Tumor Progression and Therapy. *Clin Cancer Res* (2016) 22(3):540–5. doi: 10.1158/1078-0432.CCR-15-0460
12. Zhao LN, Björklund M, Caldez MJ, Zheng J, Kaldis P. Therapeutic Targeting of the Mitochondrial One-Carbon Pathway: Perspectives, Pitfalls, and Potential. *Oncogene* (2021) 40(13):2339–54. doi: 10.1038/s41388-021-01695-8
13. Carter JL, Hege K, Kalpage HA, Edwards H, Hüttemann M, Taub JW, et al. Targeting Mitochondrial Respiration for the Treatment of Acute Myeloid Leukemia. *Biochem Pharmacol* (2020) 114253:1–12. doi: 10.1016/j.bcp.2020.114253
14. Rath S, Sharma R, Gupta R, Ast , Chan C, Durham TJ, et al. MitoCarta3.0: An Updated Mitochondrial Proteome Now With Sub-Organelle Localization and Pathway Annotations. *Nucleic Acids Res* (2021) 1410(D1):D1541–7. doi: 10.1093/nar/gkaa1011
15. Yu G, Wang L-G, Han Y, He Q-Y. Clusterprofiler: An R Package for Comparing Biological Themes Among Gene Clusters. *Omics: J Integr Biol* (2012) 16(5):284–7. doi: 10.1089/omi.2011.0118
16. Wu T, Hu E, Xu S, Chen M, Guo P, Dai Z, et al. ClusterProfiler 4.0: A Universal Enrichment Tool for Interpreting Omics Data. *Innovation (NY)* (2021) 2(3):100141.
17. Subramanian A, Tamayo P, Mootha VK, Mukherjee S, Ebert BL, Gillette MA, et al. Gene Set Enrichment Analysis: A Knowledge-Based Approach for Interpreting Genome-Wide Expression Profiles. *Proc Natl Acad Sci* (2005) 102(43):15545–50. doi: 10.1073/pnas.0506580102
18. Kanehisa M, Furumichi M, Sato Y, Ishiguro-Watanabe M, Tanabe M. KEGG: Integrating Viruses and Cellular Organisms. *Nucleic Acids Res* (2021) 49(D1): D545–51. doi: 10.1093/nar/gkaa970
19. Friedman J, Hastie T, Tibshirani R. Regularization Paths for Generalized Linear Models via Coordinate Descent. *J Stat Software* (2010) 33(1):1. doi: 10.18637/jss.v033.i01
20. Charoentong P, Finotello F, Angelova M, Mayer C, Efremova M, Rieder D, et al. Pan-Cancer Immunogenomic Analyses Reveal Genotype-Immunophenotype Relationships and Predictors of Response to Checkpoint Blockade. *Cell Rep* (2017) 18(1):248–62. doi: 10.1016/j.celrep.2016.12.019
21. Hänzelmann S, Castelo R, Guinney J. GSVA: Gene Set Variation Analysis for Microarray and RNA-Seq Data. *BMC Bioinf* (2013) 14(1):1–15. doi: 10.1186/1471-2105-14-7
22. Di Martino L, Tosello V, Peroni E, Piovan E. Insights on Metabolic Reprogramming and Its Therapeutic Potential in Acute Leukemia. *Int J Mol Sci* (2021) 22(16):8738. doi: 10.3390/ijms22168738
23. Panina SB, Pei J, Kirienko NV. Mitochondrial Metabolism as a Target for Acute Myeloid Leukemia Treatment. *Cancer Metab* (2021) 9(1):1–25. doi: 10.1186/s40170-021-00253-w
24. Garcia-Manero G, Chien KS, Montalban-Bravo G. Myelodysplastic Syndromes: 2021 Update on Diagnosis, Risk Stratification and Management. *Am J Hematol* (2020) 95(11):1399–420. doi: 10.1002/ajh.25950
25. Pogosova-Agadjanyan EL, Moseley A, Othus M, Appelbaum FR, Chauncey TR, Chen I-ML, et al. AML Risk Stratification Models Utilizing ELN-2017 Guidelines and Additional Prognostic Factors: A SWOG Report. *biomark Res* (2020) 8(1):1–13. doi: 10.1186/s40364-020-00208-1
26. Bahat A, MacVicar T, Langer T. Metabolism and Innate Immunity Meet at the Mitochondria. *Front Cell Dev Biol* (2021) 9:720490. doi: 10.3389/fcell.2021.720490
27. Duan Y, Tian X, Liu Q, Jin J, Shi J, Hou Y. Role of Autophagy on Cancer Immune Escape. *Cell Commun Signaling* (2021) 19(1):1–12. doi: 10.1186/s12964-021-00769-0
28. Chen DS, Mellman I. Oncology Meets Immunology: The Cancer-Immunity Cycle. *immunity* (2013) 39(1):1–10. doi: 10.1016/j.immuni.2013.07.012
29. Ok CY, Young KH. Targeting the Programmed Death-1 Pathway in Lymphoid Neoplasms. *Cancer Treat Rev* (2017) 54:99–109. doi: 10.1016/j.ctrv.2017.01.009
30. Finn OJ. Cancer Immunology. *N Engl J Med* (2008) 358(25):2704–15. doi: 10.1056/NEJMra072739
31. Xu L, Deng C, Pang B, Zhang X, Liu W, Liao G, et al. TIP: A Web Server for Resolving Tumor Immunophenotype Profiling. *Cancer Res* (2018) 78 (23):6575–80. doi: 10.1158/0008-5472.CAN-18-0689
32. Chen C, Liang C, Wang S, Chio CL, Zhang Y, Zeng C, et al. Expression Patterns of Immune Checkpoints in Acute Myeloid Leukemia. *J Hematol Oncol* (2020) 13(1):1–5. doi: 10.1186/s13045-020-00853-x
33. Vago L, Gojo Iothers. Immune Escape and Immunotherapy of Acute Myeloid Leukemia. *J Clin Invest* (2020) 130(4):1552–64. doi: 10.1172/JCI129204
34. Zhou F, Shen Q, Claret FX. Novel Roles of Reactive Oxygen Species in the Pathogenesis of Acute Myeloid Leukemia. *J leukocyte Biol* (2013) 94(3):423–9. doi: 10.1189/jlb.0113006
35. Basak NP, Banerjee S. Mitochondrial Dependency in Progression of Acute Myeloid Leukemia. *Mitochondrion* (2015) 21:41–8. doi: 10.1016/j.mito.2015.01.006
36. Ye X, Wei X, Liao J, Chen P, Li X, Chen Y, et al. 4-Hydroxyphenylpyruvate Dioxygenase-Like Protein Promotes Pancreatic Cancer Cell Progression and Is Associated With Glutamine-Mediated Redox Balance. *Front Oncol* (2020) 10:617190. doi: 10.3389/fonc.2020.617190
37. Kuang Y, Wang Y, Cao X, Peng C, Gao H. New Prognostic Factors and Scoring System for Patients With Acute Myeloid Leukemia. *Oncol Lett* (2021) 22(6):823. doi: 10.3892/ol.2021.13084
38. Gao C, Li H, Liu C, Wu J, Zhou C, Liu L, et al. Determination of Genetic and Epigenetic Modifications-Related Prognostic Biomarkers of Breast Cancer: Genome High-Throughput Data Analysis. *J Oncol* (2021) 2021:2143362. doi: 10.1155/2021/2143362
39. Frerman FE. Acyl-CoA Dehydrogenases, Electron Transfer Flavoprotein and Electron Transfer Flavoprotein Dehydrogenase. *Biochem Soc Trans* (1988) 16 (3):416–8. doi: 10.1042/bst0160416
40. Lai X, Umbricht CB, Fisher K, Bishop J, Shi Q, Chen S. Identification of Novel Biomarker and Therapeutic Target Candidates for Diagnosis and Treatment of Follicular Carcinoma. *J Proteomics* (2017) 166:59–67. doi: 10.1016/j.jprot.2017.07.003
41. Ruiz-Pinto S, Pita G, Martín M, Alonso-Gordoa T, Barnes DR, Alonso MR, et al. Exome Array Analysis Identifies ETFB as a Novel Susceptibility Gene for Anthracycline-Induced Cardiotoxicity in Cancer Patients. *Breast Cancer Res Treat* (2018) 167(1):249–56. doi: 10.1007/s10549-017-4497-9
42. Schlaepfer IR, Joshi M. CPT1A-Mediated Fat Oxidation, Mechanisms, and Therapeutic Potential. *Endocrinology* (2020) 161(2):1–16. doi: 10.1210/endocr/bqz046
43. Shi J, Fu H, Jia Z, He K, Fu L, Wang W. High Expression of CPT1A Predicts Adverse Outcomes: A Potential Therapeutic Target for Acute Myeloid Leukemia. *EBioMedicine* (2016) 14:55–64. doi: 10.1016/j.ebiom.2016.11.025
44. Huang D, Chowdhury S, Wang H, Savage SR, Ivey RG, Kennedy JJ, et al. Multiomic Analysis Identifies CPT1A as a Potential Therapeutic Target in Platinum-Refractory, High-Grade Serous Ovarian Cancer. *Cell Rep Med* (2021) 2(12):100471. doi: 10.1016/j.xcrm.2021.100471
45. Luo M, Liu YQ, Zhang H, Luo CH, Liu Q, Wang WY, et al. Overexpression of Carnitine Palmitoyltransferase 1A Promotes Mitochondrial Fusion and Differentiation of Glioblastoma Stem Cells. *Lab Invest* (2021). doi: 10.1038/s41374-021-00724-0
46. Rios-Colon L, Kumar P, Kim S, Sharma M, Su Y, Kumar A, et al. Carnitine Palmitoyltransferase 1 Regulates Prostate Cancer Growth Under Hypoxia. *Cancers (Basel)* (2021) 13(24):1–19. doi: 10.3390/cancers13246302
47. Dalziel K. Isocitrate Dehydrogenase and Related Oxidative Decarboxylases. *FEBS Lett* (1980) 117(S1):K45–55. doi: 10.1016/0014-5793(80)80569-2
48. May JL, Kouri FM, Hurley LA, Liu J, Tommasini-Ghelfi S, Ji Y, et al. IDH3$ \alpha$ Regulates One-Carbon Metabolism in Glioblastoma. *Sci Adv* (2019) 5 (1):eaat0456. doi: 10.1126/sciadv.aat0456

49. Zeng L, Morinibu A, Kobayashi M, Zhu Y, Wang X, Goto Y, et al. Aberrant IDH3α Expression Promotes Malignant Tumor Growth by Inducing HIF-1-Mediated Metabolic Reprogramming and Angiogenesis. *Oncogene* (2015) 34(36):4758–66. doi: 10.1038/onc.2014.411
50. Weinberg SE, Sena LA, Chandel NS. Mitochondria in the Regulation of Innate and Adaptive Immunity. *Immunity* (2015) 42(3):406–17. doi: 10.1016/j.immuni.2015.02.002
51. de Souza Breda CN, Davanzo GG, Basso PJ, C\^amara NOS, Moraes-Vieira PMM. Mitochondria as Central Hub of the Immune System. *Redox Biol* (2019) 26:101255. doi: 10.1016/j.redox.2019.101255
52. Faas M, De Vos P. Mitochondrial Function in Immune Cells in Health and Disease. *Biochim Biophys Acta (BBA)-Molecular Basis Dis* (2020) 1866 (10):165845. doi: 10.1016/j.bbadis.2020.165845
53. Perl A, Hanczko R, Doherty E. Assessment of Mitochondrial Dysfunction in Lymphocytes of Patients With Systemic Lupus Erythematosus. *Autoimmunity* (2012) 900:61-89. doi: 10.1007/978-1-60761-720-4_4
54. Hajizadeh S, DeGroot J, TeKoppele JM, Tarkowski A, Collins LV. Extracellular Mitochondrial DNA and Oxidatively Damaged DNA in Synovial Fluid of Patients With Rheumatoid Arthritis. *Arthritis Res Ther* (2003) 5(5):1–7. doi: 10.1186/ar787
55. Chen J, Chernatynskaya AV, Li J-W, Kimbrell MR, Cassidy RJ, Perry DJ, et al. T Cells Display Mitochondria Hyperpolarization in Human Type 1 Diabetes. *Sci Rep* (2017) 7(1):1–11. doi: 10.1038/s41598-017-11056-9
56. Gajewski TF, Schreiber H, Fu Y-X. Innate and Adaptive Immune Cells in the Tumor Microenvironment. *Nat Immunol* (2013) 14(10):1014–22. doi: 10.1038/ni.2703
57. Pitt J, Marabelle A, Eggermont A, Soria J-C, Kroemer G, Zitvogel L. Targeting the Tumor Microenvironment: Removing Obstruction to Anticancer Immune Responses and Immunotherapy. *Ann Oncol* (2016) 27(8):1482–92. doi: 10.1093/annonc/mdw168
58. Hinshaw DC, Shevde LA. The Tumor Microenvironment Innately Modulates Cancer Progression. *Cancer Res* (2019) 79(18):4557–66. doi: 10.1158/0008-5472.CAN-18-3962
59. Pavlova NN, Thompson CB. The Emerging Hallmarks of Cancer Metabolism. *Cell Metab* (2016) 23(1):27–47. doi: 10.1016/j.cmet.2015.12.006
60. Vitale I, Manic G, Coussens LM, Kroemer G, Galluzzi L. Macrophages and Metabolism in the Tumor Microenvironment. *Cell Metab* (2019) 30(1):36–50. doi: 10.1016/j.cmet.2019.06.001
61. Powell DR, Huttenlocher A. Neutrophils in the Tumor Microenvironment. *Trends Immunol* (2016) 37(1):41–52. doi: 10.1016/j.it.2015.11.008
62. Chaput N, Conforti R, Viaud S, Spatz A, Zitvogel L. The Janus Face of Dendritic Cells in Cancer. *Oncogene* (2008) 27(45):5920–31. doi: 10.1038/onc.2008.270
63. Terrén I, Orrantia A, Vitallé J, Zenarruzabeitia O, Borrego F. NK Cell Metabolism and Tumor Microenvironment. *Front Immunol* (2019) 10:2278. doi: 10.3389/fimmu.2019.02278
64. Kumar V, Patel S, Tcyganov E, Gabrilovich DI. The Nature of Myeloid-Derived Suppressor Cells in the Tumor Microenvironment. *Trends Immunol* (2016) 37(3):208–20. doi: 10.1016/j.it.2016.01.004
65. Paluskievicz CM, Cao X, Abdi R, Zheng P, Liu Y, Bromberg JS. T Regulatory Cells and Priming the Suppressive Tumor Microenvironment. *Front Immunol* (2019) 10:2453. doi: 10.3389/fimmu.2019.02453
66. Pardoll DM. The Blockade of Immune Checkpoints in Cancer Immunotherapy. *Nat Rev Cancer* (2012) 12(4):252–64. doi: 10.1038/nrc3239
67. Ok CY, Young KH. Checkpoint Inhibitors in Hematological Malignancies. *J Hematol Oncol* (2017) 10(1):1–16. doi: 10.1186/s13045-017-0474-3
68. Xu B, Hu R, Liang Z, Chen T, Chen J, Hu Y, et al. Metabolic Regulation of the Bone Marrow Microenvironment in Leukemia. *Blood Rev* (2020) 100786:1–26. doi: 10.1016/j.blre.2020.100786
69. Curran EK, Godfrey J, Kline J. Mechanisms of Immune Tolerance in Leukemia and Lymphoma. *Trends Immunol* (2017) 38(7):513–25. doi: 10.1016/j.it.2017.04.004

Conflict of Interest: The authors declare that the research was conducted in the absence of any commercial or financial relationships that could be construed as a potential conflict of interest.

Publisher's Note: All claims expressed in this article are solely those of the authors and do not necessarily represent those of their affiliated organizations, or those of the publisher, the editors and the reviewers. Any product that may be evaluated in this article, or claim that may be made by its manufacturer, is not guaranteed or endorsed by the publisher.

frontiers in Oncology

CASE REPORT
published: 23 March 2022
doi: 10.3389/fonc.2022.799982

Repeated Lineage Switches in an Elderly Case of Refractory B-Cell Acute Lymphoblastic Leukemia With *MLL* Gene Amplification: A Case Report and Literature Review

Reina Takeda[1], Kazuaki Yokoyama[1], Tomofusa Fukuyama[1,2], Toyotaka Kawamata[1,3], Mika Ito[3], Nozomi Yusa[4], Rika Kasajima[5,6], Eigo Shimizu[7], Nobuhiro Ohno[1,3,8], Kaoru Uchimaru[1,9], Rui Yamaguchi[7], Seiya Imoto[5], Satoru Miyano[7] and Arinobu Tojo[1,3]**

[1]Department of Hematology/Oncology, Research Hospital, The Institute of Medical Science, The University of Tokyo, Tokyo, Japan, [2] Division of Cellular Therapy, The Institute of Medical Science, The University of Tokyo, Tokyo, Japan, [3] Division of Molecular Therapy, The Institute of Medical Science, University of Tokyo, Tokyo, Japan, [4] Department of Applied Genomics, Research Hospital, Institute of Medical Science, University of Tokyo, Tokyo, Japan, [5] Division of Health Medical Data Science, Health Intelligence Center, Institute of Medical Science, University of Tokyo, Tokyo, Japan, [6] Molecular Pathology and Genetics Division, Kanagawa Cancer Center Research Institute, Yokohama, Japan, [7] Laboratory of DNA Information Analysis, Human Genome Center, Institute of Medical Science, University of Tokyo, Tokyo, Japan, [8] Department of Hematology, Kanto Rosai Hospital, Kanagawa, Japan, [9] Laboratory of Tumor Cell Biology, Department of Computational Biology and Medical Science, Graduate School of the Frontier Science, The University of Tokyo, Tokyo, Japan

OPEN ACCESS

Edited by:
Spiros Vlahopoulos, University of Athens, Greece

Reviewed by:
Luca Lo Nigro, Azienda Ospedaliero Universitaria Policlinico - San Marco, Italy
Marie C. Bene, Nantes University, France
Camille Malouf, University of Edinburgh, United Kingdom
Giovanni Cazzaniga, University of Milano Bicocca, Italy
Maureen O'Brien, Cincinnati Children's Hospital Medical Center, United States

***Correspondence:**
Kazuaki Yokoyama
k-yoko@ims.u-tokyo.ac.jp
Arinobu Tojo
tojo.adm@tmd.ac.jp

Specialty section:
This article was submitted to Hematologic Malignancies, a section of the journal Frontiers in Oncology

Received: *22 October 2021*
Accepted: *07 February 2022*
Published: *23 March 2022*

Citation:
Takeda R, Yokoyama K, Fukuyama T, Kawamata T, Ito M, Yusa N, Kasajima R, Shimizu E, Ohno N, Uchimaru K, Yamaguchi R, Imoto S, Miyano S and Tojo A (2022) Repeated Lineage Switches in an Elderly Case of Refractory B-Cell Acute Lymphoblastic Leukemia With MLL Gene Amplification: A Case Report and Literature Review. Front. Oncol. 12:799982. doi: 10.3389/fonc.2022.799982

Lineage switches in acute leukemia occur rarely, and the underlying mechanisms are poorly understood. Herein, we report the case of an elderly patient with leukemia in which the leukemia started as B-cell acute lymphoblastic leukemia (B-ALL) and later changed to B- and T-cell mixed phenotype acute leukemia (MPAL) and acute myeloid leukemia (AML) during consecutive induction chemotherapy treatments. A 65-year-old woman was initially diagnosed with Philadelphia chromosome-negative B-ALL primarily expressing TdT/CD34/HLA-DR; more than 20% of the blasts were positive for CD19/CD20/cytoplasmic CD79a/cytoplasmic CD22/CD13/CD71.The blasts were negative for T-lineage markers and myeloperoxidase (MPO). Induction chemotherapy with the standard regimen for B-ALL resulted in primary induction failure. After the second induction chemotherapy regimen, the blasts were found to be B/T bi-phenotypic with additional expression of cytoplasmic CD3. A single course of clofarabine (the fourth induction chemotherapy regimen) dramatically reduced lymphoid marker levels. However, the myeloid markers (e.g., MPO) eventually showed positivity and the leukemia completely changed its lineage to AML. Despite subsequent intensive chemotherapy regimens designed for AML, the patient's leukemia was uncontrollable and a new monoblastic population emerged. The patient died approximately 8 months after the initial diagnosis without experiencing stable remission. Several cytogenetic and genetic features were commonly identified in the initial diagnostic B-ALL and in the following AML, suggesting that this case should be classified as lineage switching leukemia rather than multiple

simultaneous cancers (i.e., *de novo* B-ALL and *de novo* AML, or primary B-ALL and therapy-related myeloid neoplasm). A complex karyotype was persistently observed with a hemi-allelic loss of chromosome 17 (the location of the *TP53* tumor suppressor gene). As the leukemia progressed, the karyotype became more complex, with the additional abnormalities. Sequential target sequencing revealed an increased variant allele frequency of *TP53* mutation. Fluorescent *in situ* hybridization (FISH) revealed an increased number of *mixed-lineage leukemia* (*MLL*) genes, both before and after lineage conversion. In contrast, FISH revealed negativity for *MLL* rearrangements, which are well-known abnormalities associated with lineage switching leukemia and MPAL. To our best knowledge, this is the first reported case of acute leukemia presenting with lineage ambiguity and *MLL* gene amplification.

Keywords: lineage switch, B-ALL, AML – acute myeloid leukaemia, MPAL – mixed phenotypic acute leukaemia, MLL, gene amplicaiton, TP53, monosomy 17

INTRODUCTION

A lineage switch from acute lymphoblastic leukemia (ALL) to acute myeloid leukemia (AML) and *vice versa* is a rare event observed during the relapse of acute leukemia and is associated with dismal clinical outcomes (1–3). Lineage conversion is found more frequently in pediatric (6-9% prevalence) than in adult patients (1, 2). A high prevalence of lineage switching has been reported in infants younger than 1 year of age presenting with acute leukemia, including neonates aged younger than 1 month with congenital acute leukemia (2, 3). However, a few cases of adult lineage switching leukemia have been reported, and even fewer cases have been reported in the elderly (2, 4–6). The majority of cases of lineage switching leukemia harbor *mixed-lineage leukemia* (*MLL*, also known as *MLL1* and *KMT2A*) gene rearrangements (2–5). Several hypotheses have been proposed to explain the lineage switches and ambiguity occurring in leukemia. For instance, genetic and/or epigenetic dysregulation of lineage-specific transcription factors (e.g., *PU.1*, *CEBPA*, *PAX5*) may rewrite the differentiation programs of bi-, tri-, and oligo-potential leukemic clones (2, 7, 8). Therapies may facilitate the selection of subclones that are better equipped for survival (7, 9, 10). The tumor microenvironment could also influence the choice of cell lineage for leukemia cells *via* cytokines and metabolic parameters (2, 7). The hematopoietic microenvironment and stroma changes during developmental stages; thus, the fetal liver and adult bone marrow may differentially contribute to defining leukemia lineage fates (11). A leukemia initiating clone with a primitive cell of origin may be multipotent, producing a variety of hematopoietic lineages (2, 7). However, the precise mechanisms underlying leukemia lineage switches remain unclear.

Gene amplification occurs in various types of malignancies. Amplified genes often lead to the overexpression of proto-oncogenes, resulting in aggressive tumor development and poor prognoses (12, 13). Compared to solid tumors, gene amplification is rarely observed in hematological malignancies. The frequency of cytogenetically detectable gene amplification is approximately 1% in AML (12–14). While *MYC* is the most common amplicon gene, *MLL* gene amplification is also found in myeloid malignancies, including myelodysplastic syndrome (MDS) and AML (12–15).

Herein, we present the case of an elderly patient with Philadelphia chromosome (Ph)-negative B-cell ALL (B-ALL). The leukemia changed immunophenotypes and lineages in rapid succession, which is unusual in elderly patients. The leukemia was negative for any *MLL* rearrangement, which often occurs in leukemia cases with lineage ambiguity. Instead, *MLL* gene amplification was observed. The multi-drug resistance as well as treatment failure without achieving durable remission seen in this case could be related to the patient's highly complex karyotype and the presence of *TP53* alterations. Herein, we report a newly identified case of *MLL*-amplified leukemia with high lineage ambiguity, along with next-generation sequencing (NGS) results and a comprehensive literature review.

CASE PRESENTATION

A 65-year-old woman was referred to our hospital due to pancytopenia and disseminated intravascular coagulation (DIC). She complained of a 2-month history of fatigue. Her performance status (Eastern Cooperative Oncology Group) score upon examination was 0. She had a history of well-controlled hypertension and mild liver dysfunction, which was treated with ursodeoxycholic acid. There was no cancer or blood disease in her family history.

On admission, peripheral blood examination revealed a white blood cell (WBC) count of 2.0×10^9/L, with 4.5% neutrophils and 11.0% myeloperoxidase (MPO)-negative blasts. Anemia (hemoglobin level, 6.7 g/dL) and thrombocytopenia (platelet count, 38×10^9/L) were also detected. Her lactic dehydrogenase (LDH) level was slightly elevated at 252 IU/L (reference range, 105-211 IU/L). A mild elevation of biliary enzymes and DIC were observed as well. Physical examination and computed tomography (CT) evaluations detected no evidence of hepatosplenomegaly or lymphadenopathy. Bone marrow (BM) aspiration showed infiltration of MPO-negative

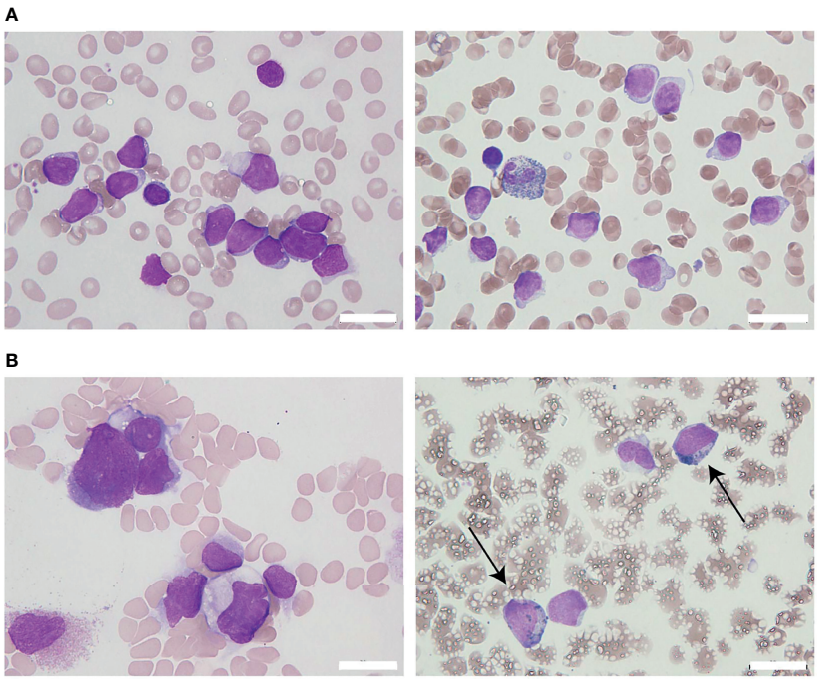

FIGURE 1 | The appearance of leukemia cells in the present case. **(A)** At initial diagnosis, the bone marrow (BM) was filled with morphologically monotonous myeloperoxidase (MPO)-negative leukemic blast cells (May–Giemsa stain [left]; MPO stain [right]; original magnification, 1,000×). **(B)** After the fourth regimen of chemotherapy, the BM presented with an increased number of MPO-positive leukemia blasts (arrows; May–Giemsa stain [left]; MPO stain [right]; original magnification, 1,000×). White bars in the right bottom portion of the figure represent 20 μm units.

blasts in 94% of the nucleated cell count (NCC) (**Figure 1A**). Flow cytometric analysis revealed that most of the blast cells were CD45 dim positive as well as highly positive for CD34, TdT, and HLA-DR. More than 20% of the blast cells were positive for CD19, CD20, cytoplasmic CD79a (cyCD79a), cytoplasmic CD22, CD13, and CD71. A small fraction of the population (up to approximately 10%) was positive for CD2, CD10, CD33, and CD56, whereas test results for CD3, CD4, CD5, CD7, CD8, CD14, CD16, CD41, MPO, and glycophorin A were negative. Cytogenetic analysis identified a complex karyotype with monosomy X, monosomy 5, and monosomy 17 (**Table 1**). A screening analysis for leukemia chimeric genes was negative for *BCR-ABL* (major, minor, or micro), *E2A-PBX*, *TEL-AML1*, *MLL-AF4*, and *MLL-AF9*. These results confirmed a diagnosis of Ph-negative B-ALL. The previously validated unfavorable prognostic factors for adult ALL seen in this case were older age and a complex karyotype (16–18).

The patient initially received standard chemotherapy for adult Ph-negative B-ALL, comprised of daunorubicin, cyclophosphamide, vincristine, L-asparaginase, and prednisolone. Despite induction therapy, the BM was still occupied by leukemia cells, accounting for 79% of the NCC. This finding was considered to reflect primary induction failure. Remission was not achieved following two additional lines of conventional intensive chemotherapies for B-ALL, comprising cytarabine/etoposide/dexamethasone as well as methotrexate/cytarabine. Throughout these sequential chemotherapies, the leukemia cells were found to additionally express cytoplasmic CD3 (cyCD3), and the B/T bi-phenotypic leukemia population gradually expanded (**Figures 2A, B**). The karyotypes became more complex with extra abnormalities, including additional material of unknown origin (add) in chromosome 11q (**Table 1**). Since mixed phenotype leukemia (MPAL) often harbors *MLL*-fusion genes derived from 11q chromosomal translocations, we performed a fluorescent *in situ* hybridization (FISH) analysis evaluating *MLL* rearrangements. Interphase FISH analysis of the split signal of the *MLL* gene on chromosome 11q23 revealed that the evaluated leukemia cells were negative for *MLL* gene rearrangements, however, the majority of these cells possessed more than eight copies of the full-length *MLL* gene per nucleus. Based on data from immunophenotypic, karyotypic, and *MLL* FISH analyses, the patient's leukemia was re-classified into MPAL, not otherwise specified (NOS) in accordance with the World Health Organization (WHO) 2016 classification guidelines (19, 20).

Given the unexpected result of an increased number of *MLL* gene copies, we retrospectively investigated the status of the *MLL* gene at the time of the initial diagnosis *via* the FISH evaluation. Due to the lack of fresh cell samples, we evaluated paraffin-embedded BM specimens that were collected on admission and found *MLL* amplification without *MLL* translocation in more than 90% of the interphase cells in the initial diagnostic B-ALL

TABLE 1 | Changes in karyotype and *TP53* mutation frequency of the present case.

Days after diagnosis, and aim of analysis		Leukemia phenotype	Karyotype [number of cells] and the frequency of cytogenetically abnormal cells (%)		*TP53* mutation VAF (%)	*MLL* amplification (%)
0	Diagnosis (BM)	B-ALL	44, X, -X, add (1) (p13), add (2) (q21), -4, -5, -10, del(11)(q)?, -12, -14, -17, -18, +r1, +mar1, +mar2, +mar3, +mar4, +mar5 [3]/46, XX [4].	80 [16]/ [20]	49.5	91.5
38	1st chemo evaluation (BM)	B-ALL	43, X, -X, add(1)(p13), add(2)(q21), -4, -5, -10, add(11)(q13), -12, -14, -17, -18, +mar1, +mar2, +mar3, +mar4, +mar5 [4]/44, idem, +r1 [3]/46, XX [11].	45 [9]/ [20]	Not done	Not done
79	2nd chemo evaluation (BM)	B/T MPAL	43, X, -X, add(1)(p13), add(2)(q21), -4, -5, -10, add(11)(q13), -12, -14, -17, -18, +mar1, +mar2, +mar3, +mar4, +mar5 [2]/46, XX [5].	75 [15]/ [20]	Note done	Not done
112	3rd chemo evaluation (BM)	B/T MPAL	44, X, -X, add(1)(p13), add(2)(q21), -4, -5, add(7)(q11.2), -10, add(11)(q13), -12, -14, -17, -18, +mar1, +mar2, +mar3, +mar4, +mar5, +mar6 [1]/87, idem x2, +5, +7, +7,-add(7) x2, -13, -mar3, -mar4, -mar5, -mar6 x2, +mar4 [1]/46, XX [6]	70 [14]/ [20]	76.2	86.6
153	4th chemo evaluation (BM)	AML	45, X, -X, add(1)(p13), add(2)(q21), -4, -5, -8, -10, add(11)(q13), -12, -13, add(17)(p11.2), +mar1, +mar2, +mar3, +mar4, +mar5, +mar6 [1]/43, idem, -7, -add(17), +add(17)(p11.2), -mar6 [1]	100 [20]/ [20]	94.1	64.7
198	5th chemo evaluation (PB)	AMML	43, X, -X, add(1)(p13), add(2)(q21), -4, -5, -8, -10, add(11)(q13), -12, -13, -17, +mar5 [1]/46, XX [2]	88.2 [15]/ [17]	Not done	43.4
219	6thc chemo evaluation (PB)	AMML	43, X, -X, add(1)(p13), add(2)(q21), -4, -5, -7, -8, -10, add(11)(q13), -12, -13, -17, +6mar [1]	100 [10]/ [10]	Not done	68.1
235	Died					

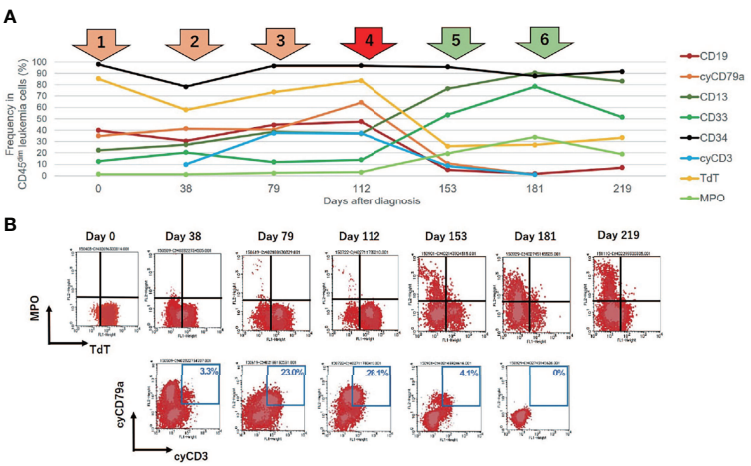

FIGURE 2 | Changes in leukemia cell immunophenotypes in the present case. Flow cytometric analysis revealed that leukemia blast cells in this case evolved immunophenotypically during sequential intensive chemotherapy. The analyzed leukemia cells were taken from bone marrow samples, with the exception of days 181 and 219 (when samples were taken from peripheral blood). **(A)** Changes in the frequency of immunophenotypic markers in CD45 dim leukemia cells. The arrows above the graph represent each chemotherapy regimen. Orange and red arrows represent intensive chemotherapy regimens for B-cell acute lymphoblastic leukemia (B-ALL), whereas green arrows indicate treatment regimens for acute myeloid leukemia (AML). After clofarabine monotherapy, administered as a fourth chemotherapy regimen (red arrow), a dynamic change in lineage marker expression was observed. **(B)** Changes in the immunophenotypic plot of CD45 dim leukemia cells (upper row, myeloid [myeloperoxidase, MPO] *vs.* lymphoid [TdT]; bottom row, B-lymphoid [cyCD79a] *vs.* T-lymphoid [cyCD3]).

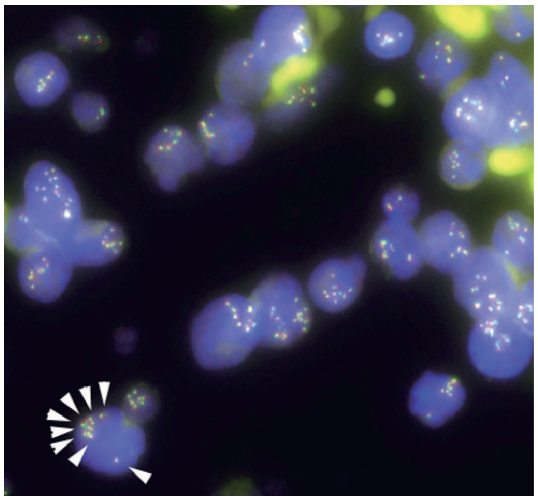

FIGURE 3 | Fluorescence *in situ* hybridization (FISH) analysis for gene rearrangements involving in the *mixed lineage leukemia* (*MLL*) gene (11q23) in the present case. *MLL* FISH data at the time of the initial B-cell acute lymphoblastic leukemia (B-ALL) diagnosis. The full-length *MLL* gene is shown *via* a yellow signal, whereas the rearranged *MLL* gene is shown *via* a pair of split signals colored green and red. A representative cell in the lower left portion of the figure shows eight full-length *MLL* signals (white arrows) in the nucleus. At the time of initial diagnosis, 91.5% of the interphase cells had at least eight copies of non-rearranged *MLL* genes. No *MLL* split signals generated by gene rearrangements were observed throughout the disease course.

cells (**Figure 3**). The *MLL* FISH signals were separately distributed and were not clustered in one location, suggesting that *MLL* loci were spread across multiple regions and chromosomes. Since the karyotyping analyses showed no chromosomal alterations directly affecting 11q23, and neither well-known hallmarks of gene amplification such as homogenously staining region (hsr) and double minutes (dmin), the aberrantly amplified *MLL* genes in this case were presumed to have been caused by multiple marker chromosomes (mar) as well as by a ring chromosome (r) (12, 13).

To overcome the refractoriness and resistance to multiple drugs of this disease presentation, clofarabine, a second-generation purine analog, was administered as a single agent in a fourth induction chemotherapy regimen. Nevertheless, leukemia cells reappeared in the peripheral blood and proliferated rapidly. A BM examination revealed hypocellular BM with infiltration of blast cells in 66% of the NCC. Unlike in the previous evaluation, more than 3% of the blast cells were positive for MPO staining (**Figure 1B**). Flow cytometric analysis showed that most of the leukemia cells were positive for CD13 and CD33, but were negative for CD19, cyCD79a, and cyCD3. The rapid increase in MPO expression and the dramatic loss of TdT expression indicated a dynamic immunophenotypic change from a lymphoid to a myeloid lineage (**Figures 2A, B**). Karyotype analysis revealed that all examined cells were abnormal and had extremely complex karyotypes. Most cytogenetic abnormalities had persisted since the time of diagnosis (**Table 1**), and new chromosomal aberrations (e.g., monosomy 8 and monosomy 13) were simultaneously detected as well. *MLL* FISH analyses demonstrated the persistence of *MLL* gene amplification without rearrangements. These findings led to the conclusive diagnosis of acute myeloid leukemia (AML), as a result of leukemia progression with a lineage conversion from MPAL, NOS (B/T bi-phenotypic leukemia).

After conversion to the myeloid lineage, the patient was treated with two lines of therapies commonly used for AML. The first line of therapy was a combination chemotherapy regimen consisting of cytarabine, anthracycline, and granulocyte-colony stimulating factor (G-CSF), and the second line of therapy was a monotherapy with gemtuzumab ozogamicin, a calicheamicin-conjugated humanized anti-CD33 monoclonal antibody. However, the leukemia did not respond to either treatment, resulting in disease deterioration with a rising cell subpopulation. Morphological and flow cytometric analyses identified this new subpopulation to be monoblastic. The cells in this monoblastic population showed high expression levels of CD13, CD33, CD14, CD45, and HLA-DR, and more than 20% of the monoblastic cells were positive for CD4, CD16, CD34 and MPO. Almost eight months (235 days) after the initial diagnosis of B-ALL and approximately three months after the lineage switch to AML, the patient died of multiple intracranial hemorrhages due to severe DIC associated with the drastic progression of AML.

To gain insight into the molecular mechanisms responsible for treatment resistance and lineage switching in the current case, we performed a targeted deep sequencing analysis. We analyzed the patient's BM samples, which were collected at three different time points during the disease course. One BM sample was collected at the time of the initial diagnosis (day 0) and the other two samples were taken before and after a dynamic lineage change (at days 112 and 153, respectively). NGS was performed using extracted DNA from each BM sample *via* the TruSight Myeloid Panel on the MiSeq platform (Illumina, San Diego, CA, USA). This panel allowed for the effective detection of myeloid neoplasm-associated hotspot mutations in the following 54 genes: *ABL1*, *ASXL1*, *ATRX*, *BCOR*, *BCORL1*, *BRAF*, *CALR*, *CBL*, *CBLB*, *CBLC*, *CDKN2A*, *CEBPA*, *CSF3R*, *CUX1*, *DNMT3A*, *ETV6*/*TEL*, *EZH2*, *FBXW7*, *FLT3*, *GATA1*, *GATA2*, *GNAS*, *HRAS*, *IDH1*, *IDH2*, *IKZF1*, *JAK2*, *JAK3*, *KDM6A*, *KIT*, *KRAS*, *MLL*, *MPL*, *MYD88*, *NOTCH1*, *NPM1*, *NRAS*, *PDGFRA*, *PHF6*, *PTEN*, *PTPN11*, *RAD21*, *RUNX1*, *SETBP1*, *SF3B1*, *SMC1A*, *SMC3*, *SRSF2*, *STAG2*, *TET2*, *TP53*, *U2AF1*, *WT1*, and *ZRSR2*. Oral epithelial cells collected *via* buccal swabs served as germline controls. Bioinformatic analysis was performed using standard procedures (21, 22). The analysis demonstrated a somatic mutation in exon5 of the *TP53* gene (c.455dupC: p.P153Afs*28) in all three samples (which, as noted above, were collected at different time points). Interestingly, the allele frequency of this *TP53* frameshift mutation gradually increased from 49.5% at time of the initial diagnosis, to 76.2% at the end of the third chemotherapy regimen, and finally to 94.1% at the end of the fourth chemotherapy regimen (when lineage conversion into AML was observed) (**Table 1**). No additional somatic or

germline mutations were detected. This study was approved by the Institutional Review Board of the Institute of Medical Science at the University of Tokyo. Written informed consent was obtained from the patient in accordance with the Declaration of Helsinki.

DISCUSSION

Herein, we describe the case of an elderly patient with acute lineage switching leukemia that transformed from B-ALL to AML. To comprehensively discuss the pathophysiology of this case, three unique features should be highlighted. The first is the high lineage ambiguity observed in this case presentation. The expression patterns of immunophenotypic markers in leukemia cells changed continuously throughout the disease course. The second feature of note is the high degree of genome instability observed in this case. More specifically, the karyotypes became more complex as the disease progressed. *MLL* gene amplification and *TP53* alterations (hemi-allelic loss and a *TP53* frameshift mutation) were present from the time of the initial diagnosis. The third characteristic of note is the severe refractoriness of the disease presentation. Multiple anti-tumor drugs failed to achieve durable remission within any of the administered chemotherapy regimens.

As shown in this case report, the immunophenotype and cell lineage changed repeatedly throughout the duration of the disease course. Although it would have been preferable to verify whether and how the status of the TCR and immunoglobulin reconstitutions changed during disease progression in order to comprehensively discuss and describe clonal evolution and the cell of origin, we are unfortunately unable to do so due to sample limitations. However, based on the persistent cytogenetic and molecular abnormalities detected in the G-band, FISH, and NGS analyses, we concluded that there were lineage conversions between clones derived from a common ancestor. The acute leukemia initially presented with B-lineage cells, with aberrant expression of an erythroid marker (CD71) and a myeloid marker (CD13). Subsequently, the leukemia evolved to become B/T bi-phenotypic. Next, a dynamic lineage switch occurred, and the leukemia transformed to a myeloid lineage. Finally, a new monoblastic population was identified. With the exception of the persistent and strong expression of CD34 (a cell surface marker for early-stage hematopoiesis), we found that the expression patterns of the immunophenotypic markers of leukemic cells were constantly changing. A series of flow cytometry data indicated that the leukemia-initiating cells in this case had the potential to express not only B-lymphoid markers (CD19, CD20, cyCD22, and CD79a), but also T-lymphoid (cyCD3), myeloid (MPO, CD13, and CD33), monocytic (CD14), and erythroid (CD71) markers. Therefore, in this case, the cell of origin may have transformed at the early stages of hematopoiesis, such as hematopoietic stem cells (HSCs) or multipotent progenitors (MPPs).

The precise mechanisms of lineage interconversion remain to be fully elucidated with respect to *MLL*-rearranged leukemia as well as other genotyped leukemias. A previous study showed that *MLL* rearrangements were prevalent in the almost 80% of pediatric B-ALL patients who experienced lineage conversion to AML after undergoing chemotherapies with or without hematopoietic stem cell transplantation (3). In addition, an increasing number of AML phenotypic relapses in patients with *MLL*-rearranged B-ALL have been reported, especially after undergoing CD19-targeting immunotherapies (including blinatumomab and chimeric antigen receptor [CAR] T-cell therapy) (9, 10, 23, 24). These clinical observations support the hypothesis that *MLL*-fusion leukemia is prone to lineage ambiguity. Considering that the overexpression of the wild-type MLL protein produced by *MLL* gene amplification shares some target genes (e.g., *HOXA*, *MEIS1*) as well as an epigenetic regulatory system (e.g., histone H3K4 trimethylation) with MLL fusion proteins (13, 25–28), *MLL* amplification may potentially play a role in leukemia lineage plasticity. Nevertheless, the differences and redundancies between *MLL* rearrangements and *MLL* amplification remain controversial. It is also unknown whether the *MLL* amplicon functions as a driver or a passenger in the process of leukemogenicity. Additional studies are warranted to investigate the biological significance of *MLL* amplification in leukemia.

MLL gene amplification is found in approximately 1% of AML cases (12–14, 29). Unlike the broad immunophenotypic repertoire of *MLL*-rearranged leukemias, *MLL*-amplified leukemia has been reported mostly in myeloid cases, including AML, MDS, and therapy-related myeloid neoplasms (t-MNs) previously treated with alkylating agents (12–15, 25, 26, 28–30). B-ALL with *MLL* amplification is extremely rare, with only a few cases described in the literature to date (29–31). Moreover, to our best knowledge, no cases of mixed lineage leukemia (MPAL) or of lineage switching leukemia with *MLL* amplification have been reported. Older age, DIC, therapy resistance, and poor outcomes were common characteristics of the previously reported cases of AML presenting with *MLL* amplification (12, 13, 15). These clinical features matched well with the present case. Interestingly, some genomic features that appeared in our case also seemed to be associated with *MLL* amplification. For example, previous cases of *MLL*-amplified AML/MDS almost always displayed highly complex karyotypes and frequently contained -5/del (5q), del(-7q), -17/del(17p), and -18 abnormalities (12, 13, 15, 25). In most *MLL*-amplified cases reported to date, karyotypes were reported to become more complex within short intervals (13, 15). These cytogenetic features were also observed in this case.

Tumor protein p53 (*TP53*) is a tumor suppressor gene located on the short arm of chromosome 17. The p53 protein is an important transcription factor that regulates cell cycle arrest, apoptosis, and the DNA damage response. Due to its function as a guardian of chromosomal stability and genome integrity, the loss and/or mutational inactivation of p53 leads to genomic instability, thus resulting in oncogene amplification and aneuploidy (15). Cancers with p53 dysfunction are typically refractory to therapy and have unfavorable prognoses. Compared with *TP53* mutations in solid tumores (which are

detected at a rate of more than 50%), the loss of or mutations in the *TP53* gene occur relatively rarely in hematological malignancies (32, 33). Among newly diagnosed patients, monosomy 17 is estimated to occur in approximately 7% of adult Ph-negative B-ALL cases (34), as well as in approximately 6% of adult AML cases (35). Moreover, the incidences of *TP53* mutations at initial diagnosis is approximately 8% in adult Ph-negative B-ALL patients (33, 36), and is approximately 8% in adult AML patients (32), respectively. In contrast, when the entity is limited to *MLL*-amplified AML/MDS, the frequency of monosomy 17 becomes remarkably higher and is estimated to reach 38% (13). Moreover, regardless of the presence or absence of cytogenetic abnormalities involving chromosome 17, the *TP53* gene is often mutated in *MLL*-amplified AML/MDS (13, 15, 25, 29). One previous study revealed that 94% of AML/MDS cases with 11q/*MLL* amplification carried *TP53* mutations (25). Hence, the loss of functional p53 may be critical to the etiology and progression of this *MLL*-amplified leukemia, including our currently reported case (25, 29).

The *TP53* gene mutation in the present case was a frameshift mutation in the DNA-binding domain that occurred concurrently with monosomy 17 since the time of the initial diagnosis. The vast majority of *TP53* mutations in malignancies (including AML and ALL) are found in the DNA binding domain (encoded by exons 5–8), with hot spots located at six particular amino acid residues, (R175, G245, R248, R249, R273, and R282) (32, 33). These are predominantly missense alternations resulting in mutant p53 proteins with one substituted amino acid; this abrogates DNA binding ability and impairs transcriptional activity (33, 37). As knowledge of *TP53* mutations in leukemogenesis has expanded in recent years, the mutant p53 protein has been found to not only plays a role as a typical tumor suppressor gene through loss-of-function alternations, but also potentially acts in a dominant negative or a gain-of-function manner (depending on mutated residues, the status of the remaining wild-type allele, and the context of the presenting cell types) (32, 37–39). *TP53* alterations are usually monoallelic. During disease progression, the remaining *TP53* wild-type gene in the second allele is also altered or lost due to mutation, monosomy of chromosome 17p/17, or loss of heterozygosity (LOH) (33) In contrast to these missense mutations, it is still unclear whether *TP53* frameshift mutations, as in our case, can be translated into C-terminus truncated mutant proteins. In addition, even though truncated p53 proteins exist, their biological functions are also still unclear. Additional investigation is warranted to clarify these points.

Lineage switching in leukemia generally occurs either at the first or second relapse (2). In contrast, lineage conversion during induction therapy without or prior to durable remission is atypical and is limited to a few reports of childhood cases (2, 3, 40–42). The clinical outcomes of leukemia cases where lineage switching occurs earlier than remission appear to be devastating. All reported patients, including our adult case, died within several months of the initial diagnosis (2, 41, 42). Currently, there is no standard recommended therapy for lineage switching leukemia and MPAL. Therefore, physicians often face challenges in the proper choice of therapy for ambiguous lineage leukemia as well as with regard to performing differential diagnoses. According to a recent retrospective study, allogenic hematopoietic stem cell transplantation (alloHSCT) in the first remission improves outcomes in adult MPAL (43). In addition, studies report that certain targeted therapies may be beneficial for child or young adult MPAL patients (20). However, caution should be exercised when using targeted therapies, as there is a theoretical risk of propagating non-targeted clones (43). For lineage switching leukemia, which patients with an extremely devastating prognosis, there have only been a few reports to date of cases experiencing long-term remission. For example, a case report of an infant patient with lineage switching leukemia showed that administering alloHSCT as a consolidation therapy following remission resulted in well-controlled disease without relapse over the course of almost 2 years of follow-up (24). In the present case, however, alloHSCT with reduced-intensity conditioning was not a viable option because of the patient's advanced age and lack of remission.

To better understand the underlying pathophysiological mechanisms and develop an effective treatment strategy based on these mechanisms, animal disease models that recapitulate human leukemic characteristics are urgently needed. Recent studies using *MLL*-rearranged leukemia mouse models have shown that the hematopoietic niche, which changes during development and aging, plays an important role in determining the lineage of leukemic cells (11, 44, 45). Contrarily, several experimental studies using specific gene-expressing mouse models have revealed that the lineage output of leukemia can be more ambiguous depending on the hematopoietic hierarchy and the developmental and aging stage of the leukemic cells (44, 46–48). Another study using MPAL patient-derived xenograft (PDX) models also supported the relationship between lineage fate and the cell of origin by demonstrating that the cell of origin, which is rooted in immature hematopoietic progenitors, primes leukemia cells for lineage promiscuity in MPAL (20). Comprehensive analyses of the genome, epigenome, and transcriptome at the single-cell level would be helpful in elucidating the precise molecular mechanisms underlying clonal evolution and cell lineage plasticity. Given the rarity and heterogeneity of lineage conversion and MPAL, the utilization of NGS should be considered in each individual patient. This may enable not only effective disease profiling but also more comprehensive treatment recommendations for precision medicine.

In summary, we report that our case of refractory B-ALL with lineage conversion to AML, which occurred in an elderly patient, exhibited lineage ambiguity and genome instability. The cell of origin may have had multi-lineage potential. Treatment may exert selective pressure that drives clonal selectivity. Leukemia subclones harboring *TP53* mono-allelic loss, *TP53* frameshift mutation, and *MLL* amplification appeared to provide advantages in terms of proliferation and treatment resistance. For rare leukemia subtypes with no established therapies, effective pathophysiology-based therapy is urgently needed.

CONCLUSION

Herein we presented a case of an elderly patient with Ph-negative B-ALL. Her leukemia was refractory to treatment and progressed with repetitive immunophenotypic changes. Dynamic lineage conversion from ALL to AML occurred after clofarabine monotherapy was provided as a fourth induction regimen. The karyotype was highly complex and rapidly increased in complexity. A monoallelic deletion and frameshift mutation in *TP53* gene accompanied by *MLL* gene amplification may have contributed to lineage plasticity and therapeutic resistance in this case. Additional accumulation of case studies, comprehensive clinical research, and basic and translational investigations are required to better understand this rare presentation of a form of leukemia that is currently without standard therapies or definitive medical guidelines. Our findings thereby guide and inform further research directions, medical guidelines, and effective clinical decision-making.

DATA AVAILABILITY STATEMENT

The datasets presented in this study can be found in online repositories. The names of the repository/repositories and accession number(s) can be found below: NBDC Human Database, JGAD000600, https://humandbs.biosciencedbc.jp/hum0318-v1.

ETHICS STATEMENT

The studies involving human participants were reviewed and approved by the Institutional Review Board of the Institute of Medical Science, the University of Tokyo. The patients/participants provided their written informed consent to participate in this study.

AUTHOR CONTRIBUTIONS

RT, KY, TF, and AT designed the study. RT, KY, TF, TK, NO, and KU participated in patient treatment and analyzed clinical data. KY, MI, NY, RK, ES, RY, SI, SM, and AT performed next-generation sequencing and analyzed the data. RT drafted the manuscript, KY and TF helped draft the manuscript. AT supervised the work and helped draft the manuscript. All authors have read and approved of the final version of the manuscript.

ACKNOWLEDGMENTS

We are deeply grateful to the physicians, nurses, and other staff at Research Hospital IMSUT and especially the patients and their families.

REFERENCES

1. Stass S, Mirro J, Melvin S, Pui CH, Murphy SB, Williams D. Lineage Switch in Acute Leukemia. *Blood* (1984) 64:701–6. doi: 10.1182/blood.V64.3.701.bloodjournal643701
2. Dorantes-Acosta E, Pelayo R. Lineage Switching in Acute Leukemias: A Consequence of Stem Cell Plasticity? *Bone Marrow Res* (2012) 2012:406796. doi: 10.1155/2012/406796
3. Rossi JG, Bernasconi AR, Alonso CN, Rubio PL, Gallego MS, Carrara CA, et al. Lineage Switch in Childhood Acute Leukemia: An Unusual Event With Poor Outcome. *Am J Hematol* (2012) 87:890–7. doi: 10.1002/ajh.23266
4. Trikalinos NA, Soupir CP, Dey BR. Lineage Switch of Acute Lymphocyctic Leukaemia With T(4(Q21;Q23) Into Acute Myeloid Leukaemia in an Adult Patient After Allogeneic Stem Cell Transplantation. *Br J Haematol* (2009) 145:262–4. doi: 10.1111/j.1365-2141.2009.07586.x
5. Wu B, Jug R, Luedke C, Su P, Rehder C, McCall C. Lineage Switch Between B-Lymphoblastic Leukemia and Acute Myeloid Leukemia Intermediated by "Occult" Myelodysplastic Neoplasm: Two Cases of Adult Patients With Evidence of Genomic Instability and Clonal Selection by Chemotherapy. *Am J Clin Pathol* (2017) 148:136–47. doi: 10.1093/ajcp/aqx055
6. Della Starza I, Ceglie G, Nunes V, Gianfelici V, Marinelli M, Fuligni F. A Case of Lineage Switch From B-Cell Acute Lymphoblastic Leukaemia to Acute Myeloid Leukaemia. Role of Subclonal/Clonal Gene Mutations. *Br J Haematol* (2016) 174:648–51. doi: 10.1111/bjh.13800
7. Hu T, Murdaugh R, Nakada D. Transcriptional and Microenvironmental Regulation of Lineage Ambiguity in Leukemia. *Front Oncol* (2017) 7:268. doi: 10.3389/fonc.2017.00268
8. Takahashi K, Wang F, Morita K, Yan Y, Hu P, Zhao P, et al. Futreal: Integrative Genomic Analysis of Adult Mixed Phenotype Acute Leukemia Delineates Lineage Associated Molecular Subtypes. *Nat Commun* (2018) 9:2670. doi: 10.1038/s41467-018-04924-z
9. Jacoby E, Nguyen SM, Fountaine TJ, Welp K, Gryder B, Qin H. CD19 CAR Immune Pressure Induces B-Precursor Acute Lymphoblastic Leukaemia Lineage Switch Exposing Inherent Leukaemic Plasticity. *Nat Commun* (2016) 7:12320. doi: 10.1038/ncomms12320
10. Aldoss I, Song JY. Extramedullary Relapse of KMT2A(MLL)-Rearranged Acute Lymphoblastic Leukemia With Lineage Switch Following Blinatumomab. *Blood* (2018) 131:2507. doi: 10.1182/blood-2018-02-834911
11. Rowe RG, Lummertz da Rocha E, Sousa P, Missios P, Morse M, Marion W, et al. The Developmental Stage of the Hematopoietic Niche Regulates Lineage in MLL-Rearranged Leukemia. *J Exp Med* (2019) 216:527–38. doi: 10.1084/jem.20181765
12. Sarova I, Brezinova J, Zemanova Z, Izakova S, Lizcova L, Malinova E, et al. Cytogenetic Manifestation of Chromosome 11 Duplication/Amplification in Acute Myeloid Leukemia. *Cancer Genet Cytogenet* (2010) 199:121–7. doi: 10.1016/j.cancergencyto.2010.02.012
13. Tang G, DiNardo C, Zhang L, Ravandi F, Khoury JD, Huh YO, et al. MLL Gene Amplification in Acute Myeloid Leukemia and Myelodysplastic Syndromes is Associated With Characteristic Clinicopathological Findings and TP53 Gene Mutation. *Hum Pathol* (2015) 46:65–73. doi: 10.1016/j.humpath.2014.09.008
14. Cuthbert G, Thompson K, McCullough S, Watmore A, Dickinson H, Telford N, et al. MLL Amplification in Acute Leukaemia: A United Kingdom Cancer Cytogenetics Group (UKCCG) Study. *Leukemia* (2000) 14:1885–91. doi: 10.1038/sj.leu.2401919
15. Andersen MK, Christiansen DH, Kirchhoff M, Pedersen-Bjergaard J. Duplication or Amplification of Chromosome Band 11q23, Including the Unrearranged MLL Gene, is a Recurrent Abnormality in Therapy-Related MDS and AML, and is Closely Related to Mutation of the TP53 Gene and to Previous Therapy With Alkylating Agents. *Genes Chromosomes Cancer* (2001) 31:33–41. doi: 10.1002/gcc.1115
16. Moorman AV, Harrison CJ, Buck GA, Richards SM, Secker-Walker LM, Martineau M, et al. Karyotype is an Independent Prognostic Factor in Adult Acute Lymphoblastic Leukemia (ALL): Analysis of Cytogenetic Data From Patients Treated on the Medical Research Council (MRC) UKALLXII/Eastern Cooperative Oncology Group (ECOG) 2993 Trial. *Blood* (2007) 109:3189–97. doi: 10.1182/blood-2006-10-051912
17. Pui CH, Evans WE. Treatment of Acute Lymphoblastic Leukemia. *N Engl J Med* (2006) 354:166–78. doi: 10.1056/NEJMra052603
18. Gökbuget N, Hoelzer D. Treatment of Adult Acute Lymphoblastic Leukemia. *Semin Hematol* (2009) 46:64–75. doi: 10.1053/j.seminhematol.2008.09.003

19. Arber DA, Orazi A, Hasserjian R, Thiele J, Borowitz MJ, Le Beau MM, et al. The 2016 Revision to the World Health Organization Classification of Myeloid Neoplasms and Acute Leukemia. *Blood* (2016) 127:2391–405. doi: 10.1182/blood-2016-03-643544
20. Alexander TB, Gu Z, Iacobucci I, Dickerson K, Choi JK, Xu B, et al. The Genetic Basis and Cell of Origin of Mixed Phenotype Acute Leukaemia. *Nature* (2018) 562:373–9. doi: 10.1038/s41586-018-0436-0
21. Yokoyama K, Shimizu E, Yokoyama N, Nakamura S, Kasajima R, Ogawa M, et al. Tojo: Cell-Lineage Level-Targeted Sequencing to Identify Acute Myeloid Leukemia With Myelodysplasia-Related Changes. *Blood Adv* (2018) 2:2513–21. doi: 10.1182/bloodadvances.2017010744
22. Takeda R, Yokoyama K, Kobayashi S, Kawamata T, Nakamura S, Fukuyama T. An Unusually Short Latent Period of Therapy-Related Myeloid Neoplasm Harboring a Rare MLL-EP300 Rearrangement: Case Report and Literature Review. *Case Rep Hematol* (2019) 2019:4532434. doi: 10.1155/2019/4532434
23. Liao W, Kohler ME, Fry T, Ernst P. Does Lineage Plasticity Enable Escape From CAR-T Cell Therapy? Lessons From MLL-R Leukemia. *Exp Hematol* (2021) 100:1–11. doi: 10.1016/j.exphem.2021.07.002
24. Rayes A, McMasters RL, O'Brien MM. Lineage Switch in MLL-Rearranged Infant Leukemia Following CD19-Directed Therapy. *Pediatr Blood Cancer* (2016) 63:1113–5. doi: 10.1002/pbc.25953
25. Zatkova A, Merk S, Wendehack M, Bilban M, Muzik EM, Muradyan A, et al. AML/MDS With 11q/MLL Amplification Show Characteristic Gene Expression Signature and Interplay of DNA Copy Number Changes. *Genes Chromosomes Cancer* (2009) 48:510–20. doi: 10.1002/gcc.20658
26. Muntean AG, Hess JL. The Pathogenesis of Mixed-Lineage Leukemia. *Annu Rev Pathol* (2012) 7:283–301. doi: 10.1146/annurev-pathol-011811-132434
27. Poppe B, Vandesompele J, Schoch C, Lindvall C, Mrozek K, Bloomfield CD, et al. Expression Analyses Identify MLL as a Prominent Target of 11q23 Amplification and Support an Etiologic Role for MLL Gain of Function in Myeloid Malignancies. *Blood* (2004) 103:229–35. doi: 10.1182/blood-2003-06-2163
28. Angelova S, Spassov B, Nikolova V, Christov I, Tzvetkov N, Simeonova M. Is Amplification of C-MYC, MLL and RUNX1 Genes in AML and MDS Patients With Trisomy 8, 11 and 21 a Factor for a Clonal Evolution in the Karyotype? *Cytol Genet* (2015) 49:165–72. doi: 10.3103/S0095452715030032
29. Bianchi JJ, Murigneux V, Bedora-Faure M, Lescale C, Deriano L. Breakage-Fusion-Bridge Events Trigger Complex Genome Rearrangements and Amplifications in Developmentally Arrested T Cell Lymphomas. *Cell Rep* (2019) 27:2847–58.e4. doi: 10.1016/j.celrep.2019.05.014
30. Racke F, Cole C, Walker A, Jones J, Heerema NA. Therapy-Related Pro-B Cell Acute Lymphoblastic Leukemia: Report of Two Patients With MLL Amplification. *Cancer Genet* (2012) 205:653–6. doi: 10.1016/j.cancergen.2012.11.001
31. Espinet B, Florensa L, Salido M, Solé F. MLL Intrachromosomal Amplification in a Pre-B Acute Lymphoblastic Leukemia. *Haematologica* (2003) 88:EIM03.
32. Molica M, Mazzone C, Niscola P, de Fabritiis P. TP53 Mutations in Acute Myeloid Leukemia: Still a Daunting Challenge? *Front Oncol* (2020) 10:610820. doi: 10.3389/fonc.2020.610820
33. Salmoiraghi S, Rambaldi A, Spinelli O. TP53 in Adult Acute Lymphoblastic Leukemia. *Leuk Lymphoma* (2018) 59:778–89. doi: 10.1080/10428194.2017.1344839
34. Lafage-Pochitaloff M, Baranger L, Hunault M, Cuccuini W, Lefebvre C, Bidet A, et al. Impact of Cytogenetic Abnormalities in Adults With Ph-Negative B-Cell Precursor Acute Lymphoblastic Leukemia. *Blood* (2017) 130:1832–44. doi: 10.1182/blood-2017-05-783852
35. Strickland SA, Sun Z, Ketterling RP, Cherry AM, Cripe LD, Dewald G, et al. Independent Prognostic Significance of Monosomy 17 and Impact of Karyotype Complexity in Monosomal Karyotype/Complex Karyotype Acute Myeloid Leukemia: Results From Four ECOG-ACRIN Prospective Therapeutic Trials. *Leuk Res* (2017) 59:55–64. doi: 10.1016/j.leukres.2017.05.010
36. Salmoiraghi S, Montalvo ML, Ubiali G, Tosi M, Peruta B, Zanghi P, et al. Mutations of TP53 Gene in Adult Acute Lymphoblastic Leukemia at Diagnosis do Not Affect the Achievement of Hematologic Response But Correlate With Early Relapse and Very Poor Survival. *Haematologica* (2016) 101:e245–8. doi: 10.3324/haematol.2015.137059
37. Sabapathy K. The Contrived Mutant P53 Oncogene - Beyond Loss of Functions. *Front Oncol* (2015) 5:276. doi: 10.3389/fonc.2015.00276
38. Boettcher S, Miller PG, Sharma R, McConkey M, Leventhal M, Krivtsov AV, et al. A Dominant-Negative Effect Drives Selection of TP53 Missense Mutations in Myeloid Malignancies. *Science* (2019) 365:599–604. doi: 10.1126/science.aax3649
39. Loizou E, Banito A, Livshits G, Ho YJ, Koche RP, Sánchez-Rivera FJ, et al. A Gain-of-Function P53-Mutant Oncogene Promotes Cell Fate Plasticity and Myeloid Leukemia Through the Pluripotency Factor FOXH1. *Cancer Discov* (2019) 9:962–79. doi: 10.1158/2159-8290.CD-18-1391
40. Ridge SA, Cabrera ME, Ford AM, Tapia S, Risueno C, Labra S, et al. Rapid Intraclonal Switch of Lineage Dominance in Congenital Leukaemia With a MLL Gene Rearrangement. *Leukemia* (1995) 9:2023–6.
41. Sakaki H, Kanegane H, Nomura K, Goi K, Sugita K, Miura M, et al. Early Lineage Switch in an Infant Acute Lymphoblastic Leukemia. *Int J Hematol* (2009) 90:653–5. doi: 10.1007/s12185-009-0446-7
42. Hershfield MS, Kurtzberg J, Harden E, Moore JO, Whang-Peng J, Haynes BF. Conversion of a Stem Cell Leukemia From a T-Lymphoid to a Myeloid Phenotype Induced by the Adenosine Deaminase Inhibitor 2'-Deoxycoformycin. *Proc Natl Acad Sci USA* (1984) 81:253–7. doi: 10.1073/pnas.81.1.253
43. Wolach O, Stone RM. Optimal Therapeutic Strategies for Mixed Phenotype Acute Leukemia. *Curr Opin Hematol* (2020) 27:95–102. doi: 10.1097/MOH.0000000000000570
44. Duguid A, Mattiucci D, Ottersbach K. Infant Leukaemia - Faithful Models, Cell of Origin and the Niche. *Dis Model Mech* (2021) 14:dmm049189. doi: 10.1242/dmm.049189
45. Antunes ETB, Ottersbach K. The MLL/SET Family and Haematopoiesis. *Biochim Biophys Acta Gene Regul Mech* (2020) 1863:194579. doi: 10.1016/j.bbagrm.2020.194579
46. Fagnan A, Bagger FO, Piqué-Borràs MR, Ignacimouttou C, Caulier A, Lopez CK, et al. Human Erythroleukemia Genetics and Transcriptomes Identify Master Transcription Factors as Functional Disease Drivers. *Blood* (2020) 136:698–714. doi: 10.1182/blood.2019003062
47. Chaudhury S, O'Connor C, Cañete A, Bittencourt-Silvestre J, Sarrou E, Prendergast Á, et al. Age-Specific Biological and Molecular Profiling Distinguishes Paediatric From Adult Acute Myeloid Leukaemias. *Nat Commun* (2018) 9:5280. doi: 10.1038/s41467-018-07584-1
48. Lopez CK, Noguera E, Stavropoulou V, Robert E, Aid Z, Ballerini P, et al. Ontogenic Changes in Hematopoietic Hierarchy Determine Pediatric Specificity and Disease Phenotype in Fusion Oncogene-Driven Myeloid Leukemia. *Cancer Discov* (2019) 9:1736–53. doi: 10.1158/2159-8290.CD-18-1463

Conflict of Interest: The authors declare that the research was conducted in the absence of any commercial or financial relationships that could be construed as a potential conflict of interest.

frontiers | Frontiers in Oncology

ORIGINAL RESEARCH
published: 14 April 2022
doi: 10.3389/fonc.2022.879471

TIM-3 Expression Level on AML Blasts Correlates With Presence of Core Binding Factor Translocations Rather Than Clinical Outcomes

Jian Hong[1†], Leiming Xia[2†], Zhenqi Huang[1], Xiaodong Yuan[3], Xinglin Liang[1], Jifei Dai[1], Zhonghui Wu[1], Li Liang[1], Min Ruan[1], Zhangbiao Long[1], Xin Cheng[1], Xiaowen Chen[1], Jing Ni[1], Jian Ge[1], Qingsheng Li[1], Qingshu Zeng[1], Ruixiang Xia[1], Yi Wang[4‡] and Mingzhen Yang[1,2*‡]*

[1] Department of Hematology, The First Affiliated Hospital of Anhui Medical University, Hefei, China, [2] Department of Hematology, The Forth Affiliated Hospital of Anhui Medical University, Hefei, China, [3] Division of Life Sciences and Medicine, Department of Organ Transplantation Center, Transplant and Immunology Laboratory, The First Affiliated Hospital of University of Science and Technology of China (USTC), University of Science and Technology of China, Hefei, China, [4] Department of Oncology, The Third Affiliated Hospital of Anhui Medical University, Hefei, China

OPEN ACCESS

Edited by:
Spiros Vlahopoulos,
University of Athens, Greece

Reviewed by:
Vadim V. Sumbayev,
University of Kent, United Kingdom
Shuxin Huang,
Jinan University, China
Nunki Hassan,
Royal North Shore Hospital, Australia

***Correspondence:**
Mingzhen Yang
yangmz89@163.com
Yi Wang
648744276@qq.com

[†]These authors have contributed equally to this work and share first authorship

[‡]These authors have contributed equally to this work and share last authorship

Specialty section:
This article was submitted to Hematologic Malignancies, a section of the journal Frontiers in Oncology

Received: 19 February 2022
Accepted: 18 March 2022
Published: 14 April 2022

Citation:
Hong J, Xia L, Huang Z, Yuan X, Liang X, Dai J, Wu Z, Liang L, Ruan M, Long Z, Cheng X, Chen X, Ni J, Ge J, Li Q, Zeng Q, Xia R, Wang Y and Yang M (2022) TIM-3 Expression Level on AML Blasts Correlates With Presence of Core Binding Factor Translocations Rather Than Clinical Outcomes. Front. Oncol. 12:879471. doi: 10.3389/fonc.2022.879471

Background: T-cell immunoglobulin and mucin domain-containing molecule 3 (TIM-3) expresses on leukemic stem and progenitor populations of non-M3 acute myeloid leukemia (AML) as well as T lymphocytes. TIM-3 is thought to be involved in the self-renewal of leukemic stem cells and the immune escape of AML cells, however its correlation with AML prognosis is still controversial and worthy of further investigation.

Methods: we simultaneously assessed TIM-3 expression levels of leukemic blasts and T lymphocytes in the bone marrow of *de novo* AML patients using flow cytometry. The correlations of TIM-3 expression between leukemic blasts and T lymphocytes and the correlations of TIM-3 expression with various patient parameters were analyzed. In addition, the Cancer Genome Atlas (TCGA) data of AML patients were acquired and analyzed to verify the results.

Results: TIM-3 expression of $CD34^+$ leukemic blasts (R^2 = 0.95, p<0.0001) and $CD34^+CD38^-$ leukemic stem cells (R^2 = 0.75, p<0.0001) were significantly and positively correlated with that of the whole population of leukemic blasts. In addition, TIM-3 expression level of leukemic blasts correlated significantly and positively with that of $CD8^+$ (R^2 = 0.44, p<0.0001) and $CD4^+$ (R^2 = 0.16, p=0.0181) lymphocytes, and higher TIM-3 expression of leukemic blasts was significantly associated with a greater proportion of peripheral $CD8^+$ T lymphocytes (R^2 = 0.24, p=0.0092), indicating that TIM-3 on leukemic blasts might alter adaptive immunity of AML patients. Regarding clinical data, the presence of core binding factor (CBF) translocations was significantly correlated with higher TIM-3 expression of leukemic blasts (CBF versus non-CBF, median 22.78% versus 1.28%, p=0.0012), while TIM-3 expression levels of leukemic blasts were not significantly associated with the remission status after induction chemotherapy (p=0.9799), overall survival (p=0.4201) or event-free survival (p=0.9873). Similar to our results, TCGA data

showed that patients with CBF translocations had significantly higher mRNA expression level of HAVCR2 (the gene encoding TIM-3) (median, 9.81 versus 8.69, $p<0.0001$), and as all patients in the cohort were divided into two groups based on the median HAVCR2 expression level, 5-year overall survivals were not significantly different (low versus high, 24.95% versus 24.54%, $p=0.6660$).

Conclusion: TIM-3 expression level on AML blasts correlates with presence of CBF translocations rather than clinical outcomes.

Keywords: TIM-3, acute myeloid leukemia, core binding factor translocation, prognosis, flow cytometry

INTRODUCTION

T-cell immunoglobulin and mucin domain-containing molecule 3 (TIM-3) is a membrane protein which was discovered initially on $CD4^+$ T helper 1 (Th1) and $CD8^+$ T cytotoxic 1 cells (1), and later on a variety of other cell types including regulatory T (Treg) cells (2), dendritic cells (3), natural killer (NK) cells (4), myeloid cells (5) and mast cells (6). TIM-3 is generally considered as a negative regulator of immune system (7), and has been investigated as a blockade target for immunotherapy of cancer in pre-clinical and clinical settings (8–10).

Interestingly, TIM-3 also expresses on leukemic stem and progenitor populations of non-M3 acute myeloid leukemia (AML) and associated with leukemic transformation of preleukemic diseases, such as myelodysplastic syndrome (MDS) and myeloproliferative neoplasm (11). TIM-3 and its ligand, galectin-9 (Gal-9), constitute an autocrine loop which drives the self-renewal of AML stem cells by activating the nuclear factor-κB (NF-κB) and β-catenin pathways (11). Besides, both TIM-3 and Gal-9 can be released in a free soluble form and involved in the immune escape of AML cells (12).

TIM-3 expression on immune cells has been reported to be associated with disease activity and prognosis in multiple types of cancers, e.g. AML (13), pediatric B-precursor acute lymphoid leukemia (14), lung cancer (2, 4). In general, higher TIM-3 expression was related to poorer prognosis. Additionally, the relation between TIM-3 expression on AML blasts and prognosis of AML was also investigated and contradictory data were published in the literature. Darwish et al. and Kamal et al. both reported TIM-3 as a biomarker of poor prognosis in AML, while Xu et al. reported that increased TIM-3 expression correlated with low-risk group and higher complete remission rate in newly diagnosed non-M3 AML patients (15–17).

According to the data mentioned above, TIM-3 expression on T cells and AML blasts are both related to prognosis of AML, and there might be an association between TIM-3 expression on T cells and AML blasts. To our knowledge, this issue has not been well investigated and published in the literature. In this study, we assessed simultaneously the TIM-3 expression on T cells and AML blasts in patients with non-M3 *de novo* AML using flow cytometry, and investigated its correlation with clinical outcomes, as well as other clinical parameters, including French-American-British (FAB) classifications, genetic abnormalities and risk stratifications. Furthermore, the Cancer Genome Atlas (TCGA) data for AML were obtained and analyzed to validate the impact of TIM-3 expression on prognosis of non-M3 AML patients.

MATERIALS AND METHODS

Patients

A total of 34 patients diagnosed with *de novo* AML (except for M3) were recruited from the Department of Hematology, the First Affiliated Hospital of Anhui Medical University (Hefei, China) between July 2018 and May 2020. The demographic and clinical data of these patients were shown in. The diagnosis and classification of these patients were based on the revised FAB classification and the 2016 World Health Organization (WHO) criteria. Smears of bone marrow aspirates were stained with Wright–Giemsa stain. Immunophenotyping analyses of leukemic cells were applied according to the "EGIL recommendations". Eight important fusion genes, including PML-RARα, AML1-ETO, CBFβ-MYH11, BCR-ABL, MLL-AF9, DEK-CAN, PLZF-RARα and NPM-MLF, were detected using reverse transcriptase-polymerase chain reaction (RT-PCR). Next-generation sequencing-based detection of somatic mutations were performed using bone marrow samples for a panel of 20 genes (ASXL1, BCOR, CEBPA, DNMT3A, EZH2, FLT3, GATA2, IDH1, IDH2, KIT, KRAS, MLL, NPM1, NRAS, PDGFRA, PHF6, RUNX1, TET2, TP53 and WT1). Karyotypic analyses were performed using conventional R-banding assay, following standard 24-hour unstimulated culture of bone marrow samples. Up to 20 cells were analyzed for clonal abnormalities according to the International System for Human Cytogenetic Nomenclature (ISCN 2005) guidelines. Patients were divided into low, intermediate and high risk groups according to the 2017 European LeukemiaNet (ELN) risk stratification by genetics. FLT3-ITD was detected using next-generation sequencing rather than PCR-based deoxyribonucleic acid analysis, therefore allelic ratio of FLT3-ITD could not be calculated and all cases of FLT3-ITD were considered as high allele ratio during ELN risk stratification.

Thirty-two Patients received induction chemotherapies and the other two patients were given supportive care. The details of chemotherapy regimens were listed in **Table 1**. The responsiveness to chemotherapy of all surviving patients (27

TABLE 1 | Demographic and clinical data of AML patients.

Patient characteristics (n=34)	
Gender, male/female	19/15
Median age, years(range)	51 (23-67)
Median WBC, $\times10^9$/L(range)	18.3 (0.5-242.3)
Median HB, g/L(range)	85.0 (34.0-127.0)
Median PLT, $\times10^9$/L(range)	38.5 (3.0-522.0)
FAB	
M1	2
M2	19
M4	5
M5	8
Karyotype	
normal	14
t(8;21) or AML1-ETO	4
inv(16) or t(16;16) or CBFβ-MYH11	4
t(9;22) or BCR-ABL	2
t(9;11) or MLLT3-KMT2A	2
complex	2
others	3
no data	3
Gene mutations	
FLT3-ITD	6
FLT3-TKD	3
NPM1	6
TET2	4
DNMT3A	5
ASXL1	3
KIT	3
NRAS	5
KRAS	1
IDH1	4
IDH2	4
single-mutated CEBPA	2
double-mutated CEBPA	4
no data	1
Risk stratification	
low	16
intermediate	5
high	11
not available	2
Treatment	
IA or DA	26
decitabine-based chemotherapy	4
CAG or DAG	2
supportive care	2

WBC, white blood cell; Hb, hemoglobin; PLT, platelet; FAB, French-American-British classification; IA, idarubicin and cytarabine; DA, daunorubicin and cytarabine; CAG, cytarabine, aclarubicin and recombinant granulocyte colony stimulating factor; DAG, daunorubicin, cytarabine and recombinant granulocyte colony stimulating factor.

out of 32) was assessed by the end of the induction chemotherapy. The assessment included a full blood work up and a bone marrow examination. Patients were classified into responders and non-responders. Responders attained complete remission (CR) or complete remission with incomplete count recovery (CRi). CR was defined as absolute neutrophilic count >1,000/μl, a platelet count ≥100,000/μl and <5% bone marrow blasts in a normocellular marrow, with no evidence of extramedullary disease. CRi was defined as <5% bone marrow blasts and no evidence of extramedullary disease without achieving the criteria of CR. Overall survival (OS) was measured from the date of diagnosis to the date of death from any cause. Event-free survival (EFS) was measured from the date of diagnosis to the date of primary refractory disease, relapse, or death from any cause. Patients with minimal residual disease were not considered relapsed for EFS determination.

The present study was approved by the Ethical Committee of the First Affiliated Hospital of Anhui Medical University and performed in accordance with the Declaration of Helsinki.

Flow Cytometric Analysis

Flow cytometry was performed on a Navios Flow Cytometer (Beckman Coulter) and analyzed using Kaluza Flow Cytometry Analysis Software (Beckman Coulter). Fluorescence-conjugated monoclonal antibodies (mAbs) against CD45 (B36294, Beckman coulter, USA), CD3 (IM2472, Beckman coulter, USA), CD8 [IM2469, (B36294, Beckman coulter, USA)], CD34 (IM2472, Beckman coulter, USA), CD38 (B92396, Beckman coulter, USA) and TIM-3 (12-3109-42, eBioscience, USA) were used to analyze the surface expression of TIM-3 on leukemic blasts and T cells in the bone marrow. The gating strategy of TIM-3 expression of leukemic blasts and T lymphocytes is shown in **Supplementary Figure 1**. Peripheral lymphocyte populations including $CD3^+$ T cells ($CD3^+$), $CD8^+$ T cells ($CD3^+CD8^+$), $CD4^+$ T cells ($CD3^+CD4^+$), B cells ($CD3^-CD19^+$), natural killer cells ($CD3^-CD16^+$ or $CD3^-CD56^+$) were assessed according to manufacturer's protocol (Tongsheng Shidai, Beijing, or Beckman coulter, USA) (**Supplementary Figure 2**). Peripheral regulatory $CD4^+$ T cells were labeled with fluorescence-conjugated mAbs against CD4, CD25 and CD127 (Beckman coulter, USA), and the percentage of $CD4^+$ Treg cells was calculated as $CD4^+CD25^+CD127^-$ cells in the $CD4^+$ cell population (**Supplementary Figure 3**). The appropriate isotypes were used as negative controls. Red blood cells in the samples were removed with red blood cell lysis buffer. Th1/Th2/Th17 cytokines in the plasma were assessed using cytometric bead array human Th1/Th2/Th17 cytokine kit according to manufacturer's protocol (BD Biosciences, USA).

TCGA Dataset

The expression data (RNA Seq V2 RSEM) of HAVCR2, the gene encoding TIM-3, from the peripheral blood of a cohort of 200 AML patients in TCGA were downloaded together with corresponding clinical data *via* cBioPortal (http://www.cbioportal.org) (18–20). In total, 157 patients were diagnosed with non-M3 AML and had HAVCR2 expression level. Their data were analyzed in this study. Regarding the risk stratification, 154 patients could be categorized into low, intermediate and high risk groups according to the 2017 ELN risk stratification by genetics, and the presence of FLT3-ITD were all considered as high allele ratio.

Statistical Analysis

Correlations of TIM-3 expression levels between different groups and TIM-3 expression level of leukemic blasts with other parameters were assessed using the spearman's rank correlation coefficient, and the linear regression was additionally carried out.

The Mann-Whitney U test was used to compare differences between two groups, and the Kruskal-Wallis test followed by Dunn's *post hoc* test was used to compare differences between multiple groups.

The probabilities of OS and EFS were estimated by the Kaplan-Meier method and compared by the log-rank test. The end point of the last follow-up for all surviving patients was September 12th, 2021. For all analyses, $p<0.05$ was considered statistically significant. The GraphPad Prism 6 (La Jolla, CA, USA) was used for data analyses.

RESULTS

TIM-3 Expression of CD8$^+$ and CD4$^+$ T Lymphocytes Correlated Positively With That of Leukemic Blasts

We assessed the TIM-3 expression on leukemic blasts of 34 patients diagnosed with *de novo* AML (except for M3) using flow cytometry, and the percentage of TIM-3 expression ranged from 0 to 68.43%. Then, we compared the TIM-3 expression of the whole population of leukemic blasts with that of CD34$^+$ leukemic blasts and CD34$^+$CD38$^-$ leukemic stem cells (LSCs). The results indicated that the TIM-3 expression of CD34$^+$ leukemic blasts (R^2 = 0.95, $p<0.0001$) and CD34$^+$CD38$^-$ LSCs (R^2 = 0.75, $p<0.0001$) were significantly and positively correlated with that of the whole population of leukemic blasts (**Figures 1A, B**). Therefore, we decided to use the TIM-3 expression of the whole population of leukemic blasts for further analyses.

In addition, we assessed the TIM-3 expression of CD8$^+$ and CD4$^+$ T lymphocytes in the bone marrow of these AML patients, and both of them correlated positively with that of leukemic blasts (CD8$^+$ T cells: R^2 = 0.44, $p<0.0001$; CD4$^+$ T cells: R^2 = 0.16, p=0.0181) (**Figures 1C, D**).

Higher TIM-3 Expression of Leukemic Blasts Was Significantly Associated With a Greater Proportion of CD8$^+$ T Lymphocytes

In order to investigate the impact of TIM-3 expression of leukemic blasts on lymphocyte subtypes, we assessed the proportions of lymphocyte subtypes (CD8$^+$ T cells, CD4$^+$ T cells, CD4$^+$ Treg cells, B cells and NK cells) and concentrations of helper T cell-1 (Th1)/Th2/Th17 cytokines (tumor necrosis factor-α, interferon-γ, interleukin-2 [IL-2], IL-4, IL-6, IL-10 and IL-17) in the peripheral blood of these AML patients. Results showed that the TIM-3 expression of leukemic blasts was significantly and positively associated with the proportion of CD8$^+$ T lymphocytes (R^2 = 0.24, p=0.0092) but not other lymphocyte subtypes (**Figure 2**). Moreover, Th1/Th2/Th17 cytokine concentrations did not correlate with the TIM-3 expression of leukemic blasts (**Supplementary Figure 4**).

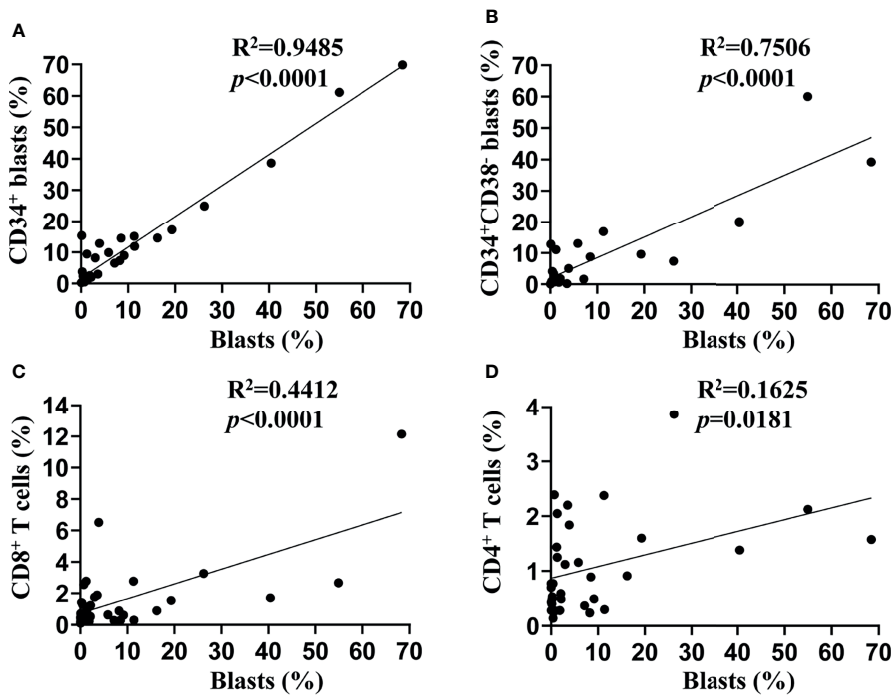

FIGURE 1 | Associations of TIM-3 expression between subtypes of leukemic blasts and T lymphocytes. TIM-3 expression levels on the surface of leukemic blasts and T lymphocytes from bone marrow samples of 34 *de novo* AML patients were assessed using flow cytometry. Linear regression was performed to show associations of TIM-3 expression level of the whole population of leukemic blasts with that of CD34$^+$ leukemic blasts **(A)**, CD34$^+$CD38$^-$ leukemic stem cells **(B)**, CD8$^+$ T lymphocytes **(C)** and CD4$^+$ T lymphocytes **(D)**.

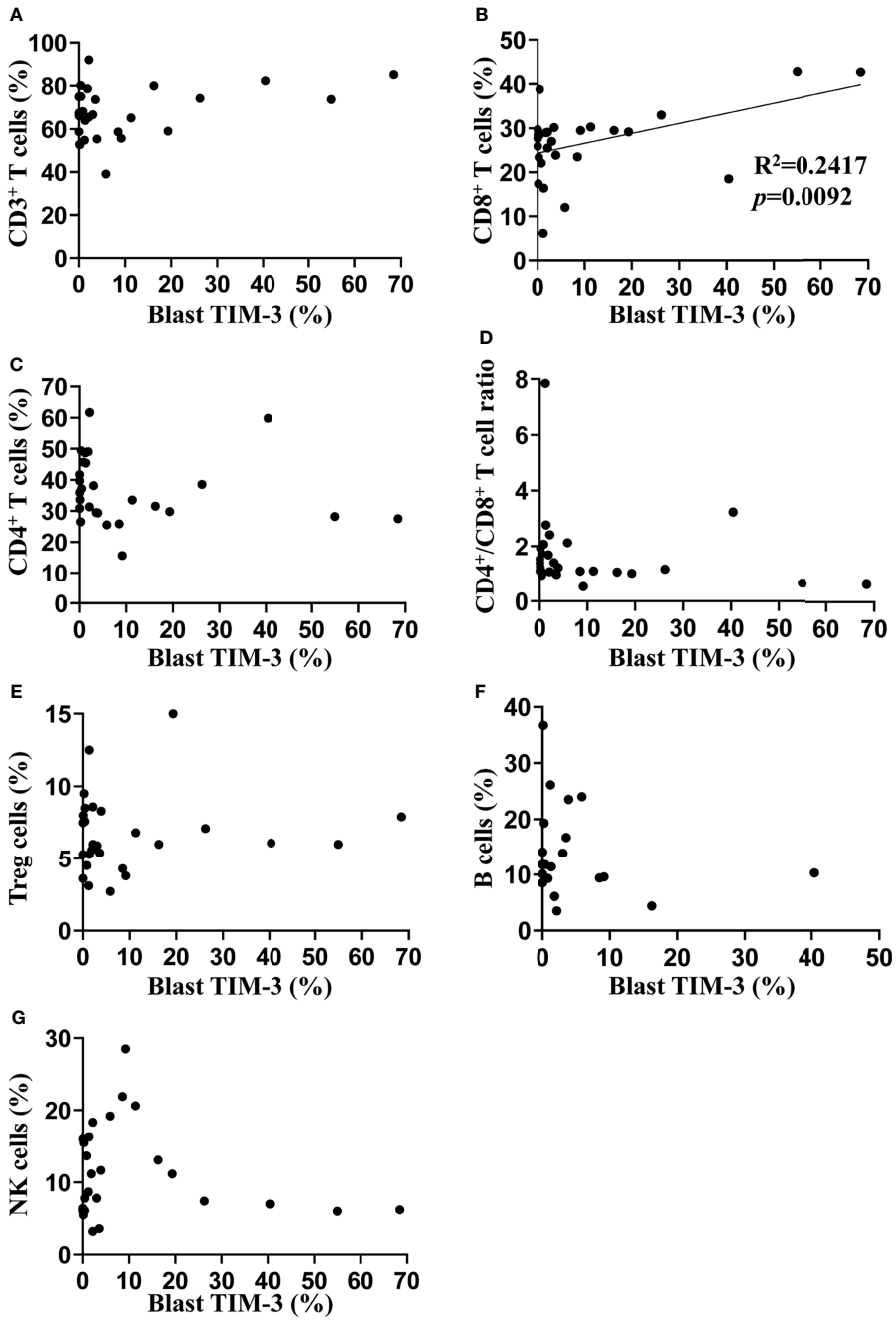

FIGURE 2 | Associations of TIM-3 expression level of leukemic blasts with proportions of peripheral lymphocyte subtypes in AML patients. Proportions of multiple lymphocyte subsets were assessed in 27 out of 34 AML patients using flow cytometry (the percentage of B cells was only available in 20 patients). Linear regression was performed to determine associations of TIM-3 expression level of leukemic blasts with percentages of $CD3^+$ T cells **(A)**, $CD3^+CD8^+$ T cells **(B)**, $CD3^+CD4^+$ T cells **(C)**, $CD4^+CD25^+CD127^-$ Treg cells **(E)**, $CD19^+$ B cells **(F)** and $CD16^+$ or $CD56^+$ NK cells **(G)**, as well as the ratio of $CD4^+/CD8^+$ T cells **(D)**.

TIM-3 Expression of Leukemic Blasts Was Associated With CBF Translocations But Not With Clinical Outcomes of AML Patients

We investigated the association of TIM-3 expression on leukemic blasts with multiple clinical characteristics of these AML patients. Data showed that TIM-3 expression levels on leukemic blasts were not significantly related to white blood cell count, hemoglobin concentration or platelet count at diagnosis (**Supplementary Figures 5A–C**). Regarding the FAB classification, a higher median TIM-3 expression level was observed in patients with

M4, however the difference among subtypes was not statistically significant (p=0.2733) (**Figure 3A**). The relation of TIM-3 expression with genetic abnormalities was investigated as well, and results showed that patients with core binding factor (CBF) translocations, including AML1-ETO and CBFβ-MYH11 fusion genes, had significantly higher TIM-3 expression level compared to those without CBF translocations (median 22.78% versus 1.28%, p=0.0012) (**Figure 3B**). In addition, although the TIM-3 expression level of three ELN risk groups had no significant difference (p=0.7399), we might observe an accumulation of patients with higher TIM-3 expression level in the low risk group (**Figure 3C**).

With respect to the relation of TIM-3 expression with clinical outcomes of these AML patients, significantly different TIM-3 expression levels were not observed between patients who achieved CR or not after the induction chemotherapy (p=0.9799) (**Figure 3D**). Moreover, all patients were divided into low and high expression groups based on the median TIM-3

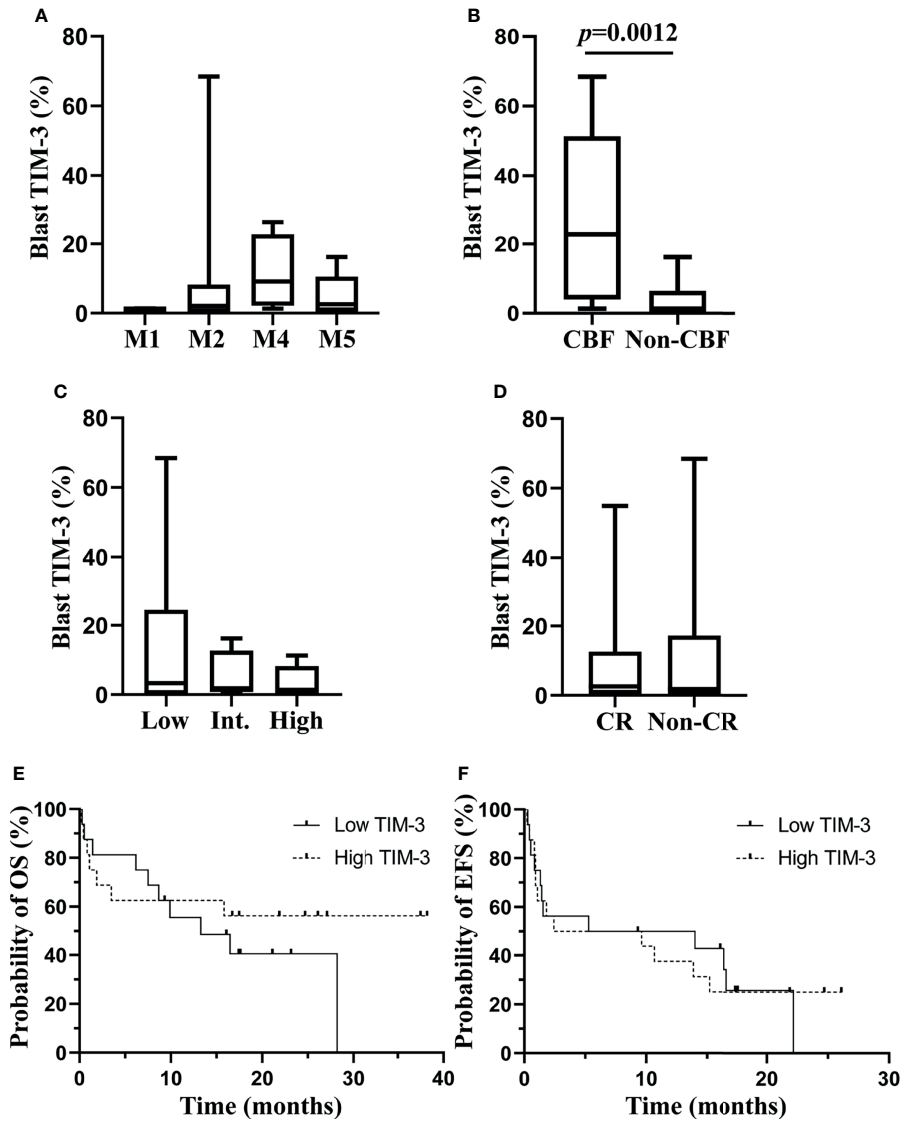

FIGURE 3 | Associations of TIM-3 expression level of leukemic blasts with clinical parameters of AML patients. TIM-3 expression levels of leukemic blasts in FAB subtypes are shown in **(A)**. TIM-3 expression levels of leukemic blasts in patients with or without CBF translocations are shown in **(B)**. TIM-3 expression levels of leukemic blasts in ELN risk groups are shown in **(C)**. A total of 32 AML patients received the induction chemotherapy, and 18 patients were CR, 9 patients were non-CR and 5 patients died during the induction chemotherapy. TIM-3 expression levels of leukemic blasts in patients who achieved CR or not after induction chemotherapy are shown in **(D)**. These patients were divided into low and high TIM-3 groups based on the median TIM-3 expression level. Probabilities of OS and EFS of two groups are shown in **(E)** and **(F)**, respectively. **(A–D)** Box and whisker plots are used to show the data. Boxes represent the interquartile range, lines inside the boxes represent the median, and whiskers represent minimum and maximum values. CBF, core-binding factor; CR, complete remission; EFS, event-free survival; Int, intermediate; OS, overall survival.

expression level, and the probabilities of 1-year OS (Low versus high, 55.56% [95% CI 75.88%-28.60%] versus 62.50% [95% CI 81.09%-34.86%], p=0.4201) and EFS (Low versus high, 50.00% [95% CI 24.52%-71.05%] versus 37.50% [95% CI 15.42%-59.77%], p=0.9873) did not differ significantly between two groups (**Figures 3E, F**).

TCGA Dataset: The mRNA Expression of TIM-3 in the Peripheral Blood of Non-M3 AML Patients Was Not Associated With Their Clinical Outcomes

In order to validate the correlation of TIM-3 expression with clinical characteristics of AML patients, we performed an independent assessment of AML patients from TCGA database. Similar to our data, The mRNA expression level (RNA Seq V2 RSEM, log2) of HAVCR2, the gene encoding TIM-3, in the peripheral blood of AML patients was not significantly associated with white blood cell count at diagnosis (p=0.4492) (**Supplementary Figure 6A**). Regarding the FAB classification, M4 subtype had the highest median HAVCR2 expression level (9.40) and M0 subtype had the lowest (7.84). A significant difference was observed among all FAB subtypes (p=0.0090) (**Figure 4A**). In addition, patients with CBF translocations had significantly higher mRNA expression level of HAVCR2 as compared to those without CBF translocations (median [range], 9.81 [8.21-10.40] versus 8.69 [3.14-11.49], p<0.0001) (**Figure 4B**). With respect to ELN risk category, the low risk group (median [range], 9.63 [3.14-11.49]) had significantly higher HAVCR2 expression level than the intermediate (8.75 [3.83-10.60]) (p=0.0302) and high (8.39 [4.84-10.19]) (p<0.0001) risk groups, however no significant difference was observed between the intermediate and high risk groups (p=0.1500) (**Figure 4C**).

In order to evaluate the impact of HAVCR2 expression levels on clinical outcomes, AML patients were first divided into low and high expression groups based on the median HAVCR2 expression level, and the probability of 5-year OS was not significantly different between two groups (low versus high, 24.95% [95% CI 14.86%-36.39%] versus 24.54% [95% CI 13.59%-37.20%], p=0.6660) (**Figure 4D**). Furthermore, patients with low, intermediate and high ELN risks were divided into low and high TIM-3 expression subgroups, respectively, and the OS did not differ significantly between two subgroups in any ELN risk group (**Supplementary Figures 6B–D**).

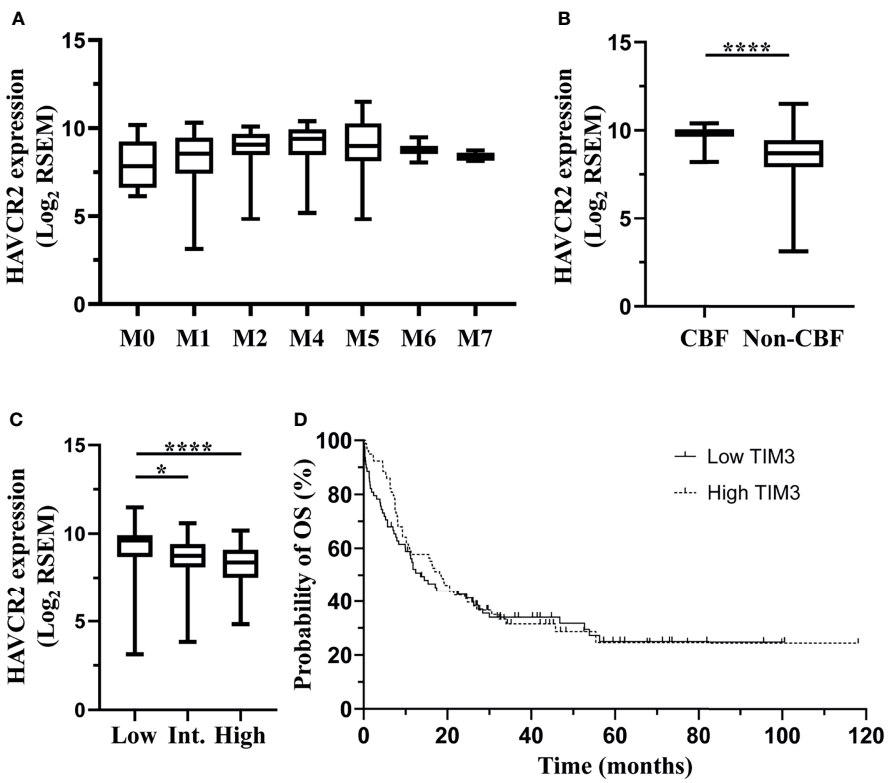

FIGURE 4 | TCGA dataset: associations of HAVCR2 mRNA expression level in the bone marrow of non-M3 AML patients with clinical parameters. Data of a cohort of 200 AML patients from The TCGA were downloaded *via* cBioPortal. Among them, 157 patients who were diagnosed with non-M3 AML and had data of HAVCR2 mRNA expression (RNA Seq V2 RSEM, log2-transformed) were analyzed in this study. HAVCR2 is the gene encoding TIM-3. HAVCR2 expression levels in FAB subtypes are shown in **(A)**. HAVCR2 expression levels in patients with or without CBF translocations are shown in **(B)**. HAVCR2 expression levels in ELN risk groups are shown in **(C)**. Patients were divided into low and high TIM-3 groups based on the median HAVCR2 expression level. Probabilities of OS of two groups are shown in **(D)**. Statistical significance is displayed as *p<0.05, ****p< 0.0001. CBF, core-binding factor; Int, intermediate; OS, overall survival.

DISCUSSION

In the present study, we simultaneously assessed the TIM-3 expression level of leukemic blasts and T lymphocytes in the bone marrow of *de novo* AML patients using flow cytometry, and found that the TIM-3 expression level of leukemic blasts correlated positively with T lymphocytes. Besides, TIM-3 expression of leukemic blasts correlated positively with the percentage of peripheral $CD8^+$ T lymphocytes. When analyzed with clinical data, higher TIM-3 expression of leukemic blasts was shown to significantly correlate with the presence of CBF translocations but not with the survival of patients, and similar results were also obtained with TCGA data.

TIM-3 is a member of the TIM family of immunoregulatory proteins. It was originally discovered in T cells and has been considered as an important checkpoint receptor. So far, four ligands, which are Gal-9, phosphatidylserine, high-mobility group protein B1 and carcinoembryonic antigen-related cell adhesion molecule 1 (CEACAM1), have been identified to bind TIM-3. Among them, Gal-9 and CEACAM1 are involved in TIM-3 mediating the inhibition and apoptosis of T cells (7). TIM-3 is a glycoprotein containing both N-linked and O-linked glycans, and glycosylation is required for Gal-9 binding (21, 22).

Besides T cells, TIM-3 also expresses on AML cells, rather than normal hematopoietic stem cells, and is involved in the self-renewal of LSCs. Autocrine Gal-9 binds to TIM-3 and subsequently activates NF-κB and β-catenin signaling, promoting LSC self-renewal (11). In addition, TIM-3 is currently thought to play a crucial role in immune escapes of AML cells. TIM-3, together with its ligand Gal-9, can be released from AML cell surface in a free soluble form through proteolysis, and impair the killing activity of NK cells and IL-2 production of T cells (12). TIM-3 also have a higher expression, together with other checkpoint receptors, like PD-1, on T cells of AML patients as compared to healthy adults (23), and this is believed to be associated with severe T cell exhaustion and disease progression (10).

Our data showed that TIM-3 expression levels on leukemic blasts varied among AML patients, which were in accordance with those of Kikushige et al. and Xu et al. (15, 24) Due to the important role of TIM-3 in AML, it would be intriguing to determine whether varied expression levels of TIM-3 on AML cells influence the immune status and prognosis of AML patients.

Our results revealed a correlation of TIM-3 expression of leukemic blasts with TIM-3 expression of both $CD8^+$ and $CD4^+$ T lymphocytes and the proportion of $CD8^+$ T lymphocytes, indicating that TIM-3 expression of leukemic blasts might alter adaptive immunity of AML patients. TIM-3 on T lymphocytes is generally considered as a marker of T cell exhaustion, especially when coexpressed with other checkpoint receptors (25). For example, $TIM\text{-}3^+PD\text{-}1^+CD8^+$ T cells in mice with advanced AML exhibited severe exhausted phenotype as defined by failure to produce IL-2, tumor necrosis factor and interferon-γ, and combined targeting of TIM-3 and PD-1 pathways was more effective in controlling the leukemia burden (10). TIM-3 was also reported to coexpress with two other checkpoint receptors LAG-3 and PD-1 on severe exhausted tumor-infiltrating lymphocytes of patients with glioblastoma (26). Therefore, we consider that our data support the notion that TIM-3 onleukemic blasts can promote an inhibitory immune environment and facilitate the immune escape of AML cells (27). In the future, it would be worthwhile to assess, together with the TIM-3 expression, the expression of other checkpoint receptors and perform the function assays of lymphocytes in AML patients, in order to further determine the effect of TIM-3 expression of leukemic blasts on adaptive immunity.

The relation of TIM-3 with AML prognosis is currently controversial. In our study, the TIM-3 expression level of leukemic blasts was neither correlated with the CR after the first induction chemotherapy nor the survival of AML patients. This data are contradictory to those of Darwish et al., Kamal et al. and Xu et al. In studies of Darwish et al. and Kamal et al., all AML subtypes including M3 were enrolled. M3 patients usually have good prognosis and hardly express TIM-3 on their leukemic blasts. This might partly explain different conclusions they got from those of our study. In the study of Xu et al., AML patients with high TIM-3 expression level achieved a higher CR rate than patients with low TIM-3 expression level (91% versus 67%, p=0.01), while the survival data were not reported. Our data, which include both treatment response after the induction chemotherapy and the survival of patients, are supposed to be more reliable. Moreover, TCGA data of 157 non-M3 AML patients were subsequently analyzed and showed that TIM-3 expression was not associated with the OS of patients, either in the whole cohort or in any ELN risk group, consistent with results of our cohort. Interestingly, Wang et al. recently reported that high TIM-3 expression levels of T and NK cells as a whole and $CD34^+CD38^-$ cells were significantly associated with a high 2-year cumulative incidence of relapse in t(8;21) AML patients (28). Unfortunately, it is impossible to confirm this finding with our data, as only few patients in our cohort have t(8;21). Further studies are needed to verify this finding and explore the underlying molecular mechanisms.

It should be noted that we assessed TIM-3 expression level on the surface of leukemic blasts in our cohort, while in TCGA data, TIM-3 mRNA expression level in the peripheral blood samples was used for analysis. In the peripheral blood of AML patients, TIM-3 expresses not only in leukemic blasts, but also in multiple other cell types, e.g. T lymphocytes, NK cells, monocytes, etc. However, leukemic blasts are the main cell population (average percentage of 39.6% in non-M3 AML patients of TCGA data), and our data also showed that TIM-3 expression of T cells, another big cell population, correlated positively with that of leukemic blasts, therefore TIM-3 mRNA expression in the peripheral blood is supposed to represent that of leukemic blasts.

CBF translocations include t(8;21)(q22;q22) and inv (16)(p13q22)/t(16;16)(p13;q22), which lead to the formation of fusion genes AML1/ETO and CBFβ/MYH11, respectively. These fusion genes disrupt the signaling of heterodimeric CBF complex in a dominant negative manner, resulting in impaired hematopoietic differentiation (29). AML with CBF translocations accounts for approximately 15% of adult AML cases and is stratified as favorable risk (30). Our results showed that CBF translocations were

associated with higher TIM-3 expression on the surface of leukemic blasts. Similar results have been reported by Jan et al. and Xu et al., and it is thought that mutations in CBF may either directly regulate TIM-3 transcription or arrest leukemic cells in a stage of differentiation with high TIM-3 expression (15, 31). Silva et al. reported that latrophilin1/protein kinase C/mammalian target of rapamycin pathway was involved in the expression of TIM-3 and its ligand Gal-9 in AML blasts, but all their experiments were performed in the cell line of THP-1, which carries KMT2A-MLLT3 fusion gene rather than CBF translocations (12). Further studies are needed to elucidate the molecular mechanism by which CBF translocations control TIM-3 expression.

Since AML with CBF translocations are considered as favorable risk, it seems that higher TIM-3 expression should be associated with good prognosis, which is not the case in our study. When we analyzed the data carefully, we found that other low-risk genetic alterations, e.g. NPM1 mutation with wild-type FLT3-ITD, usually had low TIM-3 expression level, and some intermediate-risk AML patients also had high TIM-3 expression level. Eventually, TIM-3 expression level was not related with the clinical outcome of AML patients.

Currently, TIM-3 is considered as a potential target for the treatment of myeloid malignancies. Since the autocrine Gal-9 binding to TIM-3 on the surface of leukemic blasts drives the self-renewal of AML stem cells (11), it is a potential therapeutic strategy to block TIM-3 using anti-TIM-3 mAbs. Several monoclonal antibodies (mAbs) against TIM-3, e.g. MBG453 (NCT03066648) and SHR-1702 (NCT04443751), are investigated in ongoing clinical trials and their clinical efficacy is unknown (32, 33). According to our study, it seems that TIM-3 expression on leukemic blasts does not influence the outcome of AML patients, or traditional chemotherapy can overcome the adverse impact of TIM-3 on outcomes of AML patients. Therefore, we should be cautious to expect that anti-TIM-3 mAbs further improve the clinical outcome of AML patients. However, anti-TIM-3 mAbs bound to leukemic blasts may facilitate antibody-dependent cellular phagocytosis by myeloid cells/macrophages, and they may also block TIM-3 on lymphocytes and other immune cells and potentially enhance the immune response against leukemic blasts (32). Therefore, it remains intriguing to see whether anti-TIM-3 mAbs have a therapeutic effect on myeloid malignancies.

Our study has limitations. First, the cohort size is relatively small, and further studies with larger sample size are still required to confirm these findings. Second, immunophenotyping of multiple checkpoint receptors, other than TIM-3, and function assays of lymphocytes were not performed in our study. These experiments are needed to assess adaptive immune status. Third, flow cytometry can only detect the protein of TIM-3 on the cell surface. It would be better to simultaneously assess HAVCR2 mRNA level using RT-PCR to confirm the results. Forth, western blot should be performed to assess the glycosylation status of TIM-3 in these AML samples, as glycosylation may influence the function of TIM-3, like the binding with Gal-9 (21).

In conclusion, TIM-3 expression of AML blasts correlated positively with TIM-3 expression of T lymphocytes and the proportion of $CD8^+$ T lymphocyte, indicating TIM-3 might alter adaptive immunity of AML patients. In addition, TIM-3 expression of AML blasts correlated with CBF translocations rather than the survival of patients. Therefore, TIM-3 might not be a good biomarker for non-M3 AML prognosis under current treatment modalities.

DATA AVAILABILITY STATEMENT

The raw data supporting the conclusions of this article will be made available by the authors, without undue reservation.

ETHICS STATEMENT

The studies involving human participants were reviewed and approved by The Ethical Committee of the First Affiliated Hospital of Anhui Medical University. The ethics committee waived the requirement of written informed consent for participation.

AUTHOR CONTRIBUTIONS

MY and YW conceived and designed the study. JH and LX performed the experiments, analyzed the data and wrote the manuscript. JH and XY performed TCGA data collection and analysis. JH, LX, ZH, XL, JD, ZW, LL, MR, ZL, XC, XWC, JN, JG, QL, QZ and RX performed clinical sample and data collection. All authors contributed to the article and approved the final version.

FUNDING

The study was supported by Research Fund of Anhui Institute of Translational Medicine (Grant No. 2021zhyx-C70), Clinical Medicine Discipline Construction Project of Anhui Medical University (Grant No. 2020lcxk034) and Young Scholar Program of The First Affiliated Hospital of Anhui Medical University (Grant No. 2019kj20).

SUPPLEMENTARY MATERIAL

The Supplementary Material for this article can be found online at: https://www.frontiersin.org/articles/10.3389/fonc.2022.879471/full#supplementary-material

REFERENCES

1. Monney L, Sabatos CA, Gaglia JL, Ryu A, Waldner H, Chernova T, et al. Th1-Specific Cell Surface Protein Tim-3 Regulates Macrophage Activation and Severity of an Autoimmune Disease. *Nature* (2002) 415(6871):536–41. doi: 10.1038/415536a
2. Gao X, Zhu YB, Li G, Huang HT, Zhang GB, Wang FM, et al. Tim-3 Expression Characterizes Regulatory T Cells in Tumor Tissues and Is Associated With Lung Cancer Progression. *PloS One* (2012) 7(2): e30676. doi: 10.1371/journal.pone.0030676
3. Pulido AD, Gardner A, Hiebler S, Soliman H, Rugo HS, Krummel MF, et al. Tim-3 Regulates Cd103(+) Dendritic Cell Function and Response to

Chemotherapy in Breast Cancer. *Cancer Cell* (2018) 33(1):60–+. doi: 10.1016/j.ccell.2017.11.019
4. Xu LY, Huang YY, Tan LL, Yu W, Chen DD, Lu CC, et al. Increased Tim-3 Expression in Peripheral Nk Cells Predicts a Poorer Prognosis and Tim-3 Blockade Improves Nk Cell-Mediated Cytotoxicity in Human Lung Adenocarcinoma. *Int Immunopharmacol* (2015) 29(2):635–41. doi: 10.1016/j.intimp.2015.09.017
5. Anderson AC, Anderson DE, Bregoli L, Hastings WD, Kassam N, Lei C, et al. Promotion of Tissue Inflammation by the Immune Receptor Tim-3 Expressed on Innate Immune Cells. *Science* (2007) 318(5853):1141–3. doi: 10.1126/science.1148536
6. Phong BL, Avery L, Sumpter TL, Gorman JV, Watkins SC, Colgan JD, et al. Tim-3 Enhances Fc Epsilon Ri-Proximal Signaling to Modulate Mast Cell Activation. *J Exp Med* (2015) 212(13):2289–304. doi: 10.1084/jem.20150388
7. Wolf Y, Anderson AC, Kuchroo VK. Tim3 Comes of Age as an Inhibitory Receptor. *Nat Rev Immunol* (2020) 20(3):173–85. doi: 10.1038/s41577-019-0224-6
8. Sakuishi K, Apetoh L, Sullivan JM, Blazar BR, Kuchroo VK, Anderson AC. Targeting Tim-3 and Pd-1 Pathways to Reverse T Cell Exhaustion and Restore Anti-Tumor Immunity. *J Exp Med* (2010) 207(10):2187–94. doi: 10.1084/jem.20100643
9. Borate U, Esteve J, Porkka K, Knapper S, Vey N, Scholl S, et al. Phase Ib Study of the Anti-Tim-3 Antibody Mbg453 in Combination With Decitabine in Patients With High-Risk Myelodysplastic Syndrome (Mds) and Acute Myeloid Leukemia (Aml). *Blood* (2019) 134(Supplement_1):570. doi: 10.1182/blood-2019-128178
10. Zhou Q, Munger ME, Veenstra RG, Weigel BJ, Hirashima M, Munn DH, et al. Coexpression of Tim-3 and Pd-1 Identifies a Cd8(+) T-Cell Exhaustion Phenotype in Mice With Disseminated Acute Myelogenous Leukemia. *Blood* (2011) 117(17):4501–10. doi: 10.1182/blood-2010-10-310425
11. Kikushige Y, Miyamoto T, Yuda J, Jabbarzadeh-Tabrizi S, Shima T, Takayanagi S, et al. A Tim-3/Gal-9 Autocrine Stimulatory Loop Drives Self-Renewal of Human Myeloid Leukemia Stem Cells and Leukemic Progression. *Cell Stem Cell* (2015) 17(3):341–52. doi: 10.1016/j.stem.2015.07.011
12. Silva IG, Yasinska IM, Sakhnevych SS, Fiedler W, Wellbrock J, Bardelli M, et al. The Tim-3-Galectin-9 Secretory Pathway Is Involved in the Immune Escape of Human Acute Myeloid Leukemia Cells. *Ebiomedicine* (2017) 22:44–57. doi: 10.1016/j.ebiom.2017.07.018
13. Li CX, Chen XC, Yu X, Zhu YB, Ma C, Xia R, et al. Tim-3 Is Highly Expressed in T Cells in Acute Myeloid Leukemia and Associated With Clinicopathological Prognostic Stratification. *Int J Clin Exp Pathol* (2014) 7(10):6880–8.
14. Blaeschke F, Willier S, Stenger D, Lepenies M, Horstmann MA, Escherich G, et al. Leukemia-Induced Dysfunctional Tim-3(+)Cd4(+) Bone Marrow T Cells Increase Risk of Relapse in Pediatric B-Precursor All Patients. *Leukemia* (2020) 34(10):2607–20. doi: 10.1038/s41375-020-0793-1
15. Xu LJ, Xu JG, Ma SB, Li XL, Zhu MQ, Chen SN, et al. High Tim-3 Expression on Aml Blasts Could Enhance Chemotherapy Sensitivity. *Oncotarget* (2017) 8(60):102088–96. doi: 10.18632/oncotarget.22141
16. Darwish NH, Sudha T, Godugu K, Elbaz O, Abdelghaffar HA, Hassan EE, et al. Acute Myeloid Leukemia Stem Cell Markers in Prognosis and Targeted Therapy: Potential Impact of Bmi-1, Tim-3 and Cll-1. *Oncotarget* (2016) 7(36):57811–20. doi: 10.18632/oncotarget.11063
17. Kamal AM, Nabih NA, Elleboudy NS, Radwan SM. Expression of Immune Check Point Gene Tim-3 in Patients Newly Diagnosed With Acute Myeloid Leukemia: Significance and Impact on Outcome. *Oncol Lett* (2021) 21(4):325. doi: 10.3892/ol.2021.12587
18. Cerami E, Gao JJ, Dogrusoz U, Gross BE, Sumer SO, Aksoy BA, et al. The Cbio Cancer Genomics Portal: An Open Platform for Exploring Multidimensional Cancer Genomics Data. *Cancer Discov* (2012) 2(5):401–4. doi: 10.1158/2159-8290.CD-12-0095
19. Gao JJ, Aksoy BA, Dogrusoz U, Dresdner G, Gross B, Sumer SO, et al. Integrative Analysis of Complex Cancer Genomics and Clinical Profiles Using the Cbioportal. *Sci Signal* (2013) 6(269):pl1. doi: 10.1126/scisignal.2004088
20. Ley TJ, Miller C, Ding L, Raphael BJ, Mungall AJ, Robertson AG, et al. Genomic and Epigenomic Landscapes of Adult *De Novo* Acute Myeloid Leukemia. *N Engl J Med* (2013) 368(22):2059–74. doi: 10.1056/Nejmoa1301689
21. Zhu C, Anderson AC, Schubart A, Xiong HB, Imitola J, Khoury SJ, et al. The Tim-3 Ligand Galectin-9 Negatively Regulates T Helper Type 1 Immunity. *Nat Immunol* (2005) 6(12):1245–52. doi: 10.1038/ni1271
22. Kandel S, Adhikary P, Li GF, Cheng K. The Tim3/Gal9 Signaling Pathway: An Emerging Target for Cancer Immunotherapy. *Cancer Lett* (2021) 510:67–78. doi: 10.1016/j.canlet.2021.04.011
23. Tan JX, Huang SX, Huang JY, Yu Z, Chen YC, Lu YH, et al. Increasing Tim-3 +Cd244+, Tim-3+Cd57+, and Tim-3+Pd-1+T Cells in Patients With Acute Myeloid Leukemia. *Asia Pac J Clin Oncol* (2020) 16(3):137–41. doi: 10.1111/ajco.13304
24. Kikushige Y, Shima T, Takayanagi S, Urata S, Miyamoto T, Iwasaki H, et al. Tim-3 Is a Promising Target to Selectively Kill Acute Myeloid Leukemia Stem Cells. *Cell Stem Cell* (2010) 7(6):708–17. doi: 10.1016/j.stem.2010.11.014
25. Tang R, Rangachari M, Kuchroo VK. Tim-3: A Co-Receptor With Diverse Roles in T Cell Exhaustion and Tolerance. *Semin Immunol* (2019) 42: 101302. doi: 10.1016/J.Smim.2019.101302
26. Woroniecka K, Chongsathidkiet P, Rhodin K, Kemeny H, Dechant C, Farber SH, et al. T-Cell Exhaustion Signatures Vary With Tumor Type and Are Severe in Glioblastoma. *Clin Cancer Res* (2018) 24(17):4175–86. doi: 10.1158/1078-0432.CCR-17-1846
27. Yasinska IM, Gonçalves Silva I, Sakhnevych S, Gibbs B, Raap U, Fasler-Kan E, et al. Biochemical Mechanisms Implemented by Human Acute Myeloid Leukemia Cells to Suppress Host Immune Surveillance. *Cell Mol Immunol* (2018) 15(11):989–91. doi: 10.1038/s41423-018-0047-6
28. Wang J, Yang L, Dao FT, Wang YZ, Chang Y, Xu N, et al. Prognostic Significance of Tim-3 Expression Pattern at Diagnosis in Patients With T(8;21) Acute Myeloid Leukemia. *Leuk Lymphoma* (2022) 63(1):152–61. doi: 10.1080/10428194.2021.1966785
29. Paschka P. Core Binding Factor Acute Myeloid Leukemia. *Semin Oncol* (2008) 35(4):410–7. doi: 10.1053/j.seminoncol.2008.04.011
30. Slovak ML, Kopecky KJ, Cassileth PA, Harrington DH, Theil KS, Mohamed A, et al. Karyotypic Analysis Predicts Outcome of Preremission and Postremission Therapy in Adult Acute Myeloid Leukemia: A Southwest Oncology Group/Eastern Cooperative Oncology Group Study. *Blood* (2000) 96(13):4075–83. doi: 10.1182/blood.V96.13.4075
31. Jan M, Chao MP, Cha AC, Alizadeh AA, Gentles AJ, Weissman IL, et al. Prospective Separation of Normal and Leukemic Stem Cells Based on Differential Expression of Tim3, a Human Acute Myeloid Leukemia Stem Cell Marker. *Proc Natl Acad Sci USA* (2011) 108(12):5009–14. doi: 10.1073/pnas.1100551108
32. Acharya N, Sabatos-Peyton C, Anderson AC. Tim-3 Finds Its Place in the Cancer Immunotherapy Landscape. *J Immunother Cancer* (2020) 8(1):e000911. doi: 10.1136/jitc-2020-000911
33. Zeidan AM, Komrokji RS, Brunner AM. Tim-3 Pathway Dysregulation and Targeting in Cancer. *Expert Rev Anticancer Ther* (2021) 21(5):523–34. doi: 10.1080/14737140.2021.1865814

Conflict of Interest: The authors declare that the research was conducted in the absence of any commercial or financial relationships that could be construed as a potential conflict of interest.

frontiers | Frontiers in Oncology

ORIGINAL RESEARCH
published: 12 May 2022
doi: 10.3389/fonc.2022.876556

Nrf2 Overexpression Decreases Vincristine Chemotherapy Sensitivity Through the PI3K-AKT Pathway in Adult B-Cell Acute Lymphoblastic Leukemia

Li Wang[1], Xin Liu[1], Qian Kang[2], Chengyun Pan[2], Tianzhuo Zhang[1], Cheng Feng[1], Lu Chen[1], Sixi Wei[3] and Jishi Wang[2,4]**

[1] Clinical Medical College, Guizhou Medical University, Guiyang, China, [2] Department of Hematology, Guizhou Province Institute of Hematology, Guizhou Province Laboratory of Haematopoietic Stem Cell Transplantation Centre, Affiliated Hospital of Guizhou Medical University, Guiyang, China, [3] Center for Clinical Laboratories, The Affiliated Hospital of Guizhou Medical University, Guiyang, China, [4] National Clinical Research Center for Hematologic Diseases, The First Affiliated Hospital of Soochow University, Jiangsu, China

OPEN ACCESS

Edited by:
Lokman Varisli, Dicle University, Turkey

Reviewed by:
Junmin Zhang, Lanzhou University, China
Gabriella D'Orazi, G. D'Annunzio University of Chieti-Pescara, Italy

***Correspondence:**
Jishi Wang
wangjishi9646@163.com
Sixi Wei
wsixi@gmc.edu.cn

Specialty section:
This article was submitted to Hematologic Malignancies, a section of the journal Frontiers in Oncology

Received: *15 February 2022*
Accepted: *19 April 2022*
Published: *12 May 2022*

Citation:
Wang L, Liu X, Kang Q, Pan C, Zhang T, Feng C, Chen L, Wei S and Wang J (2022) Nrf2 Overexpression Decreases Vincristine Chemotherapy Sensitivity Through the PI3K-AKT Pathway in Adult B-Cell Acute Lymphoblastic Leukemia. Front. Oncol. 12:876556. doi: 10.3389/fonc.2022.876556

Uncontrolled proliferation is an important cancer cell biomarker, which plays a critical role in carcinogenesis, progression and development of resistance to chemotherapy. An improved understanding of novel genes modulating cancer cell proliferation and mechanism will help develop new therapeutic strategies. The nuclear factor erythroid 2-related factor 2 (Nrf2), a transcription factor, decreases apoptosis when its expression is upregulated. However, the relationship between Nrf2 and Vincristine (VCR) chemotherapy resistance in B-cell acute lymphoblastic leukemia (B-ALL) is not yet established. Our results showed that Nrf2 levels could sufficiently modulate the sensitivity of B-ALL cells to VCRby regulating an apoptotic protein, i.e., the Bcl-2 agonist of cell death (BAD). Chemotherapeutic agents used for the treatment of B-ALL induced Nrf2 overactivation and PI3K-AKT pathway activation in the cells, independent of the resistance to chemotherapy; thus, a potential resistance loop during treatment for B-ALL with a drug combination is established. Therefore, B-ALL patients with a high expression of Nrf2 might mean induction chemotherapy with VCR effective little.

Keywords: nuclear factor erythroid 2-related factor 2, B-cell acute lymphoblastic leukemia, chemotherapy resistance, Vincristine, BAD, PI3K-AKT pathway

INTRODUCTION

Acute lymphoblastic leukemia (ALL) continues to be one of the most difficult-to-treat cancers in adults, particularly in terms of complete remission rates achieved using conventional therapeutic regimens. Leukemia requires a minimum of 20% blast cells in the bone marrow (BM). The incidence of ALL in adults is significantly lower, representing only 0.2% of all cancers. The prognosis is not encouraging, with an average 5-year survival rate of 20% to 40% (1–3). B-ALL accounts for approximately 75% of ALL cases. Historically, adult B-ALL patients have been associated with a

poorer prognosis than pediatric B-ALL patients (4–6). In the past 20 years, treatment algorithms similar to those for children have been developed for adults with B-ALL considering the fundamental principles of induction, early intensification, consolidation, and the presence of complications in the patients (7). Traditional chemotherapeutic approaches that include VCR, corticosteroids, and anthracyclines may not be as effective for most adults with ALL, who may also have multiple comorbidities (8). However, a previous study showed that a few adult patients completed treatment with these traditional chemotherapeutic regimens (9).

Nuclear factor erythroid 2-related factor 2 (Nrf2) is an important transcription factor and a modulator of cellular antioxidant responses, which regulates the expression of genes encoding antioxidant enzymes and exerts a protective role against a variety of oxidative changes (10, 11). Kelch-like ECH-associated protein 1 (Keap1) promotes the ubiquitination and proteasomal degradation of Nrf2, which maintains low basal levels of the Nrf2 protein (12). However, when cells are exposed to oxidative, xenobiotic, or electrophilic stress, Keap1-mediated degradation of Nrf2 is reversed (13). Subsequently, the accumulation of Nrf2 in cells increases (14). Cells have hierarchical responses to defense changes of oxidative stress and Nrf2 activated by a little increase of reactive oxygen species (ROS)/reactive nitrogen species (RNS) at the first time. With this kind of stimulated Nrf2 activated can provide apoptosis response to excessive ROS levels. In other words, Nrf2 activation cause pro-apoptotic signaling (15, 16). Previous studies have shown that the constitutive stabilisation and activation of Nrf2 is associated with poor prognosis in various human cancers, such as head and neck cancer (17), gastric cancer (18), lung cancer (19), esophageal squamous cell carcinoma (20), gallbladder cancer (21), breast cancer (22)and hepatocellular carcinomas (23, 24). Recent studies have reported additional functions of Nrf2, such as effects in drug metabolism and excretion; autophagy; proteasomal degradation; metabolism of energy, iron and amino acids; cell survival and proliferation;

Apoptosis is an active intracellular cell death virtually observed in all higher eukaryotic cell types and is abnormally repressed in many human disorders, such as tumor formation and treatment resistance in tumor cells (25). Phosphatidylinositol 3-kinase (PI3K) is a lipid kinase that controls various cellular activities by spreading intracellular signal cascades (26). In cancer treatment, PI3Ks are thought to be important causes of chemoresistance (27, 28). Protein kinase B (AKT) is another important downstream effector of PI3K signalling, modulating various pathways, including apoptosis suppression, cell growth promotion and cellular metabolism control. Therefore, the PI3K-AKT pathway is important for chemoresistance and is a hub that influences chemoresistance by inhibiting of apoptosis (26, 29). Several studies have reported that PI3K and AKT affect the apoptosis program by regulating apoptosis-related factors (30, 31). In apoptotic pathways induced by several foreign PI3K/AKT stimuli, the balance between Bcl-2 family proteins should be maintained (32). The Bcl-2 family members are antagonised by the varied pro-death proteins (e.g. BAX and BAK) or sequester BH3-only proteins, i.e. BAD (33–37). The cells' susceptibility to apoptotic stress is regulated by balancing these opposing apoptotic proteins.

Activated AKT inhibits apoptosis by phosphorylating Ser136 of BAD (the AKT target) and releasing of BAD from the Bcl-xL complex (36, 38).

Therefore, this study aimed to determine the role of Nrf2 in chemotherapeutic drug resistance among adult patients with B-ALL. Furthermore, by indirectly regulating the Bcl-2, Nrf2 inhibited the BAD protein expression through the PI3K-AKT signalling pathway, resulting in drug resistance in B-ALL cells.

MATERIALS AND METHODS

Patient Samples and Stable Cell Lines

The research employed B-ALL cells from patients at the Affiliated Hospital of Guizhou Medical University in 2019 and 2020. The samples were separated into three subgroups: "Normal donor" (n = 15), "Drug sensitive" (n = 19) and "Resistant" (n = 14). Patients with B-ALL are classified as "Drug Sensitive" if they obtain CR with standard induction treatment, or "Resistant" if they do not reach CR. Western blot and qRT-PCR were used to evaluate Nrf2 protein and mRNA levels in various subgroups. The patients' conditions were diagnosed using cytomorphology, cytochemistry, and immunophenotyping. analysed B-ALL samples were taken following hemolysis of red blood cells at diagnosis, pre-treatment, and post-induction. Then, total RNA and protein were isolated from the generated B-ALL cells and utilised for drug testing. Patients with B-ALL were classed as "drug responsive" or "resistant" to treatment. **Table 1** provides detailed patient data. The Ficoll (Solarbio Science & Technology, Beijing, PRC) density centrifugation was used to separate BMNCs from healthy donors and B-ALL patients.

TABLE 1 | The patients with B-ALL samples characteristic.

Parameter Gender (n = 33)	N	%
Male	18	54.55
Female	15	45.45
Age (year)		
18-34	8	34.78
35-64	23	69.70
≥65	2	6.06
White blood cells count (cells $\times 10^9$/L)		
<30	16	48.48
30-99	5	15.15
≥100	2	6.06
BCR-ABL (positive)	6	18.18
MLL-AF4	4	12.12
Chromosomal karyotype		
t (9;22)	1	3.03
t (4;11)	1	3.03
Normal	31	93.94
Immunophenotype		
Common-B-ALL	32	96.97
Pre-B-AL	1	3.03

Human B-ALL stable cell lines Nalm-6, Sup-b15, and RS4:11 were obtained from Guizhou Province Laboratory of Haematopoietic Stem Cell Transplantation Center. The cell lines were cultured in RPMI-1640 medium supplemented with 10% fetal bovine serum, penicillin (100 units/ml), and streptomycin (100 mg/ml) at 37°C in a humidified atmosphere with 5% CO2.

Reagents and Antibodies

Anti-Nrf2 (ab89443) purchased from Abcam (Cambridge, UK). Anti-β-actin (20536-1-AP), anti-BAD (10435-1-AP), p-CREB (12208-1-AP), LMNA (10298-1-AP) antibodies were obtained from Proteintech Group Co., Ltd. (Wuhan, PRC). Anti-AKT1 (K101311P), anti-p-AKT1(K006214P), PI3K(K106692P), p-PI3K(K006379P) antibodies were obtained from Solarbio Science & Technology(Beijing, PRC). Anti-BCL-2(AF6139), Cleaved-Caspase 3(AF7022), Caspase 3(AF6311), Cleaved-Caspase 9(AF5240), Caspase 9(AF6348) antibodies were obtained from, Affinity Biosciences (USA). Vincristine (VCR) were purchased from Topscience (Shanghai, PRC). Daunorubicin (DNR) and brusatol (an Nrf2 inhibition) were purchased from MCE (NJ, USA). The chemical inhibitor MK-2206 (MCE, NJ, USA) of the AKT (39). Fetal bovine serum and RPMI 1640 medium were obtained from Gibco (Carlsbad, CA, USA). Nuclear Protein Extraction Kit were obtained from Solarbio Science & Technology (Beijing, PRC).

Western Blot Analysis

Protein lysate was extracted from cells using RIPA lysis buffer supplemented with 1 μM PMSF (Solarbio Science & Technology, Beijing, PRC) agitated at 4°C for 30 min. The extracts were centrifuged at 12, 000 rpm for 15 min at 4°C, and the supernatant was collected. A BCA protein assay kit (Pierce, Hercules, CA, USA) was used to determine the protein concentrations. Protein (40μg) were then loaded on 10% SDS–PAGE gel, and the separated proteins were transferred onto PVDF membranes. Membranes were routinely blocked in 5% nonfat milk in PBS for 2 h with agitation and washed. Then, the membrane was blotted with primary antibodies for 2 h. After washing, the membranes were incubated with secondary antibodies for 45 min at room temperature. All protein bands were visualised with the use of the enhanced chemiluminescence (7Sea Biotech, Shanghai, PRC). The stable Nalm-6 and RS4:11 cell lines expressing LV-Nrf2 or si-Nrf2 were treated with MK-2206 (10 μM) in RPMI-1640 medium supplemented with 10% FBS for 24 h.

Quantitative Real Time-Polymerase Chain Reaction (qRT-PCR)

According to the manufacturer's instructions, total RNAs from cells were extracted using Trizol reagent (Invitrogen, Carlsbad, CA, USA). Real-time PCR was performed using the SYBR Green PCR Master Mix (TianGen Biotech, Beijing, PRC) and the PRISM 7500 real-time PCR detection system (ABI, USA). The following human primers (Generay Bioteach Co. Ltd, Shanghai, PRC) were used in this study:

β-actinF,5′-CTACCTCATGAAGATCCTCACCGA-3′;
β-actin R, 5′-TTCTCCTTAATGTCACGCACGATT-3′;
Nrf2 F, 5′-TGACAATGAGGTTTCGGCTACG-3′;
Nrf2 R, 5′-GGAGAGGATGCTGCTGAAGGAATC-3′;

Immunofluorescence and Immunohistochemical (IHC) Staining

Immunofluorescence was used to analyse Nrf2 subcellular localisation. Paraformaldehyde (4%), 4 hours, 4 temperatures. After three PBS washes, cells were permeabilised for 15 minutes with Triton X-100. After three PBS washes, cells were blocked using blocking buffer (PBS + 5% BSA) for 60 minutes and then rinsed with PBS (three times). On the third wash, cells were labeled with rabbit anti-human Nrf2 overnight. After that, the cells were either labeled with FITC-conjugated secondary antibody or phalloidin-tetramethyl rhodamine for 45 minutes. DAPI stained nuclei (4-6-diamidino- 2-phenylindole). Fluorescence microscopy was used to image cells. ICC staining required 30 minutes of formaldehyde fixation of B-ALL mononuclear cells. Three times with PBS. The cells were then penetrated into PBS with 0.1 percent Triton-X 100 for 20 minutes. After 5 minutes of repair, the antigen was sealed with 5% BSA for 1 hour at room temperature. They were then treated at 4°C overnight with dilution (1:250 rabbit anti-Nrf2). 3 PBS washes in 10 min. 1 hour incubation with horseradish peroxide second antibody (1:200) followed by 3 washes with PBS. It was incubated for 10 minutes, rinsed for 10 minutes with PBS, then stained for 1 minute with hematoxylin. Gradient ethanol dehydration, xylene transparency for 5 minutes, and lastly a microscope picture. The IHC tests were graded as described (40).

Lentiviral Transduction

Human Nrf2 overexpression clone lentiviral particle (L-Nrf2) and human Nrf2- silencing RNA (si-Nrf2) were purchased from Genechem Co., Ltd. (Shanghai, PRC). Transfection of Nrf2 was performed using the manufacturer's instructions. Cells (Nalm-6 and RS4:11), respectively transfected with empty vector (EV), were used as controls. After expansion and maintenance in RPMI-1640 medium supplemented with 10% FBS for 5 days, stable Nalm-6 and RS4:11 cell lines expressing LV-Nrf2 or si-Nrf2 were selected puromycin (1.5μg/ml and 2μg/ml respectively).

Combined Drug Analysis

Leukemia cell lines cultures were treated with DNRand VCR in the presence or absence of brusatol, added to each drug solution at fixed combination ratios. Cell viability was determined after 24–48h of treatment by CCK-8 assay as described above. To determine the synergistic, additive, or antagonistic effects of drug combinations, we used CompuSyn software (ComboSyn Inc., Paramus, NJ; www.combosyn.com) based on the method of the combination index (CI) described by Chou.25 Synergy, additivity, and antagonism were defined by a CI <1, CI = 1, or CI >1, respectively. Where indicated for some experiments, B-ALL cell lines have been treated with brusatol for 24 h at a final concentration of 1.5 μM.

Apoptosis Assay

After incubation, cells were washed in cold PBS and resuspended in buffer containing annexin V–APC and PI according to the manufacturer's instructions. The cell suspensions were analysed by flow cytometry (FCM) (BD Biosciences).

Xenografted Tumor Model

Nonobese diabetic/severe combined immunodeficiency (NOD/SCID) mice were purchased from SPF Biotechnology Co., Ltd (Beijing, China). Stably transfected Nrf2 cells that were growing in the logarithmic phase were prepared. Cells were resuspended in PBS at a concentration of 5×10^6 cells/100 μL and then subcutaneously injected into the 5-week-old mice. For *in vivo* VCR treatment, twelve mice were dived into four groups. After the xenografts reached 0.5 cm in diameter, two of the groups were treated with VCR (80 mg/kg/day for 6 days) by intraperitoneal injection (41), the others were treated with PBS. Tumor growth was monitored by measurements of the length and width and the tumor volume was calculated using the equation $(L \times W^2)/2$. After mice were placed on the platform of BLT In-Vivo Imaging System (BLT Photon Tech., Guangzhou, China), fluorescence images were captured according to the manufacturer's instructions. Animals were euthanised, tumors were excised, weighed and paraffin-embedded. All experiments on mice were approved by the Institutional Animal Care and Use Committee of Guizhou Medical University, China.

Statistical Analysis

The GraphPad Prism 7 software was used for creating graphs and for statistical analysis. Normally distributed data were expressed as mean ± standard deviation (x ± s), and a t-test was performed for the intergroup comparison; Paired sample t-test was used to compare the values of the same individual at different time points. A rank-sum test was used to compare the data that did not follow a normal distribution. $P < 0.05$ was considered statistically significant.

RESULTS

Nrf2 Is Overexpressed in Chemotherapy-Resistant Adult Patients With B-ALL

To determine the potential role of Nrf2 on chemoresistance in B-ALL, we measured the Nrf2 protein and mRNA expression in leukemia cells isolated from the BM of healthy donors and patients with B-ALL (**Table 1**). The Nrf2 protein (**Figure 1A**; $P < 0.01$) and mRNA (**Figure 1B**; $P < 0.001$) expression levels were significantly higher in the resistant subgroup than in the drug sensitive subgroup. Moreover, the Nrf2 protein and mRNA expression levels were the lowest in the cells obtained from healthy donors (**Figure 1B**; $P < 0.05$).

To further investigate the subcellular distribution of Nrf2 expression in patients' primary B-ALL cells, we used immunofluorescence staining (IF). Our results revealed that the resistant subgroup showed a higher accumulation of Nrf2 in the nuclear and cytoplasm (**Figure 1C**). Furthermore, the nuclear and cytoplasmic accumulation of Nrf2 was higher in cells obtained from B-ALL patients than in healthy donors. In patients with B-ALL, Nrf2 expression was found to be significantly related to the curative efficacy of conventional chemotherapy. The expression of the Nrf2 protein in the nucleus of resistance patients (n = 3) was higher than that in the nucleus of sensitive patients (n = 3) (**Figure 1D**; $P < 0.05$). Besides, we confirmed that Nrf2 high expression increased the HO-1 protein expression in RS4:11 cells (**Figures S1A, B**).

Nrf2 Inhibition Sensitises B-ALL Cells to VCR

To examine the role of Nrf2 in the phenomenon of drug resistance, we evaluated whether brusatol (an Nrf2 inhibitor) could enhance drug response in connection with cell viability. A western blot showing Nrf2 protein different levels of three B-ALL cell lines (Nalm-6, RS4:11, and Supb-15) and the level expression of Nrf2 in Nalm-6 and RS4:11 is similar. Supb-15 cell line has the highest expression of Nrf2 (**Figures S2A, B**). We used them treated with VCR (10^{-4},10^{-3}, 10^{-2}, 10^{-1}, 10 and 10^2 μM) and daunorubicin (DNR, 10^{-4},10^{-3}, 10^{-2}, 10^{-1}, 10 and 10^2 μM), which are drugs used in the standard treatment of B-ALL, and subsequently with brusatol (10^{-5},10^{-4},10^{-3}, 10^{-2}, 10^{-1} and 10 μM). Results from CCK-8 (cell counting kit-8) experiments indicated that brusatol administration altered the sensitivity of all B-ALL cell lines to VCR treatment (**Figure 2A**) and their combination index (CI) values were<1 (**Figure 2B**). Unlike the results observed with VCR, the combination of brusatol with DNR showed no significant change in sensitivity to DNR (**Figure 2C**); however, brusatol showed a slight increase in the sensitivity of Nalm-6 cells to DNR with a CI<1 (**Figure 2D**). In addition, we assessed the effect of drug resistance mediated by the VCR/brusatol combination by analysing the mechanism of cell death induced by treatment with sublethal doses of the individual drugs. The combination of both drugs 5 μM VCR + 1.5 μM brusatol induced a potent proapoptotic response in B-ALL cells, as seen by a significant increase in the number of apoptotic cells (by Annexin-V/PI staining) (**Figures 2E, F**). Therefore, Nrf2 overexpression decreased the sensitivity of B-ALL to VCR.

B-ALL Cells With High Expression Levels of Nrf2 Had Higher Drug Resistance to VCR

Increased Nrf2 expression has been associated with resistance to chemotherapy in B-ALL. The expression level of Nrf2 in Nalm-6 and RS4:11 cell lines was confirmed using western blot (**Figures 3A, B**) and qRT-PCR (**Figure 3C**). We examined the effect of Nrf2 expression on sensitivity to VCR. Overexpression of Nrf2 *via* lentivirus transduction resulted in reduced sensitivity of Nalm-6 and RS4:11 cells to VCR, whereas the sensitivity to VCR increased upon Nrf2 downregulation (**Figure 3D**). These data suggest that expression of Nrf2 may mediate resistance to VCR in B-ALL. These findings were confirmed using FCM. B-ALL cells overexpressing Nrf2 had reduced sensitivity to VCR treatment and decreased VCR-induced apoptosis (**Figures 3E–H**; $P < 0.01$).

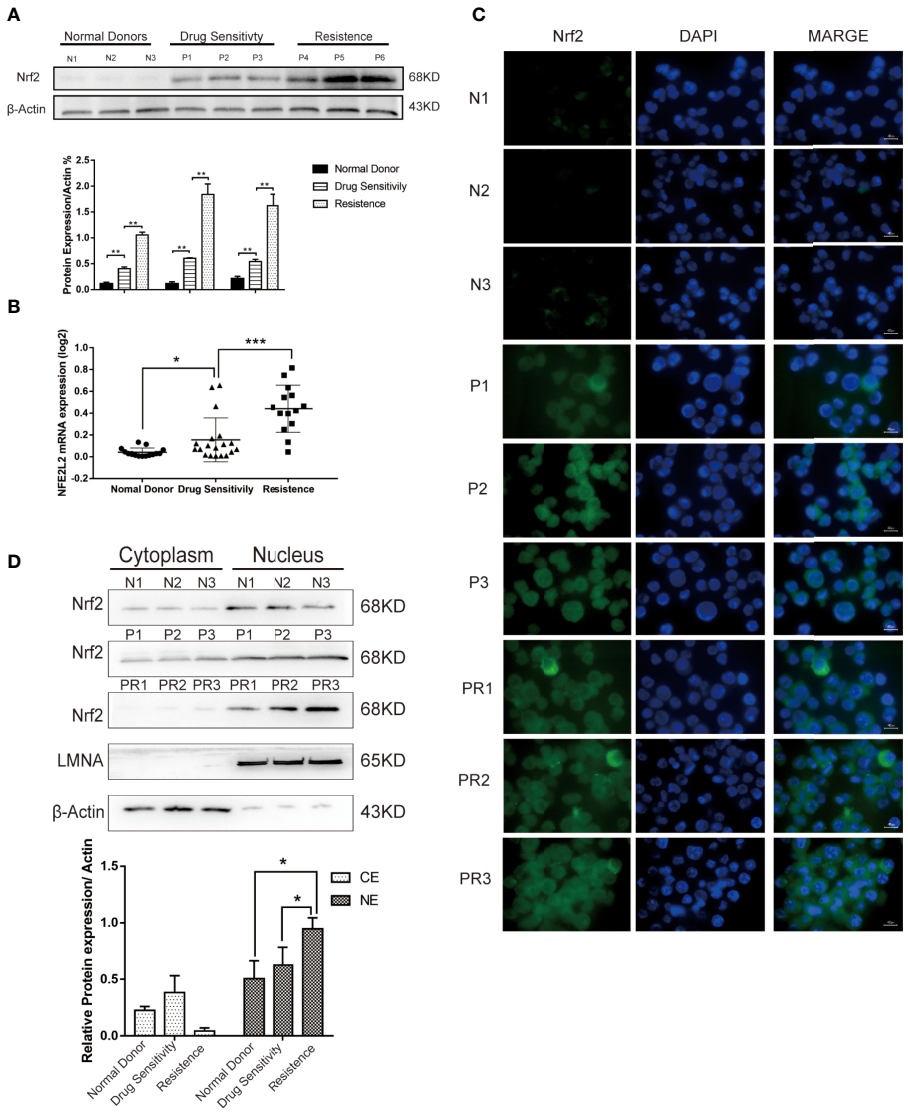

FIGURE 1 | **(A)** Expression levels of Nrf2 protein were detected in 3 donors and 6 B-ALL samples by western blot. **(B)** Quantification of Nrf2 expression in donors (n = 15) and B-ALL samples (Drug sensitivity, n = 19; Resistance, n = 14). Values are presented as mean ± SD (n = 3), *P < 0.05, **P < 0.01, ***P < 0.001. **(C)** Immunofluorescence staining analysis of the expression of Nrf2 in ALL patients (N, normal donors; P, patients of drug sensitivity; PR, patients of resistance). Green indicates Nrf2, and blue indicates DAPI. Scale bars = 10 μm. **(D)** Cytoplasmic and nuclear fractionation kit was used to obtain the cytosolic and nuclear protein. LMNA and β-Actin were considered as nuclear and cytosolic loading control, respectively (N: normal donors, P: patients of drug sensitivity, PR: patients of resistance). And bands were quantified. NE, nuclear extract. CE, Cytosolic extract. Values are presented as mean ± SD (n = 3). Significant differences are indicated by *p < 0.05 vs. Ctrl-NE group.

However, knockdown of Nrf2 using siRNA increased the sensitivity to VCR-induced cytotoxicity (**Figures 3F–H**; P < 0.05). These results indicated that Nrf2 expression was directly correlated with sensitivity to VCR treatment.

Effects of VCR Treatment on PI3K, AKT, Nrf2 and P-AKT Proteins Expressions in the PI3K-AKT Pathway in ALL Cells

To perform an in-depth investigation of this mechanism, biomarkers of the representative apoptotic signalling pathways, namely, p-PI3K and p-AKT, were detected after treating the cell with or without VCR in RS4:11 cells (**Figure 4A**) and Nalm-6 cells (**Figure 4B**). With VCR treatment, Nrf2, p-PI3K and p-AKT expression levels were significantly increased (**Figures 4C, D**, P < 0.01, P < 0.001 and P < 0.05). This observation confirms that the activation of the PI3K-AKT signal pathway is caused by VCR treatment in RS4:11 cells (**Figure 4E**) and Nalm-6 cells (**Figure 4F**). The role of Nrf2 in drug resistance in ALL cells treated with VCR was further investigated by activating the PI3K-AKT signaling pathway. Western blot was used to detect p-AKT in

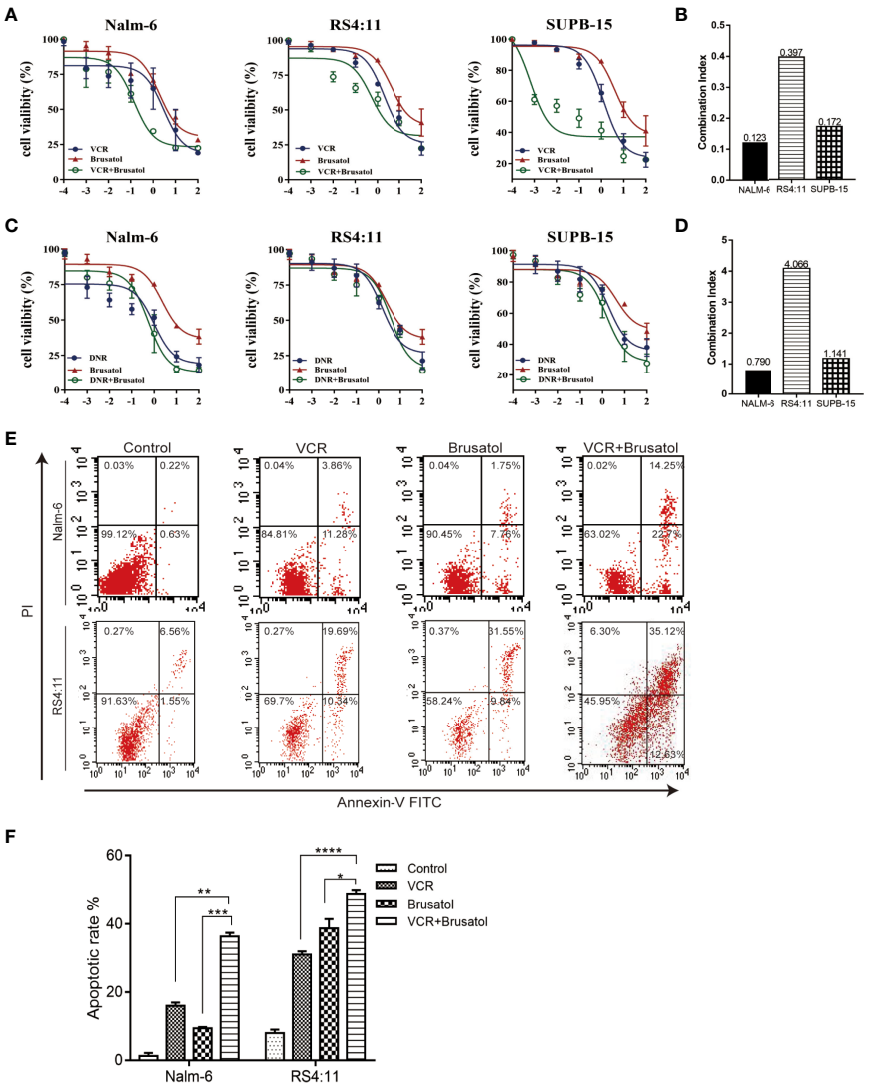

FIGURE 2 | Nrf2 inhibitor, brusatol, sensitises B-ALL cell lines to VCR. **(A)** Dose-response curves of VCR(10^{-4},10^{-3}, 10^{-2}, 10^{-1}, 10 and 10^{2} μM), brusatol (10^{-5}, 10^{-4},10^{-3}, 10^{-2}, 10^{-1} and 10 μM) and VCR (10^{-4},10^{-3}, 10^{-2}, 10^{-1}, 10 and 10^{2} μM) combination at the constant molar ratio with brusatol (1.5μM) in B-ALL cell lines. CCK-8 assay after 24 h of drug exposure determined cell viability. **(B)** Combination index (CI) values were calculated for each drug combination at effective dose ED50. **(C)** Dose-response curves of DNR (10^{-4},10^{-3}, 10^{-2}, 10^{-1}, 10 and 10^{2} μM), brusatol (10^{-5},10^{-4},10^{-3}, 10^{-2}, 10^{-1} and 10 μM) and DNR (10^{-4},10^{-3}, 10^{-2}, 10^{-1}, 10 and 10^{2} μM) combination at the constant molar ratio with brusatol (1.5μM) in B-ALL cell lines. CCK-8 assay after 24 h of drug exposure determined cell viability. Data are expressed as mean ± S.E.M. of at least three independents' experiments. **(D)** Combination index (CI) values were calculated for each drug combination at effective dose ED50. **(E, F)** The combined VCR (5 μM)/brusatol (1.5 μM) treatment increases apoptosis in B-ALL cell lines for 24h. An Analysis of apoptosis (by Annexin-V/PI staining) induced by brusatol, VCR, and their combination (at same molar ratios as in A and C) at the indicated concentrations 24 h post-treatment. *P < 0.05, **P < 0.01, ***P < 0.001,****P < 0.0001.

an empty vector and LV-Nrf2 cell group, and was found that the Nrf2 overexpression did not affect the p-AKT. Next, the protein expression levels of downstream products of this signaling pathway were examined in different groups. The results show that the expression of Bcl-2 in the LV-Nrf2 subgroup was higher than in the EV subgroup (**Figures 4 G, H**; P < 0.01, P < 0.001), and this means that Nrf2 overexpression could downregulate the BAD expression level, increasing the Bcl-2 expression level. Finally, RS4:11 cells (**Figure 4E**) and Nalm-6 cells (**Figure 4F**) were treated with MK-2206 (10 μM) for 24 h, an AKT inhibitor, and LV-Nrf2 showed it decreased BAD levels compared with those in the EV subgroup (**Figures 4G, H**; P < 0.0, P < 0.05). The expression of BAD in the LV-Nrf2+MK-2206 subgroup was lower than it in the EV+MK-2206 subgroup (**Figures 4G, H**; P < 0.05, P < 0.001). The expression of Bcl-2 in the LV-Nrf2+MK-2206 subgroup was still higher than it in the EV+MK-2206 subgroup (**Figures 4G, H**; P < 0.05, P < 0.05). Moreover, p-AKT levels were decreased in both of them, a trend that has not changed.

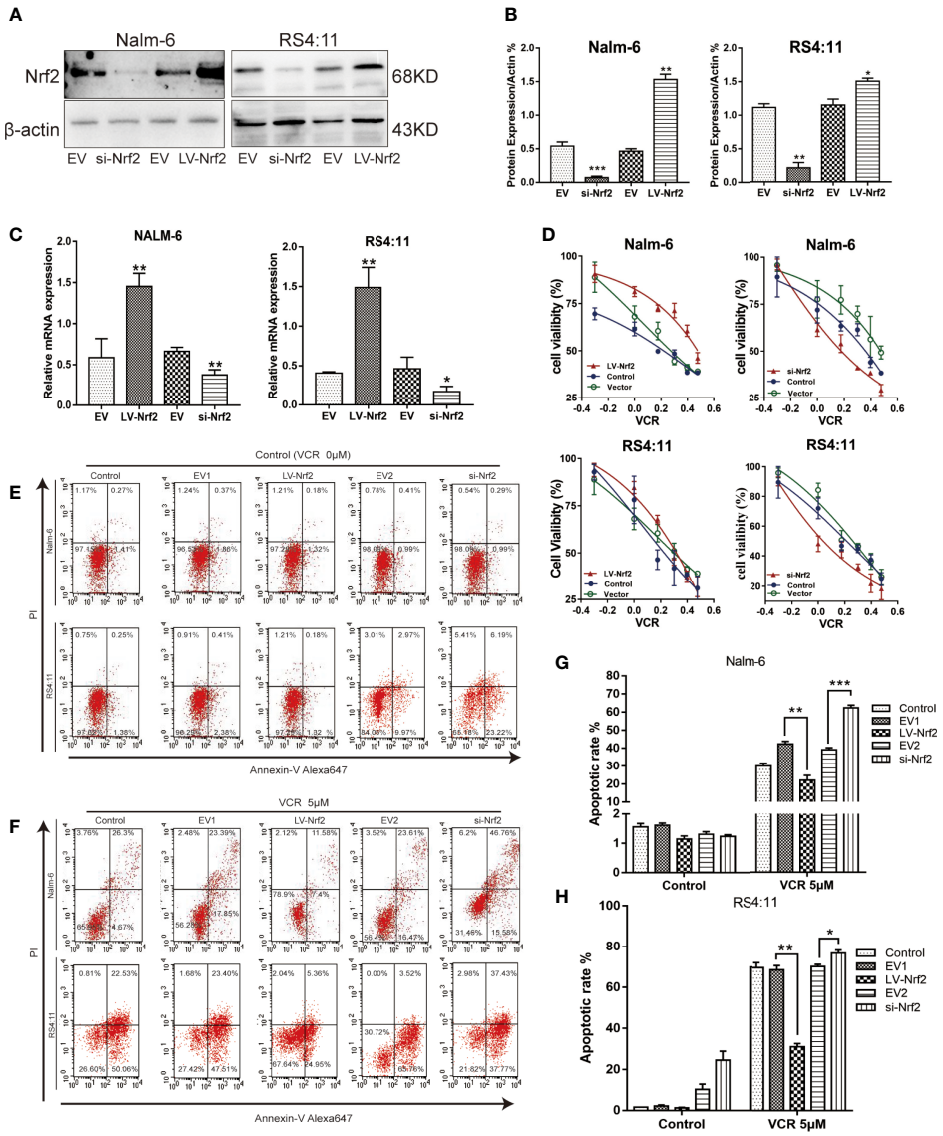

FIGURE 3 | **(A)** Nrf2 was overexpressed or silenced in Nalm-6 and RS4:11 cell lines determined by western blot analyses. **(B)** The relative grey values were shown in the histogram. **(C)** Nrf2 was overexpressed or silenced in Nalm-6 and RS4:11 cell lines determined by qRT-PCR analyses. **(D)** Dose-response curves of VCR (0, 0.05, 0.1, 0.25, 0.5, 1 and 2 μM) of LV-Nrf2 and si-Nrf2 in Nalm-6, RS4:11. CCK-8 assay after 24 h of drug exposure determined Cell viability. Data are expressed as mean ± SEM of at least three independent experiments. **(E, F)** The percentage of apoptotic cells was demonstrated by flow cytometry in both cell lines following the LV-Nrf2 and si-Nrf2 after 24h. **(G, H)** The percentage of apoptotic cells was demonstrated by flow cytometry in both cell lines following the LV-Nrf2 and si-Nrf2 after being treated with VCR (5 μM) for 24h. *P < 0.05, **P < 0.01, ***P < 0.001.

This study revealed for the first time that increased Nrf2 could reduce ALL cell sensitisation to VCR therapy by repressing BAD in the PI3K-AKT pathway (**Figure 4I**).

The Nrf2 Expression Is a Directly Associated With the Therapeutic Effects of VCR *In Vivo*

A total of 12 B-ALL xenograft models were developed by injecting EV or LV-Nrf2 transfected RS4:11 cells into NOD/SCID mice, as described, to functionally correlate Nrf2 overexpression with the response to tumor cells proliferating, growth and VCR sensitisation (**Figures 5A, B**). Moreover, VCR was administered to the mice as soon as the tumor became palpable. As shown in **Figures 5C, D** tumors in the LV-Nrf2 subgroup (n = 3) were bigger and heavier than those in the EV subgroups (n = 3; P < 0.01). Tumors in the LV-Nrf2/VCR subgroup (n = 3) were bigger and heavier than those in the EV/VCR subgroups (n = 3) (P < 0.05). The tumor volume and weight were significantly reduced in both groups treated with

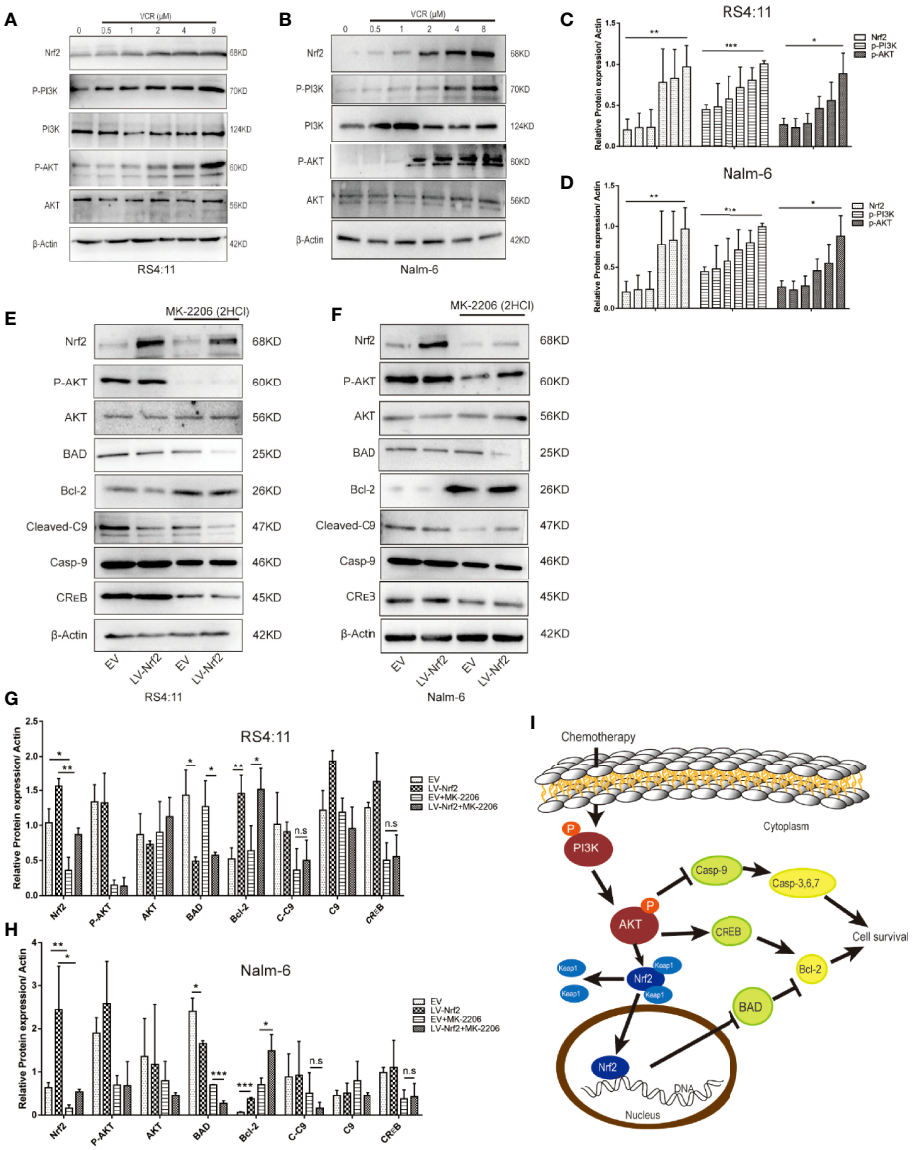

FIGURE 4 | **(A)** Representative western blot of Nrf2, p-PI3K, PI3K, p-AKT, AKT, and β-Actin in RS4:11 cells. The cells were pretreated with or without VCR (0.5,1,2,4 and 8 μM, 24 h). **(B)** Representative western blot of Nrf2, p-PI3K, PI3K, p-AKT, AKT, and β-Actin in Nalm-6 cells. The cells were pretreated with or without VCR (0.5,1,2,4 and 8 μM, 24 h). **(C, D)** The relative grey values were shown in the histogram. **(E)** After treatment with or without 10 μM MK2206 for 24 h in RS4:11 cells, protein expression levels of Nrf2, p-AKT, AKT, BAD, Bcl-2, Caspase-9, Cleaved-Caspase9 and CR_EB was evaluated by western blot analysis in the Nrf2-overexpression and EV groups. **(F)** After treatment with or without 10 μM MK2206 for 24 h in Nalm-6 cells, protein expression levels of Nrf2, p-AKT, AKT, BAD, Bcl-2, Caspase-9, Cleaved-Caspase9 and CR_EB was evaluated by western blot analysis in the Nrf2-overexpression and EV groups. **(G, H)** The relative gray values were shown in histogram. Data are presented as the mean ± SD of three independent experiments. *P < 0.05, **P < 0.01, ***P < 0.001, n.s, no significance. **(I)** Schematic representation of the molecular mechanisms proposed in the positive effect of regulate *via* Nrf2 of PI3K/Akt/Nrf2 signaling pathway in ALL cells.

VCR ($P < 0.05$). Then, an IHC assay was used to look for Nrf2 expression in paraffin-embedded tumor tissues. Neither the Nrf2 overexpression group treated with or without VCR nor the EV group showed any significant differences in Nrf2 *in vivo* (**Figure 5E**). Therefore, NRF2 overexpression is suggested to results in decreased sensitivity of B-ALL cells to VCR chemotherapy.

DISCUSSION

In recent years, several studies have investigated the potential role of Nrf2 protein, which plays critical roles in carcinogenesis, tumor progression and chemotherapy resistance (35, 42, 43), but not before B-ALL. Therefore, the Nrf2 expression in healthy donors vs. drug-sensitive vs. drug-resistant was analysed in adult

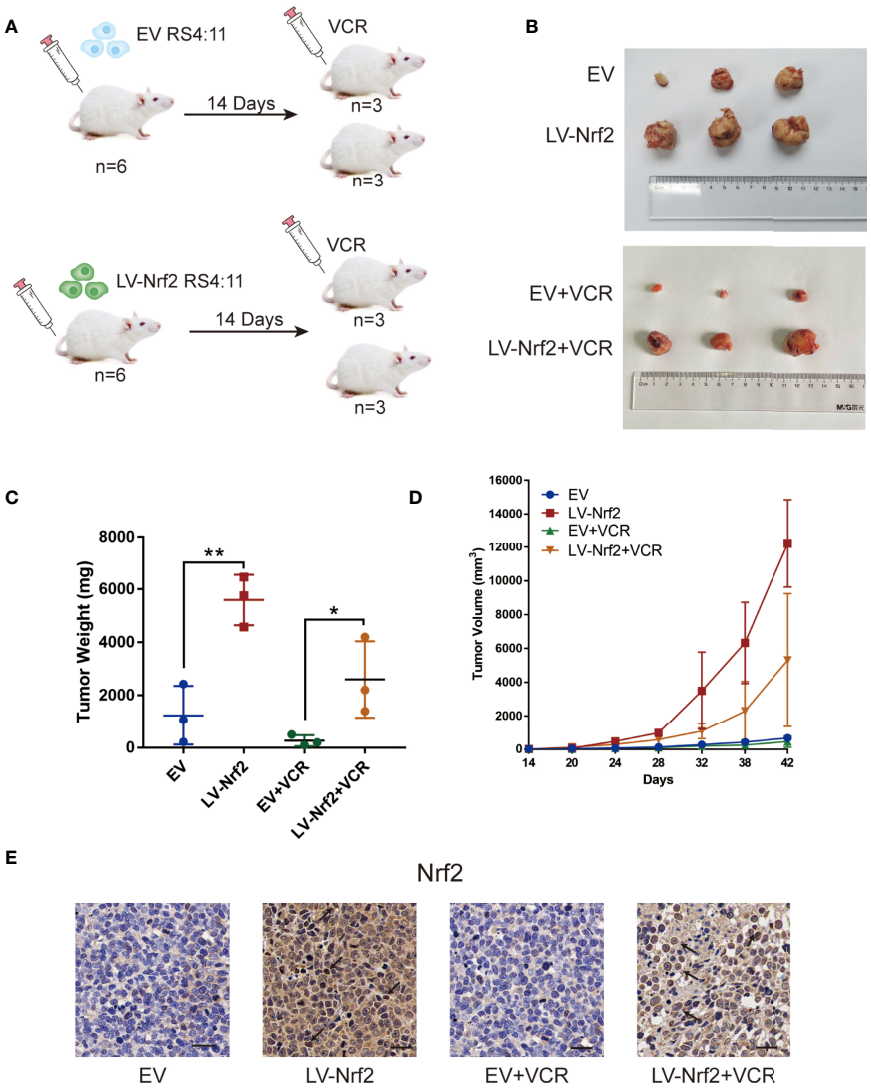

FIGURE 5 | **(A)** Model of mouse subcutaneous tumor formation. **(B)** Images of subcutaneous xenografts from mice in the EV group (n = 3), LV-Nrf2 group (n = 3), EV +VCR group (n = 3) (VCR, 80 mg/kg/day for 6 days), LV-Nrf2+VCR group (n = 3) (VCR, 80 mg/kg/day for 6 days). **(C)** Tumor weight change curves for subcutaneous xenografts. *P < 0.05, **P < 0.01. **(D)** Tumor volume growth curves for subcutaneous xenografts. **(E)** The expression of Nrf2 was examined in xenograft tumor tissue sections using immunohistochemistry (IHC) (scale bars: 50 μm).

patients with B-ALL. The basic case data are fascinating; however, they are mostly hypothesis-generating due to a paucity of longitudinal specimens. Among the main primary patient's major features, our findings revealed that chemotherapy-resistant B-ALL samples had a considerable Nrf2 overexpression and activation, which was consistent with Nrf2 descriptions in solid tumors (43, 44). Some previous studies demonstrated that Nrf2 transient knockdown or selective inhibition through the Keap1 overexpression strongly increased the susceptibility of lung cancer (44) cells to different chemotherapeutics, including cisplatin (45), doxorubicin (2, 46), and etoposide (24, 47, 48).

In this study, *in vitro* and *in vivo* niche models were employed to further examine the Nrf2 mechanism that induced chemosensitivity and to further understand their functional features in supporting adult B-ALL targets. *In vitro*, we mimicked chemotherapy with medication, employing VCR and DNR alone or combined with brusatol. Our results revealed that brusatol, an Nrf2 inhibitor, sufficiently increased the B-ALL cell sensitivity to VCR through the synergistic therapeutic effects. We recapitulate all these findings in a murine model by activating Nrf2 through tumor resistant VCR therapy. VCR is a primary drug used in induction therapy (49). Previous studies have reported (50) that specific Nrf2 inhibition *via* KEAP1 (23) or

Bcl-2 (51) strongly increased the susceptibility of tumor cell lines to different chemotherapeutics, including doxorubicin, cisplatin and etoposide. VCR and anthracycline mitoxantrone are extensively used as standard chemotherapeutics for patients with newly diagnosed and relapsed B-ALL (52, 53) which establishes the high clinical relevance of our results. This sensitisation effect was obtained by specifically inhibiting Nrf2, without the need to counteract additional detoxifying genes, indicating the significant role of Nrf2 family members in modulating drug response in B-ALL. Our findings support the use of brusatol, an Nrf2 inhibitor, combined with VCR as a novel therapeutic approach for the treatment of drug-insensitive or relapsed B-ALL.

Furthermore, gain- and loss-of-function experiments were conducted to investigate the direct impact of Nrf2 in chemotherapeutic resistance, using FCM to detect the apoptosis of different groups of B-ALL cells. Nrf2 overexpression can protect tumor cells from apoptosis and easily result in apoptosis when Nrf2 expression is repressed. This result is consistent with that of previous studies that used inhibitors. Nrf2 is shown to regulate the sensitivity of tumor cells to VCR therapy by altering their expression rather than the toxicity of inhibitors.

Nrf2 is a transcription factor, and our results establish a new possibility of chemoresistance treatments by targeting this transcriptional network that regulates the expression of apoptotic or anti-apoptotic proteins than the protein itself and using it with traditional chemotherapeutic agents. PI3K-AKT is a classical signal pathway related to apoptosis. In this study, the molecular basis underlying the resistance was investigated. Our data suggest that Nrf2 is regulated by Akt and affects the downstream products of Akt. Proteins in the apoptosis protein family, namely BAD and Bcl-2, are the most affected by Nrf2. Tumor cells with Nrf2 activation may increase antioxidant systems to mitigate oxidative stress, which in turn contributes to anti-apoptotic and drug resistance (54). Nrf2 plays a complex indispensable role in cancer growth and chemoresistance and it has been become a target for the development of anti-cancer drug (55). The influence of Nrf2 beyond redox, such as it can regulated the relation between Ca^{2+} signalling and redox homeostasis, which is correlated with proteins' sensitive to S-glutathionylation (56). Nrf2, according to regulated ROS levels, other proteins, transcription factors, signal pathways, has been established in cancers. In this study, we characterised the role of Nrf2 in B-ALL apoptotic-dependent chemotherapeutic resistance.

The transcriptional regulatory networks of many genes encoding proteins involved in chemoresistance are well-established; therefore, this approach opens new possibilities for targeted combination therapies (57). To the best of our knowledge, our findings demonstrate, for the first time, a direct relationship between Nrf2 overexpression and anti-apoptotic protein inhibition, BAD, which in the PI3K-AKT pathway that decreased response to chemotherapeutic response in adult patients with B-ALL. Therefore, Nrf2 high expression may be a predictive biomarker of the poor treatment response in adult patients with B-ALL that induction chemotherapy with VCR not effective well. In other words, it may improve the effectiveness of induction chemotherapy, which in turn may allow patients to achieve better remission. In conclusion, our results establish the therapeutic efficacy of a novel combination treatment for adult patients with chemoresistant B-ALL. Hence, novel Nrf2 inhibitors with fewer side effects that could be combined with standard chemotherapeutic agents should be developed for the treatment of drug-resistant haematological malignancies in the future.

DATA AVAILABILITY STATEMENT

The original contributions presented in the study are included in the article/**Supplementary Material**. Further inquiries can be directed to the corresponding authors.

ETHICS STATEMENT

The animal study was reviewed and approved by Guizhou Laboratory Animal Engineering Technology Center.

AUTHOR CONTRIBUTIONS

Funding acquisition, JW. Investigation, LW. Methodology, LW, XL, CF, LC. Project Administration, JW. Resources, JW. Supervision, JW, SW. validation, CP, QK, TZ. Writing—original draft, LW. Writing—review and editing, JW, SW, LW, CP, QK. The author share last authorship, SW. All authors contributed to the article and approved the submitted version.

FUNDING

The work is supported by grants from the National Natural Science Foundation of China (NO. 81960032 and NO. 82170168), the Translational Research Grant of NCRCH (2021WWB01 and 2020ZKPB03).

SUPPLEMENTARY MATERIAL

The Supplementary Material for this article can be found online at: https://www.frontiersin.org/articles/10.3389/fonc.2022.876556/full#supplementary-material

Supplementary Figure 1 | (A) The HO-1 protein levels assessed by western blot. **(B)** The relative gray values were shown in the histogram, *p<0.05.

Supplementary Figure 2 | (A) The Nrf2 protein levels in Nalm-6, RS4:11, Supb-15 were assessed by western blot. **(B)** The relative gray values were shown in the histogram.

REFERENCES

1. Wolach O, Amitai I, DeAngelo DJ. Current Challenges and Opportunities in Treating Adult Patients With Philadelphia-Negative Acute Lymphoblastic Leukaemia. *Br J Haematol* (2017) 179:705–23. doi: 10.1111/bjh.14916
2. Kantarjian H, Thomas D, O'Brien S, Cortes J, Giles F, Jeha S, et al. Long-Term Follow-Up Results of Hyperfractionated Cyclophosphamide, Vincristine, Doxorubicin, and Dexamethasone (Hyper-CVAD), a Dose-Intensive Regimen, in Adult Acute Lymphocytic Leukemia. *Cancer* (2004) 101:2788–801. doi: 10.1002/cncr.20668
3. Sive JI, Buck G, Fielding A, Lazarus HM, Litzow MR, Luger S, et al. Outcomes in Older Adults With Acute Lymphoblastic Leukaemia (ALL): Results From the International MRC UKALL XII/ECOG2993 Trial. *Br J Haematol* (2012) 157:463–71. doi: 10.1111/j.1365-2141.2012.09095.x
4. Gökbuget N. Treatment of Older Patients With Acute Lymphoblastic Leukemia. *Hematology* (2016) 2016:573–9. doi: 10.1182/asheducation-2016.1.573
5. Rowe JM. Induction Therapy for Adults With Acute Lymphoblastic Leukemia: Results of More Than 1500 Patients From the International ALL Trial: MRC UKALL XII/ECOG E2993. *Blood* (2005) 106:3760–7. doi: 10.1182/blood-2005-04-1623
6. Geyer MB, Hsu M, Devlin SM, Tallman MS, Douer D, Park JH. Overall Survival Among Older US Adults With ALL Remains Low Despite Modest Improvement Since 1980: SEER Analysis. *Blood* (2017) 129:1878–81. doi: 10.1182/blood-2016-11-749507
7. Larson RA, Dodge RK, Burns CP, Lee EJ, Stone RM, Schulman P, et al. A Five-Drug Remission Induction Regimen With Intensive Consolidation for Adults With Acute Lymphoblastic Leukemia: Cancer and Leukemia Group B Study 8811. *Blood* (1995) 85:2025–37. doi: 10.1182/blood.V85.8.2025.bloodjournal8582025
8. Kozlowski P, Lennmyr E, Ahlberg L, Bernell P, Hulegårdh E, Karbach H, et al. Age But Not Philadelphia Positivity Impairs Outcome in Older/Elderly Patients With Acute Lymphoblastic Leukemia in Sweden. *Eur J Haematol* (2017) 99:141–9. doi: 10.1111/ejh.12896
9. Jabbour E, Short NJ, Ravandi F, Huang X, Daver N, DiNardo CD, et al. Combination of Hyper-CVAD With Ponatinib as First-Line Therapy for Patients With Philadelphia Chromosome-Positive Acute Lymphoblastic Leukaemia: Long-Term Follow-Up of a Single-Centre, Phase 2 Study. *Lancet Haematol* (2018) 5:e618–27. doi: 10.1016/S2352-3026(18)30176-5
10. Suzuki T, Muramatsu A, Saito R, Iso T, Shibata T, Kuwata K, et al. Molecular Mechanism of Cellular Oxidative Stress Sensing by Keap1. *Cell Rep* (2019) 28:746–58.e4. doi: 10.1016/j.celrep.2019.06.047
11. Taguchi K, Motohashi H, Yamamoto M. Molecular Mechanisms of the Keap1-Nrf2 Pathway in Stress Response and Cancer Evolution: Molecular Mechanisms of the Keap1-Nrf2 Pathway. *Genes Cells* (2011) 16:123–40. doi: 10.1111/j.1365-2443.2010.01473.x
12. Tebay LE, Robertson H, Durant ST, Vitale SR, Penning TM, Dinkova-Kostova AT, et al. Mechanisms of Activation of the Transcription Factor Nrf2 by Redox Stressors, Nutrient Cues, and Energy Status and the Pathways Through Which it Attenuates Degenerative Disease. *Free Radic Biol Med* (2015) 88:108–46. doi: 10.1016/j.freeradbiomed.2015.06.021
13. Kobayashi A, Kang M-I, Okawa H, Ohtsuji M, Zenke Y, Chiba T, et al. Oxidative Stress Sensor Keap1 Functions as an Adaptor for Cul3-Based E3 Ligase To Regulate Proteasomal Degradation of Nrf2. *Mol Cell Biol* (2004) 24:7130–9. doi: 10.1128/MCB.24.16.7130-7139.2004
14. Huang H-C, Nguyen T, Pickett CB. Phosphorylation of Nrf2 at Ser-40 by Protein Kinase C Regulates Antioxidant Response Element-Mediated Transcription. *J Biol Chem* (2002) 277:42769–74. doi: 10.1074/jbc.M206911200
15. Hayes JD, Dinkova-Kostova AT, Tew KD. Oxidative Stress in Cancer. *Cancer Cell* (2020) 38:167–97. doi: 10.1016/j.ccell.2020.06.001
16. Sajadimajd S, Khazaei M. Oxidative Stress and Cancer: The Role of Nrf2. *Curr Cancer Drug Targets* (2018) 18:538–57. doi: 10.2174/1568009617666171002144228
17. Roh J-L, Jang H, Kim EH, Shin D. Targeting of the Glutathione, Thioredoxin, and Nrf2 Antioxidant Systems in Head and Neck Cancer. *Antioxid Redox Signal* (2017) 27:106–14. doi: 10.1089/ars.2016.6841
18. Jeddi F, Soozangar N, Sadeghi MR, Somi MH, Shirmohamadi M, Eftekhar-Sadat A-T, et al. Nrf2 Overexpression Is Associated With P-Glycoprotein Upregulation in Gastric Cancer. *BioMed Pharmacother Biomed Pharmacother* (2018) 97:286–92. doi: 10.1016/j.biopha.2017.10.129
19. Ma C-S, Lv Q-M, Zhang K-R, Tang Y-B, Zhang Y-F, Shen Y, et al. NRF2-GPX4/SOD2 Axis Imparts Resistance to EGFR-Tyrosine Kinase Inhibitors in Non-Small-Cell Lung Cancer Cells. *Acta Pharmacol Sin* (2021) 42:613–23. doi: 10.1038/s41401-020-0443-1
20. Ma S, Paiboonrungruan C, Yan T, Williams KP, Major MB, Chen XL. Targeted Therapy of Esophageal Squamous Cell Carcinoma: The NRF2 Signaling Pathway as Target. *Ann N Y Acad Sci* (2018) 1434:164–72. doi: 10.1111/nyas.13681
21. Zhang L, Wang N, Zhou S, Ye W, Jing G, Zhang M. Propofol Induces Proliferation and Invasion of Gallbladder Cancer Cells Through Activation of Nrf2. *J Exp Clin Cancer Res CR* (2012) 31:66. doi: 10.1186/1756-9966-31-66
22. Almeida M, Soares M, Ramalhinho AC, Moutinho JF, Breitenfeld L, Pereira L. The Prognostic Value of NRF2 in Breast Cancer Patients: A Systematic Review With Meta-Analysis. *Breast Cancer Res Treat* (2020) 179:523–32. doi: 10.1007/s10549-019-05494-4
23. Suzuki T, Motohashi H, Yamamoto M. Toward Clinical Application of the Keap1-Nrf2 Pathway. *Trends Pharmacol Sci* (2013) 34:340–6. doi: 10.1016/j.tips.2013.04.005
24. Wang J, Lu Q, Cai J, Wang Y, Lai X, Qiu Y, et al. Nestin Regulates Cellular Redox Homeostasis in Lung Cancer Through the Keap1–Nrf2 Feedback Loop. *Nat Commun* (2019) 10:5043. doi: 10.1038/s41467-019-12925-9
25. Kerr JF, Wyllie AH, Currie AR. Apoptosis: A Basic Biological Phenomenon With Wide-Ranging Implications in Tissue Kinetics. *Br J Cancer* (1972) 26:239–57. doi: 10.1038/bjc.1972.33
26. Fischer B, Frei C, Moura U, Stahel R, Felley-Bosco E. Inhibition of Phosphoinositide-3 Kinase Pathway Down Regulates ABCG2 Function and Sensitizes Malignant Pleural Mesothelioma to Chemotherapy. *Lung Cancer Amst Neth* (2012) 78:23–9. doi: 10.1016/j.lungcan.2012.07.005
27. Ge J, Liu Y, Li Q, Guo X, Gu L, Ma ZG, et al. Resveratrol Induces Apoptosis and Autophagy in T-Cell Acute Lymphoblastic Leukemia Cells by Inhibiting Akt/mTOR and Activating P38-MAPK. *BioMed Environ Sci BES* (2013) 26:902–11. doi: 10.3967/bes2013.019
28. Liu B, Wang C, Chen P, Cheng B, Cheng Y. RACKI Induces Chemotherapy Resistance in Esophageal Carcinoma by Upregulating the PI3K/AKT Pathway and Bcl-2 Expression. *OncoTar Ther* (2018) 11:211–20. doi: 10.2147/OTT.S152818
29. Liu R, Chen Y, Liu G, Li C, Song Y, Cao Z, et al. PI3K/AKT Pathway as a Key Link Modulates the Multidrug Resistance of Cancers. *Cell Death Dis* (2020) 11:797. doi: 10.1038/s41419-020-02998-6
30. Liu C, Chen K, Wang H, Zhang Y, Duan X, Xue Y, et al. Gastrin Attenuates Renal Ischemia/Reperfusion Injury by a PI3K/Akt/Bad-Mediated Anti-Apoptosis Signaling. *Front Pharmacol* (2020) 11:540479. doi: 10.3389/fphar.2020.540479
31. Sochalska M, Tuzlak S, Egle A, Villunger A. Lessons From Gain- and Loss-Of-Function Models of Pro-Survival Bcl2 Family Proteins: Implications for Targeted Therapy. *FEBS J* (2015) 282:834–49. doi: 10.1111/febs.13188
32. Goan Y-G, Wu W-T, Liu C-I, Neoh C-A, Wu Y-J. Involvement of Mitochondrial Dysfunction, Endoplasmic Reticulum Stress, and the PI3K/AKT/mTOR Pathway in Nobiletin-Induced Apoptosis of Human Bladder Cancer Cells. *Mol Basel Switz* (2019) 24:E2881. doi: 10.3390/molecules24162881
33. Korsmeyer SJ, Wei MC, Saito M, Weiler S, Oh KJ, Schlesinger PH. Pro-Apoptotic Cascade Activates BID, Which Oligomerizes BAK or BAX Into Pores That Result in the Release of Cytochrome C. *Cell Death Differ* (2000) 7:1166–73. doi: 10.1038/sj.cdd.4400783
34. Kuwana T, Bouchier-Hayes L, Chipuk JE, Bonzon C, Sullivan BA, Green DR, et al. BH3 Domains of BH3-Only Proteins Differentially Regulate Bax-Mediated Mitochondrial Membrane Permeabilization Both Directly and Indirectly. *Mol Cell* (2005) 17:525–35. doi: 10.1016/j.molcel.2005.02.003
35. Karathedath S, Rajamani BM, Musheer Aalam SM, Abraham A, Varatharajan S, Krishnamurthy P, et al. Role of NF-E2 Related Factor 2 (Nrf2) on Chemotherapy Resistance in Acute Myeloid Leukemia (AML) and the Effect of Pharmacological Inhibition of Nrf2. *PloS One* (2017) 12:e0177227. doi: 10.1371/journal.pone.0177227
36. Dewson G, Ma S, Frederick P, Hockings C, Tan I, Kratina T, et al. Bax Dimerizes *via* a Symmetric BH3:groove Interface During Apoptosis. *Cell Death Differ* (2012) 19:661–70. doi: 10.1038/cdd.2011.138

37. Gavathiotis E, Suzuki M, Davis ML, Pitter K, Bird GH, Katz SG, et al. BAX Activation is Initiated at a Novel Interaction Site. *Nature* (2008) 455:1076–81. doi: 10.1038/nature07396
38. Zaltsman Y, Shachnai L, Yivgi-Ohana N, Schwarz M, Maryanovich M, Houtkooper RH, et al. MTCH2/MIMP Is a Major Facilitator of tBID Recruitment to Mitochondria. *Nat Cell Biol* (2010) 12:553–62. doi: 10.1038/ncb2057
39. Hirai H, Sootome H, Nakatsuru Y, Miyama K, Taguchi S, Tsujioka K, et al. MK-2206, an Allosteric Akt Inhibitor, Enhances Antitumor Efficacy by Standard Chemotherapeutic Agents or Molecular Targeted Drugs *In Vitro* and *In Vivo*. *Mol Cancer Ther* (2010) 9:1956–67. doi: 10.1158/1535-7163.MCT-09-1012
40. Guo C, Gao C, Zhao D, Li J, Wang J, Sun X, et al. A Novel ETV6-miR-429-CRKL Regulatory Circuitry Contributes to Aggressiveness of Hepatocellular Carcinoma. *J Exp Clin Cancer Res* (2020) 39:70. doi: 10.1186/s13046-020-01559-1
41. Sato W, Fukazawa N, Suzuki T, Yusa K, Tsuruo T. Circumvention of Multidrug Resistance by a Newly Synthesized Quinoline Derivative, MS-073. *Cancer Res* (1991) 51:2420–4.
42. Lin P, Ren Y, Yan X, Luo Y, Zhang H, Kesarwani M, et al. The High NRF2 Expression Confers Chemotherapy Resistance Partly Through Up-Regulated DUSP1 in Myelodysplastic Syndromes. *Haematologica* (2019) 104:485–96. doi: 10.3324/haematol.2018.197749
43. Rushworth SA, Zaitseva L, Murray MY, Shah NM, Bowles KM, MacEwan DJ. The High Nrf2 Expression in Human Acute Myeloid Leukemia Is Driven by NF-κb and Underlies its Chemo-Resistance. *Blood* (2012) 120:5188–98. doi: 10.1182/blood-2012-04-422121
44. Bialk P, Wang Y, Banas K, Kmiec EB. Functional Gene Knockout of NRF2 Increases Chemosensitivity of Human Lung Cancer A549 Cells In Vitro and in a Xenograft Mouse Model. *Mol Ther Oncol* (2018) 11:75–89. doi: 10.1016/j.omto.2018.10.002
45. Sun X, Wang S, Gai J, Guan J, Li J, Li Y, et al. SIRT5 Promotes Cisplatin Resistance in Ovarian Cancer by Suppressing DNA Damage in a ROS-Dependent Manner *via* Regulation of the Nrf2/HO-1 Pathway. *Front Oncol* (2019) 9:754. doi: 10.3389/fonc.2019.00754
46. Takeuchi J, Kyo T, Naito K, Sao H, Takahashi M, Miyawaki S, et al. Induction Therapy by Frequent Administration of Doxorubicin With Four Other Drugs, Followed by Intensive Consolidation and Maintenance Therapy for Adult Acute Lymphoblastic Leukemia: The JALSG-ALL93 Study. *Leukemia* (2002) 16:1259–66. doi: 10.1038/sj.leu.2402526
47. Xu B, Wang S, Li R, Chen K, He L, Deng M, et al. Disulfiram/copper Selectively Eradicates AML Leukemia Stem Cells *In Vitro* and *In Vivo* by Simultaneous Induction of ROS-JNK and Inhibition of NF-κb and Nrf2. *Cell Death Dis* (2017) 8:e2797–7. doi: 10.1038/cddis.2017.176
48. Gagliardi M, Cotella D, Santoro C, Corà D, Barlev NA, Piacentini M, et al. Aldo-Keto Reductases Protect Metastatic Melanoma From ER Stress-Independent Ferroptosis. *Cell Death Dis* (2019) 10:902. doi: 10.1038/s41419-019-2143-7
49. Richard-Carpentier G, Kantarjian H, Jabbour E. Recent Advances in Adult Acute Lymphoblastic Leukemia. *Curr Hematol Malig Rep* (2019) 14-2:106–18. doi: 10.1007/s11899-019-00503-1
50. Wang X-J, Sun Z, Villeneuve NF, Zhang S, Zhao F, Li Y, et al. Nrf2 Enhances Resistance of Cancer Cells to Chemotherapeutic Drugs, the Dark Side of Nrf2. *Carcinogenesis* (2008) 29:1235–43. doi: 10.1093/carcin/bgn095
51. Nguyen LXT, Troadec E, Kalvala A, Kumar B, Hoang DH, Viola D, et al. The Bcl-2 Inhibitor Venetoclax Inhibits Nrf2 Antioxidant Pathway Activation Induced by Hypomethylating Agents in AML. *J Cell Physiol* (2019) 234:14040–9. doi: 10.1002/jcp.28091
52. Testi AM, Canichella M, Vitale A, Piciocchi A, Guarini A, Starza ID, et al. Adolescent and Young Adult Acute Lymphoblastic Leukemia. Final Results of the Phase II Pediatric-Like GIMEMA LAL-1308 Trial. *Am J Hematol* (2021) 96:292–301. doi: 10.1002/ajh.26066
53. Jabbour E, Sasaki K, Ravandi F, Huang X, Short NJ, Khouri M, et al. Chemoimmunotherapy With Inotuzumab Ozogamicin Combined With Mini-Hyper-CVD, With or Without Blinatumomab, is Highly Effective in Patients With Philadelphia Chromosome-Negative Acute Lymphoblastic Leukemia in First Salvage. *Cancer* (2018) 124:4044–55. doi: 10.1002/cncr.31720
54. Grek CL, Zhang J, Manevich Y, Townsend DM, Tew KD. Causes and Consequences of Cysteine S-Glutathionylation. *J Biol Chem* (2013) 288:26497–504. doi: 10.1074/jbc.R113.461368
55. Xue D, Zhou X, Qiu J. Emerging Role of NRF2 in ROS-Mediated Tumor Chemoresistance. *BioMed Pharmacother Biomed Pharmacother* (2020) 131:110676. doi: 10.1016/j.biopha.2020.110676
56. Takahashi N, Chen H-Y, Harris IS, Stover DG, Selfors LM, Bronson RT, et al. Cancer Cells Co-Opt the Neuronal Redox-Sensing Channel TRPA1 to Promote Oxidative-Stress Tolerance. *Cancer Cell* (2018) 33:985–1003.e7. doi: 10.1016/j.ccell.2018.05.001
57. Song C, Ge Z, Ding Y, Tan B-H, Desai D, Gowda K, et al. IKAROS and CK2 Regulate Expression of BCL-XL and Chemosensitivity in High-Risk B-Cell Acute Lymphoblastic Leukemia. *Blood* (2020) 136:1520–34. doi: 10.1182/blood.2019002655

Conflict of Interest: The authors declare that the research was conducted in the absence of any commercial or financial relationships that could be construed as a potential conflict of interest.

Publisher's Note: All claims expressed in this article are solely those of the authors and do not necessarily represent those of their affiliated organizations, or those of the publisher, the editors and the reviewers. Any product that may be evaluated in this article, or claim that may be made by its manufacturer, is not guaranteed or endorsed by the publisher.

frontiers | Frontiers in Oncology

ORIGINAL RESEARCH
published: 24 May 2022
doi: 10.3389/fonc.2022.878098

Childhood Acute B-Lineage Lymphoblastic Leukemia With CDKN2A/B Deletion Is a Distinct Entity With Adverse Genetic Features and Poor Clinical Outcomes

Jing Feng, Ye Guo, Wenyu Yang, Yao Zou, Li Zhang, Yumei Chen, Yingchi Zhang, Xiaofan Zhu and Xiaojuan Chen**

State Key Laboratory of Experimental Hematology, National Clinical Research Center for Blood Diseases, Haihe Laboratory of Cell Ecosystem, Institute of Hematology & Blood Diseases Hospital, Chinese Academy of Medical Sciences & Peking Union Medical College, Tianjin, China

OPEN ACCESS

Edited by:
Lokman Varisli,
Dicle University, Turkey

Reviewed by:
Luca Lo Nigro,
Azienda Ospedaliero Universitaria Policlinico - San Marco, Italy
Hany Ariffin,
University of Malaya, Malaysia

***Correspondence:**
Xiaofan Zhu
xfzhu@ihcams.ac.cn
Xiaojuan Chen
chenxiaojuan@ihcams.ac.cn

Specialty section:
This article was submitted to Hematologic Malignancies, a section of the journal Frontiers in Oncology

Received: *17 February 2022*
Accepted: *14 April 2022*
Published: *24 May 2022*

Citation:
Feng J, Guo Y, Yang W, Zou Y, Zhang L, Chen Y, Zhang Y, Zhu X and Chen X (2022) Childhood Acute B-Lineage Lymphoblastic Leukemia With CDKN2A/B Deletion Is a Distinct Entity With Adverse Genetic Features and Poor Clinical Outcomes. Front. Oncol. 12:878098. doi: 10.3389/fonc.2022.878098

To further emphasize the clinical–genetic features and prognosis of *CDKN2A/B* deletions in childhood acute lymphoblastic leukemia (ALL), we retrospectively analyzed 819 consecutive B-ALL patients treated with the Chinese Children's Cancer Group ALL-2015 (CCCG-ALL-2015) protocol, and fluorescence *in situ* hybridization (FISH) analysis on *CDKN2A/B* deletion was available for 599 patients. The prevalence of *CDKN2A/B* gene deletions was 20.2% (121/599) of B-ALL. *CDKN2A/B* deletions were significantly associated with older age, higher leukocyte counts, a higher percentage of hepatosplenomegaly, and a higher frequency of *BCR-ABL* ($p < 0.05$). Those patients achieved similar minimal residual disease (MRD) clearance and complete remission compared to patients without *CDKN2A/B* deletion. The *CDKN2A/B* deletions were correlated with inferior outcomes, including a 3-year event-free survival (EFS) rate (69.8 ± 4.6 vs. 89.2 ± 1.6%, $p = 0.000$) and a 3-year overall survival (OS) rate (89.4% ± 2.9% vs. 94.7% ± 1.1%, $p = 0.037$). In multivariable analysis, *CDKN2A/B* deletion was still an independent prognostic factor for EFS in total cohorts ($p < 0.05$). We also detected a multiplicative interaction between *CDKN2A/B* deletions and TP53 deletion on dismal prognosis (p-interaction < 0.05). In conclusion, *CDKN2A/B* deletion is associated with distinct characteristics and serves as a poor prognostic factor in pediatric ALL, especially in TP53 deletion carriers.

Keywords: *CDKN2A/B*, pediatric acute lymphoblastic leukemia, fluorescence *in situ* hybridization, prognosis, *TP53*

INTRODUCTION

Pediatric acute lymphoblastic leukemia (ALL) is one of the most curable malignancies, with 5-year event-free survival rates exceeding 80% in many developed countries and even exceeding 90% in high-income countries (1). With the increased understanding of genetic alterations in ALL, many molecular markers have been identified and applied to risk stratification and treatment protocols in

leukemia. *CDKN2A/B* is one of the most frequent abnormal genes in ALL and can be detected by fluorescence *in situ* hybridization (FISH), multiplex ligation-dependent probe amplification (MLPA), array-based comparative genomic hybridization (aCGH) analysis, and single-nucleotide polymorphism array (SNPA) (2–6). As a secondary genetic event in the development of leukemia, the *CDKN2A/B* deletions were found in approximately 20%–25% of B-cell precursor acute lymphoblastic leukemia (BCP-ALL) and 38.5%–50% of T-ALL patients (2, 5, 7, 8). Despite the high frequency of *CDKN2A/B* deletions in pediatric ALL, the prognostic importance of the deletions is still inconclusive. Most investigators have concluded that the deletions were associated with the recurrence of pediatric ALL (7, 9, 10), and some researchers found that the inactivation of *CDKN2A/B* did not influence the outcome of childhood B-lineage ALL (4, 11). As previous inconsistent conclusions were drawn from small cohorts, large sample-sized studies are needed to clarify the prognostic impact of *CDKN2A/B* deletion in pediatric ALL. In this study, we assessed the clinical and biological characteristics and prognostic factors of *CDKN2A/B* deletions in 662 pediatric ALL patients.

MATERIALS AND METHODS

Patients and Treatment Protocols

The cohort included 902 patients with newly diagnosed pediatric ALL who were treated according to the CCCG-ALL 2015 protocol (ClinicalTrials.gov identifier: ChiCTRIPR-14005706) (12) registered at the Blood Disease Hospital of CAMS & PUMC between May 2015 and December 2019. As the FISH test has been performed since September 2016, FISH data from 662 patients were collected in this cohort finally (**Figure 1**). The protocol described in this study was approved by the Ethics Committee, Institute of Hematology and Blood Disease Hospital, Diseases Hospital, Chinese Academy of Medical Sciences (CAMS) and Peking Union Medical College (PUMC) (No. IIT2015010-EC-1). All patients or their legal guardians signed written informed consent before treatment.

Risk Group Assignment

Patients enrolled in the CCCG-ALL-2015 study were assigned to different risk groups based on morphology and immunophenotypic and genetic features of leukemia cells. Patients were assigned to the low-risk group if they had B-cell ALL and were aged between 1 year and 10 years; had a leukocyte count of less than 50×10^9/L, a chromosome number of more than 50, or the ETV6–RUNX1 fusion gene; and did not have CNS 3 status or testicular leukemia, and had a minimal residual disease of less than 1% on day 19 of induction and less than 0.01% on day 46 of induction. Patients with a minimal residual disease of 1% or more (or ≥5% blasts morphologically without suitable markers for minimal residual disease) in bone marrow on day 46 of induction and infants younger than 6 months with KMT2A rearrangement and a leukocyte count of 300×10^9/L or more were classified as high-risk ALL. The remaining participants were assigned to the intermediate-risk group (12). All eligible patients received minimal residual disease-directed, risk-stratified treatment modified from the St Jude Children's Research Hospital Total Therapy 15 and 16 studies (13, 14) and the Shanghai Children's Medical Center ALL-2005 trial (15), with IR/HR patients receiving more intensive treatment.

FISH and Probe

Pretreatment bone marrow aspirates were taken at diagnosis and at least 1–2 ml of bone marrow aspirates was analyzed by FISH for cytogenetic abnormalities (including CDKN2A/B, KMT2A rearrangement, TP53 deletion, and BCR-ABL1), polymerase chain reaction (PCR) for fusion gene (including ETV6-RUNX1, BCR-ABL, and TCF3-PBX1) (16), and karyotyping. We analyzed interphase cells according to the instructions of the probe manufacturer (America Abbott). The *CDKN2A/B* probe spanned approximately 222 kilobases (kb) and contained many genes, including methylthioadenosine phosphorylase, *CDKN2A* (*INK4A* and *ARF*), and *CDKN2B* (*INK4B*) in the 9p21 chromosome region. The cutoff level for positive results was calculated to be 5%, and at least five hundred cells were analyzed (5, 17). Some cases with two different deleted populations (one biallelic and one monoallelic) were classified as having a biallelic deletion.

Early Treatment Response Definitions and Endpoints

To identify early prognostic factors, we evaluated leukemic blast counts in bone marrow by morphology on day 46 and minimal residual disease (MRD) on days 19 and 46 during the first induction. A total of $1–2\times10^6$ leukocytes from bone marrow were incubated with marker panel [B-lineage cells (CD10, CD19, TdT, cyμ, sIgM, CD20, cyCD22, CD22, and cyCD79a), T-lineage cells (CD1a, CD2, CD3, CD4, CD5, CD7, CD8, TCRαβ, TCRγδ, and cyCD3), or myeloid cells (CD11b, CD13, CD14, CD15, CD33, CD41, CD61, CD64, CD65, CD71, GPA, and cyMPO)] for 30 min, washed twice, and then resuspended in 100 μl of PBS. The cells were acquired on a Navios (Beckman Coulter, UK) and analyzed using Kaluza software. Samples were defined as MRD-negative if no baseline and/or different-from-normal leukemia-associated immunophenotypes (LAIP) cells could be quantitated above the limit of detection (approximately 0.01%) (18).

Diagnosis of complete remission (CR) was based solely on bone marrow morphology with a cutoff value of 5% of leukemic blasts on treatment day 46. Bone marrow MRD that is not lower than 10^{-5} was defined as positive. A poor response to prednisone was considered if the peripheral blast count on treatment day 5 was not lower than 1×10^9/L.

The primary endpoint event-free survival was calculated from the date of diagnosis until the following events: induction treatment failure, any relapse after CR, second malignancy, and death due to any cause. Overall survival was considered as the time from diagnosis to death due to any cause.

Statistical Analysis

Chi-squared test and Mann–Whitney *U* tests were used to compare categorical and continuous variables, respectively. Event-free and

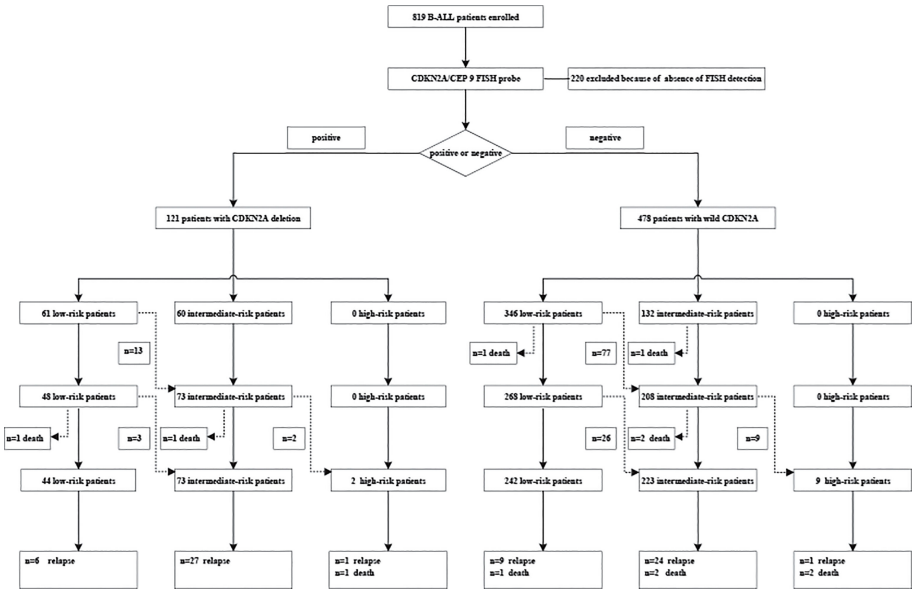

FIGURE 1 | Clinical profile.

overall survival were calculated and compared using Kaplan–Meier analysis and log-rank tests. Cox proportional hazard regression analyses were performed using univariable and multivariable regression approaches. Variables that were found statistically significant and a *p*-value of approximately 0.1 were included in multivariable Cox regression analysis. We performed subgroup analyses for prespecified baseline factors with rates of inferior events by factor interaction with the use of Cox models. Statistical significance was defined as a *p*-value of less than 0.05. All analyses were performed using SPSS v. 24. and SAS v. 9.4 software.

RESULTS

Comparison of Demographic and Clinical Characteristics of Childhood ALL With and Without *CDKN2A/B* Deletions

In total, 599 patients were included in the analysis. The final follow-up was in December 2020 and the median follow-up time was 34 months (range: 0 to 58 months). The median age was 5 years (range, 0 to 14), and the male/female ratio was 1.4 (350/249). The prevalence of *CDKN2A/B* gene deletions in B-ALL was 20.2% (121/599). Among patients with *CDKN2A/B* deletions, 57 (45.3%) harbored *CDKN2A/B* biallelic deletions, whereas 82 (54.7%) harbored monoallelic deletions, and 11 (7.3%) patients harbored both biallelic and monoallelic deletions.

Compared to patients with wild-type *CDKN2A/B* (**Table 1**), patients with *CDKN2A/B* deletions were significantly associated with older age (age >10 years; 30.6% vs. 15.2%, $p < 0.001$), a higher leukocyte count (median: 24.7 vs. 8.9×10^9/L, $p < 0.001$), a lower platelet count (median: 51 vs. 64 g/L, $p = 0.049$), and a higher percentage of hepatosplenomegaly (64.5% vs. 43.9%, $p < 0.001$). A higher rate of central nervous system status 2(CNS 2)/traumatic lumbar puncture was found among patients with *CDKN2A/B* deletion, but no statistical significance was found in the two groups. Patients with *CDKN2A/B* deletions belonged more to the intermediate-risk groups (58.7% vs. 32.6%, $p < 0.01$) than patients without *CDKN2A/B* deletions based on CCCG-ALL 2015 risk stratification. There was no significant difference between patients with biallelic deletions and monoallelic deletions. The comparison of characteristics for the two groups is shown in **Table S1**.

Correlation of *CDKN2A/B* Deletion With Other Cytogenetic Alterations

Karyotype analysis, 43 fusion genes, and FISH studies of pretreatment bone marrow were available for 599 patients. **Table 1** summarizes the correlations of *CDKN2A/B* deletions with other cytogenetic abnormalities. The *CDKN2A/B* deletion group had a higher prevalence of the *BCR/ABL* fusion gene (12.4% vs. 4.4%, $p = 0.001$). A higher co-occurrence of the *ETV6/RUNX1* fusion gene (19.8% vs. 26.8%) was found in patients with CDKN2A/B deletion; however, no statistical significance was identified. A higher incidence of chromosome < 44 (2.5% vs. 0.6%) and *TP53* deletions (8.3% vs. 4.0%) was detected by FISH, but this did not reach statistical significance ($p \geq 0.05$). The genetic feature of patients with *CDKN2A/B* gene deletions was also related to the risk stratification distribution at the first diagnosis.

The Effect of *CDKN2A/B* Gene Deletions on Early Treatment Responses

A chi-squared test showed a high rate of poor responses to prednisone (PPR) (28.1% vs. 20.9%, $p = 0.091$) in the CDKN2A/B

TABLE 1 | Characteristics of B-ALL patients with CDKN2A/B deletion and CDKN2A/B wild type.

	Total	CDKN2A/B deletion (%)	CDKN2A/B wild type (%)	*p*-value
Number	599	121 (20.2)	478 (79.8)	
Gender, male/female	350/249	63/58	287/191	0.148
Age, ≥10 years	109 (18.2)	37 (30.6)	72 (15.2)	<0.001
Leukocyte counts, $\times10^9$/L(range)	10.8 (0.7–846.5)	24.7 (0.7–846.5)	8.9 (0.74–551.2)	<0.001
Platelets, $\times10^9$/L(range)	61 (1–919)	51 (3–503)	64 (1–919)	0.049
Hepatosplenomegaly	288 (48.1)	78 (64.5)	210 (43.9)	<0.001
CNS2/traumatic lumbar puncture	66 (11.0)	17 (14.1)	49 (10.3)	0.233
Risk stratification, IR	192 (32.1)	60 (49.6)	162 (33.9)	0.001
Cytogenetic abnormalities				
Chromosome number ≥50	47 (7.8)	6 (5.0)	41 (8.6)	0.186
Chromosome number <44	6 (1.0)	3 (2.5)	3 (0.6)	0.100
ETV6-RUNX1	152 (25.4)	24 (19.8)	128 (26.8)	0.117
t(9;22)(q34;q11.2)/BCR-ABL1	36 (6.0)	15 (12.4)	21 (4.4)	0.001
t(1;19)(q23;p13.3)/TCF3-PBX1	32 (5.3)	6 (5.0)	26 (5.4)	0.834
TP53 deletion	29 (4.8)	10 (8.3)	19 (4.0)	0.050
11q23/KMT2A	11 (1.8)	1 (0.8)	10 (2.1)	0.354
PPR	134 (22.4)	34 (28.1)	100 (20.9)	0.091
MRD positive on day 19	403 (67.7)	74 (61.2)	329 (69.4)	0.083
MRD positive on day 46	108 (18.3)	22 (18.5)	86 (18.2)	0.946
CR	593 (99.0)	119 (98.4)	474 (99.2)	0.350

deletion group. No significant difference was observed between the two groups for MRD on day 19 (61.2% vs. 69.4%, $p = 0.946$) and 46 (18.5% vs. 18.2%, $p = 0.946$). The CR rate (98.4% vs. 99.2%, $p = 0.719$) for each group was equivalent.

Overall Outcomes

A high CR rate was achieved in 593 of 599 patients (99.0%) (**Figure 1**). Based on their MRD levels on days 19 and 46 during remission induction treatment, 286 (48.2%) of 593 patients were classified as having low-risk ALL, 296 (49.9%) as having intermediate-risk ALL, and 11 (1.9%) as having high-risk ALL. All six patients who did not achieve the first CR died of severe pneumonia. After remission induction, 74 patients had adverse events, including 68 relapses ($n = 54$ hematologic relapses, $n = 4$ combined hematologic and CNS relapses, $n = 2$ combined hematologic and testicular relapses, $n = 1$ combined hematologic, CNS, and testicular relapses, $n = 4$ isolated CNS relapse, $n = 2$ testicular relapse, and $n = 1$ ocular relapse). Six patients died [$n = 2$ died of severe pneumonia and emesis in remission and $n = 4$ died after chimeric antigen receptor T-cell immunotherapy (CAR-T) therapy or hematopoietic stem cell transplantation (HSCT) because of elevated MRD level]. The 3-year OS and EFS were 93.6 ± 1.1% and 85.2 ± 1.6%, respectively, for the whole series.

The Effect of *CDKN2A/B* Deletions on the Prognosis of Pediatric ALL

The *CDKN2A/B* deletion group is related to a higher relapse rate (28.1% for the deletions group vs. 7.1% for the wild-type group, $p = 0.000$) (**Table 2**). Patients with *CDKN2A/B* deletions seemed to have a higher CNS relapse rate than patients with *CDKN2A/B* deletions, although the *p*-value was not significant (3.3% vs. 1.1%, $p = 0.087$). Patients with *CDKN2A/B* deletions had lower 3-year EFS and OS rates than patients without *CDKN2A/B* deletions (3-year EFS: 69.8 ± 4.6 vs. 89.2 ± 1.6%, $p = 0.000$; and 3-year OS: 89.4% ± 2.9% vs. 94.7% ± 1.1%, $p = 0.037$) (**Figures 2A, B**). Furthermore, *CDKN2A/B* deletion serves as an independent prognosis factor (HR = 3.4 [95% CI 2.0–5.6]; $p = 0.000$) for EFS in whole cohorts (**Figure 3**). MRD on day 46 was a strong predictor (HR = 3.3 [95% CI 2.0–5.3]; $p = 0.000$) for all cases.

Outcomes Stratified by Risk Groups and *CDKN2A/B* Deletions

On the basis of the CCCG-ALL 2015 risk stratification, more patients were classified as intermediate risk in the *CDKN2A/B* deletion group at diagnosis. For patients assigned into the low-risk group, patients with *CDKN2A/B* deletions had adverse clinical outcomes (3-year EFS: 81.4 ± 5.4% vs. 91.9 ± 1.7%, $p = 0.000$; 3-year OS: 93.2 ± 3.3% vs. 97.9 ± 0.9%, $p = 0.027$)

TABLE 2 | Different types of relapse in all patients.

	Total($n = 599$)	CDKN2A/B deletion ($n = 121$)	CDKN2A/B wild type ($n = 478$)	*p*-value	χ^2 value
Relapse	68 ()	34 (28.1)	34 (7.1)	0.000	42.258
Hematological relapse	61 ()	30 (24.8)	31 (6.5)	0.000	35.384
Any CNS relapse	9 ()	4 (3.3)	5 (1.1)	0.087	–
Isolated CNS relapse	4 ()	3 (2.5)	1 (0.2)	0.028	–
Any testicular relapse	5 ()	2 (1.7)	3 (0.6)	0.266	–

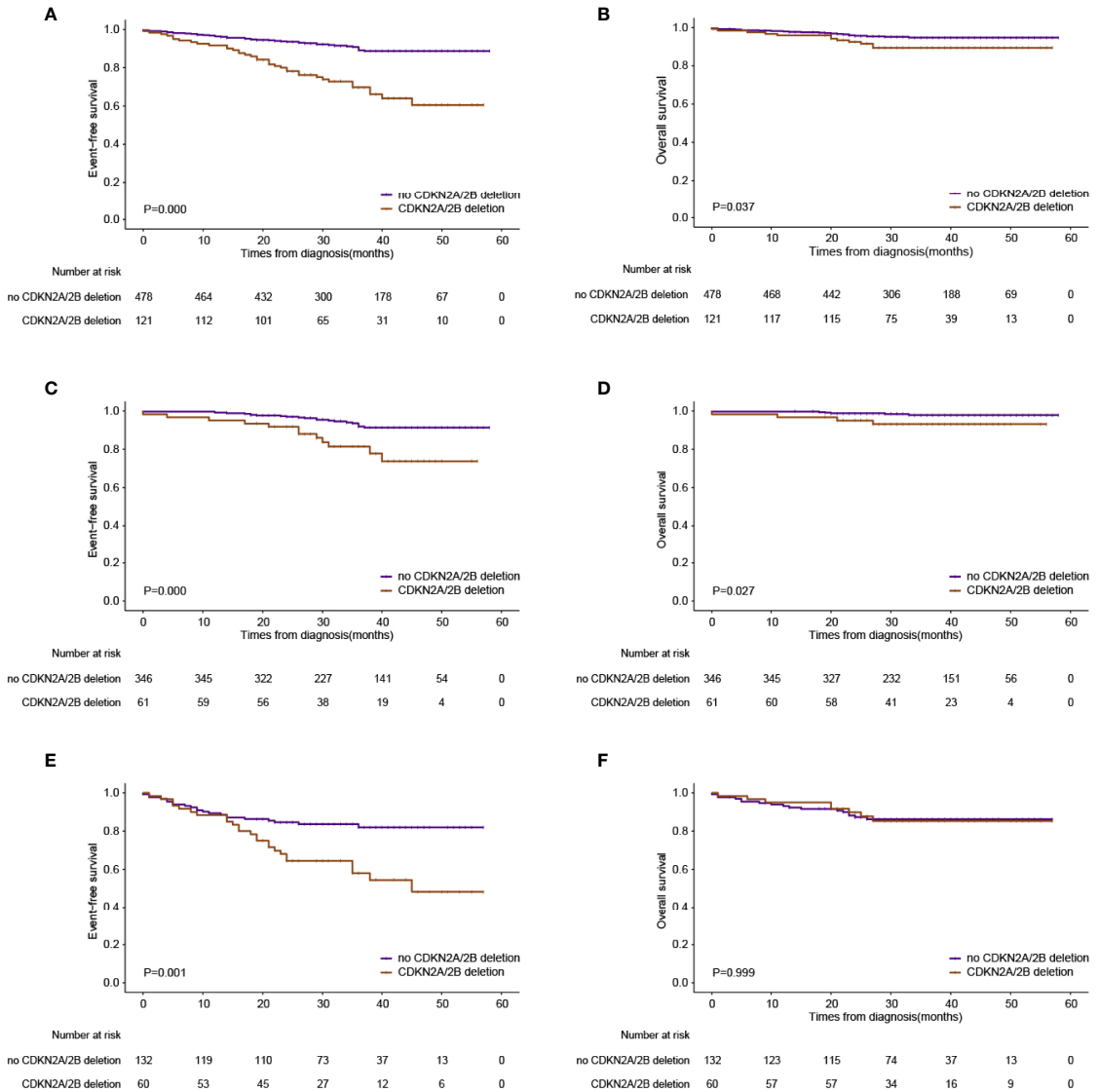

FIGURE 2 | Outcomes based on the presence or absence of CDKN2A deletions. **(A)** Event-free survival in the whole series. **(B)** Overall survival in the whole series. **(C)** Event-free survival in the low-risk group. **(D)** Overall survival in the low-risk group. **(E)** Event-free survival in the intermediate-risk group. **(F)** Overall survival in the intermediate-risk group.

compared to patients without *CDKN2A/B* deletions (**Figures 2C, D**). Intermediate-risk patients with *CDKN2A/B* deletions had inferior 3-year EFS (58.0 ± 7.1% vs. 82.0 ± 3.6%, $p = 0.001$), but no inferior 3-year OS (85.3 ± 4.9% vs. 86.3 ± 3.1%, $p = 0.999$) compared to intermediate-risk patients without *CDKN2A/B* deletions (**Figures 2E, F**).

The Joint Effect of *CDKN2A/B* Deletions and Other Baseline Factors

We performed stratified analyses by subgroups defined by major co-variables that might have been related to EFS and further quantified the effect modification of major co-variables on the influence of *CDKN2A/B* deletions in EFS, accounting for important covariates (**Table 3**). The hazard rates of *CDKN2A/B* deletions in EFS were consistent in most subgroups. The hazard rate of *CDKN2A/B* deletions for the adverse events was quite different for patients with and without *TP53* deletions (HR = 24.080 [95% CI 2.978–194.738]; $p = 0.0029$ and HR = 2.993 [95% CI 1.868–4.796]; $p < 0.0001$, respectively), while there were no significant interactions between two groups (p-interaction = 0.0631).

DISCUSSION

In this study, we present a large retrospective study of pediatric ALL patients with *CDKN2A/B* deletions treated in a single center

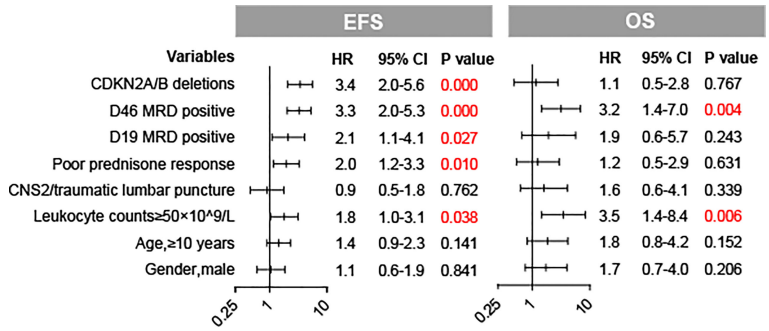

FIGURE 3 | Forest plots of the multivariate analysis of CDKN2A/B deletions and baseline factors for EFS and OS in our cohort.

and demonstrated the adverse effect of *CDKN2A/B* deletions on clinical outcomes.

The prevalence of *CDKN2A/B* deletions in our study was 20.2%, which was higher than Agarwal's research (19.8%) but lower than Sulong's research (22.0%) (2, 5). Previous investigators have reported the characteristics and clinical impact of *CDKN2A/B* deletions in pediatric ALL, and the prognostic importance of *CDKN2A/B* deletions in pediatric ALL is still controversial (2, 4, 5, 10, 19). We conducted a comprehensive analysis of *CDKN2A/B* deletions in 599 pediatric B-ALL patients. Data from our cohort showed that *CDKN2A/B* deletions were associated with older age at diagnosis, higher white blood cell counts, and prominent hepatosplenomegaly, which were consistent with the previous studies (5).

Many researchers concluded that *CDKN2A/B* deletions in childhood ALL were associated with an increased probability of relapse and death (2, 9, 10, 19–21), whereas Kima et al. and Mirebeau et al. concluded that homozygous *CDKN2A/B* deletion was not a poor prognostic factor in childhood B-ALL (4, 11). In our study, *CDKN2A/B* deletion carriers had decreased endpoints for 3-year EFS and OS compared to *CDKN2A/B* wild-type patients. Furthermore, our data showed that patients with the biallelic deletions had a worse survival rate (3-year EFS: 71.3 ± 6.0% vs. 67.7 ± 7.0% vs. 89.2 ± 1.6%, $p = 0.000$; 3-year OS:

TABLE 3 | Hazard ratio for event-free survival in prespecified subgroup.

	Total	CDKN2A/B deletion	CDKN2A/B wild type	HR (95% CI)	*p*-value	*p*-value for interaction
Number	81	37 (30.6)	44 (9.2)	4.148 (2.628–6.547)	<0.0001	
Gender						0.9523
Male	52	22 (34.9)	30 (10.5)	3.729 (2.149–6.472)	<0.0001	
Female	29	15 (25.8)	14 (7.3)	3.817 (1.842–7.910)	0.0003	
Age (years)						0.8944
<10	58	23 (27.4)	35 (7.9)	3.480 (2.056–5.891)	<0.0001	
≥10	23	14 (37.8)	9 (12.5)	3.260 (1.409–7.541)	0.0057	
Leukocyte counts						0.7870
$<50\times10^9$/L	47	16 (20.5)	31 (7.6)	3.003 (1.641–5.495)	0.0004	
$\geq50\times10^9$/L	34	21 (48.8)	13 (26.4)	2.599 (1.301–5.192)	0.0068	
CNS status at diagnosis						0.2641
CNS1	66	27 (26.2)	39 (9.1)	3.121 (1.910–5.101)	<0.0001	
CNS2/traumatic lumbar puncture	14	9 (52.9)	5 (10.2)	6.312 (2.111–18.874)	0.0010	
Risk stratification						0.7156
LR	34	12 (19.6)	22 (7.0)	3.265 (1.615–6.601)	0.0010	
IR	47	25 (41.7)	22 (13.6)	2.639 (1.487–4.683)	0.0009	
ETV6-RUNX1						0.9772
Negative	75	36 (37.1)	39 (11.1)	3.822 (2.427–6.019)	<0.0001	
Positive	6	1 (4.2)	5 (4.0)	0.903 (0.105–7.732)	0.9257	
BCR-ABL						
Negative	73	31 (29.2)	42 (9.2)	3.467 (2.179–5.515)	<0.0001	0.7067
Positive	8	6 (40.0)	2 (9.5)	4.555 (0.913–22.728)	0.0645	
TP53 deletion						0.0445
Negative	72	29 (26.1)	43 (9.4)	2.993 (1.868–4.796)	<0.0001	
Positive	9	8 (80.0)	1 (5.3)	24.080 (2.978–194.738)	0.0029	
Response to prednisone						0.9476
PGR	45	19 (21.8)	26 (6.9)	3.413 (1.888–6.171)	<0.0001	
PPR	36	18 (52.9)	18 (18.0)	3.317 (1.725–6.379)	0.0003	

922.2 ± 3.4% vs. 85.2 ± 5.2% vs. 94.7 ± 1.1%, $p = 0.025$) than patients without biallelic deletions (**Figure S1**).

The long-term outcome of pediatric ALL in China is optimal, especially for low-risk patients, and the OS rate remains 97.8% (12). Notably, in our cohorts, low-risk patients with *CDKN2A/B* deletions had inferior outcomes (3-year OS: 93.2 ± 3.3% vs. 97.9 ± 0.9%) compared to low-risk patients without *CDKN2A/B* deletions (**Figures 2C, D**). The result indicated that *CDKN2A/B* deletion patients even stratified in the low-risk group urgently needed intensive chemotherapy. Furthermore, allo-HSCT ($n = 14$) has improved overall survival than chemotherapy alone did ($n = 20$) in relapse patients with *CDKN2A/B* deletions, though no significance was observed between the two groups (3-year OS: 85.7 ± 9.4% vs. 60.5 ± 11.9%, $p = 0.192$) (**Figure S2**).

Sulong et al. reported that pediatric ALL with *CDKN2A/B* deletions had recurrent cytogenetic abnormalities including high frequencies of *TCF/PBX1*, *BCR/ABL*, hyperdiploidy, and *KMT2A*, and low frequencies of *ETV6/RUNX1* compared to patients without *CDKN2A/B* deletions (5, 11). We conclude a similar result in which *CDKN2A/B* deletion carriers had a higher prevalence of *BCR/ABL* and a low prevalence of *ETV6/RUNX1*. However, we did not find ph+ patients had inferior outcomes than ph- patients in *CDKN2A/B* deletion groups; this is most likely due to the utilization of tyrosine kinase inhibitors (TKIs) in ph+ patients for the entire duration of ALL therapy (22, 23). Pfeifer et al. demonstrated that *CDKN2A/B* deletions were adverse despite allogeneic stem cell transplantation in adult Philadelphia chromosome-positive (Ph+) ALL (24, 25); further studies in a larger cohort of pediatric Ph+ ALL with *CDKN2A/B* deletions are needed.

In our cohort, patients with *CDKN2A/B* deletions were more frequently steroid-resistant, whereas they had a better MRD clearance on day 19 of induction therapy compared with patients without *CDKN2A/B* deletions. These results differed from a study by Braun who found higher MRD levels on day 15 of induction therapy in patients with *CDKN2A/B* deletions (26). The differences in MRD clearance may be related to the patients' race, chemotherapy protocols, and examination methods. An earlier study demonstrated that *CDKN2A/B* deletions were associated with unfavorable outcomes independent of MRD level in adult patients (27). However, both MRD positive on day 46 of induction therapy and *CDKN2A/B* deletion were still independent poor indicators for childhood ALL patients in our study.

Our study also indicated that patients with *CDKN2A/B* deletion had the worst prognosis in the *TP53* deletion subgroup. A similar outcome was found by Delfau-Larue for mantle cell lymphoma; i.e., patients with both *CDKN2A/B* and *TP53* deletions had the worst prognosis (28). The *CDKN2A/B* gene controls the cell cycle through the P53-MDM pathway; thus, co-occurrence of *CDKN2A/B* deletions and *TP53* deletions might enhance the aggressiveness of disease by strongly increasing the self-renewal capacity of leukemia cells (29–31). The hypothesis needs to be proved in future research.

Several limitations exist in this study. First, because of the limited sample size and short follow-up duration in relapse patients with *CDKN2A/B* deletions, the role of allogeneic transplant in the treatment needs to be interpreted carefully. Second, for the same reason, we did not conclude whether there had been significant interactions between two *TP53* deletions and *CDKN2A/B* deletions in pediatric ALL. CDKN2A gene can control cell cycle through the P53-MDM pathway; it might be attributed to the fact that CDKN2A deletion cooperates with the *TP53* deletion to enhance the aggressiveness of the disease by strongly increasing the self-renewal capacity of leukemia cells, but there is no theory to support this hypothesis.

In conclusion, a significant proportion of pediatric ALL patients still experience relapse, particularly patients with both *CDKN2A/B* and *TP53* deletions despite the high survival rate of childhood ALL. MDM2-P53 targeted agents are still in experimental research. In addition, CDK4/6 inhibitors (e.g., palbociclib) combined with chemotherapy are in clinical trials for the management of pediatric patients with relapsed/refractory ALL (32, 33). In the future, a new therapeutic strategy (e.g., target drug) based on genetic events might be applied in some subtypes of pediatric ALL.

DATA AVAILABILITY STATEMENT

The original contributions presented in the study are included in the article/**Supplementary Material**. Further inquiries can be directed to the corresponding author.

ETHICS STATEMENT

The protocols described in this study were approved by the Ethics Committee, Institute of Hematology and Blood Disease Hospital, CAMS & PUMC. Written informed consent to participate in this study was provided by the participants' legal guardian/next of kin.

AUTHOR CONTRIBUTIONS

All authors listed have made a substantial, direct, and intellectual contribution to the work and approved it for publication.

FUNDING

The work is supported by the National Nature Science Foundation of China grants 81770175 (YCZ), 81870131 (XZ), and 81670112 (XZ).

ACKNOWLEDGMENTS

We would like to thank the patients for participating in this study.

SUPPLEMENTARY MATERIAL

The Supplementary Material for this article can be found online at: https://www.frontiersin.org/articles/10.3389/fonc.2022.878098/full#supplementary-material

REFERENCES

1. Inaba H, Mullighan CG. Pediatric Acute Lymphoblastic Leukemia. *Haematol* (2020) 105(11):2524–39. doi: 10.3324/haematol.2020.247031
2. Agarwal M, Bakhshi S, Dwivedi SN, Kabra M, Shukla R, Seth R. Cyclin Dependent Kinase Inhibitor 2A/B Gene Deletions are Markers of Poor Prognosis in Indian Children With Acute Lymphoblastic Leukemia. *Pediatr Blood Cancer* (2018) 65(6):e27001. doi: 10.1002/pbc.27001
3. Boldrin E, Gaffo E, Niedermayer A, Boer JM, Zimmermann M, Weichenhan D, et al. MicroRNA-497/195 is Tumor-Suppressive and Cooperates With CDKN2A/B in Pediatric Acute Lymphoblastic Leukemia. *Blood* (2021) 138:1953–65. doi: 10.1182/blood.2020007591
4. Kim M, Yim S-H, Cho N-S, Kang S-H, Ko D-H, Oh B, et al. Homozygous Deletion of CDKN2A (P16, P14) and CDKN2B (P15) Genes is a Poor Prognostic Factor in Adult But Not in Childhood B-Lineage Acute Lymphoblastic Leukemia: A Comparative Deletion and Hypermethylation Study. *Cancer Genet Cytogenetics* (2009) 195:59–65. doi: 10.1016/j.cancergencyto.2009.06.013
5. Sulong S, Moorman AV, Irving JAE, Strefford JC, Konn ZJ, Case MC, et al. A Comprehensive Analysis of the CDKN2A Gene in Childhood Acute Lymphoblastic Leukemia Reveals Genomic Deletion, Copy Number Neutral Loss of Heterozygosity, and Association With Specific Cytogenetic Subgroups. *Blood* (2009) 113:100–7. doi: 10.1182/blood-2008-07-166801
6. Usvasalo A, Savola S, Räty R, Vettenranta K, Harila-Saari A, Koistinen P, et al. CDKN2A Deletions in Acute Lymphoblastic Leukemia of Adolescents and Young Adults—An Array CGH Study. *Leukemia Res* (2008) 32:1228–35. doi: 10.1016/j.leukres.2008.01.014
7. Bertin R, Acquaviva C, Mirebeau D, Guidal-Giroux C, Vilmer E, Cavé H. CDKN2A, CDKN2B, and MTAP Gene Dosage Permits Precise Characterization of Mono- and Bi-Allelic 9p21 Deletions in Childhood Acute Lymphoblastic Leukemia: *CDKN2A* , *CDKN2B* , and *MTAP* Dosage in Leukemia. *Genes Chromosom Cancer* (2003) 37(1):44–57. doi: 10.1002/gcc.10188
8. Karrman K, Castor A, Behrendtz M, Forestier E, Olsson L, Ehinger M, et al. Deep Sequencing and SNP Array Analyses of Pediatric T-Cell Acute Lymphoblastic Leukemia Reveal NOTCH1 Mutations in Minor Subclones and a High Incidence of Uniparental Isodisomies Affecting CDKN2A. *J Hematol Oncol* (2015) 8:42. doi: 10.1186/s13045-015-0138-0
9. Graf Einsiedel H, Taube T, Hartmann R, Wellmann S, Seifert G, Henze G, et al. Deletion Analysis of P16inka and P15inkb in Relapsed Childhood Acute Lymphoblastic Leukemia. *Blood* (2002) 99:4629–31. doi: 10.1182/blood.V99.12.4629
10. Kees UR, Burton PR, Lu C, Baker DL. Homozygous Deletion of the P16/MTS1 Gene in Pediatric Acute Lymphoblastic Leukemia Is Associated With Unfavorable Clinical Outcome. (1997) 89(11):4161–6. doi: 10.1182/blood.V89.11.4161
11. Mirebeau D, Acquaviva C, Suciu S, Bertin R, Dastugue N, Robert A, et al. The Prognostic Significance of CDKN2A, CDKN2B and MTAP Inactivation in B-Lineage Acute Lymphoblastic Leukemia of Childhood. Results of the EORTC Studies 58881 and 5895. *haematologica* (2006) 91:881–5.
12. Yang W, Cai J, Shen S, Gao J, Yu J, Hu S, et al. Pulse Therapy With Vincristine and Dexamethasone for Childhood Acute Lymphoblastic Leukaemia (CCCG-ALL-2015): An Open-Label, Multicentre, Randomised, Phase 3, Non-Inferiority Trial. *Lancet Oncol* (2021) 22:1322–32. doi: 10.1016/S1470-2045(21)00328-4
13. Pui C-H, Campana D, Pei D, Bowman WP, Sandlund JT, Kaste SC, et al. Treating Childhood Acute Lymphoblastic Leukemia Without Cranial Irradiation. *N Engl J Med* (2009) 360:2730–41. doi: 10.1056/NEJMoa0900386
14. Jeha S, Pei D, Choi J, Cheng C, Sandlund JT, Coustan-Smith E, et al. Improved CNS Control of Childhood Acute Lymphoblastic Leukemia Without Cranial Irradiation: St Jude Total Therapy Study 16. *JCO* (2019) 37:3377–91. doi: 10.1200/JCO.19.01692
15. Liu Y, Chen J, Tang J, Ni S, Xue H, Pan C. Cost of Childhood Acute Lymphoblastic Leukemia Care in Shanghai, China. *Pediatr Blood Cancer* (2009) 53:557–62. doi: 10.1002/pbc.22127
16. Viehmann S, Borkhardt A, Lampert F, Harbott J. Multiplex PCR - a Rapid Screening Method for Detection of Gene Rearrangements in Childhood Acute Lymphoblastic Leukemia. *Ann Hematol* (1999) 78:157–62. doi: 10.1007/s002770050494
17. Wang H, Zhou Y, Huang X, Zhang Y, Qian J, Li J, et al. CDKN2A Deletions are Associated With Poor Outcomes in 101 Adults With T-Cell Acute Lymphoblastic Leukemia. *Am J Hematol* (2021) 96:312–9. doi: 10.1002/ajh.26069
18. Wood BL. Principles of Minimal Residual Disease Detection for Hematopoietic Neoplasms by Flow Cytometry: Principles of MRD. *Cytometry* (2016) 90:47–53. doi: 10.1002/cyto.b.21239
19. Kathiravan M, Singh M, Bhatia P, Trehan A, Varma N, Sachdeva MS, et al. Deletion of CDKN2A/B is Associated With Inferior Relapse Free Survival in Pediatric B Cell Acute Lymphoblastic Leukemia. *Leukemia Lymphoma* (2019) 60:433–41. doi: 10.1080/10428194.2018.1482542
20. Carter TL. Hemizygous P16ink4a Deletion in Pediatric Acute Lymphoblastic Leukemia Predicts Independent Risk of Relapse. *Blood* (2001) 97:572–4. doi: 10.1182/blood.V97.2.572
21. Dalle JH, Fournier M, Nelken B, Mazingue F, Laüi J-L, Bauters F, et al. P16ink4a Immunocytochemical Analysis is an Independent Prognostic Factor in Childhood Acute Lymphoblastic Leukemia. *Blood* (2002) 99:2620–3. doi: 10.1182/blood.V99.7.2620
22. Schultz KR, Carroll A, Heerema NA, Bowman WP, Aledo A, Slayton WB, et al. Long-Term Follow-Up of Imatinib in Pediatric Philadelphia Chromosome-Positive Acute Lymphoblastic Leukemia: Children's Oncology Group Study Aall0031. *Leukemia* (2014) 28(7):1467–71. doi: 10.1038/leu.2014.30
23. Shen S, Chen X, Cai J, Yu J, Gao J, Hu S, et al. Effect of Dasatinib vs Imatinib in the Treatment of Pediatric Philadelphia Chromosome–Positive Acute Lymphoblastic Leukemia: A Randomized Clinical Trial. *JAMA Oncol* (2020) 6:358. doi: 10.1001/jamaoncol.2019.5868
24. Pfeifer H, Raum K, Markovic S, Nowak V, Fey S, Obländer J, et al. Genomic CDKN2A/2B Deletions in Adult Ph+ ALL are Adverse Despite Allogeneic Stem Cell Transplantation. *Blood* (2018) 131:1464–75. doi: 10.1182/blood-2017-07-796862
25. Iacobucci I, Ferrari A, Lonetti A, Papayannidis C, Paoloni F, Trino S, et al. *CDKN2A/B* Alterations Impair Prognosis in Adult *BCR-ABL1*-Positive Acute Lymphoblastic Leukemia Patients. *Clin Cancer Res* (2011) 17(23):7413–23. doi: 10.1158/1078-0432.CCR-11-1227
26. Braun M, Pastorczak A, Fendler W, Madzio J, Tomasik B, Taha J, et al. Biallelic Loss of CDKN2A is Associated With Poor Response to Treatment in Pediatric Acute Lymphoblastic Leukemia. *Leukemia Lymphoma* (2017) 58:1162–71. doi: 10.1080/10428194.2016.1228925
27. Ribera J, Zamora L, Morgades M, Vives S, Granada I, Montesinos P, et al. Molecular Profiling Refines Minimal Residual Disease-Based Prognostic Assessment in Adults With Philadelphia Chromosome-Negative B-Cell Precursor Acute Lymphoblastic Leukemia. *Genes Chromosomes Cancer* (2019) 58:815–9. doi: 10.1002/gcc.22788
28. Delfau-Larue M-H, Klapper W, Berger F, Jardin F, Briere J, Salles G, et al. High-Dose Cytarabine Does Not Overcome the Adverse Prognostic Value of CDKN2A and TP53 Deletions in Mantle Cell Lymphoma. *Blood* (2015) 126:604–11. doi: 10.1182/blood-2015-02-628792
29. Zhao R, Choi BY, Lee MH, Bode AM, Dong Z. Implications of Genetic and Epigenetic Alterations of CDKN2A (P16ink4a) in Cancer. *EBioMedicine* (2016) 8:30–9. doi: 10.1016/j.ebiom.2016.04.017
30. Otsuki T, Clark HM, Wellmann A, Jaffe ES, Raffeld M. Involvement of CDKN2 (P16ink4a/MTS1) and P15ink4b/MTS2 in Human Leukemias and Lymphomas. *Cancer Res* (1995) 55(7):1436.
31. Johnson M, Dimitrov D, Vojta PJ, Barrett JC, Noda A, Pereira-Smith OM, et al. Evidence for a P53-Independent Pathway for Upregulation Ofsdi1/CIP1/WAF1/P21 RNA in Human Cells. *Mol Carcinog* (1994) 11:59–64. doi: 10.1002/mc.2940110202
32. Bride KL, Hu H, Tikhonova A, Fuller TJ, Vincent TL, Shraim R, et al. Rational Drug Combinations With CDK4/6 Inhibitors in Acute Lymphoblastic Leukemia. *haematol* (2021). doi: 10.3324/haematol.2021.279410
33. Van der Linden M, Willekes M, van Roon E, Seslija L, Schneider P, Pieters R, et al. MLL Fusion-Driven Activation of *CDK6* Potentiates Proliferation in *MLL*-Rearranged Infant ALL. *Cell Cycle* (2014) 13:834–44. doi: 10.4161/cc.27757

Conflict of Interest: The authors declare that the research was conducted in the absence of any commercial or financial relationships that could be construed as a potential conflict of interest.

this article, or claim that may be made by its manufacturer, is not guaranteed or endorsed by the publisher.

frontiers | Frontiers in Oncology

ORIGINAL RESEARCH
published: 08 June 2022
doi: 10.3389/fonc.2022.848395

Up-Regulation of TRIM32 Associated With the Poor Prognosis of Acute Myeloid Leukemia by Integrated Bioinformatics Analysis With External Validation

Xiaoyan Xu[1,2,3,4†], *Jiaqian Qi*[1,2,3,4†], *Jingyi Yang*[1,2,3,4†], *Tingting Pan*[1,2,3,4], *Haohao Han*[1,2,3,4], *Meng Yang*[1,2,3,4] *and Yue Han*[1,2,3,4*]

[1] National clinical research center for hematologic diseases, Jiangsu Institute of Hematology, The First Affiliated Hospital of Soochow University, Suzhou, China, [2] Institute of Blood and Marrow Transplantation, Collaborative Innovation Center of Hematology, Soochow University, Suzhou, China, [3] Department of Hematology, Key Laboratory of Thrombosis and Hemostasis of Ministry of Health, Suzhou, China, [4] State Key Laboratory of Radiation Medicine and Protection, Soochow University, Suzhou, China

Background: Acute myeloid leukemia (AML) is a malignant and molecularly heterogeneous disease. It is essential to clarify the molecular mechanisms of AML and develop targeted treatment strategies to improve patient prognosis.

Methods: AML mRNA expression data and survival status were extracted from TCGA and GEO databases (GSE37642, GSE76009, GSE16432, GSE12417, GSE71014). Weighted gene co-expression network analysis (WGCNA) and differential gene expression analysis were performed. Functional enrichment analysis and protein-protein interaction (PPI) network were used to screen out hub genes. In addition, we validated the expression levels of hub genes as well as the prognostic value and externally validated TRIM32 with clinical data from our center. AML cell lines transfected with TRIM32 shRNA were also established to detect the proliferation *in vitro*.

Results: A total of 2192 AML patients from TCGA and GEO datasets were included in this study and 20 differentially co-expressed genes were screened by WGCNA and differential gene expression analysis methods. These genes were mainly enriched in phospholipid metabolic processes (biological processes, BP), secretory granule membranes (cellular components, CC), and protein serine/threonine kinase activity (molecular functions, MF). In addition, the protein-protein interaction (PPI) network contains 15 nodes and 15 edges and 10 hub genes (TLE1, GLI2, HDAC9, MICALL2, DOCK1, PDPN, RAB27B, SIX3, TRIM32 and TBX1) were identified. The expression of 10 central genes, except TLE1, was associated with survival status in AML patients ($p<0.05$). High expression of TRIM32 was tightly associated with poor relapse-free survival (RFS) and overall survival (OS) in AML patients, which was verified in the bone marrow samples from our center. *In vitro*, knockdown of TRIM32 can inhibit the proliferation of AML cell lines.

OPEN ACCESS

Edited by:
Garrett Dancik, Eastern Connecticut State University, United States

Reviewed by:
Yu-Hung Wang, National Taiwan University Hospital, Taiwan
Daniela Marasco, University of Naples Federico II, Italy
Dinghua Cai, Jiangsu University, China

***Correspondence:**
Yue Han
hanyue@suda.edu.cn

[†]*These authors have contributed equally to this work and share first authorship*

Specialty section:
This article was submitted to Hematologic Malignancies, a section of the journal Frontiers in Oncology

Received: *04 January 2022*
Accepted: *23 May 2022*
Published: *08 June 2022*

Citation:
Xu X, Qi J, Yang J, Pan T, Han H, Yang M and Han Y (2022) Up-Regulation of TRIM32 Associated With the Poor Prognosis of Acute Myeloid Leukemia by Integrated Bioinformatics Analysis With External Validation. Front. Oncol. 12:848395. doi: 10.3389/fonc.2022.848395

Conclusion: TRIM32 was associated with the progression and prognosis of AML patients and could be a potential therapeutic target and biomarker for AML in the future.

Keywords: acute myeloid leukemia, weighted gene co-expression network analysis, differential gene expression analysis, TRIM32, prognosis

INTRODUCTION

Acute myeloid leukemia (AML) is the most common type of acute leukemia in adults and is a heterogeneous disease both molecularly and clinically (1). It is a malignant disease of hematopoietic stem cells characterized by clonal proliferation of immature bone marrow cells blocked at different stages of differentiation (2). The accumulation of uncontrolled leukemic blasts often disrupts normal hematopoietic function, causing severe bleeding, infection, and anemia. Therefore, timely diagnosis and prompt treatment of AML are crucial. Currently, chemotherapy and allogeneic hematopoietic stem cell transplantation (allo-HSCT) are the main treatments for AML (3). However, the prognosis of AML patients is still unsatisfactory. Finding specific molecular targets for different patients is significant for the treatment outcome and long-term prognosis of AML.

TRIM32 (Tripartite motif-containing protein 32) is a member of the Tripartite motif protein family, first identified in 1995 as a protein binding to a key activator of viral transcription HIV-1 Tat (4, 5). It is a kind of ubiquitin ligase enzyme (E3) modulating the ubiquitination of proteins. TRIM32 is known to play a crucial role in skeletal muscle stem cell differentiation and to contribute significantly to muscle homeostasis (6, 7). TRIM32 is also involved in various biological processes such as cell growth, apoptosis and immunity (8). As tumor biology continues to advance, the relationship between TRIM32 and tumor progression is receiving increasing attention. The expression of TRIM32 is upregulated in several malignancies such as gastric cancer (GC), non-small-cell lung cancer (NSCLC), and hepatocellular carcinoma (HCC) (9–11). A recent study showed that elevated expression of TRIM32 in triple-negative breast cancer (TNBC) was associated with radiation resistance and poor prognosis (12). Targeted therapy against TRIM32 could increase radiosensitivity, which may be a new potential strategy. To date, the relationship between TRIM32 and AML has not been investigated.

With the rapid development of genomic and proteomic technologies, bioinformatics has facilitated the discovery of reliable biomarkers for disease diagnosis and prognosis. Correlation networks are increasingly used in bioinformatics applications. Weighted gene co-expression network analysis (WGCNA) is one of the most compelling analyses, which was first developed in 2008 (13, 14). Rather than focusing on a single gene or an isolated biomarker, WGCNA extracts gene co-expression modules and relates them to clinical features, increasing the sensitivity to identify potential worthwhile targets for biological regulation (15). Differential gene expression analysis has recently emerged as another effective tool to indicate key driver genes for diseases (16). Therefore, combining WGCNA with differential gene expression analysis can help identify potential biomarkers for diagnosing and treating specific diseases.

In this study, we extracted mRNA expression data of AML from TCGA and GEO databases and combined WGCNA and differential gene expression analysis to find differential co-expression genes of AML. More importantly, we used functional enrichment analysis and protein-protein interaction (PPI) network to screen out hub genes. We attempted to explore the potential role of TRIM32 in AML by integrated bioinformatics analysis and the results were validated by external data from our center. Then we knocked down TRIM32 in AML cell lines to verify its function, aiming to provide a potential biomarker for future diagnosis and treatment of AML.

MATERIALS AND METHODS

Data Filtering and Processing

AML-related gene expression profiles and clinical data were extracted from the TCGA (https://portal.gdc.cancer.gov/) and GEO (https://www.ncbi.nlm.nih.gov/gds) databases. A total of 151 AML patients with RNA-seq data were enrolled from the TCGA database, which were downloaded by the *TCGAbiolinks* R package (17). As suggested by the tutorial, data filtering was performed using function *rpkm* in *edgeR* package (18).

After searching from the GEO database, another five datasets with survival outcomes were downloaded using R package *GEOquery* in this study (GSE37642, GSE76009, GSE16432, GSE12417, and GSE71014) (19). The number of patients in these five datasets was as follows: 562 in GSE37642, 534 in GSE76009, 436 in GSE16432, 405 in GSE12417, and 104 in GSE71014, respectively. As a result, a total of 2041 patients from the GEO database were included for subsequent analysis.

Weighted Gene Co-Expression Network Analysis

To improve the accuracy of network construction, the genes used for WGCNA were filtered. The R package *WGCNA* was used to conduct WGCNA between the gene expression data profiles of TCGA-LAML and GEO datasets, grouping highly co-expressed genes into modules (14). We use *pickSoftThreshold* to establish a scale-free network. A similarity matrix was built after performing the Pearson correlation of all gene pairs. The adjacency matrix was then transformed into a topological overlap matrix (TOM) and the TOM-based dissimilarity matrix for hierarchical clustering. Then, we correlated previously computed module features with clinical characteristics to identify the co-expression network's functional modules.

Differential Gene Expression Analysis

To figure out the differentially expressed genes (DEGs) between AML patients with different survival status (alive or dead), the R package *limma* was applied in the TCGA and GEO databases. The DEGs were screened with the criteria $|\log FC| \geq 1.0$ and adj. P-value < 0.05. The R package *ggplot2* and *VennDiagram* were used to draw a volcano map and Venn diagram (20).

Function and Pathway Enrichment Analysis

To determine the functional relevance of the modules, we tested whether the selected genes from the modules were enriched for specific functions or signaling pathways. Gene ontology (GO) and Kyoto Encyclopedia of Genes and Genomes (KEGG) pathway analyses were performed by the *clusterProfiler* R package (21). $p<0.05$ was considered statistically significant.

Construction of PPI and Identification of Hub Genes

We used the online database *STRING* (https://string-db.org/) to construct a protein-protein interaction (PPI) network. The PPI network was analyzed and visualized using *Cytoscape* software (v3.7.2) with an extraction score ≥ 0.4. In the PPI network, the nodes stand for proteins, and the edges represent the interactions of proteins. To identify the hub genes from the PPI network, we used the maximal clique centrality (MCC) algorithm calculated by a plugin in *Cytoscape* named *CytoHubba*. Genes with top 10 MCC values were set as hub genes.

Validation of the Expression Level and Prognostic Value of Hub Genes

To verify the reliability of the hub genes, we analyzed the expression level of hub genes in AML patients from the GEO database with different survival status (alive or dead). The expression level was represented with a boxplot for each gene. Univariate Kaplan-Meier survival analysis was done with R package *survival* to identify the prognostic value of hub genes further. Overall survival (OS) was defined as the time from diagnosis to death, regardless of the causes or last follow-up. Relapse-free survival (RFS) was defined as the time from complete remission to recurrence. Statistical significance was determined by Student's t-test for two groups and one-way ANOVA was used for comparison among multiple groups. $p<0.05$ was regarded as statistically significant.

Cells and Reagents

Human myeloid leukemia cell lines (MV4-11, MOLM13, KASUMI-1, OCI-AML3, SKM1, THP-1) were obtained from the American Tissue Culture Collection (ATCC). All cells were cultured in RPMI 1640 (Gibco, Detroit, MI, USA) medium, supplemented with 10% fetal bovine serum (Gibco, Detroit, MI, USA), 1% penicillin-streptomycin (Gibco, Detroit, MI, USA) at 37 ˚C with 5% CO_2.

Patient Samples and Characteristics

Bone marrow samples were obtained from 46 patients with newly diagnosed AML and 11 healthy donors (HD) from the First Affiliated Hospital of Soochow University between April 2020 and March 2021. The induction chemotherapy is a standard first-line treatment including an IA/DA regimen (Either idarubicin 8-12 mg/m^2 or daunorubicin 60-90 mg/m^2 on days 1-3 and cytarabine at 100mg/m^2 on days 1-7). For some older patients or patients with organ dysfunction, CAG or revised CAG (IAG, HAG) were administered with or without hypomethylating agents. Bone marrow mononuclear cells were isolated by Ficoll density gradient centrifugation. Basic clinical information, including age, gender, white blood cell count, hemoglobin level, platelet count, bone marrow morphology, karyotype, and molecular information was acquired from each patient. Patient risk stratification was based on 2017 ELN genetic categories. Receiver operating characteristics (ROC) curve analysis was performed based on the patient survival status to determine the optimal cut-off value of TRIM32. Informed consent was available from all patients and approved by the Medical Ethics Committee of the First Affiliated Hospital of Soochow University. The study was carried out following the Declaration of Helsinki.

Plasmid Constructs and Lentivirus Transduction

We used lentivirus vector pLKO.1-TRC-EGFP for carrying TRIM32 target shRNA and for non-silencing control. The sequence for TRIM32 shRNA was: GGUGGAAAGCUUUGGUGUU. Cells were transfected with the indicated plasmids by using calcium chloride.

Real-Time Quantitative Polymerase Chain Reaction

RT-qPCR measured the mRNA expression of TRIM32. Total RNA was extracted from Ficoll-separated mononucleated bone marrow samples in AML patients and healthy donors using TRIzol reagents (Invitrogen, USA). Reverse transcription was performed at 25°C for 10 minutes, 42°C for 15 minutes, and 85°C for 5 minutes. qPCR was performed at 95°C for 10 min, followed by 40 cycles of amplification at 95°C for 15 s and 60°C for 60 s. The GAPDH mRNA was used as an internal control. The sequences of the oligonucleotides used in this study were as follows: TRIM32, forward, 5'-CTCGG-AAGTTCTTCA CAGGCTC-3' and reverse, 5'-CTCCAGTAGTGCTA-CATCTGCC-3'; GAPDH, forward, 5'-GAGAAGGCTGGG GCTCATT-T-3' and reverse, 5'-ATGACGAACATGGG-GGCATC-3'.

Western Blot

Cells were lysed on ice for 30 min with RIPA buffer (Beyotime) containing protease and phosphatase inhibitors (Beyotime). After centrifuging at 12,000g for 15 min at 4°C, the supernatant was re-suspended in buffer and heated at 100°C for 10 min. Protein quantification was performed by a BCA protein assay kit (Thermo). Equal amounts of proteins were electrophoresed in 10% sodium dodecyl sulfate (SDS) polyacrylamide gels and then transferred onto polyvinylidene difluoride (PVDF) membranes (Pierce, USA). After being blocked with 5% non-fat dried milk in Tris-buffered saline

containing 0.1% Tween 20. The membranes were incubated at 4°C overnight with antibody TRIM32 (Abcam) and β-actin (Proteintech). After being incubated with appropriate secondary antibodies, proteins were visualized by a detection system of enhanced chemiluminescence (ECL).

Cell Proliferation Assay

Proliferation assay was performed using a Cell Counting Kit-8 (CCK-8, Bimake). Appropriately 5×10^3 cells/well were plated in a 96-well plate and cultured in complete medium. 10 μL of CCK8 reagent was added into each well and incubated for 2 hours at 37 °C with different time points of 0, 24, 48, and 72h. The absorbance was read at 450nm.

RESULTS

Construction of Gene Modules by WGCNA

The flowchart of this study is shown in **Figure 1**. To identify key gene sets for AML, we performed a WGCNA from the TCGA database as well as the GSE37642, GSE76009, GSE16432, GSE12417, and GSE71014 datasets based on the *WGCNA* package (**Table S1**). Each color represents a module. Here, 13 unique modules in TCGA-LAML (**Figure 2A**) and 8 modules in the above five GEO datasets (**Figure 2C**) were identified. **Figures 2B, D** showed heat maps of module-trait relationships, indicating that the green modules in TCGA and the brown modules in the GEO dataset were highly distinguishable between tumors and normal individuals (green modules: r=0.27, p=8e-04, brown modules: r=0.034, p=0.2).

Identification of Genes Between the DEGs and Co-Expression Modules

A total of 624 DEGs in TCGA (**Figure 3A**) and 338 DEGs in the five GEO datasets (**Figure 3B**) were screened by the *limma* package with |logFC|≥1.0 and adj. p<0.05 as cut-off criteria. 1122 co-expressed genes were extracted from these significant modules based on WGCNA analysis (850 genes in the green module genes and 272 genes in the brown module). Finally, 20 overlapping genes were obtained at the intersection of the DEGs list and the two co-expression modules (**Figure 3C**).

Function Enrichment Analysis for Genes in Co-Expression Module

To comprehensively understand the potential function of these genes in the co-expression modules, the GO (**Figure 4A**) and KEGG (**Figure 4B**) enrichment analyses for the genes in the brown module were performed using the R package "*ClusterProfiler*." GO analysis divides genes into three categories: biological processes (BP), cellular components (CC), and molecular functions (MF). In BP, genes were enriched in phospholipid metabolic processes, neutrophil degranulation, and activation. In the CC category, many genes were involved in secretory granule membranes, endocytic vesicles, and

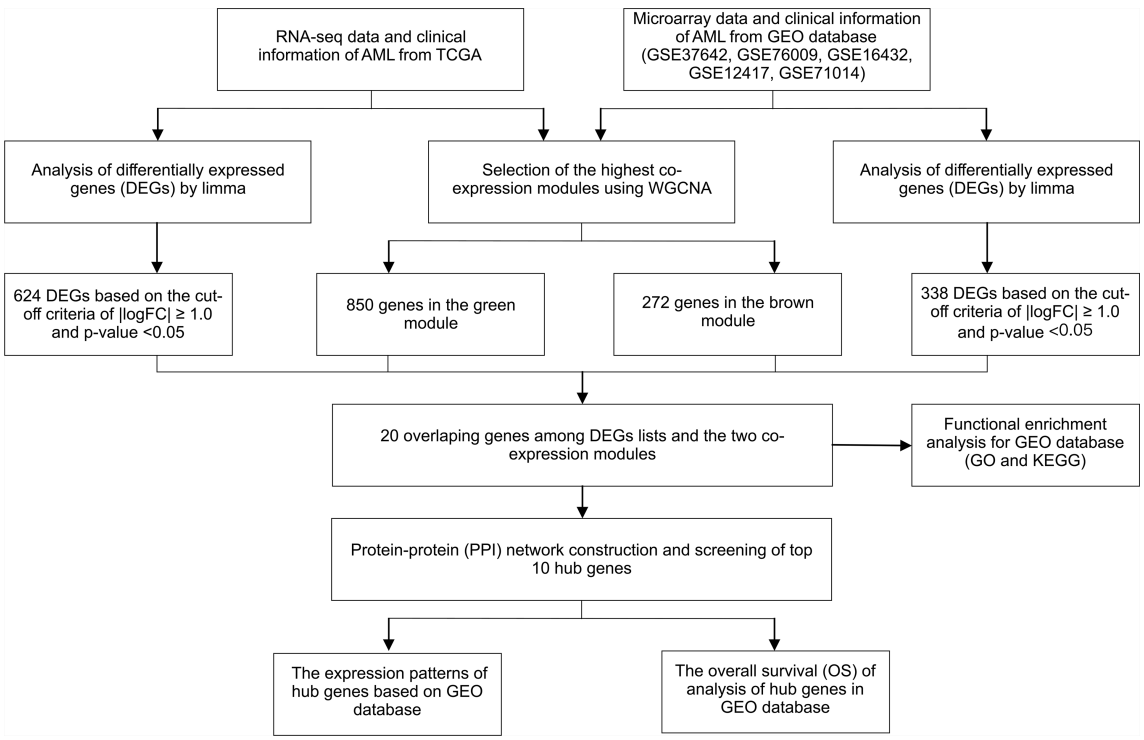

FIGURE 1 | Study design and workflow of this study.

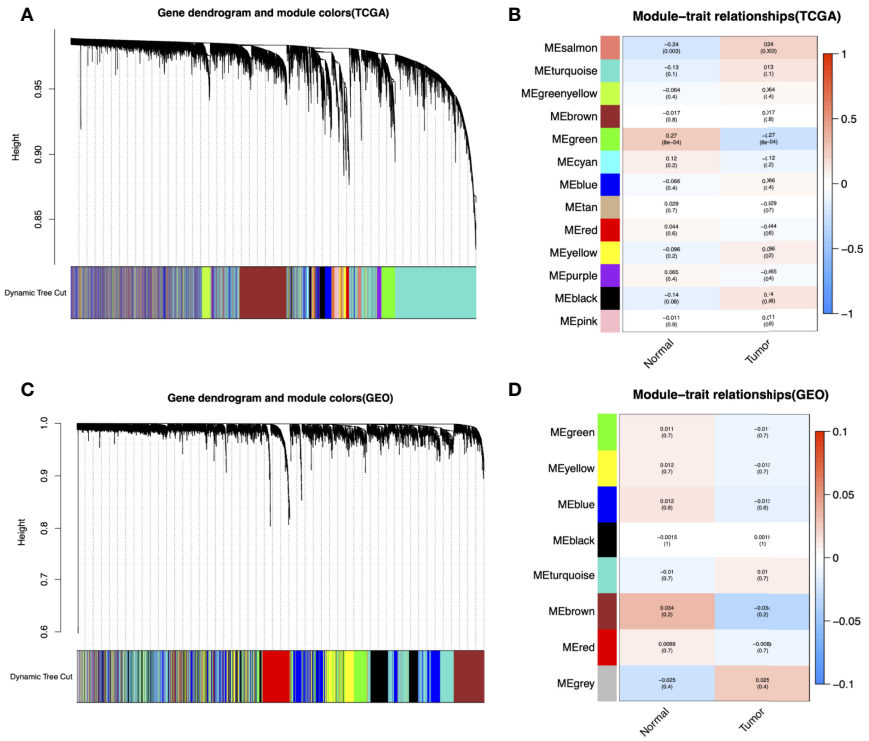

FIGURE 2 | Identification of modules associated with the clinical information in the TCGA-LAML and GEO datasets (GSE37642, GSE76009, GSE16432, GSE12417, GSE71014). The Cluster dendrogram of co-expression network modules was ordered by a hierarchical clustering of genes based on the 1-TOM matrix in TCGA-LAML **(A)** and GEO datasets **(C)**. Each module was assigned different colors. Module-trait relationships in TCGA-LAML **(B)** and GEO datasets **(D)**. Each row corresponds to a color module and column corresponds to a clinical trait (cancer and normal). Each cell contains the corresponding correlation and P-value.

glutamatergic synapses. In addition, protein serine/threonine kinase activity and DNA-binding transcription factor binding were mainly involved in MF. KEGG showed that genes were enriched in choline metabolism in cancer.

Hub Genes Identified in the PPI Network

To investigate the correlation between DEGs and co-expression modules, we performed protein-protein interaction (PPI) analysis through the *STRING* database, and a PPI network containing 15 nodes and 15 edges was created in **Figure 4C**. In addition, the top 10 hub genes with MCC scores in the PPI network were calculated using Cytoscape's CytoHubba plugin, which included TLE1, GLI2, HDAC9, MICALL2, DOCK1, PDPN, RAB27B, SIX3, TRIM32, and TBX1 (**Figure 4D**).

Expression Level and Prognostic Value of the Hub Genes

To further determine the expression levels of hub genes in AML patients with different survival status (alive or dead), we mapped the expression in the GEO database. In addition to TLE1, four hub genes (DOCK1, GLI2, RAB27B, and TRIM32) were highly expressed in those who died, while the remaining five hub genes (HDAC, MICALL2, PDPN, SIX3, and TBX1) were expressed at lower levels (**Figure 5**). Then, to further explore the prognostic value of these ten hub genes, we performed a Kaplan-Meier survival analysis *via* the *survival* R package of the GEO dataset and was illustrated in **Figure 6**. The increased expression levels of DOCK1, GLI2, and TRIM32 were highly correlated with poor prognosis in AML ($p<0.05$).

Validation of the Gene Expression and Prognosis of TRIM32

To date, the role of TRIM32 has not been reported in AML previously. Thus, we validated the role of TRIM32 with the clinical data of patients from our center. The mRNA levels of TRIM32 in 46 AML and 11 HD bone marrow samples were also detected by RT-qPCR. As shown in **Figure 7A**, TRIM32 expression was significantly upregulated in AML compared with that in HD ($p<0.05$). All patients were divided into two groups based on the optimal cut-off value of TRIM32 determined by the ROC curve (AUC: 0.682, sensitivity:91.7%, specificity: 43.3%) (**Figure S1**). The clinicopathological characteristics of these patients were summarized in **Table 1**. The expression of TRIM32 was correlated with biallelic CEBPA and PTPN11 mutation. Patients with lower expression of TRIM32 were more likely to achieve complete remission (CR) after the first induction therapy. Additionally, patients with elevated expression of TRIM32 were more frequently found in the

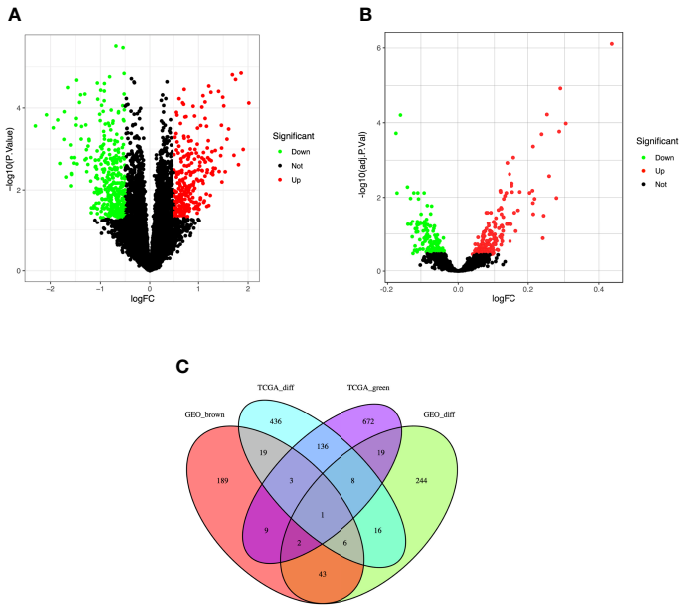

FIGURE 3 | Identification of differentially expressed genes (DEGs) among the TCGA and GSE37642, GSE76009, GSE16432, GSE12417, GSE71014 datasets of AML with the cut-off criteria of |logFC| ≥ 1.0 and adj. P < 0.05. **(A)** Volcano plot of DEGs in the TCGA dataset. **(B)** Volcano plot of DEGs in the GSE37642, GSE76009, GSE16432, GSE12417, GSE71014 dataset. **(C)** The Venn diagram of genes among DEG lists and co-expression module. In total, 20 overlapping genes in the intersection of DEG lists and two co-expression modules.

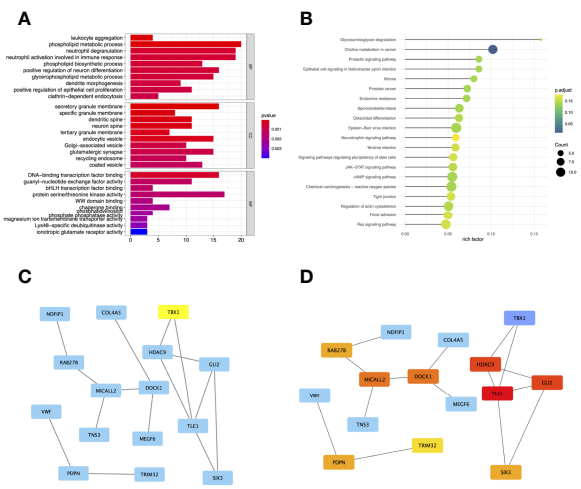

FIGURE 4 | Gene Ontology (GO) **(A)** and Kyoto Encyclopedia of Genes and Genomes (KEGG) **(B)** enrichment analysis for the genes in the brown module. The color represents the adjusted p-values (BH), and the size of the spots represents the gene number. Visualization of the protein-protein interaction (PPI) network and the candidate hub genes. **(C)** PPI network of the genes between DEG lists and two co-expression modules. The blue nodes represent the genes. Edges indicate interaction associations between nodes. **(D)** Identification of the hub genes from the PPI network using maximal clique centrality (MCC) algorithm. Edges represent the protein-protein associations. The red nodes represent genes with a high MCC sores, while the yellow node represent genes with a low MCC sore.

adverse-risk group based on 2017ELN. The results of univariate and multivariate analyses of risk factors for OS were shown in **Table 2**. Older age, not achieving CR after first induction therapy, not receiving HSCT, gene mutation status (PTPN11^{mt}, RUNX1^{mt} and IDH1^{mt}) and high expression of TRIM32 were associated with poor OS in univariate analysis (**Figure 7B**). However, TRIM32 did not play an independent role in OS while RUNX1 mutation proved to be an independent risk factor for worse OS after multivariate analysis (HR:7.441, 95% CI: 1.595-34.712, p=0.011). Receiving HSCT was an independent

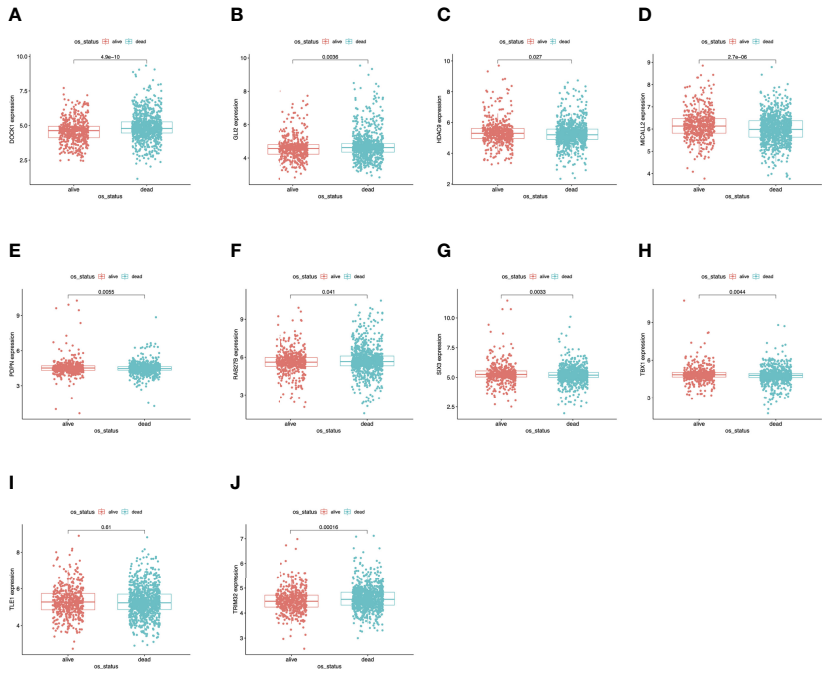

FIGURE 5 | Validation of expression levels of the ten hub genes among AMLs from the GEO database. **(A)** Gene expression value DOCK1 among samples of GEO. **(B)** Gene expression value GLI2 among samples of GEO. **(C)** Gene expression value HDAC9 among samples of GEO. **(D)** Gene expression value MICALL2 among samples of GEO. **(E)** Gene expression value PDPN among samples of GEO. **(F)** Gene expression value RAB27B among samples of GEO. **(G)** Gene expression value SIX3 among samples of GEO. **(H)** Gene expression value TBX1 among samples of GEO. **(I)** Gene expression value TLE1 among samples of GEO. **(J)** Gene expression value TRIM32 among samples of GEO.

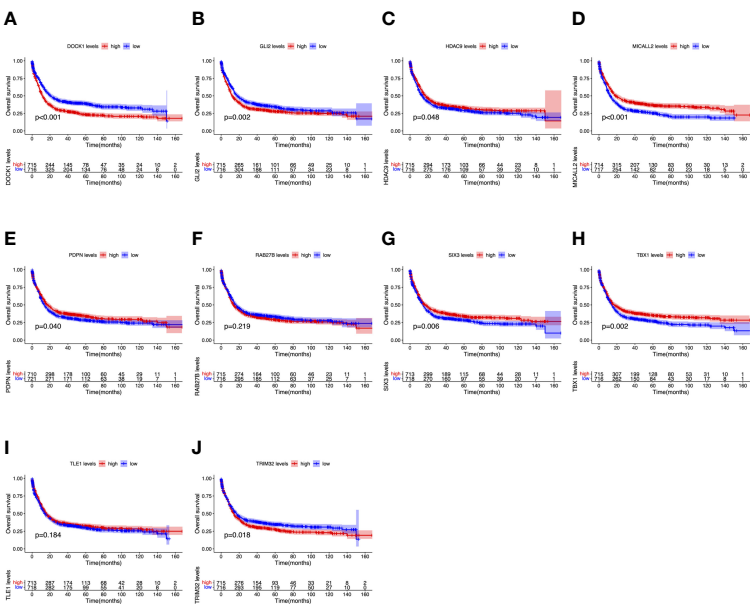

FIGURE 6 | Overall survival (OS) analysis of ten hub genes in AML patients from the GEO database. **(A)** Survival analysis for DOCK1 in AML. **(B)** Survival analysis for GLI2 in AML. **(C)** Survival analysis for HDAC9 in AML. **(D)** Survival analysis for MICALL2 in AML. **(E)** Survival analysis for PDPN in AML. **(F)** Survival analysis for RAB27B in AML. **(G)** Survival analysis for SIX3 in AML. **(H)** Survival analysis for TBX1 in AML. **(I)** Survival analysis for TLE1 in AML. **(J)** Survival analysis for TRIM32 in AML. The patients were stratified into high-level group (red) and low-level group (blue) according to median expression of the gene. Log-rank $P < 0.05$ was a statistically significant difference.

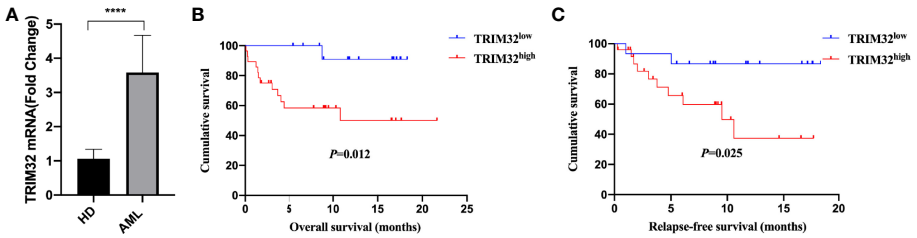

FIGURE 7 | Validation of the gene expression and prognosis of TRIM32. **(A)** Expression of TRIM32 gene in 46 AML patients and 11 HD bone marrow samples by RT-qPCR. Overall survival **(B)** and relapse-free survival **(C)** between high and low expression of the gene TRIM32. **** means $P<0.0001$.

TABLE 1 | Relationship between the expression of TRIM32 and clinicopathological features.

Variables	Totalno.(%)	TRIM32^{low} (n = 15)	TRIM32^{high} (n = 31)	P value
Gender (n, %)				0.766
Male	29 (63.0)	9 (60.0)	20 (64.5)	
Female	17 (37.0)	6 (40.0)	11 (35.5)	
Age, years				0.519
Median (Range)	48 (17-78)	44 (17-65)	50 (22-78)	
WBC count, *10^9/L				0.246
Median (Range)	19.6 (1.7-169.0)	14.75 (2.5-169)	22.21 (1.68-159.16)	
Hemoglobin, g/L				0.089
Median (Range)	72 (42-128)	90 (50-117)	70 (42-128)	
Platelet count, *10^9/L				0.888
Median (Range)	50 (4-312)	46 (8-250)	51 (4-312)	
Blast in bone marrow (%)				0.605
<50	16 (34.8)	6 (40.0)	10 (32.3)	
≥50	30 (65.2)	9 (60.0)	21 (67.7)	
Karyotype				0.880
Favorable	4 (8.7)	1 (6.7)	3 (9.7)	
Intermediate	38 (82.6)	13 (86.7)	25 (80.6)	
Adverse	4 (8.7)	1 (6.7)	3 (9.7)	
Fusiongenes				0.419
Favorable	7 (15.2)	2 (13.3)	5 (16.1)	
Intermediate	37 (80.4)	13 (86.7)	24 (77.4)	
Adverse	2 (4.3)	0 (0.0)	2 (6.5)	
2017 ELN				0.062
Favorable	3 (6.5)	0 (0.0)	3 (9.7)	
Intermediate	27 (58.7)	12 (80.0)	15 (48.4)	
Adverse	16 (34.8)	3 (20.0)	13 (41.9)	
CR1				***0.005***
Yes	14 (30.4)	1 (6.7)	13 (41.9)	
No	25 (54.3)	13 (86.7)	12 (38.7)	
NA	7 (15.2)	1 (6.7)	6 (19.4)	
Biallelic CEBPA Mut*	10 (24.4)	6 (42.9)	4 (14.8)	***0.047***
DNMT3A Mut*	11 (26.8)	3 (21.4)	8 (29.6)	0.569
NPM1 Mut*	12 (29.3)	5 (35.7)	7 (25.9)	0.514
FLT3-ITD Mut*	15 (36.6)	5 (35.7)	10 (37.0)	0.934
FLT3-TKD Mut*	3 (7.3)	0 (0.0)	3 (11.1)	0.105
TET2 Mut*	7 (17.1)	3 (21.4)	4 (14.8)	0.598
EZH2 Mut*	3 (7.3)	2 (14.3)	1 (3.7)	0.232
NRAS Mut*	9 (22.0)	2 (14.3)	7 (25.9)	0.380
PTPN11 Mut*	5 (12.2)	0 (0.0)	5 (18.5)	***0.033***
RUNX1 Mut*	4 (9.8)	1 (7.1)	3 (11.1)	0.678
KIT Mut*	3 (7.3)	1 (7.1)	2 (7.4)	0.975
IDH1 Mut*	3 (7.3)	1 (7.1)	2 (7.4)	0.975
IDH2 Mut*	3 (7.3)	2 (14.3)	1 (3.7)	0.232

*CR1, complete remission (CR) after first induction therapy. A P value of less than 0.05 is indicated in italics and bold. * Next generation sequencing data is missing from 5 patients. NA, notavailable.*

TABLE 2 | Univariate and multivariate analysis of risk factors for OS.

Variables	Univariate analysis			Multivariate analysis	
	No. of patients	1-year-OS (%)	P value	HR(95%CI)	P value
Gender (n, %)			0.960		
Male	25	73.3			
Female	17	62.7			
Age, years			***0.019***	−−	0.089
<45	18	87.7			
≥45	24	52.3			
WBC count, *10^9/L			0.224		
<100	38	65.6			
≥100	4	NA			
Hemoglobin, g/L			0.487		
<100	36	66.5			
≥100	6	80.0			
Platelet count, *10^9/L			0.255		
<100	35	61.9			
≥100	7	66.7			
Blast in bone marrow (%)			0.611		
<50	15	66.1			
≥50	27	71.5			
Karyotype			0.420		
Fav/int	38	70.6			
Adv	4	50.0			
CR1[#]			***0.007***	−−	0.458
Yes	14	86.0			
No	23	48.0			
Consolidation therapy			***0.001***	0.104(0.020-0.531)	***0.007***
HSCT	19	94.4			
Chemotherapy	23	26.6			
PTPN11*			0.064	−−	0.400
Mut	5	40.0			
WT	33	74.5			
RUNX1*			***0.003***	7.441(1.595-34.712)	***0.011***
Mut	4	25.0			
WT	34	75.4			
IDH1*			0.076	−−	0.093
Mut	3	33.3			
WT	35	73.8			
Expression of TRIM32			***0.012***	−−	0.112
Low	14	90.9			
High	28	54.1			

*A total of 42 patients were included in the OS analysis (4 patients were excluded for the lack of OS data). CR1, complete remission (CR) after first induction therapy. A P value of less than 0.05 is indicated in italics and bold. *Next generation sequencing data is missing from 4 patients with OS data. [#]Response to induction chemotherapy was unknown in 5 patients with OS data. NA, not available.*

protective factor (HR:0.104, 95%CI: 0.020-0.531, p=0.007). Similar results were observed for RFS shown in **Table 3**. Patients with overexpression of TRIM32 experienced a remarkably worse RFS in **Figure 7C** (p=0.025), although it was not an independent prognostic factor. Taken together, both the external database and clinical data in our center show that TRIM32 does have a certain influence on the prognosis of AML, whose role needs to be further studied.

TRIM32 Is Highly Expressed in AML Cells and Promote AML Cell Proliferation *in Vitro*

We investigated the relative expression of TRIM32 mRNA levels in six AML cell lines (MV4-11, MOLM13, KASUMI-1, OCI-AML3, SKM1, THP-1) and bone marrow of HD (**Figure 8A**). TRIM32 was highly expressed in AML cells compared with HD. We also measured the protein level of TRIM32 in these cell lines (**Figure 8B**). To assess the potential role of TRIM32 in proliferation in AML cell lines, we chose THP-1 and KASUMI-1with higher expression of TRIM32 to stably knockdown TRIM32 using a lentiviral delivery system. The efficiency of the shRNA in THP-1 was verified by RT-qPCR (**Figure 8C**) and western blot (**Figure 8D**). Compared with the empty vector (pLKO.1), shRNA knockdown of TRIM32 significantly inhibited proliferation *in vitro* as indicated by CCK-8 assay (**Figure 8E**). Similar results were obtained in another AML cell line KASUMI-1 shown in **Figure S2**.

DISCUSSION

Acute myeloid leukemia (AML) is a highly malignant disease and remains the most common form in adults, accounting for about 32% of all adult leukemia cases (22). The underlying molecular

TABLE 3 | Univariate and multivariate analysis of risk factors for RFS.

Variables	Univariate analysis			Multivariate analysis	
	No. of patients	1-year-RFS (%)	P value	HR(95%CI)	P value
Gender (n, %)			0.307		
Male	15	73.0			
Female	25	47.4			
Age, years			***0.014***	——	0.148
<45	17	84.4			
≥45	23	48.2			
WBC count, $*10^9$/L			0.195		
<100	36	58.5			
≥100	4	NA			
Hemoglobin, g/L			0.442		
<100	34	58.7			
≥100	6	83.3			
Platelet count, $*10^9$/L			0.880		
<100	32	64.5			
≥100	8	60.0			
Blast in bone marrow (%)			0.793		
<50	13	65.3			
≥50	27	59.0			
Karyotype			0.974		
Fav/int	37	61.5			
Adv	3	66.7			
Consolidation therapy			***0.004***	0.175(0.047-0.658)	***0.010***
HSCT	19	42.4			
Chemotherapy	21	82.0			
PTPN11*			1.000		
Mut	4	66.7			
WT	33	61.7			
RUNX1*			0.451		
Mut	3	NA			
WT	34	61.0			
IDH1*			0.320		
Mut	3	NA			
WT	34	59.8			
Expression of TRIM32			***0.025***	——	0.128
Low	15	86.7			
High	25	44.5			

*A total of 40 patients were included in the RFS analysis (6 patients were excluded for the lack of RFS data). A P value of less than 0.05 is indicated in italics and bold. * Next generation sequencing data is missing from 3 patients with RFS data. NA, not available.*

mechanism of the initiation and progression of AML is still poorly understood (23). With the rapid development of high-throughput sequencing technologies, we can extract a large volume of genomic data from patient samples, contributing to a better understanding of the underlying mechanism and providing novel molecular targets for the treatment of AML.

In this study, a total of 2192 patients in TCGA and GEO datasets were analyzed. We obtained 20 overlapping genes in the intersection of DEGs lists and two co-expression modules (green and brown module) from TCGA and GEO datasets (GSE37642, GSE76009, GSE16432, GSE12417, and GSE71014) based on integrated bioinformatics analysis. Using GO and KEGG enrichment analysis by R package "*ClusterProfiler*", genes were enriched in phospholipid and choline metabolic process. In addition, the 10 hub genes with the highest MCC scores in the PPI network were screened, including TLE1, GLI2, HDAC9, MICALL2, DOCK1, PDPN, RAB27B, SIX3, TRIM32, and TBX1. These hub genes were dysregulated in AML patients with different survival status (alive or dead). The higher levels of DOCK1, GLI2, and TRIM32 expression were closely associated with worse prognosis in AML. Ultimately, the expression levels and survival analysis of TRIM32 were validated. Knockdown of TRIM32 significantly inhibited proliferation of AML cell lines *in vitro*.

Nowadays, correlation networks are increasingly used in bioinformatics application (14). WGCNA has become a popular method for revealing the correlation patterns among genomic data and summarizing modules of highly correlated genes (24). WGCNA has been widely applied in various biological researches to identify candidate biomarkers or therapeutic targets, especially in cancers, e.g., breast cancer, hepatocellular carcinoma, and colorectal cancer (25–28). Several survival-specific lncRNAs and mRNAs of AML were identified based on WGCNA method with RNAseq data from TCGA (29). Chen et al. concluded that lncRNA-LOC646762 through the endocytosis signaling pathway might act as a survival biomarker for adult AML. Another study revealed that 15 hub genes were crucial for AML progression by comparing AML samples from TCGA with standard control samples from the Genotype-Tissue Expression (GTEx) database using WGCNA (30). Finally, overexpression of

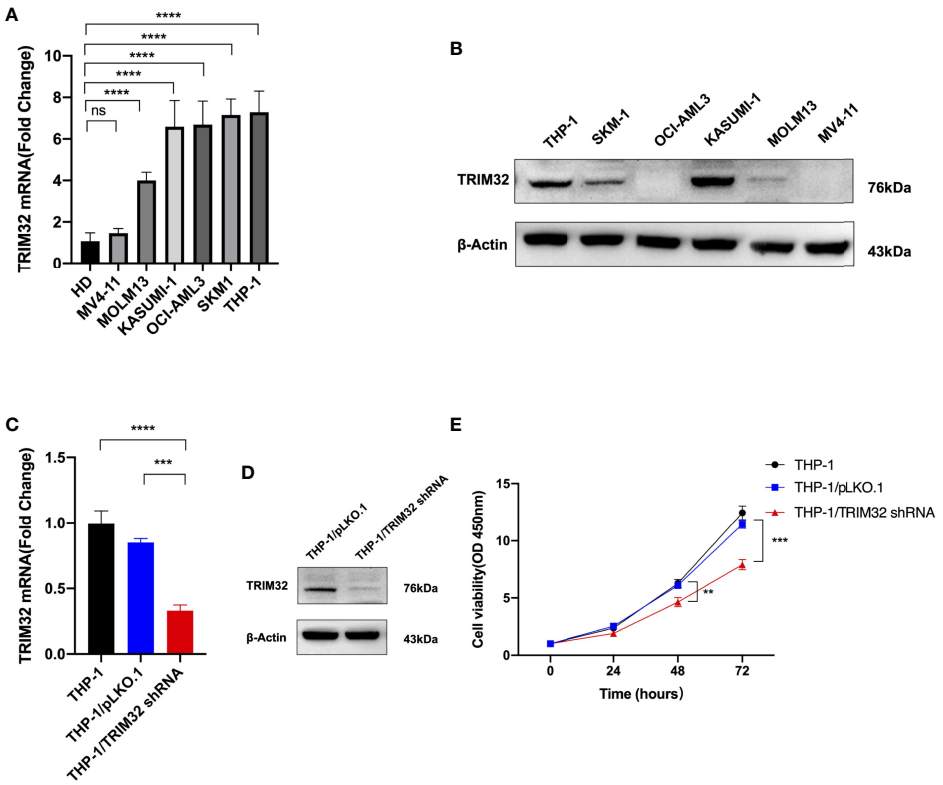

FIGURE 8 | Expression level of TRIM32 was detected in six AML cell lines by RT-qPCR **(A)** and western blot **(B)**. Transfection efficiency of TRIM32 shRNA was validated in THP-1 using RT-qPCR **(C)** and western blot **(D)**. **(E)** Cell proliferation was determined by CCK-8 assay. ** means $P<0.01$, *** means $P<0.001$, **** means $P<0.0001$, ns, no significance.

CEACAM5, one of the hub genes, was proved to be an unfavorable factor for prognosis.

In the present study, we focused on the hub gene TRIM32 since both DOCK1 and GLI2 had been discussed as adverse prognostic markers of AML in previous articles (31–34). To the best of our knowledge, it is the first time to report and validate the role of TRIM32 in AML. Tripartite motif protein (TRIM) is a highly conserved and rapidly evolving family, which plays a vital role in cell growth, apoptosis and immunity. TRIM32 is a member of the TRIM family, first discovered in 1995 as a ubiquitin ligase enzyme (E3) (4). Actin, c-Myc, and ABI2 (Ab1 interactor 2) have been proved to be substrates for TRIM32 (35–37). TRIM32 is implicated in diverse diseases, especially in malignancies (9, 11, 38, 39). According to previous studies, aberrant overexpression of TRIM32 was depicted in human skin cancer cells (40). Moreover, TRIM32 was a significant predictor of the prognosis of hepatocellular carcinoma (HCC), and the overexpression of TRIM32 may induce HCC patients' resistance to oxaliplatin (11). Liu et al. identified TRIM32 as a novel tumor suppressor p53 target gene and negatively regulated p53-mediated stress responses (41). TRIM32 overexpression promoted cell oncogenic transformation and tumorigenesis in mice in a largely p53-dependent manner. Another study found that TRIM32 can enhance retinoic acid receptor α (RARα)-mediated transcriptional activity and stabilize RARα in human promyelogenous leukemia cell line HL60 (42). Based on integrated bioinformatics analysis, our study is the first to reveal that TRIM32 is highly expressed in human AML, correlating with a poor prognosis. Furthermore, we validated the finding in human AML cell lines and patient samples in our center. Previous studies demonstrated that overexpression of TRIM32 could promote proliferation of lung cancer cells by activating JAK2/STAT3 signaling pathway (38). Both abnormal activations of JAK kinase and STAT are involved in multiple hematological malignant, especially leukemia (43). Recently, a variety of studies have proved that TRIM32 is closely related to glucose metabolism both in normal and tumor tissues by interaction with two enzymes involved in glycolysis (44). Elevated expression of TRIM32 contributes to a high rate of glycolysis with increased lactate production, which is like the Warburg effect in tumors. Metabolic reprogramming is also common in AML. However, the mechanism of oncogene TRIM32 in AML needs to be further verified by a series of fundamental experiments in the future.

In conclusion, we discovered ten hub genes enriched in human AML through integrated bioinformatics analysis. Based on WGCNA and differential gene expression analysis, TRIM32 was identified to be closely related to human AML, which could be used as a potential therapeutic target and prognostic biomarker for AML in the future.

DATA AVAILABILITY STATEMENT

The datasets presented in this study can be found in online repositories. The names of the repository/repositories and accession number(s) can be found in the article/**Supplementary Material**.

ETHICS STATEMENT

The studies involving human participants were reviewed and approved by Medical Ethics Committee of the First Affiliated Hospital of Soochow University. The patients/participants provided their written informed consent to participate in this study.

AUTHOR CONTRIBUTIONS

XX and JQ designed the study, analyzed the data, and wrote the manuscript draft. JY contributed to searching the database. TP, HH and MY contributed to data analysis. YH participated in the whole process of this study, supervised and revised the manuscript. All authors contributed to the article and approved the submitted version.

FUNDING

This work was supported by National Natural Science Foundation of China (81873432 and 82070143), grants from the Jiangsu Province of China (BE2021645), and the Priority Academic Program Development of Jiangsu Higher Education Institutions (PAPD).

SUPPLEMENTARY MATERIAL

The Supplementary Material for this article can be found online at: https://www.frontiersin.org/articles/10.3389/fonc.2022.848395/full#supplementary-material

REFERENCES

1. Aitken MJL, Ravandi F, Patel KP, Short NJ. Prognostic and Therapeutic Implications of Measurable Residual Disease in Acute Myeloid Leukemia. *J Hematol Oncol* (2021) 14(1):137. doi: 10.1186/s13045-021-01148-5
2. Short NJ, Rytting ME, Cortes JE. Acute Myeloid Leukaemia. *Lancet* (2018) 392(10147):593–606. doi: 10.1016/S0140-6736(18)31041-9
3. Leonard JP, Martin P, Roboz GJ. Practical Implications of the 2016 Revision of the World Health Organization Classification of Lymphoid and Myeloid Neoplasms and Acute Leukemia. *J Clin Oncol* (2017) 35(23):2708–15. doi: 10.1200/JCO.2017.72.6745
4. Ichimura T, Taoka M, Shoji I, Kato H, Sato T, Hatakeyama S, et al. 14-3-3 Proteins Sequester a Pool of Soluble TRIM32 Ubiquitin Ligase to Repress Autoubiquitylation and Cytoplasmic Body Formation. *J Cell Sci* (2013) 126(Pt 9):2014–26. doi: 10.1242/jcs.122069
5. Fridell RA, Harding LS, Bogerd HP, Cullen BR. Identification of a Novel Human Zinc Finger Protein That Specifically Interacts With the Activation Domain of Lentiviral Tat Proteins. *Virology* (1995) 209(2):347–57. doi: 10.1006/viro.1995.1266
6. Wang M, Luo W, Zhang Y, Yang R, Li X, Guo Y, et al. Trim32 Suppresses Cerebellar Development and Tumorigenesis by Degrading Gli1/sonic Hedgehog Signaling. *Cell Death Differ* (2020) 27(4):1286–99. doi: 10.1038/s41418-019-0415-5
7. Nicklas S, Otto A, Wu X, Miller P, Stelzer S, Wen Y, et al. TRIM32 Regulates Skeletal Muscle Stem Cell Differentiation and is Necessary for Normal Adult Muscle Regeneration. *PloS One* (2012) 7(1):e30445. doi: 10.1371/journal.pone.0030445
8. Bawa S, Piccirillo R, Geisbrecht ER. TRIM32: A Multifunctional Protein Involved in Muscle Homeostasis, Glucose Metabolism, and Tumorigenesis. *Biomolecules* (2021) 11(3). doi: 10.3390/biom11030408
9. Wang C, Xu J, Fu H, Zhang Y, Zhang X, Yang D, et al. TRIM32 Promotes Cell Proliferation and Invasion by Activating Beta-Catenin Signalling in Gastric Cancer. *J Cell Mol Med* (2018) 22(10):5020–8. doi: 10.1111/jcmm.13784
10. Du Y, Zhang W, Du B, Zang S, Wang X, Mao X, et al. TRIM32 Overexpression Improves Chemoresistance Through Regulation of Mitochondrial Function in non-Small-Cell Lung Cancers. *Onco Targets Ther* (2018) 11:7841–52. doi: 10.2147/OTT.S176689
11. Cui X, Lin Z, Chen Y, Mao X, Ni W, Liu J, et al. Upregulated TRIM32 Correlates With Enhanced Cell Proliferation and Poor Prognosis in Hepatocellular Carcinoma. *Mol Cell Biochem* (2016) 421(1-2):127–37. doi: 10.1007/s11010-016-2793-z
12. Ma Y, Zhang H, Chen C, Liu L, Ding T, Wang Y, et al. TRIM32 Promotes Radioresistance by Disrupting TC45-STAT3 Interaction in Triple-Negative Breast Cancer. *Oncogene* (2022) 41(11):1589–99. doi: 10.1038/s41388-022-02204-1
13. Shi WJ, Zhuang Y, Russell PH, Hobbs BD, Parker MM, Castaldi PJ, et al. Unsupervised Discovery of Phenotype-Specific Multi-Omics Networks. *Bioinformatics* (2019) 35(21):4336–43. doi: 10.1093/bioinformatics/btz226
14. Langfelder P, Horvath S. WGCNA: An R Package for Weighted Correlation Network Analysis. *BMC Bioinf* (2008) 9:559. doi: 10.1186/1471-2105-9-559
15. Yang R, Du Y, Wang L, Chen Z, Liu X. Weighted Gene Co-Expression Network Analysis Identifies CCNA2 as a Treatment Target of Prostate Cancer Through Inhibiting Cell Cycle. *J Cancer* (2020) 11(5):1203–11. doi: 10.7150/jca.38173
16. Liu W, Gan CY, Wang W, Liao LD, Li CQ, Xu LY, et al. Identification of lncRNA-Associated Differential Subnetworks in Oesophageal Squamous Cell Carcinoma by Differential Co-Expression Analysis. *J Cell Mol Med* (2020) 24(8):4804–18. doi: 10.1111/jcmm.15159
17. Colaprico A, Silva TC, Olsen C, Garofano L, Cava C, Garolini D, et al. TCGAbiolinks: An R/Bioconductor Package for Integrative Analysis of TCGA Data. *Nucleic Acids Res* (2016) 44(8):e71. doi: 10.1093/nar/gkv1507
18. Robinson MD, McCarthy DJ, Smyth GK. Edger: A Bioconductor Package for Differential Expression Analysis of Digital Gene Expression Data. *Bioinformatics* (2010) 26(1):139–40. doi: 10.1093/bioinformatics/btp616
19. Davis S, Meltzer PS. GEOquery: A Bridge Between the Gene Expression Omnibus (GEO) and BioConductor. *Bioinformatics* (2007) 23(14):1846–7. doi: 10.1093/bioinformatics/btm254
20. Chen H, Boutros PC. VennDiagram: A Package for the Generation of Highly-Customizable Venn and Euler Diagrams in R. *BMC Bioinf* (2011) 12:35. doi: 10.1186/1471-2105-12-35
21. Yu G, Wang LG, Han Y, He QY. Clusterprofiler: An R Package for Comparing Biological Themes Among Gene Clusters. *OMICS* (2012) 16(5):284–7. doi: 10.1089/omi.2011.0118
22. Yilmaz H, Toy HI, Marquardt S, Karakulah G, Kucuk C, Kontou PI, et al. In Silico Methods for the Identification of Diagnostic and Favorable Prognostic Markers in Acute Myeloid Leukemia. *Int J Mol Sci* (2021) 22(17). doi: 10.3390/ijms22179601
23. Prada-Arismendy J, Arroyave JC, Rothlisberger S. Molecular Biomarkers in Acute Myeloid Leukemia. *Blood Rev* (2017) 31(1):63–76. doi: 10.1016/j.blre.2016.08.005
24. Zhang B, Horvath S. A General Framework for Weighted Gene Co-Expression Network Analysis. *Stat Appl Genet Mol Biol* (2005) 4:Article17. doi: 10.2202/1544-6115.1128

25. Tang J, Kong D, Cui Q, Wang K, Zhang D, Gong Y, et al. Prognostic Genes of Breast Cancer Identified by Gene Co-Expression Network Analysis. *Front Oncol* (2018) 8:374. doi: 10.3389/fonc.2018.00374
26. Wang D, Liu J, Liu S, Li W. Identification of Crucial Genes Associated With Immune Cell Infiltration in Hepatocellular Carcinoma by Weighted Gene Co-Expression Network Analysis. *Front Genet* (2020) 11:342. doi: 10.3389/fgene.2020.00342
27. Qiu X, Cheng SH, Xu F, Yin JW, Wang LY, Zhang XY. Weighted Gene Co-Expression Network Analysis Identified MYL9 and CNN1 are Associated With Recurrence in Colorectal Cancer. *J Cancer* (2020) 11(8):2348–59. doi: 10.7150/jca.39723
28. Li CY, Cai JH, Tsai JJP, Wang CCN. Identification of Hub Genes Associated With Development of Head and Neck Squamous Cell Carcinoma by Integrated Bioinformatics Analysis. *Front Oncol* (2020) 10:681. doi: 10.3389/fonc.2020.00681
29. Chen CT, Wang PP, Mo WJ, Zhang YP, Zhou W, Deng TF, et al. Expression Profile Analysis of Prognostic Long non-Coding RNA in Adult Acute Myeloid Leukemia by Weighted Gene Co-Expression Network Analysis (WGCNA). *J Cancer* (2019) 10(19):4707–18. doi: 10.7150/jca.31234
30. Zhu R, Lin W, Tang L, Hu Y. Identification of Hub Genes Associated With Adult Acute Myeloid Leukemia Progression Through Weighted Gene Co-Expression Network Analysis. *Aging (Albany NY)* (2021) 13(4):5686–97. doi: 10.18632/aging.202493
31. Zhang G, Zhang J, Yang X, Zhang X, Yang S, Wang J, et al. High Expression of Dedicator of Cytokinesis 1 Adversely Influences the Prognosis of Acute Myeloid Leukemia Patients Undergoing Allogeneic Hematopoietic Stem Cell Transplantation. *Cancer Manag Res* (2019) 11:3053–60. doi: 10.2147/CMAR.S192845
32. Sha K, Lu Y, Zhang P, Pei R, Shi X, Fan Z, et al. Identifying a Novel 5-Gene Signature Predicting Clinical Outcomes in Acute Myeloid Leukemia. *Clin Transl Oncol* (2021) 23(3):648–56. doi: 10.1007/s12094-020-02460-1
33. Wellbrock J, Latuske E, Kohler J, Wagner K, Stamm H, Vettorazzi E, et al. Expression of Hedgehog Pathway Mediator GLI Represents a Negative Prognostic Marker in Human Acute Myeloid Leukemia and Its Inhibition Exerts Antileukemic Effects. *Clin Cancer Res* (2015) 21(10):2388–98. doi: 10.1158/1078-0432.CCR-14-1059
34. Xu Y, Wang P, Li M, Wu Z, Li X, Shen J, et al. Natural Small Molecule Triptonide Inhibits Lethal Acute Myeloid Leukemia With FLT3-ITD Mutation by Targeting Hedgehog/FLT3 Signaling. *BioMed Pharmacother* (2021) 133:111054. doi: 10.1016/j.biopha.2020.111054
35. Nicklas S, Hillje AL, Okawa S, Rudolph IM, Collmann FM, van Wuellen T, et al. A Complex of the Ubiquitin Ligase TRIM32 and the Deubiquitinase USP7 Balances the Level of C-Myc Ubiquitination and Thereby Determines Neural Stem Cell Fate Specification. *Cell Death Differ* (2019) 26(4):728–40. doi: 10.1038/s41418-018-0144-1
36. Kano S, Miyajima N, Fukuda S, Hatakeyama S. Tripartite Motif Protein 32 Facilitates Cell Growth and Migration *via* Degradation of Abl-Interactor 2. *Cancer Res* (2008) 68(14):5572–80. doi: 10.1158/0008-5472.CAN-07-6231
37. Shieh PB, Kudryashova E, Spencer MJ. Limb-Girdle Muscular Dystrophy 2H and the Role of TRIM32. *Handb Clin Neurol* (2011) 101:125–33. doi: 10.1016/B978-0-08-045031-5.00009-8
38. Yin H, Li Z, Chen J, Hu X. Expression and the Potential Functions of TRIM32 in Lung Cancer Tumorigenesis. *J Cell Biochem* (2019) 120(4):5232–43. doi: 10.1002/jcb.27798
39. Luo Q, Wu X, Nan Y, Chang W, Zhao P, Zhang Y, et al. TRIM32/USP11 Balances ARID1A Stability and the Oncogenic/Tumor-Suppressive Status of Squamous Cell Carcinoma. *Cell Rep* (2020) 30(1):98–111 e5. doi: 10.1016/j.celrep.2019.12.017
40. Horn EJ, Albor A, Liu Y, El-Hizawi S, Vanderbeek GE, Babcock M, et al. RING Protein Trim32 Associated With Skin Carcinogenesis has Anti-Apoptotic and E3-Ubiquitin Ligase Properties. *Carcinogenesis* (2004) 25 (2):157–67. doi: 10.1093/carcin/bgh003
41. Liu J, Zhang C, Wang XL, Ly P, Belyi V, Xu-Monette ZY, et al. E3 Ubiquitin Ligase TRIM32 Negatively Regulates Tumor Suppressor P53 to Promote Tumorigenesis. *Cell Death Differ* (2014) 21(11):1792–804. doi: 10.1038/cdd.2014.121
42. Sato T, Okumura F, Iguchi A, Ariga T, Hatakeyama S. TRIM32 Promotes Retinoic Acid Receptor Alpha-Mediated Differentiation in Human Promyelogenous Leukemic Cell Line HL60. *Biochem Biophys Res Commun* (2012) 417(1):594–600. doi: 10.1016/j.bbrc.2011.12.012
43. Wang L, Zhang H, Lei D. microRNA-146a Promotes Growth of Acute Leukemia Cells by Downregulating Ciliary Neurotrophic Factor Receptor and Activating JAK2/STAT3 Signaling. *Yonsei Med J* (2019) 60(10):924–34. doi: 10.3349/ymj.2019.60.10.924
44. Bawa S, Brooks DS, Neville KE, Tipping M, Sagar MA, Kollhoff JA, et al. Drosophila TRIM32 Cooperates With Glycolytic Enzymes to Promote Cell Growth. *Elife* (2020) 9. doi: 10.7554/eLife.52358

Conflict of Interest: The authors declare that the research was conducted in the absence of any commercial or financial relationships that could be construed as a potential conflict of interest.

Publisher's Note: All claims expressed in this article are solely those of the authors and do not necessarily represent those of their affiliated organizations, or those of the publisher, the editors and the reviewers. Any product that may be evaluated in this article, or claim that may be made by its manufacturer, is not guaranteed or endorsed by the publisher.

frontiers | Frontiers in Oncology

ORIGINAL RESEARCH
published: 08 June 2022
doi: 10.3389/fonc.2022.874168

Molecular Characterization of a First-in-Human Clinical Response to Nimesulide in Acute Myeloid Leukemia

*Victória Tomaz[1], Karina Griesi-Oliveira[1], Renato D. Puga[2], Bruno J. Conti[1], Fabio P. S. Santos[3], Nelson Hamerschlak[3] and Paulo V. Campregher[3]**

[1] Experimental Research Laboratory, Hospital Israelita Albert Einstein, São Paulo, Brazil, [2] Medicina Personalizada, Grupo Pardini, São Paulo, Brazil, [3] Centro de Hematologia e Oncologia Familia Dayan-Daycoval, Hospital Israelita Albert Einstein, São Paulo, Brazil

Acute myeloid leukemia (AML) is a hematologic malignancy associated with high morbidity and mortality. Here we describe a case of a patient with AML who presented a partial response after utilization of the non-steroidal anti-inflammatory drug nimesulide. The response was characterized by complete clearance of peripheral blood blasts and an 82% decrease of bone marrow blasts associated with myeloblast differentiation. We have then shown that nimesulide induces *in vitro* cell death and cell cycle arrest in all AML cell lines (HL-60, THP-1, OCI-AML2, and OCI-AML3). Weighted Correlation Network Analysis (WGCNA) of serial whole-transcriptome data of cell lines treated with nimesulide revealed that the sets of genes upregulated after treatment with nimesulide were enriched for genes associated with autophagy and apoptosis, and on the other hand, the sets of downregulated genes were associated with cell cycle and RNA splicing. Serial transcriptome of bone marrow patient sample confirmed the upregulation of genes associated with autophagy after the response to nimesulide. Lastly, we demonstrated that nimesulide potentiates the cytotoxic *in vitro* effect of several Food and Drug Administration (FDA)-approved chemotherapy drugs used in AML, including cytarabine.

Keywords: acute myeloid leukemia, anti-inflammatory agents, nimesulide, RNA-Seq, autophagy

OPEN ACCESS

Edited by:
Lokman Varisli,
Dicle University, Turkey

Reviewed by:
Ken Mills,
Queen's University Belfast, United Kingdom
Maria Salazar-Roa,
Complutense University of Madrid, Spain
Jiong Hu,
Ruijin Hospital, Shanghai, China

***Correspondence:**
Paulo V. Campregher
paulo.campregher@einstein.br

Specialty section:
This article was submitted to Hematologic Malignancies, a section of the journal Frontiers in Oncology

Received: *11 February 2022*
Accepted: *16 March 2022*
Published: *08 June 2022*

Citation:
Tomaz V, Griesi-Oliveira K, Puga RD, Conti BJ, Santos FPS, Hamerschlak N and Campregher PV (2022) Molecular Characterization of a First-in-Human Clinical Response to Nimesulide in Acute Myeloid Leukemia. Front. Oncol. 12:874168. doi: 10.3389/fonc.2022.874168

INTRODUCTION

Despite therapeutic advances in recent years, acute myeloid leukemia (AML) is still associated with high morbidity and mortality, with most patients succumbing to the disease (1, 2). AML treatment arsenal comprises chemotherapy, hypomethylating agents, targeted therapies, and hematopoietic stem cell transplantation (HSCT) (3). While remission can be induced in most patients, the only curative approach for the majority of individuals with AML remains HSCT. Nevertheless, the morbidity associated with HSCT and the median age at diagnosis of 68 years make a significant proportion of patients ineligible for such treatment (4, 5). Therefore, new treatment strategies are needed in AML.

Drug repurposing, that is, the identification of new uses for existing drugs, is a strategy with the potential to improve treatment outcomes with significantly cheaper, faster, and safer preclinical and clinical development protocols (6). Several investigators have already explored such strategy with successful examples, such as the repositioning of thalidomide for the treatment of multiple myeloma and

the subsequent development of the thalidomide analog lenalidomide, the use of rituximab for rheumatoid arthritis treatment, and the use of aspirin, a COX inhibitor, as secondary prevention in colorectal cancer (7–10).

There is preclinical evidence that non-steroidal anti-inflammatory drugs (NSAIDs) have anti-proliferative and pro-apoptotic effects in AML cell lines and xenograft models (11–13). In addition, studies have shown that the COX-2 inhibitor nimesulide, in addition to inducing *in vitro* leukemic cell death, also induces myeloid differentiation (12). There is also evidence that glucocorticoids associated with chemotherapy may have a role in the treatment of specific subsets of AML, with at least one study demonstrating improved overall and disease-free survival in patients with hyperleukocytic AML (14).

In this article, we report the first-in-human clinical response to nimesulide in AML and provide insights into the mechanisms of action involved in this effect through whole exome, transcriptome, and cell culture experiments.

MATERIALS AND METHODS

Patient Biological Sample

Peripheral blood and bone marrow samples were obtained from an AML patient after the informed consent form was signed. Blood count was performed on an XP-300 hematology analyzer (Sysmex, Kobe, Japan), and the bone marrow smear was processed according to the standards of the diagnostic medical laboratory. Bone marrow mononuclear cells (BMMC) were obtained using Ficoll-Paque (Sigma-Aldrich, St. Louis, MO, USA) and used for immunophenotyping, DNA, and total RNA extraction for whole-exome and transcriptome sequencing (**Supplementary Methods**).

Cell Culture

The leukemic cell lines HL-60, THP-1, OCI-AML2, and OCI-AML3 were obtained from American Type Culture Collection (ATCC; Manassas, VA, USA) or Leibniz Institute DSMZ (German Collection of Microorganisms and Cell Cultures GmbH) and cultured in RPMI-1640 medium containing 10% fetal bovine serum, 2 mM of L-glutamine, 100 U/ml of penicillin, and 100 μg/ml of streptomycin (all Gibco, Grand Island, NY, USA) at 37°C in a 5% CO_2-humidified atmosphere.

Compounds

The drugs nimesulide (Oficinal Pharmacy, São Paulo, SP, BR), prednisolone (Biossynthetic, São Paulo, SP, BR), and cytarabine (Libbs, , São Paulo, SP, BR) were used in the cellular experiments. Nimesulide was diluted in dimethyl sulfoxide (DMSO) in a 10-mM stock solution, and prednisolone and cytarabine, presented in liquid form, were diluted in RPMI medium immediately before being applied to the cells. Food and Drug Administration (FDA)-approved drug library (Selleck Chemicals, Houston, TX, USA) was used for drug screening in combination with nimesulide.

Flow Cytometry Assays

The eBioscience™ Annexin V Apoptosis Detection Kit FITC (Invitrogen, Carlsbad, CA, USA) was used for the detection of early and late apoptosis in treated cell lines, following the manufacturer's instructions. For the cell cycle analysis, treated cells were washed with cold phosphate-buffered saline (PBS) twice and fixed with 70% cold ethanol at 4°C overnight. After cells were washed again with PBS twice, they were incubated with PBS containing 10 mg/ml of RNase at 37°C for 30 min, followed by DNA staining with 1 mg/ml of propidium iodide (all Invitrogen). After being left in a dark place at 4°C for 10 min, the cell DNA content was evaluated using a flow cytometer to analyze the distribution of DNA content in cell cycle phases. All experiments were performed using flow cytometer FACScan Fortessa (BD Biosciences, San Jose, CA, USA) and recorded at least 10,000 events/sample. The analysis of the experiments was performed by FlowJo software.

Drug Screening and Cell Viability Assay

To identify potential effects of small molecules in combination with nimesulide, an FDA-approved drug library was purchased from Selleck Chemicals for a high-throughput drug screening with selected drugs to assess the roles of drugs in cells lines. The following drugs approved for the treatment of AML were selected: azacitidine (1 μM), gilteritinib fumarate (0.1 μM), cladribine (10 μM), doxorubicin hydrochloride (6.7 μM), mitoxantrone hydrochloride (0.33 μM), fludarabine (0.09 μM), thioguanine (1.78 μM), and decitabine (0.5 μM). All drugs were diluted in RPMI 1640 culture medium (Gibco) to obtain all the above concentrations, based on the lowest concentration found in the literature. Cell viability was analyzed using the CellTiter-Glo® Luminescent Cell Viability Assay (Promega, Madison, WI, USA) according to the manufacturer's instructions. After 24 h of incubation of cell line with drugs alone or in combination with nimesulide, the cells were incubated for 10 min with Cell Titer-Glo reagent and then assayed by a luminescence plate reader. The ATP content of cells was calculated using the ATP standard curve in a preconfigured CellTiter-Glo protocol on GloMax® Discover Microplate Reader (Promega).

RNA Extraction and Sequencing

RNA was extracted with RNeasy Mini Kit (Qiagen, Hilden, Germany), and the library preparation and sequencing were performed at the Oklahoma Medical Research Foundation Genomics Core (USA) (**Supplementary Methods**). Sequencing was performed for groups treated with nimesulide and prednisolone alone, in combination, and for the control group (DMSO), in two independent experiments. Three samples from the patient were also sequenced at different times of the disease: at diagnosis (transcriptome 1), on D+21 after the start of nimesulide (transcriptome 2), and on D+63 after the start of nimesulide (transcriptome 3). The bioinformatics pipeline used for processing the sequenced samples is available in the **Supplementary Material**.

Gene Co-Expression Network Analysis

The Weighted Correlation Network Analysis (WGCNA) package from R (15) was employed to construct the gene co-expression network and identify the co-expression modules related to the treatments. For the construction of the networks and module assignment, the parameters adopted, using the function blockwiseModule, for the two analyzes were as follows: power =

20, networkType = "signed", minModuleSize = 150, mergecutHeight = 0.15 verbose = 6, minKMEtoStay = 0.5, nThreads = 24, and maxBlockSize = 20,000. The top ~10,000 genes with the highest variance among those genes considered as expressed were selected. For each module, the gene expression levels of each sample were summarized into an eigengene value, which was then used to assess the correlation of a module with proposed treatments in the leukemic cell lines. The significance value for these correlations was considered the value of $p < 0.05$ divided by the number of modules generated for each experiment. For experiment 1, p-value ≤0.0022 was considered, and for experiment 2, p-value ≤0.0027. The function userListEnrichment from WGCNA was used to evaluate the overlap between the modules identified in experiments 1 and 2. The functional enrichment analysis of the differentially expressed modules of the WGCNA was performed using the Database for Integrated Annotation, Visualization and Discovery (DAVID) v6.8, and for the protein–protein enrichment test of the WGCNA modules, the analysis of functional enrichment of protein–protein interaction networks (STRING) v11.0 was used. The functional categories observed were from the Gene Ontology (GO) Consortium, and they were related to biological processes, cellular components, and molecular functions. The KeggCharts, which show the distribution of genes between the Kyoto Encyclopedia of Genes and Genomes (KEGG) biochemical pathways, were also analyzed.

Analysis of the Patient's Transcriptomes

The strategy used to compare the molecular findings from cell line transcriptomes with the patient's transcriptomes was the CAMERA (16) package. The transcriptome data at time points 2 and 3 of the patient were compared with the transcriptome data at time point 1 in order to generate an expression difference ratio between these times. These expression ratio values were used to rank the genes by foldchange, from the highest to lowest, and then the CAMERA package was used, which performs a differential expression analysis, in which a p-value is assigned, in order to identify whether genes from a given set are assigned non-randomly within this ranking. This analysis was performed comparing the two patient rankings with the modules differentially expressed in the WGCNA.

Statistical Analysis

For flow cytometry assays, ANOVA statistical test was used, followed by Tukey's test for multiple comparisons. The statistical computations were conducted using GraphPad Prism 7.0, and the significance level adopted was 5% ($p < 0.05$). For the bioinformatics analysis, statistical methods specific to each computer program were used.

RESULTS

Clonal Dynamics and Partial Response of a Patient With Acute Myeloid Leukemia After Use of Nimesulide

A 52-year-old female was evaluated for asthenia, and her complete blood counts revealed a hemoglobin level of 10.1 g/dL, white blood cell (WBC) count of 4,740/mm^3 (7% blasts, 1% metamyelocytes, 4% bands, 52% neutrophils, 30% lymphocytes, and 6% monocytes) and a platelet count of 139,000/mm^3. Bone marrow evaluation was compatible with the diagnosis of AML with 56% blasts on bone marrow smear. Blast immunophenotyping was positive for CD117, CD64, CD36, CD33, HLA-DR, and negative for CD34. Cytogenetics analysis revealed a diploid karyotype (46, XX), and whole-exome sequencing revealed the following driver mutations NPM1:NM_002520:c.861_862insTGCT:p.L287fs, DNMT3A: NM_175629:c.1658delA:p.N553fs, IDH1:NM_005896:c.G395A: p.R132H, NRAS : NM_002524:c.G38T:p.G13V, and PTPN11: NM_080601:c.G794A:p.R265Q with wild-type FLT3 and CEBPA. Her final diagnosis was AML with mutated NPM1, and the European LeukemiaNet risk stratification was a favorable risk (17). The patient decided to receive only palliative care without specific AML treatment. Eleven days after her initial diagnosis, the patient developed gingival infiltration that required a minor oral procedure, and nimesulide 200 mg/day was prescribed for pain control. A few days after the start of nimesulide, she presented a progressive decrease in her peripheral blood blast count and improvements in her stamina. She had also been using prednisolone 30 mg/day for 3 months due to idiopathic knee arthritis. Therefore, the medical team decided to keep both drugs in a continuous fashion given the unexpected clinical response. Seventy-two days after the start of nimesulide treatment, her peripheral blood blast count went from 12,000 blasts/mm^3 to undetectable levels (**Figure 1A**). A bone marrow evaluation 21 days after nimesulide start revealed two immunophenotypic distinct blast populations, with 27% blasts presenting the same phenotype found at diagnosis and 27% of a second blast population characterized by increased expression of CD13, CD15, and CD11b and negativity for HLA-DR and CD117 (**Figure 1B**), compatible with blast differentiation. A third bone marrow evaluation 63 days after nimesulide revealed only 10% blasts with the same phenotype seen at diagnosis, characterizing a partial response (**Figure 1C**). In order to evaluate the clonal dynamics of mutations associated with the response to nimesulide, we performed whole-transcriptome sequencing at diagnosis and at two different times after the start of nimesulide (D+21 and D+63) and whole-exome sequencing at diagnosis and after the start of nimesulide (D+63).

The analysis of bone marrow whole exome at diagnosis suggests an ancestral clone harboring the DNMT3A mutation with an allele frequency of 34.5%; a second subclone with IDH1 and NRAS with allele frequencies of 27% and 26%, respectively; and the third subclone with NPM1 and PTPN11 with allele frequencies approximately 5% (**Figure 1D**). When comparing the sequencing at diagnosis and on D+63, we observe the maintenance of all five mutations with similar allele frequencies, despite an 82% reduction in the blast percentage (**Figure 1D**), strongly suggesting myeloid differentiation, in agreement with the immunophenotyping data. Transcriptome analysis of bone marrow at diagnosis and on D+21 and D+63 reveals a heterogeneous pattern of expression change of the mutated transcripts, with a progressive increase in the expression of mutated DNMT3A, a progressive decreased expression of mutated NPM1 and NRAS, and an initial increase

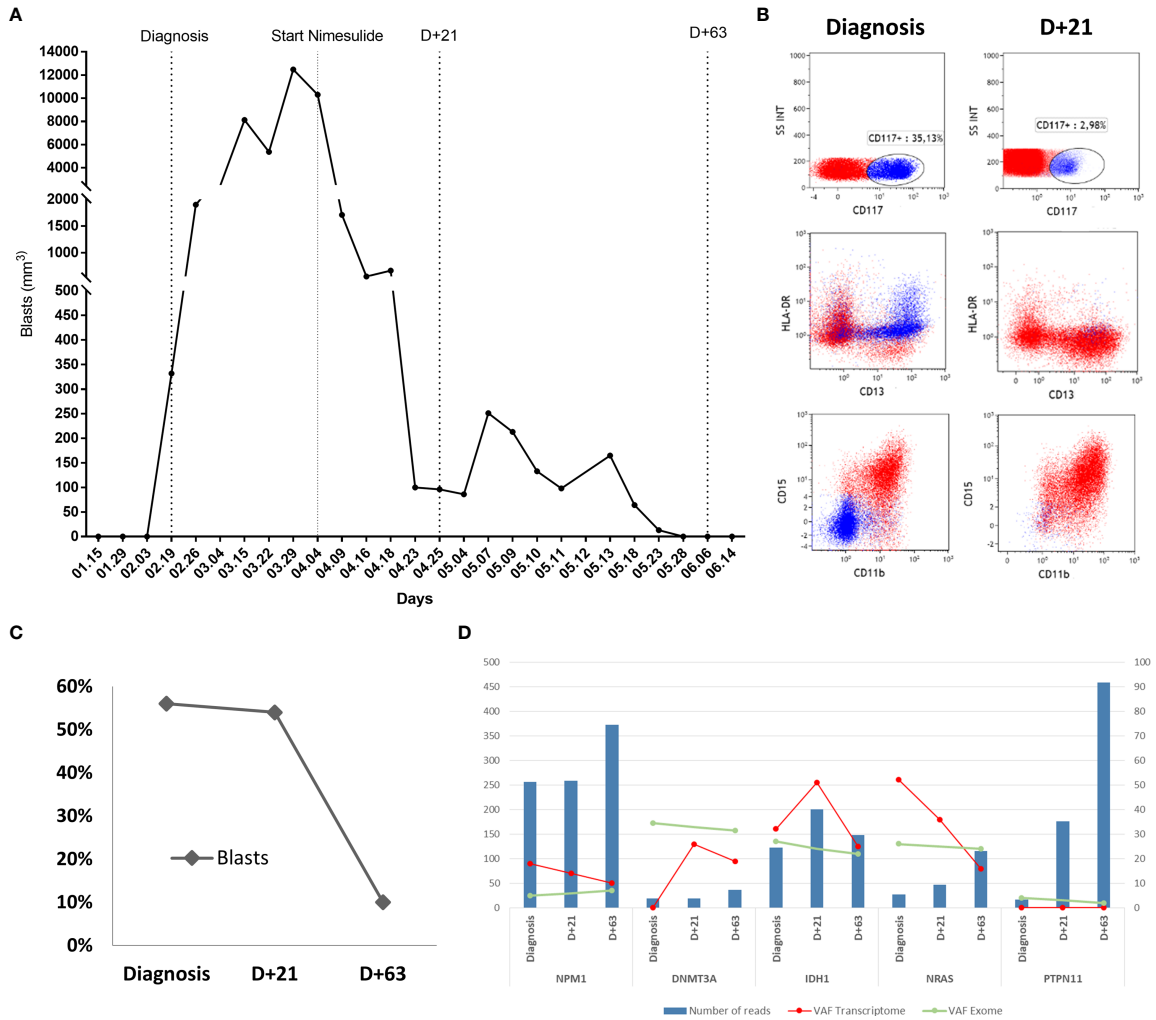

FIGURE 1 | Patient's response to the use of nimesulide. **(A)** Graph of absolute values of blasts in the patient's peripheral blood at diagnosis and after starting nimesulide use. **(B)** Dot plot graphs of the expression of HLA-DR, CD117, CD15, CD13, and CD11b markers in the patient's bone marrow leukemic blast population at diagnosis and D+21 after starting nimesulide. **(C)** Percentage of blasts in the patient's bone marrow at diagnosis and after days of nimesulide use (D+21 and D+63). **(D)** Graph showing the total number of reads (reads coverage) of NPM1, DNMT3A, IDH1, NRAS, and PTPN11 in the patient's three transcriptomes (Diagnosis, D+21, and D+63) represented in the bars in blue and the allelic frequency of variants (VAF) of the respective mutations from transcriptomes (red line) and whole-exome sequencing (green line). The left y-axis represents the values of the numbers of reads (blue bars), and the right y-axis refers to the transcriptome (red line) and exome (green line) VAF values.

followed by decreasing expression of mutated IDH1 (**Figure 1D**). Expression of mutated PTPN11 was not detected at any time point.

After 3 months of nimesulide treatment, peripheral blood blasts started increasing again, and the patient passed away 8 months after diagnosis due to progressive AML.

Anti-Inflammatory Compounds Induce Cell Death and Cell Cycle Arrest in Acute Myeloid Leukemia Cell Lines

To investigate the effect of nimesulide and prednisolone in AML, we treated HL-60, THP-1, OCI-AML2, and OCI-AML3 cells lines with these drugs at 100 μM. To assess the effect on the cell cycle at 24 h, we evaluated the DNA content and fluorescence intensity in the sub-G0 (cell death), G0/G1, S, and G2/M phases (**Supplementary Figure 1**). We observed that treatment with nimesulide alone increased the number of cells in sub-G0 (dead cells) when compared to the control, and the combination of nimesulide with prednisolone causes a statistically significant increase in sub-G0 cells when compared to the treatment of nimesulide alone with the exception of cell line OCI-AML3 (**Figure 2**). On the contrary, isolated prednisolone treatment did not cause cell death or changes in the cell cycle (**Figure 2**). The OCI-AML3 cell line, which is also resistant to cytarabine, was less sensitive to treatment with anti-inflammatory drugs than the other cell lines. Overall, we found a significant induction

of cell death at 24 h after the treatment with nimesulide alone and in combination with prednisolone.

To characterize the mechanism of cell death, the proportions of early and late apoptotic cells were evaluated by flow cytometry after treatments for 24 h (**Supplementary Figures 2**). We can observe in the cell lines a significant decrease in live cells when comparing controls with treatment with nimesulide alone, with the exception of OCI-AML3, which proved more resistant to treatment (**Figure 3**). Treatment with prednisolone alone did not induce apoptosis in cell lines; however, it increased the proportion of cells in late apoptosis in THP-1, OCI-AML2, and OCI-AML3 cell lines. Treatment with anti-inflammatory drugs did not induce a significant increase in early apoptotic cells; nevertheless, it causes more cell death than cytarabine in THP-1 and OCI-AML3. In addition, nimesulide enhanced the effect of cytarabine, a standard chemotherapy agent for the treatment of AML in cell death induction in all cell lines. In the cell lines more sensitive to cytarabine, HL-60, and OCI-AML2, the addition of nimesulide to the treatment led to the death of almost all leukemic cells (**Figures 3A, C**).

Gene Co-Expression Network Analysis Reveals Mechanisms Associated With Anti-Leukemia Effect of Anti-Inflammatory Drugs

In order to find a common mechanism behind the induction of cell death in AML cell lines after treatment with nimesulide alone

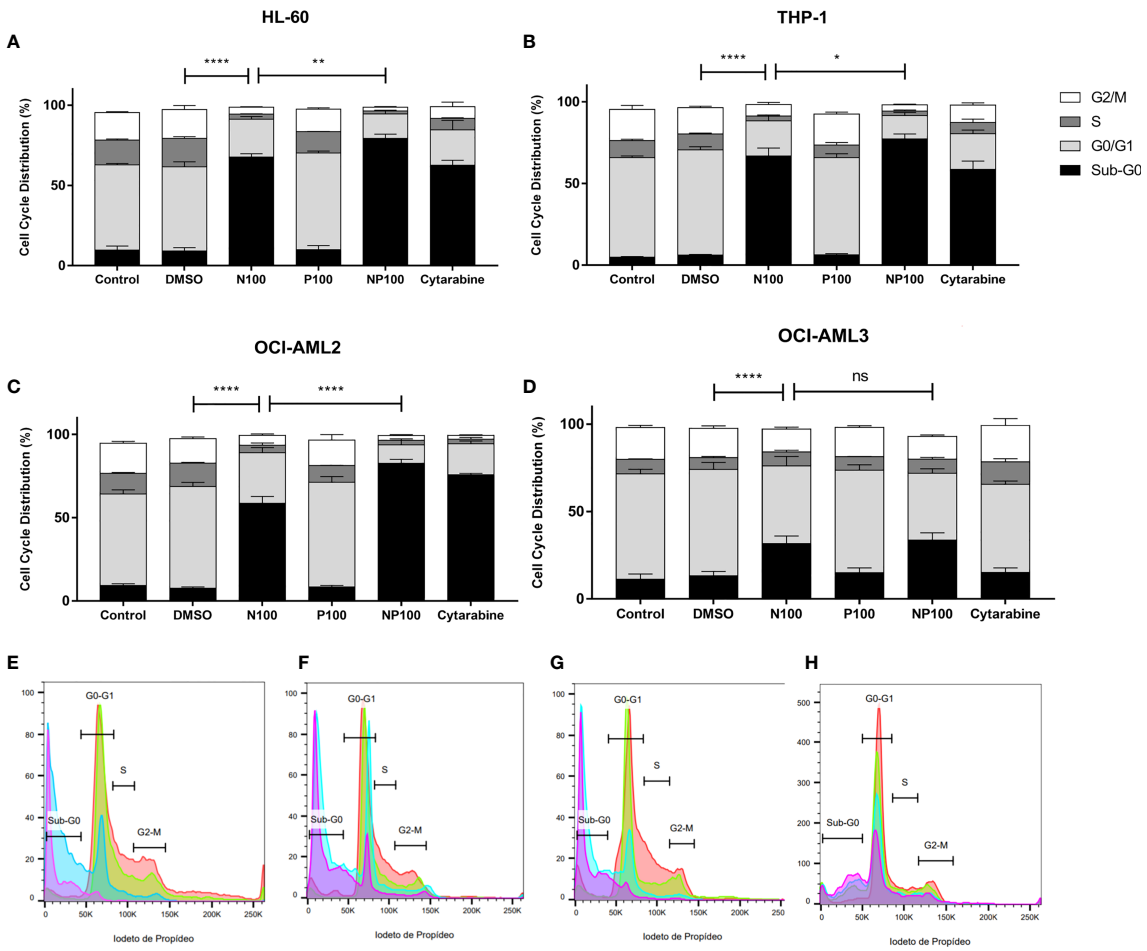

FIGURE 2 | Effect of nimesulide, prednisolone, and cytarabine treatment after 24 h in the cell cycle and death. **(A–D)** Bar graph showing the percentage of cells in each phase of the cell cycle in HL-60, THP-1, OCI-AML2, and OCI-AML3, respectively. **(E–H)** Representative histogram of the phases of the cell cycle in HL-60, THP-1, OCI-AML2, and OCI-AML3, respectively. The color red in the histogram represents the non-treatment controls, blue for nimesulide 100 μM of treatment, green for prednisolone 100 μM of treatment, and purple for nimesulide in combination with prednisolone 100 μM. Data shown are representative of 2 independent experiments and presented as mean ± SEM (n = 4). The p-value was determined using the two-way ANOVA multiple comparisons with Turkey's correction, *p < 0.05; **p < 0.01; ****p < 0.001. Control: non-treated cells; DMSO: treated with DMSO (dilution vehicle); N100: nimesulide 100 μM; P100: prednisolone 100 μM; NP100: combination of nimesulide and prednisolone 100 μM; Cytarabine: treated with cytarabine 2.5 μM. DMSO, dimethyl sulfoxide. ns, not significant.

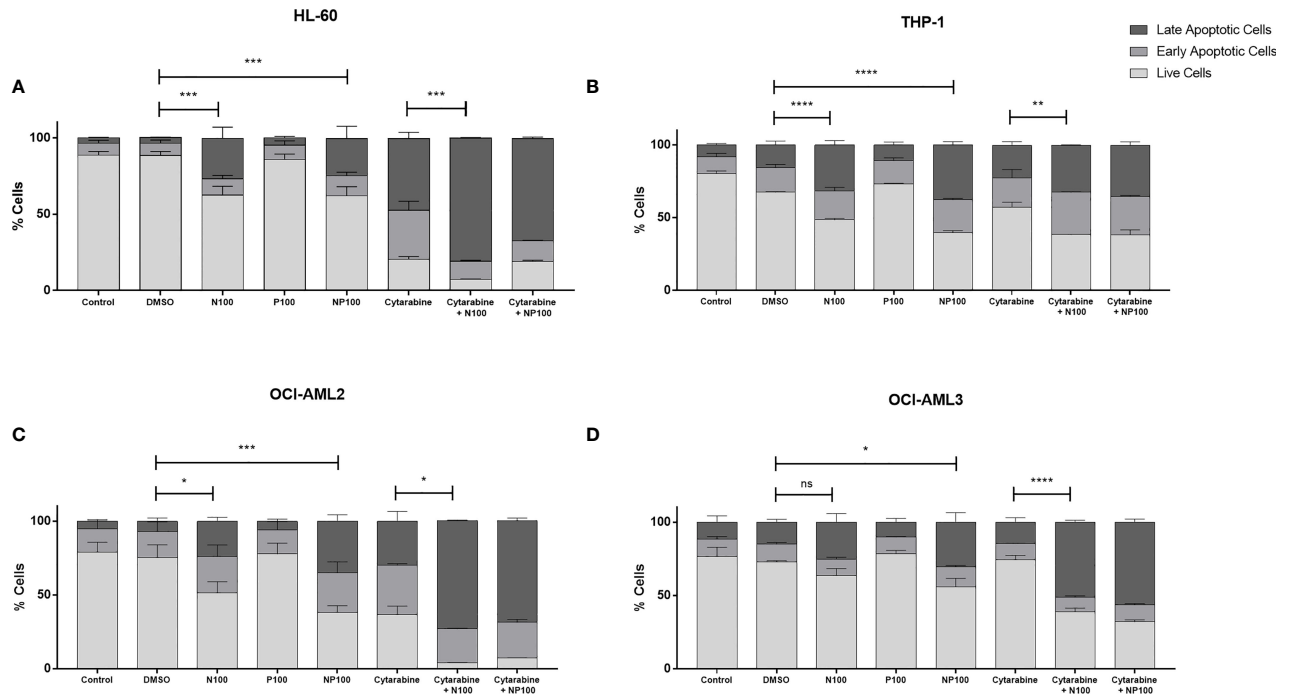

FIGURE 3 | Pro-apoptotic effect of treatment with nimesulide, prednisolone, and cytarabine. Bar graph showing the percentage of apoptotic cells in each cell line. **(A)** HL-60, **(B)** THP-1, **(C)** OCI-AML2, and **(D)** OCI-AML3 after treatment with the drugs alone and in combination for 24 h. The data presented are representative of 2 independent experiments and presented as mean ± SEM (n = 5). The p-value was determined using the two-way ANOVA multiple comparisons with Turkey's correction, *p < 0.05; **p < 0.01; ***p < 0.001; ****p < 0.001. Control: non-treated cells; DMSO: treated with DMSO (dilution vehicle); N100: nimesulide 100 μM; P100: prednisolone 100 μM; NP100: combination of nimesulide and prednisolone 100 μM; Cytarabine: treated with cytarabine 2.5 μM; Cytarabine+N100; combination of nimesulide 100 μM and cytarabine 2.5 μM; Cytarabine+NP100: combination of nimesulide and prednisolone 100 μM and cytarabine 2.5 μM. DMSO, dimethyl sulfoxide. ns, not significant.

and in combination with prednisolone, we decided to perform whole-transcriptome sequencing for each condition. All samples had at least 30 million reads and a Phred Score above Q30. We then performed principal component analysis (PCA) on raw gene expression data, normalized by FPKM (**Supplementary Figure 3**) to evaluate the clustering behavior and to remove possible outliers. We considered four experimental treatment groups (DMSO, prednisolone, nimesulide, and prednisolone plus nimesulide) from two separate experiments (duplicates). We observed that OCI-AML3 clustered significantly distantly from the three other cell lines; therefore, we decided to exclude OCI-AML3 from subsequent analysis. PCA also showed that the samples were clustered by experiment. In order to avoid data distortion while trying to correct this batch effect, we processed and analyzed the data from the two experiments separately, using experiment 2 analysis as a validation of experiment 1.

Due to the biological and genetic heterogeneities of AML cell lines, it is expected that they present dysregulation of different genes, which, however, probably participate in similar functional networks. In order to explore the data in a system-level context, we used WGCNA (18) analysis to assign genes with similar expression patterns into a module. The construction of the network and the gene assignment were obtained by selecting the ~10,000 genes with the greatest variation among the expressed genes, and then, the dendrogram representing the separation of the modules through colors was generated (**Figure 4A**). The gene expression levels for each generated module were then summarized by the first principal component (eigengene module) for each sample, and then we evaluated the correlation of the eigengene module with our variables of interest: treatment (treated vs. untreated cells), cell death level (DMSO vs. prednisolone vs. nimesulide vs. prednisolone plus nimesulide), and cell line (HL60, THP-1, and OCI-AML2). With this analysis, we identified which gene networks (eigengene modules), represented on the y-axis of **Figure 4E**, are correlated with cell lines, treatment, and death levels. The defined significance values were assigned by dividing p = 0.05 by the number of modules generated.

WGCNA of experiment 1 revealed twenty-two modules of co-expressed genes. We observed three modules that showed a significant correlation (p-adj ≤ 0.0022) with death levels: downregulated Lightyellow module (p = 0.00052), whose expression levels are inversely correlated with death levels, and upregulated modules Tan (p = 0.000038) and Lightcyan (p = 0.00025), which showed a positive correlation (**Figure 4E**). In addition to the correlation seen from the three modules with the levels of death, we can observe from the bar plots (**Figures 4B–D**)

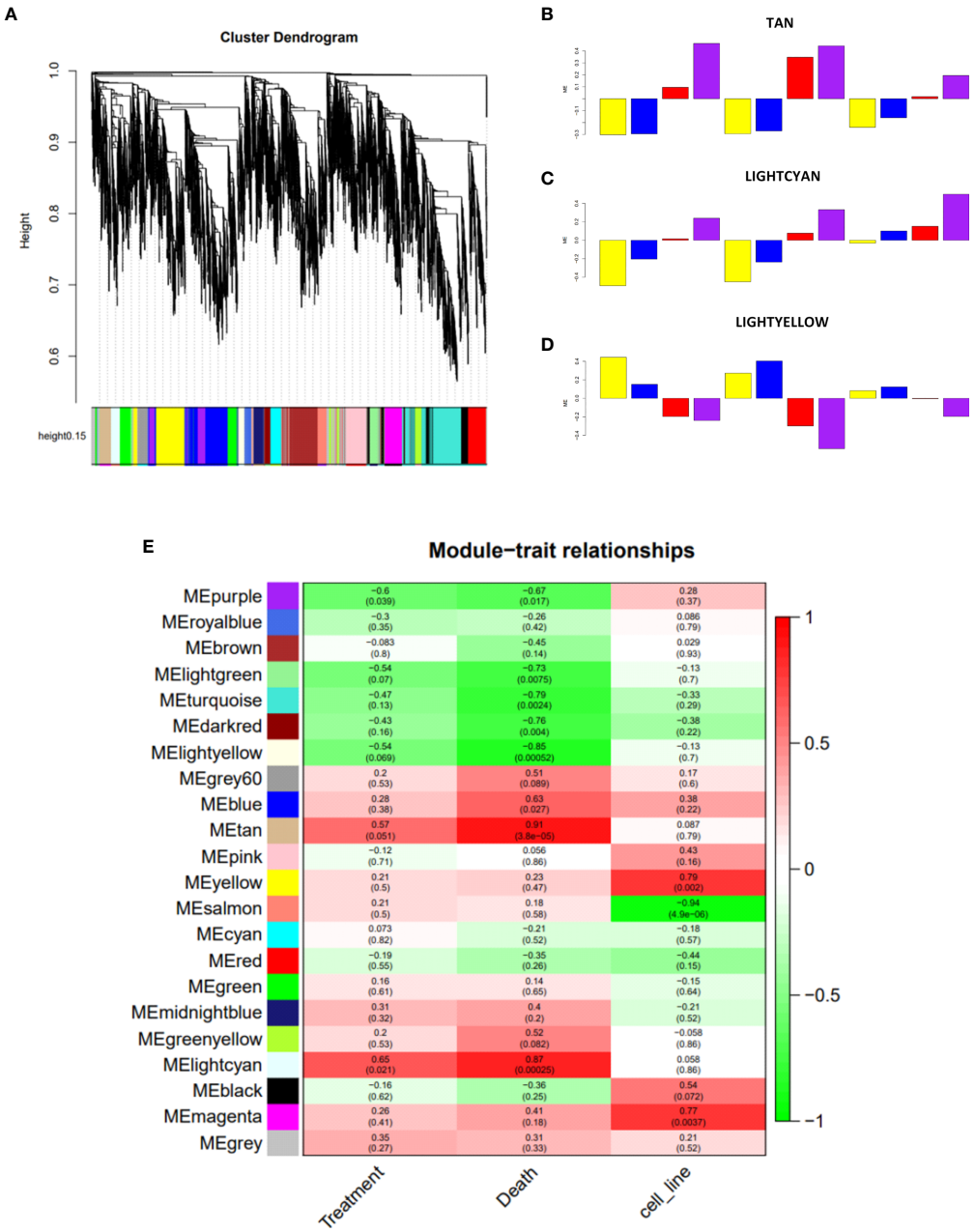

FIGURE 4 | Construction of co-expression network of experiment 1. **(A)** Network analysis dendrogram showing clustering of genes based on topological overlap for identification of modules of co-regulated genes in experiment 1. **(B–D)** Bar plots of the samples representing their variation against the significant modules Tan, Lightcyan, and Lightyellow, respectively. The color of the bar is associated with the group: DMSO (yellow), treatment with prednisolone (blue), treatment with nimesulide (red), and treatment with nimesulide plus prednisolone (purple). The representation of cell lines in bar plots is in the order HL-60, THP-1, and OCI-AML2. **(E)** Module–trait relationships showing the sets of genes (modules) generated for experiment 1 and correlation of the detected modules with the variables treatment, death, and cell line. Each row represents a module eigengene; each column to a trait. Each cell contains the corresponding correlation and p-value. DMSO, dimethyl sulfoxide.

how the expression of each sample of the three cell lines behaves in the face of treatments. The figures show that samples treated with DMSO (yellow bar) and prednisolone (blue bar) are inversely correlated with nimesulide alone (red bar) and combined with prednisolone (purple bar) treatments. The drug combination has a stronger correlation with modules than nimesulide alone. The same WGCNA was performed for experiment 2, and modules were generated and correlated with the same variables (**Supplementary Figure 4**). The biological nature of these significant treatment-associated modules is supported by evidence of protein–protein interaction performed by the STRING platform (**Supplementary Figure 7**).

In order to find common genes identified in both experiments, the overlap between the significant modules from experiment 1 with the significant modules from experiment 2 was determined (**Supplementary Table 1**). We observed that the upregulated Tan module overlapped with the genes of the Turquoise, Red, and Salmon modules from experiment 2; the other upregulated Lightcyan module overlapped with the Turquoise, Red, and Yellow modules; and the downregulated Lightyellow module had overlap with Cyan and Grey60 modules. The number of total genes within each module of both experiments is described in **Supplementary Table 2**.

Functional Enrichment Analysis of Modules

To explore the potential biological function of critical modules, we conducted a functional enrichment analysis. As shown in **Table 1**, the modules upregulated in experiment 1 (Lightcyan and Tan) were significantly enriched for genes related to the regulation of autophagy and apoptotic processes, and the module downregulated (Lightyellow) was significantly enriched for cell cycle and RNA splicing pathways genes. We found enrichment for these same upregulated and downregulated pathways in the modules of experiment 2 that overlapped with experiment 1, thus validating the results found in experiment 1 (**Supplementary Table 3**).

A Subset of Genes Upregulated *In Vitro* Were Also Upregulated in the Patient's Bone Marrow After Nimesulide Treatment

In order to evaluate whether the genes identified in the eigengene modules in the cell line experiments followed the same expression trend among the patient's transcriptomes before and after nimesulide treatment, we adopted the following approach. Since it was not possible to generate a statistical analysis of the patient's data as we had only one transcriptome sample for each treatment time (a total of three transcriptomes), we created two gene expression ratios based on the FPKM ratio for each gene. Ratio 1 was FPKM from D+21 after nimesulide treatment (early) divided by FPKM at diagnosis, and ratio 2 was FPKM from D+63 after nimesulide treatment (late) divided by FPKM at diagnosis. Then, both ratios were ranked from the highest to lowest in order to show at the top of the rank the genes with the highest fold-change and at the bottom of the rank the genes with the lowest fold-change (including downregulated genes). Afterward, we performed an enrichment test to see if the genes from the modules of experiment 1 (Lightyellow, Tan, and Lightcyan) generated by the WGCNA had a non-random distribution along with this ranked list, that is, if upregulated genes tended to occur more on the top or the bottom of the ranks and vice versa.

We verified that when comparing the patient's early rank with the genes from modules from experiment 1, related to autophagy (Lightcyan) and RNA splicing and cell cycle (Lightyellow), those genes presented a non-random distribution, being concentrated among the genes with the highest fold-change, with p-values of 0.003 and 0.004, respectively (**Table 2**). While the expression direction of genes related to autophagy was coherent between cell line and patient transcriptome ratio (upregulated expression), genes related to RNA splicing were not. Therefore, genes associated with autophagy were upregulated after nimesulide treatment both in the patient's transcriptome and in cell line experiments.

We have also evaluated changes in gene expression induced by nimesulide in mutated driver genes in the cell lines. The change in expression of DNMT3A was heterogeneous. While it was slightly reduced in THP1, it was marginally increased in HL60 and OCI-AML3 and significantly increased in OCI-AML3 (**Supplementary Figure 5**). The changes in gene expression of mutated alleles in the cell line OCI-AML3 were not significant (**Supplementary Figure 6**).

Nimesulide Potentiates the Effect of Drugs Approved for Acute Myeloid Leukemia Treatment

To further explore the potential of nimesulide in combination with other approved AML treatments, we evaluated the cytotoxic effects of the following drugs alone and in combination with nimesulide: azacitidine, gilteritinib fumarate, cladribine, doxorubicin hydrochloride, mitoxantrone hydrochloride, fludarabine, thioguanine, and decitabine. Nimesulide potentiates the effect of all chosen AML treatment drugs, decreasing the viability of leukemic cells by different proportions depending on the type of cell line (**Figure 5**). We consider that nimesulide potentiated the drug's action when after its addition there was twice as much death as compared to the drug alone. We observed that nimesulide potentiated the effect of the following drugs: azacitidine, gilteritinib fumarate, cladribine, and fludarabine in the HL-60 cell line; azacitidine, gilteritinib fumarate, cladribine, thioguanine, and decitabine in the THP-1 cell line; azacitidine, fludarabine, thioguanine, and decitabine in the OCI-AML2 cell line; and fludarabine in the OCI-AML3 cell line.

DISCUSSION

In the present work, we reported the first-in-human AML partial remission induced by nimesulide. The response was initially characterized by the acquisition of myeloid lineage markers CD11b, CD13, and CD15 and decreased expression of progenitor antigens, HLA-DR, and CD117 with the posterior reduction in blast count characterizing a partial response. While the patient presented an 82% reduction in bone marrow blast cell counts and complete blast clearance in peripheral blood, serial whole-exome sequencing revealed stability of variant allele frequencies, compatible with differentiation of leukemic blasts. Although rare, partial and complete remissions have been previously described in untreated AML and myelodysplastic syndrome (MDS) patients (19, 20). While the mechanisms involved in such remissions are unknown, there has been speculation about a possible immune-mediated anti-leukemic

TABLE 1 | Enriched pathways relevant to the significant modules of experiment 1.

Upregulated—Lightcyan			
Annotation cluster 1—enrichment score 2.73			
GOTERM_BP_FAT	**No. genes**	**p-Value**	**Genes**
GO:0097576: Vacuole fusion	9	5.1E–4	ATP6V1H, CLEC16A, GABARAPL1, NBR1, RAB24, VIPAS39, VPS33B, VPS39, VPS51, WDR24, WIPI2, ATG13, ATG14, ATG7, CALCOCO2, FAM160A2, FLCN, LGALS8, GAA, GOLGA2, IFT20, MCOLN1, MVB12A, MTMR14, PACS2, PRKAG1, SIRT2, SNAP23, SNAP29, SYT11, SYTL3, STX1A, STX5, TECPR1, TMEM127, TMEM175, TRIM5, TPP1, TSC1, USP30, ULK1, VAT1, ZFYVE1, ZBTB17, ZKSCAN3, ZKSCAN4
GO:0097352: Autophagosome maturation	8	1.1E–3	
GO:0048284: Organelle fusion	17	1.4E–3	
GO:0007033: Vacuole organization	22	2.5E–3	
GO:0006914: Autophagy	35	3.6E–3	
GO:0016236: Macroautophagy	21	6.1E–3	
Upregulated—Tan			
Annotation cluster 11—enrichment score 1.75			
GOTERM_BP_FAT	**No. genes**	**p-Value**	**Genes**
GO:0070059: Intrinsic apoptotic signaling pathway in response to endoplasmic reticulum stress	13	2.2E–4	BRCA1, CEBPB, CREBRF, CHAC1, DDIT3, DDIT4, EDEM1, ERCC6, FYN, JUN, RBCK1, WIPI1, XBP1, ATF3, ATF4, ASNS, ATXN3, CASP4, CTH, DPF2, ERN1, EEF2, EIF2AK3, FOXO3, GCLC, HERPUD1, IVNS1ABP, ITPR1, ITGA6, MAP2K5, MLH1, NRBF2, PMAIP1, PARP16, PPP1R15A, PPP2R5C, P2RX4, RHBDD1, RNF41, SESN2, SIAH1, SIRT1, STC2, TRIB3, TRIM39, TP63, TPT1, USP25
GO:0034976: Response to endoplasmic reticulum stress	29	1.9E–2	
GO:0097193: Intrinsic apoptotic signaling pathway	23	8.9E–2	
GO:0097190: Apoptotic signaling pathway	36	2.6E–1	
Downregulated—Lightyellow			
Annotation cluster 1—enrichment score 5.87			
GOTERM_BP_FAT	**No. genes**	**p-Value**	**Genes**
GO:0006397: mRNA processing	49	4.8E–8	BMS1, CNOT11, DCAF13, FASTKD5, DDX1, GAR1, RBM25, DBR1, DDX46, EIF4A3, HNRNPU, CCAR1, UBL5, SNRPD1, MAGOH, ZNF326, SNRPD3, TXNL4A, RBM17, THOC3, RBMXL1, SARNP, FASTKD5, STRAP, PPIH, SNRPE, SNRPF, HNRNPH3, AURKAIP1, SNRPC, LUC7L2, SRSF9, SF3B4, SLBP, U2AF1, CCNB1, POLR2B, POLR2C, LEO1, SAP18, POLR2K, HNRNPA0, LSM1, CWC15, LSM3, HNRNPM, SNRNP40, LSM6, PHF5A, HNRNPK, HNRNPC, TARDBP, HSPA1B, HSPA1A, THUMPD1, TSR3, DBR1, EXOSC3, EXOSC9, MTFMT, PIN4, RRP36, RPS27L, SLBP, TRMT10C, TGFB1, ZC3HAV1, ZBTB8OS
GO:0006396: RNA processing	63	9.9E–4	
GO:0008380: RNA splicing	44	1.2E–7	
GO:0000375: RNA splicing *via* transesterification reactions	37	1.5E–7	
GO:0000377: RNA splicing *via* transesterification reactions with bulged adenosine	36	3.5E–7	
GO:0000398: mRNA splicing *via* spliceosome	36	3.5E–7	
GO:0016071: mRNA metabolic process	53	7.4E–5	
Annotation cluster 10—enrichment score 3.9			
GOTERM_BP_FAT	**No. genes**	**p-Value**	**Genes**
GO:1901990: Regulation of mitotic cell cycle phase transition	33	9.3E–6	BUB1, BUB3, CNOT11, NAE1, NEK6, RAD1, RINT1, SKP1, TRIAP1, AURKAIP1, BIRC5, CALM2, CUL3, CCNB1, FEN1, HDAC8, NUSAP1, PIK3R4, PCNA, PSMC2, PSMC3, PSMD1, PSMD10, PSMD11, PSMD6, PSMD7, PSMD9, PSME3, PSMA2, PSMA3, PSMA4, PSMA5, PSMA6, PSMB1, PSMB2, PSMB5, RPA2, RPS27L, RNF4, TGFB1, UBE2C
GO:1901987: Regulation of cell cycle phase transition	33	2.1E–5	
GO:0010564: Regulation of cell cycle process	41	5.7E–4	
GO:0007346: Regulation of mitotic cell cycle	35	2.3E–3	

effect, since an episode of infection is commonly associated with the responses (19). We believe this was not the case in our patient, since there was no infection associated and blast differentiation has not been described and is neither expected, as a result of the immune-mediated anti-leukemic effect. An anti-leukemic effect of nimesulide has been previously demonstrated *in vitro* (11, 12) and a xenograft model (13), suggesting that this compound may become clinically relevant for AML treatment.

TABLE 2 | Correlation of the patient's ranked genes with modules of experiment 1.

Correlation	Number of genes	Expression	p-Value
Tan–Early	746	Up	0.413476285050312
Tan–Late	752	Up	0.326814219505457
Lightcyan–Early	618	Up	0.00366376723337888
Lightcyan–Late	618	Down	0.960253266351426
Lightyellow–Early	478	Up	0.00462018230578614
Lightyellow–Late	482	Down	0.653726520709975

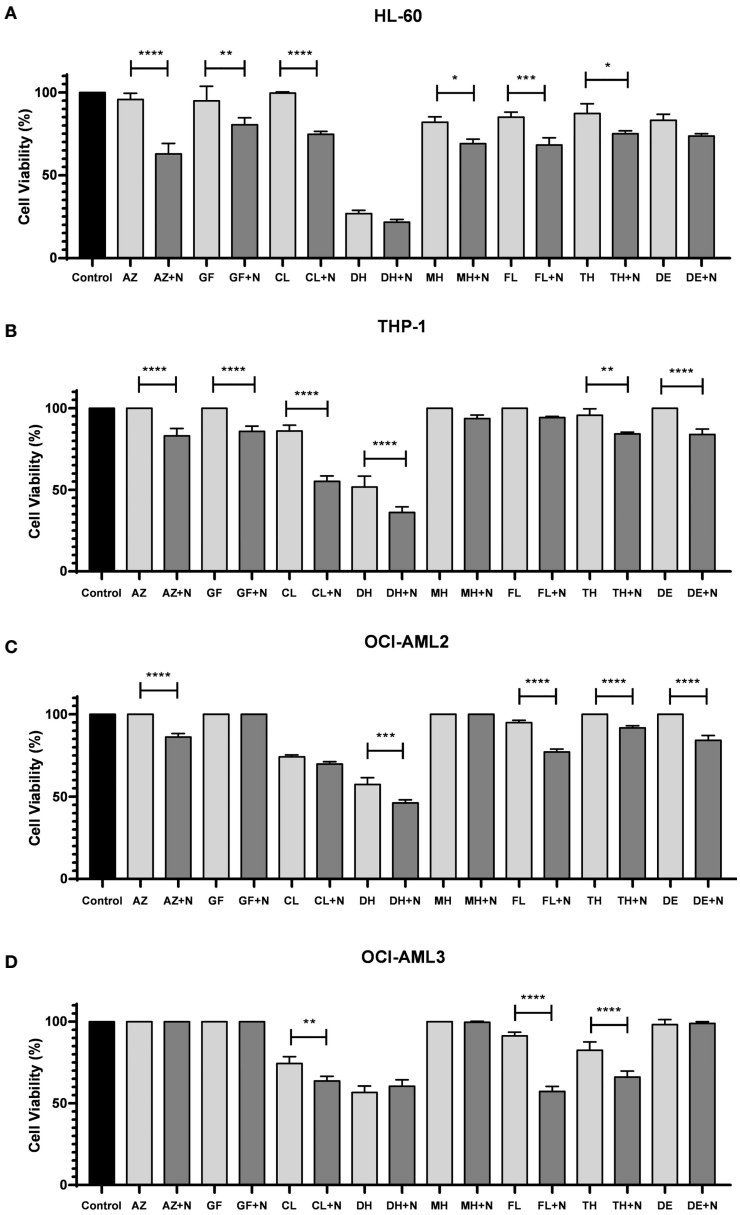

FIGURE 5 | Cell viability assay after treatment with selected FDA-approved anti-AML drugs combined with nimesulide. **(A–D)** Bar graph showing cell viability on cell lines (HL-60, THP-1, OCI-AML2, and OCI-AML3) after being treated and incubated for 24 h. Data shown are representative of an independent experiment in triplicate and presented as mean ± SD (n = 3). The p-value was determined using the one-way ANOVA comparing the drug alone and in combination with nimesulide, *$p < 0.05$; **$p < 0.01$; ***$p < 0.001$; ****$p < 0.0001$. Control: DMSO. N, nimesulide; AZ, azacitidine; GF, gilteritinib fumarate; CL, cladribine; DH, doxorubicin hydrochloride; MH, mitoxantrone hydrochloride; FL, fludarabine; TH, thioguanine; DE, decitabine; FDA, Food and Drug Administration; AML, acute myeloid leukemia; DMSO, dimethyl sulfoxide.

We recognize that the duration of the response was short, lasting approximately 3 months, but it is worth mentioning that even venetoclax and midostaurin, both FDA-approved therapies for AML, showed limited efficacy with short duration responses as single agents (21, 22), making the combination with other drugs necessary.

We have also confirmed the previously described *in vitro* induction of cell death and cell cycle arrest in AML cell lines treated with COX-2 inhibitors, including nimesulide (11, 12), and we characterized the biological mechanisms associated with this effect. Since our patient was using prednisolone when nimesulide was started, we included samples treated with prednisolone only, nimesulide only, and the combination in our experimental design to evaluate a possible synergistic effect. Even though there are findings suggesting a role for glucocorticoids in the treatment of AML in specific settings (23, 24), we could not detect an anti-leukemic activity in our experiments with prednisolone alone, but it potentiated the pro-apoptotic and cell cycle effects of nimesulide in three out of four cell lines tested, suggesting that the combination of nimesulide and prednisolone may have had a role in the observed partial response. We could not demonstrate the previously described *in vitro* differentiation of leukemic blasts induced by COX inhibitors, including nimesulide (11, 12), since DMSO alone induced the expression of myeloid differentiation markers (data not shown). We have confirmed the previously described MYC downregulation induced by COX-inhibitors in AML (12) and revealed novel mechanisms. The most significant changes induced by treatment were upregulation of genes associated with apoptosis and autophagy and downregulation of cell cycle and RNA splicing-associated genes.

To further understand if these cellular processes identified in the *in vitro* studies were also operating in the patient's cells, we evaluated gene expression changes associated with *in vivo* partial response induced by nimesulide treatment. Genes associated with autophagy were also upregulated in the patient's cell after treatment with nimesulide, confirming the *in vitro* findings. Autophagy has context-dependent roles in cancer, and interventions to stimulate or inhibit autophagy have been proposed as cancer therapies (25–27), including AML (28), and tested in clinical trials for different tumor types (29–32). In addition, it has been previously shown that autophagy plays a crucial role in hematopoietic differentiation at several stages, including myeloid differentiation (33). Further studies are necessary to better characterize the role of autophagy in cell death induction mediated by the use of nimesulide. Another commonality between *in vitro* and *in vivo* findings was the upregulation of DNMT3A after treatment with nimesulide both in the patient sample and in the OCI3-AML cell line (**Figure 1D** and **Supplementary Figure 5**). Of note, OCI-AML3 was the closest cell line in terms of gene mutations when compared to the patient, since both have mutations in DNMT3A, NPM1, and NRAS. It is possible that DNMT3A may have a role in the response to nimesulide observed in our patients since it has been shown that DNMT3A is essential for hematopoietic differentiation (34). Nevertheless, heterozygous mutation, as observed in AML, including our patient, normally does not affect differentiation and has no phenotype in animal models (35). Further studies are necessary to clarify the role of DNMT3A in the response to nimesulide.

Finally, we recognize that nimesulide is unlikely to benefit AML patients as a single agent; therefore, we explored the potential of combining nimesulide with established anti-AML therapies. Nimesulide potentiates the effect of drugs already approved for AML, suggesting that nimesulide may have a role in combination with standard AML treatment.

In conclusion, we have described the first-in-human AML partial response induced by nimesulide and demonstrated upregulation of autophagy associated genes after treatment with nimesulide both *in vitro* and *in vivo*. In addition, we have shown that *in vitro* combination of nimesulide with anti-AML FDA-approved therapies increases cell death, suggesting a potential for the utilization of this drug in AML treatment.

DATA AVAILABILITY STATEMENT

The datasets presented in this study can be found in online repositories. The names of the repository/repositories and accession number(s) can be found below: NCBI's Sequence Read Archive (SRA) with BioProject ID: PRJNA817613 (https://www.ncbi.nlm.nih.gov/bioproject/PRJNA817613).

ETHICS STATEMENT

The studies involving human participants were reviewed and approved by Plataforma Brasil. The patients/participants provided their written informed consent to participate in this study. CAAE 50594315.7.1001.007 and CAAE 19826619.60000.0071.

AUTHOR CONTRIBUTIONS

All authors had direct contributions to the elaboration of this manuscript. The first author, VT, contributed to the performance of the *in vitro* experiments, preparation of samples for sequencing, analysis of cellular and bioinformatics data, and writing of this manuscript. RP performed the raw sequencing data alignment and the recall of variants of the patient samples and performed with KG-O the WGCNA. BC performed the drug screening experiment. The FS and NH contributed to the review of the bioinformatics and clinical data analysis, respectively. PC contributed to the creation of the experimental design of the project and critical analysis of the results and writing of this manuscript. All authors listed have made a substantial, direct, and intellectual contribution to the work and approved it for publication.

FUNDING

This work was supported by grants from Programa Nacional de Apoio à Atenção Oncológica (PRONON) and The Applebaum Foundation.

ACKNOWLEDGMENTS

We acknowledge the support of the platform Varstation for part of the genomic analysis and would like to thank the patient described in this study for her commitment to improving our understanding of her disease.

SUPPLEMENTARY MATERIAL

The Supplementary Material for this article can be found online at: https://www.frontiersin.org/articles/10.3389/fonc.2022.874168/full#supplementary-material

REFERENCES

1. Coombs CC, Tallman MS, Levine RL. Molecular Therapy for Acute Myeloid Leukaemia. *Nat Rev Clin Oncol* (2016) 13(5):305–18. doi: 10.1038/nrclinonc.2015.210
2. Datoguia TS, Velloso EDRP, Helman R, Musacchio JC, Salvino MA, Soares RA, et al. Overall Survival of Brazilian Acute Myeloid Leukemia Patients According to the European LeukemiaNet Prognostic Scoring System: A Cross-Sectional Study. *Med Oncol* (2018) 35(11):141. doi: 10.1007/s12032-018-1179-3
3. Khwaja A, Bjorkholm M, Gale RE, Levine RL, Jordan CT, Ehninger G, et al. Acute Myeloid Leukaemia. *Nat Rev Dis Primers* (2016) 2:16010. doi: 10.1038/nrdp.2016.10
4. Campregher PV, Hamerschlak N, Colturato VA, Mauad MA, Souza MP, Bouzas LFS, et al. Survival and Graft-Versus-Host Disease in Patients Receiving Peripheral Stem Cell Compared to Bone Marrow Transplantation From HLA-Matched Related Donor: Retrospective Analysis of 334 Consecutive Patients. *Eur J Haematol* (2015) 95(5):421–5. doi: 10.1111/ejh.12508
5. Shimoni A, Labopin M, Savani B, Volin L, Ehninger G, Kuball J, et al. Long-Term Survival and Late Events After Allogeneic Stem Cell Transplantation From HLA-Matched Siblings for Acute Myeloid Leukemia With Myeloablative Compared to Reduced-Intensity Conditioning: A Report on Behalf of the Acute Leukemia Working Party of European Group for Blood and Marrow Transplantation. *J Hematol Oncol* (2016) 9(1):118. doi: 10.1186/s13045-016-0347-1
6. Bertolini F, Sukhatme VP, Bouche G. Drug Repurposing in Oncology–Patient and Health Systems Opportunities. *Nat Rev Clin Oncol* (2015) 12(12):732–42. doi: 10.1038/nrclinonc.2015.169
7. Singhal S, Mehta J, Desikan R, Ayers D, Roberson P, Eddlemon P, et al. Antitumor Activity of Thalidomide in Refractory Multiple Myeloma. *N Engl J Med* (1999) 341(21):1565–71. doi: 10.1056/NEJM199911183412102
8. Richardson PG, Schlossman RL, Weller E, Hideshima T, Mitsiades C, Davies F, et al. Immunomodulatory Drug CC-5013 Overcomes Drug Resistance and Is Well Tolerated in Patients With Relapsed Multiple Myeloma. *Blood* (2002) 100(9):3063–7. doi: 10.1182/blood-2002-03-0996
9. Benson AB, Venook AP, Al-Hawary MM, Arain MA, Chen YJ, Ciombor KK, et al. Colon Cancer, Version 2.2021, NCCN Clinical Practice Guidelines in Oncology. *J Natl Compr Canc Netw* (2021) 19(3):329–59. doi: 10.6004/jnccn.2021.0012
10. Protheroe A, Edwards JC, Simmons A, Maclennan K, Selby P. Remission of Inflammatory Arthropathy in Association With Anti-CD20 Therapy for Non-Hodgkin's Lymphoma. *Rheumatol (Oxford)* (1999) 38(11):1150–2. doi: 10.1093/rheumatology/38.11.1150
11. Singh R, Cadeddu RP, Fröbel J, Wilk CM, Bruns I, Zerbini LF, et al. The Non-Steroidal Anti-Inflammatory Drugs Sulindac Sulfide and Diclofenac Induce Apoptosis and Differentiation in Human Acute Myeloid Leukemia Cells Through an AP-1 Dependent Pathway. *Apoptosis* (2011) 16(9):889–901. doi: 10.1007/s10495-011-0624-y
12. Sobolewski C, Cerella C, Dicato M, Diederich M. Cox-2 Inhibitors Induce Early C-Myc Downregulation and Lead to Expression of Differentiation Markers in Leukemia Cells. *Cell Cycle* (2011) 10(17):2978–93. doi: 10.4161/cc.10.17.16460
13. Zhang Y, Wang J, Wheat J, Chen X, Jin S, Sadrzadeh H, et al. AML1-ETO Mediates Hematopoietic Self-Renewal and Leukemogenesis Through a COX/β-Catenin Signaling Pathway. *Blood* (2013) 121(24):4906–16. doi: 10.1182/blood-2012-08-447763
14. Bertoli S, Picard M, Bérard E, Griessinger E, Larrue C, Mouchel PL, et al. Dexamethasone in Hyperleukocytic Acute Myeloid Leukemia. *Haematologica* (2018) 103(6):988–98. doi: 10.3324/haematol.2017.184267
15. Langfelder P, Horvath S. WGCNA: An R Package for Weighted Correlation Network Analysis. *BMC Bioinf* (2008) 9:559. doi: 10.1186/1471-2105-9-559
16. Wu D, Smyth GK. Camera: A Competitive Gene Set Test Accounting for Inter-Gene Correlation. *Nucleic Acids Res* (2012) 40(17):e133. doi: 10.1093/nar/gks461
17. Döhner H, Estey E, Grimwade D, Amadori S, Appelbaum FR, Büchner T, et al. Diagnosis and Management of AML in Adults: 2017 ELN Recommendations From an International Expert Panel. *Blood* (2017) 129(4):424–47. doi: 10.1182/blood-2016-08-733196
18. Ye F, Huang W, Guo G. Studying Hematopoiesis Using Single-Cell Technologies. *J Hematol Oncol* (2017) 10(1):27. doi: 10.1186/s13045-017-0401-7
19. Petti MC, Latagliata R, Breccia M, Alimena G, Spadea A, D'Andrea M, et al. Spontaneous Remission in Adult Patients With *De Novo* Myelodysplastic Syndrome: A Possible Event. *Haematologica* (2001) 86(12):1277–80. doi: 10.3324/%x
20. Rashidi A, Fisher SI. Spontaneous Remission of Acute Myeloid Leukemia. *Leuk Lymphoma* (2015) 56(6):1727–34. doi: 10.3109/10428194.2014.970545
21. Konopleva M, Pollyea DA, Potluri J, Chyla B, Hogdal L, Busman T, et al. Efficacy and Biological Correlates of Response in a Phase II Study of Venetoclax Monotherapy in Patients With Acute Myelogenous Leukemia. *Cancer Discovery* (2016) 6(10):1106–17. doi: 10.1158/2159-8290.CD-16-0313
22. Fischer T, Stone RM, Deangelo DJ, Galinsky I, Estey E, Lanza C, et al. Phase IIB Trial of Oral Midostaurin (PKC412), the FMS-Like Tyrosine Kinase 3 Receptor (FLT3) and Multi-Targeted Kinase Inhibitor, in Patients With Acute Myeloid Leukemia and High-Risk Myelodysplastic Syndrome With Either Wild-Type or Mutated FLT3. *J Clin Oncol* (2010) 28(28):4339–45. doi: 10.1200/JCO.2010.28.9678
23. Miyoshi H, Ohki M, Nakagawa T, Honma Y. Glucocorticoids Induce Apoptosis in Acute Myeloid Leukemia Cell Lines With A T(8;21) Chromosome Translocation. *Leuk Res* (1997) 21(1):45–50. doi: 10.1016/s0145-2126(96)00089-6
24. Lu L, Wen Y, Yao Y, Chen F, Wang G, Wu F, et al. Glucocorticoids Inhibit Oncogenic RUNX1-ETO in Acute Myeloid Leukemia With Chromosome Translocation T(8;21). *Theranostics* (2018) 8(8):2189–201. doi: 10.7150/thno.22800
25. Parzych KR, Klionsky DJ. An Overview of Autophagy: Morphology, Mechanism, and Regulation. *Antioxid Redox Signal* (2014) 20(3):460–73. doi: 10.1089/ars.2013.5371
26. Levy JMM, Towers CG, Thorburn A. Targeting Autophagy in Cancer. *Nat Rev Cancer* (2017) 17(9):528–42. doi: 10.1038/nrc.2017.53
27. Machado-Neto JA, Coelho-Silva JL, Santos FPS, Scheucher PS, Campregher PV, Hamerschlak N, et al. Autophagy Inhibition Potentiates Ruxolitinib-Induced Apoptosis in JAK2V617F Cells. *Invest New Drugs* (2020) 38(3):733–45. doi: 10.1007/s10637-019-00812-5
28. Spinello I, Saulle E, Quaranta MT, Pasquini L, Pelosi E, Castelli G, et al. The Small-Molecule Compound AC-73 Targeting CD147 Inhibits Leukemic Cell Proliferation, Induces Autophagy and Increases the Chemotherapeutic

Sensitivity of Acute Myeloid Leukemia Cells. *Haematologica* (2019) 104 (5):973–85. doi: 10.3324/haematol.2018.199661
29. Wolpin BM, Rubinson DA, Wang X, Chan JA, Cleary JM, Enzinger PC, et al. Phase II and Pharmacodynamic Study of Autophagy Inhibition Using Hydroxychloroquine in Patients With Metastatic Pancreatic Adenocarcinoma. *Oncologist* (2014) 19(6):637–8. doi: 10.1634/theoncologist.2014-0086
30. Rangwala R, Chang YC, Hu J, Algazy KM, Evans TL, Fecher LA, et al. Combined MTOR and Autophagy Inhibition: Phase I Trial of Hydroxychloroquine and Temsirolimus in Patients With Advanced Solid Tumors and Melanoma. *Autophagy* (2014) 10(8):1391–402. doi: 10.4161/auto.29119
31. Vogl DT, Stadtmauer EA, Tan KS, Heitjan DF, Davis LE, Pontiggia L, et al. Combined Autophagy and Proteasome Inhibition: A Phase 1 Trial of Hydroxychloroquine and Bortezomib in Patients With Relapsed/Refractory Myeloma. *Autophagy* (2014) 10(8):1380–90. doi: 10.4161/auto.29264
32. Kanzawa T, Kondo Y, Ito H, Kondo S, Germano I. Induction of Autophagic Cell Death in Malignant Glioma Cells by Arsenic Trioxide. *Cancer Res* (2003) 63(9):2103–8.
33. Riffelmacher T, Simon AK. Mechanistic Roles of Autophagy in Hematopoietic Differentiation. *FEBS J* (2017) 284(7):1008–20. doi: 10.1111/febs.13962
34. Challen GA, Sun D, Jeong M, Luo M, Jelinek J, Berg JS, et al. Dnmt3a Is Essential for Hematopoietic Stem Cell Differentiation. *Nat Genet* (2011) 44 (1):23–31. doi: 10.1038/ng.1009
35. Celik H, Mallaney C, Kothari A, Ostrander EL, Eultgen E, Martens A, et al. Enforced Differentiation of Dnmt3a-Null Bone Marrow Leads to Failure With C-Kit Mutations Driving Leukemic Transformation. *Blood* (2015) 125 (4):619–28. doi: 10.1182/blood-2014-08-594564

Conflict of Interest: Author RP was employed by company Grupo Pardini.

The remaining authors declare that the research was conducted in the absence of any commercial or financial relationships that could be construed as a potential conflict of interest.

Publisher's Note: All claims expressed in this article are solely those of the authors and do not necessarily represent those of their affiliated organizations, or those of the publisher, the editors and the reviewers. Any product that may be evaluated in this article, or claim that may be made by its manufacturer, is not guaranteed or endorsed by the publisher.

frontiers | Frontiers in Oncology

ORIGINAL RESEARCH
published: 05 July 2022
doi: 10.3389/fonc.2022.926296

Transcriptome Profiling of N7-Methylguanosine Modification of Messenger RNA in Drug-Resistant Acute Myeloid Leukemia

Bing Zhang[1], *Dong Li*[1] *and Ran Wang*[2*]

[1] Department of Pediatrics, Qilu Hospital of Shandong University, Shandong, China, [2] Department of Hematology, Qilu Hospital of Shandong University, Shandong, China

Acute myeloid leukemia (AML) is an aggressive hematological tumor caused by the malignant transformation of myeloid progenitor cells. Although intensive chemotherapy leads to an initial therapeutic response, relapse due to drug resistance remains a significant challenge. In recent years, accumulating evidence has suggested that post-transcriptional methylation modifications are strongly associated with tumorigenesis. However, the mRNA profile of m7G modification in AML and its role in drug-resistant AML are unknown. In this study, we used MeRIP-seq technology to establish the first transcriptome-wide m7G methylome profile for AML and drug-resistant AML cells, and differences in m7G between the two groups were analyzed. In addition, bioinformatics analysis was conducted to explore the function of m7G-specific methylated transcripts. We found significant differences in m7G mRNA modification between AML and drug-resistant AML cells. Furthermore, bioinformatics analysis revealed that differential m7G-modified mRNAs were associated with a wide range of cellular functions. Importantly, down-methylated m7G modification was significantly enriched in ABC transporter-related mRNAs, which are widely recognized to play a key role in multidrug resistance. Our results provide new insights into a novel function of m7G methylation in drug resistance progression of AML.

Keywords: N7-methylguanosine(m7G), messenger RNA (mRNA), drug-resistant, acute myeloid leukemia (AML), bioinformatics analysis

OPEN ACCESS

Edited by:
Spiros Vlahopoulos, University of Athens, Greece

Reviewed by:
Çagdas Aktan, Beykent University, Turkey
John Charles Rotondo, University of Ferrara, Italy

***Correspondence:**
Ran Wang
wangran_78@126.com

Specialty section:
This article was submitted to Hematologic Malignancies, a section of the journal Frontiers in Oncology

Received: *22 April 2022*
Accepted: *09 June 2022*
Published: *05 July 2022*

Citation:
Zhang B, Li D and Wang R (2022) Transcriptome Profiling of N7-Methylguanosine Modification of Messenger RNA in Drug-Resistant Acute Myeloid Leukemia. Front. Oncol. 12:926296. doi: 10.3389/fonc.2022.926296

INTRODUCTION

Acute myeloid leukemia (AML) is a heterogeneous malignant clonal disease caused by the proliferation of hematopoietic stem or progenitor cells by gene mutation. Approximately 50% of young and middle-aged patients and over 80% of elderly patients with AML die each year due to primary drug resistance, relapse after remission, and treatment-related complications (1). Although a variety of new drugs are currently undergoing clinical trials, AML therapies have not yet broken through the classic treatment of anthracyclines combined with cytarabine. Although allogeneic hematopoietic stem cell transplantation is the most effective method for AML treatment, the limitation of suitable populations restricts its application (2). Therefore, there is an urgent need for

drug development to improve the overall survival rate and quality of life of AML patients. In the past decade, researchers have identified many recurrent gene mutations involved in the coding of epigenetic regulatory proteins through gene sequencing, suggesting that the occurrence of leukemia is closely related to abnormal epigenetic modifications and that abnormal RNA methylation is an important mechanism (3, 4).

RNA methylation regulates gene expression at the post-transcriptional level and is considered another layer of epigenetic regulation similar to DNA methylation and histone modification. At present, over 150 RNA methylation modifications have been identified as post-transcriptional regulatory markers in eukaryotes, and these modifications can regulate biological metabolic processes such as RNA alternative splicing, nuclear export, stabilization, and translation (5, 6). Methylation modifications of RNA mainly include N6-methyladenosine(m6A), 5-methylcytosine C5-methylcytidine (m5C), N1-methyladenosine(m1A), and 7-methylguanosine (m7G). Among these, the m7G modification is one of the most common methylation modifications in post-transcriptional regulation and is widely distributed in the 5'cap region of tRNA, rRNA, and mRNA in eukaryotes. This modification occurs during the initial stages of transcription and before other RNA-processing events (7).

Recent studies have confirmed that m7G modification is involved in the regulation of multiple processes such as mRNA transcription, splicing, nuclear export, and translation (8, 9). However, while m5C and m6A methylation modifications have been widely studied in many diseases (10, 11), few studies have been conducted on m7G methylation. In recent years, high-throughput sequencing methods for m7G modifications within the transcriptome have gradually advanced (12, 13). In 2019, Zhang et al. developed m7G-MeRIP sequencing (MeRIP-seq) for transcriptional profiling of m7G methylation in human cells (14).

To further investigate the role of m7G in drug resistance in AML cells, we used MeRIP-seq technology to establish the first known transcriptome-wide m7G methylome profile for the AML cell line HL60 and AML drug-resistant cell line. The mRNA levels in HL60 and HL60/MX2 cells were characterized by m7G-specific analysis and in-depth bioinformatics analysis. Additionally, RNA-seq was used to detect differentially expressed genes, and a combined analysis of differentially methylated and expressed genes was performed.

In this study, our results showed that there were significant differences in the genes modified by m7G methylation in AML-resistant cells, and the number of methylated genes and peaks in drug-resistant cells was greater than those in non-resistant cells. In AML drug-resistant cells, a large number of tumor-related gene m7G methylation changes can result in altered mRNA expression. Bioinformatics analysis revealed that the methylation of the two groups was different, which may lead to variable changes in cell function. Our study suggests a possible association between AML and m7G methylation in mRNA and predicts the functional changes that may arise from the difference in m7G methylation, which could be a breakthrough for improving AML treatment.

MATERIALS AND METHODS

Cell Lines and Cell Culture

Human promyelotic HL60 and HL60/MX2 cells were obtained from the American Type Culture Collection. The cells were grown in RPMI-1640 (Gibco, USA) supplemented with 10% heat-inactivated fetal calf serum (Gibco, USA) and 1% (v/v) antibiotics (penicillin-streptomycin) (Gibco, USA) in a humidified 5% CO_2 atmosphere at 37°C (15).

RNA Extraction and Fragmentation

Cells in the logarithmic growth phase were collected, total RNA was extracted using TRIzol reagent (Invitrogen Corporation, CA, USA) following the manufacturer's instructions, and RNA concentration was measured using a NanoDrop ND-100 (Thermo Fisher Scientific, Waltham, MA, USA). The purity of the RNA was evaluated based on its OD260/OD280 ratio. If the OD260/OD280 value range was 1.8 ~ 2.1, the RNA purity was qualified. Denaturing agarose gel electrophoresis was used to measure the RNA integrity and gDNA contamination.

Merip Library Construction and Sequencing

m7G-IP-Seq service was provided by CloudSeq Inc. (Shanghai, China). mRNA was isolated from total RNA with oligo(dT) magnetic beads (ThermoFisher) and subjected to immunoprecipitation using the GenSeqTM m7G-IP Kit (GenSeq Inc., China) according to the manufacturer's instructions. Briefly, RNA was decapped with tobacco decapping enzyme and randomly fragmented to ~200 nt using RNA fragmentation reagents. Protein A/G beads were coupled to the m7G antibody by rotation at room temperature for 1 h. RNA fragments were incubated with bead-linked antibodies and rotated at 4°C for 4 h. The RNA/antibody complexes were then digested with proteinase K, and the eluted RNA was purified by phenol:chloroform extraction. RNA libraries for IP and input samples were constructed using the NEBNext Ultra II Directional RNA Library Prep Kit (New England Biolabs, Inc., USA) according to the manufacturer's instructions. Libraries were qualified using an Agilent 2100 Bioanalyzer and sequenced on a NovaSeq platform (Illumina).

Sequencing Data Analysis of m7G Modification Peaks

Paired-end reads were harvested from the Illumina NovaSeq 6000 sequencer and quality was controlled by Q30. Cutadapt software (v1.9.3) was used for 3' adaptor trimming, removing low-quality reads, and obtaining high-quality clean reads (16). First, clean reads of the input libraries were aligned to the reference genome (UCSC HG19) using STAR software (17). Then, mRNAs were identified by DCC software using STAR alignment results (18). Next, clean reads from all libraries were aligned to the reference genome using Hisat2 software (v2.0.4) (19). Methylated sites on mRNAs (peaks) were identified using MACS software (20). Differentially methylated sites were identified using diffReps (21). The peaks identified by both

software overlapping with the exons of the protein-coding genes were identified and chosen by homemade scripts.

Dreme software was used to detect the sequence of the methylation peaks to identify meaningful motifs. The E value of the motif is the enrichment P value multiplied by the number of candidate motifs tested; the enrichment P value uses Fisher's exact test method to enrich the motifs in the positive sequence. The E value of the motif is negatively correlated with its credibility; that is, the lower the E value, the higher the credibility. GO analysis and KEGG pathway enrichment analysis were performed to determine the genes of differentially methylated mRNAs.

Transcriptome Sequencing Analysis and Statistical Analysis

The high-quality reads were aligned to the human reference genome (UCSC hg19) using hisat2 software (v2.0.4). Guided by the Ensembl gtf gene annotation file, cuffdiff software (v2.2.1, part of cufflinks) was used to obtain the FPKM as the expression profiles of mRNA, and fold change and p-value were calculated based on FPKM to screen differentially expressed mRNAs. Fold change ≥ 2, p-value ≤ 0.05, and FPKM value ≥ 0.5 in at least one sample were used as the criteria for screening differential mRNA.

Statistical analysis was performed using SPSS 25.0 and GraphPad Prism 8.0. Student's two-tailed t-test was used to compare significant differences between the two groups. Differences were defined as statistically significant at $p < 0.05$.

RESULTS

General Features of m7G Methylation in HL60 and HL60/MX2 Cells

RNA sequencing and transcriptome-wide m7G methylation sequencing assays were performed in HL60 and HL60/MX2 cells. In the HL-60 group, we found 8070 clean methylation peaks representing transcripts of 5571 genes. A total of 8122 peaks were identified in the HL60/MX2 group, corresponding to 5979 gene transcripts. Notably, only 495 identical peaks appeared in both groups. HL60/MX2 group had 7627 unique peaks and 7575 missing peaks compared to HL60, indicating that the m7G methylation modification features were significantly different between HL60 and HL60/MX2 cells. The average number of peaks per gene among the unique methylated genes in HL60 cells was 2.47, compared to 2.19 in HL60/MX2 cells (**Figures 1A, B**).

Distribution Characteristics of m7G Methylation

Analysis of the distribution of m7G peaks of mRNA on different chromosomes found that there were differences in the number and distribution of m7G peaks on each chromosome. Among these, the number of m7G peaks on chromosomes 1 and 2 was the highest and the number of m7G peaks on chromosome 21 was the lowest. From the comparison of m7G peaks between the two groups, the most obvious differences were identified on chromosomes 6 and 19. In addition, autosome methylation levels were generally higher than those of the sex chromosomes in both groups (**Figures 1C, D**). As shown in **Figure 1E**, when we counted the number of m7G peaks for each mRNA in the two groups, we found that most methylated mRNAs in HL60 and HL60/MX2 cells had only one m7G peak (70.8% and 74.3%, respectively). In the two groups, approximately 20% of the genes recorded two m7G peaks, and less than 10% of the genes contained more than three m7G peaks, which was consistent with previous studies of methylation in other diseases (22, 23). We performed a statistical analysis of the length of the methylation peak, and our results revealed that there was no statistically significant difference between the two groups. The average length of the methylation peak was 114.82 nt (**Figure 1F**).

Analysis of Differentially-Regulated m7G Methylation Genes

To explore the differential expression of m7G methylated genes in HL60 and HL60/MX2 cells, we performed statistical analysis on the m7G-modified genes of the two groups. A difference of more than two times ($P \leq 0.00001$) was considered methylation upregulation or downregulation. Compared with HL60 cells, m7G methylation was upregulated in 427 genes and downregulated in 452 genes in HL60/MX2 cells. The top 15 upregulated and downregulated genes are listed in **Tables 1**, **2**.

Motif Analysis of m7G Methylation

In this study, DREME software was used to determine the MOTIF sequence. As shown in **Figures 2A, B**, the most conservative MOTIFs were CUGKR (K=G/U, R=G/A) and GGAAR, with E-values of 6.5e-016 and 2.0e-013 in HL-60 cells, respectively. The MOTIFs sequences of the two groups were significantly different.

Regional Analysis of m7G Methylation

We analyzed the m7G methylation site, and our results showed that the modification was distributed in all mRNA regions. Among these, the CDS region exhibited the most methylation modification, followed by the 3'UTR region, and the StartC and StopC regions demonstrated the least methylation modification (**Figures 2C, D**). The regional distribution of the differentially modified genes in HL60 and HL60-MX2 cells was similar (**Figure 2E**). As shown in **Figure 2F**, we performed a statistical analysis of the peak density modified by m7G methylation. The results showed that the number of m7G peaks in the two groups was similar in the CDS region. Compared to HL60-MX2 cells, HL60 cells showed fewer m7G peaks in the 5'UTR region and more in the 3'UTR region.

Conjoint Analysis of Differentially Expressed m7G-Methylated Genes and mRNA Expressed Genes

RNA sequencing analysis revealed that there were statistically significant differences in the expression of 4801 genes in HL60/MX2 cells compared with HL60 cells, among which 1451 genes were upregulated and 3350 genes were downregulated. Scatter

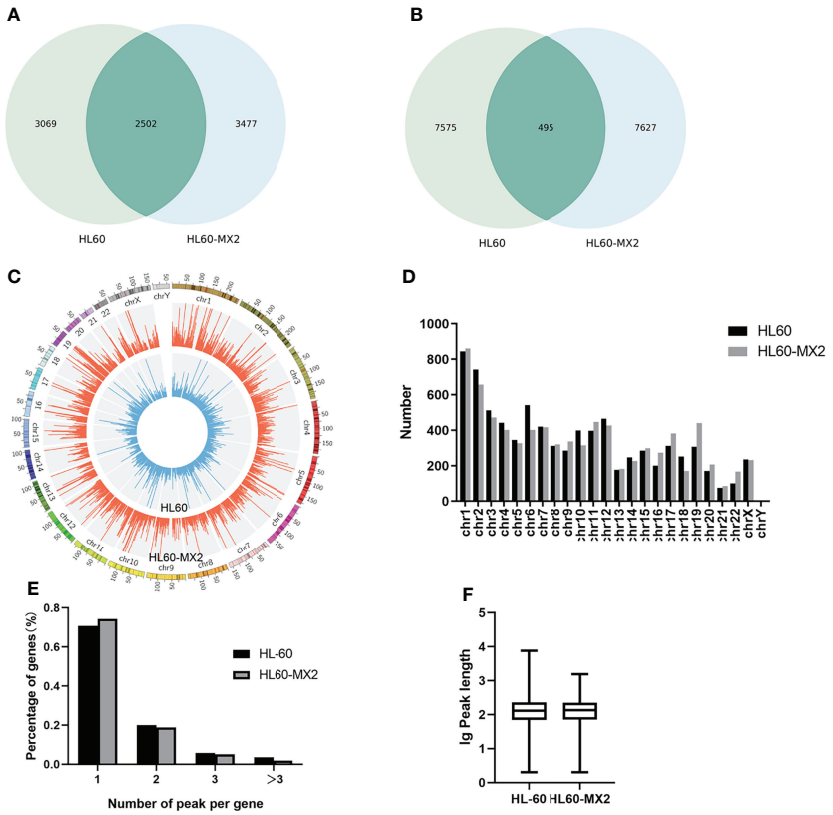

FIGURE 1 | Overview of m7G methylation in HL60 and HL60/MX2 cells. **(A)** Venn diagram of m7G genes in HL60 and HL60/MX2 cells. **(B)** Venn diagram of m7G peaks in HL60 and HL60/MX2 cells. **(C)** Visualization of m7G at the chromosome level in HL60 and HL60/MX2 cells. **(D)** The number of m7G peaks in HL60 and HL60/MX2 cells on each chromosome. **(E)** The number of m7G peaks on each mRNA. **(F)** The length of the m7G methylation peaks in HL60 and HL60/MX2 cells.

plots were used to represent the differentially expressed mRNAs between the two groups (**Figure 3A**). We conducted a conjoint analysis of the degree of m7G methylation and mRNA expression. The results showed that among the 116 genes with low mRNA expression, the degree of m7G methylation was significantly upregulated for 38 genes and significantly downregulated for 78 genes (fold-change > 2, $p < 0.001$), referred to as 'hypo-up' and 'hypo-down'. Among the 108 genes with high mRNA expression, the m7G methylation degree was significantly upregulated for 38 genes and significantly downregulated for 70 genes, referred to as 'hyper-up' and 'hyper-down' (**Figure 3B**).

TABLE 1 | Top 15 up-methylated genes (HL60/MX2 vs HL60).

Chromosome	txStart	txEnd	Gene name	Fold change
chr1	1822258	1822556	GNB1	6345.1
chr9	112020456	112020577	EPB41L4B	2873.8
chr6	78400372	78400400	MEI4	2616
chr15	59949013	59949200	GTF2A2	2597.6
chr1	184774757	184775060	FAM129A	2468.7
chrX	47430841	47431220	ARAF	2220.1
chr12	2706602	2706662	CACNA1C	2137.2
chr20	44175905	44175960	EPPIN	2082
chr19	42569374	42569400	GRIK5	2026.7
chr9	35826061	35826158	FAM221B	1962.3
chr21	45457672	45457808	TRAPPC10	1861
chr6	36790833	36790874	CPNE5	1787.3
chr1	160793970	160794042	LY9	1741.3
chr2	84928401	84928463	DNAH6	1566.3
chr9	38395736	38395920	ALDH1B1	1317.7

TABLE 2 | Top 15 down-methylated genes (HL60/MX2 vs HL60).

Chromosome	txStart	txEnd	Gene name	Fold change
chr10	50662525	50662720	ERCC6	3552.4
chr7	2338979	2339072	SNX8	3117.9
chr5	31508727	31508760	DROSHA	2629.2
chr11	14316305	14316408	RRAS2	2422.9
chr17	26925482	26925520	SPAG5	2390.3
chr6	160665501	160666480	SLC22A2	2325.1
chr8	7308085	7308422	SPAG11B	2292.5
chr10	69751955	69752080	HERC4	2042.8
chr14	20482881	20483352	OR4K14	1988.5
chr18	10739221	10740000	PIEZO2	1912.4
chr7	150270681	150271041	GIMAP4	1901.6
chr3	148939441	148939832	CP	1771.2
chr18	53070851	53071226	TCF4	1760.4
chr9	102742001	102742360	ERP44	1738.7
chr1	222757469	222757580	TAF1A	1716.9

Bioinformatics Analysis of m7G Methylation Genes

To investigate the pathophysiological role of m7G methylation modification in the induction of drug resistance in AML cells, we performed GO enrichment and KEGG pathway analyses on different m7G methylation genes in HL60/MX2 and HL60 cells. As shown in **Figure 4**, in terms of biosynthetic biological processes (BP), the up-methylated m7G genes in HL60/MX2

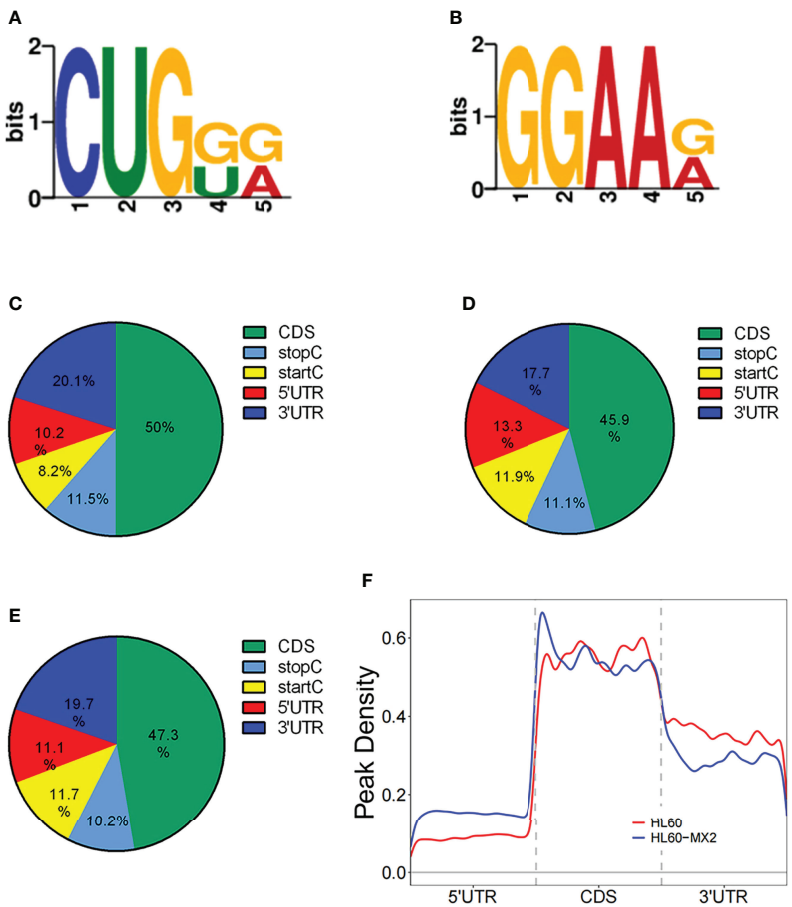

FIGURE 2 | Motif and regional analysis of m7G methylation. **(A)** Motif with minimum E-value of m7G in HL-60 cells. **(B)** Motif with minimum E-value of m7G in HL60/MX2 cells. **(C)** Pie chart of m7G peaks in different regions of mRNA in HL-60 cells. **(D)** Pie chart of m7G peaks in different regions of mRNA in HL60/MX2 cells. **(E)** Pie chart of m7G peaks in different regions of mRNA in differentially modified genes of the two groups. **(F)** Analysis of the peak density modified by m7G methylation.

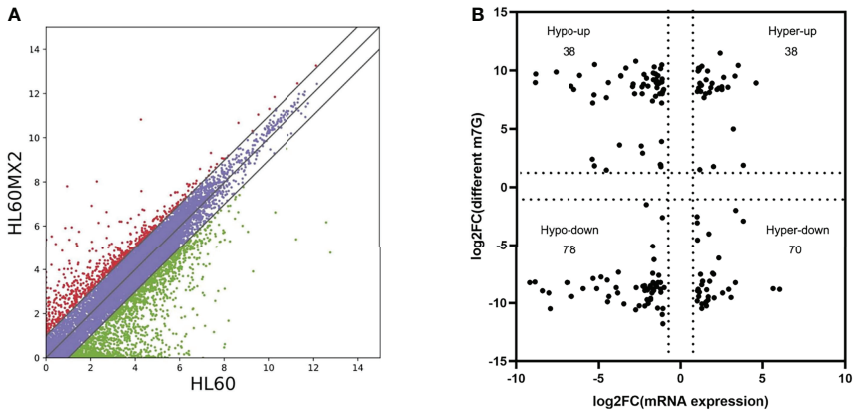

FIGURE 3 | Joint analysis of m7G methylation and transcriptome. **(A)** Scatter plots of the differentially expressed mRNAs between HL60 and HL60/MX2 cells. **(B)** Conjoint analysis of m7G methylation and the transcriptome of mRNA expression.

cells were mainly related to the regulation of proteolysis, regulation of hydrolase activity, and cellular protein metabolic process, while down-methylated m7G genes were mainly related to plasma membrane-bounded cell projection organization, cell projection organization, cellular component organization or biogenesis. In terms of molecular functions (MF), the up-methylated m7G genes were mainly related to purine ribonucleoside triphosphate binding, purine ribonucleotide binding, purine nucleotide binding, and ribonucleotide binding, while down-methylated m7G genes were mainly related to ATP-dependent microtubule motor, dynein intermediate chain binding, and motor activity. For the cellular components, the up-methylated m7G genes were mainly related to cytoplasm, pore complex, and plasma membrane-bounded cell projection, while down-methylated m7G genes were mainly related to axoneme, ciliary plasm, axonemal dynein complex, and cytoskeleton.

KEGG analysis results revealed that the mRNAs with up-methylated m7G modification in HL60-MX2 cells were primarily involved in hypertrophic cardiomyopathy, complement and coagulation cascades, and the GnRH signaling pathway (**Figure 5A**). The mRNAs with down-methylated m7G modification were significantly enriched in ABC transporters, valine, leucine, and isoleucine degradation, and amino acid biosynthesis (**Figure 5B**). Each graph in **Figures 4**, **5** lists the top ten most dominant genes in each category.

DISCUSSION

Epigenetic modification of genes is a hot topic in the study of tumor pathogenesis. Recent studies have shown that epigenetic abnormalities, including RNA methylation (24), DNA methylation (25), histone covalent modification (26), and non-coding RNAs, play important roles in the occurrence and development of tumors.

At present, methylation of some genes has been shown to be related to the occurrence and progression of hematological tumors, and the detection of gene methylation is also of great significance to the judgment of prognosis. For example, the presence of DNA hypermethylation of RASSF6 and RASSF10 always indicates a poor prognosis in acute lymphoblastic leukemia (ALL) (27). Methyltransferase-like 3 (METTL3) is a core m6A catalytic enzyme (28). Lin et al. found that, compared with normal hematopoietic stem cells, the mRNA and protein expression levels of METTL3 in leukemia cells of patients with acute myeloid leukemia (AML) were significantly increased. The high expression of METTL13 promoted its target genes, including c-MYC and BCL2, and increased m6A methylation of PTEN-promoted mRNA translation (29).

Recently, m7G methylation modifications have attracted increasing attention. Methyltransferase-like 1 (METTL1) is a writer of m7G methylation (30). Recent studies also reported that METTL1 is involved in tumor development by promoting mRNA processing in an m7G-dependent manner (31). In addition, METTL1 overexpression has been shown to be associated with poor prognosis and downregulation of tumor suppressors in hepatocellular carcinoma (32). In terms of the occurrence, development, and drug resistance of leukemia, there have been many studies on RNA methylation, but they have all focused on m5C and m6A modifications (33–35). Currently, there is a lack of research on m7G methylation modification of mRNA in leukemia.

In this study, we sequenced the m7G methylation peaks of mRNA in AML cells (HL60) and drug-resistant AML cells (HL60-MX2) using MeRIP-seq and analyzed the differences between the two groups. We identified over 10,000 m7G peaks and nearly 10,000 m7G methylated genes and found significant differences in m7G methylation modification status in HL60 and HL60-MX2 cells. The common modified genes were only 27%, the common modification peaks were only ~3%, and the overall methylation level in HL60-MX2 cells was higher than that in

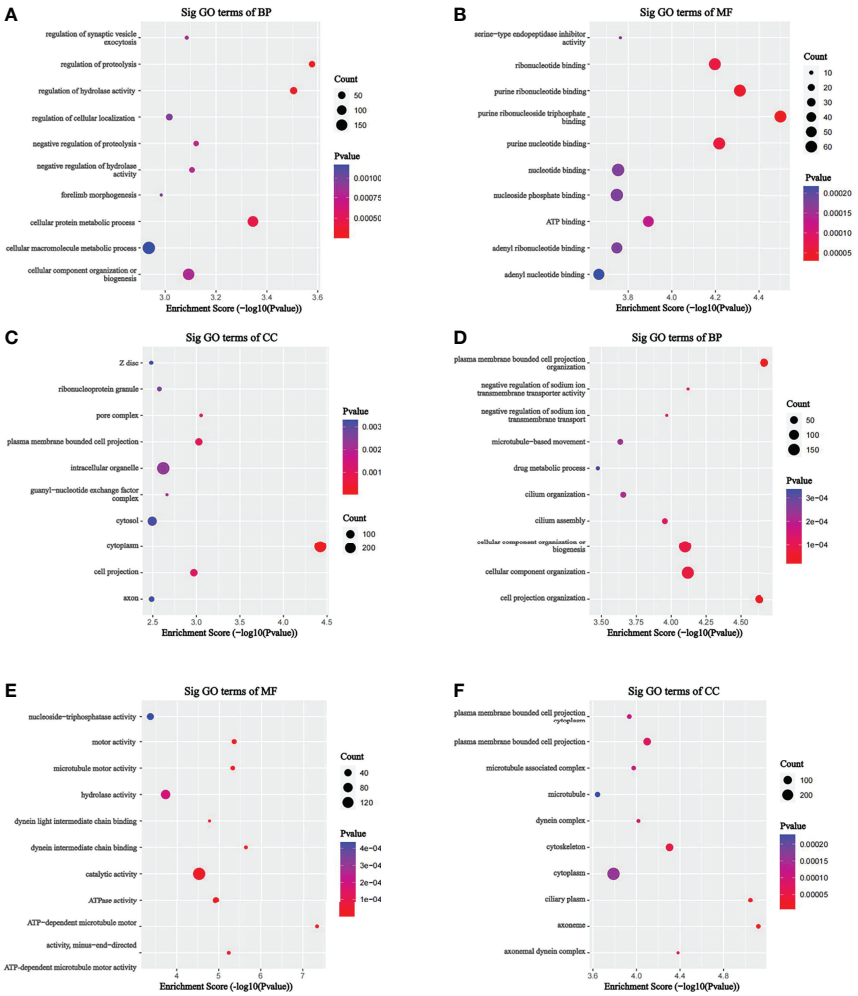

FIGURE 4 | GO analysis on different m7G methylation genes of HL60 and HL60/MX2 cells. **(A-C)** GO enrichment analysis of up-methylated m7G genes in HL60/MX2 cells. **(D-F)** GO enrichment analysis of down-methylated m7G genes in HL60/MX2 cells. GO, gene ontology; BP, biological process; CC, cellular component; MF, molecular function.

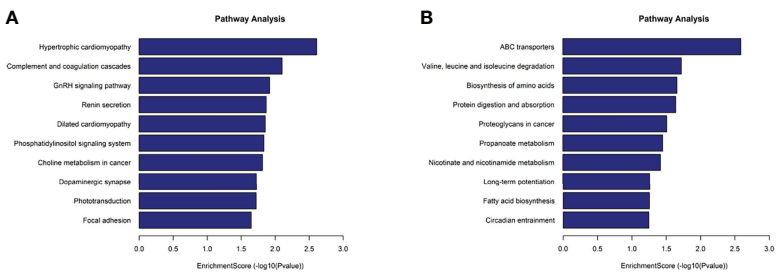

FIGURE 5 | KEGG analysis on different m7G methylation genes of HL60 and HL60/MX2 cells. **(A)** Major enriched KEGG pathway of up-methylated m7G in HL60-MX2 cells. **(B)** Major enriched KEGG pathway of down-methylated m7G in HL60-MX2 cells.

HL60 cells. This suggests that m7G methylation may be involved in the regulation of drug resistance in AML cells.

Epigenetic modification is an important area of study in tumor pathogenesis. Recent research has shown that epigenetic abnormalities, including RNA methylation, DNA methylation, histone covalent modification, and miRNA abnormalities, play an important role in the occurrence and development of tumors (26). At present, methylation of some genes has been shown to be related

to the occurrence and progression of hematological tumors, and detection of gene methylation is also of great significance to the judgment of prognosis. ARAF, a member of the RAF kinase family, is involved in tumor development by activating mitogen-activated protein kinase (MAPK) in various malignancies including lung, colorectal, pancreatic, and breast cancers (36). Our results showed that ARAF was significantly upregulated in m7G methylation in HL60/MX2 cells. Among genes with downregulated methylation in HL60/MX2, ERCC6 was directly involved in regulating the response to 5-FU chemotherapy in colorectal cancer (37). However, the role of m7G methylation in the above genes in AML pathogenesis and drug resistance remains unclear. In our study, analysis of m7G methylation modification motifs revealed significant differences between drug-resistant AML cells and non-resistant AML cells, suggesting that the differences in methylation modification between the two groups may be related to the category of m7G methylase. However, this still requires further experimental confirmation.

A large number of studies have shown that the distribution of methylation sites in different regions of mRNA is crucial to mRNA stability and translation regulation. Meyer et al. observed that m6A modification sites were enriched near stop codons and in 3' UTRs, and found that m6A modification enriched in 3' UTRs could affect the binding of microRNAs, indicating that methylation modification could play a role at the post-transcriptional level (38). A recent study found that a significant increase in HSPA1A mRNA and protein expression is regulated by m6A modification, which may be related to increased m6A methylation in the CDS region of HSPA1A, promoting mRNA stability (39). Our study found that most m7G methylation occurred in the CDS region in both AML and drug-resistant AML cells, and most of the methylation differences between the two groups occurred in the CDS region. Whether m7G methylation affects mRNA stability and expression regulation in AML pathogenesis and drug resistance has not yet been confirmed; therefore, more complex experiments are required for further study.

Multidrug resistance (MDR) has become a major reason for tumor chemotherapy failure (40). MDR refers to the cross-resistance of tumor cells to chemotherapeutic drugs, as well as other chemotherapeutic drugs with different structures and functions (41). The mechanism of MDR is an important topic of basic and clinical tumor research. The expression of drug transport pumps, especially the overexpression of ATP-binding cassette transporters (ABC transporters), is closely related to tumor MDR. Importantly, ABC transporter proteins are considered the major reason for MDR in AML (42). Increasing evidence suggests that altered expression of ABC transporters contributes not only to MDR but also to cancer initiation, progression, and metastasis (43, 44). Previous studies have demonstrated that aberrant DNA methylation of ABC transporters is present in a variety of neoplastic diseases, including MDR leukemia cell lines (45, 46). However, the effect of RNA methylation on ABC transporters remains unclear. Interestingly, our KEGG analysis results showed significant downregulation of m7G methylation in ABC transporter-related genes of HL60-MX2 cells, which may suggest that downregulation of m7G methylation could positively regulate ABC transporter-related genes in AML cells, leading to cell drug resistance. For more than 30 years, researchers have attempted to use MDR inhibitors in cancer chemotherapy without success. However, blocking ABC transporter activity has been shown to be effective *in vitro*, since the toxicity of the inhibitor drug limited its clinical application (47). Our study provides a new perspective for future investigators to study the role of m7G methylation in drug resistance of AML cells to discover new therapeutic targets.

DATA AVAILABILITY STATEMENT

The datasets presented in this study can be found in online repositories. The names of the repository/repositories and accession number(s) can be found below: https://www.ncbi.nlm.nih.gov/geo/query/acc.cgi?acc=GSE201096.

AUTHOR CONTRIBUTIONS

All authors listed have made a substantial, direct, and intellectual contribution to the work and approved it for publication. All authors contributed to the article and approved the submitted version.

FUNDING

This work was supported by the National Natural Science Foundation of China (no. 81473484).

REFERENCES

1. Burnett A, Wetzler M, Lowenberg B. Therapeutic Advances in Acute Myeloid Leukemia. *J Clin Oncol* (2011) 29(5):487–94. doi: 10.1200/JCO.2010.30.1820
2. Rashidi A, Weisdorf DJ, Bejanyan N. Treatment of Relapsed/refractory Acute Myeloid Leukaemia in Adults. *Br J Haematol* (2018) 181(1):27–37. doi: 10.1111/bjh.15077
3. Ning B, Li W, Zhao W, Wang R. Targeting Epigenetic Regulations in Cancer. *Acta Biochim Et Biophys Sin* (2016) 48(1):97–109. doi: 10.1093/abbs/gmv116
4. Wouters BJ, Delwel R. Epigenetics and Approaches to Targeted Epigenetic Therapy in Acute Myeloid Leukemia. *Blood* (2016) 127(1):42–52. doi: 10.1182/blood-2015-07-604512
5. Roundtree IA, Evans ME, Pan T, He C. Dynamic RNA Modifications in Gene Expression Regulation. *Cell* (2017) 169(7):1187–200. doi: 10.1016/j.cell.2017.05.045
6. Liu N, Zhou KI, Parisien M, Dai Q, Diatchenko L, Pan T. N6-Methyladenosine Alters RNA Structure to Regulate Binding of a Low-Complexity Protein. *Nucleic Acids Res* (2017) 45(10):6051–63. doi: 10.1093/nar/gkx141
7. Cowling VH. Regulation of mRNA Cap Methylation. *Biochem J* (2009) 425 (2):295–302. doi: 10.1042/BJ20091352
8. Pei Y, Shuman S. Interactions Between Fission Yeast mRNA Capping Enzymes and Elongation Factor Spt5. *J Biol Chem* (2002) 277(22):19639–48. doi: 10.1074/jbc.M200015200

9. Song B, Tang Y, Chen K, Wei Z, Rong R, Lu Z, et al. M7ghub: Deciphering the Location, Regulation and Pathogenesis of Internal mRNA N7-methylguanosine (M7g) Sites in Human. *Bioinformatics* (2020) 36 (11):3528–36. doi: 10.1093/bioinformatics/btaa178
10. Huang Z, Pan J, Wang H, Du X, Xu Y, Wang Z, et al. Prognostic Significance and Tumor Immune Microenvironment Heterogenicity of M5c RNA Methylation Regulators in Triple-Negative Breast Cancer. *Front Cell Dev Biol* (2021) 9:657547. doi: 10.3389/fcell.2021.657547
11. Zhao H, Xu Y, Xie Y, Zhang L, Gao M, Li S, et al. M6A Regulators Is Differently Expressed and Correlated With Immune Response of Esophageal Cancer. *Front Cell Dev Biol* (2021) 9:650023. doi: 10.3389/fcell.2021.650023
12. Chu JM, Ye TT, Ma CJ, Lan MD, Liu T, Yuan BF, et al. Existence of Internal N7-Methylguanosine Modification in mRNA Determined by Differential Enzyme Treatment Coupled With Mass Spectrometry Analysis. *ACS Chem Biol* (2018) 13(12):3243–50. doi: 10.1021/acschembio.7b00906
13. Malbec L, Zhang T, Chen YS, Zhang Y, Sun BF, Shi BY, et al. Dynamic Methylome of Internal mRNA N(7)-Methylguanosine and Its Regulatory Role in Translation. *Cell Res* (2019) 29(11):927–41. doi: 10.1038/s41422-019-0230-z
14. Zhang LS, Liu C, Ma H, Dai Q, Sun HL, Luo G, et al. Transcriptome-Wide Mapping of Internal N(7)-Methylguanosine Methylome in Mammalian mRNA. *Mol Cell* (2019) 74(6):1304–16.e8. doi: 10.1016/j.molcel.2019.03.036
15. Kik K, Wasowska-Lukawska M, Oszczapowicz I, Szmigiero L. Cytotoxicity and Cellular Uptake of Doxorubicin and Its Formamidine Derivatives in HL60 Sensitive and HL60/MX2 Resistant Cells. *Anticancer Res* (2009) 29 (4):1429–33.
16. Zhuravlev E, Sergeeva M, Malanin S, Amirkhanov R, Semenov D, Grigoryeva T, et al. RNA-Seq Transcriptome Data of Human Cells Infected With Influenza A/Puerto Rico/8/1934 (H1N1) Virus. *Data Brief* (2020) 33:106604. doi: 10.1016/j.dib.2020.106604
17. Dobin A, Davis CA, Schlesinger F, Drenkow J, Zaleski C, Jha S, et al. STAR: Ultrafast Universal RNA-Seq Aligner. *Bioinformatics* (2013) 29(1):15–21. doi: 10.1093/bioinformatics/bts635
18. Cheng J, Metge F, Dieterich C. Specific Identification and Quantification of Circular RNAs From Sequencing Data. *Bioinformatics* (2016) 32(7):1094–6. doi: 10.1093/bioinformatics/btv656
19. Kim D, Langmead B, Salzberg SL. HISAT: A Fast Spliced Aligner With Low Memory Requirements. *Nat Methods* (2015) 12(4):357–60. doi: 10.1038/nmeth.3317
20. Zhang Y, Liu T, Meyer CA, Eeckhoute J, Johnson DS, Bernstein BE, et al. Model-Based Analysis of ChIP-Seq (MACS). *Genome Biol* (2008) 9(9):R137. doi: 10.1186/gb-2008-9-9-r137
21. Shen L, Shao NY, Liu X, Maze I, Feng J, Nestler EJ. DiffReps: Detecting Differential Chromatin Modification Sites From ChIP-Seq Data With Biological Replicates. *PLoS One* (2013) 8(6):e65598. doi: 10.1371/journal.pone.0065598
22. Zhang Q, Zheng Q, Yu X, He Y, Guo W. Overview of Distinct 5-Methylcytosine Profiles of Messenger RNA in Human Hepatocellular Carcinoma and Paired Adjacent Non-Tumor Tissues. *J Trans Med* (2020) 18(1):245. doi: 10.1186/s12967-020-02417-6
23. Zhang Y, Geng X, Xu J, Li Q, Hao L, Zeng Z, et al. Identification and Characterization of N6-Methyladenosine Modification of CircRNAs in Glioblastoma. *J Cell Mol Med* (2021) 25(15):7204–17. doi: 10.1111/jcmm.16750
24. Cui Q, Shi H, Ye P, Li L, Qu Q, Sun G, et al. M(6)A RNA Methylation Regulates the Self-Renewal and Tumorigenesis of Glioblastoma Stem Cells. *Cell Rep* (2017) 18(11):2622–34. doi: 10.1016/j.celrep.2017.02.059
25. Meng Q, Lu YX, Ruan DY, Yu K, Chen YX, Xiao M, et al. DNA Methylation Regulator-Mediated Modification Patterns and Tumor Microenvironment Characterization in Gastric Cancer. *Mol Ther Nucleic Acids* (2021) 24:695–710. doi: 10.1016/j.omtn.2021.03.023
26. Werner RJ, Kelly AD, Issa JJ. Epigenetics and Precision Oncology. *Cancer J* (2017) 23(5):262–9. doi: 10.1097/PPO.0000000000000281
27. Younesian S, Shahkarami S, Ghaffari P, Alizadeh S, Mehrasa R, Ghavamzadeh A, et al. DNA Hypermethylation of Tumor Suppressor Genes RASSF6 and RASSF10 as Independent Prognostic Factors in Adult Acute Lymphoblastic Leukemia. *Leukemia Res* (2017) 61:33–8. doi: 10.1016/j.leukres.2017.08.016
28. Wang X, Feng J, Xue Y, Guan Z, Zhang D, Liu Z, et al. Corrigendum: Structural Basis of N(6)-Adenosine Methylation by the METTL3-METTL14 Complex. *Nature* (2017) 542(7640):260. doi: 10.1038/nature21073
29. Lin S, Choe J, Du P, Triboulet R, Gregory RI. The M(6)A Methyltransferase METTL3 Promotes Translation in Human Cancer Cells. *Mol Cell* (2016) 62 (3):335–45. doi: 10.1016/j.molcel
30. Teng PC, Liang Y, Yarmishyn AA, Hsiao YJ, Lin TY, Lin TW, et al. RNA Modifications and Epigenetics in Modulation of Lung Cancer and Pulmonary Diseases. *Int J Mol Sci* (2021) 22(19):10592. doi: 10.3390/ijms221910592
31. Pandolfini L, Barbieri I, Bannister AJ, Hendrick A, Andrews B, Webster N, et al. METTL1 Promotes Let-7 MicroRNA Processing *via* M7G Methylation. *Mol Cell* (2019) 74(6):1278–90.e9. doi: 10.1016/j.molcel.2019.03.040
32. Tian QH, Zhang MF, Zeng JS, Luo RG, Wen Y, Chen J, et al. METTL1 Overexpression is Correlated With Poor Prognosis and Promotes Hepatocellular Carcinoma *via* PTEN. *J Mol Med* (2019) 97(11):1535–45. doi: 10.1007/s00109-019-01830-9
33. Qing Y, Su R, Chen J. RNA Modifications in Hematopoietic Malignancies: A New Research Frontier. *Blood* (2021) 138(8):637–48. doi: 10.1182/blood.2019004263
34. Cheng JX, Chen L, Li Y, Cloe A, Yue M, Wei J, et al. RNA Cytosine Methylation and Methyltransferases Mediate Chromatin Organization and 5-Azacytidine Response and Resistance in Leukaemia. *Nat Commun* (2018) 9 (1):1163. doi: 10.1038/s41467-018-03513-4
35. Li Z, Qian P, Shao W, Shi H, He XC, Gogol M, et al. Suppression of M(6)A Reader Ythdf2 Promotes Hematopoietic Stem Cell Expansion. *Cell Res* (2018) 28(9):904–17. doi: 10.1038/s41422-018-0072-0
36. Lin W, Tong C, Zhang W, Cen W, Wang Y, Li J, et al. Silencing ARAF Suppresses the Malignant Phenotypes of Gallbladder Cancer Cells. *BioMed Res Int* (2020) 2020:3235786. doi: 10.1155/2020/3235786
37. Zhao Z, Zhang G, Li W. Elevated Expression of ERCC6 Confers Resistance to 5-Fluorouracil and Is Associated With Poor Patient Survival in Colorectal Cancer. *DNA Cell Biol* (2017) 36(9):781–6. doi: 10.1089/dna.2017.3768
38. Meyer KD, Saletore Y, Zumbo P, Elemento O, Mason CE, Jaffrey SR. Comprehensive Analysis of mRNA Methylation Reveals Enrichment in 3' UTRs and Near Stop Codons. *Cell* (2012) 149(7):1635–46. doi: 10.1016/j.cell.2012.05.003
39. Wang J, Gao F, Zhao X, Cai Y, Jin H. Integrated Analysis of the Transcriptome-Wide M6A Methylome in Preeclampsia and Healthy Control Placentas. *PeerJ* (2020) 8:e9880. doi: 10.7717/peerj.9880
40. Li YJ, Lei YH, Yao N, Wang CR, Hu N, Ye WC, et al. Autophagy and Multidrug Resistance in Cancer. *Chin J Cancer* (2017) 36(1):52. doi: 10.1186/s40880-017-0219-2
41. Liang Y, Liu ZY, Wang PY, Li YJ, Wang RR, Xie SY. Nanoplatform-Based Natural Products Co-Delivery System to Surmount Cancer Multidrug-Resistant. *J Controlled Release Off J Controlled Release Society* (2021) 336:396–409. doi: 10.1016/j.jconrel
42. Vasconcelos FC, de Souza PS, Hancio T, de Faria FCC, Maia RC. Update on Drug Transporter Proteins in Acute Myeloid Leukemia: Pathological Implication and Clinical Setting. *Crit Rev Oncol/Hematol* (2021) 160:103281. doi: 10.1016/j.critrevonc.2021.103281
43. Nobili S, Lapucci A, Landini I, Coronnello M, Roviello G, Mini E. Role of ATP-Binding Cassette Transporters in Cancer Initiation and Progression. *Semin Cancer Biol* (2020) 60:72–95. doi: 10.1016/j.semcancer.2019.08.006
44. Domenichini A, Adamska A, Falasca M. ABC Transporters as Cancer Drivers: Potential Functions in Cancer Development. *Biochim Biophys Acta Gen Subj* (2019) 1863(1):52–60. doi: 10.1016/j.bbagen.2018.09.019
45. Moreira MA, Bagni C, de Pinho MB, Mac-Cormick TM, dos Santos Mota M, Pinto-Silva FE, et al. Changes in Gene Expression Profile in Two Multidrug Resistant Cell Lines Derived From a Same Drug Sensitive Cell Line. *Leukemia Res* (2014) 38(8):983–7. doi: 10.1016/j.leukres.2014.06.001
46. Bram EE, Stark M, Raz S, Assaraf YG. Chemotherapeutic Drug-Induced ABCG2 Promoter Demethylation as a Novel Mechanism of Acquired Multidrug Resistance. *Neoplasia* (2009) 11(12):1359–70. doi: 10.1593/neo.91314
47. Nanayakkara AK, Follit CA, Chen G, Williams NS, Vogel PD, Wise JG. Targeted Inhibitors of P-Glycoprotein Increase Chemotherapeutic-Induced

Mortality of Multidrug Resistant Tumor Cells. *Sci Rep* (2018) 8(1):967. doi: 10.1038/s41598-018-19325-x

Conflict of Interest: The authors declare that the research was conducted in the absence of any commercial or financial relationships that could be construed as a potential conflict of interest.

Publisher's Note: All claims expressed in this article are solely those of the authors and do not necessarily represent those of their affiliated organizations, or those of the publisher, the editors and the reviewers. Any product that may be evaluated in this article, or claim that may be made by its manufacturer, is not guaranteed or endorsed by the publisher.

frontiers | Frontiers in Oncology

TYPE Brief Research Report
PUBLISHED 09 September 2022
DOI 10.3389/fonc.2022.959243

OPEN ACCESS

EDITED BY
Garrett Dancik,
Eastern Connecticut State University,
United States

REVIEWED BY
Ibrahim C. Haznedaroglu,
Hacettepe University Hospital, Turkey
Livius Penter,
Dana–Farber Cancer Institute,
United States

*CORRESPONDENCE
Deepak Ben Vangala
deepak.vangala@rub.de

†These authors have contributed equally to this work and share first authorship

SPECIALTY SECTION
This article was submitted to Hematologic Malignancies, a section of the journal Frontiers in Oncology

RECEIVED 01 June 2022
ACCEPTED 12 August 2022
PUBLISHED 09 September 2022

CITATION
Nilius-Eliliwi V, Tembrink M, Gerding WM, Lubieniecki KP, Lubieniecka JM, Kankel S, Liehr T, Mika T, Dimopoulos F, Döhner K, Schroers R, Nguyen HHP and Vangala DB (2022) Broad genomic workup including optical genome mapping uncovers a *DDX3X: MLLT10* gene fusion in acute myeloid leukemia.
Front. Oncol. 12:959243.
doi: 10.3389/fonc.2022.959243

Broad genomic workup including optical genome mapping uncovers a *DDX3X*: *MLLT10* gene fusion in acute myeloid leukemia

Verena Nilius-Eliliwi[1†], Marco Tembrink[2†], Wanda Maria Gerding[2], Krzystof P. Lubieniecki[2], Joanna M. Lubieniecka[2], Stefanie Kankel[3], Thomas Liehr[3], Thomas Mika[1], Fotios Dimopoulos[1], Konstanze Döhner[4], Roland Schroers[1], Hoa Huu Phuc Nguyen[2] and Deepak Ben Vangala[1*]

[1]Department of Medicine, Hematology and Oncology, Knappschaftskrankenhaus, Ruhr-University Bochum, Bochum, Germany, [2]Human Genetics, Ruhr-University Bochum, Bochum, Germany, [3]Jena University Hospital, Friedrich Schiller University, Institute of Human Genetics, Jena, Germany, [4]Department of Internal Medicine III, University Hospital Ulm, Ulm, Germany

In acute myeloid leukemia (AML), treatment decisions are currently made according to the risk classification of the European LeukemiaNet (ELN), which is based on genetic alterations. Recently, optical genome mapping (OGM) as a novel method proved to yield a genome-wide and detailed cytogenetic characterization at the time of diagnosis. A young female patient suffered from a rather unexpected aggressive disease course under FLT3 targeted therapy in combination with induction chemotherapy. By applying a "next-generation diagnostic workup" strategy with OGM and whole-exome sequencing (WES), a *DDX3X: MLLT10* gene fusion could be detected, otherwise missed by routine diagnostics. Furthermore, several aspects of lineage ambiguity not shown by standard diagnostics were unraveled such as deletions of *SUZ12* and *ARPP21*, as well as T-cell receptor recombination. In summary, the detection of this particular gene fusion *DDX3X: MLLT10* in a female AML patient and the findings of lineage ambiguity are potential explanations for the aggressive course of disease. Our study demonstrates that OGM can yield novel clinically significant results, including additional information helpful in disease monitoring and disease biology.

KEYWORDS

acute myeloid leukemia, optical genome mapping, *DDX3X*, *MLLT10*, FLT3-ITD, SUZ12, ARPP21, biphenotypic leukemia

Introduction

Acute myeloid leukemia (AML) is a common hematologic malignancy with a mortality rate of approximately 50% (1, 2). Treatment has improved in recent years with the introduction of new drugs that target specific proteins altered by distinct genetic aberrations. This progress and the increasing knowledge of risk stratification urge for more accurate genetic testing at diagnosis and relapse. Treatment decisions are currently made in line with the risk classification of the European LeukemiaNet (ELN), which is based on disease-specific genetic alterations (3).

In a recent study, we compared standard cytogenetic methods with optical genome mapping (OGM) as a novel diagnostic method for structural genome analysis in AML and myelodysplastic syndrome (MDS) (4). Briefly, ultrahigh–molecular weight (UHMW) DNA is prepared and labeled genome-wide and sequence-specific with a fluorochrome dye. After being loaded on a chip and linearized through nanochannels by electrophoresis, the labeled DNA is captured by a fluorescence microscope and processed by different software algorithms against the human GRCh37/hg19 labeling pattern. Furthermore, different pipelines are used to detect structural variants (SVs) and copy number variants (CNVs). The coverage of this method is about 300×, and the mosaicism detection level currently is about 2% for SVs and 8% for CNVs, with a substantial number of CNVs also covered in the SV pipeline (4). Besides a substantial gain of relevant information by OGM compared to classical karyotyping, here, we detected a *DDX3X: MLLT10* gene fusion in a 21-year-old female AML patient. To date, description of *DDX3X: MLLT10* in AML is restricted to a few cases in male patients (5). Also, in acute lymphoblastic leukemia (ALL), where the fusion is more commonly involved, it is mainly found in male individuals (6, 7). To the best of our knowledge, this is the first time this aberration is described in a female AML patient. Strikingly, *DDX3X* is a gene that escapes X-inactivation in women (8). Accordingly, Brandimarte et al. (6) hypothesized that *DDX3X* translocations might be a leukemic driver due to the lack of a second gene copy in male individuals (6, 9). Apart from that, both genes, *DDX3X* and *MLLT10*, separately have been observed to play a role in a whole range of different hematologic and solid malignancies (10–12).

Based on cytomorphology, immunophenotypic analysis, and histopathology, the disease in our patient was classified as CD33+, CD34+, CD38+, CD117+ AML with aberrant CD7 expression. By OGM, different genetic alterations related to T-lineage commitment were unraveled. Interestingly, the disease course appeared to be worse than expected. To improve our understanding of the aberrations and their contribution to leukemogenesis, we further analyzed the bone marrow sample by fluorescence *in situ* hybridization (FISH), whole-exome sequencing (WES), and consecutive OGM analysis. The purpose of this report is to provide insights into the benefits of a "next-generation diagnostic workup" for hematologic diseases using two different genome-wide high-resolution technologies and to find out whether its application might result in additional information useful for clinical decision-making.

Methods

Genetic standard diagnostics, such as karyotyping and PCR panels, are presented in the *Results* section and were performed at the University Hospital Knappschaftskrankenhaus Bochum and in collaborating laboratories. The patient gave written informed consent for genetic diagnostics and publication of results.

Optical genome mapping

OGM was performed as part of a recently published study at the initial time point (first time point) of AML diagnosis with bone marrow aspirate (BMA) and analyzed using Bionano Access v1.6. After the end of leukocyte nadir following reinduction treatment, consecutive OGM analysis of BMA was performed (second time point). UHMW DNA was isolated using an isolation kit from Bionano Genomics following the manufacturer's protocol. The DNA motif CTTAAG was labeled fluorescently by direct label and stain technology using a pattern recognition enzyme according to the manufacturer's instructions [direct labeling enzyme 1 (DLE-1), Bionano Genomics]. Optical scans were performed on a Saphyr platform (Bionano Genomics) using a G2.3 chip. Raw molecule data generated by OGM from samples collected at two different time points were computed using the Rare Variant pipeline (RVP) of Bionano Solve v3.7 and analyzed by the latest Bionano Access release v1.7, adding allele frequency estimates for SVs and an optimized nomenclature. OGM data showed an effective post-analysis 403-fold coverage at the initial time point and a 395-fold coverage after induction therapy. Quality metrics were reached for both samples. GRCh37/hg19 human genome reference was used for alignment.

Output SVs and CNVs were filtered against masks for known regions of high variance and default confidence cutoffs in Bionano Access v1.7 (insertion 0, deletion 0, inversion 0.7, duplication -1, intra-fusion 0.05, inter-translocation 0.05). SVs were filtered for absence in a control population consisting of 179 healthy controls provided by the manufacturer (Bionano Genomics). The remaining SVs were evaluated for their confidence, uniqueness, gene annotation overlaps, and presence in the Database of Genomic Variants (DGV). T-cell receptor (TCR) loci SVs were reported without filtering against controls, as somatic mutations are part of physiological T-cell maturation processes. All CNVs after CNV mask filtering using

default confidence cutoffs (0.5 Mbp for size and 0.99 for confidence) were reported.

Fluorescence *in situ* hybridization

To confirm the gene fusion *DDX3X: MLLT10*, FISH analysis on interphase nuclei was performed. FISH probes were hybridized to bone marrow smears according to manufacturer's instructions (MetaSystems, Altlussheim, Germany). A 193-kilobase probe covering the whole *DDX3X* locus including STS markers HUMSWX1304/RH1146 to DBX was synthesized (DDX3X-20-AQ; Empire Genomics), and a commercially available probe for the detection of *KMT2A:: MLLT10* [XL t (10;11) MLLT10/KMT2A DF, MetaSystems, Altlussheim, Germany] was applied.

Whole-exome sequencing

A WES library was constructed using SureSelectXT Human All Exon V7 (Agilent Technologies) and sequenced on NovaSeq 6000 instrument (Illumina). Sequence alignment, variant calling, and annotation were performed using Varvis bioinformatics pipeline v1.20.0 (Limbus Medical Technologies). For evaluation of myeloid cancer-related mutations, the coding sequences of 54 genes based on a commercially available myeloid NGS panel (TruSight Myeloid Sequencing Panel, Ilumina) and four case-specific genes based on OGM results (*DDX3X*, *MLLT10*, *NF1*, *SUZ12*) were analyzed for SNVs and CNVs. All detected SNVs with a population frequency <1% in gnomAD database were extracted and rated according to current cancer sequence variant interpretation standards of AMP consensus for myeloid cancer-related genes. *DDX3X:MLLT10* breakpoint search was done using the Varvis alignment by manual inspection in Integrative Genome Viewer (IGV), and fusion was confirmed using BLAT search tool University of California Santa Cruz (UCSC) and Sanger Sequencing (3500xL Genetic Analyzer, Applied Biosystems) (detailed information in Supplementary Material 1) (13, 14).

T-cell receptor clonality and junction analysis

To confirm clonal TCR TRD V(D)J recombination, Sanger sequencing was performed using primers for the amplification of *TRDV1* and *TRDJ1* generated using sequences of a EuroClonality-NGS validation study (sequences available upon request) (15). Sequencing was performed on a 3500xL Genetic Analyzer (Applied Biosystems). Sequence was analyzed using IMGT/V-Quest v3.5.29 incorporating TCR mutation junction analysis and reading frame evaluation (16).

Results

Patient characteristics and disease course

At initial diagnosis (first time point) in December 2020, the 21-year-old female patient presented with peripheral leukocytosis of 81 × 10^9/L accompanied by thrombocytopenia concomitant to a bone marrow infiltration of >90% with myelomonocytic blasts including some Auer rods (Figures 1A, B). Immunohistological workup revealed a weak expression of lysozyme and myeloperoxidase. Flow cytometry showed the expression of CD33, CD34, CD38, HLA-DR, and CD117, as well as aberrant expression of CD7 (Figure 1C). CD1a, surface and cytosolic CD3, and TCR were not detected. Cytogenetics reported a normal karyotype in the bone marrow sample, but only three metaphases could be evaluated. Molecular fragment length analysis subsequent to PCR amplification showed *FLT3*-ITD^{high} (ratio 0.759) and biallelic heterozygous *CEBPA* mutations. Fusion genes were not detected in a standard RT-PCR panel (Menotype AMLplexQS) and neither *IDH1*, *IDH2*, *NPM1*, *FLT3*-TKD (PCR/fragment length analysis) nor *ASXL1*, *RUNX1*, *TP53* [next-generation sequencing (NGS)] mutations were reported.

Based on these initial diagnostic results, the patient was grouped as high risk according to ELN 2017 risk classification and included in a clinical trial receiving gilteritinib in addition to the standard "3 + 7" induction therapy (daunorubicin 180 mg/m^2 and cytarabine 1,400 mg/m^2). Although not reaching a blast clearance after initial induction, the patient was allowed to stay on study and was reinduced with daunorubicin (180 mg/m^2) and intermediate-dose cytarabine (12 g/m^2). However, despite combining intensive chemotherapy and targeted *FLT3*-ITD treatment with a Tyrosine Kinase Inhibitor (TKI), complete remission could not be achieved by this approach and the patient showed a persistence of blasts of about 20% (second time point) similar immunophenotypic expression profile (Supplementary Figure S1). Thus, salvage therapy according to FLAG-Eto-protocol (fludarabine 150 mg/m^2, cytarabine 10 g/m^2, etoposide 300 mg/m^2, granulocyte colony stimulating factor (G-CSF) starting day 10) was initiated. Fortunately, complete remission was reached, and after identification of an human leukocyte antigen (HLA)-matched unrelated donor, the patient proceeded to allogeneic hematopoietic stem cell transplantation (allo-HSCT) following conditioning treatment including fludarabine (150 mg/m^2) and treosulfan (36 g/m^2). Graft versus Host Disease (GvHD) prophylaxis consisted of antithymocyte globulin (ATG), methotrexate (MTX), and ciclosporin A. After recovering without any major complications, maintenance treatment with sorafenib was started.

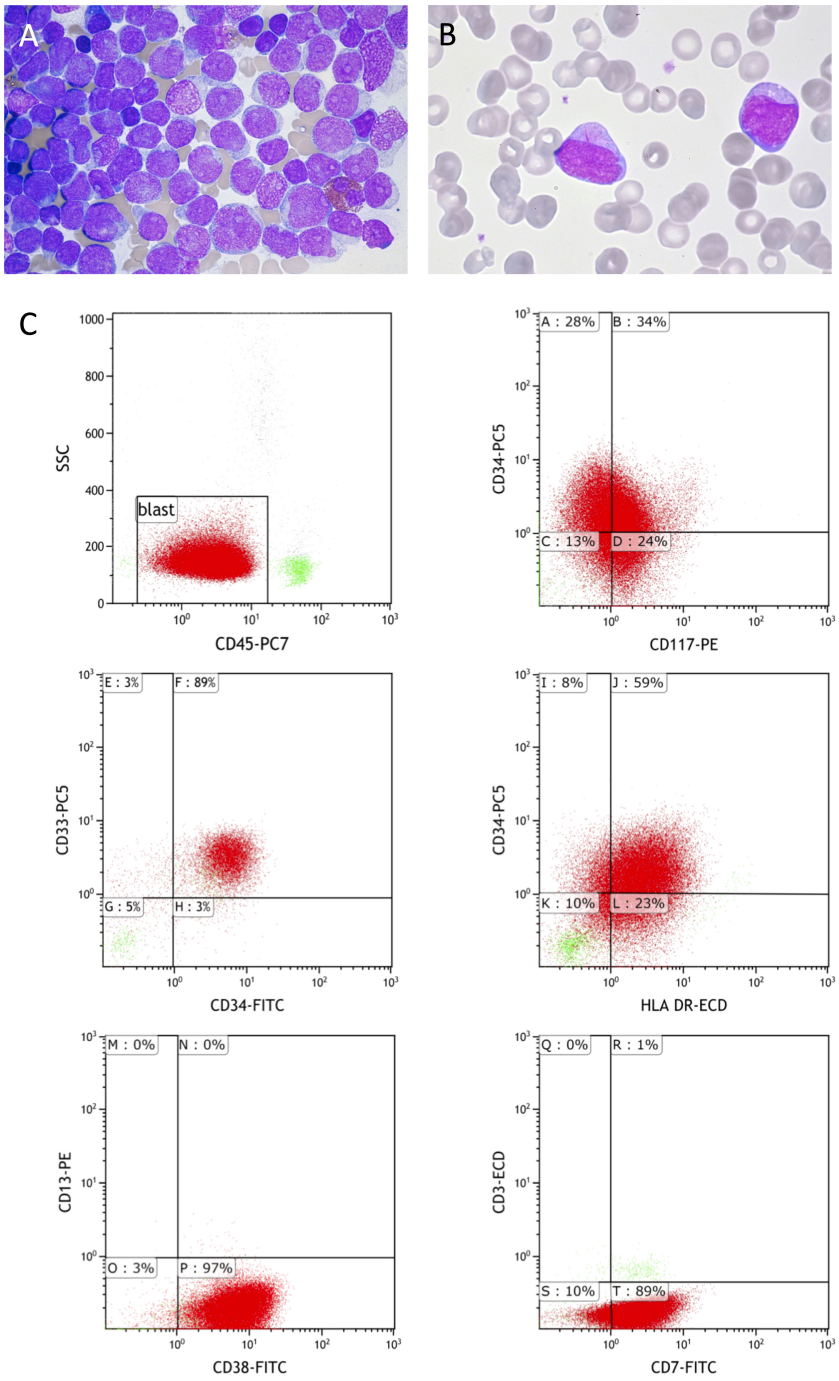

FIGURE 1
Cytology and immunophenotyping at initial diagnosis. Cytology of bone marrow **(A)** and peripheral blood **(B)** at initial diagnosis showing a subtotal infiltration of myelomonocytic blasts **(A)** and a blast with an Auer rod **(B)**. Immunophenotyping of bone marrow aspirate by flow cytometry **(C)** showing the gating strategy and relevant markers leading to the diagnosis of AML. ECD, extracellular domaine; SSC, Side scatter; PE, Phycoerythrine; FITC, Fluoresceinisothiocyanate.

TABLE 1 Clinical characteristics.

	First time point initial diagnosis	Second time point after reinduction therapy
Leukocyte count/L	81×10^9	5×10^9
Hb mmol/l	8.14	6.09
Thrombocyte count/µl	99,000	205,000
Histopathology	>90% blasts	30% blasts
Cytology	>90% blasts, single Auer rods	20% blasts, no Auer rods
Flow cytometry	>90% blasts: CD33, CD34, CD38, HLA-DR, CD117, CD7 pos. CD1a, CD3, cyCD3 neg.	12% blasts: CD33, CD34, CD38, HLA-DR, CD117 pos. CD1a, CD3, cyCD3, CD7 neg.
Karyotyping	46,XX [3]	46,XX [27]
FLT3-ITD	0.76 *FLT3*-ITD^{high}	0.05 *FLT3*-ITD^{low}
RT-PCR panel/Fragment length analysis	*CEBPA* mut. biallelic, heterozygous	*CEBPA* mut. biallelic, heterozygous

Most important findings by standard diagnostics of both time points. RT-PCR panel covering the following aberrations: *FLT3*-TKD, *NPM1*, *CBFB-MYH11*, *RUNX1-RUNX1T1*, *PML-RARA*, *CEBPA*, *IDH1*, *IDH2*, *BCR-ABL*, *KMT2A-MLLT3*.
Hb, hemoglobin; ITD, internal tandem duplication.

Interestingly, the patient developed hyperglycemia and was diagnosed with maturity-onset diabetes of the young (MODY) type 3 that correlated with the detection of a germline *HNF1A* variant (NM_000545.8 c.457C>T), previously rated as pathogenic using gene American College of Medical Genetics and Genomics (ACMG) criteria (17). Currently, 400 days after allo-HSCT, the patient is weaned off immunosuppressants, has recovered fully, and remains molecularly disease-free. Patient characteristics are summarized in Table 1.

Optical genome mapping

In consecutive analyses, 23 and 28 SVs that were absent in healthy control samples were identified in our patient. After sorting out SVs commonly present in the DGV, SVs with low confidence, duplicate SVs, and SVs not overlapping annotated genes, eight SVs remained. All of them were detected at both diagnostic time points. Variant allele frequencies (VAFs) of the SVs of interest ranged from 42% to 53% (first time point) and from 8% to 16% (second time point), corresponding to heterozygous presence in blasts; the histologically estimated blast proportions were given as >90% and 20%–30%, respectively.

A balanced rearrangement overlapping *MLLT10* and *DDX3X* was represented in OGM by five interchromosomal-translocation SVs and one intrachromosomal-translocation SV with VAFs between 45% and 53%. As revealed by OGM, a complex rearrangement involving three chromosomes was found, involving chromosomes X, 10, and 6, resulting in a *5'-DDX3X: MLLT10-3'* gene fusion on X-chromosome visualized in Figures 2A, B. Segments of different sizes are exchanged between chromosome Xp (1.14 Mbp) and 10p (0.46 Mbp). Additionally, a deleted piece of 8.68 Mbp of chromosome 6q material was found to be inserted into the derivative chromosome 10p.

Furthermore, a 1.4-Mbp deletion including the Cosmic Cancer Gene Census hallmark genes *NF1* and *SUZ12* was detected at both time points of OGM analysis (18). These SVs were also confirmed by corresponding copy number losses (manually detectable at the first and second time points but only called above the confidence threshold at the first time point due to the lower allele fraction at the second time point). Moreover, an 84-kbp SV deletion including the 5' part of *ARPP21* was detected in 42% and 8% allelic fraction at the first time point and second time point, respectively. The 3' region containing one of two different genomic loci for microRNA 128 (miRNA128-2) and a polymerase III intronic promoter region allowing for *ARPP21*-independent transcription were preserved (19, 20).

SVs of the TCR regions *TRA(D)*, *TRG*, and *TRB* were analyzed without filtering against controls. At *TRA(D)* locus, two different SV deletions were identified at both time points with corresponding VAF proportions compared to histologically determined blast percentages. One of these SVs seemed to represent a somatic *TRDV1-TRDJ1* V(D)J recombination. The TRG locus contained one matching SV deletion with VAFs of 96% and 49% at both time points, respectively, which were likely overestimated by the software (196 and 16 molecules representing SV). Insertion SVs found at the TRB locus were less meaningful (5 and 3 insertion SV calls).

Sanger sequencing confirmed the suspected *TRDV1-TRDJ1* recombination. Sequence analysis using IMGT/V-Quest-tool called an out-of-frame/nonsense mutation and junction analysis suspected *TRDD2* and *TRDD3* involvement.

Fluorescence *in situ* hybridization

In order to confirm OGM results regarding the *DDX3X: MLLT10* gene fusion, FISH analysis was performed on interphase nuclei for the visualization of *MLLT10* and *DDX3X*

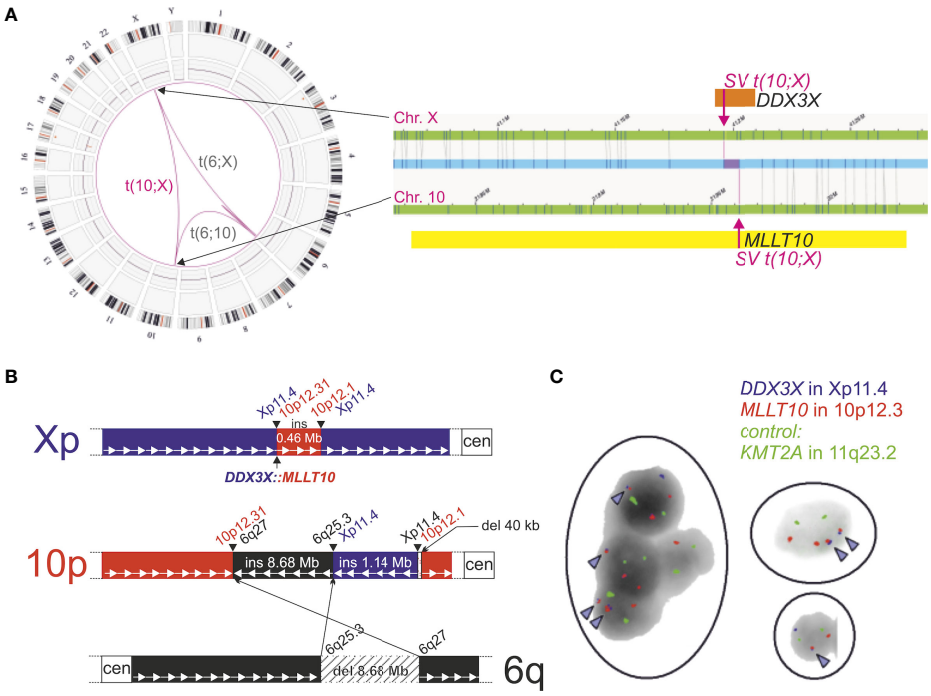

FIGURE 2
Detection of *DDX3X: MLLT10* gene fusion by optical genome mapping at the first time point and confirmation by FISH analysis. **(A)** Circos Plot (left) and detailed chromosome view SV visualization (right) of *DDX3X: MLLT10* in Bionano Access v1.7 (Translocation Confidence: inter: 0.65, intra: 0.3) filtered for absence in controls. **(B)** Schematic overview of structural rearrangement. A 0.46-Mbp fragment of Chr. 10p including *MLLT10* is transferred to Chr. Xp, fusing it to *DDX3X*. Furthermore, on Chr. 10p, an 8.68-Mbp fragment of Chr. 6q and a 1.14-Mbp fragment of Xp are inserted. Next to this insertion, a 40-kbp fragment is deleted. Both insertions are inverted and not in frame. **(C)** Interphase FISH analysis on bone marrow smear demonstrates *DDX3X: MLLT10* gene fusion. Red signals (corresponding to *MLLT10* at 10p12.13) and blue signals (corresponding to *DDX3X* at Xp11.4) are visualized adjacently and are indicated by arrowheads. In addition, green *KMT2A* control signals are not located in proximity to red *MLLT10* hybridization signals, indicating the lack of involvement of *KMT2A* in the structural rearrangement. Analyzed cell nuclei reveal heterogeneous hybridization signals due to subclonal events.

loci (Figure 2C). Additionally, a probe for *KMT2A* was co-hybridized to examine a potential rearrangement involving *MLLT10's* most common fusion partner *KMT2A*. These results confirmed the *DDX3X: MLLT10* gene fusion without evidence for involvement of the *KMT2A* gene in this rearrangement.

Whole-exome sequencing

After filtering for coding mutations, sequencing errors, and occurrence in <1% of gnomAD, seven SNVs and one CNV remained after analysis of the Cancer Virtual Panel.

One N-terminal frameshift mutation in *CEBPA* was called by Varvis software [c.308dup; p.Gly104fs, 35.3% allele frequency (AF)]. Another N-terminal frameshift mutation in *CEBPA* was not called (minimum called AF 7% at high coverage) but visible in approximately 7% of reads of the alignment visualized in IGV (c.116_117delinsA; p.Pro39fs) (14).

The *FLT3*-ITD was called with an AF of 57.7%. A 1.37-Mbp spanning loss including *NF1* and *SUZ12* was also detected by Varvis software (CN 1, no mosaic). In the remaining copy of *NF1*, no mutations were detected. On the other hand, in *SUZ12*, a c.682C>T (p.Pro228Ser) missense mutation at AF of 89.7% was detected (tier 3 VUS), which is absent in gnomAD. This result corresponded to the CNV loss in >90% blast material.

Furthermore, an *MLLT10*:c.2665G>A p.Val889Met missense mutation in exon 21 (tier 3 VUS) was observed, which is extremely rare in gnomAD. Also, the *DDX3X: MLLT10* genomic breakpoint in exon 4 (*DDX3X*) and intron 10 (*MLLT10*) was manually visible in the alignment and proven by Sanger sequencing.

Combining those genetic diagnostic methods led to the finding of several additional aberrations. *DDX3X: MLLT10* gene fusion and deletions in *NF1*, *SUZ12*, and *ARPP21* were detected with OGM and confirmed by WES. The gene fusion was additionally seen with FISH. Clonal TRD recombination as detected by OGM was validated using Sanger sequencing. The *FLT3*-ITD and biallelic *CEBPA* mutation found by standard RT-PCR were confirmed by WES.

Discussion

Acute leukemias have undergone tremendous changes regarding diagnostics and to a lesser extent treatments over the last years. We have recently described OGM as a potential tool to detect SVs on a genome-wide level with sufficient depth and high concordance to currently used methods as classical karyotyping (4). By implementing OGM in our diagnostic algorithm in combination with WES as part of an exemplary next-generation diagnostic workup, we could detect a *DDX3X: MLLT10* gene fusion, to the best of our knowledge, for the first time in a female AML patient. Both genes, *DDX3X* and *MLLT10*, have been previously described to be involved in hematological and non-hematological neoplasia (10, 11).

In detail, *DDX3X* has previously been described as a regulator of RNA metabolism (21). Its role as a tumor suppressor and simultaneously as an oncogenic driver is complex and yet to be fully understood (10). The helicase interacts with important key pathways including p53 and kirsten rat sarcoma virus homologue (KRAS) (22–25). Somatic mutations were found in a variety of cancers including medulloblastoma and hematological neoplasia such as acute and chronic lymphocytic leukemia (26, 27). *DDX3X* appears to be epigenetically silenced in renal cell carcinoma and has been discussed as a potential therapeutic target (28, 29).

Rearrangements involving the *MLLT10* gene are recurrent in ALL (more common in T-lineage ALL) and less often in AML (typically pediatric) (12, 30, 31). Regardless of the partner gene, *MLLT10* rearrangements appear to be associated with an adverse outcome in AML (5). MLLT10 is involved in histone modification by regulating the function of the histone methyltransferase DOT1L, the only methyltransferase known to methylate H3K79. In *MLLT10*-rearranged leukemia, DOT1L induces the transcription of genes involved in cell cycle progression (especially genes in the Homeobox A Cluster) (32–34). This might in the future have clinical implications, as a recent phase I trial with pinometostat, as a specific inhibitor of DOT1L, showed some promising results (35).

As in most ALL cases, reports of *DDX3X: MLLT10* fusions in AML are restricted to a few cases in male patients (5, 6). Apart from the *DDX3X: MLLT10* gene fusion, OGM could also unravel deletions in *ARPP21*, *NF1*, and *SUZ12*. SUZ12 is part of the polycomb repressive complex 2 (PRC2) that in turn is responsible for the methylation of H3K27 (36, 37). This methylation enables DOT1L with its complex to bind and exert its function as a transcription initiator for H3K79 (34). Thus, the *SUZ12* deletion and the *DDX3X: MLLT10* gene fusion might act synergistically in histone modification and could explain the aggressive course of disease (Figure 3).

ARPP21 is known to positively regulate *PHF6*-mRNA. It has a physiological counterpart, miRNA128, which is among others located at the 3′ end of *ARPP21* (20). OGM here clearly shows that the deletion does not affect miRNA128 and its intronic polymerase III-dependent open reading frame (19). Altogether, this might lead to a downregulation of *PHF6*-mRNA, which is a known tumor suppressor (38, 39).

Intriguingly, most of the findings uncovered by our next-generation diagnostic workup have rarely been associated with AML but are more common in early T-lineage ALL. In pediatric T-lineage ALL, *DDX3X* is the second most common fusion partner for *MLLT10* after *PICALM* (40). Furthermore, *SUZ12* and *PHF6* have been described in the context of T-ALL, with *PHF6* being one of the most frequently mutated or deleted genes in T-lymphoblastic leukemia and less often in AML and other myeloid neoplasia (38, 41, 42). Furthermore, OGM showed deletion SVs in the TCR regions representing clonal V(D)J recombinations. Clonal recombination of TRD and TRB could be indicative of an early stage in T-cell development. Combined with the immunophenotypic findings of CD34 and CD38 as well as lack of CD1a expression, these findings support the hypothesis that the leukemic blasts are in a pro-thymocyte (DN2) state (43, 44).

Lineage attribution today is mostly based on immunophenotyping, and AML and ALL are further classified according to genetic alterations relevant for further prognosis. This in turn leads to treatment protocols that 1) are lineage-specific, 2) are more or less intensive according to the genetic risk stratification, and 3) might include targeted therapies if actionable variants are detected. In the case described here, despite an aberrant CD7 expression in flow cytometry, routine diagnostics including cytology (Auer rods), immunohistology (myeloperoxidase and lysozyme expression), immunophenotyping by flow cytometry (Figure 1, Supplementary Figure S1), and the mutational profile (*FLT3*-ITD, *CEBPA*) led to the diagnosis of an AML. This is in line with the WHO 2016 classification, and even the older criteria of the European Group for the Immunological Classification of Leukemias (EGIL) would not have diagnosed a mixed-phenotype acute leukemia (MPAL) but an AML with aberrant coexpression of lymphatic markers due to the CD7 expression (45, 46). However, although being by far more prevalent in AML, neither Auer rods nor *FLT3*-ITD or *CEBPA* variants are exclusive to myeloid differentiation but have been previously described in ALL, especially in early T-cell precursor (ETP)-ALL (47–50).

In clinical practice, commitment to a diagnosis is necessary for defining the optimal treatment. Despite the arguably best available treatment protocol by adding FLT3-targeted therapy to standard "7 + 3" induction, treatment response was unsatisfying, without sufficient blast clearance. However, FLAG-containing regimens with consolidating allogeneic transplantation and sorafenib maintenance treatment in case of activating *FLT3*

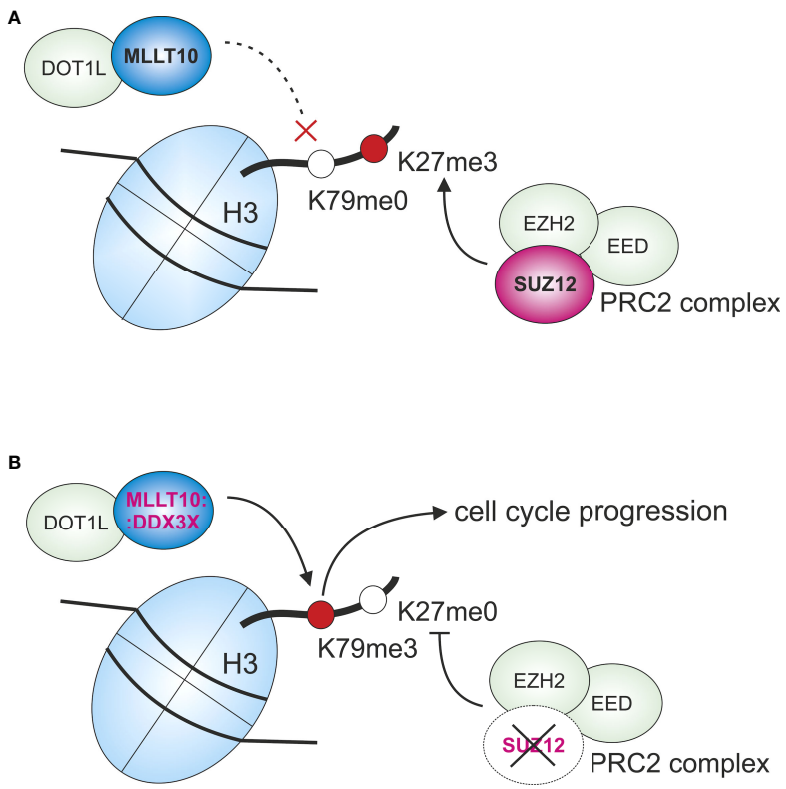

FIGURE 3
Graphic overview of interactions regarding histone 3 methylation with the participation of SUZ12 and MLLT10 under physiological conditions **(A)** and in the leukemic cells as suspected here **(B)**. **(A)** Under physiological conditions, PRC2 complex with SUZ12 and EED, and EZH2 methylates H3K27. This methylation abrogates the binding of DOT1L complex. **(B)** With SUZ12 being deleted, H3K27 is not methylated, which leads to binding of DOT1L complex and thereby to methylation of H3K79. This binding is probably additionally intensified because of *DDX3X: MLLT10* gene fusion, enabling transcription of genes that promote, among other effects, cell cycle progression, e.g., *HOXA* genes. H, histone; Me, methylated.

mutations not only are regular salvage approaches in refractory AML but also have been described as a successful therapy in ETP-ALL (51).

The immunophenotypic profile (including immunohistochemistry and flow cytometry) in this case was indicative of a myeloid differentiation (Figure 1C, Figure 4). Treatment with FLAG-Eto as salvage therefore was a straightforward approach. Compared to that, the initial diagnosis of a T-lineage disease not only would have led to a different treatment protocol but also might have changed the approach in the treatment-refractory situation with substances such as nelarabine. Thus, our here proposed broad genomic workup utilizing whole-genome cytogenetics and WES might in the future lead to a more distinct classification of disease and might help to overcome the flaws of immunophenotyping in certain situations. The detection of genetic changes typical for myeloid and early lymphoid differentiation as presented here could hint to a stem cell-like myeloid-lymphoid precursor, as has been very recently proposed by Genescà and Starza (52). This in turn could lead to more personalized approaches in treatment, omitting unwanted toxicities and improving the outcome for the patient (53).

Without OGM as a whole genome-based method with high resolution and deep coverage, the *DDX3X: MLLT10* gene fusion and other genetic aberrations not covered by routine diagnostics would have been missed. In this work, FISH, WES, and Sanger sequencing were applied as conformational diagnostics. Notably, the FISH probes used are far from any routine use. Thus, not only does OGM have the potential to improve the detection of novel aberrations but also it renders multiple other methods somewhat uncalled for.

In summary, by implementing OGM as a cytogenomic method, we detected SVs in genes involved in histone modification (*DDX3X: MLLT10*, *SUZ12)*, offering a

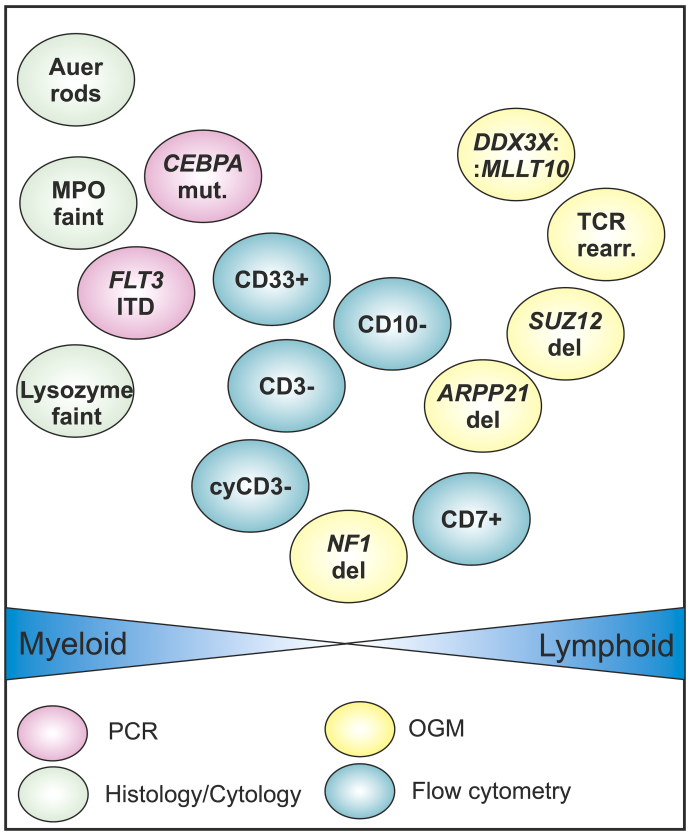

FIGURE 4
Graphical overview of selected diagnostic results obtained by different methodologies: results by optical genome mapping (OGM) are stained in yellow, PCR panel results in pink, histology results in green, and flow cytometry results in blue. The findings are positioned depending on their probability of occurrence in myeloid and lymphoid cells. The positioning reflects a general orientation and is not scaled. OGM findings are rather found on the lymphoid side. Cy, cytoplasmic; del, deletion; ITD, internal tandem duplication; MPO, myeloperoxidase.

functional explanation for aggressiveness of disease in this case. Furthermore, these and other detected variants (*ARPP21*, TCR variants) in combination with mutated myeloid genes also typical for ETP-ALL clearly hint lineage ambiguity, which was missed by routine diagnostic procedures relying on immunophenotyping for lineage discrimination. In conclusion, a next-generation diagnostic approach as proposed here has the potential to not only detect novel genetic variants but also improve risk stratification and thus individualized treatment.

Data availability statement

The data presented in the study are deposited under http://zenodo.org under accession number 6421158 387.

Ethics statement

This study was reviewed and approved by Ethik-Kommission der Medizinischen Fakultät der Ruhr-Universität Bochum Gesundheitscampus 33. The patients/participants provided their written informed consent to participate in this study. Written informed consent was obtained from the individual(s) for the publication of any potentially identifiable images or data included in this article.

Author contributions

VN-E, MT, WG and DBV prepared the manuscript. FD, TM, VN-E, DBV, RS and KD collected patient data. KL, MT and JL analyzed WES data. TL and SK performed and analyzed FISH experiments. HN, RS and DBV contributed to conception and

design of the study. All authors contributed to the article and approved the submitted version.

Funding

We thank FORUM of the Faculty of Medicine at the Ruhr-University Bochum for funding MT (medical doctoral thesis program) and VN-E as part of the Female Clinician Scientist program.

Acknowledgments

Thanks to Iris Over for expert technical assistance and the patient for participating in the study.

Conflict of interest

DV received speaker's honoraria from Roche, consultant's honoraria from Pfizer, Bristol Myers Squibb and Gilead as well as travel support and congress registration fees from Gilead and Celgene.

The remaining authors declare that the research was conducted in the absence of any commercial or financial relationships that could be construed as a potential conflict of interest.

Publisher's note

Supplementary material

The Supplementary Material for this article can be found online at: https://www.frontiersin.org/articles/10.3389/fonc.2022.959243/full#supplementary-material

SUPPLEMENTARY FIGURE 1
Immunophenotyping of bone marrow aspirate from the second time point before salvage chemotherapy. Despite a visible neutrophile-cloud compared to initial diagnosis, the blast-population with a similar expression profile is still clearly visible.

References

1. Shah A, Andersson TML, Rachet B, Björkholm M, Lambert PC. Survival and cure of acute myeloid leukaemia in England, 1971-2006: a population–based study. *Br J Haematol* (2013) 162:509–16. doi: 10.1111/BJH.12425

2. Available at: https://www.krebsdaten.de/Krebs/DE/Content/Publikationen/Krebs_in_Deutschland/kid_2019/krebs_in_deutschland_2019.pdf?_.

3. Döhner H, Estey E, Grimwade D, Amadori S, Appelbaum FR, Büchner T, et al. Diagnosis and management of AML in adults: 2017 ELN recommendations from an international expert panel. *Blood* (2017) 129(4):424–47. doi: 10.1182/blood-2016-08-733196

4. Gerding WM, Tembrink M, Nilius-Eliliwi V, Mika T, Dimopoulos F, Ladigan-Badura S, et al. Optical genome mapping reveals additional prognostic information compared to conventional cytogenetics in AML/MDS patients. *Int J Cancer* (2022) 384(10):924–35. doi: 10.1002/IJC.33942

5. Ries RE, Leonti AR, Triche TJ, Gerbing RB, Hirsch BA, Raimondi SC, et al. Structural variants involving MLLT10/AF10 are associated with adverse outcome in AML regardless of the partner gene - a COG/Tpaml study. *Blood* (2019) 134:461–1. doi: 10.1182/blood-2019-125943

6. Brandimarte L, la Starza R, Gianfelici V, Barba G, Pierini V, di Giacomo D, et al. DDX3X-MLLT10 fusion in adults with NOTCH1 positive T-cell acute lymphoblastic leukemia. *Haematologica* (2014) 99:64–6. doi: 10.3324/haematol.2013.101725

7. Brandimarte L, Pierini V, di Giacomo D, Borga C, Nozza F, Gorello P, et al. New MLLT10 gene recombinations in pediatric T-acute lymphoblastic leukemia. *Blood* (2013) 121:5064–7. doi: 10.1182/blood-2013-02-487256

8. Yang F, Babak T, Shendure J, Disteche CM. Global survey of escape from X inactivation by RNA-sequencing in mouse. *Genome Res* (2010) 20:614–22. doi: 10.1101/gr.103200.109

9. Dunford A, Weinstock DM, Savova V, Schumacher SE, Cleary JP, Yoda A, et al. Tumor-suppressor genes that escape from X-inactivation contribute to cancer sex bias. *Nat Genet* (2017) 49:10–16. doi: 10.1038/ng.3726

10. He Y, Zhang D, Yang Y, Wang X, Zhao X, Zhang P, et al. A double-edged function of DDX3, as an oncogene or tumor suppressor, in cancer progression (Review). *Oncol Rep* (2018) 39:883–92. doi: 10.3892/or.2018.6203

11. Mo J, Liang H, Su C, Li P, Chen J, Zhang B. DDX3X: structure, physiologic functions and cancer. *Mol Cancer* (2021) 20:1–20. doi: 10.1186/s12943-021-01325-7

12. Forgione MO, McClure BJ, Yeung DT, Eadie LN, White DL. MLLT10 rearranged acute leukemia: Incidence, prognosis, and possible therapeutic strategies. *Genes Chromosomes Cancer* (2020) 59:709–21. doi: 10.1002/gcc.22887

13. Kent WJ. BLAT–the BLAST-like alignment tool. *Genome Res* (2002) 12:656–64. doi: 10.1101/GR.229202

14. Robinson JT, Thorvaldsdóttir H, Winckler W, Guttman M, Lander ES, Getz G, et al. Integrative genomics viewer. *Nat Biotechnol* (2011) 29:24–6. doi: 10.1038/nbt.1754

15. Brüggemann M, Kotrová M, Knecht H, Bartram J, Boudjogrha M, Bystry V, et al. Standardized next-generation sequencing of immunoglobulin and T-cell receptor gene recombinations for MRD marker identification in acute lymphoblastic leukaemia; a EuroClonality-NGS validation study. *Leukemia* (2019) 33:2241–53. doi: 10.1038/s41375-019-0496-7

16. Brochet X, Lefranc MP, Giudicelli V. IMGT/V-QUEST: the highly customized and integrated system for IG and TR standardized V-J and V-D-J sequence analysis. *Nucleic Acids Res* (2008) 36:W503-8. doi: 10.1093/nar/gkn316

17. Althari S, Najmi LA, Bennett AJ, Aukrust I, Rundle JK, Colclough K, et al. Unsupervised Clustering of Missense Variants in HNF1A Using Multidimensional Functional Data Aids Clinical Interpretation. *Am J Hum Genet* (2020) 107(4):670–82. doi: 10.1016/j.ajhg.2020.08.016

18. Tate JG, Bamford S, Jubb HC, Sondka Z, Beare DM, Bindal N, et al. COSMIC: the catalogue of somatic mutations in cancer. *Nucleic Acids Res* (2019) 47:D941–7. doi: 10.1093/NAR/GKY1015

19. Monteys AM, Spengler RM, Wan J, Tecedor L, Lennox KA, Xing Y, et al. Structure and activity of putative intronic miRNA promoters. *RNA* (2010) 16:495–505. doi: 10.1261/RNA.1731910

20. Rehfeld F, Maticzka D, Grosser S, Knauff P, Eravci M, Vida I, et al. The RNA-binding protein ARPP21 controls dendritic branching by functionally opposing the miRNA it hosts. *Nat Commun* (2018) 9:1–13. doi: 10.1038/s41467-018-03681-3

21. Soto-Rifo RTh´ T, , Ohlmann T. The role of the DEAD-box RNA helicase DDX3 in mRNA metabolism. *WIREs RNA* (2013) 4:369–85. doi: 10.1002/wrna.1165

22. Wu DW, Liu WS, Wang J, Chen CY, Cheng YW, Lee H. Reduced p21WAF1/CIP1 *via* alteration of p53-DDX3 pathway is associated with poor relapse-free survival in early-stage human papillomavirus-associated lung cancer. *Clin Cancer Res* (2011) 17:1895–905. doi: 10.1158/1078-0432.CCR-10-2316

23. Wu DW, Lee MC, Wang J, Chen CY, Cheng YW, Lee H. DDX3 loss by p53 inactivation promotes tumor malignancy *via* the MDM2/Slug/E-cadherin pathway and poor patient outcome in non-small-cell lung cancer. *Oncogene* (2014) 33:1515–26. doi: 10.1038/onc.2013.107

24. Sun M, Zhou T, Jonasch E, Jope RS. DDX3 regulates DNA damage-induced apoptosis and p53 stabilization. *Biochim Biophys Acta* (2013) 1833:1489–97. doi: 10.1016/J.BBAMCR.2013.02.026

25. Chen WJ, Wang WT, Tsai TY, Li HK, Lee YHW. DDX3 localizes to the centrosome and prevents multipolar mitosis by epigenetically and translationally modulating p53 expression. *Sci Rep* (2017) 7:1–20. doi: 10.1038/S41598-017-09779-W

26. Jones DTW, Jäger N, Kool M, Zichner T, Hutter B, Sultan M, et al. Dissecting the genomic complexity underlying medulloblastoma. *Nature* (2012) 488:100–5. doi: 10.1038/NATURE11284

27. Ojha J, Secreto CR, Rabe KG, van Dyke DL, Kortum KM, Slager SL, et al. Identification of recurrent truncated DDX3X mutations in chronic lymphocytic leukaemia. *Br J Haematol* (2015) 169:445–8. doi: 10.1111/bjh.13211

28. Wang L, Lawrence MS, Wan Y, Stojanov P, Sougnez C, Stevenson K, et al. SF3B1 and other novel cancer genes in chronic lymphocytic leukemia. *N Engl J Med* (2011) 365:2497–506. doi: 10.1056/NEJMOA1109016

29. Lin TC. DDX3X is epigenetically repressed in renal cell carcinoma and serves as a prognostic indicator and therapeutic target in cancer progression. *Int J Mol Sci* (2020) 21:1–13. doi: 10.3390/IJMS21082881

30. ben Abdelali R, Asnafi V, Petit A, Micol JB, Callens C, Villarese P, et al. The prognosis of CALM-AF10-positive adult T-cell acute lymphoblastic leukemias depends on the stage of maturation arrest. *Haematologica* (2013) 98:1711–7. doi: 10.3324/HAEMATOL.2013.086082

31. Borel C, Dastugue N, Cances-Lauwers V, Mozziconacci M-J, Prebet T, Vey N, et al. PICALM-MLLT10 acute myeloid leukemia: a French cohort of 18 patients. *Leuk Res* (2012) 36:1365–9. doi: 10.1016/j.leukres.2012.07.008

32. Deshpande AJ, Deshpande A, Sinha AU, Chen L, Chang J, Cihan A, et al. AF10 regulates progressive H3K79 methylation and HOX gene expression in diverse AML subtypes. *Cancer Cell* (2014) 26:896–908. doi: 10.1016/j.ccell.2014.10.009

33. Uğurlu-Çimen D, Odluyurt D, Sevinç K, Özkan-Küçük NE, Özçimen B, Demirtaş D, et al. AF10 (MLLT10) prevents somatic cell reprogramming through regulation of DOT1L-mediated H3K79 methylation. *Epigenet Chromatin* (2021) 14:1–13. doi: 10.1186/S13072-021-00406-7/FIGURES/5

34. Chen S, Yang Z, Wilkinson AW, Deshpande AJ, Sidoli S, Krajewski K, et al. The PZP domain of AF10 senses unmodified H3K27 to regulate DOT1L-mediated methylation of H3K79. *Mol Cell* (2015) 60:319–27. doi: 10.1016/j.molcel.2015.08.019

35. Stein EM, Garcia-Manero G, Rizzieri DA, Tibes R, Berdeja JG, Savona MR, et al. The DOT1L inhibitor pinometostat reduces H3K79 methylation and has modest clinical activity in adult acute leukemia. *Blood* (2018) 131:2662–9. doi: 10.1182/BLOOD-2017-12-818948

36. Erokhin M, Chetverina O, Győrffy B, v. TV, Mogila V, AA S, et al. Clinical correlations of polycomb repressive complex 2 in different tumor types. *Cancers (Basel)* (2021) 13:1–26. doi: 10.3390/CANCERS13133155/S1

37. Cao R, Wang L, Wang H, Xia L, Erdjument-Bromage H, Tempst P, et al. Role of histone H3 lysine 27 methylation in polycomb-group silencing. *Science* (2002) 298:1039–43. doi: 10.1126/SCIENCE.1076997

38. Wang J, Leung JWC, Gong Z, Feng L, Shi X, Chen J. PHF6 regulates cell cycle progression by suppressing ribosomal RNA synthesis. *J Biol Chem* (2013) 288:3174–83. doi: 10.1074/JBC.M112.414839

39. Hsu YC, Chen TC, Lin CC, Yuan CT, Hsu CL, Hou HA, et al. Phf6-null hematopoietic stem cells have enhanced self-renewal capacity and oncogenic potentials. *Blood Adv* (2019) 3:2355. doi: 10.1182/BLOODADVANCES.2019000391

40. Liu Y, Easton J, Shao Y, Maciaszek J, Wang Z, Wilkinson MR, et al. The genomic landscape of pediatric and young adult T-lineage acute lymphoblastic leukemia. *Nat Genet* (2017) 49:1211–8. doi: 10.1038/NG.3909

41. Chen B, Jiang L, Zhong ML, Li JF, Li BS, Peng LJ, et al. Identification of fusion genes and characterization of transcriptome features in T-cell acute lymphoblastic leukemia. *Proc Natl Acad Sci USA* (2017) 115:373–8. doi: 10.1073/pnas.1717125115

42. Kurzer JH, Weinberg OK. PHF6 mutations in hematologic malignancies. *Front Oncol* (2021) 11:704471. doi: 10.3389/fonc.2021.704471

43. Halkias J, Melichar HJ, Taylor KT, Robey EA. Tracking migration during human T cell development. *Cell Mol Life Sci* (2014) 71:3101–17. doi: 10.1007/S00018-014-1607-2/FIGURES/3

44. Dik WA, Pike-Overzet K, Weerkamp F, de Ridder D, de Haas EFE, Baert MRM, et al. New insights on human T cell development by quantitative T cell receptor gene rearrangement studies and gene expression profiling. *J Exp Med* (2005) 201:1715–23. doi: 10.1084/JEM.20042524

45. Arber DA, Orazi A, Hasserjian R, Thiele J, Borowitz MJ, le Beau MM, et al. The 2016 revision to the world health organization classification of myeloid neoplasms and acute leukemia. *Blood* (2016) 127:2391–405. doi: 10.1182/blood-2016-03-643544

46. Bene MC, Castoldi G, Knapp W, Ludwig WD, Matutes E, Orfao A, et al. Proposals for the immunological classification of acute leukemias. European group for the immunological characterization of leukemias (EGIL). *Leukemia* (1995) 9:1783–6.

47. Neumann M, Coskun E, Fransecky L, Mochmann LH, Bartram I, Farhadi Sartangi N, et al. FLT3 mutations in early T-cell precursor ALL characterize a stem cell like leukemia and imply the clinical use of tyrosine kinase inhibitors. *PloS One* (2013) 8:1–10. doi: 10.1371/journal.pone.0053190

48. Zhang J, Ding L, Holmfeldt L, Wu G, Heatley SL, Payne-Turner D, et al. The genetic basis of early T-cell precursor acute lymphoblastic leukaemia. *Nature* (2012) 481:157–63. doi: 10.1038/nature10725

49. Li Y, Yang W, Wang W, Lin D, Wei H, Wang Y, et al. Auer rods in mixed phenotype acute leukemia, t/myeloid: A report of three cases. *Leukemia Res Rep* (2021) 15:1–3. doi: 10.1016/j.lrr.2021.100236

50. Alexander TB, Gu Z, Iacobucci I, Dickerson K, Choi JK, Xu B, et al. The genetic basis and cell of origin of mixed phenotype acute leukaemia. *Nature* (2018) 562:373–406. doi: 10.1038/s41586-018-0436-0

51. Bataller A, Garrote M, Oliver-Caldés A, López-Guerra M, Colomer D, Aymerich M, et al. Early T-cell precursor lymphoblastic leukaemia: response to FLAG-IDA and high-dose cytarabine with sorafenib after initial refractoriness. *Br J Haematol* (2019) 185:755–7. doi: 10.1111/bjh.15601

52. Genescà E, la Starza R. Early T-cell precursor ALL and beyond: Immature and ambiguous lineage T-ALL subsets. *Cancers (Basel)* (2022) 14:1–17. doi: 10.3390/cancers14081873

53. Turk S, Turk C, Akbar MW, Kucukkaraduman B, Isbilen M, Canli SD, et al. Renin angiotensin system genes are biomarkers for personalized treatment of acute myeloid leukemia with doxorubicin as well as etoposide. *PLoS One* (2020) 15:1–17. doi: 10.1371/journal.pone.0242497

frontiers | Frontiers in Oncology

TYPE Original Research
PUBLISHED 12 September 2022
DOI 10.3389/fonc.2022.947492

OPEN ACCESS

EDITED BY
Spiros Vlahopoulos,
University of Athens, Greece

REVIEWED BY
Armando Reyes-Palomares,
Complutense University
of Madrid, Spain
Junmin Li,
Shanghai Institute
of Hematology, China

*CORRESPONDENCE
Meng Lv
drlvmeng@bjmu.edu.cn
Li-Juan Hu
hulijuan3619@163.com

SPECIALTY SECTION
This article was submitted to
Hematologic Malignancies,
a section of the journal
Frontiers in Oncology

RECEIVED 18 May 2022
ACCEPTED 11 August 2022
PUBLISHED 12 September 2022

CITATION
Zhao Y, Niu L-T, Hu L-J and Lv M
(2022) Comprehensive analysis of
ECHDC3 as a potential biomarker and
therapeutic target for acute myeloid
leukemia: Bioinformatic analysis and
experimental verification.
Front. Oncol. 12:947492.
doi: 10.3389/fonc.2022.947492

Comprehensive analysis of ECHDC3 as a potential biomarker and therapeutic target for acute myeloid leukemia: Bioinformatic analysis and experimental verification

Yijing Zhao, Li-Ting Niu, Li-Juan Hu* and Meng Lv*

Peking University People's Hospital, Peking University Institute of Hematology, National Clinical Research Center for Hematologic Disease, Beijing Key Laboratory of Hematopoietic Stem Cell Transplantation, Beijing, China

Background: Enoyl-CoA hydratase domain containing 3 (ECHDC3) increased in $CD34^+$ progenitor cells of acute myeloid leukemia (AML) cells after chemotherapy. However, the prognostic significance and function of ECHDC3 in AML remain to be clarified.

Methods: In the training cohort, 24 AML (non-acute promyelocytic leukemia, APL) patients were enrolled in Peking University People's Hospital and tested for ECHDC3 in enriched $CD34^+$ cells at diagnosis. In the validation set, 351 bone marrow RNA-seq data of non-APL AML were obtained by two independent online datasets (TCGA-LAML and BEAT-AML). LASSO regression model was conducted to a new prediction model of ECHDC3-related genes. In addition, the ECHDC3 signature was further explored by GO, KEGG, GSEA, and immuno-infiltration analysis. By RNA interference, the function of ECHDC3 in mitochondrial DNA (mt-DNA) transcriptome and chemoresistance was further explored, and the GSE52919 database re-verified the ECHDC3 chemoresistance feature.

Results: By Kaplan-Meier analysis, patients with $ECHDC3^{high}$ demonstrated inferior overall survival (OS) compared to those with $ECHDC3^{low}$ both in the training (2-year OS, 55.6% *vs.* 100%, p = 0.011) and validation cohorts (5-year OS, 9.6% *vs.* 24.3%, p = 0.002). In addition, $ECHDC3^{high}$ predicted inferior OS in the subgroup of patients with ELN 2017 intermediated (int) risk (5-year OS, 9.5% *vs.* 26.3%, p = 0.039) or FLT3 +NPM1– adverse (adv) risk (4-year OS, 6.4% *vs.* 31.8%, p = 0.003). In multivariate analysis, ECHDC3 was an independent risk factor of inferior OS (HR 1.159, 95% CI 1.013–1.326, p = 0.032). In the prediction model combining ECHDC3 and nine selected genes (RPS6KL1, RELL2, FAM64A, SPATS2L, MEIS3P1, CDCP1, CD276, IL1R2, and OLFML2A) by Lasso regression, patients with high risk showed inferior 5-year OS (9.3% *vs.* 23.5%, p < 0.001). Bioinformatic analysis suggested that ECHDC3 alters the bone marrow microenvironment by inducing NK, resting mast cell, and monocyte differentiation. Knocking down ECHDC3 in AML cells by RNAi promoted the death of leukemia cells with cytarabine and doxorubicin.

Conclusion: These bioinformatic analyses and experimental verification indicated that high ECHDC3 expression might be a poor prognostic biomarker for non-APL AML, which might be a potential target for reverting chemoresistance.

KEYWORDS

ECHDC3, acute myeloid leukemia, immune cell infiltration, re-stratification, chemoresistance

Introduction

Acute myeloid leukemia (AML) is a heterogeneous disease characterized by different molecular subtypes with different prognoses and responses to treatment. Patients up to the age of 60 years reported 5-year survival rates of 30%–35% and <10%–15% for older patients (age 60 years and older) (1). The "3 + 7 regimen" (3 days of daunorubicin + 7 days of cytarabine) has long been considered the standard of care, resulting in long-term cures of 30%–40% among younger patients with AML. Therefore, finding a new target biomarker to change the therapy model from "one-set-fits-all" to "individualized stratified treatment" is an urgent problem needed to be solved (2).

Targeting mitochondrial metabolism was considered the most promising treatment for AML (3). Fatty acid metabolism is a key energy pathway for the survival of AML cells in the adipocyte-abundant bone marrow (BM) microenvironment. Adipocytes are the prevalent stromal cell type in adult BM, and leukemia cells continuously adapt to deficiency of nutrients acquiring chemoresistant profiles in the BM microenvironment (4). The latest data show that inhibition of fatty acid metabolism re-sensitizes resistant leukemia stem cells to venetoclax with azacitidine (5, 6). Enoyl-CoA hydratase domain containing 3 (ECHDC3), broadly expressed in adipocytes, is predicted to be active in the mitochondrion, involving fatty acid biosynthesis and lipid metabolism (7). Our team firstly reported that ECHDC3 was upregulated in $CD34^+$ progenitors of chemoresistant AML (8), whereas the prognostic significance and function of ECHDC3 in AML have yet to be clarified.

By integrating bioinformatic analysis and experimental verification, this study aims to characterize the prognostic significance of ECHDC3 in AML and its role in chemoresistance and immune microenvironment.

Materials and methods

Patients and samples

According to the Declaration of Helsinki, the study was approved by the ethics review board of Peking University People's Hospital, and enrolled patients provided written informed consent. All the enrolled patients were diagnosed and treated at Peking University People's Hospital, Beijing, China.

The inclusion criteria are as follows: (i) newly diagnosed *de novo* AML (non-acute promyelocytic leukemia, APL), age 16–70 years; (ii) no previous antineoplastic therapy; (iii) ECOG performance score ≤ 2, without other major coexisting illnesses such as severe kidney and liver insufficiency.

BM samples were acquired before the first induction chemotherapy. Cell sorting and mass spectrometry measurements were followed as published study (8). The diagnosis, classifications, and risk stratification were based on European Leukemia Net (ELN) recommendations (9). Induction, consolidation, and allogeneic hematopoietic stem cell transplant (allo-HSCT) followed our previous report (10).

Cell lines culture conditions

The human AML cell lines K562 were purchased from the American Type Culture Collection (ATCC) agent in China. All the cell lines have passed the STR authentication. Cell lines were cultured in RPMI 1640 medium (Thermo Fisher Scientific, Cat#11875093, USA) containing 10% FBS (Thermo Fisher Scientific, Cat#12483020, USA) and 1× antibiotic–antimycotic (Thermo Fisher Scientific, Cat#15240096, USA). Cells were grown at 37°C in a humidified atmosphere with 5% CO_2.

Online data acquisition

The clinical and transcription matrix of AML was downloaded from the TCGA database (https://portal.gdc.cancer.gov/) and the Beat AML database (http://www.vizome.org/aml/). We retrieved 154 non-APL AML BM mRNA sequence data (excluded 16 APL and 3 incomplete data) and corresponding clinicopathological characteristics from the TCGA. Additionally, 197 BM mRNA sequence data (excluded 9 APL and 25 incomplete data) were retrieved from the Beat AML database (BEAT-AML). The GSE52919 database (https://

www.ncbi.nlm.nih.gov/geo/) was performed to analyze the correlation of ECHDC3 expression with cytarabine (Ara-C) sensitivity in AML samples.

Lasso regression analysis, risk model establishment, and validation

Lasso regression was constructed by the glmnet R package according to the method previously published by our institute (11). In brief, 249 differentially expressed genes (DEGs) were identified by the comparison of ECHDC3 high and low expression samples according to the criteria $|\log_2 FC|>1$ and adjusted $p < 0.05$. LASSO regression was then applied to remove redundant prognostic genes based on the coefficient and partial likelihood deviance for developing the prognostic model. ECHDC3 and other Nine hub genes (RPS6KL1, RELL2, FAM64A, SPATS2L, MEIS3P1, CDCP1, CD276, IL1R2, and OLFML2A) were ultimately retained. Then, the hub genes were used to construct a risk signature based on the coefficient for each patient according to the following formula: $RS = \sum_{i=1}^{n} Coef(i) X(i)$, where Coef($i$) denotes the coefficient, and $X(i)$ is the z-score transformed relative expression level for each DEG. To validate the established model, the prognostic risk score of each patient was calculated using the formula, and, according to the median score, patients were classified into high- and low-risk groups. Then, time-dependent receiver operating characteristic (ROC) curve (tdROC) and Kaplan-Meier survival curve analysis were performed to verify this risk score system (Figures 4C, D).

Gene function analysis

Gene ontology (GO) and Kyoto Encyclopedia of Genes and Genomes (KEGG) enrichment analysis of differentially expressed ECHDC3 were performed using the R package "cluster profile". GO terms were classified as molecular functions (MFs), biological processes (BP), and cellular components (CCs). Both p- and q-values less than 0.05 were considered to indicate statistically significant differences. Gene set enrichment analysis (GSEA) was performed to find enriched term differences.

Immune infiltration analysis

The gene transcriptome data were used to estimate the content of multiple immune cells infiltrated in the BM microenvironment. CIBERSORT in combination with the LM22 signature matrix was used to estimate the fractions of 22 human immune cell phenotypes between AML samples with high or low ECHDC3 expression. The CIBERSORT analysis was conducted in R software by the CIBERSORT R script (version 1.03). The correlation analysis of the index was completed using the Spearman's test.

ECHDC3 knockdown

ECHDC3 siRNA was designed and synthesized by GenePharma (Shanghai, China). The plasmid was then transfected into the K562 cell lines. Opti-MEM medium and Lipofectamine L300015 reagent were used for the transfection of siRNA according to the manufacturer's instructions. After transfection, whole-cell cDNAs were synthesized, and quantitative real-time PCR was performed to verify the ECHDC3 expression level.

Cell viability assay

Ara-C (cytarabine) and doxorubicin (DOX) were purchased from Selleck Chemicals (Selleck, USA). Cell viability was determined by CCK-8 assay (Bimake, Cat#B34034, USA). The cells were seeded in a density of 2×10^4 cells/100 µl in a 96-well plate and incubated at 37°C for 48 h. Ten microliters of CCK-8 was added to each well of the 96-well plate, followed by further incubation for 1 h. The absorbance was measured at 450 nm. The cell viability was calculated using GraphPad Prism software.

Mitochondria transcriptome

Whole-cell cDNAs were synthesized, and quantitative real-time PCR was performed using the FastStart Universal SYBR Green Master mix (Millipore Sigma, MA, USA) with a StepOnePlus real-time PCR system (ABI Prism 7900HT; Applied Biosystems, USA). The threshold cycle (Ct) values of target genes were normalized over the Ct of β-actin in whole-cell lysate. For comparison, the siCT group was set as 1 unless otherwise indicated. Primers used for real-time PCR and quantitative real-time PCR are listed in Table S1.

Statistical analysis

R software 4.05 and GraphPad Prism 8.0.2 were mainly used for laboratory data statistical analysis. Comparisons between the two groups were performed using the Mann-Whitney *U*-test for continuous variables and the X2 test for categorical data. $P < 0.05$ marked with *, $P < 0.01$ marked with **, and $P < 0.005$ marked with *** are considered significant. The survival functions were estimated by the Kaplan-Meier method using the log-rank test with asymmetric 95% confidence intervals (CIs). Variables included in the multivariate analysis (MVA) were selected by

the backward elimination process with a criterion of P < 0.10 for retention. Age is linear with estimates of HRs for 10-year difference.

The total study design is illustrated in Figure 1.

Results

High ECHDC3 predicts inferior OS in the training and validation cohort

In the training cohort, 24 AML (APL) patients were enrolled between September 2019 and September 2020, followed up to July 2022. According to the median protein level of ECHDC3 in enriched $CD34^+$ cells at diagnosis, patients were divided into "$ECHDC3^{high}$" and "$ECHDC3^{low}$" groups, and the baseline characteristics were similar between the two groups (Table S2). By median follow-up of 23.7 months, 11 patients experienced relapse, which corresponds to a 2-year probability of relapse at 45.8% (95% CI, 24.1–65.1), in which 5 patients achieved CR2 and preceding to allo-HSCT. None of these patients had non-relapse mortality. OS was significantly lower in the $ECHDC3^{high}$ group than in the $ECHDC3^{low}$ (2-year OS, 55.6% *vs.* 100%; 95% CI, 23.1–79.0 *vs.* 100%; p = 0.011, Figure 2A). There was a trend that $ECHDC3^{high}$ conferred inferior leukemia-free survival (2-year LFS, 41.7% *vs.* 66.7%, p = 0.178, Figure S1A) but without statistical significance.

In the validation set, 351 BM RNA-seq data of non-APL AML were obtained by two independent online datasets (TCGA-LAML and BEAT-AML). Patients were divided into "$ECHDC3^{high}$" and $ECHDC3^{low}$" groups according to the median expression level of ECHDC3 in BM, and the baseline characteristics were listed in Table 1. OS was significantly lower in the $ECHDC3^{high}$ group than in the $ECHDC3^{low}$ (5-year OS, 9.6% *vs.* 24.3%; p = 0.002; Figure 2B). Correspondingly, the alive patients showed a lower ECHDC3 expression level compared to dead patients (P = 0.0009; Figure 2C). Of the RNA-seq data of 180 peripheral blood (PB) samples of non-APL AML in BEAT-AML, $ECHDC3^{high}$ also showed inferior 5-year OS (3.5% *vs.* 14.8%; 95% CI, 23.1–79.0 *vs.* 100%; p = 0.045; Figure S1B).

In the validation set, the expression of ECHDC3 was analyzed by age and ELN risk groups. Patients more than 60 showed higher ECHDC3 levels compared to those less or equal to 60 (p = 0.023; Figure 2D). In different risk subgroups, patients of int risk or adv risk showed a higher level of ECHDC3 compared with those of favorable (fav) risk (p < 0.001; p < 0.001; respectively; Figure 2E); meanwhile, there was no significant difference in ECHDC3 level between int- and adv-risk groups (p=0.23).

Furthermore, to test whether ECHDC3 would be a useful biomarker in re-stratification of AML patients, subgroup analysis was carried out in fav-, int-, and adv-risk AML, as well as in patients with or without NPM1/FLT3 mutation. $ECHDC3^{high}$ predicted inferior 5-year OS in the subgroup of patients with ELN int-risk (9.5% *vs.* 26.3%, p = 0.039; Figure 2F) but not in the fav-risk or adv-risk groups (Figures S1C, D). In addition, $ECHDC3^{high}$ predicted inferior 5-year OS in the subgroup of FLT3+NPM1− adv-risk AML (6.4% *vs.* 31.8%, p = 0.003; Figure 2G). There was a trend that $ECHDC3^{high}$ related to inferior 3-year OS of FLT3−NPM1+ fav-risk AML (31.7% *vs.* 54.8%, p = 0.077, Figure S1E) but without significance. Meanwhile, ECHDC3 did not affect OS in FLT3−NPM1− or FLT3+NPM1+ AML patients (Figures S1F, G).

As an expression of ECHDC3 in BM was associated with a high percentage of blast cells in PB and a low percentage of blast cells in BM (Figures S1H; Table 1), while there was a trend that a

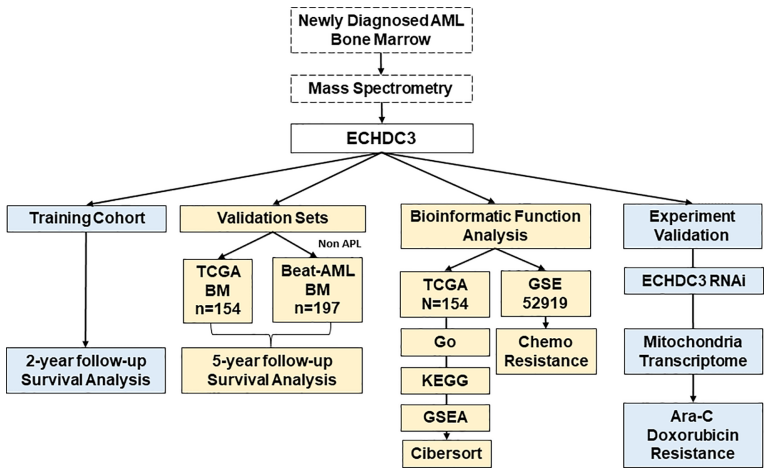

FIGURE 1
The flow chart of the study design and analysis.

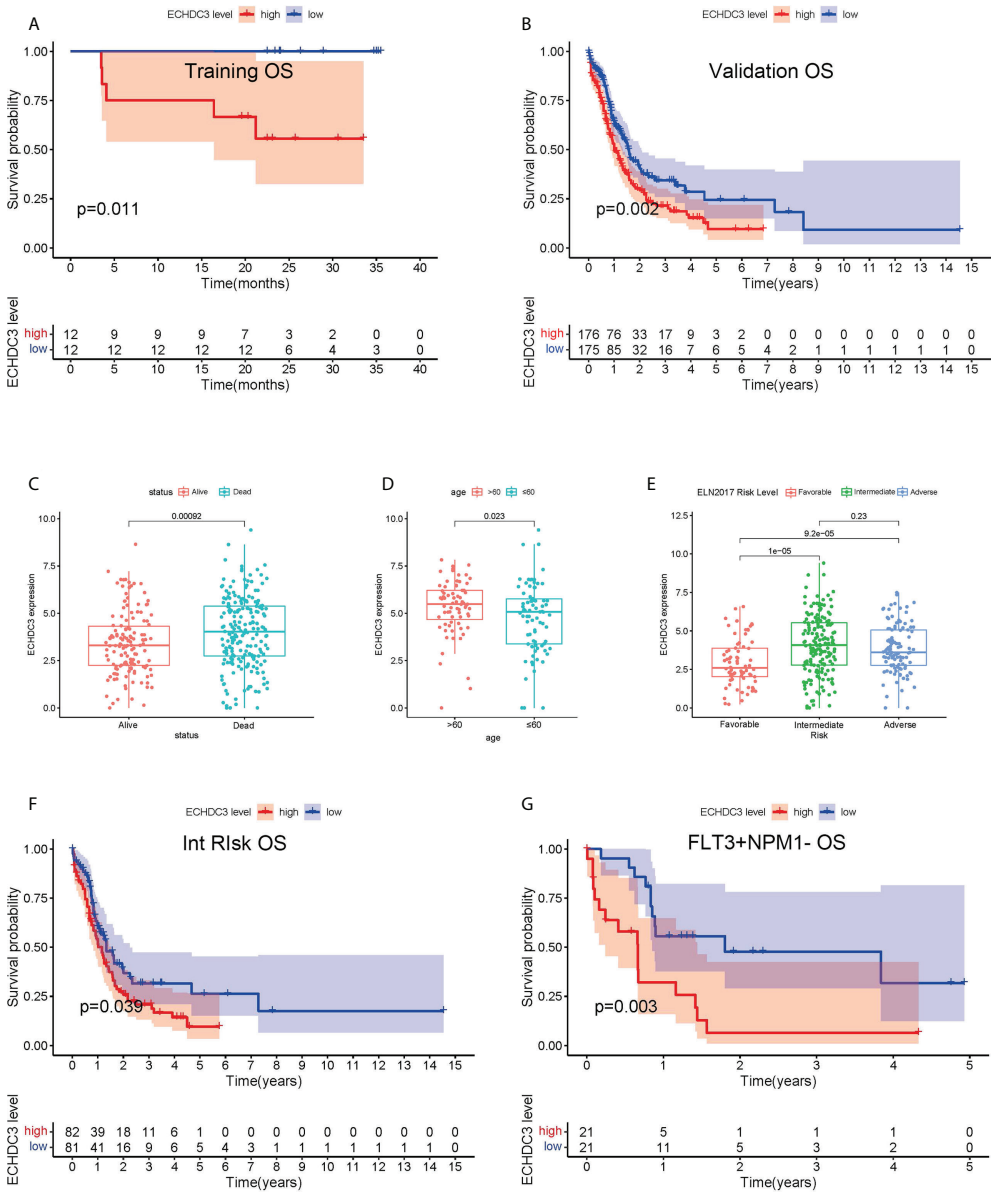

FIGURE 2
Prognostic value of ECHDC3 expression in training and validation. **(A)** Overall survival of non-APL AML patients in the training cohort (*de novo* AML patients). **(B)** Overall survival of non-APL AML patients in validation sets (TCGA-LAML and BEAT-AM bone marrow samples). **(C)** ECHDC3 expression in subgroups of alive and dead patients in validation sets. **(D)** ECHDC3 expression in subgroups of age >60 and age <=60 in validation sets. **(E)** ECHDC3 expression in subgroups of fav, int, and adv ELN risk in validation sets. **(F)** Overall survival of ELN int-risk AML in validation sets. **(G)** Overall survival of FLT3+NPM1– AML in validation sets.

high percentage of blast cells in PB rather than BM might be associated with inferior OS (Figure S1I, J), subgroup analysis was carried out addressing the percentage of blast cells in PB, which indicated that ECHDC3^{high} would be a useful biomarker predicting 5-year OS in the subgroup with a high ($p < 0.001$) rather than a low percentage of blast cells ($p = 0.537$) in PB (Figures S1K, L).

Among the confounding factors in univariate analysis, ECHDC3, age, and risk stratification level were chosen for MVA (Figure 3A). ECHDC3 was confirmed as an independent prognostic factor for OS (HR 1.159, 95% CI 1.013–1.326, $p = 0.032$; Figure 3B). Age is another independent prognostic factor (HR 1.291, 95% CI 1.114– 1.496, $p < 0.001$). Meanwhile, ELN risk might be an independent prognostic factor without

TABLE 1 Patient characteristics of validation sets.

	ECHDC3 High (n =176)	ECHDC3 Low (n = 175)	P
Sex, male/female	100/76	94/81	0.4898
Median age, years (range)	61 (21–88)	42.5 (18–61)	<0.0001*
Median PB blasts, %	67 (0–99)	47 (0–99.2)	0.0004*
Median WBC, × 109/L	22.95 (1–297)	17.9 (0.5–427.46)	0.0724
Median BM blasts, % (range)	36 (0–98)	62 (0–98)	<0.0001*
FAB classifications			<0.0001*
M0	13	6	
M1	30	18	
M2	30	12	
M4	34	17	
M5	26	14	
M6	2	0	
M7	3	1	
NA	38	107	
Risk level			0.1714
Favorable	22	48	
Intermediate	102	71	
Adverse	49	55	
NA	3	1	

*means statistic difference was observed.
NA, Not Available.

statistical significance (HR 1.365, 95% CI 0.972–1.915, p = 0.072; Figure 3B).

The combination of ECHDC3 and other risk factors improves the accuracy of survival prediction

As ECHDC3, age, and ELN risk were independent risk factors for OS, then we combined these three factors as a new prognostic model and tested it in non-APL AML patients of TCGA-LAML datasets (excluding four cases due to missing data). Adding ECHDC3 expression to age and ELN risk improved the area under the curve (AUC) from 0.657 to 0.671 of ROC (Figure 4A). A risk-score model combining ECHDC3, age, and ELN risk was developed based on a linear combination of each parameter (Coef) weighted by the regression coefficient derived from the univariate Cox regression analysis (β). The equation was calculated as $RS = \sum_{i=1}^{154} Coef\ (i) * \beta\ (i)$ .According to the median risk score, patients with high-risk scores have inferior 5-year OS (7.6% *vs*. 27.7%, p < 0.001; Figure 4B).

In non-APL AML patients of TCGA-LAML datasets, a total of 249 survival correlated genes (according to the criteria |log2FC| > 1 and adjusted p < 0.05) performed 6-fold cross-validation and 9 genes in addition to ECHDC3 were finally found with regression coefficients, namely, RPS6KL1, RELL2, FAM64A, SPATS2L, MEIS3P1, CDCP1, CD276, IL1R2, and OLFML2A (Figures S2A–C). Each gene was an independent prognostic factor by two-way interactions checked between the factors with the main effect in chi-square analysis (Figure S2D). Next, the prognostic model was established with Lasso regression to improve the predicted accuracy for overall survival in AML. The equation is calculated as $RS = \sum_{i=1}^{154} Coef\ (i) * gene\ expression\ (i)$, and that is Y = ECHDC3 × 0.0127-RPS6KL1 × 0.0006 + RELL2 × 0.0256-FAM64A × 0.0823 + SPATS2L × 0.0611-MEIS3P1 × 0.0284 + CDCP1 × 0.0296 + CD276 × 0.0099 + IL1R2 ×0.0033 + OLFML2A × 0.1069 in this study. Y ≥ 3.090 is categorized as "high risk" (Figures S2E–F). The AUC of the ROC curve following this risk model is 0.792 (Figure 4C). Patients with high-risk score have inferior 5-year OS (9.3% *vs*. 23.5%, p < 0.001; Figure 4D).

Bioinformatic analysis of ECHDC3 function

GSEA was performed to identify numbers of hallmark terms enriched in the high ECHDC3_exp and low ECHDC3_exp groups. The top 6 Hallmark terms identified in the low ECHDC3_exp group were mainly immune-related (Figure S3A), namely, complement system, IL6 signaling, IFN-α, IFN-γ, P53, and xenobiotic metabolism. Additionally, Figure 5A showed the KEGG term enriched in high ECHDC3_exp and low ECHDC3_exp groups.

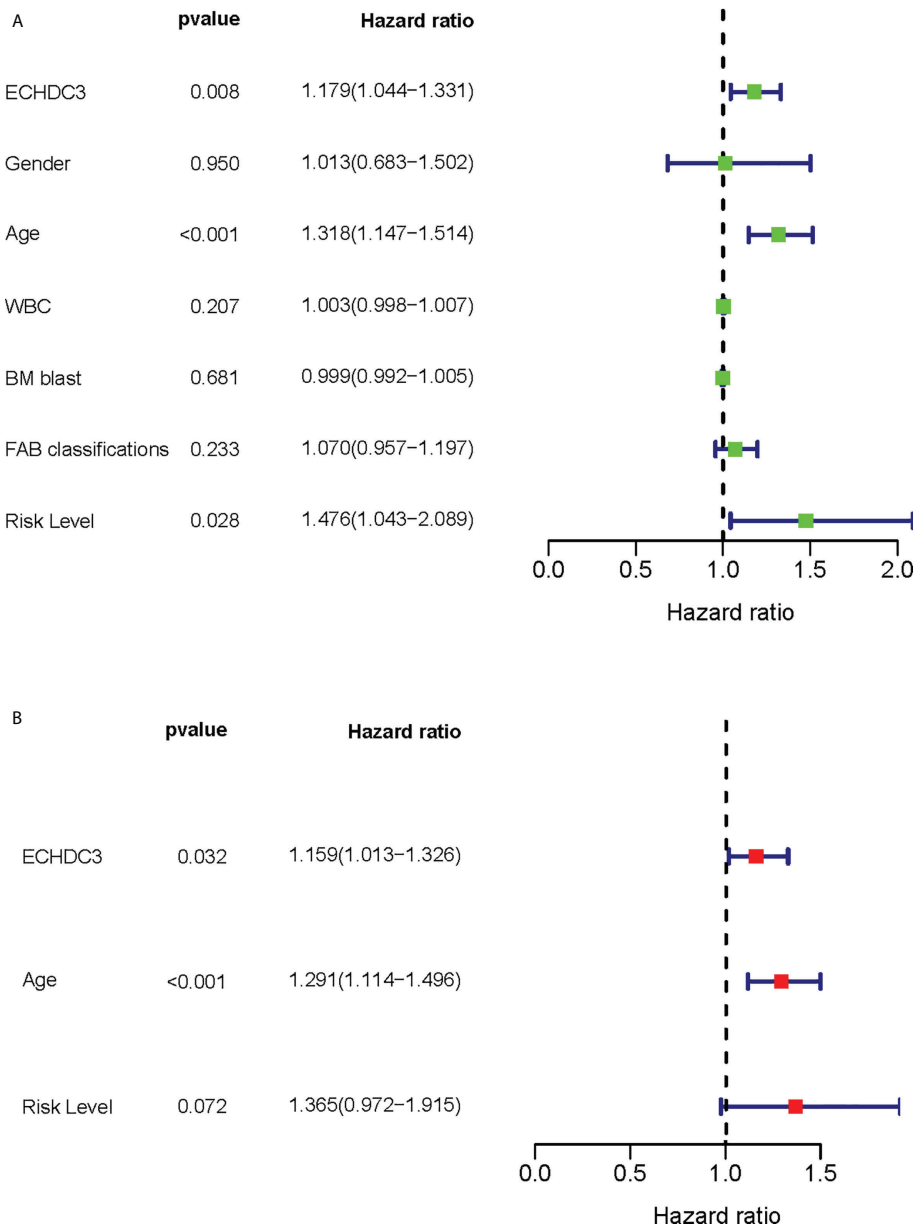

FIGURE 3
Cox regression analysis of ECHDC3 expression in validation sets. **(A)** Univariate Cox regression analysis for identification of AML patients' clinical character in validation sets. **(B)** Multivariate Cox regression analysis for identification of AML patients' clinical character in validation sets.

The top 40 DEGs, including 20 upregulated genes and 20 downregulated genes in ECHDC3^{high} and ECHDC3^{low} groups, were demonstrated in the heatmap (Figure S3B). By comparison of the top KEGG pathways enriched in DEGs in ECHDC3^{high} and ECHDC3^{low} groups, it showed that these marker genes mainly enriched in the phagosome, the intestinal immune network for IgA production, cell adhesion molecules, viral myocarditis, viral myocarditis, allograft rejection, antigen presentation, type I diabetes mellitus, and staphylococcus aureus infection (Figure S3C). GO analysis further declared the potential function of the DEGs (Figure S3D). The DEGs were most significantly enriched in the BP term of "positively regulation of cytokine production" and "regulation of leukocytes proliferation", in addition to the CC term of "collagen-containing extracellular matrix" and "external side of plasma membrane". In MF term, genes were enriched of "amide

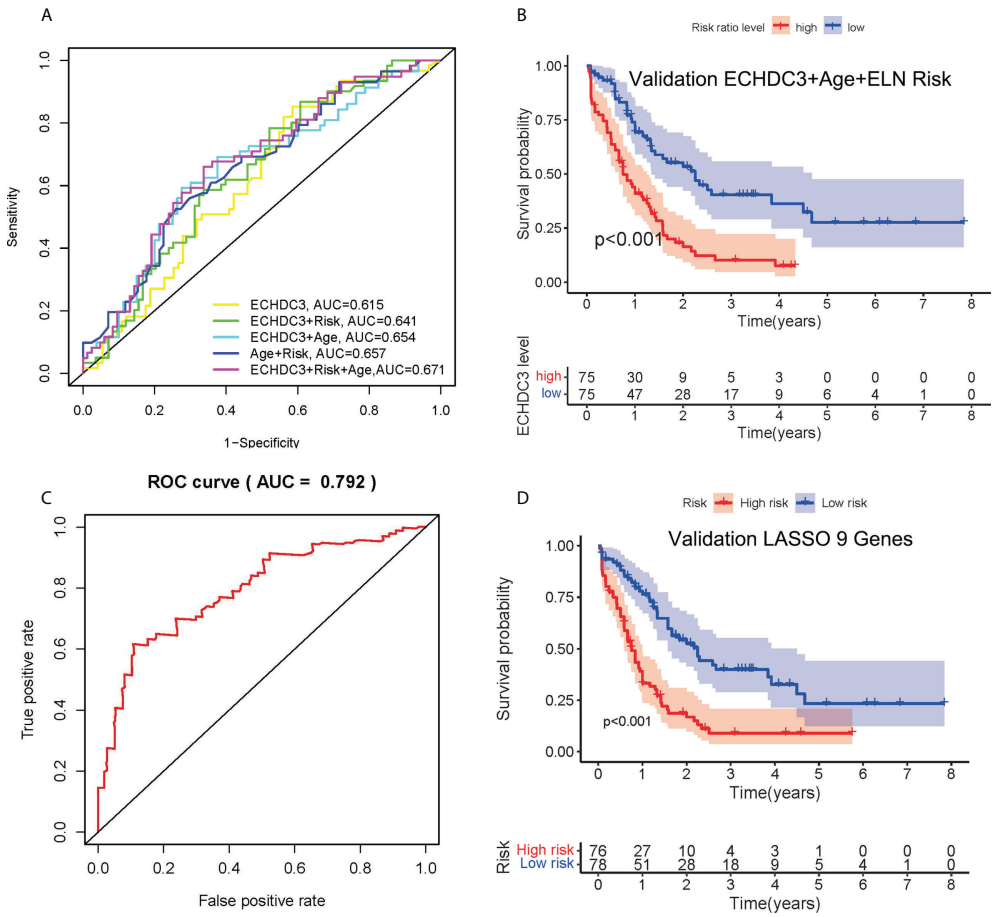

FIGURE 4
Combination of ECHDC3 and other risk factors in the prediction. **(A)** Time-dependent ROC analysis by combination of ECHDC3+age+ELN risk **(B)** Overall survival comparing high *vs*. low risk in the new model of ECHDC3 + age + ELN risk. **(C)** Time-dependent ROC analysis in the new model by LASSO regression. **(D)** Overall survival comparing high *vs*. low risk in the new model by LASSO regression.

binding" and "peptide binding". These results indicated that the DEGs were distributed in the immune system–related processes and pathways, which have been proved to play a pivotal role in the immune microenvironment. The top 8 enriched GO terms and demonstrated represents genes were demonstrated in Figure 5B.

The immune landscape between ECHDC3^{high} and ECHDC3^{low} groups

In the BM microenvironment, immune infiltrating cells controlled the fate of AML cells. In this study, the composition of significant tumor-infiltrating immune cells was assessed by the CIBERSORT algorithm in the AML BM RNA-seq dataset. The histogram of immune infiltrating cells was shown in Figure S4A. Moreover, resting NK cells (p = 0.009), monocytes (p = 0.041), naïve CD4$^+$ T cells (p = 0.065), and resting mast cell (p= 0.039) had significant differences in the immune cell fractions between the two groups ECHDC3^{high} and ECHDC3^{low} (Figure 6). Next, the co-expression analysis using prognostic tumor-infiltrating immune cells in the AML cohort with ECHDC3^{high} and ECHDC3^{low} was performed. From Figures S4B–C, we can see that monocytes have a negative correlation with resting CD4$^+$ T memory cells and CD8$^+$ T cells in the immune phenotype profiles, whereas resting NK cells were positively correlated with T regulatory cells and resting CD4$^+$ T memory cells. Considering all the interpreted results, higher ECHDC3 expression may induce NK, mast cell resting, and monocyte differentiation, and ECHDC3 may directly alter the BM microenvironment cell infiltration.

The human leukocyte antigen (HLA) system is an important part of the immune system, and HLA encodes cell surface molecules specialized to present antigenic peptides to the T-

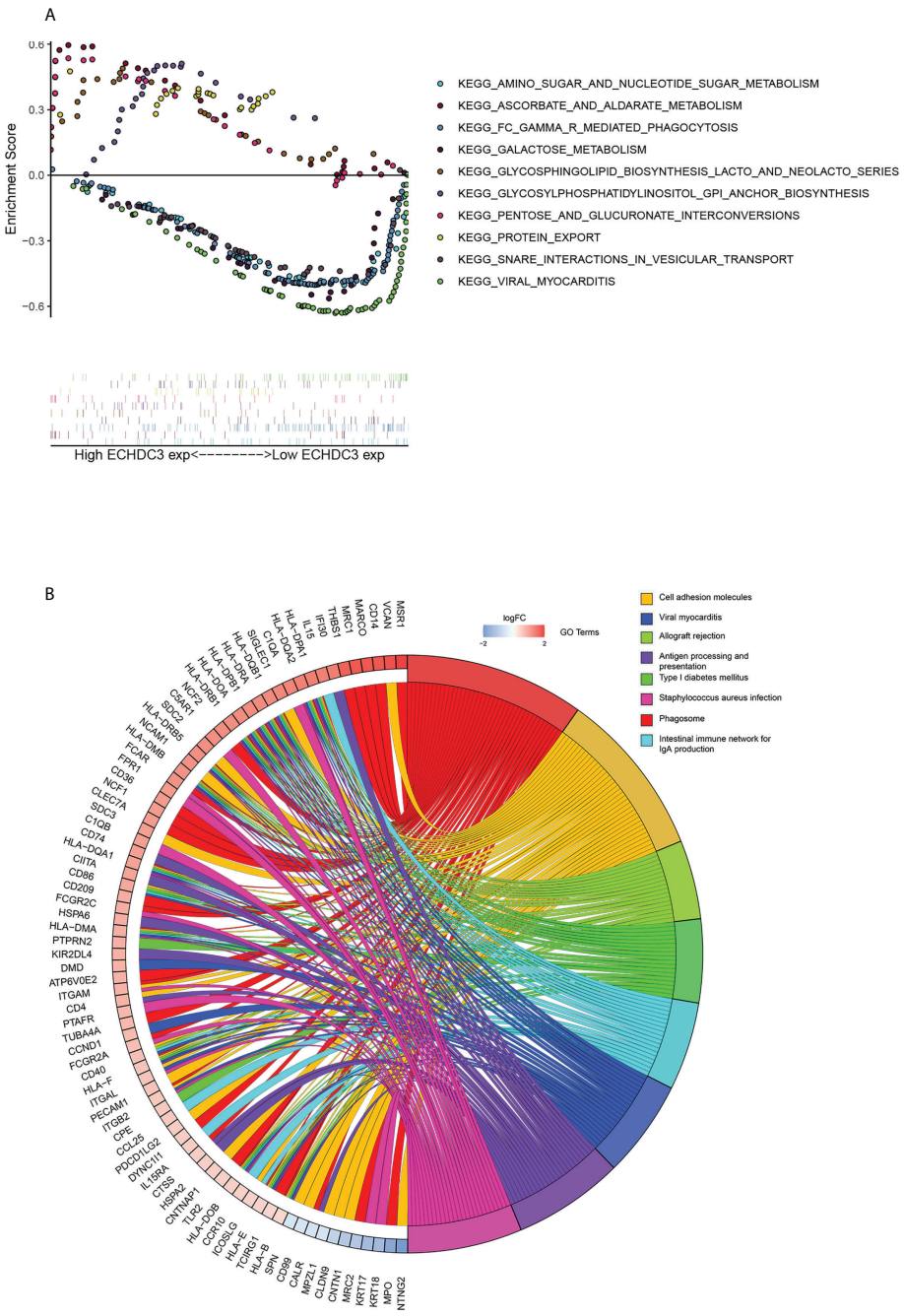

FIGURE 5
Bioinformatic analysis of ECHDC3 function. **(A)** Enriched KEGG pathways in ECHDC3^{high} and ECHDC3^{low} AML patients by GSEA. **(B)** GO Chord plot: ECHDC3 differentially expressed genes were linked *via* ribbons to the assigned terms, blue-to-red coding indicated logFC.

cell receptor (TCR) on T cells (12). Immune checkpoints are regulators of the immune system. These pathways are crucial for self-tolerance, which prevents the immune system from attacking cells indiscriminately. However, some cancers can protect themselves from attack by stimulating immune checkpoint targets (13). The expression information of the HLA family and immune checkpoints was shown (Figures 7A, B), which indicated that the HLA family and immune checkpoints were significantly different between the ECHDC3^{high} and ECHDC3^{low} groups. As can be seen in

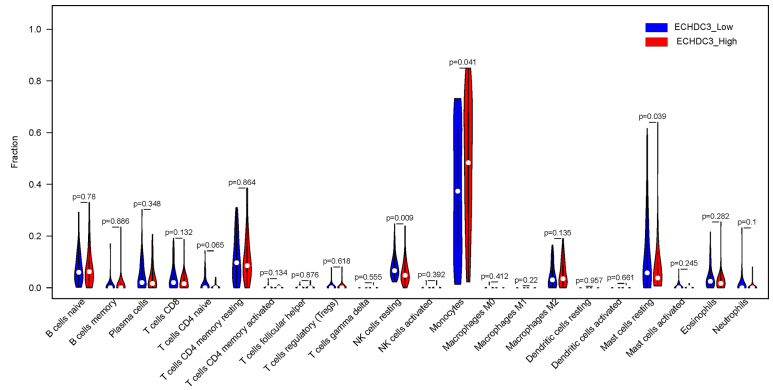

FIGURE 6
Different immune cells between ECHDC3^{high} and ECHDC3^{low} AML patients.

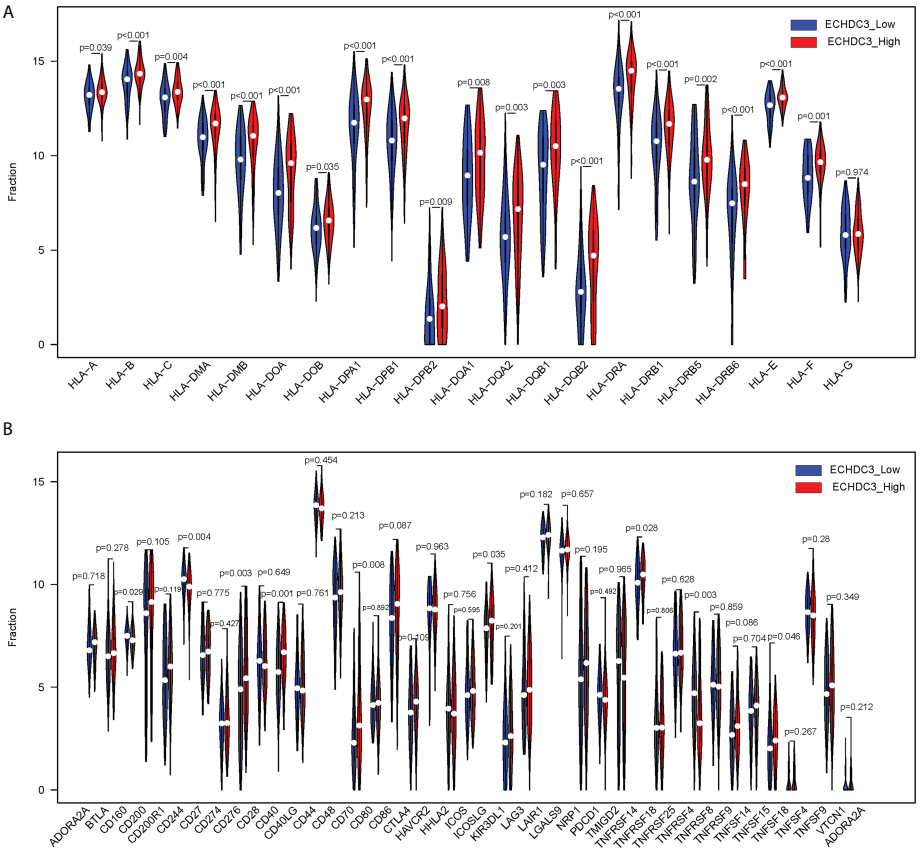

FIGURE 7
Comparison of HLA gene expression and immune checkpoint gene expression between ECHDC3 high and low subgroup. **(A)** HLA gene expression in ECHDC3 high and low subgroups. **(B)** Immune checkpoint gene expression in ECHDC3 high and low subgroups.

Figure 7B, TNF superfamily member 15 (TNFSF15) and CD40 were significantly upregulated in the ECHDC3^{high} subgroup with $p < 0.001$, whereas TNF superfamily member 4 (TNFSF4) were significantly downregulated ($p = 0.003$).

ECHDC3 promote chemoresistance

In the GSE52919 database, patients with Ara-C resistance showed higher ECHDC3 expression compared with sensitive patients ($p = 0.0136$; Figure 8A).

To verify the role of ECHDC3 in mt-DNA transcriptome and chemoresistance by experiments, ECHDC3 was knocked down by RNAi (SiECHDC3-351 and SiECHDC3-417) in the K562 cell lines (Figure 8B). The mt-DNA transcriptomes (MT-CO1, MT-CO2, ND1, ND2, and ND3) did not alter by inhibiting ECHDC3 (Figure 8C), whereas knocking down of ECHDC3 promoted the death of leukemia cells in either Ara-C at 0.1–1 μM or DOX at 0.04–0.16 μg/ml (Figures 8D–G).

Discussion

Previous studies about ECHDC3 were mainly focused on its role in Alzheimer's disease (14), acute coronary syndrome (15), and acute peanut allergic reactions (16), rather than on hematological malignancies. By extension of our previous finding of changed ECHDC3 expression in chemoresistant AML, the current study made a comprehensive analysis with bioinformatic analysis and experimental verification, supporting ECHDC3 as a novel biomarker predicting poor-prognosis AML, which might further improve risk stratification in AML

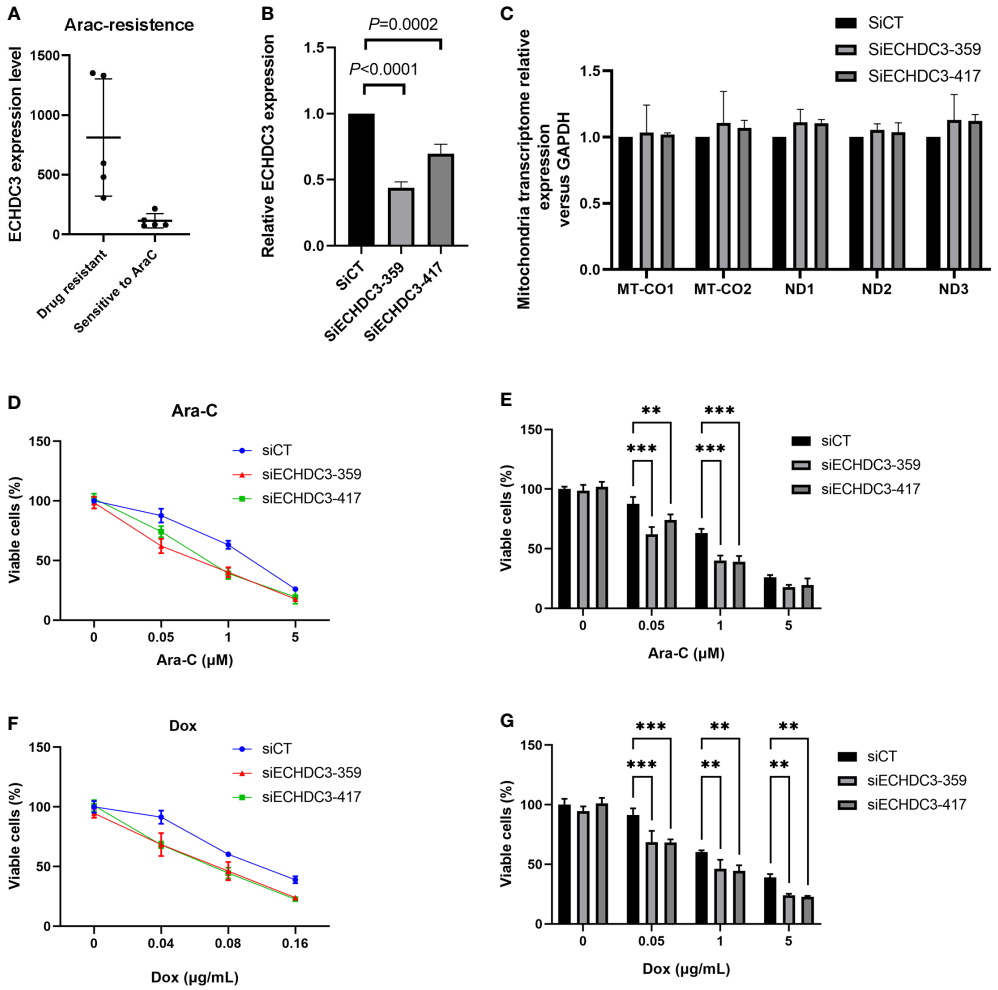

FIGURE 8
ECHDC3 in chemoresistance. **(A)** Higher ECHDC3 promotes chemoresistance by analyzing the GSE52919 database. **(B)** Knocking down ECHDC3 by RNAi. **(C)** Comparison of mt-DNA transcriptome by knocking down ECHDC3. **(D, E)** Cell viability treated with Ara-C. **(F, G)** Cell viability treated with doxorubicin. ***P<0.001, **P<0.01.

subgroups. Both bioinformatic analysis and experiment supported the role of ECHDC3 in mediating chemoresistance, and bioinformatic analysis suggested that ECHDC3 alters the BM microenvironment, which warranted further exploration of ECHDC3 in AML in near future.

The present paper presents a set of evidence for proving that ECHDC3 is a poor prognostic biomarker and a therapeutic target of AML through proteomics, genomics, and mitochondrial transcriptomics. Improvement in AML patient stratification is critical in clinical practice. Next-generation sequencing technologies are gradually implemented in the clinical setting to facilitate diagnosis and treatment decisions in AML. Currently, ELN 2017 criteria have been widely applied as the standard risk stratification method to guide treatment in the first complete remission period in AML (17), and the latest ELN 2022 recommendation has just been published (18). In the present study, we firstly demonstrated the expression of ECHDC3 as an independent prognostic factor in addition to the current risk stratification system. As the expression of ECHDC3 is related to patients' age (>60 *vs.* ≤60) as well as to ELN risk stratification (int/adv *vs.* fav), the question of whether ECHDC3 would be an independent biomarker is raised. Firstly, it is demonstrated that ECHDC3 and age remained the only two independent risk factors for inferior OS in MVA. Secondly, a new prediction model established by integrating ECHDC3 with basic characteristics including age and ELN risk groups further improved the accuracy of survival prediction, which highlighted the possibility of integration of ECHDC3 as an independent risk factor into risk stratification system in the future. Nevertheless, the current study did not follow the latest ELN 2022 criteria; therefore, the meaning of ECHDC3 in AML under ELN 2022 criteria is needed to be further validated by a larger cohort in the future.

Moreover, because allo-HSCT is generally considered a favorable consolidation treatment option in adv-risk AML, whereas chemotherapy is the preferred therapy in fav AML in the absence of persisting measurable residual diseases (MRD), it remained controversial whether allo-HSCT should be recommended as a priority in patients with int-risk AML. Several groups addressed this question by adding other gene profiles to the ELN 2017 criteria. Hu et al. established a prognostic nomogram characterized by white blood cell count ($\geq 10\times10^9$/L at diagnosis), mutated DNMT3A, and genes involved in signaling pathways, which divided int AML into two subgroups that could predict that the high-risk subgroup was associated with inferior OS and relapse-free survival (RFS), whereas allo-HSCT reduced the relapse risk of high-risk patients (3-year RFS: allo-HSCT: 40.0 *vs.* chemotherapy, P = 0.010) (19). Eisfeld et al. refined ELN 2017 by adding mutated BCOR, mutated SETBP1, and mutated IDH2 and removed NPM1mut with $FLT3^{high}$ in int AML; the outcome of 131 patients in the new int-risk group improved in comparison with that of the original int-risk group (n = 189) concerning both DFS (3-year rates: 32% *vs.* 22%) and OS (3-year rates: 41% *vs.* 31%) (20). ELN 2022 re-classified FLT3+ with mutation or wild-type NPM1 as int risk instead of previous adv risk (18). Therefore, it is important to further divide int-risk AML into subgroups with diverse relapse risks. In the present study, the expression of ECHDC3 could divide int-risk AML and FLT3+NPM1+AML into two subgroups with distinct survival rates, which might improve the prediction of the survival and guide post-remission treatment in int-risk AML.

Considering the negative effect of high ECHDC3 expression on the survival of AML patients, it becomes an important question why and how ECHDC3 promotes AML. By bioinformatic analysis and experimental verification, the current study preliminarily supported that ECHDC3 might be associated with chemoresistance in AML treatment. Although ECHDC3 was predicted to be active in the mitochondrion, knocking down ECHDC3 in the current study did not change the mt-DNA transcriptome, which remained to be explored in the future.

It is critical to develop a novel immune therapy targeting the BM microenvironment of AML. As important cytotoxic and cytokine-producing components of the innate immune system, NK cells might become key effector cells in immunotherapy for AML. Our group demonstrated that expanded clinical-grade membrane-bound IL-21/4-1BBL NK cell products could exhibit activity against AML *in vivo* (21). However, in the AML immune microenvironment, there are prominent immunosuppressive barriers, which result in dysfunction and exhaustion of NK cells (22). Resting NK cells are generally less lytic against target cells than *in vitro* interleukin 2 (IL-2)–activated NK cells. It has been revealed that the NK function is related to the levels of the fatty acids, and treatment of NK cells with saturated fatty acids or arachidonic acid significantly enhanced killing receptor expressions and decreased inhibitory NK (KIR) receptors, whereas docosahexaenoic and eicosapentaenoic acids increased KIR (23). For the first time, we found that the BM microenvironment immune phenotype was related to the fatty acid metabolism gene ECHDC3, which might contribute to its negative effect on the survival of AML patients by inhibiting NK function, which remained to be explored *in vivo* and *in vitro* research in near future.

In addition, monocyte differentiation is also of great importance in the immune microenvironment of AML, especially considering its closing relationship with monocytic myeloid-derived suppressor cells (M-MDSCs). Immature myeloid cells are characterized by the ability to suppress immune responses and expand during cancer (24). As M-MDSCs are morphologically and phenotypically similar to monocytes, it is the immune suppression that allows MDSCs to be distinguished from other myeloid cell populations. Coculture of the AML cell lines or primary AML cells with donor PB mononuclear cells expanded M-MDSCs and prevented monocyte differentiation, probably by MUC1-mediated tumor-

derived extracellular vehicles (25). In clinical studies, it has been reported that tumor-activated ILC2s secreted IL-13 to induce M-MDSCs and support tumor growth, whereas ATRA treatment reversed the increase of ILC2-MDSCs in AML (26). The intensity of the immune response triggered by ECHDC3 may help us understand the immune microenvironment of AML.

Conclusion

In sum, this study firstly described ECHDC3 as a negative AML prognosis predictor, which might refine the risk stratification of AML, especially in int AML. ECHDC3 is also involved in chemoresistance and shaping the immune microenvironment of AML, which could be a potential target for chemoresistance reverting and immune microenvironment remodeling for AML patients in the future.

Data availability statement

The original contributions presented in the study are included in the article/Supplementary Material. Further inquiries can be directed to the corresponding authors.

Ethics statement

This study was reviewed and approved by the ethics review board of Peking University People's Hospital (2022PHB030). The patients provided their written informed consent to participate in this study.

Author contribution

YZ, L-JH, and ML participated in the study design. YZ and L-TN participated in experiments. YZ and ML analyzed the data and wrote the manuscript. All authors contributed to the article and approved the submitted version.

Funding

This work was supported by: The national key research and development plan of China (2021YFA1100902), National Natural Science Foundation of China (Grant No. 82100168, 82070182, 82070181), Beijing Nova Program of Science and Technology (No. Z211100002121058, Z191100001119120), Peking University People's Hospital Research and Development Funds (RS2020-03, RDY2020-29), Peking University Medicine Fund of Fostering Young Scholars' Scientific and Technological Innovation and supported by "the Fundamental Research Funds for the Central Universities" (BMU2021PYB005), China Scholarship Council (202106015007).

Acknowledgments

We appreciated Dr. Xingchen Li (Department of Obstetrics and Gynecology, Peking University People's Hospital) providing help in the data analysis.

Conflict of interest

The authors declare that the research was conducted in the absence of any commercial or financial relationships that could be construed as a potential conflict of interest.

Publisher's note

Supplementary material

The Supplementary Material for this article can be found online at: https://www.frontiersin.org/articles/10.3389/fonc.2022.947492/full#supplementary-material

SUPPLEMENTARY FIGURE 1
Prognostic value of ECHDC3 expression in specific subgroups **(A)** Leukemia-free survival of non-APL AML patients in training cohort (*de novo* AML patients) **(B)** Overall survival of non-APL AML patients in validation sets (TCGA-LAML and BEAT-AM peripheral blood samples) **(C)** Overall survival of fav-risk AML patients in validation sets **(D)** Overall survival of adv-risk AML patients in validation sets **(E)** Overall survival of FLT3–NPM1+ AML patients in validation sets **(F)** Overall survival of FLT3–NPM1– AML patients in validation sets **(G)** Overall survival of FLT3+NPM1+ AML patients in validation sets **(H)** Distribution of Blast cells in PB or BM in validation sets **(I)** Overall survival of non-APL AML patients in validation sets according to PB blast **(J)** Overall survival of non-APL AML patients in validation sets according to BM blast **(K)** Overall survival of patients in validation sets with high PB blast **(L)** Overall survival of patients in validation sets with low PB blast.

SUPPLEMENTARY FIGURE 2
LASSO regression **(A)** The interrelation of 4 key genes acquired from LASSO regression **(B)** The evaluation progress of gene selection in LASSO regression **(C)** Heatmap of 9 key genes expression acquired from LASSO regression **(D)** Two-way interactions checked between the factors with the main effect in Lasso regression.

SUPPLEMENTARY FIGURE 3
Bioinformatic analysis of ECHDC3 function **(A)** Hallmark gene sets enrichment analyses for $ECHDC3^{high}$ and $ECHDC3^{low}$ AML patients by GSEA. **(B)** Heatmap of the deferentially expressed gene related to ECHDC3 expression. **(C)** KEGG

Cluster plot displaying a circular dendrogram of the clustering of the ECHDC3 expression profiles. The inner ring shows the colored logFC, and the outer ring is assigned functional terms. **(D)** Identification of AML subtype-specific GO terms. Top 10 GO terms enriched in the Biological Process (BP), Molecular Function (MF), and Cellular Component (CC).

SUPPLEMENTARY FIGURE 4

Immune landscape between ECHDC3^{high} and ECHDC3^{low} groups **(A)** The heat map visualized the percentage abundance of tumor-infiltrating immune cells in each sample. **(B)** Immune cell infiltration correlation matrix. **(C)** Correlation matrix of all 22 immune cell proportions.

References

1. Kantarjian H, Kadia T, DiNardo C, Daver N, Borthakur G, Jabbour E, et al. Acute myeloid leukemia: Current progress and future directions. *Blood Cancer J* (2021) 11(2):41. doi: 10.1038/s41408-021-00425-3

2. Bloomfield CD, Estey E, Pleyer L, Schuh AC, Stein EM, Tallman MS, et al. Time to repeal and replace response criteria for acute myeloid leukemia? *Blood Rev* (2018) 32(5):416–25. doi: 10.1016/j.blre.2018.03.006

3. Panina SB, Pei J, Kirienko NV. Mitochondrial metabolism as a target for acute myeloid leukemia treatment. *Cancer Metab* (2021) 9(1):17. doi: 10.1186/s40170-021-00253-w

4. Tabe Y, Saitoh K, Yang H, Sekihara K, Yamatani K, Ruvolo V, et al. Inhibition of fao in aml Co-cultured with bm adipocytes: Mechanisms of survival and chemosensitization to cytarabine. *Sci Rep* (2018) 8(1):16837. doi: 10.1038/s41598-018-35198-6

5. Stevens BM, Jones CL, Pollyea DA, Culp-Hill R, D'Alessandro A, Winters A, et al. Fatty acid metabolism underlies venetoclax resistance in acute myeloid leukemia stem cells. *Nat Cancer* (2020) 1(12):1176–87. doi: 10.1038/s43018-020-00126-z

6. Jones CL, Stevens BM, Culp-Hill R, Dalessandro A, Krug A, Goosman M, et al. Inhibition of fatty acid metabolism re-sensitizes resistant leukemia stem cells to venetoclax with azacitidine. *Blood* (2019) 134(Supplement_1):1272. doi: 10.1182/blood-2019-125773

7. Sharma NK, Chuang Key CC, Civelek M, Wabitsch M, Comeau ME, Langefeld CD, et al. Genetic regulation of enoyl-coa hydratase domain-containing 3 in adipose tissue determines insulin sensitivity in African americans and europeans. *Diabetes* (2019) 68(7):1508–22. doi: 10.2337/db18-1229

8. Niu LT, Wang YQ, Wong CCL, Gao SX, Mo XD, Huang XJ. Targeting ifn-Gamma-Inducible lysosomal thiol reductase overcomes chemoresistance in aml through regulating the ros-mediated mitochondrial damage. *Transl Oncol* (2021) 14(9):101159. doi: 10.1016/j.tranon.2021.101159

9. Dohner H, Estey E, Grimwade D, Amadori S, Appelbaum FR, Buchner T, et al. Diagnosis and management of aml in adults: 2017 eln recommendations from an international expert panel. *Blood* (2017) 129(4):424–47. doi: 10.1182/blood-2016-08-733196

10. Lv M, Wang Y, Chang YJ, Zhang XH, Xu LP, Jiang Q, et al. Myeloablative haploidentical transplantation is superior to chemotherapy for patients with intermediate-risk acute myelogenous leukemia in first complete remission. *Clin Cancer Res: an Off J Am Assoc Cancer Res* (2019) 25(6):1737–48. doi: 10.1158/1078-0432.CCR-18-1637

11. Yu J, Xie M, Ge S, Chai P, Zhou Y, Ruan J. Hierarchical clustering of cutaneous melanoma based on immunogenomic profiling. *Front Oncol* (2020) 10:580029. doi: 10.3389/fonc.2020.580029

12. Choo SY. The hla system: Genetics, immunology, clinical testing, and clinical implications. *Yonsei Med J* (2007) 48(1):11–23. doi: 10.3349/ymj.2007.48.1.11

13. Pardoll DM. The blockade of immune checkpoints in cancer immunotherapy. *Nat Rev Cancer* (2012) 12(4):252–64. doi: 10.1038/nrc3239

14. Tan MS, Yang YX, Xu W, Wang HF, Tan L, Zuo CT, et al. Associations of alzheimer's disease risk variants with gene expression, amyloidosis, tauopathy, and neurodegeneration. *Alzheimer's Res Ther* (2021) 13(1):15. doi: 10.1186/s13195-020-00755-7

15. Silbiger VN, Luchessi AD, Hirata RD, Lima-Neto LG, Cavichioli D, Carracedo A, et al. Novel genes detected by transcriptional profiling from whole-blood cells in patients with early onset of acute coronary syndrome. *Clin Chim Acta Int J Clin Chem* (2013) 421:184–90. doi: 10.1016/j.cca.2013.03.011

16. Watson CT, Cohain AT, Griffin RS, Chun Y, Grishin A, Hacyznska H, et al. Integrative transcriptomic analysis reveals key drivers of acute peanut allergic reactions. *Nat Commun* (2017) 8(1):1943. doi: 10.1038/s41467-017-02188-7

17. Dohner H, Estey EH, Amadori S, Appelbaum FR, Buchner T, Burnett AK, et al. Diagnosis and management of acute myeloid leukemia in adults: Recommendations from an international expert panel, on behalf of the European leukemianet. *Blood* (2010) 115(3):453–74. doi: 10.1182/blood-2009-07-235358

18. Dohner H, Wei AH, Appelbaum FR, Craddock C, DiNardo CD, Dombret H, et al. Diagnosis and management of aml in adults: 2022 eln recommendations from an international expert panel. *Blood* (2022) 129(4):424–447. doi: 10.1182/blood.2022016867

19. Hu X, Wang B, Chen Q, Huang A, Fu W, Liu L, et al. A clinical prediction model identifies a subgroup with inferior survival within intermediate risk acute myeloid leukemia. *J Cancer* (2021) 12(16):4912–23. doi: 10.7150/jca.57231

20. Eisfeld AK, Kohlschmidt J, Mims A, Nicolet D, Walker CJ, Blachly JS, et al. Additional gene mutations may refine the 2017 European leukemianet classification in adult patients with *De novo* acute myeloid leukemia aged <60 years. *Leukemia* (2020) 34(12):3215–27. doi: 10.1038/s41375-020-0872-3

21. Zhao XY, Jiang Q, Jiang H, Hu LJ, Zhao T, Yu XX, et al. Expanded clinical-grade membrane-bound il-21/4-1bbl nk cell products exhibit activity against acute myeloid leukemia in vivo. *Eur J Immunol* (2020) 50(9):1374–85. doi: 10.1002/eji.201948375

22. Myers JA, Miller JS. Exploring the nk cell platform for cancer immunotherapy. *Nat Rev Clin Oncol* (2021) 18(2):85–100. doi: 10.1038/s41571-020-0426-7

23. De Sanctis JB, Dumut DC, Radzioch D, Hajduch M. Functionally relevant differences in plasma fatty acid composition and expression of cytotoxic and inhibitory nk cell receptors between healthy young and healthy elder adults. *Nutrients* (2020) 12(12):3641. doi: 10.3390/nu12123641

24. Lv M, Wang K, Huang XJ. Myeloid-derived suppressor cells in hematological malignancies: Friends or foes. *J Hematol Oncol* (2019) 12(1):105. doi: 10.1186/s13045-019-0797-3

25. Pyzer AR, Stroopinsky D, Rajabi H, Washington A, Tagde A, Coll M, et al. Muc1-mediated induction of myeloid-derived suppressor cells in patients with acute myeloid leukemia. *Blood* (2017) 129(13):1791–801. doi: 10.1182/blood-2016-07-730614

26. Trabanelli S, Chevalier MF, Martinez-Usatorre A, Gomez-Cadena A, Salome B, Lecciso M, et al. Tumour-derived Pgd2 and Nkp30-B7h6 engagement drives an immunosuppressive Ilc2-mdsc axis. *Nat Commun* (2017) 8(1):593. doi: 10.1038/s41467-017-00678-2

frontiers | Frontiers in Oncology

TYPE Original Research
PUBLISHED 21 September 2022
DOI 10.3389/fonc.2022.932709

OPEN ACCESS

EDITED BY
J. Luis Espinoza,
Kanazawa University, Japan

REVIEWED BY
Vincenzo Lionetti,
Sant'Anna School of Advanced Studies, Italy
Emmanuel Roilides,
Aristotle University of Thessaloniki, Greece
Abdulsalam Adegoke,
University of Southern Mississippi, United States

*CORRESPONDENCE
Junfei Chen
18764029625@163.com

SPECIALTY SECTION
This article was submitted to Hematologic Malignancies, a section of the journal Frontiers in Oncology

RECEIVED 30 April 2022
ACCEPTED 25 August 2022
PUBLISHED 21 September 2022

CITATION
Zhang Y, Ning HN, Zheng WY, Liu J, Li FH and Chen JF (2022) Lung microbiome in children with hematological malignancies and lower respiratory tract infections. *Front. Oncol.* 12:932709. doi: 10.3389/fonc.2022.932709

Lung microbiome in children with hematological malignancies and lower respiratory tract infections

Yun Zhang[1], Haonan Ning[1], Wenyu Zheng[1], Jing Liu[2], Fuhai Li[1] and Junfei Chen[3]*

[1]Department of Pediatrics, Qilu Hospital of Shandong University, Jinan, China, [2]Department of Biostatistics, School of Public Health, Cheeloo College of Medicine, Shandong University, Jinan, China, [3]Department of Pediatric Surgery, Qilu Hospital of Shandong University, Jinan, China

Background: Respiratory infectious complications remain a major cause of morbidity and mortality in children with hematological malignancies. Knowledge regarding the lung microbiome in aforementioned children is limited.

Methods: A prospective cohort was conducted, enrolling 16 children with hematological malignancies complicated with moderate-to-severe lower respiratory tract infections (LRTIs) versus 21 LRTI children with age, gender, weight, and infection severity matched, with no underlying malignancies, to evaluate the lung microbiome from bronchoalveolar lavage fluid samples in different groups.

Results: The lung microbiome from children with hematological malignancies and LRTIs showed obviously decreased α and β diversity; increased microbial function in infectious disease:bacteria/parasite; drug resistance:antimicrobial and human pathogenesis than the control group; a significantly reduced proportion of *Firmicutes*, *Bacteroidota*, *Actinobacteriota*; increased *Proteobacteria* at the phylum level; and distinctly elevated *Parabacteroides*, *Klebsiella*, *Grimontia*, *Escherichia_Shigella*, *unclassified_Enterobacteriaceae* at the genus level than the control group. Furthermore, it was revealed that α diversity (Shannon), β diversity (Bray–Curtis dissimilarity), *Proteobacteria* at the phylum level, and *unclassified_Enterobacteriaceae* and *Escherichia_Shigella* at the genus level were significantly negatively associated with hospitalization course whereas *Firmicutes* at the phylum level was established positively correlated with the hospitalization course.

Conclusions: Children with hematological malignancies and LRTIs showed obviously decreased α and β diversity, significantly increased function in infectious disease pathogenesis, antimicrobial drug resistance, and unfavorable environment tolerance. Moreover, α diversity (Shannon), β diversity (Bray–Curtis dissimilarity), and *Proteobacteria* may be used as negative correlated predictors for hospitalization course in these children whereas *Firmicutes* may be utilized as a positive correlated predictor.

KEYWORDS

lung microbiome, bronchoalveolar lavage fluid, children, hematological malignancies, lower respiratory tract infection, drug resistance, microbial tolerance, unfavorable environment

1. Introduction

Over the past decades, major advances have been made in therapy for childhood hematological malignancies (1, 2), especially acute lymphoblastic leukemia, resulting in obviously higher 10-year survival rates than before (2–5). However, respiratory infectious complications remain a major cause of morbidity and mortality in the aforementioned children (3, 6–8). In particular, children undergoing chemotherapy with hematological malignancies are at a high risk of more severe infections with prolonged clinical treatment course and profound immunity condition.

Empirical antibiotherapy with wide-spectrum bactericidal drugs within early phase in febrile children with malignancies is always the more willing choice for pediatric clinicians, the guidelines of vast medical institutions and multitudinous countries to avoid further progression and exacerbation (9–11). In view of the adverse effects from the frequent use of wide-spectrum antibiotics in a high grade, such as dysbiosis throughout multiple systems, opportunistic infections, and expensive treatment payment, pathogen-targeted antibiotic therapy based on validated pathogen-detected results become increasingly urgent for global clinicians. In contrast to the limitations of a conventional culture-dependent technique, the lower rate of positive results, longer test course, and critical requirement for objective samples, emerging 16s RNA tests show advantages unfolding the full view of one individual microbiome (12–14), revealing the microbial changes in infectious loci within a certain group of individuals.

There are limited data regarding the lung microbiome from samples of the pediatric malignancy group, and most of the general information is extrapolated from adult studies. Further studies are needed to establish the optimal approach to the diagnosis and management of children with hematological respiratory infections. Thus, in this study, we sought to characterize the lung microbiome from bronchoalveolar lavage fluid (BALF) samples in a cohort of 16 children with hematological malignancies and moderate-to- severe lower respiratory tract infections (LRTIs) versus 21 LRTI controls with age, gender, weight, and infection severity matched and without any underlying malignancies.

2. Methods

2.1 Clinical cohort and sample collection

From January 2020 to October 2021, we prospectively enrolled a convenience sample of consecutive malignancy children with moderate-to-severe LRTIs and, at the same time, LRTI children without any underlying diseases as controls, with age, gender, weight, infection severity matched, who all needed bronchoscopy and alveolar lavage in pediatric departments at Qilu Hospital of Shandong University and who had focal findings on a lung CXR or CT scan diagnosed as LRTIs and had bronchoscopy lavage management within the first two days after hospitalization. LRTIs were defined as more than one of the following: new or different cough or sputum production, chest pain, dyspnea, tachypnea, or abnormal auscultatory findings (15). Hematological malignancies were all pathologically diagnosed based on bone marrow cytology smears, lymph node biopsy, and immunophenotyping. All enrolled children were eligible for the indications of the Guidelines of Pediatric Flexible Bronchoscopy in China (2018 version): (1) laryngeal stridor; (2) recurrent or persistent wheeze; (3) local stridor; (4) chronic cough of unknown cause; (5) recurrent respiratory tract infection; (6) suspicious foreign body aspiration; (7) hemoptysis; (8) difficulty in weaning mechanical ventilation; and (9) abnormal imaging results in lungs: (1) dysplasia or malformation in trachea or bronchi; (2) atelectasis; (3) emphysema; (4) mass lesions of lungs; (5) diffuse lesions of lungs; (6) mediastinal emphysema; (7) space-occupying focus of mediastinum or airway; (8) dysplasia of blood vessels, lymphangion, or esophagus; (9) differentiating the diagnosis of lesions in pleural cavity; (10) pathogenic diagnosis and treatment of infections in lungs;(11) thoracic trauma with suspicious airway rupture; (12) interventional therapy with bronchoalveolar lavage; (13) assessment and management of airway in a perioperative period; (14) assistance of endotracheal intubation and gastric intubation; and (15) other conditions for differentiating diagnosis. In addition, all cases underwent bronchoalveolar lavage until they were excluded by contraindications (such as severe cardiopulmonary hypofunction, severe arrythmia, high fever, severe hemoptysis, and severe malnutrition). Exclusion criteria included details as follows: (1) inability to obtain

informed consent; (2)predisposing bronchoscopy and alveolar lavage in other hospitals within the same infection medical course; (3) immunodeficiency; (4) chronic corticosteroid use; (5) chronic lung disease; (6) sickle cell disease; (7) congenital heart disease; (8) patients dependent on tracheostomy; and (9) neuromuscular disorders impacting respiration. The study was approved by Qilu Hospital of Shandong University Institutional Review Board (Protocol KYLL-2020(KS)-211), and written informed consent was provided by all participants' legal guardians. Upon enrollment, we collected BALF for the study of the lung microbiome with simultaneous blood samples for the quantification of the host inflammatory response and immune state.

2.2 Laboratory analyses

We extracted bacterial DNA directly from frozen BALF samples and amplified the V3–V4 hypervariable region of the bacterial 16S ribosomal RNA (rRNA) for sequencing on the Illumina Novaseq platform. Simultaneously, we performed quantitative PCR (qPCR) of the V3–V4 to obtain number of 16S rRNA gene copies per sample (surrogate for bacterial load). The default set of criteria was used to remove low-quality and chimeric reads. The remaining reads were subject to a close reference operational taxonomic unit (OTU) picking (97% identity cutoff). As for plasma biomarkers, we performed routine tests (white blood cells, neutrophils, red blood cell count, hemoglobin, platelets, alanine transaminase, etc.), inflammatory biomarkers (CRP, PCT, et al.) and correlated measurements. The WBC count, ANC, and ESR assays were performed on the CELL-DYN Sapphire (Abbott Diagnostics, Lake Forest, IL). CRP assays were performed on the Dimension Vista 1500 (Siemens Medical Solutions USA, Inc, Malvern, PA, USA) with a functional sensitivity of 0.29 mg/dl. Biomarkers were concentrations in blood measured at the Center for Clinical Research of Qilu Hospital of Shandong University.

2.3 Sequencing data quality controls

First, Trimmomatic (16) (version 0.33) was used to filter the quality of the raw data, then use Cutadapt (version 1.9.1) to identify and remove primer sequences, and then use FLASH (version 1.2.11) to splice the paired-end reads, with chimeras were removed (UCHIME, version 8.1), resulting in high-quality sequences for subsequent analysis. The original off-machine subreads were corrected to obtain CCS (Circular Consensus Sequencing) sequences (SMRT Link, version 8.0), and then using the Lima (v1.7.0) software, the CCS sequences of different samples were identified by barcode sequences and chimeras were removed to obtain high-quality CCS sequence.

2.4 Amplicon generation

The diluted genomic DNA was used as a template; specific primers with Barcode were used according to the selection of the sequencing region; Phusion® High-Fidelity PCR Master Mix with GC Buffer was used. The PCR was performed using efficient and high-fidelity enzymes to ensure amplification efficiency and accuracy. The primer corresponding area is as follows: 16S V3 +V4 338F 5'- ACTCCTACGGGAGGCAGCA-3', 806R 5'-GGACTACHVGGGTWTCTAAT-3'.

2.5 PCR product mixing and purification

The samples were mixed at the same concentration according to the concentration of the PCR product, thoroughly mixed, and the PCR product was detected by 2% agarose gel electrophoresis, and GeneJET gel (Thermo Scientific) was used. The product was recovered.

2.6 Data analysis

2.6.1 Sequencing data processing

The raw data obtained by the Illumina MiSeq/HiSeq sequencing platform have some low-quality data that will interfere with the final result. Therefore, it is necessary to preprocess the offline data before further analysis. The specific processing steps are as follows: pata splitting, PE reads stitching, Tags filter and Tags to chimera sequences. The PE read splicing is performed with the application of Usearch v10.0 to split the data for the reading of each sample. Raw Tags are also the stitching sequences obtained.

2.6.2 Operational taxonomic unit cluster and species annotation

All of the Effective Tags sequences of all samples were clustered using Usearch v10.0 software (17), providing clustering with 97% consensus sequences to become OTU results, which purpose is to study the compositional diversity information of the species of the sample. A sequence in the same OTU is considered to be sequence-derived from one of the same taxon as the hypothetical taxon. When Usearch constructs OTUs, it selects the sequence with the highest frequency according to its algorithm principles and uses these RDP Classifier and GreenGene database for species annotation analysis to study the phylogenetic relationship between OTUs and uses KRONA for species identification. The results of the annotations are visualized. Based on the species annotation, the number of sequences for each sample at each classification level is calculated, and the sequence of species constitutes a histogram.

To facilitate a further study of the phylogenetic relationships of OTUs and the structural differences of major flora between different samples (groups), phylogenetic relationship data for the first 10 genera of OTUs corresponding to the maximum relative abundance were selected and combined with each OTU. With the relative abundance and species annotation confidence for representative sequences, the results of the integration can visualize the diversity of the species composition of the study. According to the type labeling and abundance information of all samples of the genus level, select the top 35 abundance genera and their abundance information in each sample to draw a heat map, and collect clusters from the difference between the classification information and the sample to identify Focus on more species or samples in the study sample. Select the phylogenetic relationship data of the OTUs corresponding to the top 10 relatives of the largest relative abundance and the relative abundance information of their corresponding OTUs to achieve a vertical clustering of samples at the OTU level to examine the differences between different samples or Similarity.

2.6.3 α diversity

α Diversity is used to analyze community diversity within a sample and includes three indicators: dilution curve, species richness, and community diversity (18). The sample complexity index was calculated and plotted using Qiime2 software. The rarefaction curve is used to indicate whether the amount of sequencing data of the sample is reasonable and indirectly reflects the richness of the substance in the sample. It is a curve obtained by randomly extracting a certain amount of sequencing data from a sample to calculate the number of species they represent based on the number of species and the amount of data. In the dilution curve, when the curve tends to be flat, it means that more data will only produce a small amount of new OTUs, indicating that the amount of sequencing data is reasonable.

2.6.4 β diversity

Principal component analysis (PCA) is a method for the dimensionality reduction of multidimensional data and the most important elements and structures in the data by applying variance decomposition (19). It is applied to reduce the dimension of the original variables using the QIIME2 software package. It can reflect the difference of multidimensional data on the two-dimensional coordinate map, and the method of selecting the two coordinate axes that can reflect the difference between samples is selected from the PCA results. The closer the sample is in the PCA plot, the more similar its community composition. UPGMA (unweighted pair-group method with arithmetic mean) is a commonly used cluster analysis method in environmental biology. It requires a transformation from the distance matrix to a new set of orthogonal axes, where the maximum variation factor is represented by the first principal coordinate, the second maximum is represented by the second primary coordinate, and so on. UPGMA clustering is a hierarchical clustering method that uses average links and can be used to interpret the distance matrix.

2.6.5 Function prediction analyses

PICRUSt2 (20) is a computational method that uses marker gene data and a reference genome database to predict the functional composition of environmental microbes, which is based on IMG microbial genome data to predict the functional potential of microbial communities during phylogeny through phylogenetic and functional correlations. Its working principle is summarized in Supplementary Figure 1.

BugBase is a biological-level coverage that predicts functional pathways within the complex microbiome and Methods for biologically interpretable phenotypes. BugBase first normalizes OTUs by the predicted 16S copy number and then predicts microbial phenotypes using the provided precomputed files. First, for each sample in the biological dataset, the relative abundance of the trait across the full range of coverage thresholds is estimated (0–1 in 0.01 increments). Then, BugBase selects the coverage threshold with the highest variance among all samples for each feature in the user data. After thresholds are set, BugBase generates the final organism-level trait prediction table, which contains the predicted relative abundance of the trait for each sample.

2.6.6 Data processing and statistical analyses

From the derived 16S sequences, we applied a custom pipeline for OTU classification and performed analyses at phylum, class, order, family, genus, and species levels, respectively. Statistical analysis groups were compared using the Fisher exact or chi-square tests for categorical data or the Wilcoxon rank sum test for continuous data. A general linear model (GLM) was constructed between demographic and baseline clinical variables and the temporal variability of α and β diversity among subjects. The correlation analysis between two indicators was done using Spearman correlation analysis. The false discovery rate (FDR) method was used to adjust P-values for multiple testing wherever applicable (21). All tests were two tailed and a P-value <0.05 was considered to be statistically significant. IBM SPSS statistics (version 21.0; International Business Machine Corp.) was used. The ecologic analyses of α diversity (Shannon index) and β diversity (Manhattan distances with permutational ANOVA [Permanova] at 1,000 permutations) were conducted using the R vegan package and visualized with principal-coordinate analysis plots.

3. Results

3.1 Cohort description

A total of 16 children with malignancies and moderate-to-severe LRTIs (median age, 4.6 years, 62.5% male) contributed to the observation group (75% acute lymphoblastic leukemia, 12.5% acute myelogenous leukemia, 6.25% B-cell lymphoblastic lymphoma, 6.25% Burkitt's lymphoma), in addition to the control group of 21 children with LRTIs only (median age, 3.9 years, 42.9% male) (Table 1) (the chemotherapy information of children with malignancy and LRTIs is listed in Table 2). For both groups, bronchoscopy was strongly needed for moderate-to-severe LRTIs. Comparison samples including blood and BALF from the samples of 16 observation-group objects and 21 control-group objects were used in our experiment pipelines.

With respect to the pathogen of LRTIs in the observation group, there were two bacterial infection cases (one case of penicillin-sensitive *Staphylococcus aureus* infection defined by a BALF culture, one case of *Haemophilus influenzae* infection defined by BALF PCR), two mycoplasma pneumoniae-infected cases defined by BALF PCR, two viral infection cases (one case of adenovirus infection and one case of coronavirus infection defined both by BALF PCR), and two suspicious fungal infection cases defined by positive serum (1,3)-beta-D-glucan test (G test), the galactomannan test (GM test) plus a high level of the BALF GM test (>1.50 ODI) (22) without other conventional diagnostic bases of fungal infection, with eight cases of no pathogens tested. In the control group, there were seven bacterial infection cases [one case of *Branhamella catarrhalis* infection defined by a BALF culture, two cases of *H. influenzae* infection defined by a BALF culture, and four cases of *S. pneumoniae* infection defined by a BALF culture (n=1) and BALF PCR (n=3)], five mycoplasma pneumoniae-infected cases defined by BALF PCR, and two viral infection cases (one case of parainfluenza virus infection and one case of herpes virus infection defined both by BALF PCR), with seven cases of no pathogens tested.

As for the pulmonary function tests, children under 6 years old were only given tidal breath pulmonary function (e.g., VT/kg, tPTEF/tE, and VPEF/VE). Children older than 6 years were given a pulmonary function test (e.g., FEV1/FVC, FEV1, MEF75, MEF50, MEF25, MEF75/25, and FVC). Among the 16 children with malignancy and LRTIs, there were 7 children who were given a routine pulmonary function test and 9 children who were given a tidal breath pulmonary function test. Among the control group, there were 9 children who were given a routine pulmonary function test and 12 children who were given a tidal breath pulmonary function test. With regard to the phenotypes in pulmonary function tests, in children with malignancy and LRTIs, there were two mediate obstructive ventilation dysfunction, two mediate–severe obstructive ventilation dysfunction, three mild restrictive ventilation dysfunction, and four mediate restrictive ventilation dysfunction, while there were other five children in this group with common pulmonary function. Within the control group, there were three mild obstructive ventilation dysfunction, three mediate obstructive ventilation dysfunction, two severe obstructive ventilation dysfunction, two mild restrictive ventilation dysfunction, and two severe obstructive plus mild restrictive ventilation dysfunction, while for the rest nine children in this group, with common pulmonary function.

About the phenotypes of CT scan, there were 11 pneumonia and 5 bronchopneumonia in children with malignancy and LRTI group, with 2 pneumonia cases complicated with pleural effusions and 1 pneumonia case complicated with pulmonary cavitation. Furthermore, within this group, there were 1 single left lesion, 4 single right lesions, and 11 bilateral lesions. Meanwhile, in the control group, there were 9 pneumonia and 12 bronchopneumonia in children, with 1 pneumonia case complicated with pleural effusions. Within the control group, there were 5 single left lesions, 2 single right lesions, and 14 bilateral lesions.

3.2 Description of the clinical features in lower respiratory tract infection children with/without hematological malignancies

There were no significant differences noted in the age, weight, height, gender, predisposition of antibiotics before hospitalization, white blood cell count, absolute neutrophil count, C-reactive protein, alanine transaminase, lactate dehydrogenase, positive BALF cultures, FEV1/FVC, FEV1, MEF75, MEF50, MEF25, MEF75/25, FVC, tPTEF/tE, VPEF/VE, and death during LRTIs between the observation group and the control group (Table 1). Meanwhile, LRTI children with hematological malignancies revealed to have less red blood cell count (median, 2.67 $\times 10^{12}$/L *vs.* 4.61 $\times 10^{12}$/L, p<0.001), lower hemoglobin level (median, 84g/L *vs.* 125g/L,p<0.001), less platelet count(median, 244 $\times 10^{9}$/L *vs.* 328 $\times 10^{9}$/L, p<0.001), higher incidence of positive cultures of non-respiratory samples (25% *vs.* 0%, p=0.015), lower VT/kg(median, 8.9 *vs.* 12.4, ml/kg, p=0.002, <0.01), and longer entire lower respiratory tract infection course (median, 31 *vs.* 13,p=0.001, <0.01) and hospitalization course (median, 17.5 *vs.* 7, p<0.001) than those with LRTIs but without hematological malignancies (Table 1).

TABLE 1 Comparison of the demographics, clinical course, features, and outcome of lower respiratory tract infection (LRTI) children with/without hematological malignancies.

Characteristics		Children with hematological malignancies and sLRTI (N = 16)	Children with sLRTI only (N = 21)	P-value*
Age, median (IQR), years		4.6 (3.5–7.7)	3.9 (1.7–8.1)	0.471
Weight, median (IQR), kg		16.8 (14.0–24.0)	19.0 (10.4–29.5)	0.923
Height, median (IQR),cm		105.5 (98.0–127.3)	105.0 (85.0–135.0)	0.581
Males, n (%)		10 (62.5)	9 (42.9)	0.236
Malignancy subtype, n (%)	ALL	12 (75.0)	–	–
	AML	2 (12.5)	–	–
	B-LBL	1 (6.25)	–	–
	BL	1 (6.25)	–	–
Course of lower respiratory tract infection before hospitalization, median (IQR), d		5 (1–15)	4 (3–11)	0.805
Course of antibiotics before hospitalization, median (IQR), d		3 (1–14)	7 (0–18)	0.916
Course of entire lower respiratory tract infection, median (IQR), d		31 (19–38)	13 (11–20)	**0.001**
WBC, median (IQR), $\times10^9$/L		3.30 (2.13–21.49)	7.55 (5.26–13.17)	0.456
ANC, median (IQR), $\times10^9$/L		1.42 (0.58–5.92)	2.79 (1.95–6.75)	0.059
RBC, median (IQR), $\times10^{12}$/L		2.67 (2.13–3.52)	4.61 (4.21–4.91)	**0.000**
Hb, median (IQR), g/L		84 (64–113)	125 (119–132)	**0.000**
PLT, median (IQR), $\times10^9$/L		244 (35–310)	328 (313–416)	**0.000**
CRP, median (IQR), mg/L		15.29 (1.91–81.47)	2.06 (0.25–14.4)	**0.044**
ALT, median (IQR), g/L		15 (10–45)	13 (9–22)	0.421
LDH, median (IQR), g/l		303 (237–356)	335 (292–412)	0.217
Positive BALF cultures, n (%)		1 (6.3)	4 (19.0)	0.259
Positive cultures other than BALF, n (%)		4 (25.0)	0 (0)	**0.015**
FEV1/FVC, %, median (IQR), (n)**		106.6 (100.5–115.1), (7)	108.5 (98.6-113.1), (9)	0.965
FEV1, %, median (IQR), (n)**		90.2 (78.7–102.6), (7)	85.7 (74.9-94.5), (9)	0.480
MEF75, %, median (IQR), (n)**		73.9 (60.9–83.8), (7)	69.0 (64.4–95.8), (9)	0.895
MEF50, %, median (IQR), (n)**		68.4 (64.3–99.8), (7)	70.0 (52.3–100.8), (9)	0.965
MEF25, %, median (IQR), (n)**		71.5 ()58.3–98.8), (7)	73.5 (52.7–95.0), (9)	0.895
MEF75/25, %, median (IQR), (n)**		70.2 (64.3–101.7), (7)	71.0 (60.3–98.5), (9)	0.965
FVC, ml, median (IQR), (n)**		90.1 (79.0–95.0), (7)	80.0 (66.5–93.3), (9)	0.402
VT/kg, ml/kg, median (IQR), (n)**		8.9 (5.8–11.2), (9)	12.4 (11.1–14.4), (12)	**0.002**
tPTEF/tE, %, median (IQR), (n)**		18.3 (15.7–36.6), (9)	19.7 (14.0–36.9), (12)	0.865
VPEF/VE, %, median (IQR), (n)**		20.4 (18.9–37.6), (9)	24.2 (19.6–33.6), (12)	0.777
Hospitalization course, median, d		17.5 (4–52)	7 (4–14)	**0.000**
Death during sLRTI, n (%)		1 (6.3)	0 (0)	0.245

sLRTI, severe lower respiratory tract infection; ALL, acute lymphoblastic leukemia; AML, acute myelogenous leukemia; B-LBL, B-cell lymphoblastic lymphoma; BL, Burkitt's lymphoma; WBC, white blood cell count; ANC, absolute neutrophil count; RBC, red blood cell count; Hb, hemoglobin; PLT, platelet; CRP, C reactive protein; ALT, alanine transaminase; LDH, lactate dehydrogenase; BALF, bronchoalveolar lavage fluid.
*Statistically significant p-values($p < 0.05$) are shown in bold.
**Children under 6 years old were only given tidal breath pulmonary function. Children older than 6 years were given a pulmonary function test.

3.3 Lung microbiome communities in lower respiratory tract infection children with or without hematological malignancies

From DNA sequences of the V3 and V4 hypervariable regions of the 16S rRNA gene, a total of 700 OTUs were clustered by the identity of 97% cutoff after rarefaction to make species annotation. There were 79,854–112,096 raw reads, 73,966-104,672 clean reads and 54,778–95,159 effective reads analyzed of each sample. The mean Q30(%) was 95.96% and the mean Q20(%) was 98.93%. The samples of bronchoalveolar lavage fluid (BALF) from LRTI children with hematological malignancies had a much lower number of 16S reads than samples from control group(p=0.001, <0.01) (Figure 1), whereas the mutual OTUs of samples from the observation group were much more than those from the control group (Figure 2). The microbiome composition

TABLE 2 Chemotherapy information of children with hematological malignancies and LRTIs.

Malignancies subtype (n)	Disease group		Malignancy course/m	Present chemotherapy phase when enrolled	
ALL (12)	Mediate risk	5 (42%)	3 (0.55–20)*	Induction phase	6 (50%)
				Consolidation phase	2 (16.7%)
	Low risk	7 (58%)		Maintenance phase	4 (33.4%)
AML (2)	Low risk	2 (100%)	1/1.5	Induction phase	2 (100%)
B-LBL (1)	Stage III		15	Consolidation phase	
BL (1)	Stage IV		10	3 days after the end of chemotherapy	

*Median (IQR).

between the two groups was significantly different. Inconsistent with the previous studies of the lung microbiome, the vast majority of OTUs in LRTI children with hematological malignancies belonged to *Proteobacteria* (76%), *Firmicutes* (12%), *Bacteroidota* (7%), and *Actinobacteriota* (2%) at the phylum level, while the most abundant in LRTI children without hematological malignancies belonged to *Firmicutes* (53%), *Proteobacteria* (19%), *Bacteroidota* (12%), and *Actinobacteriota* (6%), similar to other studies. At the genus level, the top two in LRTI children with hematological malignancies belonged to *unclassified_Enterobacteriaceae* (49%) and *Escherichia_Shigella* (17%), whereas the vast two in LRTI children without hematological malignancies were *Streptococcus* (12%) and *Caproiciproducens* (6%) (Figure 3). Other common genera, such as *Moraxella* (5%), *Bacillus*(4%), *Oceanobacillus* (4%), and *Rothia*(4%), were among the most abundant genera of BALF identified in children without malignancies, while in children with malignancies, they were *Streptococcus* (6%), *Grimontia* (4%) and *Klebsiella*(3%), *Bacteroides* (3%), and *Parabacteroides* (3%).

3.4 α diversity of lung microbiome in lower respiratory tract infection children with or without hematological malignancies

Overall, the α (within-subject) diversity between LRTI children with or without hematological malignancies was significantly different (ACE p=0.000, Shannon p=0.000, Chao1 p=0.000, and Simpson p=0.000, p<0.01) (Table 3). LRTI children with hematological malignancies were found with a much lower number of OTUs and a smaller Shannon index than that of the control group (Figure 4). The richness and evenness of species from the BALF of LRTI children with hematological malignancies decreased significantly than those of the control group (Figure 5).

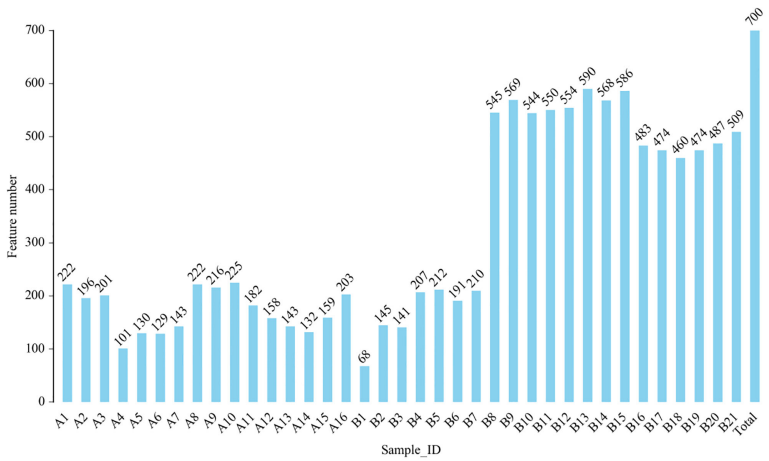

FIGURE 1
Comparison of operational taxonomic units (OTUs) in bronchoalveolar lavage fluid (BALF) from lower respiratory tract infection (LRTI) children with/without hematological malignancies. P = 0.001, < 0.01, feature number of group **A(A1-16)** was obviously lower than that of group **B(B1-21)**. A1–16 stand for the BALF samples of LRTI children with hematological malignancies, while B1–21 stand for the samples of LRTI children without malignancies.

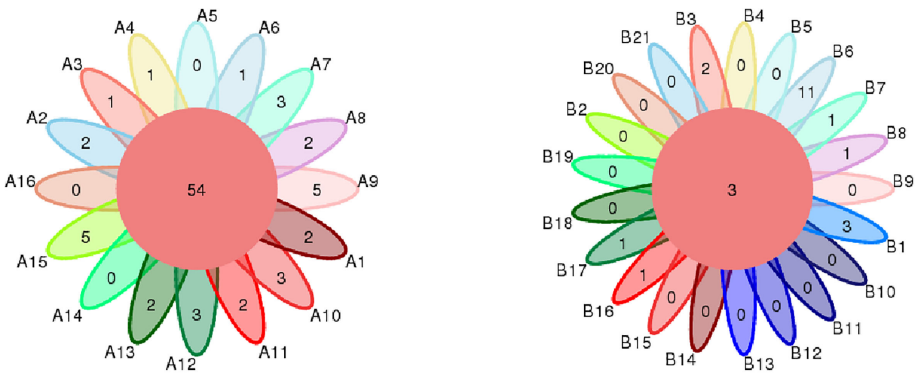

FIGURE 2
Comparison of mutual OTUs of samples from LRTI children with/without hematological malignancies. The left figure reflects BALF samples of LRTI children with hematological malignancies (Group A); the right figure reflects BALF samples of LRTI children without hematological malignancies (Group B). Mutual OTUs (the core of flower) of group **A** were more than that of group **B**.

For the comparison of abundances in common species at the phylum or genus levels, respectively, between two groups, obvious differences were found in *Proteobacteria, Firmicutes*, *Actinobacteriota*, and *Bacteroidota* at the phylum level, in addition with significant differences at the genus level, in *Escherichia_Shigella*, *unclassified_Enterobacteriaceae, Streptococus, Rothia, Klebsiella*, *Bacteroides*, and *Parabacteroides* (Table 2). We performed the correlation analysis of α diversity (Shannon) across different species at the phylum and genus levels, respectively. At the phylum level, *Proteobacteria* was obviously negatively associated with *Firmicutes* (r=-0.909, p=0.000, <0.01) and *Bacteroidota* (r=-0.518, p=0.001, <0.01); in addition to that, *Firmicutes* and *Bacteroidota* were significantly positively correlated with each other (r=0.456, p=0.005, <0.01). At the genus level, *Escherichia_Shigella* was significantly positively associated with *unclassified_Enterobacteriaceae* (r=792, p=0.000, <0.01), *Klebsiella* (r=0.458, p=0.004, <0.01), and *Parabacteroides* (r=0.354, p=0.032, <0.05), while *unclassified_Enterobacteriaceae* was obviously positively correlated with *Klebsiella* (r=0.415, p=0.011, <0.05). In addition, *Klebsiella* versus *Parabacteroides* (r=0.624, p=0.000, <0.01) and *Streptococcus* versus *Rothia* (r=0.478, p=0.003, <0.01) both had significantly positive correlation.

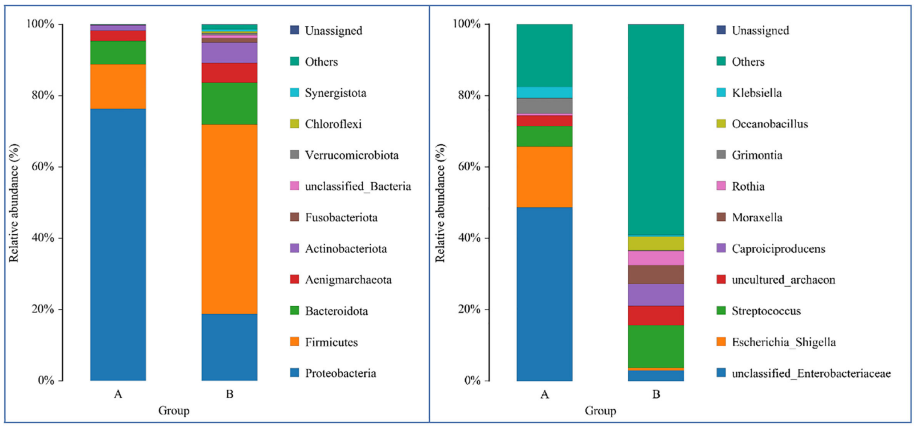

FIGURE 3
Comparison of LRTI children with/without hematological malignancies at the phylum/genus level. The bar chart on the left was the comparison at the phylum level, while the bars on the right were at the genus level. Bar A reflects BALF samples of LRTI children with hematological malignancies; Bar B reflects BALF samples of LRTI children without hematological malignancies.

10.3389/fonc.2022.932709

TABLE 3 Comparison of α diversity between LRTI children with/without hematological malignancies.

α diversity		Sum of ranks		P- value*
		Children with malignancy and sLRTI (N = 20)	Children with sLRTI only (N = 21)	
ACE		183	520	**0.000**
Chao1		182	521	**0.000**
Simpson*		184	519	**0.000**
Shannon index		183	520	**0.000**
Abundance (phylum level)	*Proteobacteria*	459	244	**0.000**
	Firmicutes	156	547	**0.000**
	Actinobacteriota	206	497	**0.002**
	Bacteriodota	230	473	**0.023**
Abundance (genus level)	*Escherichia Shigella*	472	231	**0.000**
	unclassified Enterobacterioriaceae	468	235	**0.000**
	Streptococcus	289	414	0.660
	Rothia	293	410	0.751
	Klebsiella	432	271	**0.000**
	Bacteroides	314	389	0.774
	Parabacteroides	404	299	**0.002**

*Comparison of the Simpson index in two groups were eligible for Student's t-test (p = 0.000, < 0.05), equal with the p-value by the Wilcoxon rank sum test.
Statistically significant p-values (p < 0.05) are shown in bold.

3.5 β diversity of lung microbiome in lower respiratory tract infection children with or without hematological malignancies

For the β (between-subject) diversity (Bray–Curtis) analysis, there was a significant difference between two groups (p=0.046, <0.05). The β diversity of BALF samples from LRTI children with hematological malignancies revealed high similarity, while samples from the control group showed higher heterogeneity within the group, with a relatively mutual difference from those from the observation group (Figure 6). There were obvious similarities within each group and significant differences between the two groups (Figure 7, 8) (PERMANOVA, R:0.623, p:0.001, p<0.01). As for the linear discriminant analysis effect size (LFeSe) analysis of biomarkers between the two groups, distinct microbial populations were found in bacterial exacerbation among LRTI children with hematological malignancies, with an obvious decreased proportion of *Firmicutes*, *Bacteroidota*, *Aenigmarchaeon*, and *Actinobacteriota* and a significantly increased proportion of *Proteobacteria* at the phylum level. At the genus level, among LRTI children with hematological malignancies, there were obviously decreased proportions of *Caproiciproducens*,

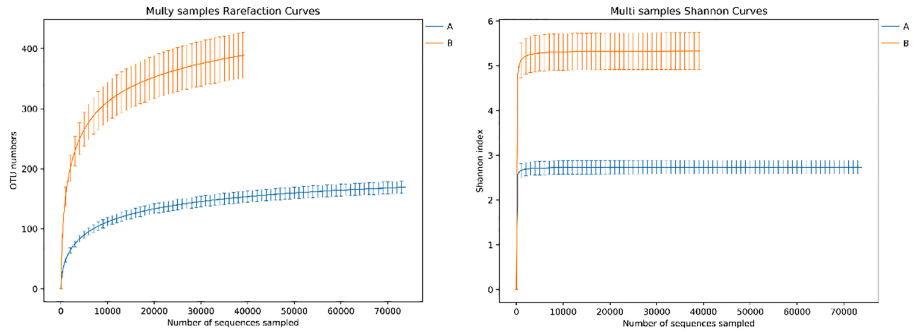

FIGURE 4
Rarefaction curve and Shannon index curve between samples of LRTI children with/without hematological malignancies. Curve A reflects BALF samples of LRTI children with hematological malignancies; Curve B reflects BALF samples of LRTI children without hematological malignancies.

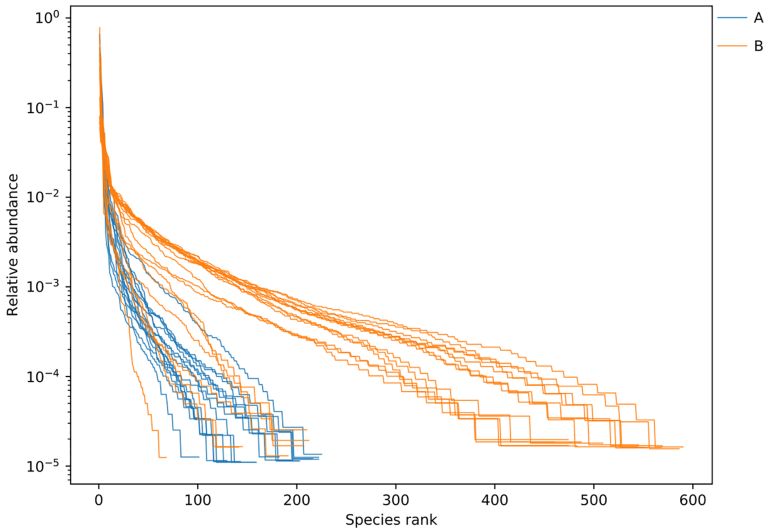

FIGURE 5
Rank abundance curve between samples of LRTI children with/without hematological malignancies. Curve A reflects BALF samples of LRTI children with hematological malignancies; Curve B reflects BALF samples of LRTI children without hematological malignancies. Width of each curve means the species richness of certain samples; smoothness means the species evenness of certain samples.

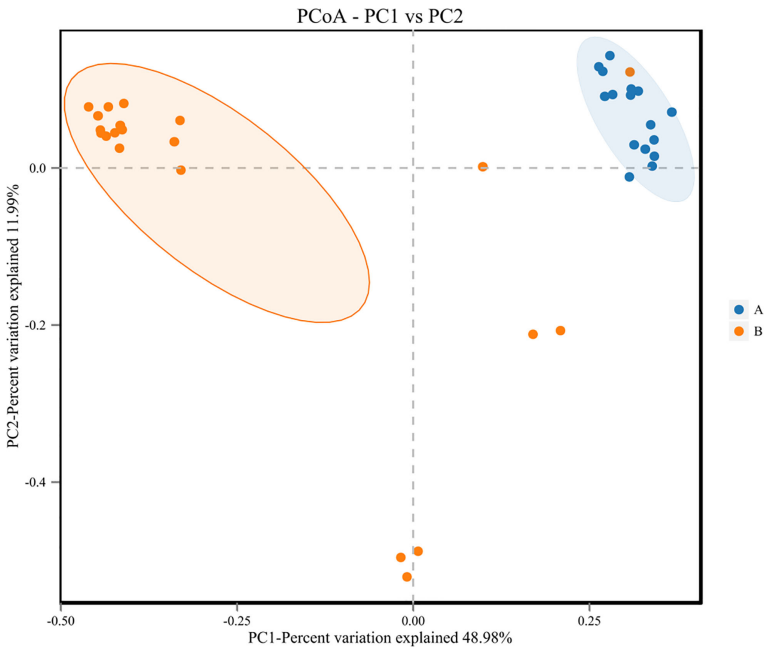

FIGURE 6
Principal Co-ordinates Analysis (PCoA) of samples of LRTI children with/without hematological malignancies. Dots A reflect BALF samples ofLRTI children with hematological malignancies; Dots B reflect BALF samples of LRTI children without hematological malignancies.

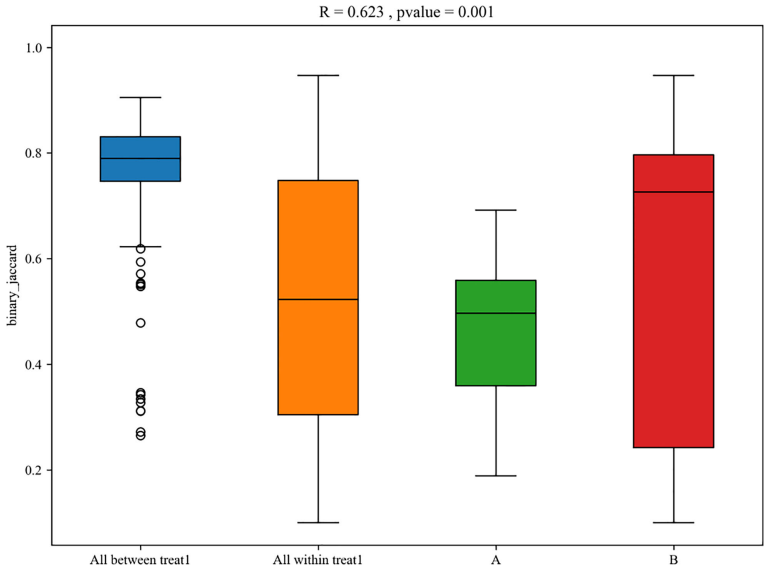

FIGURE 7
Box plot of PERMANOVA between samples of LRTI children with/without hematological malignancies. A mean BALF samples ofLRTI children with hematological malignancies; B mean BALF samples of LRTI children without hematological malignancies. Treat 1 means the differences(the basis of maignancies and the correlated conditions) between the two groups.

Oceanobacillus, *Bacillus*, *unclassified_Caloramatoracceae*, *Proteiniphilum*, and *Vibrio* and distinct elevated proportions of *Parabacteroides*, *Klebsiella*, *Grimontia*, *Escherichia_Shigella*, and *unclassified_Enterobacteriaceae* (Figure 9).

3.6 Function analysis of lung microbiome in lower respiratory tract infection children with or without hematological malignancies

As for the function analysis, BugBase phenotype prediction, species from LRTI children with hematological malignancies have significantly higher abundance than those from children without malignancies in a potentially pathogenic ability (Mann–Whitney–Wilcoxon test, FDR-corrected p-value: 1.087313e-09), facultatively anaerobic ability (Mann–Whitney–Wilcoxon test, FDR-corrected p-value: 6.213218e-10), and stress tolerance ability (Mann–Whitney–Wilcoxon test, FDR-corrected p-value: 1.087313e-09) (Figure 10). For the Kyoto Encyclopedia of Genes and Genomes (KEGG) metabolic pathway analysis between the samples of LRTI children with or without malignancies, there were significant differences in the function of drug resistance: antimicrobial (p-value: 1.01e-11), infectious disease:bacterial (p-value: 1.86e-11), and infectious disease:parasite (p-value: 3.61e-02), all of which were higher in the observation group, whereas there was a mildly decreased function of infectious disease:viral in the lung microbiome of LRTI children with hematological malignancies than that of the control group (p-value: 1.68e-03) (Figure 11). For Functional Annotation of Prokaryotic Taxa (FAPROTAX) analysis between these two groups, in terms of mammal_gut (p-value: 1e-15), human_gut (p-value: 1e-15) and human_pathogen_all (p-value: 6.38e-03), LRTI children with hematological malignancies showed a significantly increased microbial function than the control group (Figure 12).

3.7 Correlation between clinical factors and lung microbiome in lower respiratory tract infection children with or without hematological malignancies

We performed multivariate analysis to identify clinical factors significantly associated with microbial α and β diversity. Among all enrolled clinical factors, alanine transaminase (p=0.012, <0.05) and hemoglobin (p=0.004, <0.05) were significantly correlated with α diversity (Shannon), while the predisposition course of antibiotics before hospitalization (α diversity, p=0.025, <0.05; β diversity, p=0.042, <0.05) revealed an obvious correlation with both α (Shannon) and β (Bray–Curtis dissimilarity) diversity among all samples (Supplementary Table 1).

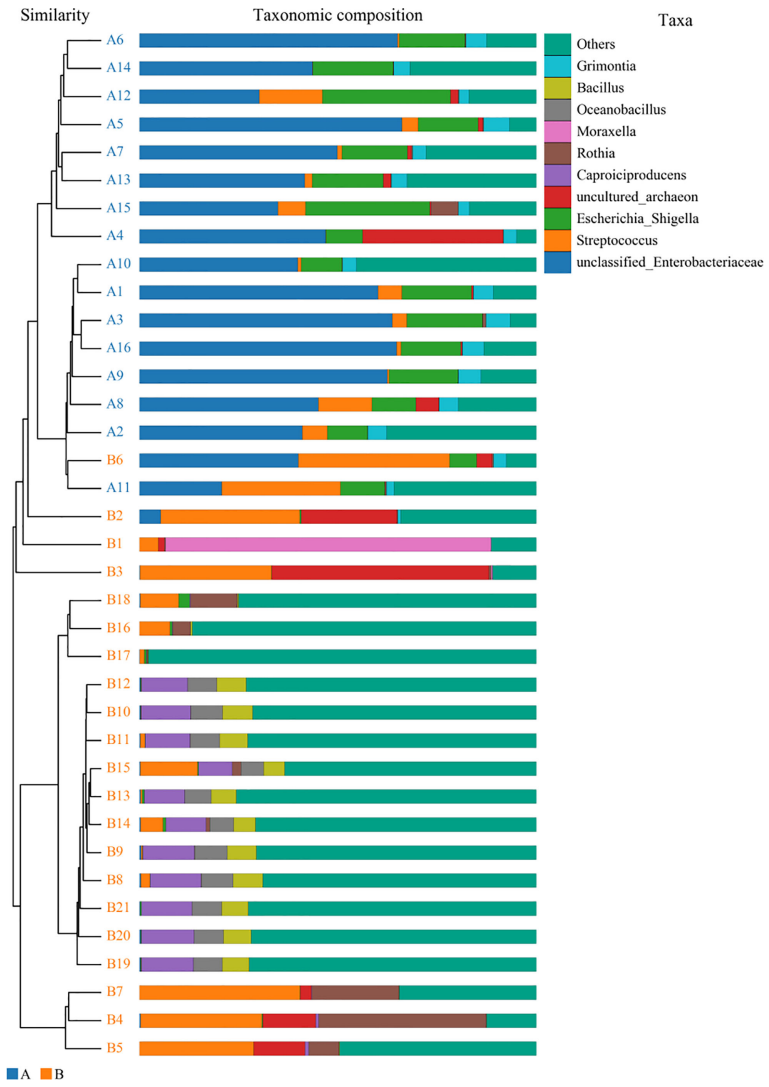

FIGURE 8
Unweighted pair-group method with arithmetic mean analysis. A1–16 mean the BALF samples of LRTI children with hematological malignancies, while B1–21 stand for the samples of LRTI children without hematological malignancies.

3.8 Correlation between clinical factors, lung microbiome in lower respiratory tract infection children with or without hematological malignancies versus hospitalization course

Multivariate analysis was performed to identify the correlation between the hospitalization course and the abundances of certain species at the phylum or genus levels, respectively, revealing that *Streptococcus* is correlated with the hospitalization course (R^2 = 0.335, p=0.036, <0.05). In addition, we performed multivariate analysis to investigate the association of clinical factors and the hospitalization course, establishing that absolute neutrophil count (p=0.038, <0.05), alanine transaminase (p=0.007, <0.01), hemoglobin (p=0.008, <0.01), platelet count (p=0.037, <0.05), the predisposition course of antibiotics before hospitalization (p=0.037, <0.05), and gender (p=0.044, <0.05) are respectively correlated with the hospitalization course. For Spearman correlation analysis between the hospitalization course versus α diversity, β diversity, and the abundances of certain species at the phylum or genus level, α diversity (Shannon) (r=-0.520, p=0.001, <0.01), β diversity (Bray–Curtis dissimilarity) (r=-0.413, p=0.011, <0.05), the abundances of *Firmicutes* (r=0.336, p=0.042, <0.05), *Proteobacteria* (r=-0.357, p=0.030, <0.05) at the phylum level, abundances of *unclassified_Enterobacteriaceae* (r=-0.448, p=0.005, <0.01), and *Escherichia_Shigella* (r=-0.386,

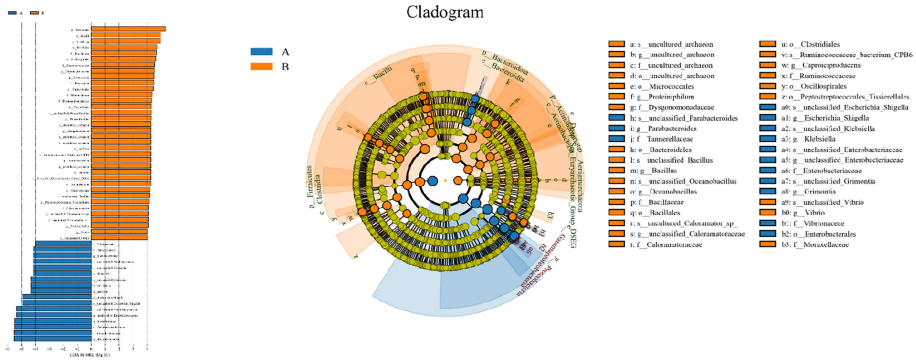

FIGURE 9
Line discriminant analysis effect size and cladogram. A reflect BALF samples of LRTI children with hematological malignancies; B reflect BALF samples of LRTI children without hematological malignancies.

p=0.018, <0.05) at the genus level showed a significant association with the hospitalization course (Figure 13).

Discussion

This study firstly compared the lung microbiome and the demographic characteristics of children with hematological malignancies and LRTIs versus children with LRTIs and no any malignancies. Between the two groups with age, weight, height, gender, and predisposed antibiotics course before hospitalization all matched, significant differences were found in the red blood cell count, hemoglobin, platelet count, C-reactive protein, ratio of positive culture other than bronchoalveolar lavage fluid(BALF) and hospitalization course. Among microbiome of all BALF samples from the two groups, LRTI children with hematological malignancies showed obviously decreased α and β diversity, significantly increased function in infectious disease:bacteria/parasite, drug resistance:antimicrobial and human pathogenesis than control group (LRTI children without any hematological malignancies), distinctly reduced proportion of *Firmicutes*, *Bacteroidota*, *Actinobacteriota*, increased *Proteobacteria* at the phylum level, and obviously elevated proportion of *Parabacteroides*, *Klebsiella*, *Grimontia*, *Escherichia_Shigella*, *unclassified_Enterobacteriaceae* at the genus level than the control group. Besides, it was revealed that α diversity(Shannon), β diversity(Bray Curtis dissimilarity), *Proteobacteria* at the phylum level, *unclassified_Enterobacteriaceae* and *Escherichia_Shigella* at the genus level, significantly negatively associated with hospitalization course, whereas *Firmicutes* at the phylum level established a positive correlation with hospitalization course.

Consistent with previous studies (23, 24), LRTI children with hematological malignancies were easier to get immunity and hemocyte exacerbations when attacked by LRTIs than other children with similar infectious conditions. In this study, children with malignancies turned out with significantly lower level of red blood cell count, hemoglobin, platelet count, and obviously higher level of C-reactive protein, ratio of a positive non-BALF culture, lower level of tidal volume per kilogram, and longer entire lower respiratory tract infection course and

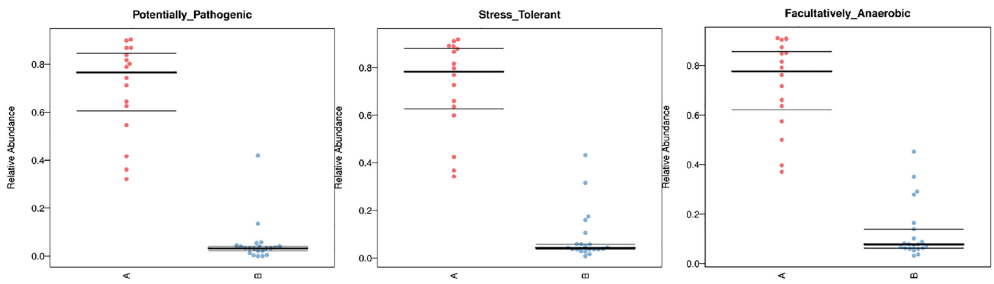

FIGURE 10
BugBase phenotype prediction. A reflect BALF samples of LRTI children with hematological malignancies; B reflect BALF samples of LRTI children without hematological malignancies.

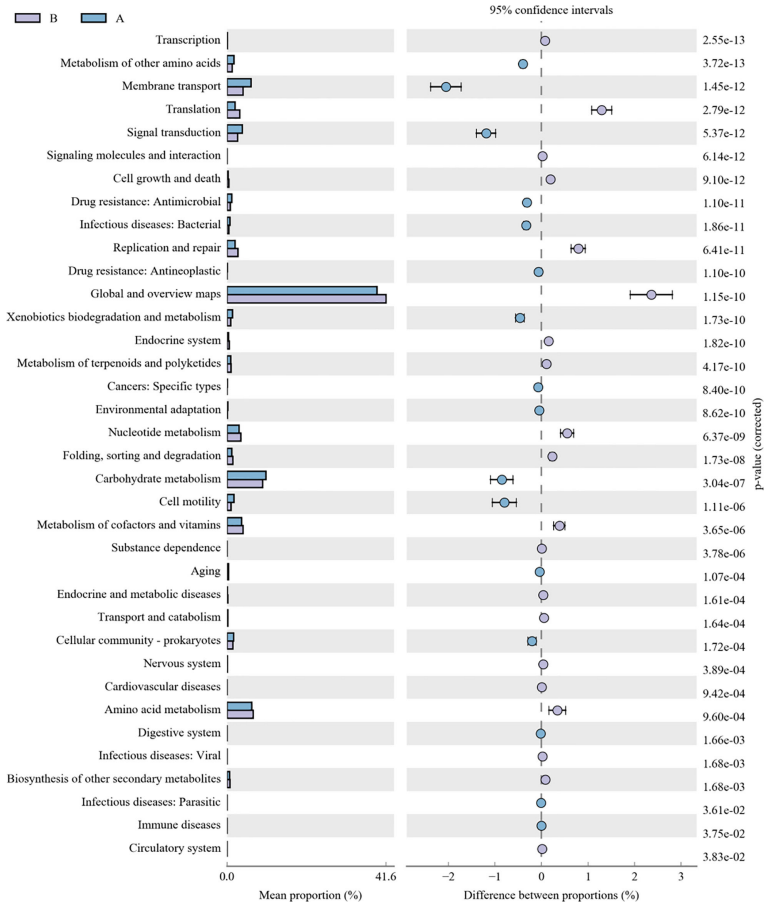

FIGURE 11
KEGG analysis of LRTI children with/without hematological malignancies. A reflect BALF samples of LRTI children with hematological malignancies; B reflect BALF samples of LRTI children without hematological malignancies.

hospitalization course. Nonetheless, in a large cohort study of acute respiratory infections in children and adolescents with acute lymphoblastic leukemia, patients with viral LRTIs had a significantly lower nadir absolute lymphocyte count compared with those with viral upper respiratory tract infections (8). Further, larger sample–sized and multicentered studies are in great demand about this field. Moreover, children with malignancies showed a higher ratio of pulmonary infiltration other than bronchopulmonary infiltration, higher percentage of bilateral loci in CT, and pulmonary complications than in the control group. Given the results of this study, on one hand, the immunity system of children with hematological malignancies seemed more fragile on the account of chemotherapy and malignancies' pathogenic mechanism. On the other hand, in previous studies and daily clinical work, common pathogens observed among children with hematological malignancies used to be variable from those among other children, with much stronger virulence and invasion ability than common community-acquired pathogens. It should be noted that in this study children with malignancies and LRTIs older than 6 years old seemed have equal pulmonary function with the age-matched control group, while children with malignancies and LRTIs under 6 years old showed significantly lower level of tidal volume per kilogram, a restrictive pulmonary dysfunction indicator, than the age-matched control group. Based on the previous studies about the worsening trend in pulmonary function for children with hematological malignancies (25–27), we have reason to believe that younger children with malignancies and LRTIs seem to worsen more in restrictive pulmonary dysfunction than age-matched children with only LRITs. This may be related with the more unstable and immature situation in younger children, yet more large cohort studies for this aspect are still greatly needed in the future.

α (within-subject) Diversity was found significantly decreased in LRTI children with hematologic malignancies than the control group, with both the abundance and OTUs lower than the control group. More frequent hospital visits, upper or lower tract infections, empirical antimicrobial

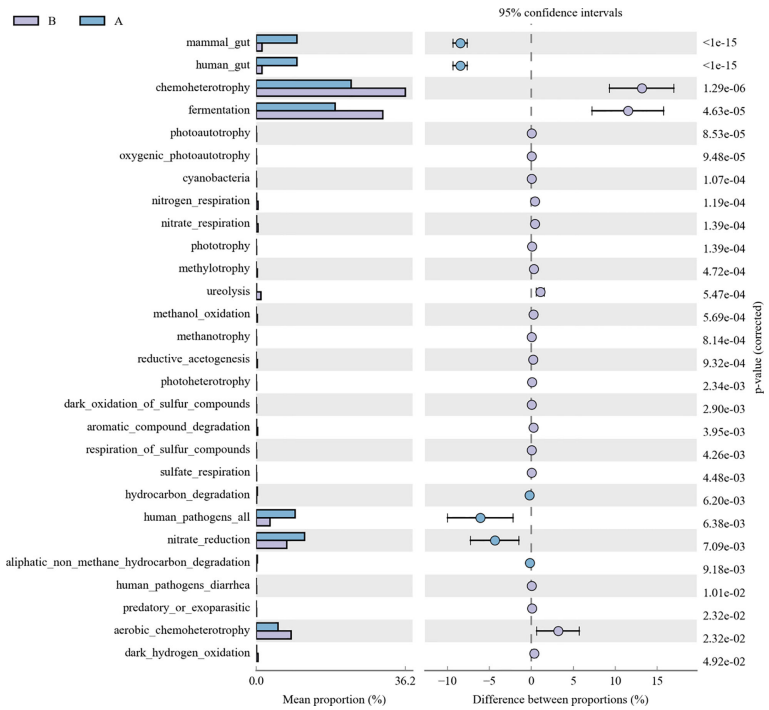

FIGURE 12
FAPROTAX analysis of LRTI children with/without hematological malignancies. A reflect BALF samples of LRTI children with hematological malignancies; B reflect BALF samples of LRTI children without hematological malignancies.

treatment than other children, and even chemotherapy may account for this distinct difference. Unlike other studies about the common airway microbiome composition of other diseases (15, 28–31), in this study, LRTI children with hematological malignancies revealed higher abundance in *Proteobacteria*, yet lower abundance in *Firmicutes*, *Actinobacteriota*, and *Bacteroidota* at the phylum level and, at the genus level, obviously higher abundance in *Escherichia_Shigella*, *unclassified_Enterobacteriaceae, Klebsiella*, and *Parabacteroides*, the majority of which were pathogens of intestinal flora, but lower abundance in *Streptococus, Rothia, and Bacteroides*. As reported in other studies (32, 33), there were always variable correlations between the abundances of certain species at different levels. In our study, *Proteobacteria* was obviously negatively associated with *Firmicutes* and *Bacteroidota*; in addition to that, *Firmicutes* and *Bacteroidota* were significantly positively correlated with each other. At the genus level, *Escherichia_Shigella* was significantly positively associated with *unclassified_Enterobacteriaceae, Klebsiella*, and *Parabacteroides*; in addition, *unclassified_Enterobacteriaceae* was obviously positively correlated with *Klebsiella*. Furthermore, *Klebsiella* versus *Parabacteroides* and *Streptococcus* versus *Rothia* both had a significantly positive correlation.

There were significant differences in the β (between-subject) diversity (Bray–Curtis) between two groups, the microbiome composition in BALF samples of LRTI children with hematological malignancies revealed high similarity within the group, while the composition in the samples of the control group showed more heterogeneity with each other within the group, which still have mutual similarity within the group and dissimilarity from the samples of the observation group (PERMANOVA, R:0.623, p:0.001, p<0.01). The biomarker analysis (LFeSe) of each group established that there were distinct species in each group eligible to be the reliable indicators. For the hematological malignancy group, *Proteobacteria* at the phylum level and *Parabacteroides*, *Klebsiella*, *Grimontia*, *Escherichia_Shigella*, and *unclassified_Enterobacteriaceae* at the genus level were validated. In addition, among the control group, *Firmicutes*, *Bacteroidota*, *Aenigmarchaeon*, and *Actinobacteriota* at the phylum level and *Caproiciproducens*, *Oceanobacillus*, *Bacillus*, *unclassified_Caloramatoracceae*, *Proteiniphilum*, and *Vibrio* at the genus level were good biomarkers. It turned out that microbial biomarkers for different diseases varied a lot (29, 31, 34–36), supporting that the tiny partially explored microbiome correlated with pathogenesis and progression of variable diseases work through numerous pathways.

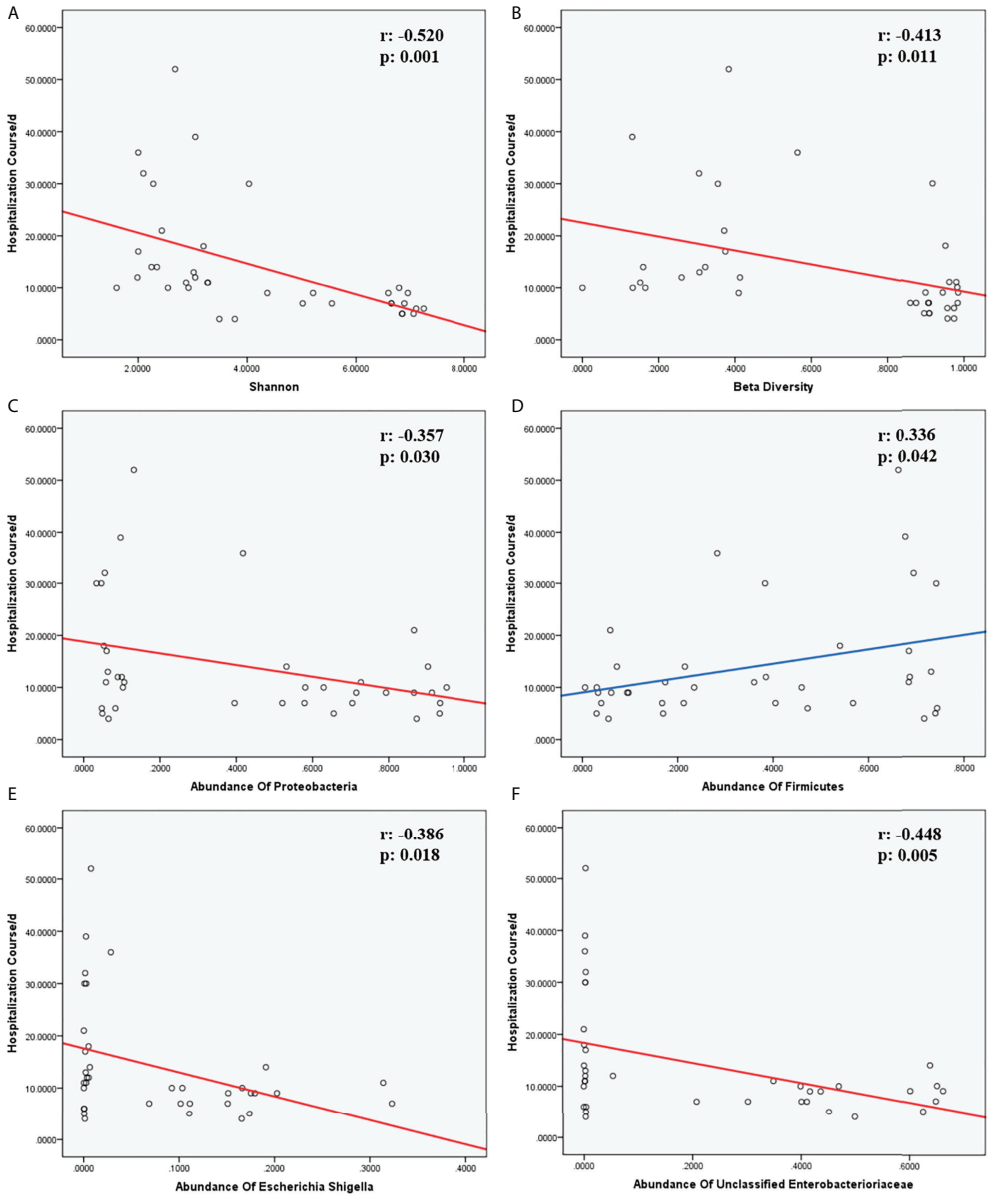

FIGURE 13
Correlation of hospitalization course and indicators. **(A, B)** were the correlation of α and β diversity and hospitalization course. **(C, D)** were the correlation of species and hospitalization course at the phylum level. **(E, F)** were the correlation of species and hospitalization course at the genus level. The r-value and p-value in Spearman correlation analysis were marked on the top-right corner in each chart. Fitting curves with a negative correlation were in red; fitting curves with a positive correlation were in blue.

As for function prediction analysis, BugBase phenotype prediction showed the lung microbiome from LRTI children with hematological malignancies having an elevated potentially pathogenic ability, facultatively anaerobic ability, and stress tolerance ability. For the KEGG metabolic pathway analysis, the function in drug resistance: antimicrobial, infectious disease: bacterial, and infectious disease:parasite was found obviously stronger in the microbiome from LRTI children with hematological malignancies. Furthermore, for FAPROTAX analysis, in terms of mammal_gut, human_gut, and human_pathogen_all, samples from LRTI children with hematological malignancies were indicated to be more superior than the control group. Altogether, the three kinds of microbiome function analysis in children with hematological malignancies were established with stronger microbial function in pathogenesis (bacteria or parasite) ability, survival ability even

in unfavorable environments, and antimicrobial drug resistance ability, leading to more frequent, severe, and refractory respiratory infections in these children. In the UKPCCMP cohort (37), researchers did not identify any increased risk of severe/critical infection in children with hematological compared with non-hematological malignancies, consistent with the slightly decreased function in the infectious disease: viral of the microbiome from the observation group in our study. What cannot be ignored is that the microbiome from LRTI children with hematological malignancies showed stronger function in mammal_gut and human_gut to a certain extent, reminding us about the gut–lung axis theory of microbiomes (38–40).

About the correlation of clinical factors and microbiome α diversity and β diversity, the predisposition course of antibiotics before hospitalization was indicated to be associated with both α and β diversity. The easier choice for empirical antimicrobial drugs in front of febrile episodes in children with hematological malignancies may be the major cause to this situation, which was comprehensible and common nowadays, whereas, in this study, alanine transaminase revealed a significant correlation with α diversity, which was scarcely reported in previous studies (32, 41–43). There was a great need for further study about this term.

The hospitalization course was complicated with variable factors, such as disease severity, disease complications, disease pathogen, treatment plan, immunity condition, and adjuvant therapy, yet, in general, a hospitalization course could simply stand for the smoothness of disease management, consistent with other previous studies (28). For the correlation analysis of the hospitalization course and lung microbiome, it was established that the α diversity, β diversity, abundance of *Proteobacteria* at the phylum level, and abundance of *unclassified_Enterobacteriaceae* and *Escherichia_Shigella* at the genus level were negatively associated with the hospitalization course, whereas the abundance of *Firmicutes* was positively correlated with the hospitalization course. That indicated that the lower α diversity; β diversity; and the abundance of *Proteobacteria*, *unclassified_Enterobacteriaceae*, and *Escherichia_Shigella*, the longer and rougher the course and the higher payment would happen in LRTIs children.. However, the more *Firmicutes* children with LRTIs have in the lung microbiome, the more smoothly treating course they would have.

Taken together, what made the changes in this study existing were still unknown. There was evidence that smoking was shown to restrict the ability of alveolar macrophages to phagocytose and kill bacteria, changing the homeostasis of the lung microbiome (44). Children with hematological malignancies had chemotherapy for treatment and uncommon immunity conditions from the pathogenesis of hematological malignancies. Either of these two factors could do more harm than smoking to the lung microbiome, resulting in lung dysbiosis. Moreover, there is quantity evidence that the components of the enteric microflora, specifically Gram-negative bacilli, may also make up a component of the lung microflora (45, 46). The disruption of intestinal–pulmonary crosstalk is linked to increased susceptibility to airway diseases and infections (47). Furthermore, the concept of the gut–bone marrow–lung axis has gained increasing attention with the discovery of the influence of SCFAs on bone marrow hematopoiesis (48, 49). The latest study also exhibited that the lung microbiome regulates brain autoimmunity, breaking through the so-called tight security of the brain (50), which indicated that the lung microbiome could also affect other organs or systems. Therefore, changes in the gut microbiome or bone marrow, immunity cells, and so on could be the potential origin of lung dysbiosis in children with malignancies and LRTIs, which could also cause a chain reaction to other organs, systems, or back onto the gut and bone marrow. Anyhow, along with many researchers, we have been committed to continuous studies for discovering the final trick.

Our study has several important strengths. Firstly, we reported the microbiome features from 16 BALF samples from children with hematological malignancies complicated with LRTIs, with age, weight, height, gender, and disease severity–matched children as the control group(children with LRTIs without any basement diseases). We found distinctly different α diversity, β diversity, abundance of certain species in BALF samples from LRTI children with hematological malignancies, indicating that the lung microbiome of children with hematological malignancies developed a stronger ability in pathogenesis, antimicrobial drug resistance, and unfavorable environment tolerance. To some extent, we could take advantage of macrobiotic biomarker (α diversity, β diversity, the abundance of *Proteobacteria*, *unclassified_Enterobacteriaceae*, *Escherichia_Shigella*, or *Firmicutes*) tests to predict the hospitalization course according to the significant correlation between them.

There were limitations in this study. Firstly, the sample size was limited since the samples are not so easy to obtain. A future larger cohort with more samples from multiple airway loci in children will be of great value. Secondly, the data in this study were collected with one single center so that results may not be generalizable. Validation across centers is important. Thirdly, this study was limited to the lack of the gut microbiome data for deeper research. Further study including the lung and gut microbiome is under way to uncover whether gut dysbiosis is consistent with the lung's and which system would be the origin of these changes. Fourthly, children with hematological malignancies complicated with LRTIs compared with the control group had hematological malignancies and chemotherapy as additional factors; the difference between two groups could not be simply ascribed to any single factor. We have begun a longitudinal observation on the sputum and oral swab of children at the time of initially being diagnosed as hematological malignancies and other certain time nodes during chemotherapy to support the conclusion in this study and promote further study in this field.

In summary, this study firstly characterizes the lung microbiome of children with or without hematological malignancies complicated with LRTI. LRTI children with hematological malignancies had a decreased α and β diversity; significantly reduced abundance of *Firmicutes*, *Bacteroidota*, *Actinobacteriota*; increased *Proteobacteria* at the phylum level; and distinctly elevated abundance of *Parabacteroides*, *Klebsiella*, *Grimontia*, *Escherichia_Shigella*, and *unclassified_Enterobacteriaceae* at the genus level, significantly increased function in infectious disease pathogenesis, antimicrobial drug resistance, and unfavorable environment tolerance, than the LRTI children without any malignancies. Furthermore, α diversity (Shannon), β diversity (Bray–Curtis dissimilarity), *Proteobacteria* at the phylum level, and *unclassified_Enterobacteriaceae* and *Escherichia_Shigella* at the genus level were significantly negatively associated with the hospitalization course whereas *Firmicutes* at the phylum level was positively correlated with the hospitalization course.

Data availability statement

The original contributions presented in the study are publicly available. This data can be found here: https://doi.org/10.5061/dryad.wm37pvmr3.

Ethics statement

This study was reviewed and approved by Qilu Hospital of Shandong University Institutional Review Board. Written informed consent to participate in this study was provided by the participants' legal guardian/next of kin.

Author contributions

YZ initiated the study, participated in the design and coordination, and drafted the manuscript. WYZ and HNN did equal roles in data management. JL provided statistical support. FHL and JFC helped to initiate the study and edit the manuscript. We are grateful to the entire research team. Finally, we are especially grateful to the patients and families whose data had been enrolled in the study. All authors contributed to the article and approved the submitted version.

Funding

This research received grant from Natural Science Foundation for Youths of Shandong Province (ZR2020QH055) and Qilu Hospital of Shandong University Scientific Research Fund Youth Project (2017QLQN32).

Conflict of interest

The authors declare that the research was conducted in the absence of any commercial or financial relationships that could be construed as a potential conflict of interest.

Publisher's note

All claims expressed in this article are solely those of the authors and do not necessarily represent those of their affiliated organizations, or those of the publisher, the editors and the reviewers. Any product that may be evaluated in this article, or claim that may be made by its manufacturer, is not guaranteed or endorsed by the publisher.

Supplementary material

The Supplementary Material for this article can be found online at: https://www.frontiersin.org/articles/10.3389/fonc.2022.932709/full#supplementary-material

References

1. Pui CH, Pei D, Campana D, Cheng C, Sandlund JT, Bowman WP, et al. A revised definition for cure of childhood acute lymphoblastic leukemia. *LEUKEMIA*. (2014) 28:2336–43. doi: 10.1038/leu.2014.142

2. Pillai V, Tallarico M, Bishop MR, Lim MS. Mature T- and NK-cell non-Hodgkin lymphoma in children and young adolescents. *Brit J Haematol* (2016) 173:573–81. doi: 10.1111/bjh.14044

3. Katsimpardi K, Papadakis V, Pangalis A, Parcharidou A, Panagiotou JP, Soutis M, et al. Infections in a pediatric patient cohort with acute lymphoblastic leukemia during the entire course of treatment. *SUPPORT Care CANCER*. (2006) 14:277–84. doi: 10.1007/s00520-005-0884-6

4. Buhtoiarov IN. Pediatric Lymphoma. *Pediatr Rev* (2017) 38:410–23. doi: 10.1542/pir.2016-0152

5. Derqaoui S, Boujida I, Marbouh O, Rouas L, Hessissen L, Lamalmi N. Non Hodgkin Lymphoma Among Children: Pathological Aspects and Diagnostic Challenges. *Clin Pathol* (2022) 17:15. doi: 10.1177/2632010X221090156

6. Srinivasan A, Gu Z, Smith T, Morgenstern M, Sunkara A, Kang G, et al. Prospective Detection of Respiratory Pathogens in Symptomatic Children With Cancer. *Pediatr Infect Dis J* (2013) 32:e99–e104. doi: 10.1097/INF.0b013e31827bd619

7. Dror T, Akerman M, Noor A, Weinblatt ME, Islam S, Glasser CL. Seasonal variation of respiratory viral infections: a comparative study between children with cancer undergoing chemotherapy and children without cancer. *Pediatr Hematol Oncol* (2021) 38:444–55. doi: 10.1080/08880018.2020.1871137

8. Hakim H, Dallas R, Zhou Y, Pei D, Cheng C, Flynn PM, et al. Acute respiratory infections in children and adolescents with acute lymphoblastic leukemia. *Cancer-Am Cancer Soc* (2016) 122:798–805. doi: 10.1002/cncr.29833

9. Lehrnbecher T. Treatment of fever in neutropenia in pediatric oncology patients. *Curr Opin Pediatr* (2019) 31:35–40. doi: 10.1097/MOP.0000000000000708

10. Kebudi R, Kizilocak H. Febrile Neutropenia in Children with Cancer: Approach to Diagnosis and Treatment. *Curr Pediatr Rev* (2018) 14:204–9. doi: 10.2174/1573396314666180508121625

11. Lehrnbecher T, Fisher BT, Phillips B, Beauchemin M, Carlesse F, Castagnola E, et al. Clinical Practice Guideline for Systemic Antifungal Prophylaxis in Pediatric Patients With Cancer and Hematopoietic Stem-Cell Transplantation Recipients. *J Clin Oncol* (2020) 38:3205–16. doi: 10.1200/JCO.20.00158

12. Sanschagrin S, Yergeau E. Next-generation Sequencing of 16S Ribosomal RNA Gene Amplicons. *J Visualized Experiments.* (2014) 90):51709. doi: 10.3791/51709

13. Kim H, Kim S, Jung S. Instruction of microbiome taxonomic profiling based on 16S rRNA sequencing. *J Microbiol* (2020) 58:193–205. doi: 10.1007/s12275-020-9556-y

14. Bolyen E, Rideout JR, Dillon MR, Bokulich NA, Abnet CC, Al-Ghalith GA, et al. Reproducible, interactive, scalable and extensible microbiome data science using QIIME 2. *Nat Biotechnol* (2019) 37:852–7. doi: 10.1038/s41587-019-0209-9

15. Jain S, Williams DJ, Arnold SR, Ampofo K, Bramley AM, Reed C, et al. Community-Acquired Pneumonia Requiring Hospitalization among U.S. Children. *New Engl J Med* (2015) 372:835–45. doi: 10.1056/NEJMoa1405870

16. Bolger AM, Lohse M, Usadel B. Trimmomatic: a flexible trimmer for Illumina sequence data. *Bioinformatics.* (2014) 30:2114–20. doi: 10.1093/bioinformatics/btu170

17. Edgar RC. UPARSE: highly accurate OTU sequences from microbial amplicon reads. *Nat Methods* (2013) 10:996–8. doi: 10.1038/nmeth.2604

18. Grice EA, Kong HH, Conlan S, Deming CB, Davis J, Young AC, et al. Topographical and temporal diversity of the human skin microbiome. *Science.* (2009) 324:1190–2. doi: 10.1126/science.1171700

19. Liu W, Zhang R, Shu R, Yu J, Li H, Long H, et al. Study of the Relationship between Microbiome and Colorectal Cancer Susceptibility Using 16SrRNA Sequencing. *BioMed Res Int* (2020) 2020:7828392. doi: 10.1155/2020/7828392

20. Douglas GM, Maffei VJ, Zaneveld JR, Yurgel SN, Brown JR, Taylor CM, et al. PICRUSt2 for prediction of metagenome functions. *Nat Biotechnol* (2020) 38:685–8. doi: 10.1038/s41587-020-0548-6

21. Korthauer K, Kimes PK, Duvallet C, Reyes A, Subramanian A, Teng M, et al. A practical guide to methods controlling false discoveries in computational biology. *Genome Biol* (2019) 20(1):118. doi: 10.1186/s13059-019-1716-1

22. de Heer K, Gerritsen MG, Visser CE, Leeflang MM. Galactomannan detection in broncho-alveolar lavage fluid for invasive aspergillosis in immunocompromised patients. *Cochrane Database Syst Rev* (2019). doi: 10.1002/14651858.CD012399.pub2

23. Lin B, Kennedy B, McBride J, Dalla Pozza L, Trahair T, McCowage G, et al. Long-term morbidity of respiratory viral infections during chemotherapy in children with leukaemia. *Pediatr Pulm.* (2019) 54:1821–9. doi: 10.1002/ppul.24456

24. Srinivasan A, Gu Z, Smith T, Morgenstern M, Sunkara A, Kang G, et al. Prospective Detection of Respiratory Pathogens in Symptomatic Children With Cancer. *Pediatr Infect Dis J* (2013) 32:e99–e104. doi: 10.1097/INF.0b013e31827bd619

25. Tantawy AAG, Elbarbary N, Ahmed A, Mohamed NA, Ezz-Elarab S. Pulmonary Complications in Survivors of Childhood Hematological Malignancies: Single-Center Experience. *Pediatr Hemat Oncol* (2011) 28:403–17. doi: 10.3109/08880018.2011.576905

26. Fanfulla F, Locatelli F, Zoia MC, Giorgiani G, Bonetti F, Spagnolatti L, et al. Pulmonary complications and respiratory function after bone marrow transplantation in children. *Eur Respir J* (1997) 10:2301–6. doi: 10.1183/09031936.97.10102301

27. Inaba H, Yang J, Pan J, Stokes DC, Krasin MJ, Srinivasan A, et al. Pulmonary dysfunction in survivors of childhood hematologic malignancies after allogeneic hematopoietic stem cell transplantation. *Cancer-Am Cancer Soc* (2010) 116:2020–30. doi: 10.1002/cncr.24897

28. Man WH, van Houten MA, Mérelle ME, Vlieger AM, Chu MLJN, Jansen NJG, et al. Bacterial and viral respiratory tract microbiota and host characteristics in children with lower respiratory tract infections: a matched case-control study. *Lancet Respir Med* (2019) 7:417–26. doi: 10.1016/S2213-2600(18)30449-1

29. Kitsios GD, Yang H, Yang L, Qin S, Fitch A, Wang X, et al. Respiratory Tract Dysbiosis Is Associated with Worse Outcomes in Mechanically Ventilated Patients. *Am J Resp Crit Care* (2020) 202:1666–77. doi: 10.1164/rccm.201912-2441OC

30. Harris M, Clark J, Coote N, Fletcher P, Harnden A, McKean M, et al. British Thoracic Society guidelines for the management of community acquired pneumonia in children: update 2011. *Thorax.* (2011). doi: 10.1136/thoraxjnl-2011-200598

31. Ahmed B, Cox MJ, Cuthbertson L, James P, Gardner L, Cookson W, et al. Comparison of the airway microbiota in children with chronic suppurative lung disease. *BMJ Open Respir Res* (2021) 8:e001106. doi: 10.1136/bmjresp-2021-001106

32. Wang Z, Singh R, Miller BE, Tal-Singer R, Van Horn S, Tomsho L, et al. Sputum microbiome temporal variability and dysbiosis in chronic obstructive pulmonary disease exacerbations: an analysis of the COPDMAP study. *Thorax.* (2018) 73:331–8. doi: 10.1136/thoraxjnl-2017-210741

33. Wang Z, Bafadhel M, Haldar K, Spivak A, Mayhew D, Miller BE, et al. Lung microbiome dynamics in COPD exacerbations. *Eur Respir J* (2016) 47:1082–92. doi: 10.1183/13993003.01406-2015

34. Garrett WS. Cancer and the microbiota. *Science.* (2015) 348:80–6. doi: 10.1126/science.aaa4972

35. Invernizzi R, Lloyd CM, Molyneaux PL. Respiratory microbiome and epithelial interactions shape immunity in the lungs. *Immunology.* (2020) 160:171–82. doi: 10.1111/imm.13195

36. Man WH, de Steenhuijsen Piters WAA, Bogaert D. The microbiota of the respiratory tract: gatekeeper to respiratory health. *Nat Rev Microbiol* (2017) 15:259–70. doi: 10.1038/nrmicro.2017.14

37. Millen GC, Arnold R, Cazier JB, Curley H, Feltbower R, Gamble A, et al. COVID-19 in children with haematological malignancies. *Arch Dis Child.* (2022) 107:186–8. doi: 10.1136/archdischild-2021-322062

38. Dickson RP, Singer BH, Newstead MW, Falkowski NR, Erb-Downward JR, Standiford TJ, et al. Enrichment of the lung microbiome with gut bacteria in sepsis and the acute respiratory distress syndrome. *Nat Microbiol* (2016) 1(10):16113. doi: 10.1038/nmicrobiol.2016.113

39. Sencio V, Barthelemy A, Tavares LP, Machado MG, Soulard D, Cuinat C, et al. Gut Dysbiosis during Influenza Contributes to Pulmonary Pneumococcal Superinfection through Altered Short-Chain Fatty Acid Production. *Cell Rep* (2020) 30:2934–2947.e6. doi: 10.1016/j.celrep.2020.02.013

40. Wedgwood S, Gerard K, Halloran K, Hanhauser A, Monacelli S, Warford C, et al. Intestinal Dysbiosis and the Developing Lung: The Role of Toll-Like Receptor 4 in the Gut-Lung Axis. *Front Immunol* (2020) 11:357. doi: 10.3389/fimmu.2020.00357

41. Leitao FF, Takiguchi H, Akata K, Ra SW, Moon JY, Kim HK, et al. Effects of Inhaled Corticosteroid/Long-Acting beta2-Agonist Combination on the Airway Microbiome of Patients with Chronic Obstructive Pulmonary Disease: A Randomized Controlled Clinical Trial (DISARM). *Am J Respir Crit Care Med* (2021) 204:1143–52. doi: 10.1164/rccm.202102-0289OC

42. Kehrmann J, Veckollari B, Schmidt D, Schildgen O, Schildgen V, Wagner N, et al. The lung microbiome in patients with pneumocystosis. *BMC Pulm Med* (2017) 17(1):170. doi: 10.1186/s12890-017-0512-5

43. Huang W, Wu M, Huang C, Liu S, Chen H, Chen Y, et al. Dynamics of the lung microbiome in intensive care patients with chronic obstructive pulmonary disease and community-acquired pneumonia. *Sci Rep-Uk.* (2020) 10(1):11046. doi: 10.1038/s41598-020-68100-4

44. King TJ, Savici D, Campbell PA. Phagocytosis and killing of Listeria monocytogenes by alveolar macrophages: smokers versus nonsmokers. *J Infect Dis* (1988) 158:1309–16. doi: 10.1093/infdis/158.6.1309

45. Soler N, Torres A, Ewig S, Gonzalez J, Celis R, El-Ebiary M, et al. Bronchial microbial patterns in severe exacerbations of chronic obstructive pulmonary disease (COPD) requiring mechanical ventilation. *Am J Respir Crit Care Med* (1998) 157:1498–505. doi: 10.1164/ajrccm.157.5.9711044

46. Lode H, Allewelt M, Balk S, De Roux A, Mauch H, Niederman M, et al. A prediction model for bacterial etiology in acute exacerbations of COPD. *INFECTION.* (2007) 35:143–9. doi: 10.1007/s15010-007-6078-z

47. Keely S, Talley NJ, Hansbro PM. Pulmonary-intestinal cross-talk in mucosal inflammatory disease. *Mucosal Immunol* (2012) 5:7–18. doi: 10.1038/mi.2011.55

48. Trompette A, Gollwitzer ES, Pattaroni C, Lopez-Mejia IC, Riva E, Pernot J, et al. Dietary Fiber Confers Protection against Flu by Shaping Ly6c(-) Patrolling Monocyte Hematopoiesis and CD8(+) T Cell Metabolism. *Immunity.* (2018) 48:992–1005.e8. doi: 10.1016/j.immuni.2018.04.022

49. Trompette A, Gollwitzer ES, Yadava K, Sichelstiel AK, Sprenger N, Ngom-Bru C, et al. Gut microbiota metabolism of dietary fiber influences allergic airway disease and hematopoiesis. *Nat Med* (2014) 20:159–66. doi: 10.1038/nm.3444

50. Hosang L, Canals RC, van der Flier FJ, Hollensteiner J, Daniel R, Flügel A, et al. The lung microbiome regulates brain autoimmunity. *Nature.* (2022) 603:138–44. doi: 10.1038/s41586-022-04427-4

frontiers | Frontiers in Oncology

TYPE Original Research
PUBLISHED 07 October 2022
DOI 10.3389/fonc.2022.966920

OPEN ACCESS

EDITED BY
Ioannis Voutsas,
Hospital Agios Savvas, Greece

REVIEWED BY
Feng Jiang,
Fudan University, China
Wei Song,
Wuhan University, China

*CORRESPONDENCE
Fujue Wang
404338834@qq.com

†These authors share first authorship

SPECIALTY SECTION
This article was submitted to Hematologic Malignancies, a section of the journal Frontiers in Oncology

RECEIVED 11 June 2022
ACCEPTED 23 September 2022
PUBLISHED 07 October 2022

CITATION
Li P, Li J, Wen F, Cao Y, Luo Z, Zuo J, Wu F, Li Z, Li W and Wang F (2022) A novel cuproptosis-related LncRNA signature: Prognostic and therapeutic value for acute myeloid leukemia. *Front. Oncol.* 12:966920. doi: 10.3389/fonc.2022.966920

A novel cuproptosis-related LncRNA signature: Prognostic and therapeutic value for acute myeloid leukemia

Pian Li[1†], Junjun Li[2†], Feng Wen[2], Yixiong Cao[2], Zeyu Luo[2], Juan Zuo[2], Fei Wu[2], Zhiqin Li[2], Wenlu Li[2] and Fujue Wang[2,3*]

[1]The First Affiliated Hospital, Department of Oncology Radiotherapy, Hengyang Medical School, University of South China, Hengyang, China, [2]The First Affiliated Hospital, Department of Hematology, Hengyang Medical School, University of South China, Hengyang, China, [3]Department of Hematology, West China Hospital of Sichuan University, Chengdu, China

Background: Cuproptosis is a type of programmed cell death that is involved in multiple physiological and pathological processes, including cancer. We constructed a prognostic cuproptosis-related long non-coding RNA (lncRNA) signature for acute myeloid leukemia (AML).

Methods: RNA-seq and clinical data for AML patients were acquired from The Cancer Genome Atlas (TCGA) database. The cuproptosis-related prognostic lncRNAs were identified by co-expression and univariate Cox regression analysis. The least absolute shrinkage and selection operator (LASSO) was performed to construct a cuproptosis-related lncRNA signature, after which the AML patients were classified into two risk groups based on the risk model. Kaplan-Meier, ROC, univariate and multivariate Cox regression, nomogram, and calibration curves analyses were used to evaluate the prognostic value of the model. Then, expression levels of the lncRNAs in the signature were investigated in AML samples by quantitative polymerase chain reaction (qPCR). KEGG functional analysis, single-sample GSEA (ssGSEA), and the ESTIMATE algorithm were used to analyze the mechanisms and immune status between the different risk groups. The sensitivities for potential therapeutic drugs for AML were also investigated.

Results: Five hundred and three lncRNAs related to 19 CRGs in AML samples from the TCGA database were obtained, and 21 differentially expressed lncRNAs were identified based on the 2-year overall survival (OS) outcomes of AML patients. A 4-cuproptosis-related lncRNA signature for survival was constructed by LASSO Cox regression. High-risk AML patients exhibited worse outcomes. Univariate and multivariate Cox regression analyses demonstrated the independent prognostic value of the model. ROC, nomogram, and calibration curves analyses revealed the predictive power of the signature. KEGG pathway and ssGSEA analyses showed that the high-risk group had

higher immune activities. Lastly, AML patients from different risk groups showed differential responses to various agents.

Conclusion: A cuproptosis-related lncRNA signature was established to predict the prognosis and inform on potential therapeutic strategies for AML patients.

KEYWORDS

cuproptosis-related Genes (CRGs), long non-coding RNAs (lncRNAs), acute myeloid leukemia (AML), prognostic value, chemotherapy and immunotherapy

Introduction

Acute myeloid leukemia (AML) is a highly heterogeneous leukemia that is associated with abnormalities in genetics, epigenetics, and cytogenetics (1). Over the last four decades, chemotherapy has remained the main treatment option for AML, However, most patients exhibit dismal outcomes and less than one-third of adult patients acquired durable remission (2). With the recent advances in molecular biology as well as the discovery of drivers for leukemogenesis and due to a better understanding of the AML, including the tumor environment (TME) and immune landscape, clinical trials, as well as novel therapies are now being promoted (2–4). Therefore, identification of novel prognostic and therapeutic targets will inform on development of personalized therapies for AML patients.

Cuproptosis is a recently defined type of cell death that differs from the well-known programmed cell death types, such as apoptosis, ferroptosis, pyroptosis, and necroptosis (5–8). Cuproptosis is involved in various physiological and pathological processes, including multiple cancers, and both copper ion carriers as well as copper chelators have potent anticancer activity (7). Disulfiram with copper selectively eradicated AML stem cells by activating the ROS-JNK while inhibiting the NF-κB and Nrf2 pathways (9). However, the role cuproptosis and its regulation in AML remains unclear.

Long non-coding RNAs (lncRNAs) are transcripts longer than 200 nucleotides, which are classified as non-coding RNAs, and are involved in the epigenetic regulation of gene expressions (10). They are associated with distinct cell death types and are implicated in several cancer types, including AML (10–15). Various lncRNAs are involved in leukemia and are potential diagnostic or prognostic biomarkers as well as therapeutic targets (16). However, the relationship between cuproptosis-related genes (CRGs) and lncRNAs in leukemia has yet to be reported.

We established a cuproptosis-related lncRNA signature using The Cancer Genome Atlas (TCGA) database to serve as a prognostic marker and to elucidate on the mechanism of cuproptosis in AML patients.

Materials and methods

Data collection and processing

RNA-seq data corresponding to the clinical data for 151 AML patients from the TCGA-LAML database were downloaded in the FPKM format (https://portal.gdc.cancer.gov) (17). The annotation of lncRNAs was obtained from the GENCODE (https://www.gencodegenes.org/) (18). Patients diagnosed with the M3 subtype according to the French-American-British (FAB) classification and those without complete clinical information were excluded from this study. Finally, 129 AML patients were included in this study, and their clinicopathological characteristics are shown in Table S1. To construct a prognostic cuproptosis-related lncRNA signature, 129 AML samples were randomized into a training set (93 cases) and validation set (36 cases) using "caret" R package.

Screening for cuproptosis-related lncRNAs

Nineteen CRGs (Table S2) were obtained from the literatures (5, 9, 19). Genetic alterations of CRGs in AML patients from the TCGA database were investigated using the cBioPortal database (https://www.cbioportal.org/). Correlations between cuproptosis-related lncRNAs in AML patients were determined using "limma" R package with a correlation coefficient of > 0.4 and $p < 0.001$ were set as the threshold. AML patients in the training set were assigned into two groups according to 2-year overall survival (OS) time based on clinical experience and previous studies (20, 21). Differentially expressed lncRNAs were identified using "DEGseq" R package with $p < 0.05$ and $|\log \text{fold change (log FC)}| \geq 1$ as the filter criteria.

Construction of a prognostic cuproptosis-related lncRNA signature for AML patients

Univariate Cox regression analysis was performed to screen for cuproptosis-related lncRNAs associated with survival from the identified differentially expressed lncRNAs (FDR < 0.05). Then, LASSO Cox regression analysis was performed with 10-fold cross-validation to establish the cuproptosis-related lncRNA signature. Analysis of the proportional hazards (PH) hypothesis and multicollinearity of covariates estimated by the variance inflation factor (VIF) were performed. LncRNAs that satisfied the PH hypothesis ($p > 0.05$) and VIF < 2 were selected to construct the signature *via* multivariate Cox regression (22). The risk score was calculated as follows:

Risk Score

$$= \sum_{i=1}^{n} \beta \times \text{lncRNA} \qquad \text{expression}$$

Whereby β is the regression coefficient. Regulatory networks of CRGs and the screened lncRNAs were analyzed and displayed using the "ggalluvial" R package.

Independent prognostic role of the cuproptosis-related lncRNA signature for AML patients

Univariate and multivariate Cox regression analyses were performed to determine the independent prognostic value of the constructed cuproptosis-related lncRNA risk model. Multiple clinical factors, including sex, age, white blood cell counts (WBCs), FAB classification, blasts in bone marrow (BM), and molecular risk stratification, were considered during the analysis. A nomogram for 1-, 3-, and 5-year OS was plotted with the above factors using the "rms" R package, and calibration curves analyses were performed to assess the accuracy of prediction.

Quantitative polymerase chain reaction (qPCR)

We had previously collected bone marrow samples for 50 newly diagnosed AML patients and peripheral blood samples for 6 healthy volunteers, and conducted a study for *TRPM4* gene in *MLL*-rearranged AML. Informed consents were obtained from all the participants and the Ethical Committee of the West China Hospital of Sichuan University had approved the study (1).

We used the partially reserved cDNA of mononuclear cells from bone marrow or peripheral blood samples to investigate the expressions of lncRNAs in the signature. The qPCR assay was performed using 2 × SYBR Green qPCR Master Mix (Bimake, China, B21203) on a LightCycler 480 II instrument (Roche, Switzerland). Relative expressions of the lncRNAs were normalized to *GAPDH* and calculated using the $2^{-\Delta\Delta Ct}$ method. The primers used in this study are shown in Table S3.

Gene set enrichment analysis (GSEA)

Functional enrichments analysis between the low- and high-risk subgroups were analyzed using the GSEA 4.2.2 software with the curated gene set (kegg.v7.5.symbols.gmt) based on the criterion: |NES| > 1.5, NOM $p < 0.05$ and FDR< 0.25.

Evaluation of immune infiltration status and tumor environment (TME)

To investigate the immune infiltration status of AML patients with different risk groups, single-sample gene set enrichment analysis (ssGSEA) was performed using "GSVA" R package to calculate the infiltration scores for 16 immune cells and 13 immune-related function activation (23). Thereafter, a comparison of TME scores was performed and expressions of immune checkpoints between different risk groups analyzed using "ggpubr" R package.

Assessment of the potential therapeutic drugs

Based on the half-maximal inhibitory concentration (IC50) on Genomics of Drug Sensitivity in Cancer (GDSC) (https://www.cancerrxgene.org/) and clinical gene expression data, "pRRophetic" R package was used to predict the sensitivity of the potential therapeutic drugs for the AML patients in the two risk subgroups (24, 25).

Statistical analysis

The R software (v4.1.3) was used to construct a risk model and for statistical analyses. Univariate and multivariate Cox regression analyses were performed to evaluate the independent prognostic value of clinical factors and risk model for AML patients. The Kaplan-Meier method with the two-side log-rank test was used to compare the OS time. Student's t-test or Mann-Whitney test were used to determine the relationship between the risk score and clinical factors. For comparisons of immune cell infiltrations and immune scores between the two risk groups, the Mann-Whitney test was used. $p < 0.05$ was the threshold for significance.

Results

Identification of cuproptosis-related lncRNAs in AML patients

The workflow of this study is shown in Figure 1. Mutant statuses of the 19 CRGs in AML patients from the TCGA database were analyzed by the cBioPortal database, which revealed that almost all CRGs had no significant genetic alterations (Figure S1). 503 lncRNAs that were associated with the 19 CRGs in AML samples from the TCGA database were obtained (Figure 2A). The correlations and regulation between CRGs and these lncRNAs are shown in Table S4. Next, 93 AML patients in the training set were assigned into two subgroups according to OS < 2 years (n = 55) and ≥ 2 years (n = 38) criteria. Twenty-one significantly differentially expressed lncRNAs were identified (Figures 2B, C).

A cuproptosis-related lncRNA prognostic model for the AML patients

Univariate Cox regression analysis was performed using the 21 differentially expressed lncRNAs in the training set and 13 lncRNAs (AC018552.3, AC026904.1, AC093278.2, AC133961.1, AL137186.1, AP000790.1, AP003064.2, HMGA2-AS1, LINC00987, LINC01679, LINC02757, SOCS2-AS1, Z98257.1) were found to be significantly associated with OS and an increased risk for AML (all adjusted *p*-value < 0.05 and HR > 1) (Table 1 and Figure 3A). Then, a 4-lncRNA signature for prognosis was established based on LASSO regression (Figures 3B, C) and multivariate Cox regression (Figure 3D). We performed the multicollinearity test with all VIF < 2 (Table S5) and checked for violations of the proportional hazard (PH) hypothesis (Table S6 and Figure S2). All covariates in the multivariate Cox regression satisfied the PH hypothesis and multicollinearity test. Risk Score = $0.3233 \times AC093278.2_{expression} + 0.6025 \times AC133961.1_{expression} + 1.2585 \times LINC01679_{expression} + 0.3490 \times LINC02757_{expression}$. Regulatory relationships between CRGs and the four lncRNAs are shown with a Sankey chart (Figure 3E).

Performance of the signature for AML patients in the TCGA database

Based on the risk score, 93 AML patients were assigned into low- and high-risk groups (n = 47 and n = 46, respectively). Principal component analysis (PCA) and t-distributed Stochastic

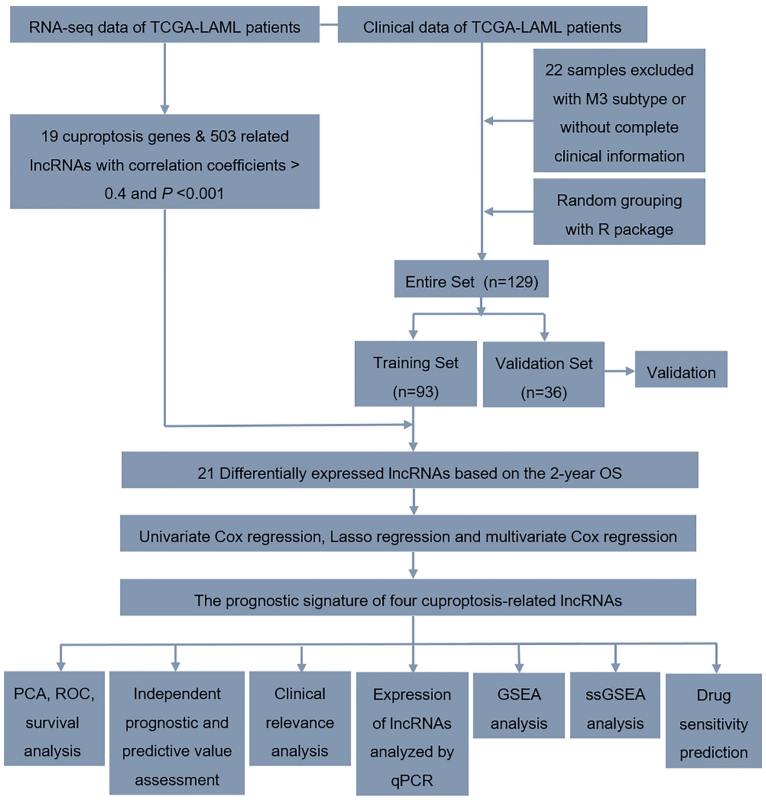

FIGURE 1
Workflow of the study design.

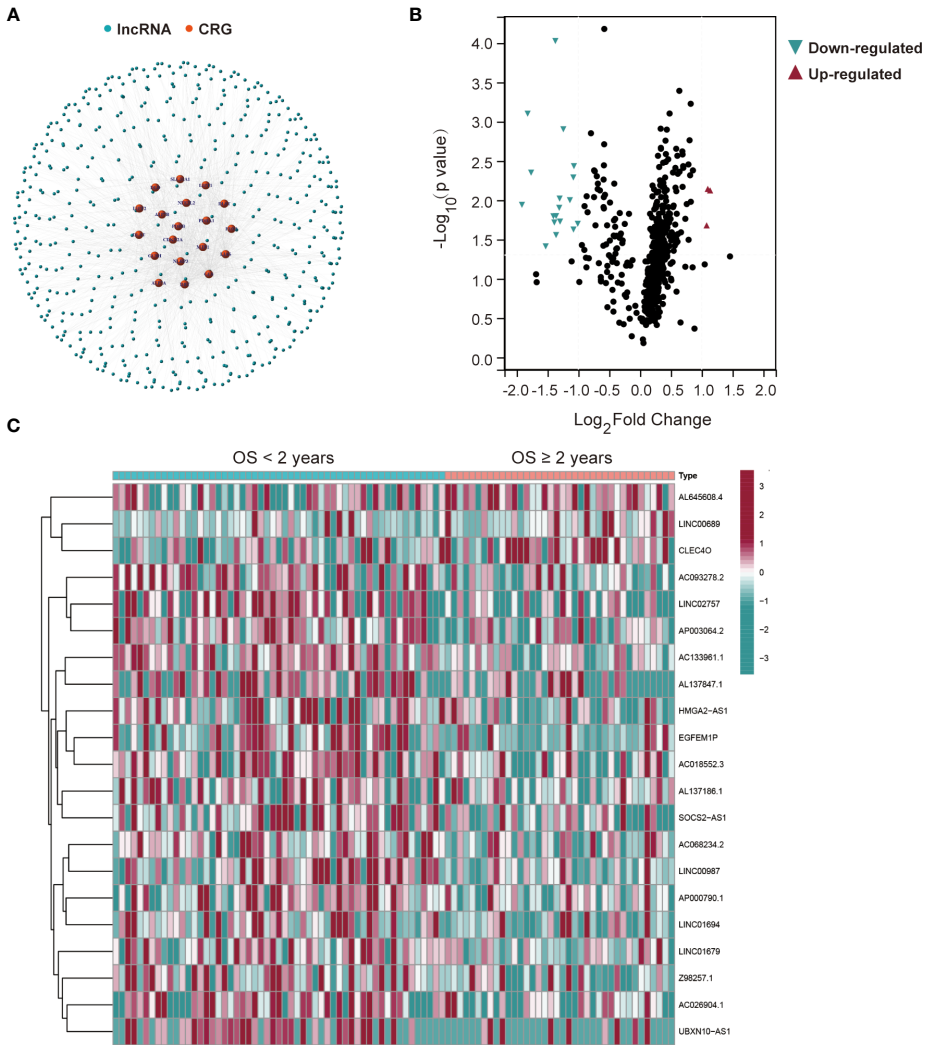

FIGURE 2
Twenty-one differentially expressed cuproptosis-related lncRNAs in AML patients from the TCGA database. **(A)** The network between 19 cuproptosis-related genes (CRGs) and 503 lncRNAs in AML patients (correlation coefficients > 0.4 and $p < 0.001$). **(B)** Differentially expressed lncRNAs for AML patients based on the OS < or ≥ 2 years. **(C)** A heatmap of the twenty-one differentially expressed lncRNAs.

Neighbor Embedding (t-SNE) were performed. It was found that AML patients in distinct risk groups could be separated into two clusters (Figures 4A, B). Compared to the low-risk group, more death events and a shorter OS time were observed in the high-risk group (Figures 4C-E). Sensitivity and specificity of this novel prognostic model for AML patients were assessed using the receiver operating characteristic (ROC) method, and the area under the ROC curve (AUC) found to be 0.867, 0.814 and 0.760 for 1-, 2-, 3-year survival, respectively (Figure 4F), suggesting a high predictive power of the signature in the training set.

We used the same algorithm to compute the risk scores in testing and entire sets. Findings from risk score distribution plot and scatter plot analyses were in accordance with those from the training set (Figures 5A-D). Kaplan-Meier curve analyses revealed that high-risk AML patients had worse survival outcomes (Figures 5E, F). Additionally, AUCs for 1-, 2- and 3-year OS were 0.694, 0.617 and 0.594 in the testing set (Figure 5G), and 0.815, 0.754 and 0.717 in the entire set (Figure 5H), respectively. These findings imply a good performance of the signature for prognostic prediction.

Independent prognostic value of the cuproptosis-related lncRNA signature for AML patients

Univariate and multivariate Cox regression analyses were performed to identify the independent prognostic factors for

TABLE 1 Univariate Cox regression of 13 lncRNAs for the OS of AML patients.

Ensemble Accession	lncRNA	HR (95%CI)	Adjusted *P*-value
ENSG00000261633	AC018552.3	1.149 (1.089-1.847)	0.009
ENSG00000253140	AC026904.1	1.562 (1.217-2.005)	< 0.001
ENSG00000261269	AC093278.2	1.410 (1.222-1.774)	0.003
ENSG00000251009	AC133961.1	1.745 (1.368-2.225)	< 0.001
ENSG00000229664	AL137186.1	1.115 (1.021-1.217)	0.016
ENSG00000214788	AP000790.1	1.715 (1.201-2.450)	0.003
ENSG00000255446	AP003064.2	1.154 (1.003-1.327)	0.045
ENSG00000197301	HMGA2-AS1	1.047 (1.002-1.094)	0.039
ENSG00000237248	LINC00987	1.416 (1.114-1.801)	0.005
ENSG00000237989	LINC01679	3.380 (1.935-5.902)	< 0.001
ENSG00000255363	LINC02757	4.245 (1.932-9.327)	< 0.001
ENSG00000246985	SOCS2-AS1	1.039 (1.001-1.079)	0.044
ENSG00000227066	Z98257.1	1.505 (1.236-1.833)	< 0.001

HR, Hazard Ratio.

AML patients in the TCGA cohort. Seven factors were considered in the analyses, including sex (Male vs. Female), FAB classification (M4/M5 vs. Non-M4/M5 subtype), age (≥ 60 vs. < 60 years old), blasts in BM (≥ 70% vs. < 70%), WBC counts (≥ 30 vs. < 30×10^9/L), molecular risk stratification (Poor vs. Good/Intermediate) and the established lncRNA risk model (high- vs. low-risk group). Univariate Cox regression showed that age, molecular risk stratification and the lncRNA risk model were associated with worse prognostic outcomes (HR = 2.4051, 95% CI: 1.5685–3.6879; HR = 1.7108, 95% CI: 1.0893–2.6868; HR = 2.5301, 95% CI: 1.6471–3.8993 (Figure 6A). The multivariable Cox regression further established the independent prognostic value of the risk model (HR = 3.2867, 95% CI: 2.0414–5.2914) (Figure 6B). A nomogram for 1-, 3-, and 5-year OS was plotted based on the above 7 factors. The TCGA-AB-2846 sample was taken as an example for assessment of the nomogram. The patient was a 57 years old female with M4/M5 subtype, WBC counts 13.6×10^9/L, 61% blasts in the bone marrow, good molecular risk group and belonging to the low-risk group. The patient had 301 as her risk score and showed a possibility of 85.4%, 71.9% and 61.1% for the OS > 1-, 3-, and 5-year, respectively (Figure 6C). Calibration curves analyses further confirmed the accuracy of this predictive model (Figure 6D).

Association between the cuproptosis-related lncRNA signature and clinicopathological features of AML patients

After constructing the cuproptosis-related lncRNA signature, we investigated its association with clinicopathological characteristics of AML patients, including sex, FAB classification, age, blasts in BM, WBC counts, molecular risk stratification, the status of gene mutations or rearrangements of *FLT3, NPM1, DNMT3A, NRAS/KRAS*, *TP53*, *WT1*, *KIT*, *MLL, CBFβ-MYH11, RUNX1-RUNX1T1*. It was found that AML patients with age > 60 years old, M4/M5 subtype, *TP53* mutation fusion and *MLL* rearranged had significantly higher risk scores while those with *RUNX1-RUNX1T1* had a lower risk score, and there were no significant differences between the risk score and other clinical variables (Figure 7).

Expression levels of four cuproptosis-related lncRNAs investigated by qPCR in AML samples

qPCR was performed to examine the expressions of the four cuproptosis-related lncRNAs in 24 AML and 6 healthy control samples. Our results showed that the expression levels of the four lncRNAs were relatively higher in AML than that in controls. Besides AC093278.2, other three lncRNAs revealed a significant increase in AML patients (Figure 8).

KEGG pathway analysis for high and low-risk AML patients

To explore the functional mechanism between the two risk groups, enriched KEGG pathways were determined using the GSEA software. Fifty-six and two pathways were enriched in high- and low-risk groups, respectively (all |NES| > 1.5, NOM p < 0.05 and FDR < 0.25) (Table S7). Nearly all of the top eleven enriched pathways in the high-risk group were significantly

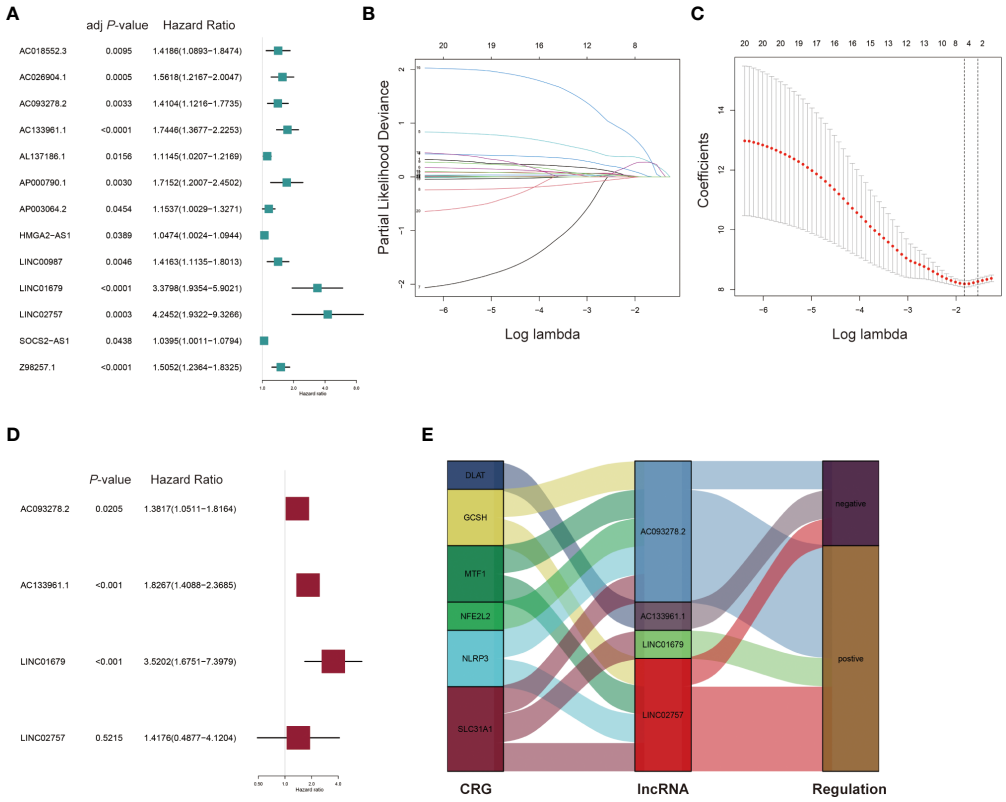

FIGURE 3
Construction of the prognostic cuproptosis-related lncRNA signature for AML patients in the training set. **(A)** Univariate Cox regression analysis for the prognostic cuproptosis-related lncRNAs. **(B, C)** Identification of prognostic cuproptosis-related lncRNAs in AML patients with 10-fold cross-validation for variable selection in LASSO (Least Absolute Shrinkage and Selection Operator) Cox regression. **(D)** Multivariate Cox regression analysis of the four cuproptosis-related lncRNAs for the prognosis of AML patients. **(E)** The Sankey diagram of cuproptosis-related genes (CRGs) and related lncRNAs.

correlated with the immune response (Figure 9), which provides the rationale for immune analysis in this risk model.

Immune infiltration status and TME of AML patients in different risk groups

The ssGSEA algorithm was used to assess the status and differences in immune cell infiltrations and immune-related function activation between AML patients in low- and high-risk groups. In Figures 10A, B cells, $CD8^+$ T cells, natural killer (NK) cells, plasmacytoid DCs (pDCs), T helper cells, Th1 cells, tumor-infiltrating lymphocytes (TIL), and regulatory T cells (Tregs) were significantly upregulated in the high-risk group (all $p < 0.05$). APC co-inhibition and co-stimulation, CCR, checkpoint, cytolytic activities, inflammation promotion, MHC class I, para-inflammation, T cell co-inhibition and co-stimulation, and Type I IFN responses were highly increased in the high-risk group (all $p < 0.05$, Figure 10B). Immune and ESTIMATE scores revealed different TME for AML patients in high-risk and low-risk groups (Figures 10C-E). Elevated expressions of multiple immune checkpoints were prevalent in the high-risk group (Figure 10F).

Prediction of potential therapeutic drugs for AML patients in different risk groups

The sensitivity of various chemotherapeutic or targeted drugs for AML patients within different risk groups was predicted. In Figure 11, high-risk AML patients had a high IC50 for cytarabine, methotrexate, etoposide, and ABT-263, and a lower IC50 for rapamycin and bortezomib. The targets and involved pathways for these drugs are shown in Table S8.

Discussion

As a newly defined type of programmed cell death, the exact role of cuproptosis in various cancer types has yet to be

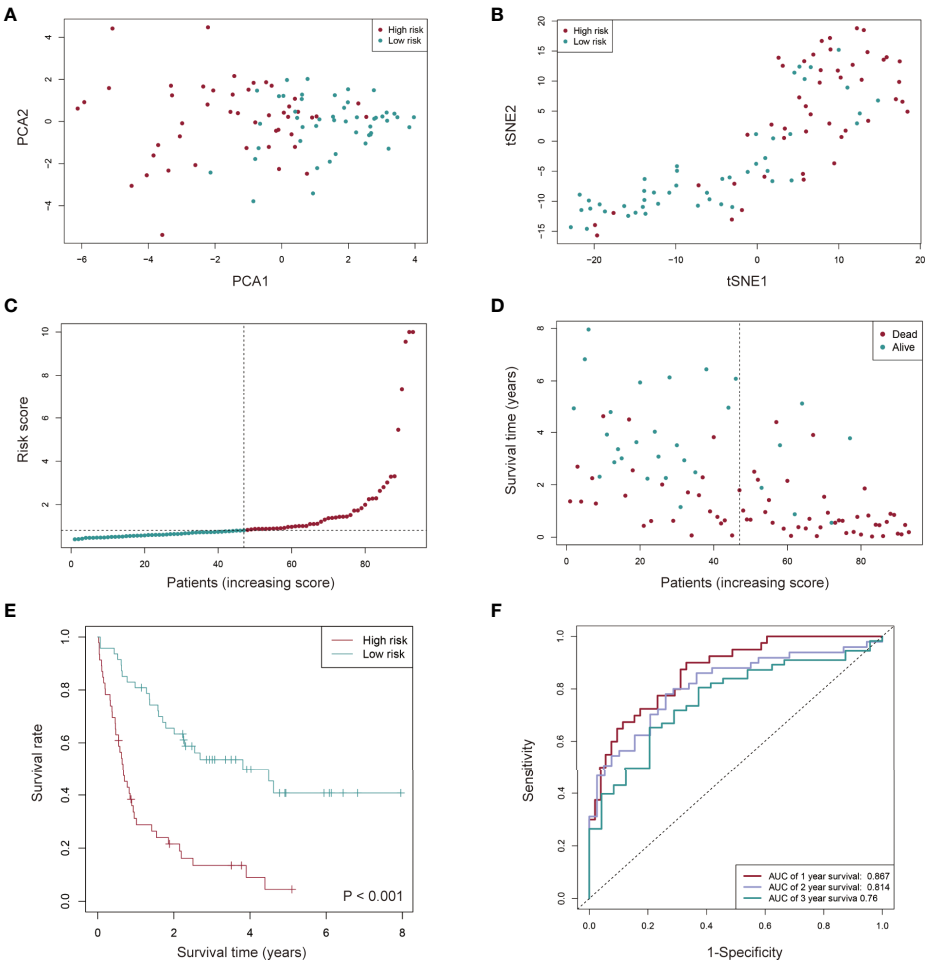

FIGURE 4
Prognostic value of the cuproptosis-related lncRNA signature in AML patients from the TCGA cohort. **(A, B)** AML patients in distinct risk groups could be separated into two clusters based on the PCA (Principal component analysis) **(A)** and t-distributed stochastic neighbor embedding (t-SNE) method **(B)**. **(C, D)** Distribution of the risk score **(C)** and survival time of each patient **(D)**. **(E)** Kaplan-Meier survival analysis of overall survival (OS) for AML patients with low- and high-risk groups. **(F)** The sensitivity and specificity of the prognostic model for AML patients assessed using the 1-, 2-, and 3-year ROC (receiver operating characteristic) curves and AUC (area under curve).

conclusively established; moreover, studies have not elucidated on the relationship between cuproptosis and lncRNA in AML. Therefore, we aimed at constructing a novel prognostic model that is based on cuproptosis-related lncRNAs for improved outcomes in AML patients.

In this study, CRGs were obtained from literatures and mutation analyses did not reveal significant genetic alterations for these genes in AML patients from the TCGA database. Next, 503 cuproptosis-related lncRNAs were identified using correlation analyses. To construct a cuproptosis-related prognostic model, 129 AML patients from the TCGA database were randomized into training and validation sets. Based on clinical experience and literatures, 93 AML patients in the training set were assigned into two groups using 2-year OS as the cutoff, and 21 differentially expressed lncRNAs were obtained. Out of the 21 lncRNAs, 13 were identified using univariate Cox regression to have a prognostic potential. To avoid overfitting, LASSO regression was performed to obtain a 4-cuproptosis-related lncRNA signature. The PCA, Kaplan-Meier survival and AUC analyses were performed to verify the distinguishing ability and accuracy of the established lncRNA signature. Then, validation and entire sets were used to confirm the prognostic value of the risk model. Moreover, multivariate Cox regression analyses were performed to confirm the independent prognostic value of the four lncRNA signatures for AML patients. Older patients, *TP53* mutation fusion or *MLL*

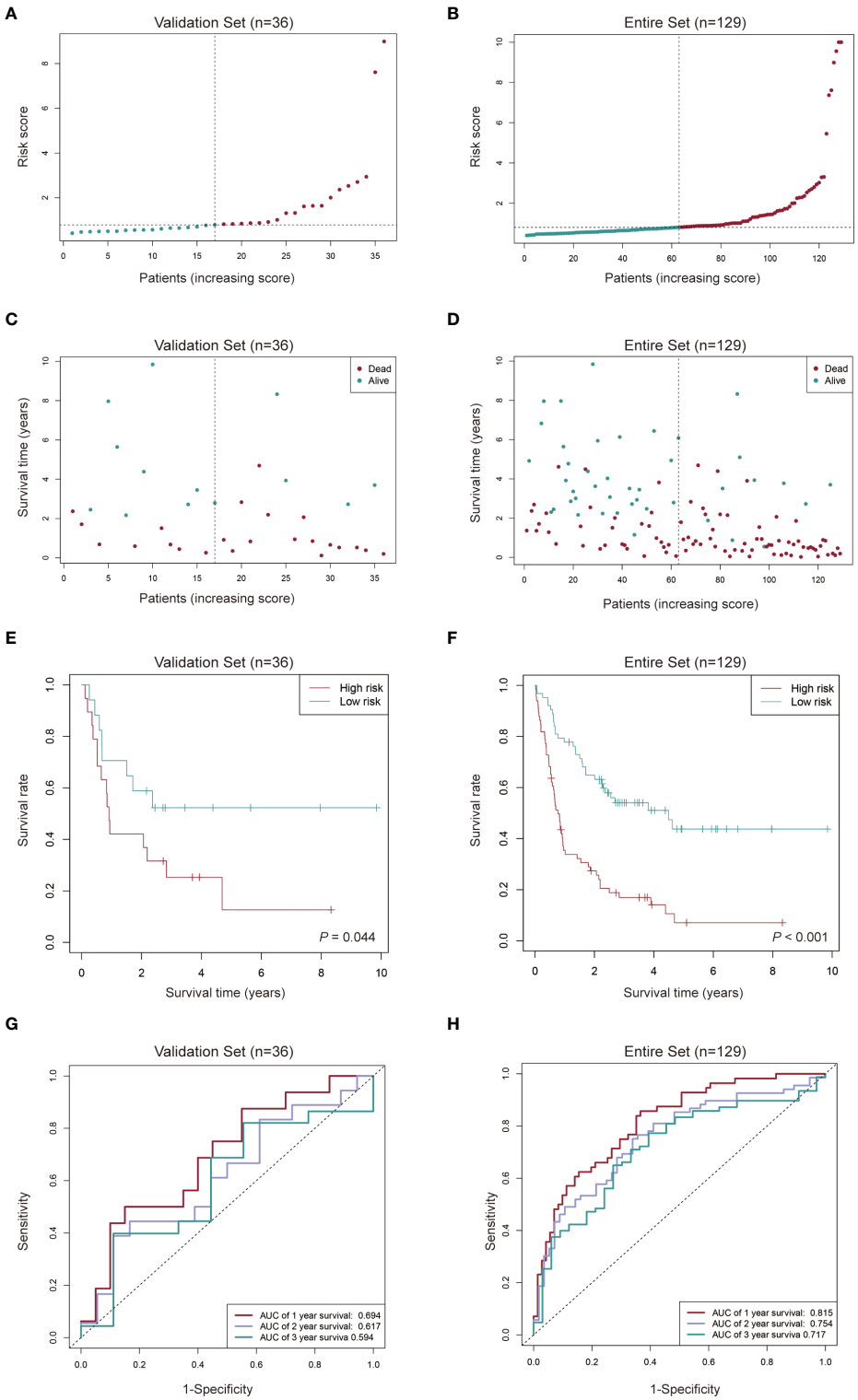

FIGURE 5
Evaluation of the cuproptosis-related lncRNA signature in the validation set and the entire set. **(A-D)** Distribution of the risk score and survival time of each patient in the validation set **(A, C)** and entire set **(B, D)**. **(E, F)** Kaplan-Meier curve analysis of the signature in the validation set **(E)** and entire set **(F)**. **(G, H)** ROC curves and their AUC values showed 1-, 2-, and 3-year predictions in the validation set **(G)** and entire set **(H)**.

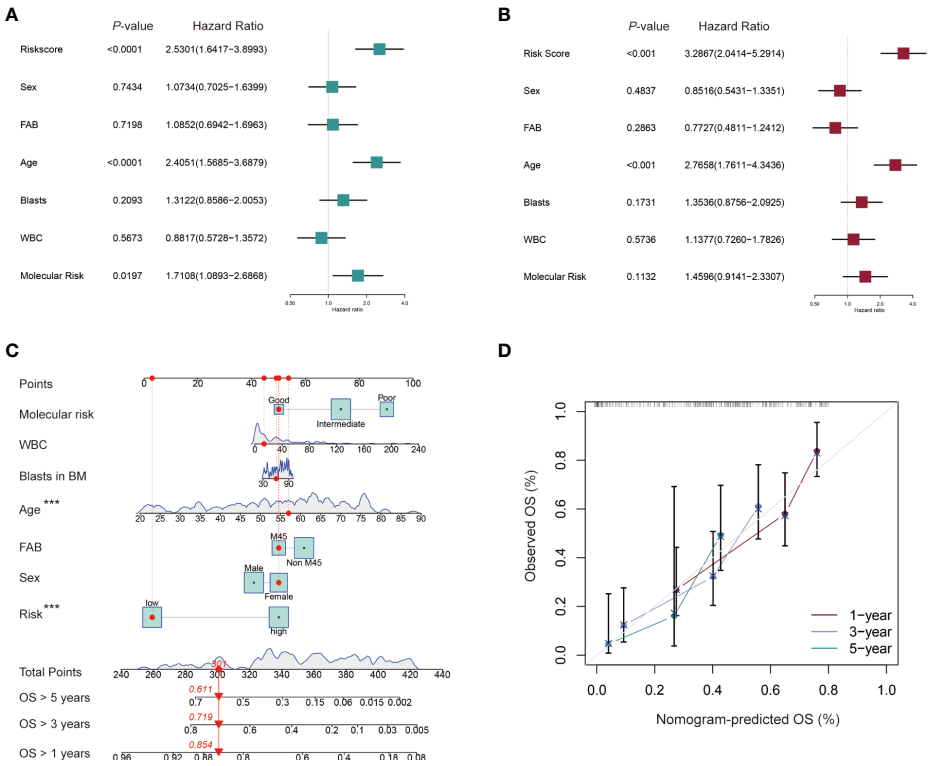

FIGURE 6
Independent prognostic role of the cuproptosis-related lncRNA signature for AML patients. **(A, B)** Univariate and multivariate Cox regression analysis of clinical factors including sex, French-American-British (FAB) subtype, age, blasts in bone marrow (BM), white blood counts (WBC), and molecular risk stratification and risk score for OS. **(C)** Nomogram that integrated the risk score and clinical factors predicts the probability of the 1-, 3-, and 5-year OS. **(D)** The calibration curves for 1-, 3-, and 5-year OS.

rearranged, which are independent adverse prognostic factors for AML patients (2), had higher risk scores, and those with *RUNX1-RUNX1T1*, a favorable fusion gene, had lower risk scores. Furthermore, expressions of AC133961.1, LINC01679 and LINC02757 were found to be significantly increased in AML patients compared to healthy controls by qPCR assay.

Among the 4 cuproptosis-related lncRNA signatures, LINC01679 was initially identified in a 4 lncRNAs-based prognostic model for classification and prediction of survival in patients with prostate cancer (PCa) (26). A study (27) investigated the role of LINC01679 in PCa and found that patients with low expressions of LINC01679 had worse survival outcomes. Mechanistically, LINC01679, serving as a competitive endogenous RNA (ceRNA) inhibits PCa development and progression by regulating the miR-3150a-3p/SLC17A9 axis. Notably, LINC01679 was found to be a protective factor for PCa in both studies. In this study, LINC01679 was associated with increased risk for AML, suggesting that LINC01679 may have distinct roles in various cancer types. In previous studies, AC093278.2 was found to be an immune-related lncRNA for kidney renal clear cell carcinoma (28), while AC133961.1 was reported to be a ferroptosis-related lncRNA in AML with diagnostic and adverse prognostic roles (11). In addition, LINC02757 discovered in this study were not reported previously, of which the role needs to be further elucidated.

To investigate the functional mechanism of the constructed cuproptosis-related lncRNA signature for AML prognosis, KEGG pathway analysis was performed using the GSEA software. Multiple signaling pathways, especially immune-related processes, were found to be significantly enriched in the high-risk group. Previously, a variety of genes signatures associated with tumor immune microenvironment and immunotherapy response for pediatric or adult AML patients were established (29–33), and studies have reported on potential clinical benefits of immunotherapy against AML, including targeting CD33, CD123, and several immune checkpoint inhibitors (ICIs) (4, 34). In this study, we found high immune cell infiltrations and immune-related function activations in high-risk AML patients. The presence of T cells at the tumor

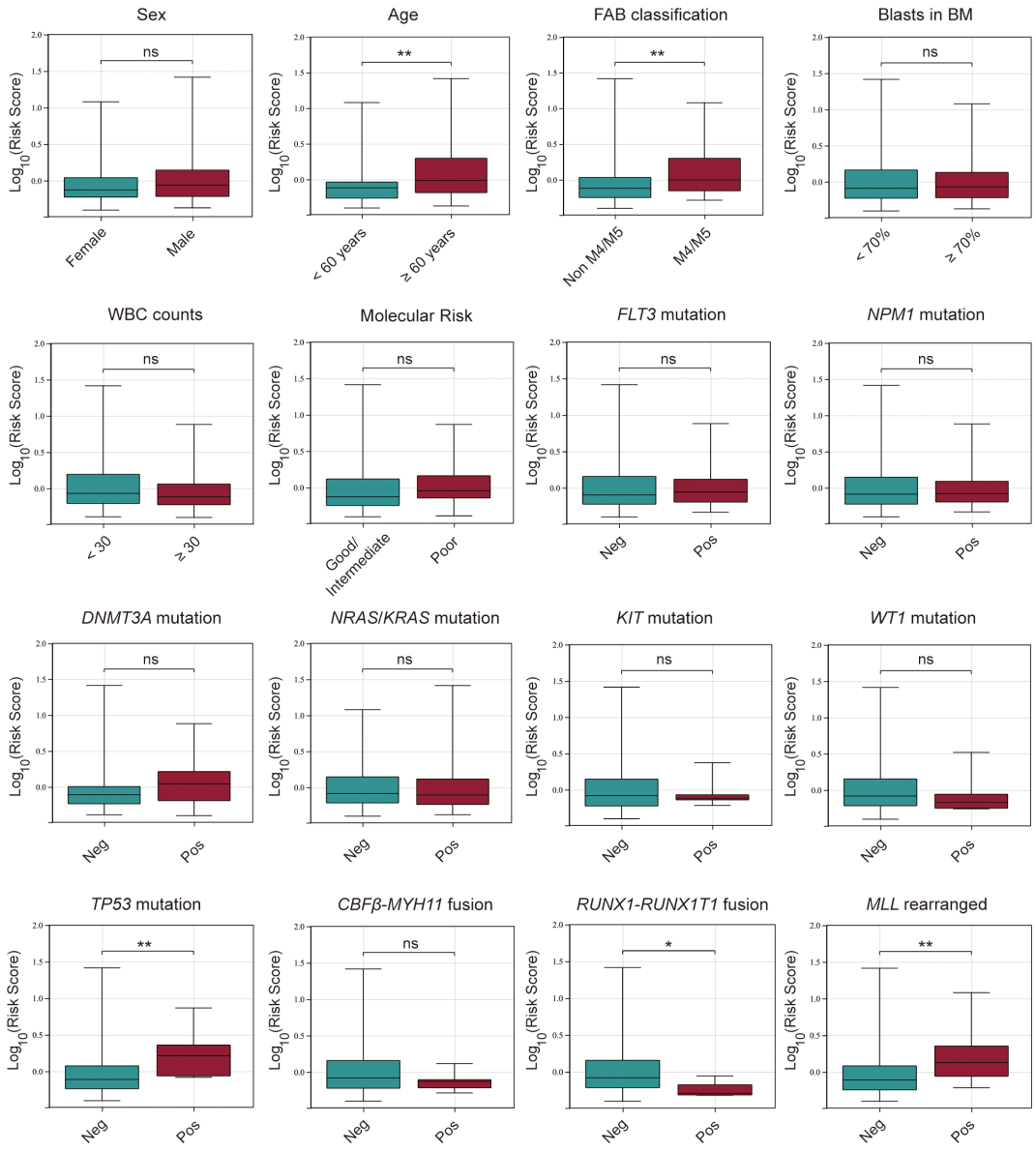

FIGURE 7
Association between the risk score and various clinicopathological factors in AML patients from the TCGA database. ns, no significance; *p < 0.05; **p < 0.01.

site is critical for immune recognition and elimination of AML cells, and a higher percentage of CD8+ T cells in BM were predictive of responses to ICIs combined with a hypomethylating agent in AML patients (3, 35). The proportion of NK cells in the BM of AML patients effectively predicted their prognostic outcomes and a combination of NK cell-based immunotherapies with an MCL1 inhibitor showed synergistic anti-leukemia effects *in vitro* (36). Elevated pDC infiltrations are associated with immune escape and may be used for risk stratification for AML and to transdifferentiate leukemia in AML microenvironments (37, 38). Tregs were shown to be major contributors to defective immune responses, with increased Treg levels being associated with worse outcomes in AML (39, 40). Intriguingly, expressions of multiple well-known checkpoints were found to be significantly upregulated in high-risk AML patients.

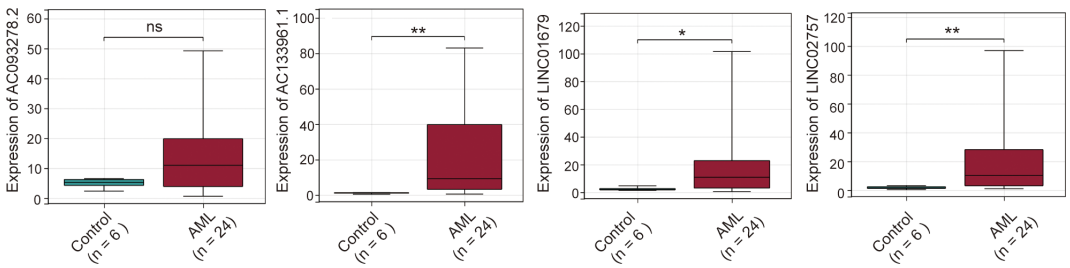

FIGURE 8
Expression levels of four cuproptosis-related lncRNAs in AML samples. ns:xFF1A;no significance; *$p < 0.05$; **$p < 0.01$.

Programmed cell death 1 (PD-1), encoded by the PDCD1 gene, and its ligands PD-L1 (also known as CD274) and PD-L2 (also known as PDCD1LG2 or CD273), plays a crucial role in maintaining self-tolerance and are associated with immune escape in cancer by inhibiting the direct cytotoxic activities of effector $CD8^+$ T cells on tumor cells (34). Elevated expressions of PD-1, PD-L1, and PD-L2 were associated with worse OS in AML patients (41), while the inhibition of the PD-1/PD-L1 pathway combined with hypomethylating agents or chemotherapy was found to be feasible and effective for newly diagnosed and refractory/relapsed (R/R) AML patients (3). CTLA-4, associated with the attenuation of T cell activation by preventing CD28 on T cells from binding its co-stimulatory counterparts (CD80 and CD86) on antigen-presenting cells (APCs) (34), demonstrated a modest efficacy for AML *in vitro* and *in vivo* upon blocking (4). Overall, the developed cuproptosis-related lncRNA signature elucidates on the relationship between cuproptosis and immunity as well as the rationale for the use of immunotherapy in AML patients.

Finally, drug sensitivities for AML patients in different risk groups were predicted. AML patients in the high-risk group showed a lower sensitivity to a range of anti-leukemia agents/drugs, including cytarabine, methotrexate, etoposide, and ABT-263 (a BCL-2 inhibitor, also called Navitoclax), while they responded better to several other drugs like rapamycin, bortezomib, Erlotinib, even though some of them are currently not in clinical use for treatment of AML. Based on our cuproptosis-related lncRNA risk model and the above findings, we concluded that a combination of immunotherapy with chemotherapy or other target inhibitors will provide a precise and personalized treatment strategy for AML patients.

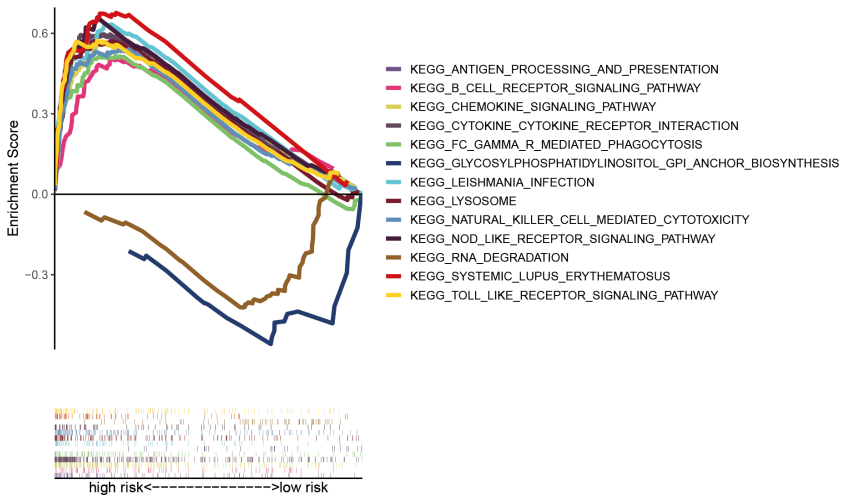

FIGURE 9
Significantly enriched KEGG pathways in AML patients with low- and high-risk groups analyzed using GSEA software.

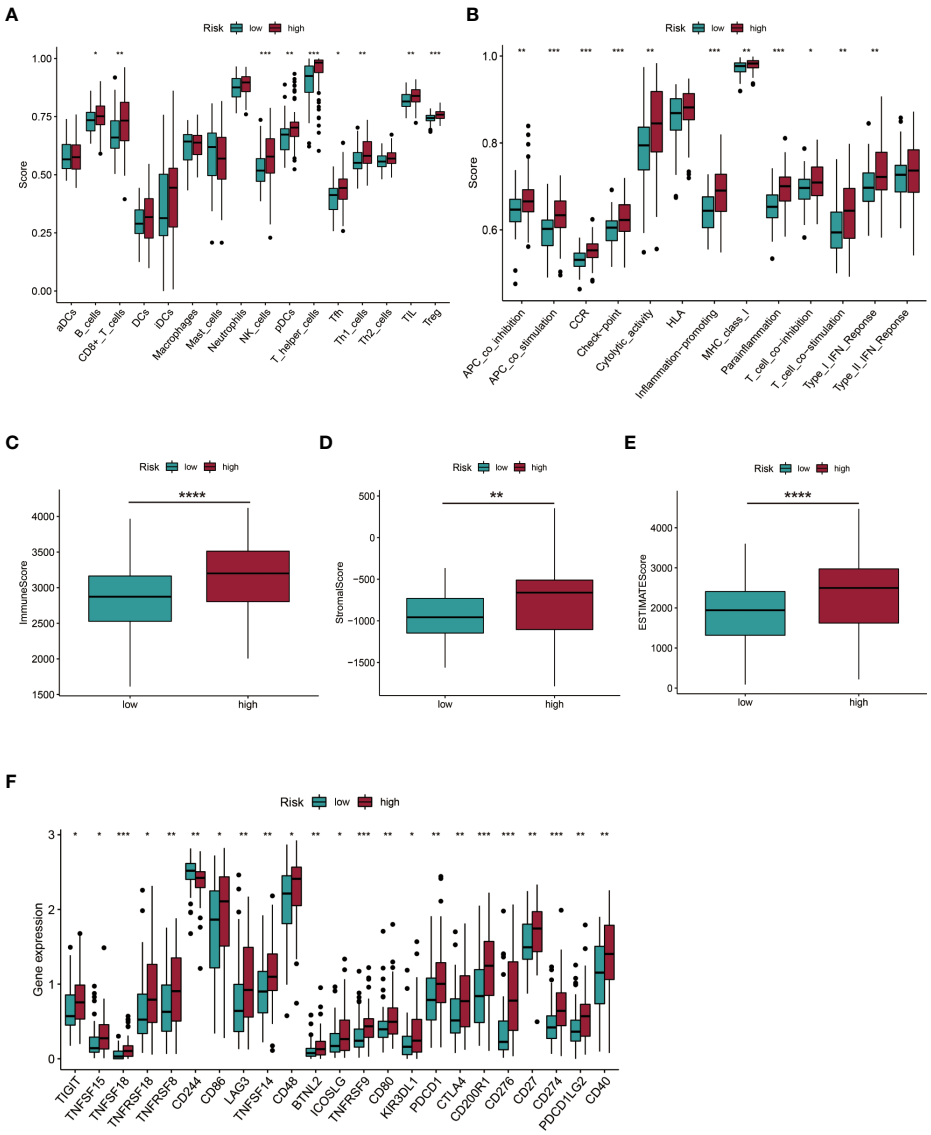

FIGURE 10
Investigation of immune cell infiltration and the tumor environment (TME). **(A, B)** Immune cell infiltration and immune-related function activation in the low- and high-risk group of AML patients. **(C-E)** Comparison of immune-related scores between low- and high-risk groups. **(F)** Twenty-three differentially expressed checkpoints between low- and high-risk groups. *$P < 0.05$; **$P < 0.01$; ***$P < 0.005$; ****$P < 0.001$.

This study has some limitations. First, we used the AML samples from the TCGA database and only conducted internal validation, since there was a lack of a suitable externally validated cohort to evaluate the effectiveness and reliability of the cuproptosis-related lncRNA signature. Moreover, we investigated the expressions of lncRNAs in the signature with a small sample size, and did not perform experiments to investigate the functions of the cuproptosis-related lncRNAs. Therefore, the established risk model established should be further tested by other researchers. Despite these limitations, this is the first study to construct a cuproptosis-related lncRNA signature for AML patients, and the risk model provides rational therapeutic strategies.

Conclusion

We constructed a prognostic cuproptosis-related lncRNA signature for AML patients. The model provides an independent prognostic value, and novel insights into the potential therapeutic strategies, including immunotherapy for AML patients.

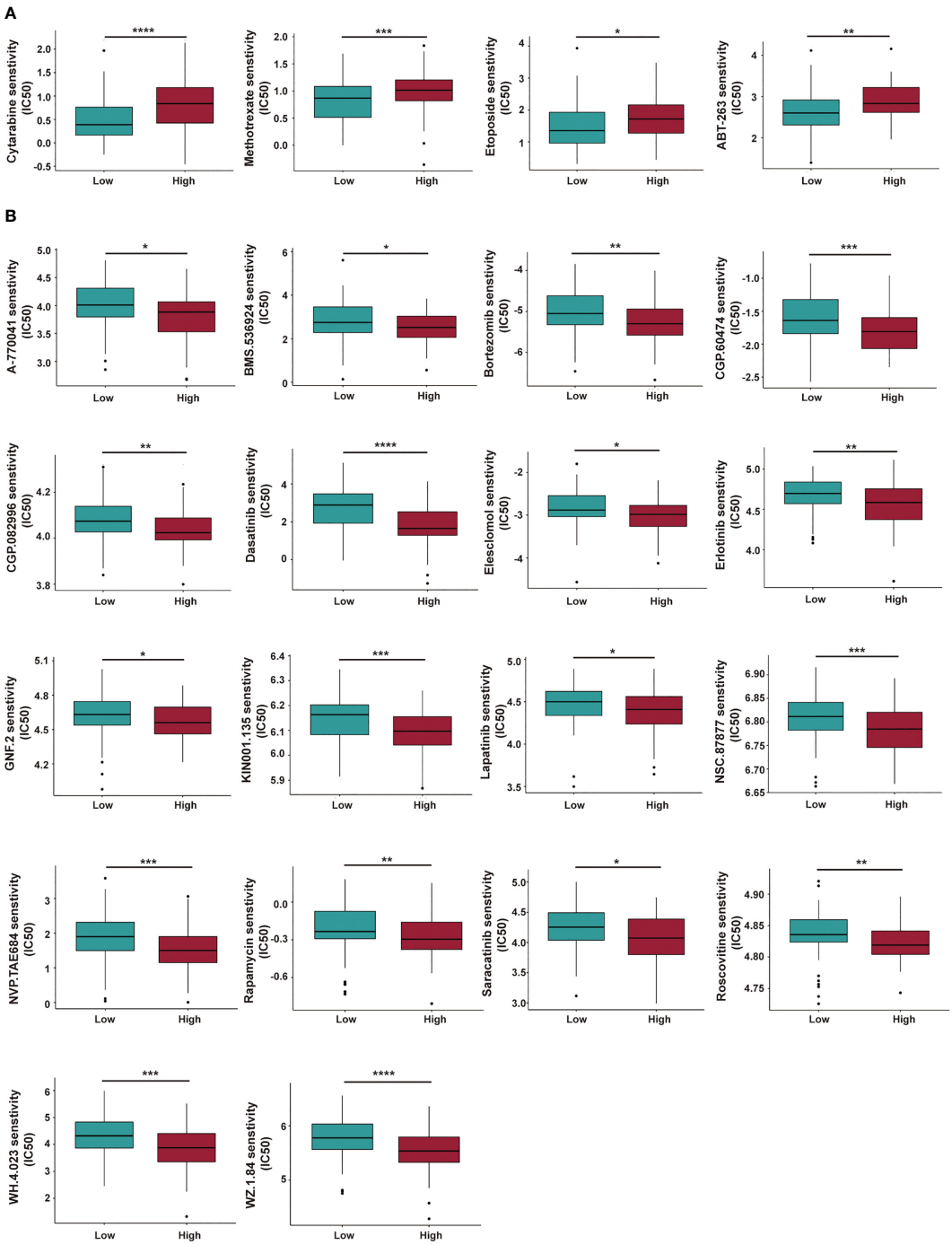

FIGURE 11
Investigation of chemotherapeutic and targeted therapy for AML patients with low- and high-risk groups. **(A, B)** The high-risk AML patients have a higher IC50 **(A)** and lower IC50 **(B)** for multiple potential drugs based on the GDSC database. IC50: Half-maximal Inhibitory Concentration. GDSC, Genomics of Drug Sensitivity in Cancer. *$P < 0.05$; **$P < 0.01$; ***$P < 0.005$; ****$P < 0.001$.

Data availability statement

The datasets presented in this study can be found in online repositories. The names of the repository/repositories and accession number(s) can be found in the article/Supplementary Material.

Ethics statement

The studies involving human participants were reviewed and approved by ethical committee of the West China Hospital of Sichuan University. The patients/participants provided their written informed consent to participate in this study. Written informed consent was obtained from the individual(s) for the publication of any potentially identifiable images or data included in this article.

Author contributions

FJW conceived and designed this study, reviewed, and revised the manuscript. PL and JJL conducted the data analysis and wrote the original draft. FWen, YXC, ZYL, and JZ contributed in methodology and data collection. FWu, ZQL, and WLL performed qPCR and data analysis. All authors contributed to the article and approved the submitted version.

Funding

This study was supported by the Natural Science Foundation of Hunan Province (2021JJ40501, 2020JJ8095) and the Health Commission Foundation of Hunan Province (202203044326, 202214014454).

Acknowledgments

We are thankful to Li Wang, Ph.D. (from the Department of, Zhongshan University, Guangzhou, China) for providing guidance of data processing. We also thank Bullet Edits Limited for the linguistic editing and proofreading of the manuscript.

Conflict of interest

The authors declare that the research was conducted in the absence of any commercial or financial relationships that could be construed as a potential conflict of interest.

Publisher's note

All claims expressed in this article are solely those of the authors and do not necessarily represent those of their affiliated organizations, or those of the publisher, the editors and the reviewers. Any product that may be evaluated in this article, or claim that may be made by its manufacturer, is not guaranteed or endorsed by the publisher.

Supplementary material

The Supplementary Material for this article can be found online at: https://www.frontiersin.org/articles/10.3389/fonc.2022.966920/full#supplementary-material

References

1. Wang F, Wu P, Gong S, Chen Y, Gao J, Wang S, et al. Aberrant Trpm4 expression in mll-rearranged acute myeloid leukemia and its blockade induces cell cycle arrest *via* Akt/Gli1/Cyclin D1 pathway. *Cell Signal* (2020) 72:109643. doi: 10.1016/j.cellsig.2020.109643

2. Newell LF, Cook RJ. Advances in acute myeloid leukemia. *BMJ* (2021) 375: n2026. doi: 10.1136/bmj.n2026

3. Vago L, Gojo I. Immune escape and immunotherapy of acute myeloid leukemia. *J Clin Invest* (2020) 130(4):1552–64. doi: 10.1172/JCI129204

4. Liu H. Emerging agents and regimens for aml. *J Hematol Oncol* (2021) 14 (1):49. doi: 10.1186/s13045-021-01062-w

5. Tsvetkov P, Coy S, Petrova B, Dreishpoon M, Verma A, Abdusamad M, et al. Copper induces cell death by targeting lipoylated tca cycle proteins. *Science* (2022) 375(6586):1254–61. doi: 10.1126/science.abf0529

6. Tang D, Chen X, Kroemer G. Cuproptosis: A copper-triggered modality of mitochondrial cell death. *Cell Res* (2022) 32:417–8. doi: 10.1038/s41422-022-00653-7

7. Oliveri V. Selective targeting of cancer cells by copper ionophores: An overview. *Front Mol Biosci* (2022) 9:841814. doi: 10.3389/fmolb.2022.841814

8. Yu P, Zhang X, Liu N, Tang L, Peng C, Chen X. Pyroptosis: Mechanisms and diseases. *Signal Transduct Target Ther* (2021) 6(1):128. doi: 10.1038/s41392-021-00507-5

9. Xu B, Wang S, Li R, Chen K, He L, Deng M, et al. Disulfiram/Copper selectively eradicates aml leukemia stem cells in vitro and in vivo by simultaneous induction of ros-jnk and inhibition of nf-kappab and Nrf2. *Cell Death Dis* (2017) 8 (5):e2797. doi: 10.1038/cddis.2017.176

10. Zeng H, Wu H, Yan M, Tang L, Guo X, Zhao X. Characterization of a 4 lncrnas-based prognostic risk scoring system in adults with acute myeloid leukemia. *Leuk Res* (2020) 88:106261. doi: 10.1016/j.leukres.2019.106261

11. Zheng Z, Wu W, Lin Z, Liu S, Chen Q, Jiang X, et al. Identification of seven novel ferroptosis-related long non-coding rna signatures as a diagnostic biomarker for acute myeloid leukemia. *BMC Med Genomics* (2021) 14(1):236. doi: 10.1186/s12920-021-01085-9

12. Li D, Liang J, Cheng C, Guo W, Li S, Song W, et al. Identification of M6a-related lncrnas associated with prognoses and immune responses in acute myeloid leukemia. *Front Cell Dev Biol* (2021) 9:770451. doi: 10.3389/fcell.2021.770451

13. Zhao Z, Liu H, Zhou X, Fang D, Ou X, Ye J, et al. Necroptosis-related lncrnas: Predicting prognosis and the distinction between the cold and hot tumors in gastric cancer. *J Oncol* (2021) 2021:6718443. doi: 10.1155/2021/6718443

14. Xiao R, Yang M, Tan Y, Ding R, Li D. Identification of five immune-related lncrnas predicting survival and tumor microenvironment characteristics in breast cancer. *Comput Math Methods Med* (2021) 2021:6676692. doi: 10.1155/2021/6676692

15. Liu S, Luo D, Luo J, Liang H, Zhi Y, Wang D, et al. Construction of a pyroptosis-related signature for prognostic prediction and characterization of immune microenvironment in acute myelogenous leukemia. *Int J Gen Med* (2022) 15:2913–27. doi: 10.2147/IJGM.S352062

16. Gao J, Wang F, Wu P, Chen Y, Jia Y. Aberrant lncrna expression in leukemia. *J Cancer* (2020) 11(14):4284–96. doi: 10.7150/jca.42093

17. Cancer Genome Atlas Research N, Weinstein JN, Collisson EA, Mills GB, Shaw KR, Ozenberger BA, et al. The cancer genome atlas pan-cancer analysis project. *Nat Genet* (2013) 45(10):1113–20. doi: 10.1038/ng.2764

18. Frankish A, Diekhans M, Ferreira AM, Johnson R, Jungreis I, Loveland J, et al. Gencode reference annotation for the human and mouse genomes. *Nucleic Acids Res* (2019) 47(D1):D766–D73. doi: 10.1093/nar/gky955

19. Dong J, Wang X, Xu C, Gao M, Wang S, Zhang J, et al. Inhibiting Nlrp3 inflammasome activation prevents copper-induced neuropathology in a murine model of wilson's disease. *Cell Death Dis* (2021) 12(1):87. doi: 10.1038/s41419-021-03397-1

20. Lin SY, Hu FF, Miao YR, Hu H, Lei Q, Zhang Q, et al. Identification of Stab1 in multiple datasets as a prognostic factor for cytogenetically normal aml: Mechanism and drug indications. *Mol Ther Nucleic Acids* (2019) 18:476–84. doi: 10.1016/j.omtn.2019.09.014

21. Dao FT, Wang J, Yang L, Qin YZ. Development of a poor-Prognostic-Mutations derived immune prognostic model for acute myeloid leukemia. *Sci Rep* (2021) 11(1):4856. doi: 10.1038/s41598-021-84190-0

22. Yan Z, He M, He L, Wei L, Zhang Y. Identification and validation of a novel six-gene expression signature for predicting hepatocellular carcinoma prognosis. *Front Immunol* (2021) 12:723271. doi: 10.3389/fimmu.2021.723271

23. Rooney MS, Shukla SA, Wu CJ, Getz G, Hacohen N. Molecular and genetic properties of tumors associated with local immune cytolytic activity. *Cell* (2015) 160(1-2):48–61. doi: 10.1016/j.cell.2014.12.033

24. Geeleher P, Cox NJ, Huang RS. Clinical drug response can be predicted using baseline gene expression levels and in vitro drug sensitivity in cell lines. *Genome Biol* (2014) 15(3):R47. doi: 10.1186/gb-2014-15-3-r47

25. Yang W, Soares J, Greninger P, Edelman EJ, Lightfoot H, Forbes S, et al. Genomics of drug sensitivity in cancer (Gdsc): A resource for therapeutic biomarker discovery in cancer cells. *Nucleic Acids Res* (2013) 41(Database issue): D955–61. doi: 10.1093/nar/gks1111

26. Zhang P, Tan X, Zhang D, Gong Q, Zhang X. Development and validation of a set of novel and robust 4-Lncrna-Based nomogram predicting prostate cancer survival by bioinformatics analysis. *PLos One* (2021) 16(5):e0249951. doi: 10.1371/journal.pone.0249951

27. Mi YY, Sun CY, Zhang LF, Wang J, Shao HB, Qin F, et al. Long non-coding rnas Linc01679 as a competitive endogenous rnas inhibits the development and progression of prostate cancer *Via* regulating the mir-3150a-3p/Slc17a9 axis. *Front Cell Dev Biol* (2021) 9:737812. doi: 10.3389/fcell.2021.737812

28. Sun Z, Jing C, Xiao C, Li T. Long non-coding rna profile study identifies an immune-related lncrna prognostic signature for kidney renal clear cell carcinoma. *Front Oncol* (2020) 10:1430. doi: 10.3389/fonc.2020.01430

29. Jiang F, Mao Y, Lu B, Zhou G, Wang J. A hypoxia risk signature for the tumor immune microenvironment evaluation and prognosis prediction in acute myeloid leukemia. *Sci Rep* (2021) 11(1):14657. doi: 10.1038/s41598-021-94128-1

30. Jiang F, Wang XY, Wang MY, Mao Y, Miao XL, Wu CY, et al. An immune checkpoint-related gene signature for predicting survival of pediatric acute myeloid leukemia. *J Oncol* (2021) 2021:5550116. doi: 10.1155/2021/5550116

31. Zhu R, Tao H, Lin W, Tang L, Hu Y. Identification of an immune-related gene signature based on immunogenomic landscape analysis to predict the prognosis of adult acute myeloid leukemia patients. *Front Oncol* (2020) 10:574939. doi: 10.3389/fonc.2020.574939

32. Wang S, Yang L, Liu Y, Xu Y, Zhang D, Jiang Z, et al. A novel immune-related competing endogenous rna network predicts prognosis of acute myeloid leukemia. *Front Oncol* (2020) 10:1579. doi: 10.3389/fonc.2020.01579

33. Yan H, Qu J, Cao W, Liu Y, Zheng G, Zhang E, et al. Identification of prognostic genes in the acute myeloid leukemia immune microenvironment based on tcga data analysis. *Cancer Immunol Immunother* (2019) 68(12):1971–8. doi: 10.1007/s00262-019-02408-7

34. Tabata R, Chi S, Yuda J, Minami Y. Emerging immunotherapy for acute myeloid leukemia. *Int J Mol Sci* (2021) 22(4):1944. doi: 10.3390/ijms22041944

35. Daver N, Garcia-Manero G, Basu S, Boddu PC, Alfayez M, Cortes JE, et al. Efficacy, safety, and biomarkers of response to azacitidine and nivolumab in Relapsed/Refractory acute myeloid leukemia: A nonrandomized, open-label, phase ii study. *Cancer Discov* (2019) 9(3):370–83. doi: 10.1158/2159-8290.CD-18-0774

36. Dai YJ, He SY, Hu F, Li XP, Zhang JM, Chen SL, et al. Bone marrow infiltrated natural killer cells predicted the anti-leukemia activity of Mcl1 or Bcl2 inhibitors in acute myeloid leukemia. *Mol Cancer* (2021) 20(1):8. doi: 10.1186/s12943-020-01302-6

37. Faget J, Bendriss-Vermare N, Gobert M, Durand I, Olive D, Biota C, et al. Icos-ligand expression on plasmacytoid dendritic cells supports breast cancer progression by promoting the accumulation of immunosuppressive Cd4+ T cells. *Cancer Res* (2012) 72(23):6130–41. doi: 10.1158/0008-5472.CAN-12-2409

38. Zhu L, Wang P, Zhang W, Li Q, Xiong J, Li J, et al. Plasmacytoid dendritic cell infiltration in acute myeloid leukemia. *Cancer Manag Res* (2020) 12:11411–9. doi: 10.2147/CMAR.S260825

39. Ustun C, Miller JS, Munn DH, Weisdorf DJ, Blazar BR. Regulatory T cells in acute myelogenous leukemia: Is it time for immunomodulation? *Blood* (2011) 118 (19):5084–95. doi: 10.1182/blood-2011-07-365817

40. Delia M, Carluccio P, Mestice A, Brunetti C, Albano F, Specchia G. Impact of bone marrow aspirate tregs on the response rate of younger newly diagnosed acute myeloid leukemia patients. *J Immunol Res* (2018) 2018:9325261. doi: 10.1155/2018/9325261

41. Chen C, Liang C, Wang S, Chio CL, Zhang Y, Zeng C, et al. Expression patterns of immune checkpoints in acute myeloid leukemia. *J Hematol Oncol* (2020) 13(1):28. doi: 10.1186/s13045-020-00853-x

frontiers | Frontiers in Oncology

TYPE Original Research
PUBLISHED 14 November 2022
DOI 10.3389/fonc.2022.1017947

OPEN ACCESS

EDITED BY
Spiros Vlahopoulos,
University of Athens, Greece

REVIEWED BY
Dirk Schneider,
Johannes Gutenberg University Mainz, Germany
Kirill Nadezhdin,
Columbia University, United States

*CORRESPONDENCE
Jörg P. Müller
Joerg.mueller@med.uni-jena.de

SPECIALTY SECTION
This article was submitted to Hematologic Malignancies, a section of the journal Frontiers in Oncology

RECEIVED 12 August 2022
ACCEPTED 25 October 2022
PUBLISHED 14 November 2022

CITATION
Schwarz M, Rizzo S, Paz WE, Kresinsky A, Thévenin D and Müller JP (2022) Disrupting PTPRJ transmembrane-mediated oligomerization counteracts oncogenic receptor tyrosine kinase FLT3 ITD.
Front. Oncol. 12:1017947.
doi: 10.3389/fonc.2022.1017947

Disrupting PTPRJ transmembrane-mediated oligomerization counteracts oncogenic receptor tyrosine kinase FLT3 ITD

Marie Schwarz[1], Sophie Rizzo[2], Walter Espinoza Paz[2], Anne Kresinsky[1,3], Damien Thévenin[2] and Jörg P. Müller[1*]

[1]Institute for Molecular Cell Biology, CMB - Center for Molecular Biomedicine, University Hospital Jena, Jena, Germany, [2]Department of Chemistry, Lehigh University, Bethlehem, PA, United States, [3]Leibniz Institute on Aging, Fritz Lipmann Institute, Jena, Germany

The receptor protein tyrosine phosphatase (RPTP) PTPRJ (also known as DEP-1) has been identified as a negative regulator of the receptor tyrosine kinase FLT3 signalling *in vitro*. The inactivation of the *PTPRJ* gene in mice expressing the constitutively active, oncogenic receptor tyrosine kinase FLT3 ITD aggravated known features of leukaemogenesis, revealing PTPRJ's antagonistic role. FLT3 ITD mutations resulting in constitutively kinase activity and cell transformation frequently occur in patients with acute myeloid leukaemia (AML). Thus, *in situ* activation of PTPRJ could be used to abrogate oncogenic FLT3 signalling. The activity of PTPRJ is suppressed by homodimerization, which is mediated by transmembrane domain (TMD) interactions. Specific Glycine-to-Leucine mutations in the TMD disrupt oligomerization and inhibit the Epidermal Growth Factor Receptor (EGFR) and EGFR-driven cancer cell phenotypes. To study the effects of PTPRJ TMD mutant proteins on FLT3 ITD activity in cell lines, endogenous PTPRJ was inactivated and replaced by stable expression of PTPRJ TMD mutants. Autophosphorylation of wild-type and ITD-mutated FLT3 was diminished in AML cell lines expressing the PTPRJ TMD mutants compared to wild-type-expressing cells. This was accompanied by reduced FLT3-mediated global protein tyrosine phosphorylation and downstream signalling. Further, PTPRJ TMD mutant proteins impaired the proliferation and *in vitro* transformation of leukemic cells. Although PTPRJ's TMD mutant proteins showed impaired self-association, the specific phosphatase activity of immunoprecipitated proteins remained unchanged. In conclusion, this study demonstrates that the destabilization of PTPRJ TMD–mediated self-

association increases the activity of PTPRJ *in situ* and impairs FLT3 activity and FLT3-driven cell phenotypes of AML cells. Thus, disrupting the oligomerization of PTPRJ *in situ* could prove a valuable therapeutic strategy to restrict oncogenic FLT3 activity in leukemic cells.

KEYWORDS

transmembrane domain oligomerization, receptor protein tyrosine phosphatase (RPTP), DEP-1, receptor tyrosine kinase (RTK), oncogenic FLT3 ITD, signal transduction, AML

Introduction

The receptor tyrosine kinase (RTK) FLT3 (fms-like tyrosine kinase 3) is predominantly expressed in early hematopoietic progenitor cells of both myeloid and lymphoid lineage (1–3). and is activated by its ligand FL. Wild-type (wt) FLT3 is present at the plasma membrane in the form of inactive monomers, whose auto-inhibited conformation is maintained by interactions between the juxtamembrane (JM) and kinase domains (4, 5). Binding of homo-dimeric FL induces receptor dimerization and trans-autophosphorylation on intracellular tyrosine residues (6, 7), The ligand-induced receptor phosphorylation results in the recruitment of adapter and scaffolding proteins that mediate the activation of phosphatidylinositol 3-kinase (PI3K)/protein kinase B (AKT) and rapidly accelerated fibrosarcoma (RAF)/mitogen-activated protein kinase (MAPK) signalling pathways (4, 8–10).

Activating mutations of FLT3 occur in approximately 25 – 30% of acute myeloid leukaemia (AML) patients. Internal tandem duplications (ITD) within the FLT3 JM domain constitute the most prevalent type of mutation and are associated with a poor patient prognosis. ITD mutations are characterized as in-frame duplications in the region encoding the receptor's JM domain (11–13). As a consequence, FLT3 ITD mutations presumably disrupt the auto-inhibitory activity of the JM domain (4, 5), leading to ligand-independent dimerization, auto-phosphorylation, and constitutive activation of the receptor (10, 11, 14). In contrast to the wt receptor and due to its constitutive kinase activity, ITD-mutated FLT3 is predominantly retained in the endoplasmic reticulum (ER) and Golgi compartments (15–17), from where it strongly promotes activation of signal transducer and activator of transcription 5 (STAT5) (15–17). Due to a residual pool of FLT3 ITD reaching the plasma membrane, constitutive activation of AKT and extracellular signal-regulated kinases 1/2 (ERK1/2) signalling can also be found (16, 18, 19).

FLT3 ITD promotes factor-independent growth and blocks the differentiation of myeloblastic cells *in vitro (*9, 10, 20*).* Moreover, it has been shown to induce leukemic cell transformation *in vitro* (10) and to drive the developmentof myeloproliferative disease in murine bone marrow transplantation models (14, 21). Furthermore, FLT3 ITD induces the production of high levels of reactive oxygen species (ROS) *via* STAT5-mediated activation and enhanced expression of NADPH oxidase (NOX) 4 (22, 23). This contributes to FLT3 ITD–driven cellular proliferation and transformation by several mechanisms, including the oxidative inactivation of the antagonistic PTP DEP-1 (22, 24, 25).

Protein tyrosine phosphatases (PTPs) are important modulators of reversible protein tyrosine phosphorylation, counterbalancing the action of protein tyrosine kinases (26, 27). PTPRJ, also known as DEP-1, CD148 or RPTPη, is an RPTP encoded by the *PTPRJ* gene. It is composed of a single PTP domain, a transmembrane segment, and an extracellular domain that contains eight fibronectin type III repeats, and the mature protein is highly N-glycosylated (28, 29).

PTPRJ is an essential negative regulator of growth factor signalling and, therefore, of cell proliferation and migration processes (30–33). For instance, PTPRJ restricts the activity of the platelet-derived growth factor β receptor (30, 31, 34), vascular endothelial growth factor receptor (32, 35) hepatocyte growth factor receptor MET (33, 36), epidermal growth factor receptor (EGFR) (37, 38), and FLT3 (39, 40). This highlights the role of PTPRJ as a candidate tumor-suppressor, especially in the context of RTK-driven cancers (41, 42). For example, PTPRJ has been shown to suppress the proliferation of glioblastoma cells by attenuating EGFR signalling and internalization (37). Furthermore, PTPRJ deficiency has been implied to promote meningioma cell motility and invasiveness (31, 43, 44) and to contribute to FLT3 ITD–driven leukemic cell transformation (24).

Besides indirect mechanisms such as modulation of expression levels or subcellular distribution, the specific activity of PTPs can be regulated by ligand binding, oxidation, or dimerization (27, 45). Binding of ligands to the extracellular domains of RPTPs has been shown to modulate specific PTP activity. PTPRJ can be activated by TSP1, but it is mechanistically not understood (46, 47). On the contrary, reactive oxygen species (ROS) can reversibly oxidize the catalytic cysteine of PTPs, leading to the formation of sulfenic acid derivates, sulfenylamides, or disulfides and thereby inactivating the PTP (48–50).

Upon stimulation, some RTKs induce the production of ROS and thus transiently inhibit antagonistic PTPs from allowing for efficient signal propagation (45). In particular, pathological ROS production by oncogenic RTKs can remove regulatory constraints from counteracting PTPs through this mechanism (22, 49, 51) as seen for the ROS-mediated inactivation of PTPRJ in FLT3 ITD–positive leukemic cells (22, 24).

For some RPTPs, including RPTPα, SAP1, and PTPRJ, TMD-mediated interactions have been demonstrated to contribute to dimerization (52–54). Homodimerization of the RPTP at the plasma membrane is typically associated with inactivation of the PTP (52, 53, 55) due to blocked access to the catalytic site (45, 56, 57). In mutational studies of PTPRJ TMD, the residues G979, G983, and G987 have been identified as major mediators of self-association (38, 54) through a specific contact interface consistent with a double GxxxG zipper motif. In accordance with a dimerization-mediated suppression of PTP activity, disruption of those PTPRJ TMD interactions by introducing G-to-L mutations was shown to enhance PTPRJ association with and dephosphorylation of EGFR (38). This is supported by structural analyses on the PTPRJ rat homolog that suggest that a wedge-like segment would block substrate access to the catalytic site in dimers, similar to RPTPα D1 (58).

Given the tumor-suppressing function of PTPs such as PTPRJ, strategies to enhance PTP activity have been developed by exploiting their regulatory mechanisms, such as ligand binding or oligomerization (26, 59). Given the enhanced activity of PTPRJ following stimulation with its ligand TSP1 (60, 61), PTPRJ–activating therapies may be developed by targeting the PTPRJ ectodomain, for example, with monoclonal antibodies (33) or peptide agonists (62, 63). Based on the structure-function relationship of PTPRJ TMD–mediated oligomerization described above, Bloch et al. designed agonistic peptides that bind to PTPRJ TMD and disrupt it its interactions (38). *In vitro* treatment of EGFR-driven cancer cells with those peptide agonists was shown to decrease PTPRJ self-association, enhance its activity on EGFR, and ultimately inhibit EGFR-driven cancer cell migration (38).

Several PTPs are known to be involved in the regulation of FLT3 signalling. SHP2 has been shown to positively regulate ERK1/2 and STAT5 activation downstream of FLT3 (7, 64, 65). In contrast, other phosphatases, including SHP1, PTP1B, and CD45, have been found to restrict FLT3 activity (66, 67). PTPRJ was first characterized as an antagonist of FLT3 in an shRNA-based screen to identify PTPs regulating FLT3 activity. Depletion of PTPRJ in THP-1 and 32D cells expressing wt FLT3 was demonstrated to enhance FL-induced FLT3 autophosphorylation and ERK1/2 signalling, ultimately stimulating proliferation and clonal growth (39). FLT3 was also established as a *bona fide* substrate of PTPRJ based on *in vitro* dephosphorylation of immunoprecipitated FLT3 by recombinant PTPRJ and direct interaction evidenced by co-immunoprecipitation and *in situ* proximity ligation assay (PLA). These studies also indicated that PTPRJ could play a role in suppressing both basal and ligand-induced activity of FLT3 (39, 40).

Here we show that despite disruption of PTPRJ oligomerization of PTPRJ Gly-to-Leu TMD mutations at positions G979, G983, and G987 specific phosphatase activity of immunoprecipitated PTPRJ proteins was not altered. Stable expression of PTPRJ TMD mutants in leukemic cells inactivated for their endogenous PTPRJ expression resulted in diminished phosphorylation of wt and ITD-mutated FLT3 compared to cells expressing wt PTPRJ. This was accompanied by reduced FLT3-mediated global protein tyrosine phosphorylation and FLT3-mediated downstream signalling. Lastly, PTPRJ TMD mutant proteins impaired the proliferation and *in vitro* transformation of leukemic cells.

Material and methods

Cell lines, cytokines, and antibodies

The human leukemic cell lines THP-1 (expressing wt FLT3) and MV4-11 (expressing FLT3 ITD) were cultured in RPMI-1640 supplemented with stabilized glutamine, 10% heat-inactivated FCS. The IL-3-dependent murine myeloid cell line 32D clone 3 (32D) (German Collection of Microorganisms and Cell Cultures (DSMZ), Braunschweig, Germany) was maintained in RPMI 1640 medium supplemented with sodium pyruvate (5 mg/ml), 10% heat-inactivated fetal calf serum (FCS), L-glutamine (2 mM), and IL-3 (1 ng/ml). 32D cells stably expressing FLT3 ITD were kindly provided by Drs. R. Grundler and J. Duyster (Technical University Munich, Germany) (14). All cell lines were inactivated for endogenous PTPRJ production using CRISPR/Cas9-mediated gene inactivation. Biallelic gene disruption, further described as PTPRJ KO, was confirmed by sequencing and immunologically. The human embryonal kidney cell line HEK293T (obtained from the DSMZ, Braunschweig, Germany) was cultured in DMEM/F12 supplemented with stabilized glutamine, 10% fetal calf serum (FCS) (Invitrogen, Darmstadt, Germany). Cells were cultured in a humidified incubator at 37°C with 5% CO_2.

Recombinant human FL and murine IL-3 were purchased from PeproTech Ltd., London, UK.

Anti-P-AKT (Ser-473) (catalogue no. 9271), anti-P-p44/42 MAPK (Thr-202/Tyr-204) (catalogue no. 9106), anti-ERK1/2 (catalogue no. 9107) anti- STAT5 (catalogue no. 9310) and anti-P-FLT3 Y591 (3461)) were from Cell Signalling Technology (Frankfurt, Germany). Anti-AKT (sc-8312) and anti-STAT5 (sc-835) were purchased from Santa Cruz, and anti-P-STAT5 (ab32364) was from Abcam. Polyclonal anti-FLT3 antibody (from goat, AF768) recognizing the extracellular domain of the murine protein, anti-DEP-1 antibody (from goat, AF1934) recognizing murine DEP-1 and cross-reacting with human DEP-1 were obtained from R&D Systems (Wiesbaden,

Germany). ß-actin antibody (A5441) was from Sigma-Aldrich. Antibodies recognizing phosphotyrosine (05-321) were purchased from Upstate Biotechnology, Inc. (Milton Keynes, UK). Human FLT3 was detected with polyclonal rabbit antibodies, kindly provided by Lars Rönnstrand (Lund, Sweden). Immune detection of HA-tagged DEP-1 was done with antibody 3724 from Cell Signaling Technology (Leiden, The Netherlands). Antibodies recognizing ß-actin or vinculin were obtained from Sigma. HRP-coupled secondary anti-mouse IgG and anti-rabbit IgG antibodies were from KPL (Gaithersburg, MD). HRP-coupled secondary anti-goat IgG (sc2056) was from Santa Cruz Biotechnology. HA-tagged DEP-1 proteins were immunoprecipitated using an α-HA-tag antibody (kindly provided by Sebastian Drube, Institute of Immunology, University Hospital Jena).

DNA expression vectors

Retroviral pBABE vectors expressing human PTPRJ wt or G-L TMD mutants were published earlier (38). For efficient immunoprecipitation 3'-end of the gene was replaced by a human hemagglutinin (HA) tag derived from pcDNA3.1-PTPRJ-HA (our laboratory collection). Obtained plasmids were sequence validated.

Production of pseudoviral particles, cell transduction, and cell establishment

For the generation of retroviral particles, HEK293T cells were transfected with pBABE plasmids encoding PTPRJ and pVSVg and pGag/Pol packaging vectors using polyethylenimine (PEI). Retroviral particles were collected 24, 48, and 72 h post-transfection. Cell-free culture supernatants were concentrated using Amicon Ultra-15 Centrifugal Filter Units (Millipore, # UFC903024). THP-1, MV4-11, or 32D FLT3 ITD PTPRJ KO cells were infected three times with the pseudotyped particles in the presence of 8 mg/ml polybrene (1,5-dimethyl-1,5-diazaundecamethylene polymethobromide, AL-118, #10,768-9, Sigma-Aldrich). Cell lines were cultivated for at least 3 weeks post-transduction.

To enrich cells re-expressing PTPRJ, transduced cells were stained with APC-coupled anti-PTPRJ (CD148) antibody and subsequently purified by flow cytometric cell sorting according to their PTPRJ surface levels. APC signal was measured at 633/660 nm ex/em using a BD FACS Canto and FACS Diva v7.0 software (BD). Data were analyzed in FlowJo v10.8.0 (BD). Similar PTPRJ levels were monitored using immunoblotting. Not all cell populations could be sorted to an equivalent PTPRJ level. Thus, only data from cells with comparable PTPRJ levels were used here.

Analysis of signal transduction

For analysis of cell signalling, cells were starved for 4 hours. FLT3 ITD–expressing cell lines 32D FLT3 ITD, and MV4-11 were treated with 0.5 µM of the NAD(P)H oxidase inhibitor diphenyleneiodonium (DPI) or mock (DMSO) for the starvation period. As a control, cells were incubated with the FLT3 inhibitor AC220 (20 nM). FLT3 wt expressing THP-1 cells were starved for 4 hours in RPMI medium without FCS, stimulated with FL (200 ng/ml), and harvested sharply 5 min post-stimulation. Stimulation was stopped by transferring the cells to 1.5 ml tubes on ice and subsequently washed once with cold PBS.

Cell pellets were re-suspended in the RIPA lysis buffer (containing 1% Nonidet P-40, 0.25% deoxycholate, 50 mM Tris, pH 7.4, 0.15 M NaCl, 1 mM EDTA freshly supplemented with protease and phosphatase inhibitors) was used. Cells were lysed by vigorous up-and-down pipetting and incubation for 15 min on ice. Then, lysates were cleared by centrifugation (20 min, 13,300 rpm, 4°C). The protein concentration of cleared lysates was measured using a bicinchoninic acid assay (Pierce BCA Protein Assay Kit, Thermo Fisher Scientific) following the manufacturer's protocol. Samples were prepared in an appropriate sample buffer.

For reliable detection of FLT3 signals, lysates were purified by wheat germ agglutinin (WGA) precipitation. Therefore, 100 – 180 µg of lysate were diluted with immunoprecipitation buffer supplemented with protease and phosphatase inhibitors to a total volume of 700 µl. After adding 30 µl of equilibrated WGA agarose beads (50% slurry, Vector Laboratories, #AL-1023-2), samples were incubated for 3 to 4 hours at 4°C by overhead rotation. Beads were pelleted (3000 rpm, 2 – 3 min, 4°C), and the supernatant was discarded. Beads were washed twice in immunoprecipitation buffer, and precipitated proteins were eluted in 15 µl sample buffer at 95°C for 5 min. To detect other signalling proteins, 15 – 20 µg of lysate were prepared in sample buffer and incubated at 95°C for 5 min. SDS-PAGE and semi-dry blotting were performed as described above.

SDS-PAGE and immunoblotting

Comparable amounts of proteins were loaded on polyacrylamide (PAA) gels at indicated concentrations. Using standard SDS-PAGE, proteins were separated according to their molecular weight and subsequently blotted to nitrocellulose membrane (Amersham Protran Premium 0.2 µM NC, # 10600001) by tank blotting or semi-dry blotting depending on the size of the proteins of interest. After blotting, membranes were washed, incubated with blocking buffer, and incubated in primary antibody solutions overnight at 4°C. Subsequently, blots were washed, incubated with appropriate

horseradish peroxidase–coupled secondary antibodies, and incubated with ECL substrate. The chemiluminescent signal was detected using a LAS-4000 imager (Fujifilm) and quantified using Multi Gauge V3.0 software (Fujifilm). Membranes were first probed with phospho-site specific antibodies and re-probed using the respective α-pan-protein antibody. To re-probe blots, membranes were incubated with Restore PLUS Western Blot Stripping Buffer (Thermo Fisher Scientific, 46430), washed, and re-probed with primary antibody incubation overnight at 4°C.

PTPRJ phosphatase activity assay

HEK293T cells were seeded in 100 mm dishes and transfected with pBABE-PTPRJ-HA, or empty control plasmids. Cells were harvested using 0.05% Trypsin-EDTA 48 hours post-transfection, washed with cold PBS and lysed with 600 µl PTP lysis buffer (50 mM HEPES pH 7.5; 150 mM NaCl; 5 mM EDTA pH 8.0; 0.5% (v/v) NP40; 1 mM DTT; 5 mM NaF) supplemented with protease inhibitors. Immunoprecipitation of PTPRJ-HA proteins was carried out from 600 to 1000 µg protein lysate with HA antibody (4 – 8 µg) for 2 hours at 4°C by overhead rotating. Immune complexes were immobilized on Protein G-Sepharose beads (Immobilized Protein G, Thermo Fisher Scientific, #. 20399). Beads were washed with lysis buffer (centrifugation 2 – 3 min, 3000 rpm) and incubated with immune complexes for 2 hours at 4°C by overhead rotation. Beads were pelleted (2 – 3 min, 3000 rpm, 4°C), and the supernatant was discarded.

For enzymatic assays, beads were washed once with lysis buffer and twice with PTP reaction buffer (50 mM Sodium Acetate pH 9.0 with freshly added 0.5 mg/ml BSA, 0.5 mM DTT and with or without 5 mM pNPP [Acros Organics; 12886.0100] or 25 µM DiFMUP [Invitrogen; D6567]). Next, samples were incubated in 100 µl complete PTP reaction buffer for 10 – 15 min at 37°C and 750 rpm. A blank (buffer only) was included, and 0.2 mM sodium vanadate was added to one sample to inhibit protein phosphatase activity as a control. After incubation, beads were pelleted, and 50 µl of supernatant were transferred to a 96-well plate (transparent plate for pNPP, and white chimney plate for DiFMUP). The reaction was stopped by adding 50 µl 0.4 N NaOH. Substrate reaction was measured by absorbance at 405 nm for pNPP and fluorescence at 360/465 nm excitation/emission for DiFMUP on a TECAN Infinite F200 plate reader.

To quantify the immunoprecipitated material, samples were subjected to SDS-PAGE and tank blotting. Thus, beads were washed once with PBS, and immune complexes eluted in sample buffer by incubation at 60°C for 10 min. Membranes were immunologically probed against PTPRJ or HA.

Assessing TMD-TMD interaction with the DN-AraTM transcriptional reporter assay

The DNA sequences coding for the TMD of FLT3 and PTPRJ were cloned into either pAraTMwt (coding for AraC) or pAraTMDN (coding for the inactive form of AraC, AraC*) plasmids, as previously described (38). Unless otherwise stated, standard molecular biology techniques were used, and all constructs were verified by DNA sequencing (Genewiz, Inc.). The protein sequences for both FLT3 and PTPRJ used in AraTM assays contains five extracellular residues, the putative TMD as predicted by MPEx (underlined below) (68), and 20 cytoplasmic juxtamembrane residues:

FLT3 - QDNISFYATIGVCLLFIVVLTLLICHKYKKQFRY ESQLQMVQVTG

PTPRJ - QDPGVICGAVFGCIFGALVIVTVGGFIFWRKK RKDAKNNEVSFSQIKP

The constructs and the reporter plasmid (pAraGFPCDF) were co-transformed into the AraC-deficient *E. coli* strain SB1676 and streaked onto selective plates. Colonies were picked from each construct and grown in LB media for 8 h at 30 °C. Each culture was diluted into selective autoinduction media and grown for an additional 16 h at 30 °C. A series of 2-fold dilutions of the cultures were prepared in a black 96-well, clear-bottom plate. Absorption at 580 (10) nm and GFP fluorescence emission spectra (excitation maximum 485 (20) nm and emission maximum at 530 (30) nm were collected using an Infinite® 200 PRO Plate Reader (Tecan). The results are reported as the ratio of fluorescence emission at 530 nm to absorbance at 580 nm and normalized to the negative control (empty plasmids and reporter plasmid). Immunoblotting was performed using HRP-conjugated anti-maltose binding protein (MBP) monoclonal antibody at 1:10000 dilution (New England Biolabs, #E8038) to verify expression levels of each construct.

Analysis of cell proliferation and viability

For MV4-11 cells, proliferation and viability were analyzed by trypan blue count and flow cytometry using cell counting beads. For viability assessment, 2x 10 µl per sample was taken, and the percentage of dead cells was measured by automated trypan blue count (Countess II FL, Invitrogen). For flow cytometric cell count, samples were mixed with 10 µl 123count eBeads (Invitrogen, catalog no. 01-1234-42) and measured on a BD FACS Canto.

The transformative capacity of cells was analyzed by colony-forming unit (CFU) assay. Cells were grown in a 1.27% methylcellulose-containing, semi-solid medium. Cells were

seeded in triplicates at a density of 500 cells/well (MV4-11, THP-1) or 400 cells/well (32D FLT3 ITD) in 24-well plates. The remaining wells were filled with PBS, and plates were placed in humidity chambers for cultivation. After 7 to 10 days, colonies were stained by adding 50 µl of iodonitrotetrazolium chloride solution (4 mg/ml) dropwise to the wells. After overnight incubation, plates were scanned on an HP Scanjet G4050 photo scanner, and the number of colonies was counted using ImageJ v1.53k software (National Institutes of Health).

Results

The TMD residues G979, G983, and G987 of PTPRJ have been previously identified as major mediators of PTPRJ self-association (38) (54). Glycine-to-leucine (G-to-L) mutations of those residues destabilize PTPRJ oligomerization and increase phosphatase activity towards EGFR by promoting substrate access (38). We hypothesized that TMD mutants of PTPRJ would have similar effects on FLT3 phosphorylation and signalling.

To assess if an altered activity of PTPRJ TMD mutants would interfere with cellular signal transduction processes, model cell systems expressing the FLT3 wt (THP-1), constitutive active oncogenic FTL3 ITD (MV4-11), or ectopic FLT3 ITD (32D) were used. Leukemic human THP-1 cells allow to study the effects of PTPRJ on the FLT3 wt receptor. Both, the human leukemic cell lines MV4-11 expressing biallelic FLT3 ITD as well as murine 32D, stably transduced with FLT3 ITD are factor independent cells lines. They rely on the constitutive kinase activity of mutant FLT3 ITD and are routinely used by us and others to study effects on modified FLT3 ITD kinase activity (22, 64, 66, 69–72). Since PTPRJ is a well-characterized antagonistic phosphatase for FLT3 proteins, these cell systems provide clear input about the *in situ* activity of mutant PTPRJ. To prevent interference from endogenous wt PTPRJ, we inactivated chromosomally encoded PTPRJ in these cells using CRISPR/Cas9. Biallelic gene inactivation was confirmed by DNA sequencing, and the absence of PTPRJ production was confirmed by immunoblotting (data not shown). Subsequently the cell lines were transduced with retroviral particles encoding PTPRJ wild type or G-to-L TMD mutant PTPRJ variants. In order to compare the effect of altered oligomerization on FLT3 activity and downstream signaling, cell lines were sorted for similar phosphatase expression by flow cytometric cell sorting using CD148-APC-mediated PTPRJ surface labeling. Unfortunately, stable cell populations with similar PTPRJ protein levels could not be obtained in all cell populations modified. Thus, only cell lines with similar PTPRJ protein levels were used in the study (Supplementary Figure 1).

PTPRJ TMD mutants decrease FLT3 phosphorylation

If PTPRJ TMD mutants show enhanced phosphatase activity *in situ*, diminished FLT3 phosphorylation and downstream signalling would be expected. In THP-1 cells, expression of PTPRJ G979L or G983L resulted in significantly reduced FL-mediated receptor phosphorylation at position Y591 in comparison to wt PTPRJ, indicating decreased FLT3 activity in those cells (Figure 1A) (39). Because FLT3 ITD induces high levels of cellular ROS with subsequent oxidative inactivation of PTPRJ (Godfrey 2012, Jayavelu 2016), cell lines expressing FLT3 ITD (MV4-11 and 32D) were treated with DPI during starvation to quench ROS production. While a weak reduction of Y591 phosphorylation could be observed in response to the expression of PTPRJ TMD mutants in MV4-11 cells (Figure 1B), the expression of G983L PTPRJ in 32D FLT3 ITD cells resulted in significantly reduced FLT3 phosphorylation (Figure 1C).

Mutations in the TMD of PTPRJ affect receptor oligomerization states but not PTP activity

To address the question, of whether altered PTP oligomerization is due to altered substrate accessibility or due to altered specific enzymatic activity, PTPRJ variants were immunoprecipitated and specific phosphatase activity was determined. In comparison to wt PTPRJ immunoprecipitated HA-tagged PTPRJ TMD mutants showed no significant changes in activity towards pNPP and DiFMUP (Figure 2). Thus, it can be concluded that the observed diminished FLT3 dephosphorylation is not due to an altered specific PTP activity of the PTPRJ TMD mutants but most likely to changes in PTPRJ.

We then sought to assess whether FLT3 and PTPRJ may interact through direct TM interaction and whether introducing the glycine-to-leucine mutations not only disrupts PTPRJ self-association but also promotes interaction between the TMDs of PTPRJ and FLT3. To do so, we used the dominant-negative AraC-based transcriptional reporter assay (DN-AraTM), an assay reporting on the propensity of TMD to self-associate and heterodimerize in cell membranes (38, 73–77). When the TMD of FLT3 was expressed as a fusion to AraC, a strong GFP signal was observed, indicating that the TMD has a high propensity to self-associate (Figure 3; lane 1). On the other hand, when FLT3-AraC* was co-expressed as a competitor to FLT3-AraC, a significant decrease in GFP signal was observed (Figure 3; lane 2), consistent with specific TMD-TMD interactions. The results show that while wt PTPRJ has a propensity to associate with FLT3 (Figure 3; lane 3), it does so

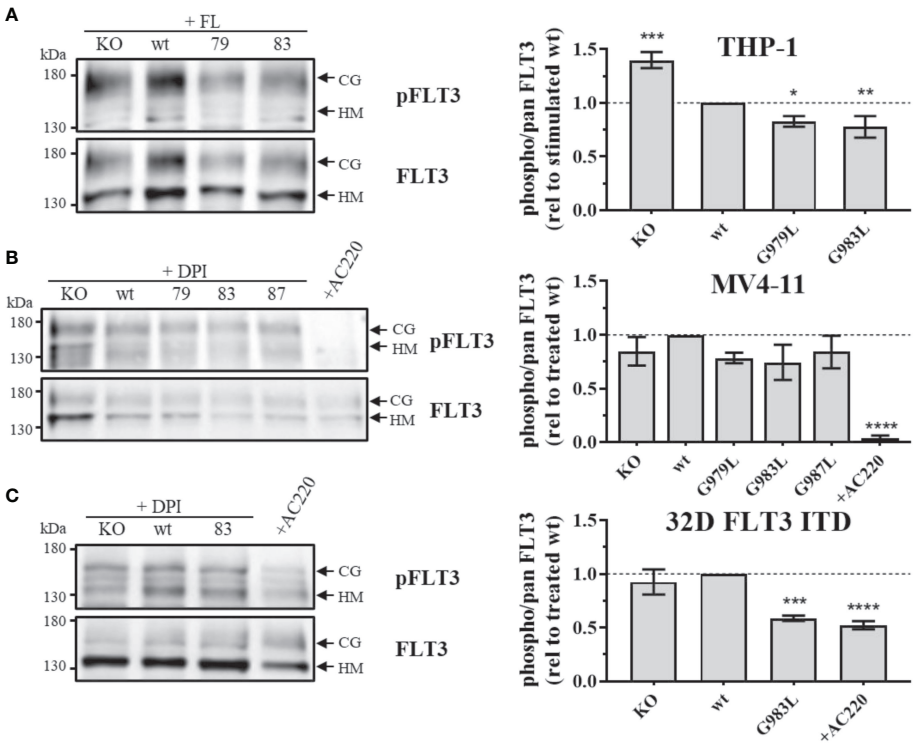

FIGURE 1
Phosphorylation of FLT3 in MV4-11, THP-1, and 32D FLT3 ITD PTPRJ KO AML cell lines stably re-expressing PTPRJ wt or TMD G979L, G983L, or G987L mutants. Cells were starved for 4 h in serum-free medium and lysed in RIPA buffer. During starvation, MV4-11 and 32D FLT3 ITD cells were treated with DPI (0.5 μM) or AC220 (20 nM), as indicated. THP-1 cells were stimulated with FL (200 ng/ml, 5 min) before harvest. FLT3 was enriched from 100 – 180 μg lysate by wheat germ agglutinin precipitation and subjected to SDS-PAGE and immunoblotting. Blots were first probed by phospho-site specific antibodies recognizing FLT3 pY591 and re-probed for total FLT3. **(A–C)** *Left:* Representative immunoblots (n = 3) are shown. Positions of immature, high mannose (HM, 130 kDa) and mature, complex glycosylated (CG, 160 kDa) forms of FLT3 are indicated by arrows. Positions of 130 and 180 kDa molecular weight standard bands are shown on the left side of the blots. 79 – G979L; 83 – G983L; 87 – G987L. *Right*: Quantification of specific FLT3 phosphorylation. Values were calculated as the ratio of phosphorylated to total receptor (sum of HM and CG signal) and normalized to DPI-treated or FL-stimulated wt. All values are given as mean ± standard deviation, n = 3. Statistics: one-way ANOVA, followed by Dunnett's multiple comparisons tests; *p ≤ 0.05; **p ≤ 0.01; ***p ≤ 0.001; ****p ≤ 0.0001 compared to wt.

to a lesser extent than FLT3 itself (Figure 3; lane 2 vs. lane 3). Importantly, the PTPRJ mutants show a significant decrease in GFP signal compared to wt PTPRJ, consistent with a more productive association with FLT3 (Figure 3; lane 3 vs. lanes 4-6).

Altogether, these results suggest that PTPRJ's self-association prevents its access to FLT3 and that disrupting it through TMD mutations promotes interaction with FLT3 and subsequent receptor dephosphorylation.

PTPRJ TMD mutants decrease FLT3 downstream signalling

To further investigate the effect of PTPRJ mutations on FLT3 activity, phosphorylation of signalling proteins downstream of FLT3 was analyzed. Whereas wt FLT3 signals mainly through PI3K/AKT and RAF/MAPK cascades upon ligand stimulation, constitutively active FLT3 ITD predominantly induces STAT5 signalling due to altered localization in the ER (8, 9, 16, 19).

In THP-1 cells, strong activation of AKT and ERK1/2 could be observed upon FL stimulation (Figure 4A), illustrating the main signalling pathways of wt FLT3. No phosphorylation of STAT5 at position Y694 was detected (data not shown). FL-induced phosphorylation of ERK1/2 MAPK kinases was significantly decreased in cells expressing PTPRJ G979L and G983L compared to wt PTPRJ. But no alteration in AKT S473 phosphorylation could be observed. In MV4-11 cells, endogenously expressed FLT3 ITD induces STAT5 activation, as indicated by prominent Y694 phosphorylation, and activation through ERK1/2 and AKT, albeit less pronounced (Figure 4B). FLT3 ITD mediated activation of these pathways was confirmed

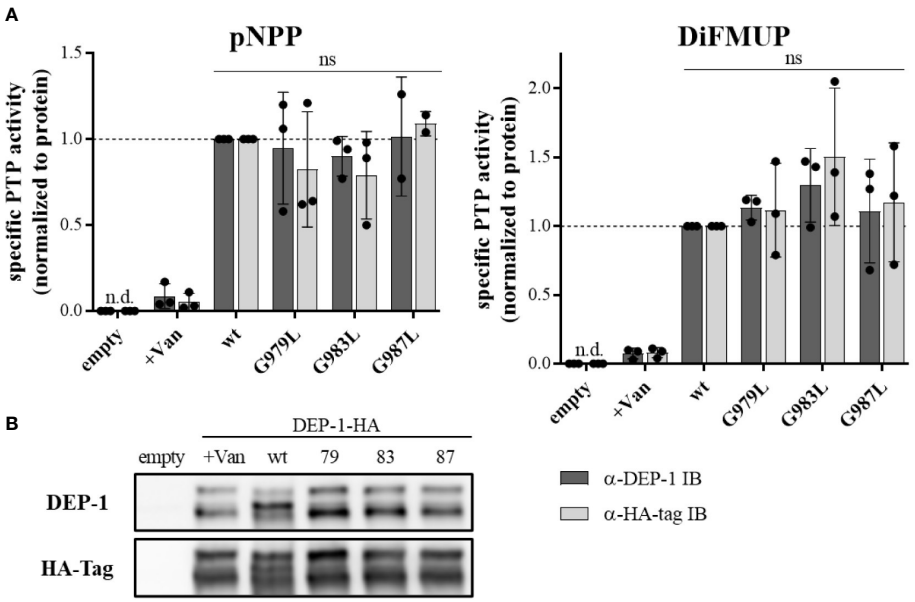

FIGURE 2
Specific PTP activity of wt and TMD mutant PTPRJ remains unchanged PTPRJ-HA proteins were immunoprecipitated from transiently transfected HEK293T cells with pBABE-PTPRJ-HA constructs (wt, G979L, G983L, and G987L) 48 hours post-transfection. Cell lysates were probed with phosphatase substrate mimetics pNPP or DiFMUP for 10 – 15 min at 37°C. Vanadate was added to controls (0.2 mM, +Van) to inhibit phosphatase activity. Substrate cleavage was measured by absorbance at 405 nm (pNPP) or fluorescence at 360/465 nm ex/em (DiFMUP). The amount of immunoprecipitated protein was analyzed by immunoblotting using antibodies recognizing PTPRJ and HA-tag. **(A)** Specific PTP activity of PTPRJ variants relative to respective wt is shown. Values were calculated as absorbance, or fluorescence measurements minus blank (buffer only) normalized to the amount of immunoprecipitated protein, based on quantification of PTPRJ or HA-tag immunoblots (IB). The individual values of three independent experiments (for pNPP G987L n = 2) are shown by closed circles, columns, and error bars represent mean ± standard deviation. Statistics: two-way ANOVA and Dunnett's multiple comparisons test; (ns, not significant; n.d., not detectable). **(B)** A representative immunoblot is shown (n = 3). 79 – G979L; 83 – G983L; 87 – G987L.

by the substantial reduction of STAT5, AKT, and ERK1/2 phosphorylation upon treatment with the FLT3 inhibitor AC220. Treatment with DPI to prevent the ROS-mediated inhibition of PTPRJ resulted in reduced STAT5 and ERK1/2 phosphorylation, confirming the restored PTPRJ phosphatase activity. Overexpression of FLT3 ITD in 32D cells resulted in strong constitutive activation of STAT5 as well as RAF/MAPK and, more weakly, PI3K/AKT signalling (Figure 4C). Abrogation of activation upon AC220 treatment demonstrated FLT3 ITD mediated induction. Similarly to MV4-11 cells, DPI treatment showed diminished STAT5 phosphorylation, indicating PTPRJ activation.

Despite the significant reduction in FLT3 Y591 phosphorylation upon expression of the PTPRJ TMD mutants (Figure 1), reduction of FLT3 ITD downstream signalling could only be observed in 32D FLT3 ITD cells expressing PTPRJ G983L, in which a decrease in ERK1/2 phosphorylation is observed in response to DPI treatment (Figure 4C). Taken together, diminished ERK1/2 phosphorylation in wt and FLT3 ITD cell lines expressing PTPRJ TMD mutants further indicates activation of PTPRJ upon abrogation of oligomerization.

PTPRJ TMD mutants decrease FLT3-driven cell proliferation and clonal growth

To study the phenotypic consequences of the enhanced activity of PTPRJ TMD mutants towards FLT3, proliferation, viability, and transformation capacity of MV4-11 cells were assessed. The overexpression of wtPTPRJ did not result in an impaired proliferation of MV4-11 cells compared to cell with inactivated endogenous PTPRJ. In contrast, proliferation was significantly decreased in the MV4-11 cell lines expressing PTPRJ TMD mutants (albeit to a different extent) when compared to wt PTPRJ (Figure 5A). The G983L mutation, which has been previously shown to be the most impactful in disrupting PTPRJ oligomerization and in inhibiting EGFR-driven phenotypes (38), exhibited the most substantial effect on the proliferative capacity of all mutants. On the other hand, the expression of the TMD mutants did not significantly impact cell viability. (Figure 5B).

Constitutive activity of FLT3 ITD drives cellular transformation *via* AKT, STAT5, and RAS pathways (10, 78). PTPRJ depletion and

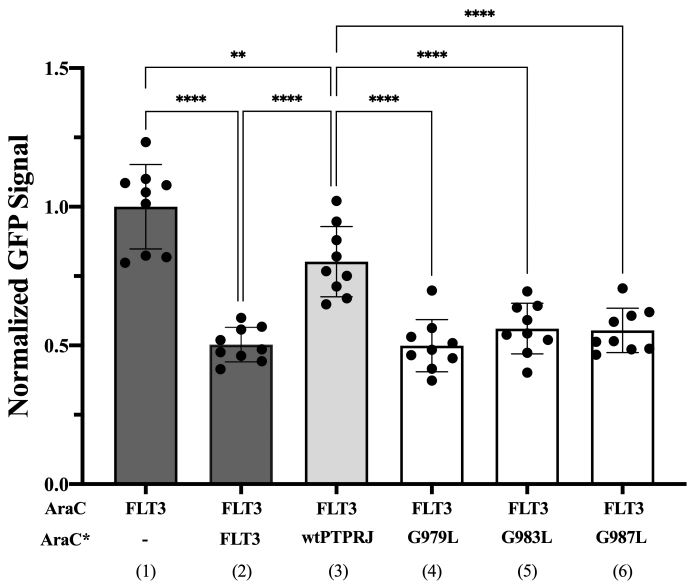

FIGURE 3
Quantifying FLT3 self-association and hetero-interaction with wt PTPRJ and 3 TMD point mutants using the DN-AraTM assay. GFP signal is normalized to the signal of FLT3 (1), and the results are shown as mean ± S.E. (n=9). Pair-wise statistical significance (1 vs. 3 and 2 vs. 3) was assessed using an unpaired t-test (at 95% confidence intervals). Results were normalized, taking into account the slight differences in expression level measured by immunoblotting (Supplementary Figure 2). Statistical significance was assessed using one-way ANOVA followed by Dunnett's multiple comparisons test at 95% confidence intervals. ****$p \leq 0.0001$; **$p \leq 0.01$.

ROS-induced inhibition have been previously shown to promote leukemic cell transformation due to elevated activity of FLT3 and downstream signalling (22, 24, 39). We hypothesized that disrupting PTPRJ oligomerization and thereby presumably enhancing its activity could impair FLT3-driven transformation of AML cells. Therefore, *in vitro, the* transformative capacity of cell lines stably expressing PTPRJ TMD mutants was analyzed compared to wt PTPRJ cells. Cells were grown in semisolid, cytokine-free methylcellulose medium, and colony formation was quantified after 7-10 days. MV4-11 cells exhibited a significantly reduced clonal growth in methylcellulose for all three PTPRJ TMD mutants compared to wt (Figure 6), indicating restriction of FLT3 ITD activity. The strongest impairment of transformation capacity was observed in PTPRJ G983L–expressing cells. 32D FLT3 ITD cell lines demonstrated IL3-independent, FLT3 ITD–driven clonal growth, as previously described (10, 72). Colony formation was only insignificantly reduced in PTPRJ G983L–expressing cells compared to wt.

PTPRJ TMD mutations induce alterations in global protein tyrosine phosphorylation

Next, we addressed how altered PTPRJ self-association influenced global protein tyrosine phosphorylation in cells expressing either wt FLT3 or FLT3 ITD. Possible changes could be attributed directly to enhanced PTPRJ phosphatase activity and inhibition of FLT3 kinase activity.

First, global protein phosphorylation was analyzed by immunoblotting using pY-site-specific antibodies. To abrogate FLT3-independent signalling events, cells were starved for 4 hours in serum- and cytokine-free medium. MV4-11 and 32D cells with constitutively active FLT3 ITD were then harvested directly, whereas wt FLT3 in THP-1 cells was first stimulated with FL (200 ng/ml, 5 min). Cells were then lysed, and lysates were analyzed by SDS-PAGE and immunoblotting. In THP-1 cells, global pY increased by more than 2-fold upon FL stimulation, illustrating phosphorylation events downstream of activated wt FLT3 (Supplementary Figure 3A). Upon ligand stimulation, protein tyrosine phosphorylation of cells stably expressing PTPRJ G983L was significantly reduced compared to PTPRJ wt cells.

To quench cellular ROS levels of FLT3 ITD–expressing cells, DPI was added during starvation before analysis of protein phosphorylation. Here, no consistent effect of DPI treatment on MV4-11 cells regarding global protein tyrosine phosphorylation was observed (Supplementary Figure 3B). In 32D FLT3 ITD cells expressing PTPRJ wt or G983L, pY was slightly decreased upon DPI treatment, suggesting restored PTPRJ phosphatase activity (Supplementary Figure 3C).

In DPI-treated and untreated MV4-11 cells, the global protein tyrosine phosphorylation was found to be slightly reduced in PTPRJ G983L cells compared to wt, but without a

10.3389/fonc.2022.1017947

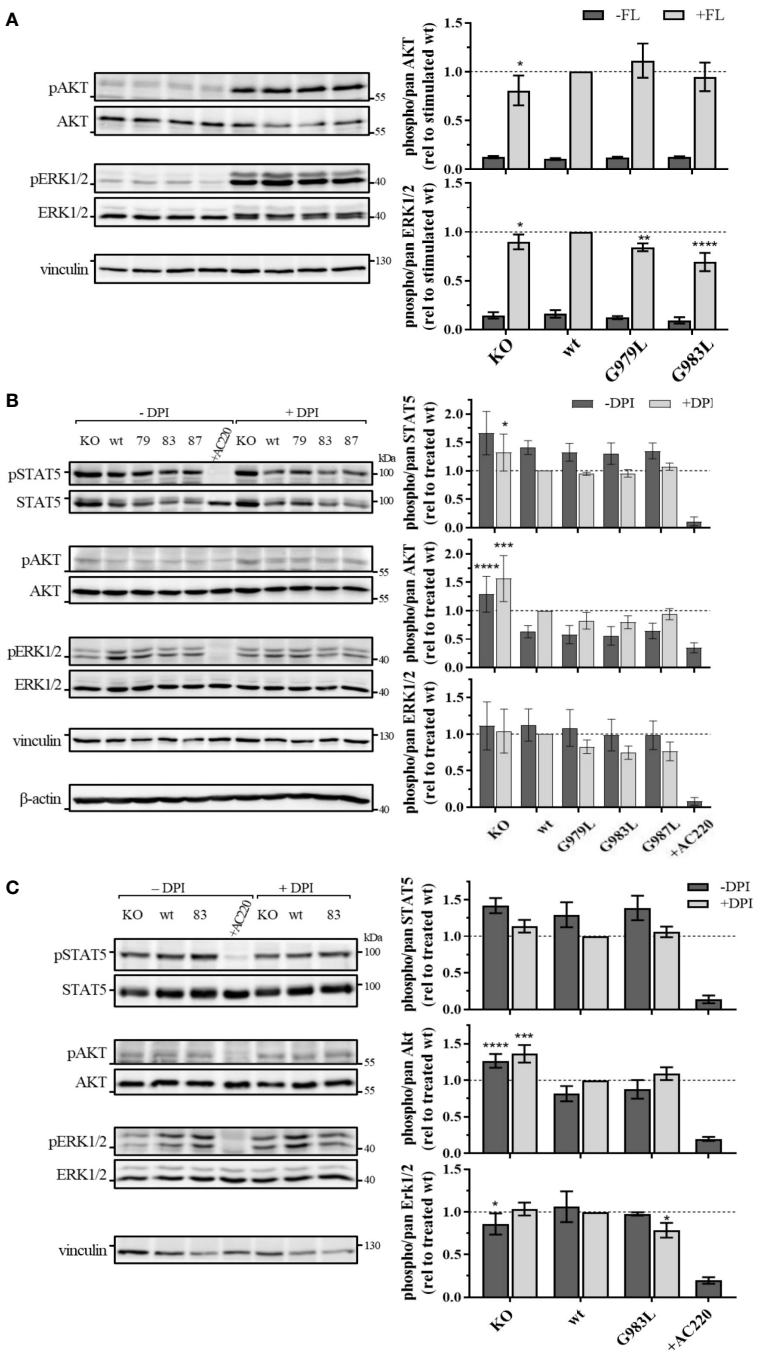

FIGURE 4
Signaling analysis of THP-1 **(A)** MV4-11 **(B)** and 32D FLT3 ITD cells expressing TMD mutant PTPRJ. **(A)** THP-1 PTPRJ KO cells or cells re-expressing PTPRJ wt, G979L, or G983L were starved for 4 h in serum-free medium, then stimulated with 200 ng/ml FLT3 ligand for 5 min (+FL) or left unstimulated (−FL) and lysed in RIPA buffer. **(B, C)** MV4-11 and 32D FLT3 ITD PTPRJ KO cells or cells re-expressing PTPRJ wt, G979L, G983L, or G987L were starved for 4 h in serum-free medium and treated with DPI (0.5 μM), AC220 (20 nM), or mock (DMSO), as indicated, then lysed in RIPA buffer. Equivalent amounts of protein samples were separated by SDS-PAGE and blotted to a nitrocellulose membrane. Blots were first probed by phospho-site specific antibodies recognizing pSTAT5 (Y694), pAKT (S473), and pERK1/2 (T202/Y204). Blots were re-probed for total STAT5, AKT, and ERK1/2 and subsequently analyzed with antibodies recognizing vinculin (124 kDa) and beta-actin (42 kDa) as a loading control. *Left*: Representative immunoblots are shown. Dashes indicate positions of molecular weight standard bands. 79 – G979L; 83 – G983L; 87 – G987L *Right*: Quantification of specific phosphorylation of AKT, ERK1/2, and STAT5 in relation to the total protein level. Values were normalized to FL-stimulated or DPI treated wt and are given as mean ± standard deviation, n = 3 - 4. Statistics: two-way ANOVA and Dunnett's multiple comparisons test; *p ≤ 0.05; **p ≤ 0.01; ***p ≤ 0.001; ****p ≤ 0.0001 compared to respective wt.

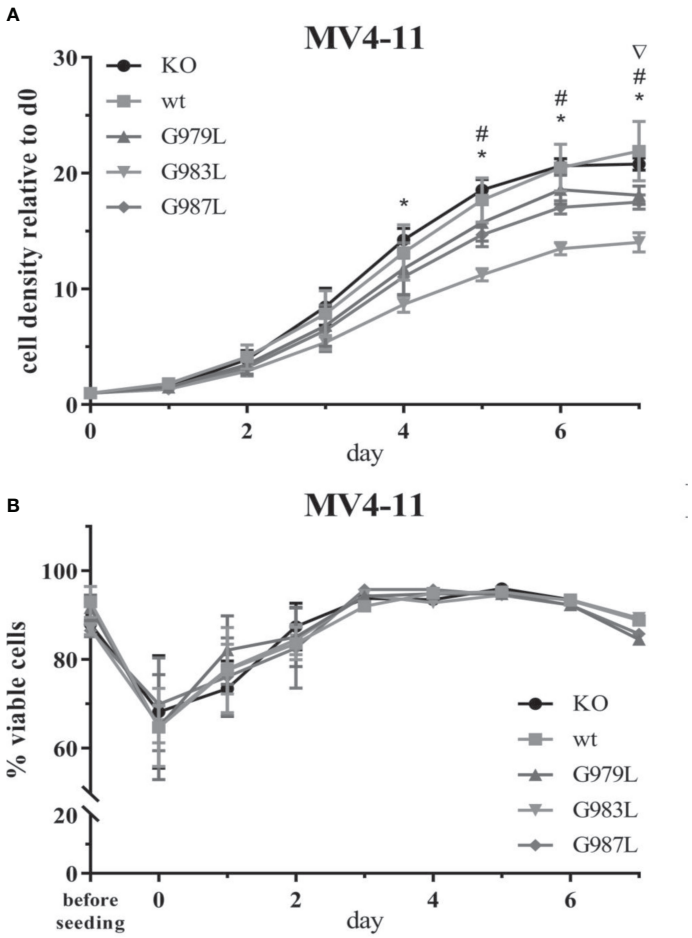

FIGURE 5
Proliferation and viability of MV4-11 cells expressing TMD mutant PTPRJ proteins. A+B) MV4-11 PTPRJ KO cells re-expressing wt PTPRJ or G-to-L mutants were seeded in duplicates in a 6-well plate. Cells were counted 4 hours after seeding (= day 0) and then every 24 hours for 7 days. **(A)** Cell density was determined by flow cytometry by measuring the number of viable cells in relation to the number of counting beads. The graphs show cell density relative to day 0. Values are given as mean ± standard deviation, n = 3. Statistics: repeated-measures two-way ANOVA and Dunnett's multiple comparisons test; significant differences ($p \leq 0.05$) of TMD mutants G979L (∇); G983L (*); and G987L (#) to wt PTPRJ are indicated. **(B)** Percentage of viable cells, measured by automated trypan blue count, is shown. Values are given as mean ± standard deviation, with n = 3 for d0 – 2 and n = 1 for d3 – 7.

statistically significant difference (Supplementary Figure 3B). The clear reduction in pY upon treatment with the FLT3 inhibitor AC220 demonstrates the dependency of observed phosphorylation events on FLT3 ITD activity. In contrast, in 32D FLT3 ITD cells, no differences in global pY of cells expressing PTPRJ wt and TMD were observed, irrespective of DPI treatment (Supplementary Figure 3C). As expected, 32D FLT3 ITD PTPRJ KO cells showed an increased global pY compared to 32D FLT3 ITD cells re-expressing PTPRJ. Surprisingly, AC220 treatment only slightly reduced protein phosphorylation in 32D FLT3 ITD cells, suggesting fewer FLT3 ITD–dependent phosphorylation events or incomplete inhibition of FLT3 activity.

Taken together, these findings with MV4-11 cells indicate increased dephosphorylation of PTPRJ targets and impaired FLT3 signalling in the presence of PTPRJ TMD mutants, especially G983L.

Discussion

PTPRJ has been shown to act as an antagonistic regulator on FLT3 activity *in vitro* and *in vivo* (39, 79). and its oligomerization has been demonstrated to hinder its activity (38, 58). Therefore, disruption of its PTPRJ oligomerization could result in an *in situ* activation of its activity and would consequently result in

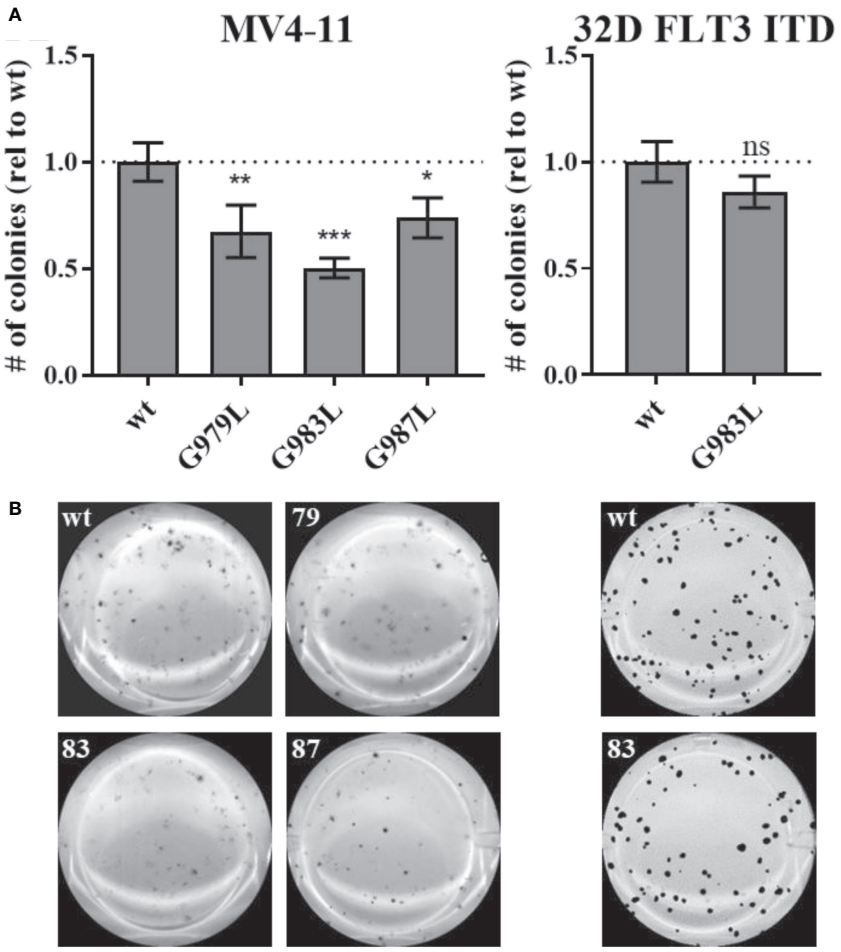

FIGURE 6
Clonal growth of FLT ITD cells expressing TMD mutant PTPRJ proteins. MV4-11 and 32D FLT3 ITD PTPRJ KO cells re-expressing PTPRJ wt, G979L, G983L, or G987L were seeded in triplicates in 1.27% methylcellulose-containing, cytokine-free medium. Colonies were stained with iodonitrotetrazolium chloride after 7 days (32D FLT3 ITD) or 10 days incubation (MV4-11) and quantified using Image (J) **(A)** Number (#) of colonies per well relative (rel) to wt is shown. Values are given as mean ± standard deviation, n = 3. Statistics for MV4-11: one-way ANOVA and Dunnett's multiple comparisons test; *p ≤ 0.05; **p ≤ 0.01; ***p ≤ 0.001 compared to respective wt (ns; not significant). Statistics for 32D FLT3 ITD: unpaired two-tailed t-test; * p ≤ 0.05. **(B)** Representative images of whole wells are shown. 79 – G979L; 83 – G983L; 87 – G987L.

decreased FLT3 receptor phosphorylation. Data presented here elucidated the effects on FLT3 signalling of TMD mutations known to disrupt PTPRJ oligomerization. First, determination of the specific phosphatase activity of immunoprecipitated PTPRJ revealed no alteration of phosphatase activity of mutant PTPRJ. Using our established leukemic model cell lines inactivated for endogenous PTPRJ but stably re-expressing TMD mutated PTPRJ variants phosphorylation of FLT3/FLT3 ITD and downstream targets, as well as cellular proliferation, viability, and clonal growth, were studied. Diminished phosphorylation of wt FLT3 and FLT3 ITD in AML cell lines re-expressing PTPRJ TMD mutants compared to cells expressing wt PTPRJ was accompanied by reduced downstream signalling *via* ERK1/2 and selective PTPRJ substrates as shown by mass spectrometry. Lastly, PTPRJ TMD mutant proteins impaired proliferation and *in vitro* transformation of leukemic MV4-11 cells. These findings reveal an enhanced activity of PTPRJ TMD mutant proteins *in situ*. Of the three studied PTPRJ G-to-L substitutions, G983L (a TMD mutation shown to be the most disruptive of PTPRJ oligomerization) seemed to have the most potent effects on FLT3 activity and tyrosine phosphorylation as well as cellular proliferation and clonal growth.

Wild type FLT3 and FLT3 ITD have been established as *bona fide* substrates of PTPRJ (24, 39, 40). Accordingly, PTPRJ depletion in wt FLT3-expressing 32D and THP-1 cell lines has been shown to increase FL-stimulated FLT3 phosphorylation (e.g., at Y589, Y591, or Y842). In contrast, PTPRJ–overexpressing cells were characterized by decreased receptor phosphorylation (39). Similarly, co-expression of PTPRJ and FLT3 ITD in HEK293T cells diminished FLT3 ITD phosphorylation in ROS-quenched

cells (39). As expected, our immunoblotting results revealed significantly decreased phosphorylation of wt FLT3 and FLT3 ITD at the PTPRJ regulated Y591 site (39) in leukemic cells expressing PTPRJ TMD mutants. Phosphorylation of this residue is considered a hallmark of FLT3 kinase activation and is presumed to be involved in relieving the autoinhibitory conformation of the FLT3 JM domain (4, 5). Y591 becomes phosphorylated by autocatalysis upon ligand stimulation and is constitutively phosphorylated in FLT3 ITD (16, 80, 81).

Chemical *in situ* crosslinking was used to reveal the effect of TMD G-to-L replacements on their oligomerization at the membrane. It should be noted that immunologically detected high molecular weight of crosslinked PTPRJ-HA could represent PTPRJ homodimers but could include other proteins. Analyses by Iuliano et al. using a mostly identical BS3-crosslinking protocol identified the crosslinked PTPRJ species as homodimers (82). However, another study based on PTPRJ TMD protein chimeras with staphylococcal nuclease observed higher order oligomers in SDS micelles in addition to dimers (54). By analysing specific PTP activity of immunoprecipitated PTPRJ, no distinct effects of PTPRJ TMD mutations could be detected. Moreover, our results show that the TMDs of FLT3 and PTPRJ have a propensity to interact with each other and that the PTPRJ TMD mutants enhance this interaction. Together, our findings indicate that the PTPRJ G-to-L mutations promote the dephosphorylation of FLTR3 (and thus reducing its activity) not by affecting PTPRJ's specific phosphatase activity but by destabilizing its self-association and favouring its access to FLT3 in the cellular membrane as a monomer. Moreover, our results suggest that decreased FLT3 activity might also result from a disruption of FLT3 dimer by PTPRJ TMD mutants (Figure 3**; lane 1 vs. lanes 4-6**).

While PTPRJ is presumed to be primarily localized at the plasma membrane (37, 46, 83), FLT3 ITD is retained in its immature HM form in the ER/Golgi system (17, 66). The maturation efficiency of FLT3 ITD has been demonstrated to be inversely correlated to its tyrosine phosphorylation (17, 66). PTP such as SHP1 and PTP1B have been found to dephosphorylate FLT3 ITD (66). In agreement with those findings, increased activity of the PTPRJ G983L mutant on FLT3 tended to enhance FLT3 ITD maturation. In addition, maturation seemed to be slightly decreased in *PTPRJ* KO cells, consistent with observations in bone marrow cells isolated from *PTPRJ* KO FLT3 ITD knock-in mice (84).

While treatment with the FLT3 inhibitor AC220 completely abrogated FLT3 ITD auto-phosphorylation in MV4-11 cells, it surprisingly reduced receptor phosphorylation in 32D FLT3 ITD cells only by ca. 50%. However, downstream signalling of FLT3 ITD in AC220-treated 32D cells was diminished, demonstrating that FLT3 activity was efficiently suppressed despite the residual pY591 signal. Those findings are consistent with a previous study using identical treatment conditions and cell lines (70). In a similar FLT3 overexpression system in 32D cells, Kellner and colleagues characterized FLT3 ITD to have a slower protein turnover than the wt receptor (71). This increased half-life of FLT3 ITD could explain why phosphorylated protein was still detectable in AC220-treated cells.

Like receptor phosphorylation, ERK1/2 phosphorylation downstream of wt FLT3 has been previously described to be enhanced in PTPRJ–depleted THP-1 or 32D cells (39). Likewise, signalling *via* STAT5 increases upon PTPRJ knockdown in DPI-treated 32D FLT3 ITD cells (24). As expected, ERK1/2 phosphorylation at T202/Y204 was impaired in both wt FLT3 and FLT3 ITD harbouring cell lines upon expression of PTPRJ TMD mutants. In addition to reduced activation downstream of inhibited FLT3, this could be partly due to the enhanced action of PTPRJ on ERK1/2 Y204, which has been previously identified as a direct target of PTPRJ phosphatase activity (85). In contrast, AKT activation was mostly unchanged by the expression of PTPRJ TMD mutant proteins.

Physiological alterations in leukemic cell lines due to the enhanced activity of PTPRJ TMD mutants were demonstrated. In particular, PTPRJ has been previously shown to play a role in suppressing FLT3-mediated leukemic cell transformation (22, 24, 39). Reactivating PTPRJ by counteracting ROS has been found to attenuate the clonal growth of 32D FLT3 ITD cells (22, 24). Furthermore, shRNA-mediated depletion of PTPRJ has been shown to induce FL-stimulated colony formation of 32D cells stably expressing wt FLT3 (39). Here, FLT3 ITD–driven clonal growth was reduced for MV4-11 cells stably expressing PTPRJ TMD mutants, and the same trend was observed with 32D FLT3 ITD cells. Similarly, the reactivation of PTPRJ's PTP activity by blocking ROS has been demonstrated to prolong survival in a murine model of FLT3 ITD–driven myeloproliferative disease (22, 24).

Expression of PTPRJ TMD mutants in MV4-11 cells significantly impaired their proliferation, again indicating enhanced activity of TMD mutant PTPRJ against FLT3 ITD and/or other targets. In contrast, expression of PTPRJ G983L did not affect the proliferation of 32D FLT3 ITD cells within the four days of observation. This could result from high ROS levels and subsequent oxidative inactivation of PTPRJ. It also seems possible that prolonged growth of cells might be required due to the strong stimulatory effect of overexpressed FLT3 ITD on proliferation. Similarly, the impact of PTPRJ depletion on FL-induced proliferation of 32D FLT3wt cells has been previously found to be only moderate when scored after three days but much more pronounced after five days (39).

Total pY immunoblotting provided insight into the effect of PTPRJ on global Tyr phosphorylation. Immunoblotting revealed global pY to be significantly reduced in THP-1 cells expressing PTPRJ G983L compared to PTPRJ wt. The same trend was observed in MV4-11 cells. Thus, our data indicate enhanced PTP activity of TMD mutant PTPRJ and/or reduced FLT3 activity in those cells. Taken together, our findings provide clear evidence that disrupting PTPRJ TMD–mediated self-association may be used as a tool to restrict oncogenic FLT3 activity. Therefore, the

potential application of PTPRJ TMD-targeting peptides (38) in treating FLT3 ITD–positive AML should be investigated further.

Data availability statement

The original contributions presented in the study are included in the article/Supplementary Material. Further inquiries can be directed to the corresponding author.

Author contributions

JPM and DT conceived the project; MS, SR, WE, and AK performed the experiments. MS, DT, and JPM wrote the manuscript. All authors contributed to the article and approved the submitted version.

Funding

This work was supported by the Deutsche Forschungsgemeinschaft, grant Mu955/14-1 and Mu955/15-1 to JM, and by the National Institute of General Medical Sciences [grant number R01GM139998] to DT.

Conflict of interest

The authors declare that the research was conducted in the absence of any commercial or financial relationships that could be construed as a potential conflict of interest.

Publisher's note

Supplementary material

The Supplementary Material for this article can be found online at: https://www.frontiersin.org/articles/10.3389/fonc.2022.1017947/full#supplementary-material

SUPPLEMENTARY FIGURE 1
Stable re-expression of PTPRJ in AML cell lines. PTPRJ wt and G-to-L variants were stably expressed in MV4-11, THP-1, and 32D FLT3 ITD PTPRJ KO cells by retroviral transduction. Cells were sorted for similar PTPRJ surface expression levels using flow cytometric based on PTPRJ detection. **(A)** PTPRJ surface expression. Cells were stained with APC-coupled α-CD148 (PTPRJ) antibody, and the APC signal was measured flow cytometrically. Histograms show cell-bound APC fluorescence intensity (APC-A). **(B)** Cellular PTPRJ expression level. Cell lysates were separated by SDS-PAGE, blotted, and analyzed with antibodies recognizing PTPRJ. For loading control, antibodies recognizing vinculin (124 kDa) and beta-actin (42 kDa) or Ponceau staining (not shown) were used. Graphs show PTPRJ signal normalized to loading control (ctrl), relative (rel) to respective wt. Values are given as mean ± standard deviation, with n = 5 – 6 for MV4-11 and n = 3 for THP-1 and 32D, except for MV4-11 and THP-1 parental n = 1. Statistics: one-way ANOVA and Dunnett's multiple comparisons test; * $p \leq 0.05$ compared to respective wt. ns – not significant. Representative immunoblots are shown below graphs. Positions of 40 and 130 kDa bands of molecular weight standard are indicated. 79 – G979L; 83 – G983L; 87 – G987L.

SUPPLEMENTARY FIGURE 2
Representative immunoblot analysis against MBP used to normalize the DN-AraTM assay results. Bacteria are always transformed with both AraC* and AraC-containing plasmids. The dash (-) represents an empty vector without the TMD construct of interest.

SUPPLEMENTARY FIGURE 3
Global protein tyrosine phosphorylation pattern of DEP-1 wt and TMD mutant expressing cell lines. THP-1 **(A)**, MV4-11 **(B)**, and 32D FLT3 ITD **(C)** PTPRJ KO cells or cells re-expressing DEP-1 wt, G979L, G983L, and G987L were starved for 4 h in serum- and cytokine-free medium and lysed in RIPA buffer. During starvation, MV4-11 and 32D FLT3 ITD cells were treated with DPI (0.5 μM), AC220 (+AC, 20 nM), or mock (DMSO), as indicated. THP-1 cells were stimulated with FL (200 ng/ml, 5 min) before harvest. Equivalent amounts of protein samples (15 – 20 μg) were separated by SDS-PAGE, blotted to a nitrocellulose membrane, and analyzed for global tyrosine phosphorylation using α-pY antibody (4G10). Blots were re-probed for vinculin (124 kDa) or beta-actin (42 kDa) as loading control. *Right*: Quantification of total tyrosine phosphorylation normalized to loading control (Ctrl), relative (rel) to DPI-treated or FL-stimulated wt is shown. Values are given as mean ± standard deviation, n = 3 – 4. Statistics: two-way ANOVA and Dunnett's multiple comparisons test; * $p \leq 0.05$; ** $p \leq 0.01$ compared to respective wt. *Left:* Representative immunoblots are shown. Position of molecular weight standard bands from 35 – 180 kDa are indicated by dashes left and right of blots. 79 – G979L; 83 – G983L; 87 – G987L.

References

1. Matthews W, Jordan CT, Wiegand GW, Pardoll D, Lemischka IR. A receptor tyrosine kinase specific to hematopoietic stem and progenitor cell-enriched populations. *Cell* (1991) 65(7):1143–52. doi: 10.1016/0092-8674(91)90010-V

2. Rosnet O, Schiff C, Pebusque MJ, Marchetto S, Tonnelle C, Toiron Y, et al. Human FLT3/FLK2 gene: cDNA cloning and expression in hematopoietic cells. *Blood* (1993) 82(4):1110–9. doi: 10.1182/blood.V82.4.1110.1110

3. Maroc N, Rottapel R, Rosnet O, Marchetto S, Lavezzi C, Mannoni P, et al. Biochemical characterization and analysis of the transforming potential of the FLT3/FLK2 receptor tyrosine kinase. *Oncogene* (1993) 8(4):909–18.

4. Kazi JU, Ronnstrand L. FMS-like tyrosine kinase 3/FLT3: From basic science to clinical implications. *Physiol Rev* (2019) 99(3):1433–66. doi: 10.1152/physrev.00029.2018

5. Griffith J, Black J, Faerman C, Swenson L, Wynn M, Lu F, et al. The structural basis for autoinhibition of FLT3 by the juxtamembrane domain. *Mol Cell* (2004) 13 (2):169–78. doi: 10.1016/S1097-2765(03)00505-7

6. Verstraete K, Vandriessche G, Januar M, Elegheert J, Shkumatov AV, Desfosses A, et al. Structural insights into the extracellular assembly of the hematopoietic Flt3 signaling complex. *Blood* (2011) 118(1):60–8. doi: 10.1182/blood-2011-01-329532

7. Heiss E, Masson K, Sundberg C, Pedersen M, Sun J, Bengtsson S, et al. Identification of Y589 and Y599 in the juxtamembrane domain of Flt3 as ligand-induced autophosphorylation sites involved in binding of src family kinases and the protein tyrosine phosphatase SHP2. *Blood* (2006) 108(5):1542–50. doi: 10.1182/blood-2005-07-008896

8. Grafone T, Palmisano M, Nicci C, Storti S. An overview on the role of FLT3-tyrosine kinase receptor in acute myeloid leukemia: biology and treatment. *Oncol Rev* (2012) 6(1):e8. doi: 10.4081/oncol.2012.e8

9. Hayakawa F, Towatari M, Kiyoi H, Tanimoto M, Kitamura T, Saito H, et al. Tandem-duplicated Flt3 constitutively activates STAT5 and MAP kinase and introduces autonomous cell growth in IL-3-dependent cell lines. *Oncogene* (2000) 19(5):624–31. doi: 10.1038/sj.onc.1203354

10. Mizuki M, Fenski R, Halfter H, Matsumura I, Schmidt R, Müller C, et al. Flt3 mutations from patients with acute myeloid leukemia induce transformation of 32D cells mediated by the ras and STAT5 pathways. *Blood* (2000) 96(12):3907–14. doi: 10.1182/blood.V96.12.3907

11. Kiyoi H, Ohno R, Ueda R, Saito H, Naoe T. Mechanism of constitutive activation of FLT3 with internal tandem duplication in the juxtamembrane domain. *Oncogene* (2002) 21(16):2555–63. doi: 10.1038/sj.onc.1205332

12. Nakao M, Yokota S, Iwai T, Kaneko H, Horiike S, Kashima K, et al. Internal tandem duplication of the flt3 gene found in acute myeloid leukemia. *Leukemia* (1996) 10(12):1911–8.

13. Schnittger S, Bacher U, Haferlach C, Alpermann T, Kern W, Haferlach T. Diversity of the juxtamembrane and TKD1 mutations (exons 13-15) in the FLT3 gene with regards to mutant load, sequence, length, localization, and correlation with biological data. *Genes Chromosomes Cancer* (2012) 51(10):910–24. doi: 10.1002/gcc.21975

14. Grundler R, Miething C, Thiede C, Peschel C, Duyster J. FLT3-ITD and tyrosine kinase domain mutants induce 2 distinct phenotypes in a murine bone marrow transplantation model. *Blood* (2005) 105(12):4792–9. doi: 10.1182/blood-2004-11-4430

15. Schmidt-Arras D, Böhmer SA, Koch S, Müller JP, Blei L, Cornils H, et al. Anchoring of FLT3 in the endoplasmic reticulum alters signaling quality. *Blood* (2009) 113(15):3568–76. doi: 10.1182/blood-2007-10-121426

16. Choudhary C, Olsen JV, Brandts C, Cox J, Reddy PN, Böhmer FD, et al. Mislocalized activation of oncogenic RTKs switches downstream signaling outcomes. *Mol Cell* (2009) 36(2):326–39. doi: 10.1016/j.molcel.2009.09.019

17. Yamawaki K, Shiina I, Murata T, Tateyama S, Maekawa Y, Niwa M, et al. FLT3-ITD transduces autonomous growth signals during its biosynthetic trafficking in acute myelogenous leukemia cells. *Sci Rep* (2021) 11(1):22678. doi: 10.1038/s41598-021-02221-2

18. Kothe S, Muller JP, Bohmer SA, Tschongov T, Fricke M, Koch S, et al. Features of ras activation by a mislocalized oncogenic tyrosine kinase: FLT3 ITD signals through K-ras at the plasma membrane of acute myeloid leukemia cells. *J Cell Sci* (2013) 126(Pt 20):4746–55. doi: 10.1242/jcs.131789

19. Choudhary C, Schwable J, Brandts C, Tickenbrock L, Sargin B, Kindler T, et al. AML-associated Flt3 kinase domain mutations show signal transduction differences compared with Flt3 ITD mutations. *Blood* (2005) 106(1):265–73. doi: 10.1182/blood-2004-07-2942

20. Zheng R, Friedman AD, Small D. Targeted inhibition of FLT3 overcomes the block to myeloid differentiation in 32Dcl3 cells caused by expression of FLT3/ITD mutations. *Blood* (2002) 100(12):4154–61. doi: 10.1182/blood-2002-03-0936

21. Kelly LM, Liu Q, Kutok JL, Williams IR, Boulton CL, Gilliland DG. FLT3 internal tandem duplication mutations associated with human acute myeloid leukemias induce myeloproliferative disease in a murine bone marrow transplant model. *Blood* (2002) 99(1):310–8. doi: 10.1182/blood.V99.1.310

22. Jayavelu AK, Muller JP, Bauer R, Bohmer SA, Lassig J, Cerny-Reiterer S, et al. NOX4-driven ROS formation mediates PTP inactivation and cell transformation in FLT3ITD-positive AML cells. *Leukemia* (2016) 30(2):473–83. doi: 10.1038/leu.2015.234

23. Sallmyr A, Fan J, Datta K, Kim K.T, Grosu D, Shapiro P, et al. Internal tandem duplication of FLT3 (FLT3/ITD) induces increased ROS production, DNA damage, and misrepair: implications for poor prognosis in AML. *Blood* (2008) 111 (6):3173–82. doi: 10.1182/blood-2007-05-092510

24. Godfrey R, Arora D, Bauer R, Stopp S, Muller JP, Heinrich T, et al. Cell transformation by FLT3 ITD in acute myeloid leukemia involves oxidative inactivation of the tumor suppressor protein-tyrosine phosphatase DEP-1/PTPRJ. *Blood* (2012) 119(19):4499–511. doi: 10.1182/blood-2011-02-336446

25. Jayavelu AK, Moloney JN, Bohmer FD, Cotter TG. NOX-driven ROS formation in cell transformation of FLT3-ITD-positive AML. *Exp Hematol* (2016) 44(12):1113–22. doi: 10.1016/j.exphem.2016.08.008

26. Hendriks W, Bourgonje A, Leenders W, Pulido R. Proteinaceous regulators and inhibitors of protein tyrosine phosphatases. *Molecules* (2018) 23(2):395–417. doi: 10.3390/molecules23020395

27. Östman A, Böhmer FD. Regulation of receptor tyrosine kinase signaling by protein tyrosine phosphatases. *Trends Cell Biol* (2001) 11(6):258–66. doi: 10.1016/S0962-8924(01)01990-0

28. Honda H, Inazawa J, Nishida J, Yazaki Y, Hirai H. Molecular cloning, characterization, and chromosomal localization of a novel protein-tyrosine phosphatase, HPTP eta. *Blood* (1994) 84(12):4186–94. doi: 10.1182/blood.V84.12.4186.bloodjournal84124186

29. Ostman A, Yang Q, Tonks NK. Expression of DEP-1, a receptor-like protein-tyrosine-phosphatase, is enhanced with increasing cell density. *Proc Natl Acad Sci U.S.A.* (1994) 91(21):9680–4. doi: 10.1073/pnas.91.21.9680

30. Jandt E, Denner K, Kovalenko M, Ostman A, Bohmer FD. The protein-tyrosine phosphatase DEP-1 modulates growth factor-stimulated cell migration and cell-matrix adhesion. *Oncogene* (2003) 22(27):4175–85. doi: 10.1038/sj.onc.1206652

31. Petermann A, Haase D, Wetzel A, Balavenkatraman KK, Tenev T, Guhrs KH, et al. Loss of the protein-tyrosine phosphatase DEP-1/PTPRJ drives meningioma cell motility. *Brain Pathol* (2011) 21(4):405–18. doi: 10.1111/j.1750-3639.2010.00464.x

32. Grazia Lampugnani M, Zanetti A, Corada M, Takahashi T, Balconi G, Breviario F, et al. Contact inhibition of VEGF-induced proliferation requires vascular endothelial cadherin, beta-catenin, and the phosphatase DEP-1/CD148. *J Cell Biol* (2003) 161(4):793–804. doi: 10.1083/jcb.200209019

33. Takahashi T, Takahashi K, Mernaugh RL, Tsuboi N, Liu H, Daniel TO. A monoclonal antibody against CD148, a receptor-like tyrosine phosphatase, inhibits endothelial-cell growth and angiogenesis. *Blood* (2006) 108(4):1234–42. doi: 10.1182/blood-2005-10-4296

34. Kovalenko M, Denner K, Sandstrom J, Persson C, Gross S, Jandt E, et al. Site-selective dephosphorylation of the platelet-derived growth factor beta-receptor by the receptor-like protein-tyrosine phosphatase DEP-1. *J Biol Chem* (2000) 275 (21):16219–26. doi: 10.1074/jbc.275.21.16219

35. Patel JP, Gonen M, Figueroa ME, Fernandez H, Sun Z, Racevskis J, et al. Prognostic relevance of integrated genetic profiling in acute myeloid leukemia. *N Engl J Med* (2012) 366(12):1079–89. doi: 10.1056/NEJMoa1112304

36. Palka HL, Park M, Tonks NK. Hepatocyte growth factor receptor tyrosine kinase met is a substrate of the receptor protein-tyrosine phosphatase DEP-1. *J Biol Chem* (2003) 278(8):5728–35. doi: 10.1074/jbc.M210656200

37. Tarcic G, Boguslavsky SK, Wakim J, Kiuchi T, Liu A, Reinitz F, et al. An unbiased screen identifies DEP-1 tumor suppressor as a phosphatase controlling EGFR endocytosis. *Curr Biol* (2009) 19(21):1788–98. doi: 10.1016/j.cub.2009.09.048

38. Bloch E, Sikorski EL, Pontoriero D, Day EK, Berger BW, Lazzara MJ, et al. Disrupting the transmembrane domain-mediated oligomerization of protein tyrosine phosphatase receptor J inhibits EGFR-driven cancer cell phenotypes. *J Biol Chem* (2019) 294(49):18796–806. doi: 10.1074/jbc.RA119.010229

39. Arora D, Stopp S, Bohmer SA, Schons J, Godfrey R, Masson K, et al. Protein-tyrosine phosphatase DEP-1 controls receptor tyrosine kinase FLT3 signaling. *J Biol Chem* (2011) 286(13):10918–29. doi: 10.1074/jbc.M110.205021

40. Bohmer SA, Weibrecht I, Soderberg O, Bohmer FD. Association of the protein-tyrosine phosphatase DEP-1 with its substrate FLT3 visualized by in situ proximity ligation assay. *PloS One* (2013) 8(5):e62871. doi: 10.1371/journal.pone.0062871

41. Östman A, Hellberg C, Böhmer FD. Protein-tyrosine phosphatases and cancer. *Nat Rev Cancer* (2006) 6(4):307–20. doi: 10.1038/nrc1837

42. Balavenkatraman KK, Jandt E, Friedrich K, Kautenburger T, Pool-Zobel BL, Ostman A, et al. DEP-1 protein tyrosine phosphatase inhibits proliferation and migration of colon carcinoma cells and is upregulated by protective nutrients. *Oncogene* (2006) 25(47):6319–24. doi: 10.1038/sj.onc.1209647

43. Petermann A, Stampnik Y, Cui Y, Morrison H, Pachow D, Kliese N, et al. Deficiency of the protein-tyrosine phosphatase DEP-1/PTPRJ promotes matrix metalloproteinase-9 expression in meningioma cells. *J Neurooncol* (2015) 122 (3):451–9. doi: 10.1007/s11060-015-1740-2

44. Ruivenkamp CA, Wezel van T, Zanon C, Stassen AP, Vlcek C, Csikos T, et al. Ptprj is a candidate for the mouse colon-cancer susceptibility locus Scc1 and is frequently deleted in human cancers. *Nat Genet* (2002) 31(3):295–300. doi: 10.1038/ng903

45. den Hertog J, Ostman A, Bohmer FD. Protein tyrosine phosphatases: regulatory mechanisms. *FEBS J* (2008) 275(5):831–47. doi: 10.1111/j.1742-4658.2008.06247.x

46. de la Fuente-Garcia MA, Nicolas JM, Freed JH, Palou E, Thomas AP, Vilella R, et al. CD148 is a membrane protein tyrosine phosphatase present in all hematopoietic lineages and is involved in signal transduction on lymphocytes. *Blood* (1998) 91(8):2800–9. doi: 10.1182/blood.V91.8.2800.2800_2800_2809

47. Sorby M, Sandstrom J, Ostman A. An extracellular ligand increases the specific activity of the receptor-like protein tyrosine phosphatase DEP-1. *Oncogene* (2001) 20(37):5219–24. doi: 10.1038/sj.onc.1204581

48. Denu JM, Tanner KG. Specific and reversible inactivation of protein tyrosine phosphatases by hydrogen peroxide: evidence for a sulfenic acid intermediate and implications for redox regulation. *Biochemistry* (1998) 37 (16):5633–42. doi: 10.1021/bi973035t

49. Ostman A, Frijhoff J, Sandin A, Bohmer FD. Regulation of protein tyrosine phosphatases by reversible oxidation. *J Biochem* (2011) 150(4):345–56. doi: 10.1093/jb/mvr104

50. Chiarugi P, Cirri P. Redox regulation of protein tyrosine phosphatases during receptor tyrosine kinase signal transduction. *Trends Biochem Sci* (2003) 28 (9):509–14. doi: 10.1016/S0968-0004(03)00174-9

51. Lou YW, Chen YY, Hsu SF, Chen RK, Lee CL, Khoo KH, et al. Redox regulation of the protein tyrosine phosphatase PTP1B in cancer cells. *FEBS J* (2008) 275(1):69–88. doi: 10.1111/j.1742-4658.2007.06173.x

52. Walchli S, Espanel X, Hooft van Huijsduijnen R. Sap-1/PTPRH activity is regulated by reversible dimerization. *Biochem Biophys Res Commun* (2005) 331 (2):497–502. doi: 10.1016/j.bbrc.2005.03.196

53. Tertoolen LG, Blanchetot C, Jiang G, Overvoorde J, Gadella TW Jr, Hunter T, et al. Dimerization of receptor protein-tyrosine phosphatase alpha in living cells. *BMC Cell Biol* (2001) 2:8. doi: 10.1186/1471-2121-2-8

54. Chin CN, Sachs JN, Engelman DM. Transmembrane homodimerization of receptor-like protein tyrosine phosphatases. *FEBS Lett* (2005) 579(17):3855–8. doi: 10.1016/j.febslet.2005.05.071

55. Jiang G, Hertog den J, Su J, Noel J, Sap J, Hunter T. Dimerization inhibits the activity of receptor-like protein-tyrosine phosphatase-alpha. *Nature* (1999) 401 (6753):606–10. doi: 10.1038/44170

56. Bilwes AM, Hertog den J, Hunter T, Noel JP. Structural basis for inhibition of receptor protein-tyrosine phosphatase-alpha by dimerization. *Nature* (1996) 382 (6591):555–9. doi: 10.1038/382555a0

57. Barr AJ, Ugochukwu E, Lee WH, King ON, Filippakopoulos P, Alfano I, et al. Large-Scale structural analysis of the classical human protein tyrosine phosphatome. *Cell* (2009) 136(2):352–63. doi: 10.1016/j.cell.2008.11.038

58. Matozo HC, Santos MA, Neto Oliveira M, Bleicher L, Lima LM, Iuliano R, et al. Low-resolution structure and fluorescence anisotropy analysis of protein tyrosine phosphatase eta catalytic domain. *Biophys J* (2007) 92(12):4424–32. doi: 10.1529/biophysj.106.094961

59. Fahs S, Lujan P, Kohn M. Approaches to study phosphatases. *ACS Chem Biol* (2016) 11(11):2944–61. doi: 10.1021/acschembio.6b00570

60. Takahashi K, Mernaugh RL, Friedman DB, Weller R, Tsuboi N, Yamashita H, et al. Thrombospondin-1 acts as a ligand for CD148 tyrosine phosphatase. *Proc Natl Acad Sci U.S.A.* (2012) 109(6):1985–90. doi: 10.1073/pnas.1106171109

61. Takahashi K, Sumarriva K, Kim R, Jiang R, Brantley-Sieders DM, Chen J, et al. Determination of the CD148-interacting region in thrombospondin-1. *PloS One* (2016) 11(5):e0154916. doi: 10.1371/journal.pone.0154916

62. Paduano F, Ortuso F, Campiglia P, Raso C, Iaccino E, Gaspari M, et al. Isolation and functional characterization of peptide agonists of PTPRJ, a tyrosine phosphatase receptor endowed with tumor suppressor activity. *ACS Chem Biol* (2012) 7(10):1666–76. doi: 10.1021/cb300281t

63. Ortuso F, Paduano F, Carotenuto A, Gomez-Monterrey I, Bilotta A, Gaudio E, et al. Discovery of PTPRJ agonist peptides that effectively inhibit in vitro cancer cell proliferation and tube formation. *ACS Chem Biol* (2013) 8(7):1497–506. doi: 10.1021/cb3007192

64. Müller JP, Schönherr C, Markova B, Bauer R, Stocking C, Böhmer FD. Role of SHP2 for FLT3-dependent proliferation and transformation in 32D cells. *Leukemia* (2008) 22(10):1945–8. doi: 10.1038/leu.2008.73

65. Nabinger SC, Li XJ, Ramdas B, He Y, Zhang X, Zeng L, et al. The protein tyrosine phosphatase, Shp2, positively contributes to FLT3-ITD-induced hematopoietic progenitor hyperproliferation and malignant disease in vivo. *Leukemia* (2013) 27(2):398–408. doi: 10.1038/leu.2012.308

66. Schmidt-Arras DE, Böhmer A, Markova B, Choudhary C, Serve H, Böhmer FD. Tyrosine phosphorylation regulates maturation of receptor tyrosine kinases. *Mol Cell Biol* (2005) 25(9):3690–703. doi: 10.1128/MCB.25.9.3690-3703.2005

67. Kresinsky A, Schnoder TM, Jacobsen ID, Rauner M, Hofbauer LC, Ast V, et al. Lack of CD45 in FLT3-ITD mice results in a myeloproliferative phenotype, cortical porosity, and ectopic bone formation. *Oncogene* (2019) 38:4773–87. doi: 10.1038/s41388-019-0757-y

68. Snider C, Jayasinghe S, Hristova K, White SH. MPEx: a tool for exploring membrane proteins. *Protein Sci* (2009) 18(12):2624–8. doi: 10.1002/pro.256

69. Arora D, Kothe S, Eijnden den van M, Huijsduijnen van Hooft R, Heidel F, Fischer T, et al. Expression of protein-tyrosine phosphatases in acute myeloid leukemia cells: FLT3 ITD sustains high levels of DUSP6 expression. *Cell Commun Signal* (2012) 10(1):19. doi: 10.1186/1478-811X-10-19

70. Bohmer A, Barz S, Schwab K, Kolbe U, Gabel A, Kirkpatrick J, et al. Modulation of FLT3 signal transduction through cytoplasmic cysteine residues indicates the potential for redox regulation. *Redox Biol* (2020) 28:101325. doi: 10.1016/j.redox.2019.101325

71. Kellner F, Keil A, Schindler K, Tschongov T, Hunninger K, Loercher H, et al. Wild-type FLT3 and FLT3 ITD exhibit similar ligand-induced internalization characteristics. *J Cell Mol Med* (2020) 24(8):4668–76. doi: 10.1111/jcmm.15132

72. Choudhary C, Müller-Tidow C, Berdel WE, Serve H. Signal transduction of oncogenic Flt3. *Int J Hematol* (2005) 82(2):93–9. doi: 10.1532/IJH97.05090

73. Su PC, Berger BW. A novel assay for assessing juxtamembrane and transmembrane domain interactions important for receptor heterodimerization. *J Mol Biol* (2013) 425(22):4652–8. doi: 10.1016/j.jmb.2013.07.022

74. Barton R, Palacio D, Iovine MK, Berger BW. A cytosolic juxtamembrane interface modulates plexin A3 oligomerization and signal transduction. *PloS One* (2015) 10(1):e0116368. doi: 10.1371/journal.pone.0116368

75. Sale GJ, Smith DM. Serine phosphorylations triggered by the insulin receptor. *Cell Signal* (1989) 1(3):205–18. doi: 10.1016/0898-6568(89)90038-7

76. Su PC, Berger BW. Identifying key juxtamembrane interactions in cell membranes using AraC-based transcriptional reporter assay (AraTM). *J Biol Chem* (2012) 287(37):31515–26. doi: 10.1074/jbc.M112.396895

77. Gerhart J, Thevenin AF, Bloch E, King KE, Thevenin D. Inhibiting epidermal growth factor receptor dimerization and signaling through targeted delivery of a juxtamembrane domain peptide mimic. *ACS Chem Biol* (2018) 13 (9):2623–32. doi: 10.1021/acschembio.8b00555

78. Brandts CH, Sargin B, Rode M, Biermann C, Lindtner B, Schwable J, et al. Constitutive activation of akt by Flt3 internal tandem duplications is necessary for increased survival, proliferation, and myeloid transformation. *Cancer Res* (2005) 65 (21):9643–50. doi: 10.1158/0008-5472.CAN-05-0422

79. Kresinsky A, Bauer R, Schnoder TM, Berg T, Meyer D, Ast V, et al. Loss of DEP-1 (Ptprj) promotes myeloproliferative disease in FLT3-ITD acute myeloid leukemia. *Haematologica* (2018) 103(11):e505–9. doi: 10.3324/haematol.2017.185306

80. Leischner H, Albers C, Grundler R, Razumovskaya E, Spiekermann K, Bohlander S, et al. SRC is a signaling mediator in FLT3-ITD- but not in FLT3-TKD-positive AML. *Blood* (2012) 119(17):4026–33. doi: 10.1182/blood-2011-07-365726

81. Rocnik JL, Okabe R, Yu JC, Lee BH, Giese N, Schenkein DP, et al. Roles of tyrosine 589 and 591 in STAT5 activation and transformation mediated by FLT3-ITD. *Blood* (2006) 108(4):1339–45. doi: 10.1182/blood-2005-11-011429

82. Iuliano R, Raso C, Quintiero A, Pera IL, Pichiorri F, Palumbo T, et al. The eighth fibronectin type III domain of protein tyrosine phosphatase receptor J influences the formation of protein complexes and cell localization. *J Biochem* (2009) 145(3):377–85. doi: 10.1093/jb/mvn175

83. Tsuboi N, Utsunomiya T, Roberts RL, Ito H, Takahashi K, Noda M, et al. The tyrosine phosphatase CD148 interacts with the p85 regulatory subunit of phosphoinositide 3-kinase. *Biochem J* (2008) 413(1):193–200. doi: 10.1042/BJ20071317

84. Quentmeier H, Reinhardt J, Zaborski M, Drexler HG. FLT3 mutations in acute myeloid leukemia cell lines. *Leukemia* (2003) 17(1):120–4. doi: 10.1038/sj.leu.2402740

85. Sacco F, Tinti M, Palma A, Ferrari E, Nardozza AP, Huijsduijnen van Hooft R, et al. Tumor suppressor density-enhanced phosphatase-1 (DEP-1) inhibits the RAS pathway by direct dephosphorylation of ERK1/2 kinases. *J Biol Chem* (2009) 284(33):22048–58. doi: 10.1074/jbc.M109.002758

frontiers | Frontiers in Oncology

TYPE Original Research
PUBLISHED 28 November 2022
DOI 10.3389/fonc.2022.888570

OPEN ACCESS

EDITED BY
Spiros Vlahopoulos,
University of Athens, Greece

REVIEWED BY
Li Wei,
Guangzhou Medical University Cancer Hospital, China
Baohong Yue,
Zhengzhou University, China

*CORRESPONDENCE
Xiao-Zhong Wang
wangxiaozhong@ncu.edu.cn
Bo Huang
764019522@qq.com

SPECIALTY SECTION
This article was submitted to Hematologic Malignancies, a section of the journal Frontiers in Oncology

RECEIVED 03 March 2022
ACCEPTED 08 November 2022
PUBLISHED 28 November 2022

CITATION
Zhong F-M, Yao F-Y, Liu J, Zhang H-B, Zhang J, Zhang N, Lin J, Li S-Q, Li M-Y, Jiang J-Y, Cheng Y, Xu S, Wen W, Yang Y-L, Zhang X-R, Cheng X-X, Huang B and Wang X-Z (2022) Ferroptosis-related molecular patterns reveal immune escape, inflammatory development and lipid metabolism characteristics of the tumor microenvironment in acute myeloid leukemia.
Front. Oncol. 12:888570.
doi: 10.3389/fonc.2022.888570

Ferroptosis-related molecular patterns reveal immune escape, inflammatory development and lipid metabolism characteristics of the tumor microenvironment in acute myeloid leukemia

Fang-Min Zhong[1,2], Fang-Yi Yao[1], Jing Liu[1], Hai-Bin Zhang[1], Jing Zhang[1], Nan Zhang[1], Jin Lin[1], Shu-Qi Li[1], Mei-Yong Li[1], Jun-Yao Jiang[1], Ying Cheng[1,2], Shuai Xu[1,2], Wen Wen[1,2], Yu-Lin Yang[1,2], Xue-Ru Zhang[1,2], Xue-Xin Cheng[1], Bo Huang[1]* and Xiao-Zhong Wang[1,2]*

[1]Jiangxi Province Key Laboratory of Laboratory Medicine, Department of Clinical Laboratory, The Second Affiliated Hospital of Nanchang University, Nanchang, Jiangxi, China, [2]School of Public Health, Nanchang University, Nanchang, Jiangxi, China

Background: An increasing number of studies have revealed the influencing factors of ferroptosis. The influence of immune cell infiltration, inflammation development and lipid metabolism in the tumor microenvironment (TME) on the ferroptosis of tumor cells requires further research and discussion.

Methods: We explored the relationship between ferroptosis-related genes and acute myeloid leukemia (AML) from the perspective of large sample analysis and multiomics, used multiple groups to identify and verify ferroptosis-related molecular patterns, and analyzed the sensitivity to ferroptosis and the state of immune escape between different molecular pattern groups. The single-sample gene set enrichment analysis (ssGSEA) algorithm was used to quantify the phenotypes of ferroptosis-related molecular patterns in individual patients. HL-60 and THP-1 cells were treated with ferroptosis inducer RSL3 to verify the therapeutic value of targeted inhibition of *GPX4*.

Results: Three ferroptosis-related molecular patterns and progressively worsening phenotypes including immune activation, immune exclusion and immunosuppression were found with the two different sequencing approaches. The FSscore we constructed can quantify the development of ferroptosis-related phenotypes in individual patients. The higher the FSscore is, the worse the patient's prognosis. The FSscore is also highly positively correlated with pathological conditions such as inflammation development, immune escape, lipid metabolism, immunotherapy resistance, and chemotherapy resistance and is negatively correlated with tumor mutation

10.3389/fonc.2022.888570

burden. Moreover, RSL3 can induce ferroptosis of AML cells by reducing the protein level of *GPX4*.

Conclusions: This study revealed the characteristics of immunity, inflammation, and lipid metabolism in the TME of different AML patients and differences in the sensitivity of tumor cells to ferroptosis. The FSscore can be used as a biomarker to provide a reference for the clinical evaluation of the pathological characteristics of AML patients and the design of personalized treatment plans. And *GPX4* is a potential target for AML treatment.

KEYWORDS

ferroptosis, tumor microenvironment, immune escape, inflammatory development, lipid metabolism, acute myeloid leukemia

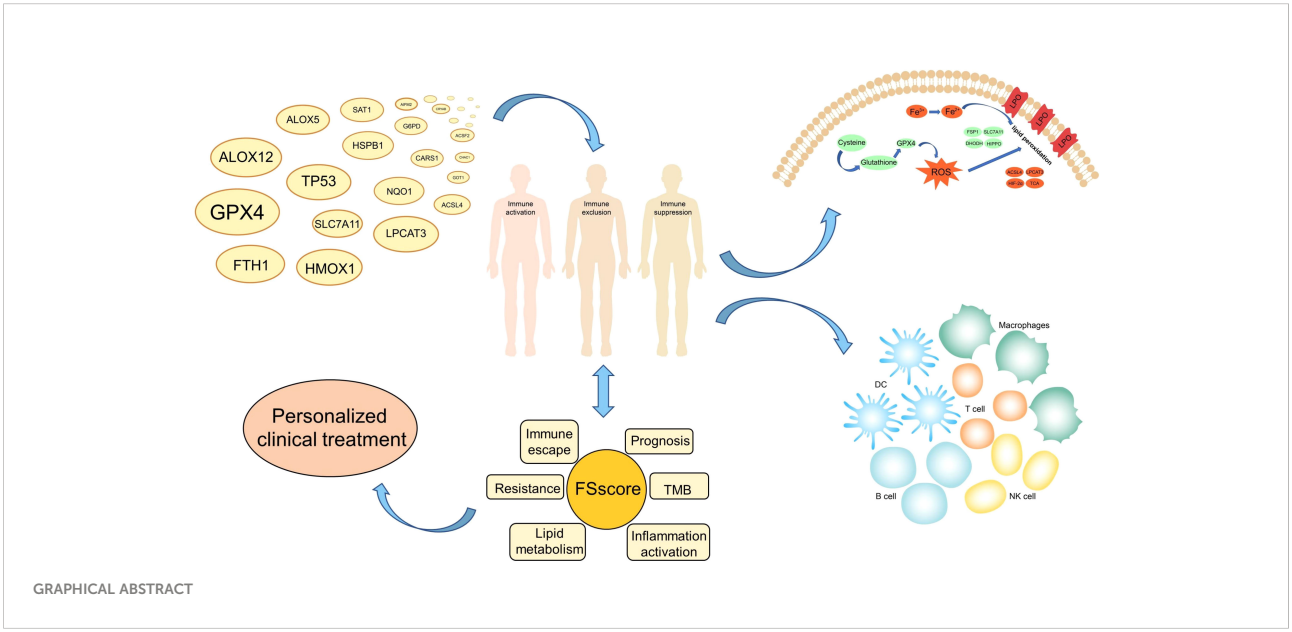

GRAPHICAL ABSTRACT

Introduction

Cell death is important for maintaining the normal growth and development of living organisms and for maintaining homeostasis. The classic cell death modes include apoptosis, autophagy and necrosis (1). In 2012, Dixon et al. proposed a new type of iron-dependent programmed cell death induced by erastin and RSL3 and other small molecules, called ferroptosis, which is mainly characterized by the generation of reactive oxygen species (ROS), lipid peroxidation and iron accumulation (2). When a specific small molecule compound interacts with a specific target in the cell, it will cause the reduction in antioxidants such as glutathione (GSH) and glutathione peroxidase 4 (*GPX4*), and the antioxidant capacity of the cell will be weakened. In addition to a large amount of ROS accumulation, under the synergistic effect of iron, lipid peroxidation of the cell membrane induces ferroptosis (3, 4). Ferroptosis is involved in many inflammatory and immune diseases and cancers (5–7). It has potential clinical value to treat diseases by using regulators that affect the occurrence of ferroptosis. Acute myeloid leukemia (AML) is the most common hematological malignant tumor. The pathogenesis mechanism is still unclear. An increasing number of studies have revealed the relationship between ferroptosis and AML. For example, ferroptosis plays an important role in the differentiation of AML induced by ATPR (8), dihydroartemisinin (DHA) induces ferroptosis of AML cells through autophagy-dependent degradation of ferritin (9), and erastin increases the sensitivity of AML cells to chemotherapy by inducing ferroptosis (10). These studies suggest that the induction of ferroptosis has potential therapeutic value for AML.

The sensitivity of cells to ferroptosis is closely related to lipid metabolism, which induces ferroptosis through lethal lipid peroxides (LPOs) accumulated by lipid peroxidation (11). There are many types of lipids, and their biological functions are quite different. The synthesis and metabolism of lipids are

precisely regulated. However, in the process of ferroptosis, polyunsaturated fatty acids (PUFAs), such as linoleic acid (LA), linolenic acid (LNA) and arachidonic acid (AA), play an important role (12); AA is particularly important, as it is very prone to peroxidation and can be oxidized to LPO (11, 13). GSH, ferroptosis suppressor protein 1 (FSP1), cystine/glutamate antiporter (system XC^-), and *GPX4* play an important regulatory role in the mechanisms that protect cells from ferroptosis caused by oxidative stress (14–17). These characteristics all indicate that the occurrence of ferroptosis is related to complex metabolic regulation, and the destruction of cellular redox homeostasis is one of the most critical factors.

How ferroptosis is regulated by immune cells and the relationship between ferroptosis induction therapy and antitumor immunity are worthy of in-depth research and discussion. The immune system includes innate immunity and adaptive immunity (18). The effect of ferroptosis on the immune system is mainly reflected in the impact on the number and function of immune cells, as well as the specific reaction and inflammatory reaction produced by immune cells after the occurrence of ferroptosis (19). In addition to tumor cells, the tumor microenvironment (TME) is also rich in a large number of immune cells, including T cells, B cells, monocytes, macrophages, dendritic cells (DCs), natural killer (NK) cells, neutrophils and myeloid-derived suppressor cells (MDSCs) (20). Many studies have revealed the relationship between ferroptosis and immune cells. For example, *TLR2* on macrophages eliminates ferroptotic cells by recognizing phosphatidylethanolamines on ferroptotic cells (21), neutrophils maintain the inflammatory response that occurs after ferroptosis in related tissues (22), and CD8+ T cells kill cancer cells by stimulating ferroptosis (23), indicating that ferroptosis plays an important role in antitumor immunity.

Ferroptosis is more likely than apoptosis to trigger an inflammatory response. For example, ferroptotic cells express more phosphatidylserine on the plasma membrane to release "eat me" signals to induce macrophage aggregation (24). The occurrence and development of inflammation is a double-edged sword in antitumor immunity (25). Acute inflammation is conducive to the protective immunity activated in anticancer therapy, while chronic inflammation provides a favorable environment for tumor cell proliferation and immune escape. Studies have shown that cancer cells evade the immune system by producing a large number of cytokines and chemokines that inhibit immune cells. For example, in patients with melanoma, pancreatic cancer, and colorectal cancer (26–28), the expression levels of the immunosuppressive cytokines *IL-10* and *TGF-β* are significantly higher than the expression levels of the immunostimulatory cytokines *IL-2*, *IL-12* and *IFN-γ*. The predominant expression of immunosuppressive cytokines causes the TME to adopt an immunosuppressive state, which in turn helps cancer cells escape immunity (29). In the blood system, the activation of inflammatory signals in hematopoietic cells and the hematopoietic niche can significantly change the connection between hematopoietic cells and their microenvironment (30). The high expression of TNF-α, *IL-6*, *TGF-β*, *IL-8* and other proinflammatory cytokines in the bone marrow can lead to negative bone marrow hematopoietic function (31, 32). A study showed that inflammation-related cytokines inhibit the proliferation of normal progenitor cells, significantly promote the growth and survival of AML cells and are not affected by the mutation status of AML cells. The abnormal expression of cytokines creates a favorable TME for AML (33).

In summary, the occurrence of ferroptosis is closely related to biological behaviors such as the immune response, inflammation development, and lipid metabolism. However, there are few research reports on the relationship between ferroptosis and the occurrence and development of AML. As a blood tumor, AML is complicated by bone marrow cell proliferation, and changes in immune and inflammatory responses occur in the peripheral blood microenvironment at all times. Therefore, a comprehensive understanding of the TME characteristics related to ferroptosis will help us improve our understanding of the abnormal hematopoietic microenvironment of AML and provide insights for clinical diagnosis, treatment and prognostic evaluation. In this study, we integrated the genome information of 992 AML specimens, including expression profile chip data and high-throughput sequencing data, and comprehensively analyzed the characteristics of immune cell infiltration, lipid metabolism, and inflammation development in the TME of AML patients. We divided patient transcriptome data into a gene chip group (GEO group) and a high-throughput sequencing group (TCGA group). Both sets of data revealed three different ferroptosis-related phenotypes in AML patients and deeply reflected that immune escape and inflammation development in AML patients gradually worsened. To better evaluate the development of ferroptosis-related phenotypes in individual patients, we constructed a gene signature (FSscore) to quantify these phenotypes. The FSscore not only reflects the TME status of AML patients but also accurately evaluates the pathological characteristics of AML patients, such as prognosis, immunotherapy, and drug resistance. Finally, we experimentally confirmed that GPX4 is a potential target for AML treatment.

Methods

Data acquisition and preprocessing

The workflow of this project was shown in Figure S1. This study included 992 AML samples containing clinical survival information and 337 healthy control samples, including samples from six GEO (Gene-Expression Omnibus) cohorts (GSE10358, GSE12417-GPL96, GSE12417-GPL570, GSE37642, GSE71014, GSE146173), The Cancer Genome Atlas-Acute Myeloid Leukemia (TCGA-LAML) cohort, and the Genome Tissue Expression (GTEx)-whole blood cohort. For the GEO cohorts of the affymetrix

platform was used, after downloading the original "CEL" file of the microarray data, we used the robust multiarray averaging (RMA) method with the "affy" package for standardization. For the microarray data of other platforms, we downloaded the normalized matrix file. For high-throughput sequencing data, we transformed the raw data into transcripts per kilobase million (TPM) values. Then, we used the combat algorithm with the "sva" package to perform batch correction on all microarray data. The normalized RNA-seq data (RSEM tpm) of the TCGA-LAML and GTEx whole blood datasets were downloaded from the UCSC XENA database (https://xenabrowser.net/datapages/). Somatic mutation data and gene copy number data were downloaded from the TCGA database (https://portal.gdc.cancer.gov/), Tumor mutation burden (TMB) calculation method: TMB = (total count of variants)/(the whole length of exons). All data were analyzed using R x64 4.1.0 and related R Bioconductor packages, and the data information is shown in Table S1. Sixty ferroptosis-related genes (FRGs) were retrieved from previous literature records (34) and are summarized in Table S2.

Unsupervised clustering for FRGs

We used the consensus clustering algorithm *via* the "ConsensusClusterPlus" package to perform unsupervised cluster analysis on the mRNA expression of 60 FRGs (35) and performed 1000 repetitions to ensure the stability of classification, which was also verified by t-distributed stochastic neighbor embedding (t-SNE).

Pathway enrichment analysis, functional annotation and protein–protein interaction (PPI) network analysis

Gene set variation analysis (GSVA) can quantify the activity of biological processes and signal pathways in different samples based on the expression of genes in the data set (36). We performed GSVA analysis on the "c2.cp.kegg.v2.2.symbols" gene set downloaded from the MSigDB database (37). An adjusted P value < 0.05 was regarded as statistically significant to analyze the biological behavior differences in ferroptosis-related molecular patterns. For ferroptosis-related genes and ferroptosis-related phenotype genes, we used the "clusterProfiler" package for functional annotation and uploaded them to the STRING database (https://string-db.org) to obtain their PPI network.

Evaluation of TME immune cell infiltration level

The CIBERSORT algorithm is based on the support vector regression method to infer the proportions of various immune cells from the mixed cells of the tumor sample (38). We used an algorithm based on LM22 gene signatures to evaluate the infiltration level of immune cells such as B cells, T cells, NK cells and macrophages.

Identification of ferroptosis-related phenotype genes

To better identify ferroptosis-related phenotypes, we adopted the empirical Bayesian approach through the "LIMMA" package to analyze the difference in gene expression between different ferroptosis-related molecular patterns (39). An adjusted P value <0.05 was used as the significance standard to determine differentially expressed genes (DEGs). The genes after the intersection of DEGs of different FRG cluster subtypes were defined as ferroptosis-related phenotype genes.

Dimension reduction and construction of ferroptosis-related phenotype gene signatures

We tried to quantify ferroptosis-related phenotypes to better assess the degree of tumor development in AML patients. First, the ferroptosis-related phenotype genes identified by the GEO group and TCGA group were intersected, and a total of 317 overlapping genes were screened. We considered these genes to be ferroptosis-related phenotype signature genes. The phenotypic genes related to the prognosis of AML patients in the GEO group and TCGA group were further screened for dimension reduction and defined as the ferroptosis-related phenotype gene set. Single-sample gene set enrichment analysis (ssGSEA) can calculate the ferroptosis-related phenotype gene set enrichment score of individual samples, indicating the degree to which these genes are synergistically upregulated or downregulated in the sample, and the degree of development of ferroptosis-related phenotypes is positively correlated with the overall expression levels of these genes. Therefore, we used ferroptosis-related phenotype gene set enrichment scores, collectively named the FSscore, to quantify ferroptosis-related phenotypes.

Correlation analysis of ferroptosis-related molecular patterns and other biological characteristics, such as immune escape, lipid metabolism, and inflammation development

To explore the sensitivity of different molecular patterns to the occurrence of ferroptosis, we collected lipid metabolism-related signaling pathways and other gene sets that have been

confirmed to be related to ferroptosis through the MSigDB database. To determine the degree of immune escape and inflammation development of molecular patterns with different phenotypes, we used a series of gene sets designed by Mariathasan et al. (40), including immune checkpoint, angiogenesis, nucleotide excision repair, DNA damage repair, mismatch repair gene sets and gene sets related to cell adhesion, tumor angiogenesis, and inflammatory response signaling pathways from the MSigDB database. MDSCs are closely related to tumor immune escape (41). From the study of Charoentong et al., we obtained the marker genes of MDSCs (42). Finally, we used the tumor immune dysfunction and exclusion (TIDE) website (http://tide.dfci.harvard.edu/) to predict the TIDE score of samples with different ferroptosis-related phenotypes to verify the immune escape level (43).

Immune checkpoint blockade response, drug sensitivity prediction, and small molecule drug screening

We collected the genomic and clinical information of two immunotherapy groups: an anti-PD-L1-treated advanced urothelial cancer cohort (IMvigor210) (40) and an anti-PD-1-treated metastatic melanoma cohort (GSE78220) (44). The gene expression data of the two cohorts were transformed to TPM values. The Genomics of Drug Sensitivity in Cancer (GDSC; https://www.cancerrxgene.org/) database was used to predict the sensitivity of all patients to 138 chemotherapy drugs, and the "pRRophetic" package was used to calculate the value of half-maximal inhibitory concentration (IC50) (45, 46). Then, we uploaded the genes that were upregulated and downregulated in immunosuppression phenotypes to the CMap database (47) and used the mode-of-action (MoA) analysis function of the website to predict the potential small molecule drugs to regulate ferroptosis-related phenotypes and targets to induce therapeutic effects.

In vitro assays

Human AML cell lines HL-60 and THP-1 were cultured in RPMI1640 medium containing 10% fetal bovine serum and 1% penicillin-streptomycin at 37°C and 5% CO2. Cell counting Kit (CCK-8) (Bioss, BA00208, USA) was used to evaluate cell viability. The cells were inoculated into 96 well flat bottom microtiter plates with a density of 20000 cells per well, and then treated with different concentrations of RSL3 or (and) ferrostatin-1 for 48 hours. After that, 10 μl CCK-8 reagent was added to each well and incubated at 37 °C for 2.5 h. The absorbance of the cells at 450 nm was measured by microplate reader. Western blot analysis was used to detect the expression of GPX4. Antibodies used were rabbit anti-GAPDH (1: 1000, #5174) from Cell Signaling Technology (Danvers, MA, USA) and anti-GPX4 (1:1000, T56959) from Abmart (Shanghai, China).

Statistical analysis

The Wilcoxon rank-sum test and Kruskal–Wallis test were used to determine the difference between two groups and multiple groups, respectively. The "survminer" package was used to determine the cutoff point of various scores and divide patients into high and low groups. The log rank test was used to determine the significance of Kaplan–Meier survival analysis. Univariate Cox regression analysis was used to calculate the hazard ratios (HRs). Multivariate Cox regression analyses further determined independent prognostic factors. The "forestplot" package was used for univariate and multivariate independent prognostic analysis. The specificity and sensitivity of the FSscore were evaluated by receiver operating characteristic (ROC) curve analysis, and the "pROC" package was further used to determine the area under the curve (AUC). The "maftools" package was used to show the characteristics of somatic mutations in TCGA-LAML patients. The chromosomal location where the copy number variation in FRGs occurred was described with the "RCircos" package. A two-sided p value < 0.05 was considered to indicate statistical significance.

Results

Variation landscape of FRGs in AML

The phenotype of organisms is mainly regulated by gene expression, and the occurrence of ferroptosis is no exception. To explore the relationship between ferroptosis and AML, we first analyzed the genetic characteristics of FRGs in AML cells. Based on the transcriptome sequencing data of tumor samples and normal blood samples from AML patients, we observed that most FRGs were upregulated in AML (Figure 1A). The high expression of these genes may play an important role in the occurrence and development of AML. We further analyzed the copy number variation (CNV) frequency of FRGs in AML patients, and 27 genes had copy number gain or loss. High expression of *PTGS2, TFRC, HSPB1, SQLE, RPL8, NCOA4, FADS2, KEAP1*, and *SLC1A5* may be related to an increase in CNV frequency (Figure 1B). Figure 1C shows the location of FRGs on the chromosome where CNVs occurred. The occurrence of leukemia is closely related to gene mutations, and we summarized the somatic mutations of FRGs. Among 134 samples, 17 had gene mutations, and TP53 had the highest mutation frequency (Figure 1D). To better explore the interaction between these genes, we further analyzed the

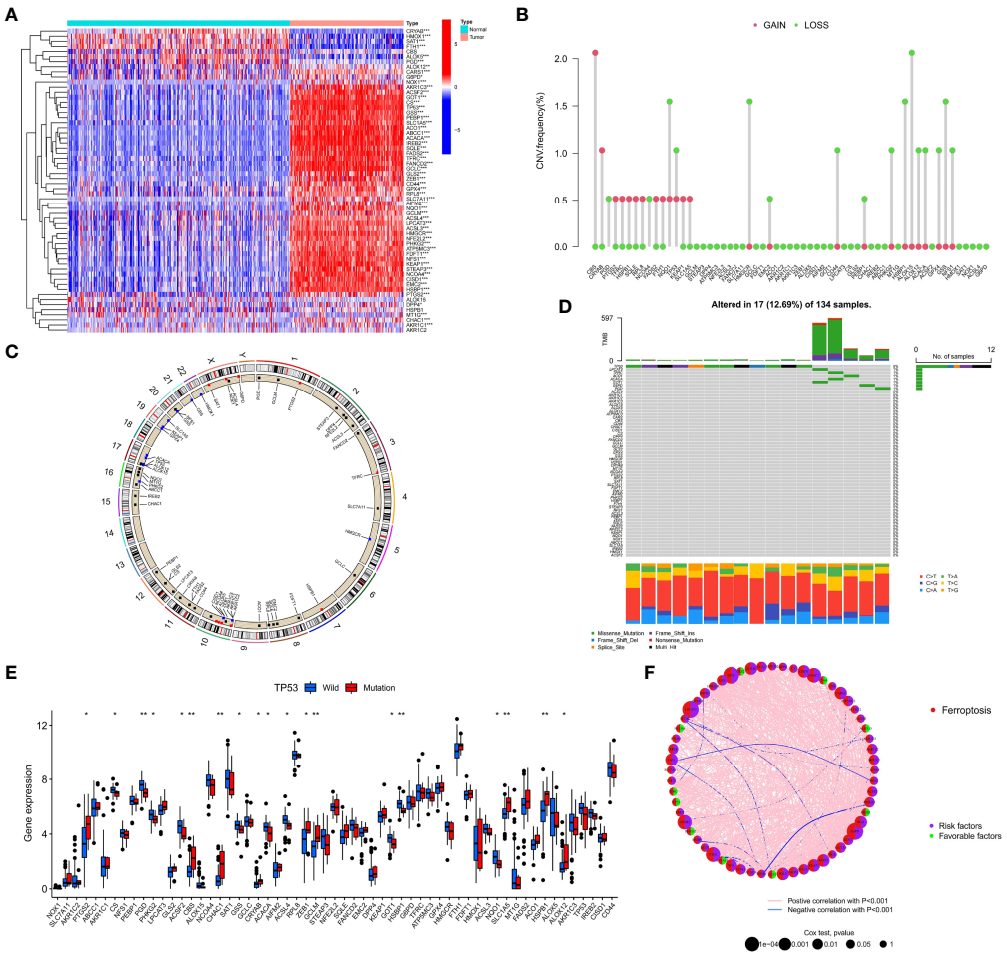

FIGURE 1
Genetic characteristics of FRGs in AML patients. **(A)** The heatmap depicts the difference in the expression of 60 FRGs in AML samples and normal samples. Wilcoxon test, *P < 0.05; **P < 0.01; *P < 0.001. **(B)** CNV frequency of FRGs in the TCGA cohort. **(C)** The position of FRGs on 23 chromosomes where CNV occurred in the TCGA cohort. **(D)** Somatic mutations of 60 FRGs in 134 TCGA-LAML patients. Each column in the waterfall diagram represents the mutation type of each patient, the upper part shows the TMB of each patient, and the right side shows the mutation frequency and mutation type ratio of FRGs. The ratio of different base transitions is shown below. **(E)** The expression of 60 FRGs in *TP53* mutation-type patients and wild-type patients, Wilcoxon test, *P < 0.05; **P < 0.01. **(F)** The interaction of FRGs in AML patients and its relationship with prognosis. Spearman correlation analysis was used to calculate the correlation between FRGs; p<0.001 indicates correlation, pink lines represent a positive correlation, and blue lines represent a negative correlation. Univariate Cox regression analysis was used to calculate the HRs to identify the relationship between FRG expression and prognosis. HR<1: Favorable factors for prognosis, indicated by a green semicircle. HR>1: Risk factors for prognosis, indicated by a purple semicircle. The size of the circle indicates the degree of association between the gene and the prognosis. The larger the circle is, the stronger the association with the prognosis.

difference in the expression of FRGs between *TP53* mutation-type and wild-type patients, the correlations among FRG expression levels, and the prognostic value of FRGs in AML patients. The results showed that compared with that in the *TP53* wild-type patient group, the expression of 9 FRGs, such as *PTGS2*, was upregulated in the mutant patient group, and the expression of 10 FRGs, such as *PGD*, was downregulated (Figure 1E). Correlation analysis showed that the expression levels of most FRGs were positively correlated; for example, *TP53* expression was positively correlated with the expression of other FRGs (Figure 1F and Table S3). Univariate Cox regression analysis showed that 10 FRGs such as *TP53* and *PHKG2*, were favorable factors in terms of the prognosis of AML (Figure 1F and Table S4). High expression of these genes indicated a better prognosis for AML patients. The remaining FRGs were risk factors. The mutation of *TP53* in AML often indicates a poor prognosis, poor cytogenetic risk and immunosuppression (48, 49). In connection with the differential expression of FRGs in AML and normal samples, we observed that *PTGS2, CBS, CHAC1, GCLM, SLC1A5, HSPB1*, and *ALOX12* were highly expressed in AML samples and patients with *TP53* mutations and also showed significant positive correlations in terms of

expression levels, indicating that they are also risk factors in terms of the prognosis of AML patients.

Based on the above results, we observed that the genetic changes in FRGs in AML samples versus normal samples, including gene structure, number, and expression, were highly heterogeneous, indicating that FRGs may have a profound impact on the occurrence and development of AML.

Identification of ferroptosis-related molecular patterns and analysis of their biological characteristics

To further analyze the influence of FRGs on the biological functions of AML, we first performed Kyoto Encyclopedia of Genes and Genomes (KEGG) enrichment analysis and found that these genes are involved in many signaling pathways related to lipid metabolism, energy metabolism and ferroptosis (Figure S2A). The PPI network also shows that FRGs have complex interactions at the protein level (Figure S2B). The high correlation between FRGs at the mRNA and protein expression levels indicates that the combined effect of these genes may have an important impact on the biological process of AML. Therefore, we performed unsupervised clustering based on the expression of FRGs in the TCGA cohort. The clustering results showed that AML patients in the TCGA cohort were divided into three different molecular patterns, named TCGA.FScluster A-C (Figure S2C, and Table S5), and t-SNE verified the stability of the clustering results (Figure S2D). We observed that most of the FRGs in FScluster B were upregulated (Figure S2E). Survival analysis showed that TCGA.FSclusters A and C were related to a better prognosis, while TCGA.FScluster B was related to a worse prognosis (Figure 2A). To verify these clustering characteristics, we expanded the number of patients

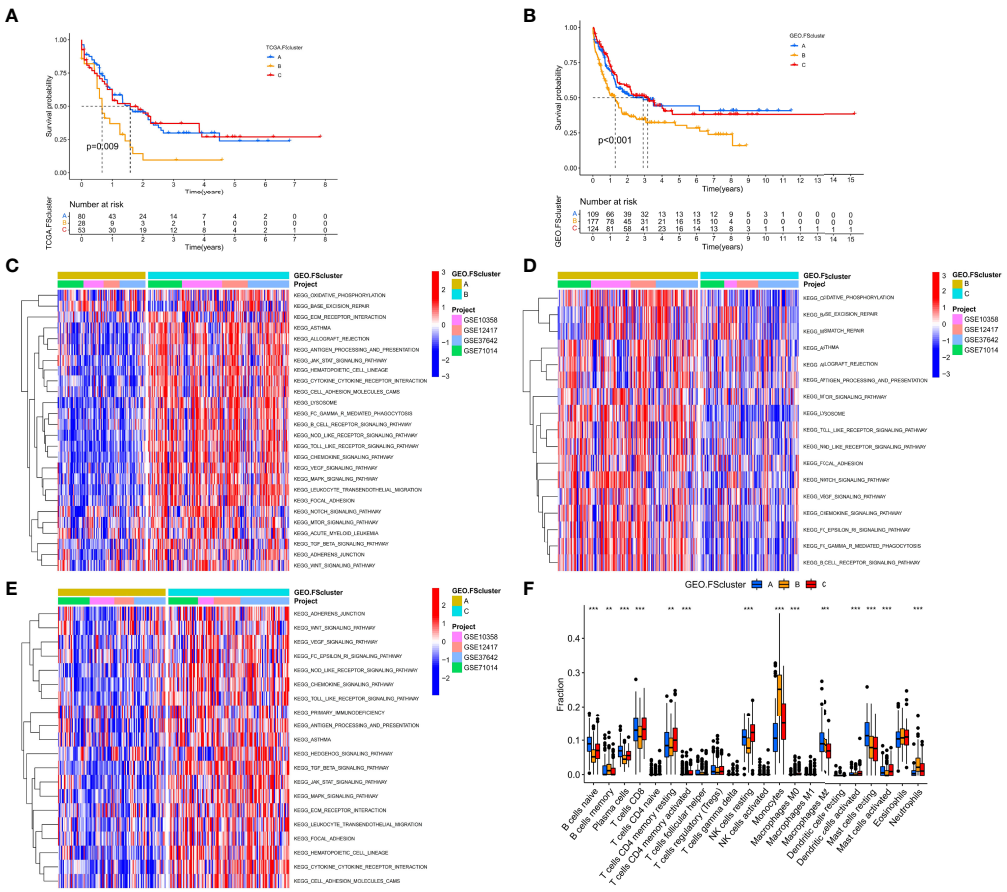

FIGURE 2
Survival analysis and biological characteristics analysis of ferroptosis-related molecular patterns. **(A)** Kaplan–Meier survival analysis of different ferroptosis-related molecular pattern groups in the TCGA cohort, log rank test. **(B)** Kaplan–Meier survival analysis of different ferroptosis-related molecular pattern groups in the GEO cohort, log rank test. **(C–E)** GSVA showed the activation levels of biological pathways in different ferroptosis-related molecular pattern groups in the GEO cohort. **(F)** The infiltration ratio of various TME cells in three ferroptosis-related molecular pattern groups in the GEO cohort, Kruskal–Wallis test, **P < 0.01; ***P < 0.001.

and performed the same analysis on the microarray data of AML patients in the GEO database. Since GSE146173 contains high-throughput sequencing data, expression data for some of the FRGs is missing in GSE37642-GPL96. These two sets of data were used for verification. We merged only the remaining AML chip data (GSE12417-GPL570, GSE10358, GSE37642, GSE71014) for the GEO group. We clustered the GEO group and obtained three completely different subgroups, named GEO.FScluster A-C (Figures S2F, G and Table S6) and verified by t-SNE (Figure S2H). Survival analysis showed that patients in GEO.FScluster B had a worse prognosis, while patients in GEO.FSclusters A and C had a better prognosis (Figure 2B).

We further analyzed the biological characteristics of the molecular patterns. GSVA showed that compared with FScluster A, FSclusters B and C were enriched a large number of inflammatory immune and cancer-promoting signaling pathways in both the TCGA group and the GEO group, and the enrichment degree of FScluster B was higher than that of FScluster C; the enriched pathways included the chemokine signaling pathway, cytokine–cytokine receptor interaction, the NOD-like receptor signaling pathway, the Toll-like receptor signaling pathway, the TGFβ signaling pathway, the JAK-STAT signaling pathway, cell adhesion and the MAPK signaling pathway (GEO group: Figures 2C–E and Table S7, TCGA group: Figures S3A–C and Table S8). In the past, inflammatory immune pathways were thought to be limited to immune cells activating immune responses, but an increasing number of studies have shown that TLRs, NLRs, chemokines and cytokines highly expressed by tumor cells can promote immune escape (32, 50, 51). Further analysis of TME cell infiltration showed that FSclusters A and C in the GEO group and TCGA group showed a large amount of innate immune cell infiltration, including NK cells, eosinophils, mast cells, dendritic cells and adaptive immune cells. Infiltrations included naïve B cells, CD8+ T cells, and resting memory CD4+ T cells (GEO group: Figure 2F and Table S9, TCGA group: Figure S3D and Table S10). FScluster B showed increased infiltration of memory B cells, monocytes, M2 macrophages and neutrophils. Both FScluster A and C patients with immune activation showed a better prognosis, while the high infiltration of inflammatory cells in FScluster B indicated the deterioration of the tumor's inflammatory microenvironment and the suppression of the patient's immune function, which are indicators of a poor prognosis.

Analysis of the sensitivity of different molecular patterns to the occurrence of ferroptosis

To explore the relationship between tumor cells and ferroptosis in AML patients with different TMEs and prognostic status, we further analyzed various factors that affect the occurrence of ferroptosis. The occurrence of ferroptosis is often accompanied by abnormal lipid metabolism. We examined the characteristics of lipid metabolism among different ferroptosis-related molecular pattern groups. In the GEO and TCGA cohorts, we observed that FScluster B had the strongest lipid metabolism, while FScluster A had the weakest lipid metabolism (GEO group: Figures S4A–C and Table S11, TCGA group: Figures S5A–C and Table S12). We conducted in-depth analysis on the GEO group with a larger number of patients and found that the fatty acid metabolism, degradation, elongation signaling and unsaturated fatty acid biosynthesis signaling pathways were significantly activated in FSclusters A and B compared to FScluster C. The occurrence of ferroptosis depends on phospholipids containing polyunsaturated fatty acid chains (PUFA-PL). The biosynthesis of unsaturated fatty acids creates conditions for the occurrence of ferroptosis. Polyunsaturated fatty acids mainly include linoleic acid, linolenic acid and arachidonic acid. We also observed that the metabolism of linoleic acid and arachidonic acid was enhanced in FScluster C. Based on the results of GSVA, we further constructed four lipid metabolism scores for unsaturated fatty acid biosynthesis, linoleic acid metabolism, α-linolenic acid metabolism and arachidonic acid metabolism, and named them the BUFAscore, LAMscore, ALAMscore and AAMscore, respectively (Table S13). Kruskal–Wallis test results showed that BUFAscore was higher in FSclusters A and B, the AAMscore and LAMscore were higher in FScluster C, and the ALAMscore was only slightly upregulated in FScluster B (Figures 3A–D). These lipid metabolism characteristics indicate that FSclusters A and B may be more sensitive to the occurrence of ferroptosis. Taken together, the biological characteristics of each subtype indicate that the massive infiltration of immune cells in FScluster A may induce ferroptosis. Although FScluster B was represented by immunosuppression, the worsening of inflammation confers a hypoxic and ROS-enriched TME, which in turn promotes lipid peroxidation and increases the sensitivity of tumor cells containing high levels of unsaturated fatty acids to ferroptosis. We constructed a hypoxia score based on the enrichment analysis of the hypoxia signaling pathway (Table S13). The difference analysis showed that the hypoxia score was the highest in FScluster B (Figure 3E). This result verified our conjecture. In the above, we observed the activation of the tumor cell inflammatory immune pathway in FScluster C, which may promote the immune escape of tumor cells, prevent the occurrence of ferroptosis induced by immune cells, and a low degree of hypoxia in the weak inflammatory environment of FScluster C, so the tumor cells in FScluster C are more resistant to ferroptosis.

We also analyzed the relationship between BUFAscore and patient prognosis in each ferroptosis-related molecular pattern group. Patients with a high BUFAscore in FSclusters A and B had poor survival (Figures S6A, B). In FScluster C, patients with a high BUFAscore had better survival, but there was no significant difference (Figure S6C). Patients in FScluster B have

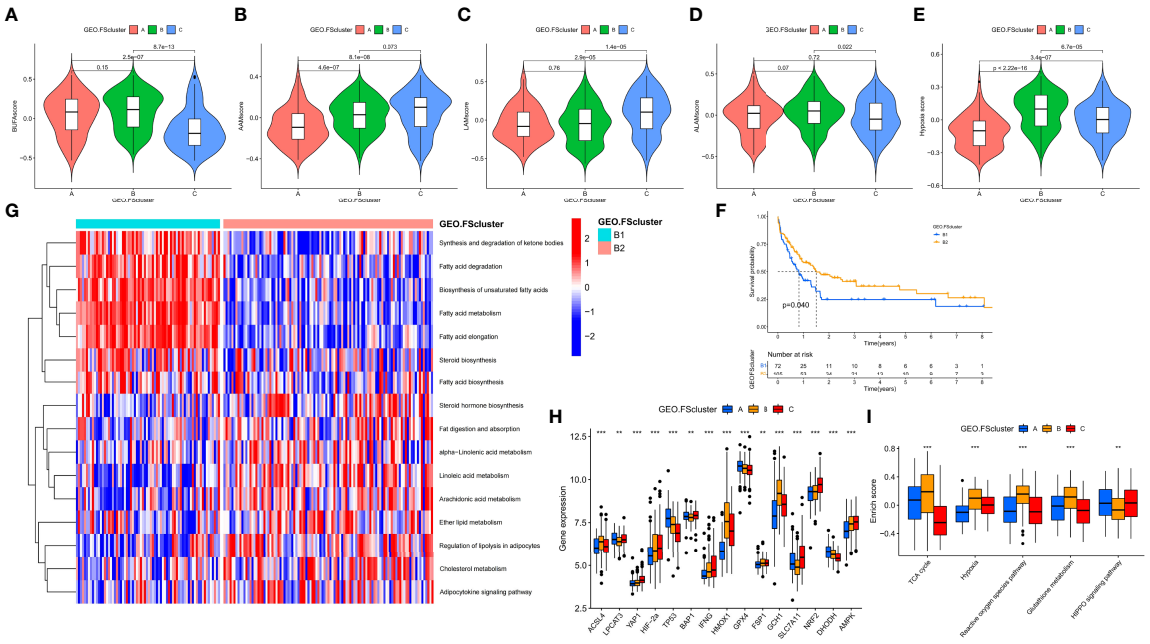

FIGURE 3
Analysis of the metabolic characteristics of unsaturated fatty acids in ferroptosis-related molecular patterns and other factors affecting ferroptosis. **(A–E)** Differences in BUFAscore, AAMscore, LAMscore, ALAMscore, and hypoxia score in different ferroptosis-related molecular pattern groups in the GEO cohort, Kruskal–Wallis test. **(F)** Kaplan–Meier survival analysis of different cluster subtypes in the FScluster B of the GEO group, log rank test. **(G)** GSVA showed the activation levels of lipid metabolism pathways in different cluster subtypes. FScluster B of the GEO group. **(H, I)** Differences in genes and signaling pathways that affect ferroptosis among different ferroptosis-related molecular patterns, Kruskal–Wallis test, **P < 0.01; ***P < 0.001.

poor prognostic characteristics, and we analyzed the relationship between lipid metabolism and prognosis in this molecular pattern. By unsupervised clustering of lipid metabolism signaling pathway enrichment scores, we further divided FScluster B into FSclusters B1 and B2 (Figures S6D, E). Survival analysis showed that patients in FScluster B1 had a worse prognosis (Figure 3F). Lipid metabolism pathway enrichment analysis showed that fatty acid metabolism and synthesis-related signaling pathways and unsaturated fatty acid biosynthesis signaling pathways were activated in FScluster B1, and unsaturated fatty acid metabolism signaling pathways, including linoleic acid, α-linolenic acid and arachidonic acid pathways, were significantly enriched in FScluster B (Figure 3G). These results indicate that with the deterioration of the TME in patients with AML, the tumor cells of patients with poor prognosis exhibit enhanced fatty acid metabolism and unsaturated fatty acid biosynthesis, and the enhanced metabolism of unsaturated fatty acids suggests a better prognosis for patients.

To better assess the propensity for the occurrence of ferroptosis between different molecular patterns, we summarized the genes and signaling pathways that promote and inhibit ferroptosis through existing research (5). *ACSL4, LPCAT3, YAP1, HIF-2α, TP53, BAP1, IFNG*, and *HOMOX1* and the TCA cycle, hypoxia, reactive oxygen signaling pathway and glutathione metabolism signaling pathways have been proven to promote the occurrence of ferroptosis. *GPX4, FSP1, GCH1, SLC7A11, NRF2, DHODH, AMPK* and the HIPPO signaling pathway have inhibitory effects. The results of the Kruskal–Wallis test showed that *ACSL4*, *HMOX1*, and *GCH1* were highly expressed in FScluster B, while FScluster A mainly showed high expression of ferroptosis inhibitory genes such as *GPX4* and DHODH. FScluster C was characterized by low expression of the ferroptosis-promoting genes *YAP1*, *HIF-2α*, and *IFNG*, and high expression of the ferroptosis-suppressor genes *SLC7A11, NRF2*, and AMPK (GEO group: Figure 3H, TCGA group: Figure S7A). The ferroptosis signaling pathway was highly activated in FScluster B, and the activity of inhibiting the ferroptosis signaling pathway was significantly reduced; the opposite was true for FSclusters A and C (GEO group: Figure 3I and Table S14, TCGA group: Figure S7B and Table S15). These results indicate that the expression of FRGs in ferroptosis-related molecular patterns is specific, and the connection between these genes and the relationship between these genes and ferroptosis in AML needs further discussion and research. However, ferroptosis-related pathways show a high degree of consistency. In cluster B, which was associated with the worst prognosis, the proferroptosis pathways were uniformly

activated, while the antiferroptosis pathways were inhibited. These findings combined with the characteristics of lipid metabolism indicate that tumors cells in FScluster B have a higher tendency to undergo ferroptosis than those in other clusters.

Phenotypic analysis of ferroptosis-related molecular patterns

To better identify and verify the phenotypes of the three ferroptosis-related molecular patterns, we first identified the DEGs shared between the molecular patterns. A total of 1883 and 1222 shared DEGs were identified in the GEO and TCGA groups, respectively (Figures S8A, B). In the GEO group and TCGA group, three different genomic subtypes were further identified through unsupervised clustering and were named GEO.geneCluster A-C and TCGA.geneCluster A-C (Figures S8C–F and Tables S5, S6). This indicates that there are indeed three molecular patterns in AML patients. We analyzed the biological and clinical characteristics of genomic subtypes. We found that the three genomic subtypes were very similar to the previously identified ferroptosis-related molecular patterns. In the GEO group, we observed that FScluster A and geneCluster A had a high degree of overlap. Some of the samples in FScluster B and in FScluster C constituted geneCluster C, and the remaining samples in FScluster B were classified into geneCluster B (Figure S9A). In the TCGA group, some samples in FScluster A corresponded to geneCluster A, some samples in FScluster C and FScluster B were in geneCluster B, and the remaining FScluster A and C samples formed geneCluster C (Figure S9B). These results seem to suggest that AML samples are divided into three biological states based on the nodes of two biological processes. Through survival analysis, it was found that in the GEO and TCGA groups, the patients with samples in geneCluster A had a better prognosis, and the patients with samples in geneCluster B and C had a worse prognosis; the patients with samples in geneCluster C were mostly derived from FScluster C but showed a worse prognosis (Figures S9C, D). We performed GSVA and TME cell infiltration analysis again on genomic subtypes, and the results showed similar biological characteristics to ferroptosis-related molecular patterns (Figures S10A–D, S11A–D). Samples in geneClusters A and C were characterized by a large number of infiltrating immune cells, and those in geneCluster B presented an immunosuppressive state and highly activated inflammation status. Samples in geneCluster C also showed enrichment of a large number of inflammatory and immune signaling pathways. Based on this, we reasonably hypothesized that the changes in the inflammatory microenvironment in geneCluster C versus geneCluster A promote further immune escape of tumor cells and that the cells in this cluster are different from solid tumor cells that can directly pass through the surrounding matrix to block the attack of immune cells. As a hematological tumor, AML creates favorable survival conditions by reshaping the bone marrow microenvironment. These changes may be reflected in the promotion of tumor angiogenesis and abnormal adhesion to the niche.

Subsequent analysis showed that AML cells in geneCluster C exhibited high expression of immune checkpoints, stimulated tumor angiogenesis, highly activated cell adhesion-related and inflammation-related signals, and more MDSC infiltration than cells characterized by other ferroptosis-related molecular patterns. These malignant changes were more obvious in the genomic subtypes (GEO group: Figures 4A, B and Table S16, TCGA group: Figures S12A, B and Table S17). These results show that compared with that in cells of geneCluster A, the AML TME in cells of geneCluster C was further deteriorated, the immune escape of AML cells was enhanced, and the expression level of DEGs shared between the ferroptosis-related molecular patterns was positively correlated with the immune and inflammatory microenvironment characteristics. Further unsupervised clustering rearranged AML patient samples and divided them into three more accurate phenotypes, which we defined as the following ferroptosis-related phenotypes: The immune activation phenotype, corresponding to FScluster A and geneCluster A, was characterized by innate immune cell and adaptive immune cell infiltration and the best patient prognosis. The immune exclusion phenotype, corresponding to FScluster C and geneCluster C, was characterized by innate and adaptive immune cell infiltration and an inflammatory microenvironment, and with the development of inflammation, immune escape increased; patient prognosis for this phenotype ranked second. The immunosuppression phenotype, corresponding to FScluster B and geneCluster B, was characterized by a high degree of inflammatory cell infiltration and inflammatory microenvironment development, with the strongest immune escape ability, and corresponded to the worst prognosis in patients. To verify the characteristics of immune escape of the three ferroptosis-related phenotypes, we analyzed a TCGA dataset, which included RNA-seq data, on the TIDE website. Through the differential analysis of the calculated TIDE scores, we found that among the ferroptosis-related molecular patterns and the genomic subtypes, cluster B had the highest score, cluster C scored second, and cluster A scored the lowest (Figures 4C, D). This result verified the immune escape characteristics of the ferroptosis-related phenotypes. We also calculated the difference in TIDE scores between FScluster C and geneCluster C and found that the TIDE score of FScluster C was higher (Figure 4E and Table S18). This is because some samples in FScluster C and some samples in FScluster A with better ferroptosis-related phenotypes constituted geneCluster C, so the overall biological status of patients with sample in geneCluster C was better than that of patients with samples in FScluster C, while the immune escape ability was weaker. Similarly, the immune escape ability of geneCluster A was also weaker than that of FScluster A (Figure 4F). These results can be explained by the distribution characteristics of AML patients with different phenotypes in each cluster.

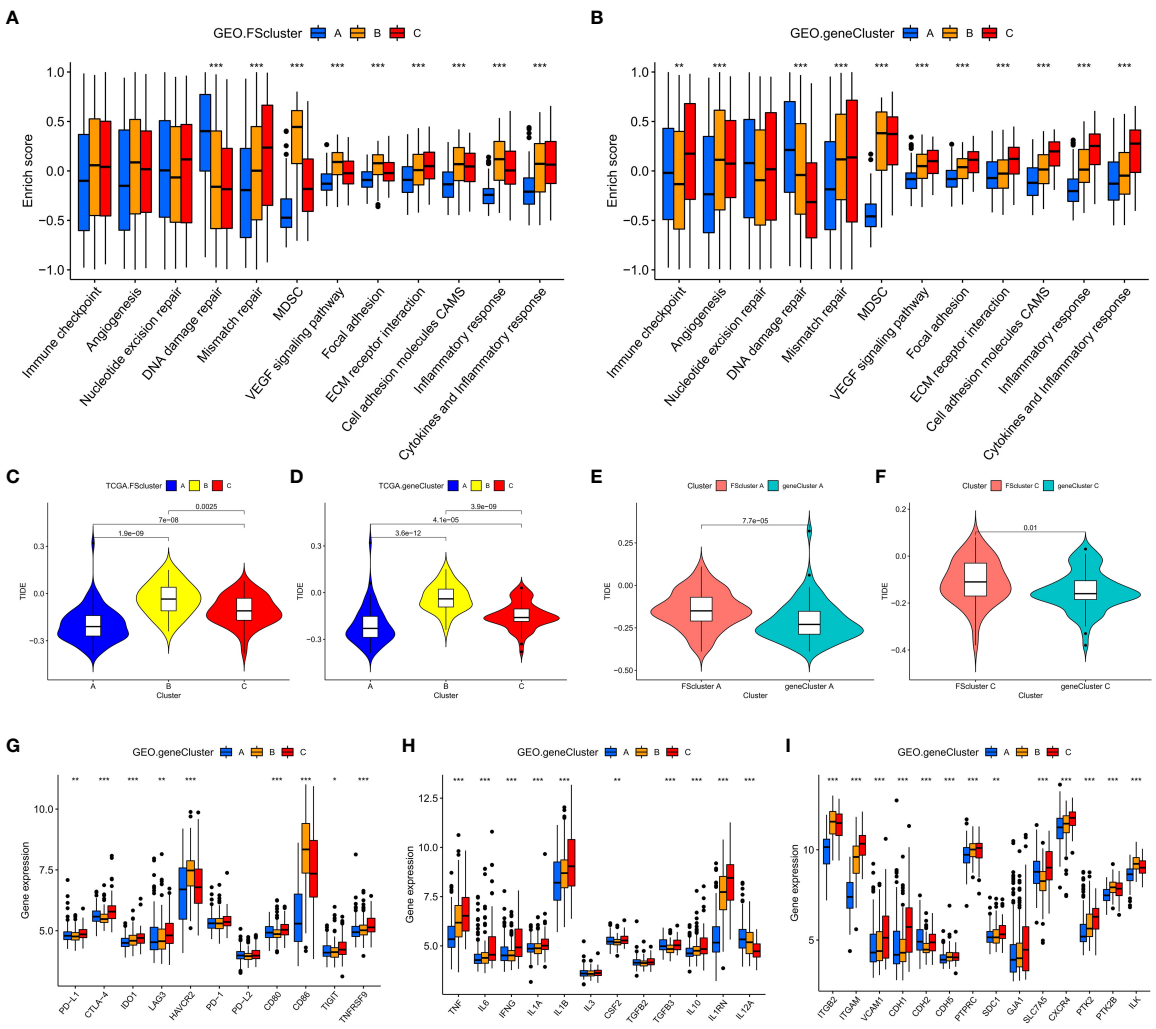

FIGURE 4
Analysis of TME characteristics associated with ferroptosis-related phenotypes. **(A, B)** Differences in pathway signatures related to tumor development and the infiltration level of MDSCs in the TME of ferroptosis-related molecular pattern and genomic subtype groups in the GEO cohort. **(C–F)** Differences in TIDE scores of ferroptosis-related molecular pattern and genomic subtype groups in the TCGA cohort. **(G–I)** Differences in gene signatures related to tumor development in the TME of ferroptosis-related molecular pattern and genomic subtype groups in the GEO cohort, G: Immune checkpoint-related genes, H: cytokines related to inflammation associated with AML, I: cell adhesion molecules associated with AML. Kruskal–Wallis test, *P < 0.05; **P < 0.01; ***P < 0.001.

Transcriptome characteristics of ferroptosis-related phenotypes

To further explore the relationship between ferroptosis-related phenotypes and immunity and inflammation. We analyzed the mRNA expression of related cytokines and chemokines in genomic subtypes. It has been reported in the literature that *PD-L1, CTLA-4, IDO1, LAG3, HAVCR2, PD-1, PD-L2, CD80, CD86, TIGIT* and *TNFRSF90* are considered immune checkpoint-related genes (40); *TNF, IL6, IFNG, IL1A, IL1B, IL3, CSF2, TGFB1, IL10, ILRN*, and *IL2A* are considered to be cytokines related to inflammation associated with AML (52); *TGFB2, ITGAM, VCAM1, CDH1, CDH2, CDH5, PTPRC, SDC1, GJA1, SLC7A5, CXCR4, PTK2, PTK2B*, and *ILK* are considered to be cell adhesion molecules associated with AML (53). We observed that genes related to immune checkpoints, inflammatory cytokines and cell adhesion molecules were highly expressed in geneClusters B and C (GEO group: Figures 4G–I, TCGA group: Figures S12C–E). These results once again indicate that there are indeed ferroptosis-related phenotypes with obvious immune and inflammatory characteristics in the occurrence and development of AML. Promoting inflammation development and cell adhesion-related signaling pathways and related genes are highly activated or highly expressed in tumor cells of patients with

an immune exclusion phenotype, because patients with this phenotype have more innate and adaptive immune cell infiltration in the TME, and tumor cells show high activity of these signaling pathways to avoid the attack of immune cells. Although these pathways are also obviously activated in AML cells of patients with an immunosuppression phenotype, their activation degree is lower than that in AML cells of the immune exclusion phenotype. This may be because immune cells with this phenotype are suppressed and there is a high degree of inflammation to promote immune escape. Therefore, there is no need to overactivate these signaling pathways or overexpress these genes.

Quantification of ferroptosis-related phenotypes and analysis of associated clinical characteristics

The ferroptosis-related phenotypes of AML patients indicate a pathological state that gradually deteriorates from immune activation to immune exclusion to immune suppression. However, the phenotype can only qualitatively assess patient stage. To better evaluate the tumor development of individual patients with AML, we used the ssGSEA method to calculate the enrichment score of the ferroptosis-related phenotype gene signatures to quantify the ferroptosis-related phenotypes with a metric named the FSscore. Gene ontology (GO) and KEGG analyses showed that these genes were closely related to immunity and inflammation (Figures 5A, B), and the PPI network also showed a high degree of interaction (Figure 5C). The Kruskal–Wallis test compared the differences in FSscore between different ferroptosis-related molecular patterns and between different genomic subtypes (Figures 5D–G). Patients with an immune activation phenotype had the lowest FSscore, followed by patients with an immune exclusion phenotype, and patients with an immunosuppression phenotype had the highest FSscore. Kaplan–Meier curve survival analysis was performed for AML patients divided into high FSscore and low FSscore groups based on the cutoff value identified by the survminer package. Among the GEO and TCGA groups, the prognosis of patients in the low FSscore group was significantly better than that of patients in the high FSscore group [GEO group, HR 3.178 (1.817-5.556); TCGA group, HR 3.533 (1.701-3.338)] (Figures 5H, I). ROC curve analysis showed that the FSscore can accurately predict the prognosis of AML patients (Figures 5J–K). The heatmap showed that the low FSscore group matched FScluster A and geneCluster A, and the high FSscore group corresponded to FScluster B-C and geneCluster B-C (Figures 6A, B). The alluvial diagram showed the differences in the attributes of individual patients (Figures 6C, D). These results shows that the FSscore can quantify the ferroptosis-related phenotypes of AML patients well.

Next, to further evaluate the ability of the FSscore to predict the prognosis of patients, we conducted an independent prognostic analysis of the FSscore together with other clinical characteristics of AML patients. Both univariate and multivariate independent prognostic analyses confirmed that the FSscore is an independent and reliable prognostic marker (Figures 6E, F). We verified the prognostic value of the FSscore in all independent cohorts of GEO group [GSE10358, HR 2.34 (0.80-6.86); GSE12417-GPL570, HR 2.60 (0.79-8.52); GSE37642, HR 2.81 (1.17-6.77); GSE71014, HR 6.93 (1.88-25.57)] (Figures S13A–D). We also verified the results in the other two sets of AML transcriptome data. Both chip data (GSE12427-GPL96, HR 0.97 (0.41-2.34)) and high-throughput sequencing data (GSE146173, HR 1.50 (0.67-3.39)) showed that patients with a high FSscore had a poorer prognosis than patients with a low FSscore (Figures S13E, F). Finally, we evaluated the prognostic value of the FSscore in 33 TCGA pancancer datasets including 10496 tumor samples. Although the analysis results showed some differences, the prognosis of patients in 12 TCGA tumor cohorts could be accurately predicted (Figure 6G). These results all show that the FSscore can be used as a good prognostic marker.

We also assessed the correlations among known signatures such as immune infiltration, lipid metabolism, inflammation and FSscore. The infiltration of monocytes, M2 macrophages, resting dendritic cells, and neutrophils showed a significant positive correlation with the FSscore, while the infiltration of B cells, T cells, mast cells, NK cells, and mast cells was negatively correlated with the FSscore (GEO group: Figure 6H, TCGA group: Figure S13G). The activity of most lipid metabolism pathways was positively correlated with the FSscore (GEO group: Figure 6I, TCGA group: Figure S13H). In the high FSscore group, pathways such as immune checkpoints, tumor angiogenesis, adhesion, and inflammation were activated, and MDSCs were highly infiltrated. In the low FSscore group, the activity of DNA damage repair signaling pathways was significantly increased (Figures 6J, K). These results clearly show that a low FSscore is closely related to immune activation, and a high FSscore is related to inflammatory cell infiltration, lipid metabolism activation, deterioration of the TME, and the enhanced immune escape ability of tumor cells through adhesion, which suggests a harsh TME. In summary, the FSscore can well assess the development status of ferroptosis-related phenotypes in AML patients and has profound guiding significance for judging the individual characteristics and clinical treatment outcomes of AML patients.

The relationship between clinicopathological factors, tumor somatic mutations and ferroptosis-related phenotypes in AML patients

The TCGA database has provided more comprehensive clinical annotations and somatic mutation data for AML patients. We further explored the relationship between

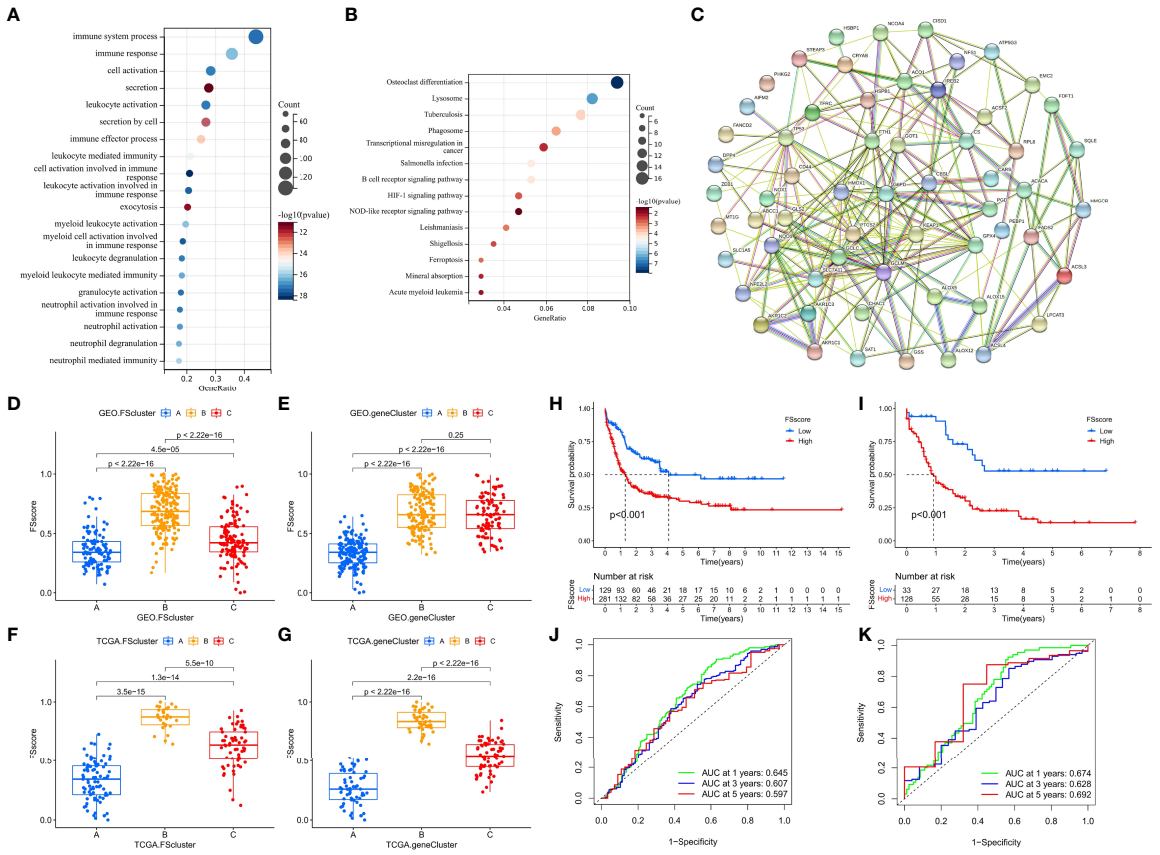

FIGURE 5
Analysis TME characteristics associated with ferroptosis-related phenotypes. **(A, B)** GO annotation and KEGG pathway enrichment analysis showed the functions of the ferroptosis-related phenotype signature genes. **(C)** PPI network of ferroptosis-related phenotype signature genes. **(D–G)** Differences in the FSscore of ferroptosis-related molecular patterns and genomic subtypes in GEO and TCGA groups, Kruskal–Wallis test. **(D–I)** Differences in the survival of patients in high and low FSscore groups in the GEO and TCGA cohorts, **(H)**: GEO group, **(I)**: TCGA group, log rank test. **(J, K)** The ROC curves showed the specificity and sensitivity of the FSscore; **(J)**: GEO group, **(K)**: TCGA group.

ferroptosis-related phenotypes and these clinical characteristics. Through Fisher's exact test, we analyzed the differences in clinicopathological factors between the high and low FSscore groups (Figure 7A and Table S19), among which cytogenetic risk, FAB classifications, and white blood cell (WBC) count were significantly different. The high FSscore group had more patients with poor cytogenetic risk, a high WBC count, and M4 and M5 classifications, while the low-risk group had a higher proportion of M1-M3 patients (Figures 7B–D). Based on the characteristics of ferroptosis-related phenotypes, we can understand these results well. The immune exclusion and immunosuppression phenotypes corresponding to a high FSscore are accompanied by higher inflammatory cell infiltration, which indicates a higher proportion of WBCs. For example, neutrophils, account for approximately 50-70% of the proportion of WBCs (54), and a high WBC count has been included as a poor prognostic factor for AML (55), so the high FSscore group showed a higher WBC count. Another validation cohort (GSE146173) also had abundant clinical information, and we observed that the high FSscore group showed the same characteristics (Figures S14A–D and Table S20).

Based on the poor cytogenetic risk of patients in the high FSscore group, we further analyzed the frequency and distribution of somatic mutations between the high and low FSscore groups in the TCGA group using the maftools package. As shown in Figures 7E, F, the overall gene mutation frequency of AML patients was not high. The low FSscore group had a lower percentage of mutated samples, and the gene mutation frequency was similar to the average expected value. The high FSscore group had a higher percentage of mutated samples. The mutation rate of the top 20 mutated genes ranged from 2%- 15%, and only a few samples in both groups showed high TMB. Spearman correlation analysis indicated that FSscore and TMB showed a significant negative correlation with each other (Figure 7G). Many studies have shown that high TMB in cancer is associated with a better prognosis (56, 57), which

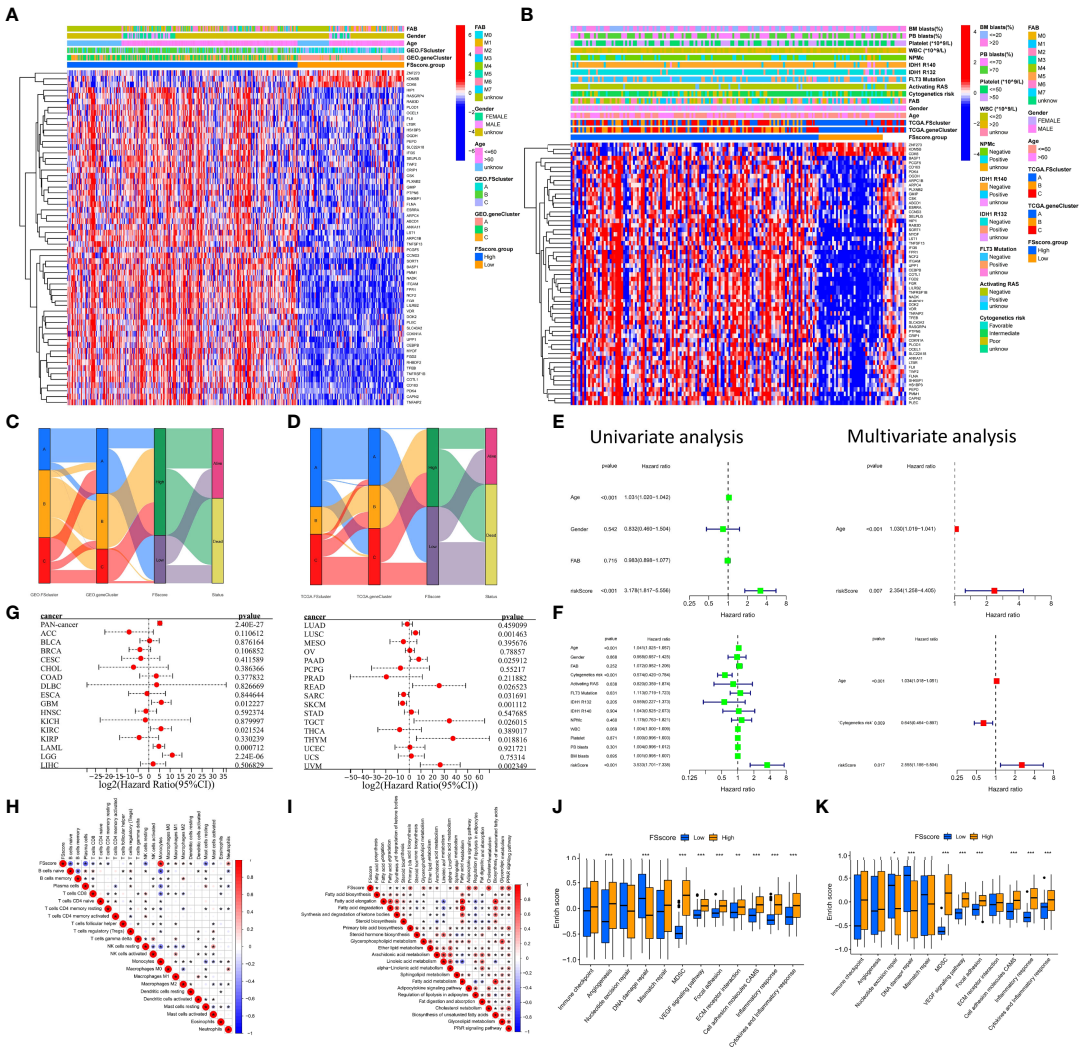

FIGURE 6
Distribution characteristics and prognostic value analysis of the FSscore, correlation analysis between characteristics of the TME and FSscore. **(A, B)** Differences in patient distribution, clinicopathological factors and phenotype signature gene expression of the high and low FSscore groups in the GEO and TCGA cohorts, the blank in the annotation of FSscore group in the TCGA cohort is due to the lack of clinical information of corresponding patients. **(C, D)** Alluvial diagram showing the changes in ferroptosis-related molecular patterns, genomic subtypes, FSscore and patient status. **(E, F)** Univariate and multivariate independent prognostic analysis of FSscore, E: GEO group, F: TCGA group. **(G)** Prognostic value of the FSscore in pancancer datasets. **(H)** Correlation analysis between the levels of TME cell infiltration and the FSscore in the GEO group. **(I)** Correlation analysis between levels of lipid metabolism and the FSscore in the GEO group. **(J, K)** Differences in pathway signatures related to tumor development and the infiltration level of MDSCs in the TME in the high and low FSscore groups. D: GEO group, E: TCGA group, Wilcoxon test. *P < 0.05; **P < 0.01, ***P < 0.001.

may be because tumor cells in patients with high TMB express more immunogens that are recognized by immune T cells and because anti-PD-1/PD-L1 treatment has a better effect in these patients. Therefore, we analyzed the relationship between FSscore and immunotherapy response in the two immune checkpoint inhibitor treatment cohorts (IMvigor210, GSE78220), and we observed that in the two cohorts, patients in the low FSscore group had a better prognosis and that the proportion of patients who responded to immunotherapy was higher (Figures 7H, I). This may indirectly prove that patients with a low FSscore have a high TMB and better response to immunotherapy. Moreover, we previously confirmed that the immune exclusion and immunosuppression phenotypes corresponding to a high FSscore are closely related to strong immune escape ability. We again quantitatively analyzed the difference in TIDE score between the high and low FSscore groups. The TIDE score was significantly higher in the high FSscore group (Figure 7J). Correlation analysis showed that the FSscore and TIDE score were highly positively correlated (Figure 7K). Finally, we explored the relationship between

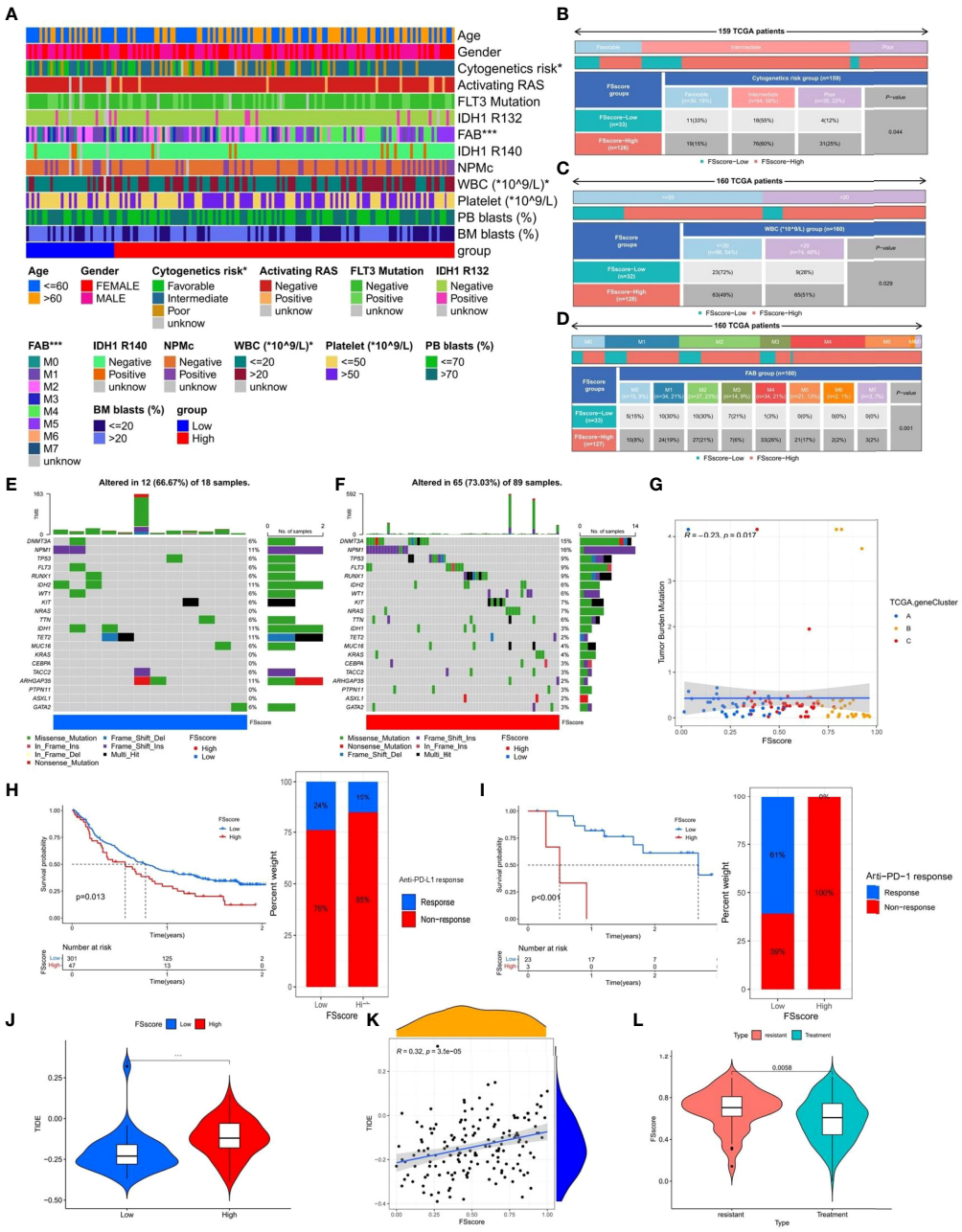

FIGURE 7
The relationship between clinicopathological factors, tumor somatic mutations, immunotherapy and FSscore. **(A–D)** Correlation analysis between clinicopathological factors and FSscore in the TCGA group, Fisher's exact test, *P < 0.05. **(E, F)** The characteristics of tumor somatic mutations in the high and low FS score groups of the TCGA group, WBC: white blood cell, PB: peripheral blood, BM: Bone marrow, IDH: isocitrate dehydrogenase, NPMc: nucleophosmin. **(G)** Correlation analysis between TMB and FSscore in the TCGA group. **(H, I)** Differences in survival of patients and the proportion of patients in high and low FSscore groups of immune checkpoint inhibitor treatment cohorts (H: IMvigor210, I: GSE78220), log rank test. **(J)** Differences in TIDE scores of the high and low FS score groups in the TCGA group. **(K)** Correlation analysis between TIDE score and FSscore in the TCGA group. **(L)** The difference in FSscore between drug-resistant and nonresistant patients. ***P < 0.001.

FSscore and chemotherapy resistance. In the GSE146173 cohort, we analyzed the difference in FSscore between drug-resistant and nonresistant patients, and the results showed that the FSscore of drug-resistant patients was significantly higher (Figure 7L). A high FSscore is accompanied by the enhanced ability of AML cells to adhere to the bone marrow niche, and it is easy to avoid the attack of chemotherapy drugs, which may be one of the reasons for the occurrence of drug resistance. The above results

indicate that the FSscore is closely related to clinical laboratory test indicators, somatic mutations, immunotherapy, immune escape, and drug resistance, which can facilitate clinical treatment decision making.

Sensitivity analysis of anticancer drugs and prediction of targeted small molecule drugs for ferroptosis-related phenotypes

Patients with a high FSscore may be accompanied by resistance to conventional chemotherapy drugs. Therefore, different clinical treatments are required for patients with different ferroptosis-related phenotypes. In the TCGA and GEO groups, we compared the sensitivity of patients with high and low FSscores to 138 anticancer drugs to assess potentially valuable treatment options. By using the pRRophetic package to predict the IC50 values of different AML patients after drug treatment based on RNA-seq data and performing differential analysis between high and low FSscore groups, we found that the sensitivity of the eight anticancer drugs [A.443654 (pan-AKT inhibitor), ABT.263 (navitoclax, Bcl-2 inhibitor), AG.014699 (rucaparib, PARP inhibitor), AKT inhibitor VIII, AP.24534 (Ponatinib, pan-BCR-ABL inhibitor), AS601245 (JNK inhibitor), AUY922 (luminespib, HSP90 inhibitor) and axitinib (VEGFR inhibitor)] were significantly different in the high and low FSscore groups of the GEO cohort (Figure S15A). The sensitivity of six anticancer drugs [ABT.263 (navitoclax, Bcl-2 inhibitor), AG.014699 (rucaparib, PARP inhibitor), AKT inhibitor VIII, AP.24534 (ponatinib, pan-BCR-ABL inhibitor), axitinib (VEGFR inhibitor), and AZ628 (Raf inhibitor) were significantly different in the high and low FSscore groups of the TCGA cohort (Figure S15B). Among them, five anticancer drugs (ABT.263, AG.014699, AKT inhibitor VIII, AP.24534, and axitinib) showed significant differences in treatment sensitivity in patients with high and low FSscores in the TCGA and GEO groups, and the IC50 values were higher in patients with high FSscores, indicating that these drugs are more appropriate for the treatment of patients with low FSscore; that is, patients with low FSscores may benefit from treatment with these drugs.

We further performed targeted small molecule drug prediction based on the gene signatures of ferroptosis-related phenotypes, selected highly expressed gene sets in immunosuppression phenotype as upregulated genes, and gene sets expressed at low levels as downregulated genes and uploaded them to the CMap database to analyze potential therapeutic drugs. With the predicted correlation P value < 0.05 as the standard, a total of 44 small molecule drugs and 29 corresponding drug mechanisms were identified (Figure S15C). The predicted candidate drugs and potential therapeutic effects can provide references for basic research and clinical trials.

GPX4 is a potential therapeutic target for AML

We observed that *GPP4* is highly expressed in AML patients and has the highest expression level in immunosuppressive phenotype, suggesting that *GPX4* may be a potential therapeutic target. Both in GEO group and TCGA group, the prognosis of patients with high expression of *GPX4* was significantly worse (Figures 8A, B). We further used RSL3, a targeted inhibitor of *GPX4*, in AML cell line HL-60 to explore the biological effects of inducing ferroptosis. Cell viability assay showed that RSL3 inhibited HL-60 cells and THP-1 cells in a dose-dependent manner (Figure 8C), and the addition of iron death inhibitor (ferrostatin-1) could partially save cell viability (Figure 8D). Western blot analysis showed that RSL3 could significantly reduce the expression of *GPX4* (Figure 8E), indicating that inhibiting *GPX4* could promote the death of HL-60 cells and THP-1 cells by inducing ferroptosis.

Discussion

AML, a hematological malignant tumor, has a high degree of heterogeneity. The complex and dynamic clonal architecture is the main reason for the refractoriness of AML (58–60). According to the FAB classification, patients can be divided into eight classifications (M0-M7) (61). AML is highly malignant, with a five-year survival rate of less than 30%, and is the most common leukemia among the elderly (62). Chemotherapy and hematopoietic stem cell transplantation (HSCT) are the most common treatments for AML (63), but drug resistance and recurrence lead to unsatisfactory treatment outcomes (64). Therefore, the development of new treatment methods to improve the effects of AML treatment has important clinical significance. As a new type of cell death mode, ferroptosis has a profound impact on the development and treatment of many diseases, especially cancers (65). Ferroptosis is closely related to the biological characteristics of the TME. Hypoxia induces the production of ROS, and the activation of lipid metabolism and the immune response create conditions for ferroptosis (66). These factors all show that tumor cells are prone to ferroptosis. Therefore, strategies for inducing ferroptosis in tumor cells and weakening the protective mechanism should have the most direct clinical value for cancer treatment, with the ultimate goal of promoting tumor cell death. In this study, we explored the genomic characteristics of FRGs in AML and their correlation with the TME and prognosis of AML patients and found that most FRGs showed high expression of mRNA levels and interactions at the protein level and were also were significantly related to the prognosis of patients. FRGs participate in many metabolic-related signaling pathways, and high expression of these FRGs may be one of the factors

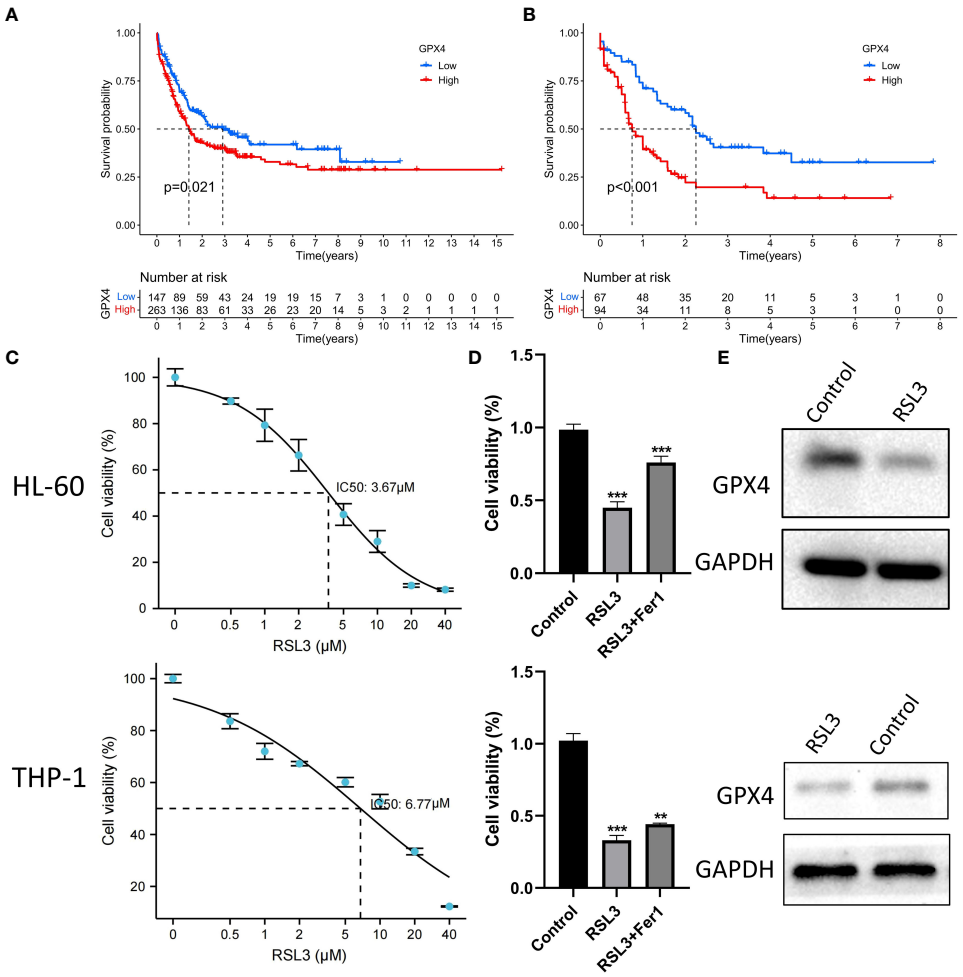

FIGURE 8
RSL3 inhibits growth of AML cells. **(A, B)** Differences in the survival of patients in high and low expression of GPX4 in the GEO and TCGA groups, A: GEO group, B: TCGA group, log rank test. **(C)** HL-60 cells and THP-1 cells were treated with RSL3 at the indicated doses for 48 h and cell viability was assayed using a CCK-8 kit. **(D)** HL-60 cells and THP-1 cell were treated with RSL3(HL-60: 5 μM; THP-1: 10μM) with or without ferrostatin-1 for 48 h and cell viability was assayed, ***P < 0.001. **(E)** Protein level of *GPX4* in HL-60 cells and THP-1 cells treated with RSL3 (HL-60: 5 μM; THP-1: 10μM) or control for 48 hours. **P < 0.01.

promoting the growth of AML tumor cells and the deterioration of the TME.

FRGs may also collaborate to induce more potent effects on AML. We observed three ferroptosis-related phenotypes in the ferroptosis-related molecular patterns and genomic subtypes; they were defined as the immune activation phenotype, immune exclusion phenotype, and immunosuppression phenotype. These phenotypes showed significant differences in characteristics such as immunity, inflammation, lipid metabolism, and prognosis and represented a progressively deteriorating pathological state. The occurrence of ferroptosis is closely related to biological factors such as immunity, inflammation, and metabolism. For example, the activation of immune cells, such as CD8+ T cells, through the secretion of INF-γ downregulates the expression of components of system XC^-, such as *SLC3A2* and *SLC7A11*, to inhibit the uptake of cystine by tumor cells, thereby promoting ferroptosis induced by the depletion of glutathione (67). Ferroptotic cancer cells containing immunogens can be recognized and engulfed by macrophages (21). Ferroptosis and inflammation are also complementary. The occurrence of ferroptosis increases the expression of *PTGS2* encoding *COX2* and further promotes the metabolism of AA to increase the secretion of inflammatory signal molecules (14); treatment of cells with the inflammatory cytokine TNF leads to continuous downregulation of *GPX4* to induce ferroptosis (68). Unsaturated fatty acids act as peroxidation substrates for ferroptosis and are also important regulators of inflammatory processes along with their metabolic enzymes (69). Samples with different ferroptosis-related phenotypes also showed different sensitivities to ferroptosis. For the immune activation phenotype, a large number of immune cells can promote the ferroptosis of tumor

cells through different induction methods; for the immunosuppression phenotype, the hypoxia of the TME increases the generation of ROS, and the high development of inflammation can also increase the sensitivity of tumor cells to ferroptosis; the immune exclusion phenotype is accompanied by immune escape and decreased inflammation, and the sensitivity to ferroptosis is relatively low. Moreover, the enrichment of unsaturated fatty acids in immune activation and immunosuppression phenotypes provides conditions for the occurrence of ferroptosis. Therefore, these results suggest that different methods can be used to induce ferroptosis in patients with different ferroptosis-related phenotypes. For patients with immune activation phenotype, we can induce ferroptosis in leukemia cells by stimulating immune cells such as CD8+ T cells to secrete more INF-γ, and inhibit the expression of ferroptosis inhibitors such as *GPX4* and *DHODH*. For immunosuppression phenotype, we can induce ferroptosis by targeting enhanced lipid peroxidation. For patients with immune exclusion phenotype, ferroptosis can be induced in leukemia cells by simultaneously activating the immune system and enhancing lipid peroxidation at the same time. These insights may provide new ideas for the treatment of drug resistance caused by clinical chemotherapy and targeted therapy.

In the subsequent analysis, we further analyzed the immune escape levels of the three ferroptosis phenotypes. Unlike solid tumors that can block the infiltration of immune cells through stromal cells to produce immune exclusion (70), AML, as a hematological tumor, can avoid the attack of immune cells through adhesion to the niche (71). The expression levels of immune checkpoints in patients with immune activation and immune suppression phenotypes are significantly higher, and the signaling pathways related to immune escape are significantly activated; they also show consistency in the transcriptome. In terms of the mechanism of promoting immune escape, tumor cells with an immune exclusion phenotype mainly prevent the infiltration of a large number of immune cells by increasing adhesion and promoting the release of inflammatory signals. On the other hand, tumor cells of the immune exclusion phenotype mainly exploit the worsening chronic inflammatory microenvironment to create favorable living conditions for themselves (72), and the immune cells of this phenotype are in a suppressed state. These results suggest that for patients with different ferroptosis-related phenotypes, AML patients can be treated by drugs that induce ferroptosis or suppress immune escape according to the corresponding phenotypic characteristics. To judge the individual characteristics of a single patient more accurately, we constructed the FSscore to quantify the degree of development of ferroptosis-related phenotypes. The FSscore can quantitatively evaluate the pathological status of patients and also has good prognostic value. We confirmed this in two groups and two other cohorts that used different sequencing methods and showed certain prognostic prediction accuracy across cancers. In terms of various pathological characteristics, a high FSscore is highly positively correlated with inflammation development, immune escape, lipid metabolism, anti-immunotherapy, chemotherapy resistance, etc., and negatively correlated with tumor mutation burden. These results all show the reference value of the FSscore for the evaluation of individual characteristics and clinical treatment of AML patients.

Finally, to explore the clinical treatment options for patients with different ferroptosis-related phenotypes, we used drug prediction to identify five anticancer drugs and nine small molecule drugs that may have therapeutic benefits for patients with low FSscores and 20 small molecule drugs that may have therapeutic benefits for patients with high FSscores. Among them, ABT.263 (navitoclax) has been confirmed to be effective for the treatment of AML in cell and mouse experiments (73–76). The combination of hyperforin and Akt inhibitor AKT inhibitor VIII significantly promotes the apoptosis of AML U937 cells (77). Second-generation tyrosine kinase inhibitors (TKIs), such as ponatinib (AP.24534), are also widely used in hematological malignancies (78). Axitinib effectively inhibits BCR-ABL1 (T315I) to treat chronic myeloid leukemia (79). Research on these drugs suggests that they can improve the treatment of hematological tumors and provide a reference for further basic research and clinical trials. In addition, we used GPX4 targeting inhibitor RSL3 to reduce the protein level of GPX4 and promote AML cell death by inducing ferroptosis, indicating that GPX4 is a potential target for AML treatment.

In summary, we found three ferroptosis-related phenotypes in AML patients based on FRG analysis and revealed the TME characteristics (such as immune escape, inflammation development, and lipid metabolism) of samples with different phenotypes. The FSscore can improve the assessment of the pathological state and prognosis of AML patients and provides reference value for the establishment of more personalized clinical treatment plans. Moreover, compared with other studies on ferroptosis in AML, our project also has its own advantages and limitations. For example, compared with the data analysis of Zhou et al. (80), our study not only used more AML samples and multi-omics data such as transcriptome, copy number variation, and gene mutation, but also verified the existence of three ferroptosis-related phenotypes in both microarray and high-throughput sequencing types, and explored the differences in TME and clinical pathological characteristics among them, the constructed scoring system can also accurately predict the prognosis of AML patients and provide some insights for the therapeutic evaluation. However, compared with the research of Yusuf et al. (81), our exploration of ferroptosis mainly focuses on the analysis of big data of bioinformatics, but there are obvious deficiencies in the exploration of regulation mechanism, which is the direction of our follow-up study, linking more regulatory mechanisms of ferroptosis in AML cells with bioinformatics data.

Conclusions

This project revealed that the occurrence of ferroptosis is closely related to the complex pathological changes in the TME. Patients with different TME features show differences in terms of ferroptosis sensitivity. Immune cell infiltration, inflammation development and lipid metabolism are important regulatory factors that affect the occurrence of ferroptosis. The comprehensive analysis of ferroptosis-related molecular patterns in individual patients can provide references for the clinical evaluation of patient pathological characteristics and the design of personalized treatment plans.

Data availability statement

The original contributions presented in the study are included in the article/Supplementary Material. Further inquiries can be directed to the corresponding authors.

Author contributions

F-MZ research design and drafing the manuscript. F-YY helping to revision the manuscript. H-BZ, JZ, JLiu, J-YJ, SX, WW, X-RZ, X-XC, Y-LY, YC, JLin, S-QL, NZ and M-YL assisted bioinformatic and statistical analysis. BH revision of the manuscript and writing guidance. X-ZW review and revision of the manuscript and writing guidance. All authors contributed to the article and approved the submitted version.

Funding

The study was funded by the National Natural Science Foundation of China (81860034, 82160405, 82160038).

Conflict of interest

The authors declare that the research was conducted in the absence of any commercial or financial relationships that could be construed as a potential conflict of interest.

Publisher's note

All claims expressed in this article are solely those of the authors and do not necessarily represent those of their affiliated organizations, or those of the publisher, the editors and the reviewers. Any product that may be evaluated in this article, or claim that may be made by its manufacturer, is not guaranteed or endorsed by the publisher.

Supplementary material

The Supplementary Material for this article can be found online at: https://www.frontiersin.org/articles/10.3389/fonc.2022.888570/full#supplementary-material

References

1. Su Z, Yang Z, Xu Y, Chen Y, Yu Q. Apoptosis, autophagy, necroptosis, and cancer metastasis. *Mol Cancer* (2015) 14:48. doi: 10.1186/s12943-015-0321-5

2. Dixon S, Lemberg K, Lamprecht M, Skouta R, Zaitsev E, Gleason C, et al. Ferroptosis: an iron-dependent form of nonapoptotic cell death. *Cell* (2012) 149:1060–72. doi: 10.1016/j.cell.2012.03.042

3. Gao M, Monian P, Pan Q, Zhang W, Xiang J, Jiang X. Ferroptosis is an autophagic cell death process. *Cell Res* (2016) 26:1021–32. doi: 10.1038/cr.2016.95

4. Xie Y, Hou W, Song X, Yu Y, Huang J, Sun X, et al. Ferroptosis: process and function. *Cell Death differentiation* (2016) 23:369–79. doi: 10.1038/cdd.2015.158

5. Jiang X, Stockwell B, Conrad M. Ferroptosis: mechanisms, biology and role in disease. *Nat Rev Mol Cell Biol* (2021) 22:266–82. doi: 10.1038/s41580-020-00324-8

6. Stockwell B, Jiang X, Gu W. Emerging mechanisms and disease relevance of ferroptosis. *Trends Cell Biol* (2020) 30:478–90. doi: 10.1016/j.tcb.2020.02.009

7. Tang D, Chen X, Kang R, Kroemer G. Ferroptosis: molecular mechanisms and health implications. *Cell Res* (2021) 31:107–25. doi: 10.1038/s41422-020-00441-1

8. Du Y, Bao J, Zhang M, Li L, Xu X, Chen H, et al. Targeting ferroptosis contributes to ATPR-induced AML differentiation *via* ROS-autophagy-lysosomal pathway. *Gene* (2020) 755:144889. doi: 10.1016/j.gene.2020.144889

9. Du J, Wang T, Li Y, Zhou Y, Wang X, Yu X, et al. DHA inhibits proliferation and induces ferroptosis of leukemia cells through autophagy dependent degradation of ferritin. *Free Radical Biol Med* (2019) 131:356–69. doi: 10.1016/j.freeradbiomed.2018.12.011

10. Yu Y, Xie Y, Cao L, Yang L, Yang M, Lotze M, et al. The ferroptosis inducer erastin enhances sensitivity of acute myeloid leukemia cells to chemotherapeutic agents. *Mol Cell Oncol* (2015) 2:e1054549. doi: 10.1080/23723556.2015.1054549

11. Doll S, Proneth B, Tyurina Y, Panzilius E, Kobayashi S, Ingold I, et al. ACSL4 dictates ferroptosis sensitivity by shaping cellular lipid composition. *Nat Chem Biol* (2017) 13:91–8. doi: 10.1038/nchembio.2239

12. Zheng J, Conrad M. The metabolic underpinnings of ferroptosis. *Cell Metab* (2020) 32:920–37. doi: 10.1016/j.cmet.2020.10.011

13. Kagan V, Mao G, Qu F, Angeli J, Doll S, Croix C, et al. Oxidized arachidonic and adrenic PEs navigate cells to ferroptosis. *Nat Chem Biol* (2017) 13:81–90. doi: 10.1038/nchembio.2238

14. Yang W, SriRamaratnam R, Welsch M, Shimada K, Skouta R, Viswanathan V, et al. Regulation of ferroptotic cancer cell death by GPX4. *Cell* (2014) 156:317–31. doi: 10.1016/j.cell.2013.12.010

15. Bersuker K, Hendricks J, Li Z, Magtanong L, Ford B, Tang P, et al. The CoQ oxidoreductase FSP1 acts parallel to GPX4 to inhibit ferroptosis. *Nature* (2019) 575:688–92. doi: 10.1038/s41586-019-1705-2

16. Sato H, Tamba M, Ishii T, Bannai S. Cloning and expression of a plasma membrane cystine/glutamate exchange transporter composed of two distinct proteins. *J Biol Chem* (1999) 274:11455–8. doi: 10.1074/jbc.274.17.11455

17. Liu J, Xia X, Huang P. xCT: A critical molecule that links cancer metabolism to redox signaling. *Mol Ther J Am Soc Gene Ther* (2020) 28:2358–66. doi: 10.1016/j.ymthe.2020.08.021

18. Iwasaki A, Medzhitov R. Control of adaptive immunity by the innate immune system. *Nat Immunol* (2015) 16:343–53. doi: 10.1038/ni.3123

19. Xu H, Ye D, Ren M, Zhang H, Bi F. Ferroptosis in the tumor microenvironment: perspectives for immunotherapy. *Trends Mol Med* (2021) 27 (9):856–67. doi: 10.1016/j.molmed.2021.06.014

20. Binnewies M, Roberts E, Kersten K, Chan V, Fearon D, Merad M, et al. Understanding the tumor immune microenvironment (TIME) for effective therapy. *Nat Med* (2018) 24:541–50. doi: 10.1038/s41591-018-0014-x

21. Luo X, Gong H, Gao H, Wu Y, Sun W, Li Z, et al. Oxygenated phosphatidylethanolamine navigates phagocytosis of ferroptotic cells by interacting with TLR2. *Cell Death differentiation* (2021) 28:1971–89. doi: 10.1038/s41418-020-00719-2

22. Yee P, Wei Y, Kim S, Lu T, Chih S, Lawson C, et al. Neutrophil-induced ferroptosis promotes tumor necrosis in glioblastoma progression. *Nat Commun* (2020) 11:5424. doi: 10.1038/s41467-020-19193-y

23. Efimova I, Catanzaro E, Van der Meeren L, Turubanova V, Hammad H, Mishchenko T, et al. Vaccination with early ferroptotic cancer cells induces efficient antitumor immunity. *J immunotherapy Cancer* (2020) 8:e001369. doi: 10.1136/jitc-2020-001369

24. Klöditz K, Fadeel B. Three cell deaths and a funeral: macrophage clearance of cells undergoing distinct modes of cell death. *Cell Death Discovery* (2019) 5:65. doi: 10.1038/s41420-019-0146-x

25. Greten F, Grivennikov S. Inflammation and cancer: Triggers, mechanisms, and consequences. *Immunity* (2019) 51:27–41. doi: 10.1016/j.immuni.2019.06.025

26. Lüscher U, Filgueira L, Juretic A, Zuber M, Lüscher N, Heberer M, et al. The pattern of cytokine gene expression in freshly excised human metastatic melanoma suggests a state of reversible anergy of tumor-infiltrating lymphocytes. *Int J Cancer* (1994) 57:612–9. doi: 10.1002/ijc.2910570428

27. Monti P, Leone B, Zerbi A, Balzano G, Cainarca S, Sordi V, et al. Tumor-derived MUC1 mucins interact with differentiating monocytes and induce IL-10highIL-12low regulatory dendritic cell. *J Immunol* (2004) 172:7341–9. doi: 10.4049/jimmunol.172.12.7341

28. Barth R, Camp B, Martuscello T, Dain B, Memoli V. The cytokine microenvironment of human colon carcinoma. lymphocyte expression of tumor necrosis factor-alpha and interleukin-4 predicts improved survival. *Cancer* (1996) 78:1168–78. doi: 10.1002/(sici)1097-0142(19960915)78:6<1168::Aid-cncr2>3.0.Co;2-6

29. Ohm J, Carbone D. VEGF as a mediator of tumor-associated immunodeficiency. *Immunologic Res* (2001) 23:263–72. doi: 10.1385/ir:23:2-3:263

30. Takizawa H, Manz M. Impact of inflammation on early hematopoiesis and the microenvironment. *Int J Hematol* (2017) 106:27–33. doi: 10.1007/s12185-017-2266-5

31. Flores-Figueroa E, Gutiérrez-Espíndola G, Montesinos J, Arana-Trejo R, Mayani H. *In vitro* characterization of hematopoietic microenvironment cells from patients with myelodysplastic syndrome. *Leukemia Res* (2002) 26:677–86. doi: 10.1016/s0145-2126(01)00193-x

32. Schinke C, Giricz O, Li W, Shastri A, Gordon S, Barreyro L, et al. IL8-CXCR2 pathway inhibition as a therapeutic strategy against MDS and AML stem cells. *Blood* (2015) 125:3144–52. doi: 10.1182/blood-2015-01-621631

33. Carey A, Edwards D, Eide C, Newell L, Traer E, Medeiros B, et al. Identification of interleukin-1 by functional screening as a key mediator of cellular expansion and disease progression in acute myeloid leukemia. *Cell Rep* (2017) 18:3204–18. doi: 10.1016/j.celrep.2017.03.018

34. Liang J, Wang D, Lin H, Chen X, Yang H, Zheng Y, et al. A novel ferroptosis-related gene signature for overall survival prediction in patients with hepatocellular carcinoma. *Int J Biol Sci* (2020) 16:2430–41. doi: 10.7150/ijbs.45050

35. Wilkerson M, Hayes D. ConsensusClusterPlus: a class discovery tool with confidence assessments and item tracking. *Bioinf (Oxford England)* (2010) 26:1572–3. doi: 10.1093/bioinformatics/btq170

36. Hänzelmann S, Castelo R, Guinney J. GSVA: gene set variation analysis for microarray and RNA-seq data. *BMC Bioinf* (2013) 14:7. doi: 10.1186/1471-2105-14-7

37. Subramanian A, Tamayo P, Mootha VK, Mukherjee S, Ebert BL, Gillette MA, et al. Gene set enrichment analysis: A knowledge-based approach for interpreting genome-wide expression profiles. *Proc Natl Acad Sci* (2005) 102:15545–50. doi: 10.1073/pnas.0506580102

38. Newman A, Liu C, Green M, Gentles A, Feng W, Xu Y, et al. Robust enumeration of cell subsets from tissue expression profiles. *Nat Methods* (2015) 12:453–7. doi: 10.1038/nmeth.3337

39. Ritchie M, Phipson B, Wu D, Hu Y, Law C, Shi W, et al. Limma powers differential expression analyses for RNA-sequencing and microarray studies. *Nucleic Acids Res* (2015) 43:e47. doi: 10.1093/nar/gkv007

40. Mariathasan S, Turley S, Nickles D, Castiglioni A, Yuen K, Wang Y, et al. TGFβ attenuates tumour response to PD-L1 blockade by contributing to exclusion of T cells. *Nature* (2018) 554:544–8. doi: 10.1038/nature25501

41. Gabrilovich D. Myeloid-derived suppressor cells. *Cancer Immunol Res* (2017) 5:3–8. doi: 10.1158/2326-6066.Cir-16-0297

42. Charoentong P, Finotello F, Angelova M, Mayer C, Efremova M, Rieder D, et al. Pan-cancer immunogenomic analyses reveal genotype-immunophenotype relationships and predictors of response to checkpoint blockade. *Cell Rep* (2017) 18:248–62. doi: 10.1016/j.celrep.2016.12.019

43. Fu J, Li K, Zhang W, Wan C, Zhang J, Jiang P, et al. Large-Scale public data reuse to model immunotherapy response and resistance. *Genome Med* (2020) 12:21. doi: 10.1186/s13073-020-0721-z

44. Hugo W, Zaretsky J, Sun L, Song C, Moreno B, Hu-Lieskovan S, et al. Genomic and transcriptomic features of response to anti-PD-1 therapy in metastatic melanoma. *Cell* (2016) 165:35–44. doi: 10.1016/j.cell.2016.02.065

45. Yang W, Soares J, Greninger P, Edelman E, Lightfoot H, Forbes S, et al. Genomics of drug sensitivity in cancer (GDSC): a resource for therapeutic biomarker discovery in cancer cells. *Nucleic Acids Res* (2013) 41:D955–961. doi: 10.1093/nar/gks1111

46. Geeleher P, Cox N, Huang R. pRRophetic: an r package for prediction of clinical chemotherapeutic response from tumor gene expression levels. *PloS One* (2014) 9:e107468. doi: 10.1371/journal.pone.0107468

47. Lamb J, Crawford E, Peck D, Modell J, Blat I, Wrobel M, et al. The connectivity map: using gene-expression signatures to connect small molecules, genes, and disease. *Sci (New York N.Y.)* (2006) 313:1929–35. doi: 10.1126/science.1132939

48. Sallman D, McLemore A, Aldrich A, Komrokji R, McGraw K, Dhawan A, et al. TP53 mutations in myelodysplastic syndromes and secondary AML confer an immunosuppressive phenotype. *Blood* (2020) 136:2812–23. doi: 10.1182/blood.2020006158

49. Bernard E, Nannya Y, Hasserjian R, Devlin S, Tuechler H, Medina-Martinez J, et al. Implications of TP53 allelic state for genome stability, clinical presentation and outcomes in myelodysplastic syndromes. *Nat Med* (2020) 26:1549–56. doi: 10.1038/s41591-020-1008-z

50. Huang B, Zhao J, Li H, He K, Chen Y, Mayer L, et al. Editor's note: Toll-like receptors on tumor cells facilitate evasion of immune surveillance. *Cancer Res* (2019) 79:4305. doi: 10.1158/0008-5472.Can-19-1889

51. Suarez G, Romero-Gallo J, Piazuelo M, Wang G, Maier R, Forsberg L, et al. Modification of helicobacter pylori peptidoglycan enhances NOD1 activation and promotes cancer of the stomach. *Cancer Res* (2015) 75:1749–59. doi: 10.1158/0008-5472.Can-14-2291

52. Binder S, Luciano M, Horejs-Hoeck J. The cytokine network in acute myeloid leukemia (AML): A focus on pro- and anti-inflammatory mediators. *Cytokine Growth factor Rev* (2018) 43:8–15. doi: 10.1016/j.cytogfr.2018.08.004

53. Gruszka A, Valli D, Restelli C, Alcalay M. Adhesion deregulation in acute myeloid leukaemia. *Cells* (2019) 8:66. doi: 10.3390/cells8010066

54. Injarabian L, Devin A, Ransac S, Marteyn B. Neutrophil metabolic shift during their lifecycle: Impact on their survival and activation. *Int J Mol Sci* (2019) 21:287. doi: 10.3390/ijms21010287

55. Newell L, Cook R. Advances in acute myeloid leukemia. *BMJ (Clinical Res ed.)* (2021) 375:n2026. doi: 10.1136/bmj.n2026

56. Samstein R, Lee C, Shoushtari A, Hellmann M, Shen R, Janjigian Y, et al. Tumor mutational load predicts survival after immunotherapy across multiple cancer types. *Nat Genet* (2019) 51:202–6. doi: 10.1038/s41588-018-0312-8

57. Goodman A, Kato S, Bazhenova L, Patel S, Frampton G, Miller V, et al. Tumor mutational burden as an independent predictor of response to immunotherapy in diverse cancers. *Mol Cancer Ther* (2017) 16:2598–608. doi: 10.1158/1535-7163.Mct-17-0386

58. Anderson K, Lutz C, van Delft F, Bateman C, Guo Y, Colman S, et al. Genetic variegation of clonal architecture and propagating cells in leukaemia. *Nature* (2011) 469:356–61. doi: 10.1038/nature09650

59. McGranahan N, Swanton C. Biological and therapeutic impact of intratumor heterogeneity in cancer evolution. *Cancer Cell* (2015) 27:15–26. doi: 10.1016/j.ccell.2014.12.001

60. Yates L, Campbell P. Evolution of the cancer genome. *Nat Rev Genet* (2012) 13:795–806. doi: 10.1038/nrg3317

61. Bennett J, Catovsky D, Daniel M, Flandrin G, Galton D, Gralnick H, et al. Proposals for the classification of the acute leukaemias. French-American-British (FAB) co-operative group. *Br J haematology* (1976) 33:451–8. doi: 10.1111/j.1365-2141.1976.tb03563.x

62. Juliusson G, Antunovic P, Derolf A, Lehmann S, Möllgård L, Stockelberg D, et al. Age and acute myeloid leukemia: real world data on decision to treat and outcomes from the Swedish acute leukemia registry. *Blood* (2009) 113:4179–87. doi: 10.1182/blood-2008-07-172007

63. Schlenk R. Post-remission therapy for acute myeloid leukemia. *Haematologica* (2014) 99:1663–70. doi: 10.3324/haematol.2014.114611

64. Döhner H, Estey E, Grimwade D, Amadori S, Appelbaum F, Büchner T, et al. Diagnosis and management of AML in adults: 2017 ELN recommendations from an international expert panel. *Blood* (2017) 129:424–47. doi: 10.1182/blood-2016-08-733196

65. Mou Y, Wang J, Wu J, He D, Zhang C, Duan C, et al. Ferroptosis, a new form of cell death: opportunities and challenges in cancer. *J Hematol Oncol* (2019) 12:34. doi: 10.1186/s13045-019-0720-y

66. Riera-Domingo C, Audigé A, Granja S, Cheng W, Ho P, Baltazar F, et al. Immunity, hypoxia, and metabolism-the ménage à trois of cancer: Implications for immunotherapy. *Physiol Rev* (2020) 100:1–102. doi: 10.1152/physrev.00018.2019

67. Wang W, Green M, Choi J, Gijón M, Kennedy P, Johnson J, et al. CD8 T cells regulate tumour ferroptosis during cancer immunotherapy. *Nature* (2019) 569:270–4. doi: 10.1038/s41586-019-1170-y

68. Wen Q, Liu J, Kang R, Zhou B, Tang D. The release and activity of HMGB1 in ferroptosis. *Biochem Biophys Res Commun* (2019) 510:278–83. doi: 10.1016/j.bbrc.2019.01.090

69. Çolakoğlu M, Tunçer S, Banerjee S. Emerging cellular functions of the lipid metabolizing enzyme 15-Lipoxygenase-1. *Cell proliferation* (2018) 51:e12472. doi: 10.1111/cpr.12472

70. Joyce J, Fearon D. T Cell exclusion, immune privilege, and the tumor microenvironment. *Sci (New York N.Y.)* (2015) 348:74–80. doi: 10.1126/science.aaa6204

71. Raaijmakers M, Mukherjee S, Guo S, Zhang S, Kobayashi T, Schoonmaker J, et al. Bone progenitor dysfunction induces myelodysplasia and secondary leukaemia. *Nature* (2010) 464:852–7. doi: 10.1038/nature08851

72. Mantovani A, Allavena P, Sica A, Balkwill F. Cancer-related inflammation. *Nature* (2008) 454:436–44. doi: 10.1038/nature07205

73. Kivioja J, Thanasopoulou A, Kumar A, Kontro M, Yadav B, Majumder M, et al. Dasatinib and navitoclax act synergistically to target NUP98-NSD1/FLT3-ITD acute myeloid leukemia. *Leukemia* (2019) 33:1360–72. doi: 10.1038/s41375-018-0327-2

74. Airiau K, Prouzet-Mauléon V, Rousseau B, Pigneux A, Jeanneteau M, Giraudon M, et al. Synergistic cooperation between ABT-263 and MEK1/2 inhibitor: effect on apoptosis and proliferation of acute myeloid leukemia cells. *Oncotarget* (2016) 7:845–59. doi: 10.18632/oncotarget.6417

75. Pons M, Zeyn Y, Zahn S, Mahendrarajah N, Page B, Gunning P, et al. Oncogenic kinase cascades induce molecular mechanisms that protect leukemic cell models from lethal effects of *De novo* dNTP synthesis inhibition. *Cancers* (2021) 13(14):3464. doi: 10.3390/cancers13143464

76. Montoya J, Turnidge M, Wai D, Patel A, Lee D, Gokhale V, et al. *In vitro* activity of a G-quadruplex-stabilizing small molecule that synergizes with navitoclax to induce cytotoxicity in acute myeloid leukemia cells. *BMC Cancer* (2019) 19:1251. doi: 10.1186/s12885-019-6464-9

77. Merhi F, Tang R, Piedfer M, Mathieu J, Bombarda I, Zaher M, et al. Hyperforin inhibits Akt1 kinase activity and promotes caspase-mediated apoptosis involving bad and noxa activation in human myeloid tumor cells. *PloS One* (2011) 6:e25963. doi: 10.1371/journal.pone.0025963

78. Shimada A. Hematological malignancies and molecular targeting therapy. *Eur J Pharmacol* (2019) 862:172641. doi: 10.1016/j.ejphar.2019.172641

79. Pemovska T, Johnson E, Kontro M, Repasky G, Chen J, Wells P, et al. Axitinib effectively inhibits BCR-ABL1(T315I) with a distinct binding conformation. *Nature* (2015) 519:102–5. doi: 10.1038/nature14119

80. Zhou F, Chen B. Prognostic significance of ferroptosis-related genes and their methylation in AML. *Hematol (Amsterdam Netherlands)* (2021) 26:919–30. doi: 10.1080/16078454.2021.1996055

81. Yusuf RZ, Saez B, Sharda A, van Gastel N, Yu VWC, Baryawno N, et al. Aldehyde dehydrogenase 3a2 protects AML cells from oxidative death and the synthetic lethality of ferroptosis inducers. *Blood* (2020) 136:1303–16. doi: 10.1182/blood.2019001808

frontiers | Frontiers in Oncology

TYPE Review
PUBLISHED 19 December 2022
DOI 10.3389/fonc.2022.1022979

OPEN ACCESS

EDITED BY
Spiros Vlahopoulos,
University of Athens, Greece

REVIEWED BY
Chao Chen,
Emory University, United States
Dan Ma,
Affiliated Hospital of Guizhou Medical University, China

*CORRESPONDENCE
Ling Gu
guling@scu.edu.cn
Ping Liao
ping_liao@nni.com.sg
Hanmin Liu
liuhm@scu.edu.cn

SPECIALTY SECTION
This article was submitted to Hematologic Malignancies, a section of the journal Frontiers in Oncology

RECEIVED 19 August 2022
ACCEPTED 01 December 2022
PUBLISHED 19 December 2022

CITATION
Gu L, Liao P and Liu H (2022) Cancer-associated fibroblasts in acute leukemia.
Front. Oncol. 12:1022979.
doi: 10.3389/fonc.2022.1022979

Cancer-associated fibroblasts in acute leukemia

Ling Gu[1,2,3]*, Ping Liao[4,5,6]* and Hanmin Liu[1,2,3,7]*

[1]Department of Pediatrics, Key Laboratory of Birth Defects and Related Diseases of Women and Children (Sichuan University), Ministry of Education, West China Second University Hospital, Sichuan University, Chengdu, China, [2]The Joint Laboratory for Lung Development and Related Diseases of West China Second University Hospital, Sichuan University and School of Life Sciences of Fudan University, West China Institute of Women and Children's Health, West China Second University Hospital, Sichuan University, Chengdu, China, [3]NHC Key Laboratory of Chronobiology, Sichuan University, Chengdu, China, [4]Calcium Signalling Laboratory, National Neuroscience Institute, Singapore, Singapore, [5]Academic & Clinical Development, Duke-NUS Medical School, Singapore, Singapore, [6]Health and Social Sciences, Singapore Institute of Technology, Singapore, Singapore, [7]Sichuan Birth Defects Clinical Research Center, West China Second University Hospital, Sichuan University, Chengdu, China

Although the prognosis for acute leukemia has greatly improved, treatment of relapsed/refractory acute leukemia (R/R AL) remains challenging. Recently, increasing evidence indicates that the bone marrow microenvironment (BMM) plays a crucial role in leukemogenesis and therapeutic resistance; therefore, BMM-targeted strategies should be a potent protocol for treating R/R AL. The targeting of cancer-associated fibroblasts (CAFs) in solid tumors has received much attention and has achieved some progress, as CAFs might act as an organizer in the tumor microenvironment. Additionally, over the last 10 years, attention has been drawn to the role of CAFs in the BMM. In spite of certain successes in preclinical and clinical studies, the heterogeneity and plasticity of CAFs mean targeting them is a big challenge. Herein, we review the heterogeneity and roles of CAFs in the BMM and highlight the challenges and opportunities associated with acute leukemia therapies that involve the targeting of CAFs.

KEYWORDS

bone marrow, tumor microenvironment, leukemia, relapsed/refractory, cancer associated fibroblasts

Abbreviations: ALL, acute lymphoid leukemia; AML, acute myeloid leukemia; APL, acute promyelocytic leukemia; BM, bone marrow; BMM, BM microenvironment; BMT, BM transplantation; CAFs, cancer associated fibroblasts; CAR, Cxcl12-abundant reticular; CAR-T, chimeric antigen receptor T; CLL, chronic lymphoid leukemia; CML, chronic myeloid leukemia; ECs, endothelial cells; ECM, extracellular matrix; EFS, event free survival; HSCs, hematopoietic stem cells; LSCs, leukemic stem cells; MSCs, mesenchymal stem cells; MDS, myelodysplastic syndrome; MM, multiple myeloma; MF, myelofibrosis; MPN, myeloproliferative neoplasms; R/R, relapsed/refractory; TME, tumor microenvironment.

1 Background

Acute leukemia is a clonal hematopoietic cancer originating in the bone marrow (BM) and can be classified into two types: acute lymphoid leukemia (ALL) and acute myeloid leukemia (AML). With the advancement of therapies, leukemia is no longer an incurable disease. In children, the 5-year event-free survival (EFS) rate is approximately 85-90% for ALL, sometimes exceeding 90% in ALL trials in developed countries (1–4), and approximately 45-65% for AML (5, 6). However, in adults, the 5-year EFS rate for ALL is only 35-45% (7, 8). The prognosis for adult AML is better in acute promyelocytic leukemia (APL), with a 5-year EFS rate exceeding 80% (9, 10). However, only 35-40% of patients with AML manage to survive for more than 5 years (10, 11). Even in the most curable pediatric ALL, 10-15% of patients do not survive because of chemo-resistance and relapse, which is named relapsed/refractory (R/R) ALL (12, 13). The proportion of R/R AML and R/R adult ALL cases is far higher than that of R/R pediatric ALL.

Until now, the treatment of leukemia has been focused on targeting leukemic cells. While the intensity of chemoradiotherapy is limited by toxic side effects, such as pancytopenia, BM transplantation (BMT) has been drawn into the therapeutic protocol to help reconstruct hematologic and immunologic capacity following high-intensity chemotherapy and radiation treatment to eradicate leukemic cells (14–16). Even so, the prognosis for patients with R/R leukemia remains poor. The exploration of innovative approaches is crucial for patients with R/R leukemia. Immunotherapy, especially chimeric antigen receptor T (CAR-T) cell and antibody therapy, improves the response rate in patients with R/R leukemia by targeting leukemic cells (1, 8, 13–19). However, the cure rate has not been noticeably improved, especially in patients with R/R AML, which highlights an urgent need for novel and synergistic therapies.

'Seed-and-soil' theory is well known in cancer research and the term was coined by Dr. Stephen Paget in 1889 (20, 21). 'Seed' and 'soil' crosstalk may push cancer progression. Remodeling of the 'soil' will make it more difficult for cancer cells but more suitable for normal cells, thus potentially helping to cure cancer. As a matter of course, the next target should be the 'soil'. 'Soil' remodeling is important for R/R leukemia patients as it may provide conditions in which cancer cells and cancer stem cells struggle to survive in (22–25). It generally accepted that the 'soil' of solid cancer, known as the tumor microenvironment (TME), is a target-rich environment (26–31). Cancer-associated fibroblasts (CAFs), the major players in the TME, have drawn much attention for their multiple functions, including extracellular matrix (ECM) remodeling, growth factor, cytokine, and chemokine production, angiogenesis regulation, and metabolism and immune system modulation (24, 32–39). In this review, we summarize the role of CAFs in acute leukemia and highlight the challenges and opportunities associated with CAF-targeting therapy.

2 Bone marrow microenvironment and CAFs

First, we must understand the 'soil' of leukemic cells and stem cells, the BM microenvironment (BMM). BMM plays a key role in regulating normal hematopoiesis, as well as chondrogenesis and osteogenesis. Initially, BMM was identified as necessary for successful BMT to reconstruct hematopoiesis. In the 1950s, few patients with leukemia benefitted from BMT (40). After the human histocompatibility antigen system was recognized, a modern era of human BMT began. From then on, the BMM has been slowly demystified.

In 1961, Fliedner et al. (41) pointed out that the recovery of hematopoiesis in rats following 1000 cGy total body irradiation required the recovery of vasculogenesis as support. Then, in 1967, Wolf and Trentin applied the term 'hemopoietic inductive microenvironment' to this event in the spleen and BM (42–44). In 1978, Raymond Schofield (45) formally proposed the 'stem cell niche' in BM as a specialized microenvironment for stem cells *in vivo*. Since the 1980s, an increasing number of studies have showed that the BM niche (also called BMM) plays a crucial role in both hematopoiesis and leukemogenesis (46–51). Traditionally, the BMM was divided into endosteal and vascular niches, which may participate in different divisions of labor (52–61). Through technological breakthroughs, such as the construction of transgenic mouse models, the development of sophisticated imaging technologies, and single-cell sequencing, the atlas of BMM is becoming clearer. BMM is a continuum in which hematopoietic stem cells (HSCs) and leukemic stem cells (LSCs) may locate in their corresponding niche. The trouble is that LSCs remodel the BMM into a leukemia-permissive microenvironment while suppressing a hematopoietic-permissive microenvironment (50, 60, 62–67). Clinically, this hypothesis is best supported by donor cell leukemia, in which leukemia originates from engrafted donor cells after allogeneic HSC transplantation, i.e., the leukemia-permissive microenvironment may initiate leukemogenesis in healthy cells (68–72). Therefore, targeting of the leukemia-permissive BMM to restore hematopoietic-permissive BMM can be a useful strategy for overcoming R/R leukemia. Herein, the next issue is to dig out the potent target cells.

2.1 The cell components of BMM

Initially, in the 1960s, Owen and Macapheson (73, 74) observed a group of pre-osteoblasts growing in the inner periosteal surface of the femur. In 1968, Friedenstein (75) and Tavassoli et al. (76) found that BMT could generate non-hematopoietic osteogenic cells. Then, in the 1980s, many papers reported fibroblast colonies originating from stromal osteogenic precursor cells in BM (77–81). In 1991, Caplan (82) termed precursor cells with multipotency properties as mesenchymal stem cells (MSCs). In the present day,

autoradiography, BM smear and biopsy, flowcytometry, *in vivo* BMT, and *in vitro* cell culture have helped us recognize the cellular components of the BMM, including MSCs, endothelial cells (ECs), adipocytes, Cxcl12-abundant reticular (CAR) cells, osteogenic cells, macrophages, fibroblasts, Schwann cells, and possibly other stromal cells (81, 83, 84). Cre-mediated lineage tracing and deletion of molecular factors helped trace cell fate and differentiation, which were still limited in a small piece of a whole. Recently, single-cell and spatial transcriptomic technologies provided the first systematic and label-free identification of cell types of the BMM (85–90). So far, we can map the cellular composition and distribution in the BMM. Different BM resident cell types are successfully allocated to endosteal, sinusoidal, arteriolar, and non-vascular niches (90). Baryawno et al. (86) first profiled all non-hematopoietic (Ter119-/CD71-/Lin-) cells in mouse BM and gained 17 clusters spanning MSCs (*Lepr*$^{+}$*Cxcl12*$^{+}$), osteolineage cells (*Bglap*$^{+}$), chondrocytes (*Acan*$^{+}$*Col2a1*$^{+}$), fibroblasts (*S100a4*$^{+}$), BMECs (*Cdh5*$^{+}$), pericytes (*Acta2*$^{+}$), and possible transitional states. Based on single-cell and spatial transcriptomics, Baccin et al. (87), identified nine cell types in BM-resident non-hematopoietic cells and demonstrated their differential localization, including two different EC clusters (*Ly6a*$^{+}$ arterial ECs and *Emcn*$^{+}$ sinusoidal ECs), CAR cells (*Lepr*^{high} Adipo-CAR and *osterix*^{high} *Lepr*^{low} Osteo-CAR), three distinct fibroblast clusters (stromal, arteriolar, and endosteal localizations), myofibroblasts, Ng2^{+} Nestin^{+} MSCs, chondrocytes (*Acan* and *Sox9*), osteoblasts (*Osteocalcin*/*Bglap* and *Col1a1*), smooth muscle cells (*Tagln* and *Acta2*), and Schwann cells (*Mog*, *Mag*).

In the BMM, MSCs and ECs are the most abundant subsets (86), and have been fully researched, especially MSCs. Fibroblasts, myofibroblasts, and Schwann cells were found to be more abundant in crushed bones than in flushed bones (87). Therefore, these cells might be ignored during regular clinical examinations without broken bones, such as BM aspiration and biopsy, due to the limited number of cells. Baryawno et al. (86) revealed that Fibroblast-1 and -2 cells are MSC-like as they expressed the progenitor marker CD34 and MSC markers (*Ly6a*, *Pdgfra*, *Thy1*, *and Cd44*), but not BMECs or pericytes genes (*Cdh5* and *Acta2*). While in the BMM of AML, *Cxcl12*, *Kitl*, and *Angpt1* were upregulated in Fibroblast-1 cells (similar to Cxcl12-secreting CAFs). CAFs are defined as fibroblasts that are located within or adjacent to cancer cells, and have been extensively studied due to the ease with which they can be obtained and cultured *in vitro* from solid cancers (24, 33, 35, 91). In the past decade, CAFs have been well recognized as a promising target in the TME (25, 33, 34, 37).

2.2 Origins of CAFs in BM

Fibroblasts are defined as interstitial cells of a mesenchymal lineage that are not epithelial, endothelial, or immune cells (34, 37, 92). The origins and roles of fibroblasts in different tissues remain ambiguous, resulting in a lack of unified biomarkers to define them (36, 93). It is generally accepted that CAFs are the main participants in ECM remodeling, wound-healing responses, immune cell recruitment, inflammation, and fibrosis (32, 34–37, 93). The origins and roles of CAFs are even more complicated than fibroblasts. So far, over 10 origins of CAFs have been found in solid tumors, including tissue-resident cells (fibroblasts, myofibroblasts, fibrocytes, epithelial cells, endothelial cells, adipocytes, smooth muscle cells, and immune cells) and BM-derived cells (MSCs, circulating fibrocytes, and immune cells) (24, 35, 37). Still, the precise origins of CAFs and CAF subgroups, and the differences between CAFs and fibroblasts in normal tissues, remain elusive due to the phenotypic and functional plasticity of these cells and the lack of well-defined lineage biomarkers (34, 37). However, based on scRNA-seq and spatial transcription technology, there is a considerable understanding of the heterogeneity of CAFs in solid cancers, such as pancreatic cancer, liver cancer, gastric cancer, head and neck cancer, and breast cancer (94–102).

Although the BMM has been studied extensively since 1978, research on CAFs in hematological malignancies is falling far behind that of solid tumors. The major reason for this is that BM biopsy specimens are relatively hard to obtain. Additionally, lineage tracing of CAFs might be more difficult in BM. According to the achievements with solid tumors, we can conclude that there are abundant resident origins of CAFs in the BMM, such as MSCs, fibroblasts, myofibroblasts, fibrocytes, smooth muscle cells, endothelial-mesenchymal transformation cells, adipocyte-mesenchymal transition cells (24, 35, 103), pericyte-fibroblast transformation cells (104, 105), monocyte-fibroblast transition cells (106, 107), macrophage-mesenchymal transformation cells (108), and leukemia cells (109–111) (Figure 1). Different cell origins of CAFs might suggest different phenotypes and roles. Additionally, most of the cell origins of CAFs in BM contain populations with multipotent differentiation capacity, which may make lineage tracing of CAFs more difficult (Figure 2). For example, MSCs can differentiate into osteoblasts, chondrocytes, and adipocytes *in vitro* and *in vivo* (82, 112, 113). Adipocytes can differentiate into myofibroblasts (103) and osteoblasts (114). CD34(+) fibrocytes are BM-derived monocyte progenitor cells, which can differentiate into adipocytes, osteoblasts, and chondrocytes (115, 116). Monocytes can differentiate into fibrocytes and macrophages (117, 118). Furthermore, the cell origins of BM MSCs currently remain unclear; a mesodermal, a neuro-ectodermal, or even a dual origin have been suggested (113). The pericytes of ectodermal origin can differentiate into MSCs (113, 119, 120). BM MSCs may arise from BM or adipose tissue (121). Similarly, activated fibroblasts can transform into MSCs, adipocytes, chondrocytes, endothelial cells, ECs, and pericytes, and can even be induced to become induced pluripotent stem cells (iPSCs) (35, 122).

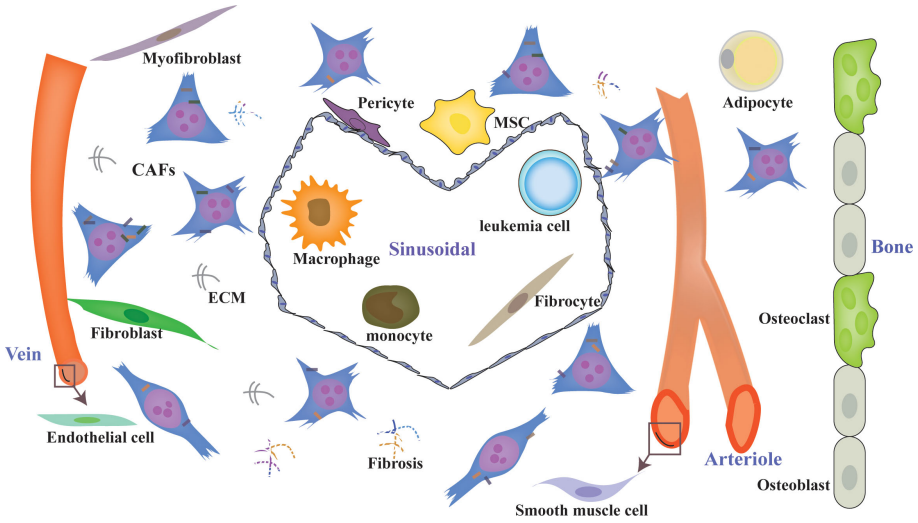

FIGURE 1
Diverse origins of CAFs in the BMM. CAFs can originate from diverse sources, such as MSCs, fibroblasts, myofibroblasts, fibrocytes, smooth muscle cells, endothelial cells, adipocyte pericytes, monocytes, macrophages, and leukemia cells, with different phenotypes. CAFs are a heterogeneous population with distinct functions in the BMM. ECM, extracellular matrix; CAFs, cancer-associated fibroblasts.

3 CAFs in the BMM of leukemia

3.1 Myelofibrosis and CAFs

First described in 1879, BM fibrosis with fibroblast infiltration and excessive ECM deposition (123, 124) is a typical type of BMM remodeling (125). Now, myelofibrosis (MF) is defined as a clonal hematopoietic BCR-ABL-negative myeloproliferative neoplasm characterized by BM fibrosis, extramedullary hematopoiesis, megakaryocytic hyperplasia, and constitutional symptoms (126). MF may be primary or secondary with a heterogeneous clinical course, ranging from a

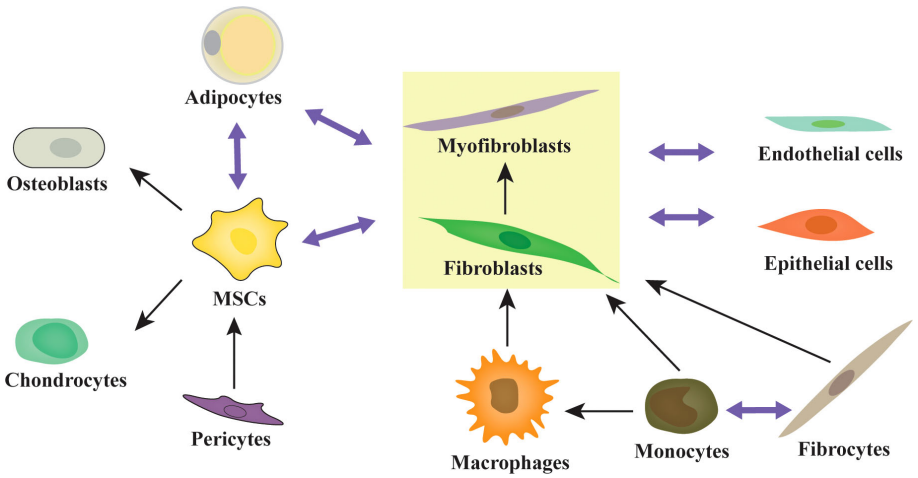

FIGURE 2
The multipotent differentiation capacity of origin cells of CAFs. Activated fibroblasts, MSCs, and adipocytes are highly plastic and exhibit multipotent capacity. MSCs can differentiate into osteoblasts, chondrocytes, adipocytes, and fibroblasts/myofibroblasts. Adipocytes can differentiate into fibroblasts/myofibroblasts and osteoblasts. Fibrocytes can differentiate into monocytes, fibroblasts/myofibroblasts, adipocytes, osteoblasts, and chondrocytes. Monocytes can differentiate into fibrocytes, macrophages, and fibroblasts/myofibroblasts. The pericytes and adipocytes can differentiate into MSCs. Similarly, activated fibroblasts can transform into MSCs, adipocytes, chondrocytes, endothelial cells, ECs, and pericytes.

chronic asymptomatic state to acute leukemic transformation, and possibly a preleukemic state (126, 127). Most forms of secondary MF collaborate with myeloproliferative neoplasms (MPN) and chronic myeloid leukemia (CML). Leukemia transformation is rare in patients with non-fibrotic MPNs but common in patients with MF (128–131). Patients with acute leukemia transformed from MF have a dismal prognosis, with a median survival time of approximately 3 months (128, 129). BM fibrosis in ALL and AML was first described in 1964 (132). Although BM fibrosis may disappear and accompany the complete remission of leukemia, a higher degree of fibrosis (measured as reticulin fibrin density) may correlate with relapse and higher minimal residual disease (MRD) in ALL, especially B-ALL (133–136), and with a poor prognosis in AML (137); however, there remains controversy (138, 139). These results imply that CAFs may play a crucial role in a part of patients with acute leukemia.

3.2 Acute leukemia and CAFs

The phenotypes and roles of BM CAFs were first reported in patients and mice with multiple myeloma (MM) in 2014 (140). The same year, Duan et al. (141) found that ALL cells may induce a dynamically transient niche in the BMM with the help of chemotherapy: beginning with Nestin$^+$ MSCs, maturating through their transition to a-SMA$^+$ cells, and terminating with fiber residues, called the NSM niche, in mice models and patients with ALL after chemotherapy. The NSM niche was associated with additional difficulties in achieving complete remission after therapy in ALL patients, i.e., the transit of Nestin$^+$ MSCs to a-SMA$^+$ CAFs might correlate with BM fibrosis and poor prognosis in ALL. In 2015, Paggetti et al. (142) reported that exosomes from chronic lymphoid leukemia (CLL) may induce the transition of BM MSCs to CAFs. In 2016, a retrospective study on BM biopsies from patients with AML showed that CAFs were widespread within the BM. Furthermore, excessive reticular fibers in the BM led to a higher frequency of relapse and mortality in primary ALL patients (143). In 2019, Burt et al. (144) pinpointed that CAFs/activated MSCs are frequently presence in ALL, which could prevent ALL cell apoptosis and death from reactive oxygen species-inducing agents by mitochondrial transfer. Exposure to Ara-C or daunorubicin may generate CAFs *in vitro* and in ALL mice models (144). Then, Pan et al. (145, 146) found that TGF-β is a key factor for BM MSCs to obtain a CAF-like phenotype in a B-ALL microenvironment, which may interact with ALL cells through an SDF1-CXCR4 signaling axis to promote the progression of B-ALL. Using single-cell sequencing, Baryawno et al. (86) revealed a decrease in Fibroblast-5s (*Sox9*, *Spp1*, *Nt5e*, *cspg4*, and *clip)*, an increase in Fibroblast-2s (*Cd34*, *Ly6a*, *Pdgfra*, *Thy1*, and *Cd44*), and a Cxcl12-secreting CAF phenotype of Fibroblast-1s (with upregulation of *Cxcl12*, *Kitl*, and *Angpt1*) in mice BM with AML. In 2021, our team established the first CAF tumor cell line, HXWMF-1 (α-SMA, vimentin, HSP47, S100A4/FSP1, FAP, PDGFRβ, and CD34 positive) (147), originated from the subcutaneous xenografts of HXEX-ALL1 (148), a cell line from a relapsed patient with B-ALL. The cell line provides firm evidence that leukemia cells may induce malignant transformation of CAFs (147). Malignant CAFs might remodel the BMM to form a more aggressive niche. Although the exact roles and underlying mechanisms of CAFs in BM remain elusive, it is clear that CAFs in BM may correlate with BM fibrosis, promote leukemia progression, and induce chemoresistance (Table 1) (86, 141, 143–146). Chemotherapeutic drugs, such as Ara-C and daunorubicin, may induce the generation of CAFs (Table 1) (141, 144). In general, CAFs in BM may have distinct phenotypes and play crucial roles in leukemogenesis and therapy resistance. Understanding the role of CAFs in BM and AL may have clinical significance as it may facilitate the identification of novel drug targets for BMM and immunotherapy.

3.3 Genetic alteration and CAFs

G-banding analysis showed that HXWMF-1 cells have 60–70 chromosomes with complex structural chromosomal abnormalities (147), which raises the question of whether there are cytogenetic abnormalities in BM stromal cells in patients with acute leukemia? Some studies reported that stromal cells in the BM of MM, myelodysplastic syndrome (MDS), AML, ALL, and CML patients had numerical and structural chromosomal abnormalities, which were different from the abnormalities of leukemic cells (149–153). However, other researchers were unable to find chromosomal abnormalities in stromal cells from different hematological diseases, including MDS, AML, ALL, CLL, and CML (154–157). Gunsilius et al. (158) reported that ECs from patients with CML expressed the *BCR-ABL* fusion gene. Zhou et al. (159) found that clonal expansion of fibroblasts with somatic copy number alterations is prevalent in patients with colorectal cancer. The genetic profile of cancer cells can affect the surrounding stoma (160), and genetic alterations have been detected in a few stroma cells in solid tumors (161–163). In general, cytogenetic alterations could appear in stromal cells in some patients with leukemia but not all. The presence of chromosomal aberrations in BM MSCs has been associated with a bad prognosis (150).

4 Why focus on CAFs

4.1 The role of CAFs

Although, studies of the BMM of malignant hematological diseases have suggested a tumor-promoting role for CAFs (140–

TABLE 1 CAFs in AL and their functions in leukemia progression.

Models	Induction factors of CAFs	CAFs subtypes	Cell origin of CAFs	Roles of CAFs	Mechanisms	Method	Correlated with BM fibrosis	References
Murine ALL models /Pediatric and Adult patients with ALL	Ara-C or DNR	a-SMA$^+$, Vimentin$^+$ (murine)/a-SMA$^+$, Nestin$^-$, CD146$^-$ (human)	MSCs with Nestin$^+$	Protect leukemic cells from chemotherapy	GDF15 mediated the niche protection	IF and IHC	Yes	Duan et al. (140)
Adult patients with AML	NA	FSP1$^+$, α-SMA$^+$, or FAP$^+$	MSCs	Protect leukemic cells from chemotherapy	GDF15 mediated the chemoprotection	IHC	Yes	Zhai et al. (142)
Adult patients with ALL /Murine B-ALL models	Ara-C or DNR	F-action$^+$, α-SMA$^+$	MSCs	Protect leukemic cells from chemotherapy	Mitochondria transfer mediated the chemoprotection.	Cell culture and IF	NA	Burt et al. (143)
Murine AML models	NA	Cd34$^+$, Ly6a$^+$, Pdgfra$^+$, Thy1$^+$ and Cd44$^+$/ Cxcl12$^+$, Kitl$^+$, and Angpt1$^+$	NA	NA	NA	Single cell sequencing	NA	Baryawno et al. (86)
Adult patients with B-ALL	TGF-β	α-SMA$^+$, FAP$^+$	MSCs	Accelerate leukemic cells migration and invasion	NA	Cell culture, IF	NA	Pan et al. (145)
Adult patients with B-ALL/ Murine B-ALL modle	TGF-β	a-SMA$^+$, FAP$^+$	MSCs	Promoting the growth and invasion of B-ALL	SDF-1/CXCR4 axis mediated the communication of CAFs and leukemia cells	IHC	Yes	Pan et al. (144)

IF, immunofluorescence; IHC, immunohistochemistry; NA, not reported.

146, 164), studies on solid tumors revealed highly heterogeneous phenotypes in CAFs, with both tumor-promoting and restraining functions (35, 36, 38, 93, 165–169), which may partly explain the failure in clinical trials of targeting CAFs as a whole (34). The former phenotype represents most of the CAF population (38), which helps reprogram malignant ECM, increase angiogenesis and neovascurization, fuel cancer cells, direct cancer cell proliferation, metastasis, and invasion, deregulate metabolism, induce epigenetic reprogramming, unlock phenotypic plasticity, promote the stemness of cancer cells, resist cell death, shape the tumor immune microenvironment, and confer therapeutic resistance (32, 33, 36, 38, 39, 91, 93, 96, 97, 99, 168, 170, 171). Therefore, CAFs may participate in constructing almost all the fourteen hallmarks of cancer proposed by Dr. Hanahan and Dr. Weinberg (172–174), including acquiring capabilities for sustaining proliferative signaling, evading growth suppressors, resisting cell death, enabling replicative immortality, tumor-promoting inflammation, inducing/accessing vasculature, activating invasion and metastasis, reprogramming cellular metabolism, avoiding immune destruction, genome instability and mutation, unlocking phenotypic plasticity, non-mutational epigenetic reprogramming, polymorphic microbiomes, and senescent cells (172). Kochetkova and Samuel (33) reviewed the published evidence and summarized that CAF-mediated differentiation may give rise to cancer-associated immune cells, adipocytes, nerves, endothelia, and vasculature. They pointed out that CAFs are well equipped to assume the role of master organizer in the cancer by interacting with cancer cells and other stromal cells and immune cells in the TME, and producing cancer-specific ECM and secretome. Therefore, targeting CAFs to destroy cancer might be a potent therapeutic protocol for improving and perfecting cancer therapy.

4.2 Targeting CAFs and the associated challenges

The first clinical trial of targeting CAFs was reported in 1994, using iodine 131-labeled monoclonal antibody F19 (^{131}I-mAbF19) to target FAP$^+$CAFs in colorectal carcinoma patients with hepatic metastasis. The results prompted the diagnostic and

therapeutic applications of mAbF19 (175). Then, an increasing number of preclinical and clinical trials of different targets and strategies were undertaken or are still in progress. However, in recent years, CAFs have been the focus of debate. There are numerous obstacles and challenges in targeting CAFs, such as a lack of specific CAF cell markers and signaling pathways, and the heterogeneous roles of CAFs. Increasing evidence has added further complication by indicating that the phenotypes of CAFs are dynamic and able to interconvert depending on tumor status, culture conditions, and therapeutic protocols (34, 93, 176–178). This presents a challenge and an opportunity, as modulating the phenotype of CAFs from tumor promoting to tumor restraining might be an attractive approach for cancer treatment (38, 93). Unfortunately, owing to the same difficulty, there are no definite and standardized markers to classify the functional subtypes of CAFs. Traditionally, α-smooth muscle actin (α-SMA) was identified as a marker of active CAFs and a prognostic factor in tumor patients; however, certain subtypes of CAFs are characterized by a far lower degree of α-SMA (176, 179, 180). Currently, a number of markers, such as α-SMA, FAP, PDGFRα/β, vimentin, S100A4 (FSP1), CAV1(caveolin 1), transgelin (TAGLN), periostin (POSTN), podoplanin (PDPN), integrin α11β1 (ITGA11), collagen type XI alpha I chain (COL11A1), and microfibril-associated protein 5 (MFAP5), are used to identify CAF populations and subgroups (24, 32, 38, 93, 179). Just as Dr. Song mentioned, CAFs are frequently defined by what they are not, typically using multiple biomarkers, resulting in an incomprehensive definition of a CAF (38). Recently, novel CAF-specific biomarkers were discovered in different cancers, such as $CD10^+GPR77^+$ CAFs in breast and lung cancer (25), G protein-coupled receptor 30^+ CAFs in prostate cancer (181), netrin $G1^+$ CAFs (182), $neuregulin^+$ CAFs (183), leucine-rich-repeat-containing 15^+ CAFs (91), $Gli1^+$ CAFs (184), $CD105^+$ CAFs in pancreatic cancer (99), and EGRhigh CAFs in adult T cell leukemia/lymphoma (185). Novel markers may help to precisely attack the tumor-promoting CAFs.

According to the target spot, there are two strategies for targeting CAFs, direct and indirect, which were recently comprehensively reviewed by Saw et al. (38). The direct targeting approach includes CAF depletion *via* cell markers, inhibition of CAF activation by targeting the signaling pathway, halting infiltration of CAFs, and reprogramming tumor-promoting CAFs to a quiescent state or tumor-restraining phenotype (24, 32, 38, 39). The indirect targeting approach includes targeting the TME, CAF-derived ECM, and downstream effectors (24, 32, 38, 39). However, parts of the clinical trials of targeting CAFs ended in failure, and in some cases, even accelerated cancer progression (34). Recently, there have been numerous studies on FAP-specific CAR-T cells, which can specifically attack FAP^+ CAFs with concomitant antitumor efficacy and no severe toxicity (24, 186–188). CAR-T, which was first described by Gross et al. (189) in 1989, can enable T cells to recognize antigens independent of major histocompatibility complex II. The first FDA-approved CAR-T cell therapy obtained a good response in aspects of patients' ALL (190, 191). CAR-T cell therapy is mainly performed in patients with hematological malignancies and is a revolutionary new treatment for cancer (192). However, responses are transient in patients as CAR-T cells may become exhausted/dysfunctional. Recently, Sakemura et al. (164) constructed a dual-targeting BCMA-FAP and BCMA-SLAMF CAR-T to target both malignant plasma cells and BM CAFs. The results showed that dual-targeting of CAR-T can overcome BM-CAF-mediated inhibition of BCMA-CAR-T (targeting plasma cells only) in an MM mice model. This study is a perfect preclinical attempt to target both cancer cells and the TME with immunotherapeutic strategies, and a brand-new attempt at targeting CAFs in the BMM. Encouragingly, the study suggests that FAP-CAR-T can be applied to target BM CAFs in hematologic malignancies to combat BMM-mediated therapy resistance.

5 Conclusions and perspectives

Studies on CAFs are exciting and critical for leukemia treatment. The challenge is to better understand the heterogeneity and plasticity of CAFs, which may help to develop novel CAF-targeting therapeutic strategies. Compared with solid tumors, the targeting of CAFs is more challenging in hematological malignancy. First, the BM biopsy samples are harder to obtain. To complicate matters further, it is difficult to obtain enough CAFs through regular BM aspiration and biopsy, whereas fibroblasts and myofibroblasts are abundant in crushed bones (87). Second, the precursor cells in the BMM are more complex and plastic, which make lineage tracing more challenging. In general, there are still many questions about CAFs in the BMM that need to be answered, including the following:

1. What kinds of CAFs in the BMM might correlate with R/R AL? What are their cell origins? Do these CAFs have chromosomal alterations?
2. Do CAFs contribute to donor cell leukemia? What kinds of CAFs might induce donor cell leukemia? What are the underlying mechanisms?
3. What kinds of ALs might induce the malignant transformation of CAFs? What are the exact roles of malignant CAFs?
4. What are the underlying mechanisms of the transition of precursor cells to CAFs? Are there any influences of therapeutic protocols on the transition of CAFs?

Author contributions

LG drafted the manuscript and prepared the figures. LG and PL conceived the review. HL designed and revised the review. All authors contributed to the article and approved the submitted version.

Funding

This work was supported by the Sichuan Science and Technology Program of China (Grant no. 2021YFH0062), and Fundamental Research Funds for the Central Universities (Grant no. SCU2019C4005).

Conflict of interest

The authors declare that the research was conducted in the absence of any commercial or financial relationships that could be construed as a potential conflict of interest.

Publisher's note

References

1. Malard F, Mohty M. Acute lymphoblastic leukaemia. *Lancet* (2020) 395 (10230):1146–62. doi: 10.1016/S0140-6736(19)33018-1

2. Jeha S, Pei D, Choi J, Cheng C, Sandlund JT, Coustan-Smith E, et al. Improved CNS control of childhood acute lymphoblastic leukemia without cranial irradiation: St Jude total therapy study 16. *J Clin Oncol* (2019) 37 (35):3377–91. doi: 10.1200/JCO.19.01692

3. Inaba H, Pui CH. Advances in the diagnosis and treatment of pediatric acute lymphoblastic leukemia. *J Clin Med* (2021) 10(9):1926. doi: 10.3390/jcm10091926

4. Hunger SP, Mullighan CG. Acute lymphoblastic leukemia in children. *N Engl J Med* (2015) 373(16):1541–52. doi: 10.1056/NEJMra1400972

5. Creutzig U, van den Heuvel-Eibrink MM, Gibson B, Dworzak MN, Adachi S, de Bont E, et al. Diagnosis and management of acute myeloid leukemia in children and adolescents: recommendations from an international expert panel. *Blood* (2012) 120(16):3187–205. doi: 10.1182/blood-2012-03-362608

6. Conneely SE, Stevens AM. Acute myeloid leukemia in children: Emerging paradigms in genetics and new approaches to therapy. *Curr Oncol Rep* (2021) 23 (2):16. doi: 10.1007/s11912-020-01009-3

7. Richard-Carpentier G, Kantarjian H, Jabbour E. Recent advances in adult acute lymphoblastic leukemia. *Curr Hematol Malig Rep* (2019) 14(2):106–18. doi: 10.1007/s11899-019-00503-1

8. Leonard J, Stock W. Progress in adult ALL: incorporation of new agents to frontline treatment. *Hematol Am Soc Hematol Educ Program* (2017) 2017(1):28–36. doi: 10.1182/asheducation-2017.1.28

9. Abaza Y, Kantarjian H, Garcia-Manero G, Estey E, Borthakur G, Jabbour E, et al. Long-term outcome of acute promyelocytic leukemia treated with all-trans-retinoic acid, arsenic trioxide, and gemtuzumab. *Blood* (2017) 129(10):1275–83. doi: 10.1182/blood-2016-09-736686

10. Kantarjian HM, Short NJ, Fathi AT, Marcucci G, Ravandi F, Tallman M, et al. Acute myeloid leukemia: Historical perspective and progress in research and therapy over 5 decades. *Clin Lymphoma Myeloma Leuk* (2021) 21(9):580–97. doi: 10.1016/j.clml.2021.05.016

11. Naina HV, Patnaik MM, Harris S. Anthracycline dose intensification in acute myeloid leukemia. *N Engl J Med* (2009) 361(26):2578. doi: 10.1056/NEJMc0910366

12. Pui CH, Yang JJ, Hunger SP, Pieters R, Schrappe M, Biondi A, et al. Childhood acute lymphoblastic leukemia: Progress through collaboration. *J Clin Oncol* (2015) 33(27):2938–48. doi: 10.1200/JCO.2014.59.1636

13. Hunger SP, Raetz EA. How I treat relapsed acute lymphoblastic leukemia in the pediatric population. *Blood* (2020) 136(16):1803–12. doi: 10.1182/blood.2019004043

14. Brown PA, Shah B, Advani A, Aoun P, Boyer MW, Burke PW, et al. Acute lymphoblastic leukemia, version 2.2021, NCCN clinical practice guidelines in oncology. *J Natl Compr Canc Netw* (2021) 19(9):1079–109. doi: 10.6004/jnccn.2021.0042

15. Pollyea DA, Bixby D, Perl A, Bhatt VR, Altman JK, Appelbaum FR, et al. NCCN guidelines insights: Acute myeloid leukemia, version 2.2021. *J Natl Compr Canc Netw* (2021) 19(1):16–27. doi: 10.6004/jnccn.2021.0002

16. Brown P, Inaba H, Annesley C, Beck J, Colace S, Dallas M, et al. Pediatric acute lymphoblastic leukemia, version 2.2020, NCCN clinical practice guidelines in oncology. *J Natl Compr Canc Netw* (2020) 18(1):81–112. doi: 10.6004/jnccn.2020.0001

17. Inaba H, Pui CH. Immunotherapy in pediatric acute lymphoblastic leukemia. *Cancer Metastasis Rev* (2019) 38(4):595–610. doi: 10.1007/s10555-019-09834-0

18. Lussana F, Gritti G, Rambaldi A. Immunotherapy of acute lymphoblastic leukemia and lymphoma with T cell-redirected bispecific antibodies. *J Clin Oncol* (2021) 39(5):444–55. doi: 10.1200/JCO.20.01564

19. Khaldoyanidi S, Nagorsen D, Stein A, Ossenkoppele G, Subklewe M. Immune biology of acute myeloid leukemia: Implications for immunotherapy. *J Clin Oncol* (2021) 39(5):419–32. doi: 10.1200/JCO.20.00475

20. Fidler IJ. The pathogenesis of cancer metastasis: the 'seed and soil' hypothesis revisited. *Nat Rev Cancer* (2003) 3(6):453–8. doi: 10.1038/nrc1098

21. Paget S. The distribution of secondary growths in cancer of the breast. 1889. *Cancer Metastasis Rev* (1989) 8(2):98–101.

22. Plaks V, Kong N, Werb Z. The cancer stem cell niche: how essential is the niche in regulating stemness of tumor cells. *Cell Stem Cell* (2015) 16(3):225–38. doi: 10.1016/j.stem.2015.02.015

23. Najafi M, Mortezaee K, Majidpoor J. Cancer stem cell (CSC) resistance drivers. *Life Sci* (2019) 234:116781. doi: 10.1016/j.lfs.2019.116781

24. Chen X, Song E. Turning foes to friends: targeting cancer-associated fibroblasts. *Nat Rev Drug Discovery* (2019) 18(2):99–115. doi: 10.1038/s41573-018-0004-1

25. Su S, Chen J, Yao H, Liu J, Yu S, Lao L, et al. CD10+GPR77+ cancer-associated fibroblasts promote cancer formation and chemoresistance by sustaining cancer stemness. *Cell* (2018) 172(4):841–56.e16. doi: 10.1016/j.cell.2018.01.009

26. Xiao Y, Yu D. Tumor microenvironment as a therapeutic target in cancer. *Pharmacol Ther* (2021) 221:107753. doi: 10.1016/j.pharmthera.2020.107753

27. Roma-Rodrigues C, Mendes R, Baptista PV, Fernandes AR. Targeting tumor microenvironment for cancer therapy. *Int J Mol Sci* (2019) 20(4):840. doi: 10.3390/ijms20040840

28. Kaymak I, Williams KS, Cantor JR, Jones RG. Immunometabolic interplay in the tumor microenvironment. *Cancer Cell* (2021) 39(1):28–37. doi: 10.1016/j.ccell.2020.09.004

29. Duan Q, Zhang H, Zheng J, Zhang L. Turning cold into hot: Firing up the tumor microenvironment. *Trends Cancer* (2020) 6(7):605–18. doi: 10.1016/j.trecan.2020.02.022

30. Peng J, Yang Q, Shi K, Xiao Y, Wei X, Qian Z. Intratumoral fate of functional nanoparticles in response to microenvironment factor: Implications on cancer diagnosis and therapy. *Adv Drug Delivery Rev* (2019) 143:37–67. doi: 10.1016/j.addr.2019.06.007

31. Chen Q, Liu G, Liu S, Su H, Wang Y, Li J, et al. Remodeling the tumor microenvironment with emerging nanotherapeutics. *Trends Pharmacol Sci* (2018) 39(1):59–74. doi: 10.1016/j.tips.2017.10.009

32. Mhaidly R, Mechta-Grigoriou F. Role of cancer-associated fibroblast subpopulations in immune infiltration, as a new means of treatment in cancer. *Immunol Rev* (2021) 302(1):259–72. doi: 10.1111/imr.12978

33. Kochetkova M, Samuel MS. Differentiation of the tumor microenvironment: are CAFs the organizer. *Trends Cell Biol* (2022) 32(4):285–94. doi: 10.1016/j.tcb.2021.11.008

34. Chen Y, McAndrews KM, Kalluri R. Clinical and therapeutic relevance of cancer-associated fibroblasts. *Nat Rev Clin Oncol* (2021) 18(12):792–804. doi: 10.1038/s41571-021-00546-5

35. Kalluri R. The biology and function of fibroblasts in cancer. *Nat Rev Cancer* (2016) 16(9):582–98. doi: 10.1038/nrc.2016.73

36. Pradhan RN, Krishnamurty AT, Fletcher AL, Turley SJ, Müller S. A bird's eye view of fibroblast heterogeneity: A pan-disease, pan-cancer perspective. *Immunol Rev* (2021) 302(1):299–320. doi: 10.1111/imr.12990

37. Sahai E, Astsaturov I, Cukierman E, DeNardo DG, Egeblad M, Evans RM, et al. A framework for advancing our understanding of cancer-associated fibroblasts. *Nat Rev Cancer* (2020) 20(3):174–86. doi: 10.1038/s41568-019-0238-1

38. Saw PE, Chen J, Song E. Targeting CAFs to overcome anticancer therapeutic resistance. *Trends Cancer* (2022) 8(7):527–55. doi: 10.1016/j.trecan.2022.03.001

39. Desbois M, Wang Y. Cancer-associated fibroblasts: Key players in shaping the tumor immune microenvironment. *Immunol Rev* (2021) 302(1):241–58. doi: 10.1111/imr.12982

40. Thomas ED, Lochte HL, Lu WC, Ferrebee JW. Intravenous infusion of bone marrow in patients receiving radiation and chemotherapy. *N Engl J Med* (1957) 257 (11):491–6. doi: 10.1056/NEJM195709122571102

41. Fliedner TM, Bond VP, Cronkite EP. Structural, cytologic and autoradiographic (H3-thymidine) changes in the bone marrow following total body irradiation. *Am J Pathol* (1961) 38:599–623.

42. Trentin JJ. Hemopoietic microenvironments. *Transplant Proc* (1978) 10 (1):77–82.

43. Curry JL, Trentin JJ, Wolf N. Hemopoietic spleen colony studies. II. erythropoiesis. *J Exp Med* (1967) 125(4):703–20. doi: 10.1084/jem.125.4.703

44. Curry JL, Trentin JJ, Cheng V. Hemopoietic spleen colony studies. 3. hemopoietic nature of spleen colonies induced by lymph node or thymus cells, with or without phytohemagglutinin. *J Immunol* (1967) 99(5):907–16.

45. Schofield R. The relationship between the spleen colony-forming cell and the haemopoietic stem cell. *Blood Cells* (1978) 4(1-2):7–25.

46. Bentley SA. Bone marrow connective tissue and the haemopoietic microenvironment. *Br J Haematol* (1982) 50(1):1–6. doi: 10.1111/j.1365-2141.1982.tb01884.x

47. Dorshkind K. Regulation of hemopoiesis by bone marrow stromal cells and their products. *Annu Rev Immunol* (1990) 8:111–37. doi: 10.1146/annurev.iy.08.040190.000551

48. Testa NG, Dexter TM. Long-term hematopoietic damage: concepts, approaches, and results relevant to the study of environmental toxins. *Environ Health Perspect* (1989) 82:51–6. doi: 10.1289/ehp.898251

49. Ayala F, Dewar R, Kieran M, Kalluri R. Contribution of bone microenvironment to leukemogenesis and leukemia progression. *Leukemia* (2009) 23(12):2233–41. doi: 10.1038/leu.2009.175

50. Le PM, Andreeff M, Battula VL. Osteogenic niche in the regulation of normal hematopoiesis and leukemogenesis. *Haematologica* (2018) 103(12):1945–55. doi: 10.3324/haematol.2018.197004

51. Medyouf H. The microenvironment in human myeloid malignancies: emerging concepts and therapeutic implications. *Blood* (2017) 129(12):1617–26. doi: 10.1182/blood-2016-11-696070

52. Acar M, Kocherlakota KS, Murphy MM, Peyer JG, Oguro H, Inra CN, et al. Deep imaging of bone marrow shows non-dividing stem cells are mainly perisinusoidal. *Nature* (2015) 526(7571):126–30. doi: 10.1038/nature15250

53. Chen JY, Miyanishi M, Wang SK, Yamazaki S, Sinha R, Kao KS, et al. Hoxb5 marks long-term haematopoietic stem cells and reveals a homogenous perivascular niche. *Nature* (2016) 530(7589):223–7. doi: 10.1038/nature16943

54. Bruns I, Lucas D, Pinho S, Ahmed J, Lambert MP, Kunisaki Y, et al. Megakaryocytes regulate hematopoietic stem cell quiescence through CXCL4 secretion. *Nat Med* (2014) 20(11):1315–20. doi: 10.1038/nm.3707

55. Itkin T, Gur-Cohen S, Spencer JA, Schajnovitz A, Ramasamy SK, Kusumbe AP, et al. Distinct bone marrow blood vessels differentially regulate haematopoiesis. *Nature* (2016) 532(7599):323–8. doi: 10.1038/nature17624

56. Goncalves KA, Silberstein L, Li S, Severe N, Hu MG, Yang H, et al. Angiogenin promotes hematopoietic regeneration by dichotomously regulating quiescence of stem and progenitor cells. *Cell* (2016) 166(4):894–906. doi: 10.1016/j.cell.2016.06.042

57. Silberstein L, Goncalves KA, Kharchenko PV, Turcotte R, Kfoury Y, Mercier F, et al. Proximity-based differential single-cell analysis of the niche to identify Stem/Progenitor cell regulators. *Cell Stem Cell* (2016) 19(4):530–43. doi: 10.1016/j.stem.2016.07.004

58. Ding L, Saunders TL, Enikolopov G, Morrison SJ. Endothelial and perivascular cells maintain haematopoietic stem cells. *Nature* (2012) 481 (7382):457–62. doi: 10.1038/nature10783

59. Mendelson A, Frenette PS. Hematopoietic stem cell niche maintenance during homeostasis and regeneration. *Nat Med* (2014) 20(8):833–46. doi: 10.1038/nm.3647

60. Ghiaur G, Wroblewski M, Loges S. Acute myelogenous leukemia and its microenvironment: A molecular conversation. *Semin Hematol* (2015) 52(3):200–6. doi: 10.1053/j.seminhematol.2015.03.003

61. Comazzetto S, Shen B, Morrison SJ. Niches that regulate stem cells and hematopoiesis in adult bone marrow. *Dev Cell* (2021) 56(13):1848–60. doi: 10.1016/j.devcel.2021.05.018

62. Behrmann L, Wellbrock J, Fiedler W. Acute myeloid leukemia and the bone marrow niche-take a closer look. *Front Oncol* (2018) 8:444. doi: 10.3389/fonc.2018.00444

63. Ladikou EE, Sivaloganathan H, Pepper A, Chevassut T. Acute myeloid leukaemia in its niche: the bone marrow microenvironment in acute myeloid leukaemia. *Curr Oncol Rep* (2020) 22(3):27. doi: 10.1007/s11912-020-0885-0

64. Duarte D, Hawkins ED, Lo Celso C. The interplay of leukemia cells and the bone marrow microenvironment. *Blood* (2018) 131(14):1507–11. doi: 10.1182/blood-2017-12-784132

65. Tettamanti S, Pievani A, Biondi A, Dotti G, Serafini M. Catch me if you can: how AML and its niche escape immunotherapy. *Leukemia* (2022) 36(1):13–22. doi: 10.1038/s41375-021-01350-x

66. Wang X, Huang S, Chen JL. Understanding of leukemic stem cells and their clinical implications. *Mol Cancer* (2017) 16(1):2. doi: 10.1186/s12943-016-0574-7

67. Schepers K, Campbell TB, Passegué E. Normal and leukemic stem cell niches: insights and therapeutic opportunities. *Cell Stem Cell* (2015) 16(3):254–67. doi: 10.1016/j.stem.2015.02.014

68. Flynn CM, Kaufman DS. Donor cell leukemia: insight into cancer stem cells and the stem cell niche. *Blood* (2007) 109(7):2688–92. doi: 10.1182/blood-2006-07-021980

69. Williams L, Doucette K, Karp JE, Lai C. Genetics of donor cell leukemia in acute myelogenous leukemia and myelodysplastic syndrome. *Bone Marrow Transplant* (2021) 56(7):1535–49. doi: 10.1038/s41409-021-01214-z

70. Shahar Gabay T, Chapal-Ilani N, Moskovitz Y, Biezuner T, Oron B, Brilon Y, et al. Donor cell leukemia: reappearance of gene mutations in donor cells - more than an incidental phenomenon. *Haematologica* (2020) 105(12):2861–3. doi: 10.3324/haematol.2019.242347

71. Scheuermann A, Moskop A, Hopp A, Bone K, Drendel HM, Talano J, et al. Pediatric donor cell acute lymphoblastic leukemia following bone marrow transplant for GATA2 mutation. *J Pediatr Hematol Oncol* (2022) 44(5):268–70. doi: 10.1097/MPH.0000000000002437

72. Wiseman DH. Donor cell leukemia: a review. *Biol Blood Marrow Transplant* (2011) 17(6):771–89. doi: 10.1016/j.bbmt.2010.10.010

73. Owen M, Macpherson S. Cell population kinetics of an osteogenic tissue. II. *J Cell Biol* (1963) 19:33–44. doi: 10.1083/jcb.19.1.33

74. Owen M. Cell population kinetics of an osteogenic tissue. I. *J Cell Biol* (1963) 19:19–32. doi: 10.1083/jcb.19.1.19

75. Friedenstein AJ, Petrakova KV, Kurolesova AI, Frolova GP. Heterotopic of bone marrow. analysis of precursor cells for osteogenic and hematopoietic tissues. *Transplantation* (1968) 6(2):230–47.

76. Tavassoli M, Crosby WH. Transplantation of marrow to extramedullary sites. *Science* (1968) 161(3836):54–6. doi: 10.1126/science.161.3836.54

77. Friedenstein AJ, Chailakhyan RK, Gerasimov UV. Bone marrow osteogenic stem cells: *in vitro* cultivation and transplantation in diffusion chambers. *Cell Tissue Kinet* (1987) 20(3):263–72. doi: 10.1111/j.1365-2184.1987.tb01309.x

78. Castro-Malaspina H, Gay RE, Resnick G, Kapoor N, Meyers P, Chiarieri D, et al. Characterization of human bone marrow fibroblast colony-forming cells (CFU-f) and their progeny. *Blood* (1980) 56(2):289–301. doi: 10.1182/blood.V56.2.289.289

79. Howlett CR, Cavé J, Williamson M, Farmer J, Ali SY, Bab I, et al. Mineralization in *in vitro* cultures of rabbit marrow stromal cells. *Clin Orthop Relat Res* (1986) 213):251–63. doi: 10.1097/00003086-198612000-00037

80. Mardon HJ, Bee J, von der Mark K, Owen ME. Development of osteogenic tissue in diffusion chambers from early precursor cells in bone marrow of adult rats. *Cell Tissue Res* (1987) 250(1):157–65. doi: 10.1007/BF00214667

81. Owen M, Friedenstein AJ. Stromal stem cells: marrow-derived osteogenic precursors. *Ciba Found Symp* (1988) 136:42–60. doi: 10.1002/9780470513637.ch4

82. Caplan AI. Mesenchymal stem cells. *J Orthop Res* (1991) 9(5):641–50. doi: 10.1002/jor.1100090504

83. Crane GM, Jeffery E, Morrison SJ. Adult haematopoietic stem cell niches. *Nat Rev Immunol* (2017) 17(9):573–90. doi: 10.1038/nri.2017.53

84. Mayani H, Guilbert LJ, Janowska-Wieczorek A. Biology of the hemopoietic microenvironment. *Eur J Haematol* (1992) 49(5):225–33. doi: 10.1111/j.1600-0609.1992.tb00053.x

85. Al-Sabah J, Baccin C, Haas S. Single-cell and spatial transcriptomics approaches of the bone marrow microenvironment. *Curr Opin Oncol* (2020) 32 (2):146–53. doi: 10.1097/CCO.0000000000000602

86. Baryawno N, Przybylski D, Kowalczyk MS, Kfoury Y, Severe N, Gustafsson K, et al. A cellular taxonomy of the bone marrow stroma in homeostasis and leukemia. *Cell* (2019) 177(7):1915–32.e16. doi: 10.1016/j.cell.2019.04.040

87. Baccin C, Al-Sabah J, Velten L, Helbling PM, Grünschläger F, Hernández-Malmierca P, et al. Combined single-cell and spatial transcriptomics reveal the molecular, cellular and spatial bone marrow niche organization. *Nat Cell Biol* (2020) 22(1):38–48. doi: 10.1038/s41556-019-0439-6

88. Severe N, Karabacak NM, Gustafsson K, Baryawno N, Courties G, Kfoury Y, et al. Stress-induced changes in bone marrow stromal cell populations revealed through single-cell protein expression mapping. *Cell Stem Cell* (2019) 25(4):570–83.e7. doi: 10.1016/j.stem.2019.06.003

89. Wolock SL, Krishnan I, Tenen DE, Matkins V, Camacho V, Patel S, et al. Mapping distinct bone marrow niche populations and their differentiation paths. *Cell Rep* (2019) 28(2):302–11.e5. doi: 10.1016/j.celrep.2019.06.031

90. Zhang P, Li X, Pan C, Zheng X, Hu B, Xie R, et al. Single-cell RNA sequencing to track novel perspectives in HSC heterogeneity. *Stem Cell Res Ther* (2022) 13(1):39. doi: 10.1186/s13287-022-02718-1

91. Dominguez CX, Müller S, Keerthivasan S, Koeppen H, Hung J, Gierke S, et al. Single-cell RNA sequencing reveals stromal evolution into LRRC15+ myofibroblasts as a determinant of patient response to cancer immunotherapy. *Cancer Discovery* (2020) 10(2):232–53. doi: 10.1158/2159-8290.CD-19-0644

92. Buechler MB, Pradhan RN, Krishnamurty AT, Cox C, Calviello AK, Wang AW, et al. Cross-tissue organization of the fibroblast lineage. *Nature* (2021) 593 (7860):575–9. doi: 10.1038/s41586-021-03549-5

93. Biffi G, Tuveson DA. Diversity and biology of cancer-associated fibroblasts. *Physiol Rev* (2021) 101(1):147–76. doi: 10.1152/physrev.00048.2019

94. Mannarapu M, Dariya B, Bandapalli OR. Application of single-cell sequencing technologies in pancreatic cancer. *Mol Cell Biochem* (2021) 476 (6):2429–37. doi: 10.1007/s11010-021-04095-4

95. Hu B, Wu C, Mao H, Gu H, Dong H, Yan J, et al. Subpopulations of cancer-associated fibroblasts link the prognosis and metabolic features of pancreatic ductal adenocarcinoma. *Ann Transl Med* (2022) 10(5):262. doi: 10.21037/atm-22-407

96. Affo S, Nair A, Brundu F, Ravichandra A, Bhattacharjee S, Matsuda M, et al. Promotion of cholangiocarcinoma growth by diverse cancer-associated fibroblast subpopulations. *Cancer Cell* (2021) 39(6):866–82.e11. doi: 10.1016/j.ccell.2021.03.012

97. Li X, Sun Z, Peng G, Xiao Y, Guo J, Wu B, et al. Single-cell RNA sequencing reveals a pro-invasive cancer-associated fibroblast subgroup associated with poor clinical outcomes in patients with gastric cancer. *Theranostics* (2022) 12(2):620–38. doi: 10.7150/thno.60540

98. Kumar V, Ramnarayanan K, Sundar R, Padmanabhan N, Srivastava S, Koiwa M, et al. Single-cell atlas of lineage states, tumor microenvironment, and subtype-specific expression programs in gastric cancer. *Cancer Discovery* (2022) 12 (3):670–91. doi: 10.1158/2159-8290.CD-21-0683

99. Hutton C, Heider F, Blanco-Gomez A, Banyard A, Kononov A, Zhang X, et al. Single-cell analysis defines a pancreatic fibroblast lineage that supports anti-tumor immunity. *Cancer Cell* (2021) 39(9):1227–44.e20. doi: 10.1016/j.ccell.2021.06.017

100. Obradovic A, Graves D, Korrer M, Wang Y, Roy S, Naveed A, et al. Immunostimulatory cancer-associated fibroblast subpopulations can predict immunotherapy response in head and neck cancer. *Clin Cancer Res* (2022) 28 (10):2094–109. doi: 10.1158/1078-0432.CCR-21-3570

101. Busch S, Andersson D, Bom E, Walsh C, Ståhlberg A, Landberg G. Cellular organization and molecular differentiation model of breast cancer-associated fibroblasts. *Mol Cancer* (2017) 16(1):73. doi: 10.1186/s12943-017-0642-7

102. Wu SZ, Roden DL, Wang C, Holliday H, Harvey K, Cazet AS, et al. Stromal cell diversity associated with immune evasion in human triple-negative breast cancer. *EMBO J* (2020) 39(19):e104063. doi: 10.15252/embj.2019104063

103. Marangoni RG, Korman B, Varga J. Adipocytic progenitor cells give rise to pathogenic myofibroblasts: Adipocyte-to-Mesenchymal transition and its emerging role in fibrosis in multiple organs. *Curr Rheumatol Rep* (2020) 22 (11):79. doi: 10.1007/s11926-020-00957-w

104. Hosaka K, Yang Y, Seki T, Fischer C, Dubey O, Fredlund E, et al. Pericyte-fibroblast transition promotes tumor growth and metastasis. *Proc Natl Acad Sci U.S.A.* (2016) 113(38):E5618–27. doi: 10.1073/pnas.1608384113

105. Feng F, Feng X, Zhang D, Li Q, Yao L. Matrix stiffness induces pericyte-fibroblast transition through YAP activation. *Front Pharmacol* (2021) 12:698275. doi: 10.3389/fphar.2021.698275

106. Haudek SB, Trial J, Xia Y, Gupta D, Pilling D, Entman ML. Fc receptor engagement mediates differentiation of cardiac fibroblast precursor cells. *Proc Natl Acad Sci U.S.A.* (2008) 105(29):10179–84. doi: 10.1073/pnas.0804910105

107. Dong Y, Yang M, Zhang J, Peng X, Cheng J, Cui T, et al. Depletion of CD8 + T cells exacerbates CD4+ T cell-induced monocyte-to-Fibroblast transition in renal fibrosis. *J Immunol* (2016) 196(4):1874–81. doi: 10.4049/jimmunol.1501232

108. Iwamoto C, Ohuchida K, Shinkawa T, Okuda S, Otsubo Y, Okumura T, et al. Bone marrow-derived macrophages converted into cancer-associated fibroblast-like cells promote pancreatic cancer progression. *Cancer Lett* (2021) 512:15–27. doi: 10.1016/j.canlet.2021.04.013

109. Shirasaki R, Tashiro H, Oka Y, Matsuo T, Yamamoto T, Sugao T, et al. Chronic myelogenous leukemia cells contribute to the stromal myofibroblasts in leukemic NOD/SCID mouse in vivo. *J Oncol* (2012) 2012:901783. doi: 10.1155/2012/901783

110. Tashiro H, Mizutani-Noguchi M, Shirasaki R, Shirafuji N. Acute myelogenous leukemia cells with the MLL-ELL translocation convert morphologically and functionally into adherent myofibroblasts. *Biochem Biophys Res Commun* (2010) 391(1):592–7. doi: 10.1016/j.bbrc.2009.11.104

111. Shirasaki R, Tashiro H, Mizutani-Noguchi M, Kawasugi K, Shirafuji N. Chronic myelogenous leukemia cells convert to myofibroblasts *in vitro*: effect of vascular endothelial growth factor on development of the microenvironment. *Leuk Res* (2011) 35(5):663–9. doi: 10.1016/j.leukres.2010.09.019

112. Pittenger MF, Discher DE, Péault BM, Phinney DG, Hare JM, Caplan AI. Mesenchymal stem cell perspective: cell biology to clinical progress. *NPJ Regener Med* (2019) 4:22. doi: 10.1038/s41536-019-0083-6

113. Andrzejewska A, Lukomska B, Janowski M. Concise review: Mesenchymal stem cells: From roots to boost. *Stem Cells* (2019) 37(7):855–64. doi: 10.1002/stem.3016

114. Lin D, Dass CR. Transdifferentiation of adipocytes to osteoblasts: potential for orthopaedic treatment. *J Pharm Pharmacol* (2018) 70(3):307–19. doi: 10.1111/jphp.12862

115. Hong KM, Burdick MD, Phillips RJ, Heber D, Strieter RM. Characterization of human fibrocytes as circulating adipocyte progenitors and the formation of human adipose tissue in SCID mice. *FASEB J* (2005) 19(14):2029–31. doi: 10.1096/fj.05-4295fje

116. Choi YH, Burdick MD, Strieter RM. Human circulating fibrocytes have the capacity to differentiate osteoblasts and chondrocytes. *Int J Biochem Cell Biol* (2010) 42(5):662–71. doi: 10.1016/j.biocel.2009.12.011

117. Niedermeier M, Reich B, Rodriguez Gomez M, Denzel A, Schmidbauer K, Göbel N, et al. CD4+ T cells control the differentiation of Gr1+ monocytes into fibrocytes. *Proc Natl Acad Sci U.S.A.* (2009) 106(42):17892–7. doi: 10.1073/pnas.0906070106

118. Reilkoff RA, Bucala R, Herzog EL. Fibrocytes: emerging effector cells in chronic inflammation. *Nat Rev Immunol* (2011) 11(6):427–35. doi: 10.1038/nri2990

119. Mangialardi G, Cordaro A, Madeddu P. The bone marrow pericyte: an orchestrator of vascular niche. *Regener Med* (2016) 11(8):883–95. doi: 10.2217/rme-2016-0121

120. Crisan M, Yap S, Casteilla L, Chen CW, Corselli M, Park TS, et al. A perivascular origin for mesenchymal stem cells in multiple human organs. *Cell Stem Cell* (2008) 3(3):301–13. doi: 10.1016/j.stem.2008.07.003

121. Zhang J, Liu Y, Yin W, Hu X. Adipose-derived stromal cells in regulation of hematopoiesis. *Cell Mol Biol Lett* (2020) 25:16. doi: 10.1186/s11658-020-00209-w

122. Raab S, Klingenstein M, Liebau S, Linta L. A comparative view on human somatic cell sources for iPSC generation. *Stem Cells Int* (2014) 2014:768391. doi: 10.1155/2014/768391

123. Greenberg BR, Woo L, Veomett IC, Payne CM, Ahmann FR. Cytogenetics of bone marrow fibroblastic cells in idiopathic chronic myelofibrosis. *Br J Haematol* (1987) 66(4):487–90. doi: 10.1111/j.1365-2141.1987.tb01332.x

124. Tomuleasa C, Selicean S, Gafencu G, Petrushev B, Pop L, Berce C, et al. Fibroblast dynamics as an *in vitro* screening platform for anti-fibrotic drugs in primary myelofibrosis. *J Cell Physiol* (2018) 233(1):422–33. doi: 10.1002/jcp.25902

125. Tefferi A. Pathogenesis of myelofibrosis with myeloid metaplasia. *J Clin Oncol* (2005) 23(33):8520–30. doi: 10.1200/JCO.2004.00.9316

126. Venugopal S, Mascarenhas J. Current clinical investigations in myelofibrosis. *Hematol Oncol Clin North Am* (2021) 35(2):353–73. doi: 10.1016/j.hoc.2020.12.003

127. Song IC, Yeon SH, Lee MW, Ryu H, Lee HJ, Yun HJ, et al. Myelofibrotic and leukemic transformation in 2016 WHO-defined Philadelphia-negative myeloproliferative neoplasm. *Blood Res* (2022) 57(1):59–68. doi: 10.5045/br.2021.2021209

128. Mughal TI, Vaddi K, Sarlis NJ, Verstovsek S. Myelofibrosis-associated complications: pathogenesis, clinical manifestations, and effects on outcomes. *Int J Gen Med* (2014) 7:89–101. doi: 10.2147/IJGM.S51800

129. Mesa RA, Li CY, Ketterling RP, Schroeder GS, Knudson RA, Tefferi A. Leukemic transformation in myelofibrosis with myeloid metaplasia: a single-institution experience with 91 cases. *Blood* (2005) 105(3):973–7. doi: 10.1182/blood-2004-07-2864

130. Kundranda MN, Tibes R, Mesa RA. Transformation of a chronic myeloproliferative neoplasm to acute myelogenous leukemia: does anything work. *Curr Hematol Malig Rep* (2012) 7(1):78–86. doi: 10.1007/s11899-011-0107-9

131. Tefferi A, Lasho TL, Jimma T, Finke CM, Gangat N, Vaidya R, et al. One thousand patients with primary myelofibrosis: the mayo clinic experience. *Mayo Clin Proc* (2012) 87(1):25–33. doi: 10.1016/j.mayocp.2011.11.001

132. Kundel DW, Brecher G, Bodey GP, Brittin GM. Reticulin fibrosis and bone infarction in acute leukemia. implications for prognosis. *Blood* (1964) 23:526–44. doi: 10.1182/blood.V23.4.526.526

133. Norén-Nyström U, Heyman M, Frisk P, Golovleva I, Sundström C, Porwit A, et al. Vascular density in childhood acute lymphoblastic leukaemia correlates to biological factors and outcome. *Br J Haematol* (2009) 146(5):521–30. doi: 10.1111/j.1365-2141.2009.07796.x

134. Norén-Nyström U, Roos G, Bergh A, Botling J, Lönnerholm G, Porwit A, et al. Bone marrow fibrosis in childhood acute lymphoblastic leukemia correlates to biological factors, treatment response and outcome. *Leukemia* (2008) 22(3):504–10. doi: 10.1038/sj.leu.2405072

135. Wallis JP, Reid MM. Bone marrow fibrosis in childhood acute lymphoblastic leukaemia. *J Clin Pathol* (1989) 42(12):1253–4. doi: 10.1136/jcp.42.12.1253

136. Nath SV, Nicholson I, Tapp H, Zola H, Zannettino AC, Revesz T. Reticulin fibres anchor leukaemic blasts in the marrow of patients with acute lymphoblastic leukaemia. *Med Hypotheses* (2011) 77(3):333–5. doi: 10.1016/j.mehy.2011.05.007

137. Zhang X, Wang F, Yu J, Jiang Z. Significance of bone marrow fibrosis in acute myeloid leukemia for survival in the real-world. *Front Oncol* (2022) 12:971082. doi: 10.3389/fonc.2022.971082

138. Bharos A, Jong AJ, Manton N, Venn N, Story C, Hodge G, et al. Bone marrow fibrosis and vascular density lack prognostic significance in childhood acute lymphoblastic leukaemia. *Leukemia* (2010) 24(8):1537–8. doi: 10.1038/leu.2010.134

139. Kuter DJ, Bain B, Mufti G, Bagg A, Hasserjian RP. Bone marrow fibrosis: pathophysiology and clinical significance of increased bone marrow stromal fibres. *Br J Haematol* (2007) 139(3):351–62. doi: 10.1111/j.1365-2141.2007.06807.x

140. Frassanito MA, Rao L, Moschetta M, Ria R, Di Marzo L, De Luisi A, et al. Bone marrow fibroblasts parallel multiple myeloma progression in patients and mice: *in vitro* and *in vivo* studies. *Leukemia* (2014) 28(4):904–16. doi: 10.1038/leu.2013.254

141. Duan CW, Shi J, Chen J, Wang B, Yu YH, Qin X, et al. Leukemia propagating cells rebuild an evolving niche in response to therapy. *Cancer Cell* (2014) 25(6):778–93. doi: 10.1016/j.ccr.2014.04.015

142. Paggetti J, Haderk F, Seiffert M, Janji B, Distler U, Ammerlaan W, et al. Exosomes released by chronic lymphocytic leukemia cells induce the transition of stromal cells into cancer-associated fibroblasts. *Blood* (2015) 126(9):1106–17. doi: 10.1182/blood-2014-12-618025

143. Zhai Y, Zhang J, Wang H, Lu W, Liu S, Yu Y, et al. Growth differentiation factor 15 contributes to cancer-associated fibroblasts-mediated chemo-protection of AML cells. *J Exp Clin Cancer Res* (2016) 35(1):147. doi: 10.1186/s13046-016-0405-0

144. Burt R, Dey A, Aref S, Aguiar M, Akarca A, Bailey K, et al. Activated stromal cells transfer mitochondria to rescue acute lymphoblastic leukemia cells from oxidative stress. *Blood* (2019) 134(17):1415–29. doi: 10.1182/blood.2019001398

145. Pan C, Fang Q, Liu P, Ma D, Cao S, Zhang L, et al. Mesenchymal stem cells with cancer-associated fibroblast-like phenotype stimulate SDF-1/CXCR4 axis to enhance the growth and invasion of b-cell acute lymphoblastic leukemia cells through cell-to-Cell communication. *Front Cell Dev Biol* (2021) 9:708513. doi: 10.3389/fcell.2021.708513

146. Pan C, Liu P, Ma D, Zhang S, Ni M, Fang Q, et al. Bone marrow mesenchymal stem cells in microenvironment transform into cancer-associated fibroblasts to promote the progression of b-cell acute lymphoblastic leukemia. *BioMed Pharmacother* (2020) 130:110610. doi: 10.1016/j.biopha.2020.110610

147. Li Y, Gu L. Establishment and characterization of HXWMF-1: the first mouse fibroblastic tumor cell line derived from leukemia-associated fibroblasts. *Cancer Cell Int* (2021) 21(1):177. doi: 10.1186/s12935-021-01870-7

148. Zhu Y, Yang R, Gao J, Zhang Y, Zhang G, Gu L. Establishment and characterization of a novel childhood acute lymphoblastic leukemia cell line, HXEX-ALL1, with chromosome 9p and 17p deletions. *Cancer Cell Int* (2019) 19:113. doi: 10.1186/s12935-019-0834-x

149. Kim Y, Jekarl DW, Kim J, Kwon A, Choi H, Lee S, et al. Genetic and epigenetic alterations of bone marrow stromal cells in myelodysplastic syndrome and acute myeloid leukemia patients. *Stem Cell Res* (2015) 14(2):177–84. doi: 10.1016/j.scr.2015.01.004

150. Blau O, Baldus CD, Hofmann WK, Thiel G, Nolte F, Burmeister T, et al. Mesenchymal stromal cells of myelodysplastic syndrome and acute myeloid leukemia patients have distinct genetic abnormalities compared with leukemic blasts. *Blood* (2011) 118(20):5583–92. doi: 10.1182/blood-2011-03-343467

151. Blau O, Hofmann WK, Baldus CD, Thiel G, Serbent V, Schümann E, et al. Chromosomal aberrations in bone marrow mesenchymal stroma cells from patients with myelodysplastic syndrome and acute myeloblastic leukemia. *Exp Hematol* (2007) 35(2):221–9. doi: 10.1016/j.exphem.2006.10.012

152. Yeh SP, Lo WJ, Lin CL, Liao YM, Lin CY, Bai LY, et al. Anti-leukemic therapies induce cytogenetic changes of human bone marrow-derived mesenchymal stem cells. *Ann Hematol* (2012) 91(2):163–72. doi: 10.1007/s00277-011-1254-8

153. Huang JC, Basu SK, Zhao X, Chien S, Fang M, Oehler VG, et al. Mesenchymal stromal cells derived from acute myeloid leukemia bone marrow exhibit aberrant cytogenetics and cytokine elaboration. *Blood Cancer J* (2015) 5:e302. doi: 10.1038/bcj.2015.17

154. Campioni D, Bardi MA, Cavazzini F, Tammiso E, Pezzolo E, Pregnolato E, et al. Cytogenetic and molecular cytogenetic profile of bone marrow-derived mesenchymal stromal cells in chronic and acute lymphoproliferative disorders. *Ann Hematol* (2012) 91(10):1563–77. doi: 10.1007/s00277-012-1500-8

155. Diaz de la Guardia R, Lopez-Millan B, Lavoie JR, Bueno C, Castaño J, Gómez-Casares M, et al. Detailed characterization of mesenchymal Stem/Stromal cells from a Large cohort of AML patients demonstrates a definitive link to treatment outcomes. *Stem Cell Rep* (2017) 8(6):1573–86. doi: 10.1016/j.stemcr.2017.04.019

156. Flores-Figueroa E, Montesinos JJ, Flores-Guzmán P, Gutiérrez-Espíndola G, Arana-Trejo RM, Castillo-Medina S, et al. Functional analysis of myelodysplastic syndromes-derived mesenchymal stem cells. *Leuk Res* (2008) 32(9):1407–16. doi: 10.1016/j.leukres.2008.02.013

157. Xie J, Chen J, Wang B, He X, Huang H. Bone mesenchymal stromal cells exhibit functional inhibition but no chromosomal aberrations in chronic myelogenous leukemia. *Oncol Lett* (2019) 17(1):999–1007. doi: 10.3892/ol.2018.9681

158. Gunsilius E, Duba HC, Petzer AL, Kähler CM, Grünewald K, Stockhammer G, et al. Evidence from a leukaemia model for maintenance of vascular endothelium by bone-marrow-derived endothelial cells. *Lancet* (2000) 355(9216):1688–91. doi: 10.1016/S0140-6736(00)02241-8

159. Zhou Y, Bian S, Zhou X, Cui Y, Wang W, Wen L, et al. Single-cell multiomics sequencing reveals prevalent genomic alterations in tumor stromal cells of human colorectal cancer. *Cancer Cell* (2020) 38(6):818–28.e5. doi: 10.1016/j.ccell.2020.09.015

160. Novo D, Heath N, Mitchell L, Caligiuri G, MacFarlane A, Reijmer D, et al. Mutant p53s generate pro-invasive niches by influencing exosome podocalyxin levels. *Nat Commun* (2018) 9(1):5069. doi: 10.1038/s41467-018-07339-y

161. Tuhkanen H, Anttila M, Kosma VM, Heinonen S, Juhola M, Helisalmi S, et al. Frequent gene dosage alterations in stromal cells of epithelial ovarian carcinomas. *Int J Cancer* (2006) 119(6):1345–53. doi: 10.1002/ijc.21785

162. Patocs A, Zhang L, Xu Y, Weber F, Caldes T, Mutter GL, et al. Breast-cancer stromal cells with TP53 mutations and nodal metastases. *N Engl J Med* (2007) 357(25):2543–51. doi: 10.1056/NEJMoa071825

163. Moinfar F, Man YG, Arnould L, Bratthauer GL, Ratschek M, Tavassoli FA. Concurrent and independent genetic alterations in the stromal and epithelial cells of mammary carcinoma: implications for tumorigenesis. *Cancer Res* (2000) 60(9):2562–6.

164. Sakemura R, Hefazi M, Siegler EL, Cox MJ, Larson DP, Hansen MJ, et al. Targeting cancer-associated fibroblasts in the bone marrow prevents resistance to CART-cell therapy in multiple myeloma. *Blood* (2022) 139(26):3708–21. doi: 10.1182/blood.2021012811

165. Özdemir BC, Pentcheva-Hoang T, Carstens JL, Zheng X, Wu CC, Simpson TR, et al. Depletion of carcinoma-associated fibroblasts and fibrosis induces immunosuppression and accelerates pancreas cancer with reduced survival. *Cancer Cell* (2014) 25(6):719–34. doi: 10.1016/j.ccr.2014.04.005

166. Rhim AD, Oberstein PE, Thomas DH, Mirek ET, Palermo CF, Sastra SA, et al. Stromal elements act to restrain, rather than support, pancreatic ductal adenocarcinoma. *Cancer Cell* (2014) 25(6):735–47. doi: 10.1016/j.ccr.2014.04.021

167. Zhang Y, Lazarus J, Steele NG, Yan W, Lee HJ, Nwosu ZC, et al. Regulatory T-cell depletion alters the tumor microenvironment and accelerates pancreatic carcinogenesis. *Cancer Discovery* (2020) 10(3):422–39. doi: 10.1158/2159-8290.CD-19-0958

168. Paulsson J, Micke P. Prognostic relevance of cancer-associated fibroblasts in human cancer. *Semin Cancer Biol* (2014) 25:61–8. doi: 10.1016/j.semcancer.2014.02.006

169. Brechbuhl HM, Finlay-Schultz J, Yamamoto TM, Gillen AE, Cittelly DM, Tan AC, et al. Fibroblast subtypes regulate responsiveness of luminal breast cancer to estrogen. *Clin Cancer Res* (2017) 23(7):1710–21. doi: 10.1158/1078-0432.CCR-15-2851

170. Li C, Teixeira AF, Zhu HJ, Ten Dijke P. Cancer associated-fibroblast-derived exosomes in cancer progression. *Mol Cancer* (2021) 20(1):154. doi: 10.1186/s12943-021-01463-y

171. Kadel D, Zhang Y, Sun HR, Zhao Y, Dong QZ, Qin LX. Current perspectives of cancer-associated fibroblast in therapeutic resistance: potential mechanism and future strategy. *Cell Biol Toxicol* (2019) 35(5):407–21. doi: 10.1007/s10565-019-09461-z

172. Hanahan D. Hallmarks of cancer: New dimensions. *Cancer Discovery* (2022) 12(1):31–46. doi: 10.1158/2159-8290.CD-21-1059

173. Hanahan D, Weinberg RA. Hallmarks of cancer: the next generation. *Cell* (2011) 144(5):646–74. doi: 10.1016/j.cell.2011.02.013

174. Hanahan D, Weinberg RA. The hallmarks of cancer. *Cell* (2000) 100(1):57–70. doi: 10.1016/s0092-8674(00)81683-9

175. Welt S, Divgi CR, Scott AM, Garin-Chesa P, Finn RD, Graham M, et al. Antibody targeting in metastatic colon cancer: a phase I study of monoclonal antibody F19 against a cell-surface protein of reactive tumor stromal fibroblasts. *J Clin Oncol* (1994) 12(6):1193–203. doi: 10.1200/JCO.1994.12.6.1193

176. Öhlund D, Handly-Santana A, Biffi G, Elyada E, Almeida AS, Ponz-Sarvise M, et al. Distinct populations of inflammatory fibroblasts and myofibroblasts in pancreatic cancer. *J Exp Med* (2017) 214(3):579–96. doi: 10.1084/jem.20162024

177. Biffi G, Oni TE, Spielman B, Hao Y, Elyada E, Park Y, et al. IL1-induced JAK/STAT signaling is antagonized by TGFβ to shape CAF heterogeneity in pancreatic ductal adenocarcinoma. *Cancer Discovery* (2019) 9(2):282–301. doi: 10.1158/2159-8290.CD-18-0710

178. Friedman G, Levi-Galibov O, David E, Bornstein C, Giladi A, Dadiani M, et al. Cancer-associated fibroblast compositions change with breast cancer progression linking the ratio of S100A4(+) and PDPN(+) CAFs to clinical outcome. *Nat Cancer* (2020) 1(7):692–708. doi: 10.1038/s43018-020-0082-y

179. Nurmik M, Ullmann P, Rodriguez F, Haan S, Letellier E. In search of definitions: Cancer-associated fibroblasts and their markers. *Int J Cancer* (2020) 146(4):895–905. doi: 10.1002/ijc.32193

180. Li H, Courtois ET, Sengupta D, Tan Y, Chen KH, Goh J, et al. Reference component analysis of single-cell transcriptomes elucidates cellular heterogeneity in human colorectal tumors. *Nat Genet* (2017) 49(5):708–18. doi: 10.1038/ng.3818

181. Zhang R, Zong J, Peng Y, Shi J, Du X, Liu H, et al. GPR30 knockdown weakens the capacity of CAF in promoting prostate cancer cell invasion via reducing macrophage infiltration and M2 polarization. *J Cell Biochem* (2021). doi: 10.1002/jcb.29938

182. Francescone R, Barbosa Vendramini-Costa D, Franco-Barraza J, Wagner J, Muir A, Lau AN, et al. Netrin G1 promotes pancreatic tumorigenesis through cancer-associated fibroblast-driven nutritional support and immunosuppression. *Cancer Discovery* (2021) 11(2):446–79. doi: 10.1158/2159-8290.CD-20-0775

183. Ogier C, Colombo PE, Bousquet C, Canterel-Thouennon L, Sicard P, Garambois V, et al. Targeting the NRG1/HER3 pathway in tumor cells and cancer-associated fibroblasts with an anti-neuregulin 1 antibody inhibits tumor growth in pre-clinical models of pancreatic cancer. *Cancer Lett* (2018) 432:227–36. doi: 10.1016/j.canlet.2018.06.023

184. Garcia PE, Adoumie M, Kim EC, Zhang Y, Scales MK, El-Tawil YS, et al. Differential contribution of pancreatic fibroblast subsets to the pancreatic cancer stroma. *Cell Mol Gastroenterol Hepatol* (2020) 10(3):581–99. doi: 10.1016/j.jcmgh.2020.05.004

185. Joo EH, Bae JH, Park J, Bang YJ, Han J, Gulati N, et al. Deconvolution of adult T-cell Leukemia/Lymphoma with single-cell RNA-seq using frozen archived skin tissue reveals new subset of cancer-associated fibroblast. *Front Immunol* (2022) 13:856363. doi: 10.3389/fimmu.2022.856363

186. Wang LC, Lo A, Scholler J, Sun J, Majumdar RS, Kapoor V, et al. Targeting fibroblast activation protein in tumor stroma with chimeric antigen receptor T cells can inhibit tumor growth and augment host immunity without severe toxicity. *Cancer Immunol Res* (2014) 2(2):154–66. doi: 10.1158/2326-6066.CIR-13-0027

187. Bughda R, Dimou P, D'Souza RR, Klampatsa A. Fibroblast activation protein (FAP)-targeted CAR-T cells: Launching an attack on tumor stroma. *Immunotargets Ther* (2021) 10:313–23. doi: 10.2147/ITT.S291767

188. Hiltbrunner S, Britschgi C, Schuberth P, Bankel L, Nguyen-Kim T, Gulati P, et al. Local delivery of CAR T cells targeting fibroblast activation protein is safe in patients with pleural mesothelioma: first report of FAPME, a phase I clinical trial. *Ann Oncol* (2021) 32(1):120–1. doi: 10.1016/j.annonc.2020.10.474

189. Gross G, Waks T, Eshhar Z. Expression of immunoglobulin-t-cell receptor chimeric molecules as functional receptors with antibody-type specificity. *Proc Natl Acad Sci U.S.A.* (1989) 86(24):10024–8. doi: 10.1073/pnas.86.24.10024

190. Maude SL, Laetsch TW, Buechner J, Rives S, Boyer M, Bittencourt H, et al. Tisagenlecleucel in children and young adults with b-cell lymphoblastic leukemia. *N Engl J Med* (2018) 378(5):439–48. doi: 10.1056/NEJMoa1709866

191. Halford Z, Anderson MK, Bennett LL, Moody J. Tisagenlecleucel in acute lymphoblastic leukemia: A review of the literature and practical considerations. *Ann Pharmacother* (2021) 55(4):466–79. doi: 10.1177/1060028020948165

192. Sterner RC, Sterner RM. CAR-T cell therapy: current limitations and potential strategies. *Blood Cancer J* (2021) 11(4):69. doi: 10.1038/s41408-021-00459-7

frontiers | Frontiers in Oncology

TYPE Review
PUBLISHED 07 February 2023
DOI 10.3389/fonc.2023.1078556

OPEN ACCESS

EDITED BY
Spiros Vlahopoulos,
University of Athens, Greece

REVIEWED BY
Zixing Chen,
First Affiliated Hospital of Soochow University, China
Liping Dou,
People's Liberation Army General Hospital, China

*CORRESPONDENCE
Hua Wang
huagnaw@163.com
Kai-Min Li
ytyhdyykytg@163.com
Jing-Hua Ma
13954599511@163.com

†These authors share first authorship

SPECIALTY SECTION
This article was submitted to Hematologic Malignancies, a section of the journal Frontiers in Oncology

RECEIVED 24 October 2022
ACCEPTED 26 January 2023
PUBLISHED 07 February 2023

CITATION
Yin P-Y, Wang R-W, Jing R, Li X, Ma J-H, Li K-M and Wang H (2023) Research progress on molecular biomarkers of acute myeloid leukemia. *Front. Oncol.* 13:1078556. doi: 10.3389/fonc.2023.1078556

Research progress on molecular biomarkers of acute myeloid leukemia

Pei-Yuan Yin[1,2†], Rui-Wen Wang[3†], Rui Jing[1†], Xing Li[2], Jing-Hua Ma[4*], Kai-Min Li[5*] and Hua Wang[1*]

[1]Hematology Department, Yantai Affiliated Hospital, Binzhou Medical University, Yantai, Shandong, China, [2]Department of Blood Supply, Yantai Center Blood Station, Yantai, Shandong, China, [3]Department of Anesthesiology, Yantai Yuhuangding Hospital, Qingdao University, Yantai, Shandong, China, [4]Department of Science and Education, Yantai Hospital of Traditional Chinese Medicine, Yantai, Shandong, China, [5]Hematology Department, Yantai Yuhuangding Hospital, Qingdao University, Yantai, Shandong, China

Acute myeloid leukemia (AML) is the most common type of adult acute leukemia. The pathophysiology of the disease has been studied intensively at the cellular and molecular levels. At present, cytogenetic markers are an important basis for the early diagnosis, prognostic stratification and treatment of AML. However, with the emergence of new technologies, the detection of other molecular markers, such as gene mutations and epigenetic changes, began to play important roles in evaluating the occurrence and development of diseases. Recent evidence shows that identifying new AML biomarkers contributes to a better understanding of the molecular mechanism of the disease and is essential for AML screening, diagnosis, prognosis monitoring, and individualized treatment response. In this review, we summarized the promising AML biomarkers from four aspects, which contributing to a better understanding of the disease. Of course, it must be soberly aware that we have not listed all biomarkers of AML. Anyway, the biomarkers we mentioned are representative. For example, mutations in TP53, FLT3, and ASXL1 suggest poor prognosis, low remission rate, short survival period, and often require allogeneic hematopoietic stem cell transplantation. The CEBPA double mutation, NPM1 and CBF mutation suggest that the prognosis is good, the remission rate is high, the survival period is long, and the effect of chemotherapy or autotherapy is good. As for other mutations mentioned in the article, they usually predict a moderate prognosis. All in all, we hope it could provide a reference for the precise diagnosis and treatment of AML.

KEYWORDS

acute myeloid leukemia, biomarker, gene mutation, chromosome, epigenetics

1 Introduction

Acute myeloid leukemia (AML) is a type of malignant tumor affecting hemopoietic stem cells/progenitor cells and is characterized by abnormal proliferation of primitive cells in bone marrow and peripheral blood. The clinical manifestations of AML include anemia, hemorrhage, infection and organ infiltration. The incidence of AML has been increasing

with the passage of time, and men are more likely to suffer from the disease than women (1). At present, cytogenetic and molecular abnormalities are still the most important prognostic factors of AML and are closely related to clinical features (age, white blood cell count and morphology), treatment response, recurrence rate and overall survival (OS) (2–4). This has laid a solid foundation for the development of disease prognostic stratification by the World Health Organization (WHO) and European Leukemia Net (ELN). At present, the five-year survival rate of all adult AML patients is less than 50%, which is even lower in elderly patients. Statistics have shown that the median OS of patients > 65 years is less than one year (5). This paper summarizes the molecular biomarkers related to AML and elaborates their clinical value in early diagnosis and prognosis. Among them, prognostic markers can estimate the severity of the disease and predict the long-term outcome of patients, whereas predictive markers allow the surveillance of treatment response and recurrence.

2 Marker source 1: Specific gene mutation-related molecules

2.1 Nucleophosmin 1

NPM1 mutation is the most common gene mutation related to AML. NPM1 is located in the long arm of chromosome 5 and encodes a multifunctional chaperone protein shuttling between the nucleus and cytoplasm. NPM1 is mainly involved in the regulation of ribosomal protein assembly and trafficking, the stabilization of the tumor suppressors p19ARF and p53 pathway, DNA repair process, genome stability, and ultimately regulates DNA transcription by altering chromatin structure. As a tumor suppressor, any mutation that disrupts its normal function will lead to the transformation of normal cells into malignancy. In addition, wild-type NPM1 protein localizes to the nucleolus in normal cells. However, the mutant protein usually mislocalizes to the cytoplasm, which is closely related to the pathogenesis of leukemia, but its specific mechanism is still unclear (6). NPM1 mutations are only found in myeloid cells and have been detected in a few cases of chronic myelomonocytic leukemia, all of which progressed to AML within one year. NPM1 mutations are most frequently detected in the M4 and M5 subtypes of AML but are rarely found in acute promyelocytic leukemia (APL). AML accounts for approximately 30% of all AML cases and 40-60% of AML cases with normal karyotypes. Clinical data showed that patients with mutant NPM1 had a higher number of myeloid progenitor cells, higher white blood cell and platelet counts, lower CD34 level, a complete remission rate (CRR) of 58-60%, and a median OS of 16.2 months (6).

ELN guidelines suggest that NPM1-mutant patients with an allelic ratio (AR) < 0.5 for FMS, such as tyrosine kinase 3-internal tandem replication (FLT3-ITD), have a good prognosis, and allogeneic hematopoietic stem cell transplantation (allo-HSCT) is not recommended after the first complete remission. According to the 2021 National Comprehensive Cancer Network (NCCN) guidelines, NPM1-mutant patients without FLT3-ITD or with FLT3-ITDlow are classified into the good prognosis group, whereas patients with NPM1 mutation and FLT3-ITDhigh are classified into the intermediate prognosis group. Therefore, it is assumed that leukemogenesis is not induced by NPM1 mutation alone but is also related to other cellular and molecular genetic changes, such as FLT3-ITD.

It has been found that NPM1 mutation accompanied by mutations in isocitrate dehydrogenase 1/2 (IDH1/2) and DNA methyltransferase 3 alpha (DNMT3A) led to poor prognosis, and it is generally believed that such mutations are secondary to the NPM1 mutation. Similar to promyelocytic leukemia-retinoic acid receptor α (PML-RARA) rearrangement, NPM1 can also serve as a marker for the surveillance of minimal residual disease (MRD) in AML patients. That is, the increase in mutant NPM1 in peripheral blood is predictive of the relapse of AML in patients with complete remission morphologically. Therefore, timely and reasonable intervention can be carried out according to the NPM1 level in MRD. For AML patients with NPM1 mutation, it is currently known that combined application of all-trans retinoic acid (ATRA) and arsenic trioxide (ATO) can degrade the mutant NPM1 protein and further induce the apoptosis of AML cells (7). Our understanding of the mechanism of targeted therapies based on NPM1 is still incomplete, and large-scale basic studies are still needed to explore the function and mechanism of NPM1 to provide a new theoretical basis for the treatment of AML.

2.2 FLT3

FLT3 is located on the long arm of chromosome 13 and is a member of the type III receptor tyrosine kinase (RTK) family. It participates in the proliferation, differentiation and apoptosis of hematopoietic cells through the extracellular domain containing ligand binding sites. FLT3 mutation is the most common RTK mutation in AML, accounting for approximately 30% of cases, of which ITD accounts for approximately 25%, and tyrosine kinase domain (TKD) point mutation accounts for only 7%. FLT3-ITD is usually common in AML with a normal karyotype, and the prognosis is poor. At the molecular level, mutant FLT3 activates downstream factors related to the STAT5, RAS/MAPK and PI3K signaling pathways.

In terms of clinical characteristics, relevant statistical data showed that the expression level of FLT3 was correlated with different National Comprehensive Cancer Network(NCCN) stratification of AML, with the lowest level in the M3 subtype and the highest level in M5. Several studies have shown that patients with FLT3 mutations are mainly characterized by high white blood cell counts in the peripheral blood, high myeloid progenitor cell counts, and poor prognosis (8–10). Among them, FLT3-ITD patients are prone to combined PML-RARA rearrangement, which rarely occurs in AML patients with complex karyotypes or core binding factor (CBF)-AML. Compared with FLT-TKD patients, FLT-ITD patients have significantly lower OS and event-free survival (EFS) and worse prognosis. A study showed that the prognosis of FLT3-mutant patients was closely correlated with the expression ratio of the mutant FLT3 allele against the wild-type FLT3 allele. The greater the ratio, the shorter the duration of remission (DOR), EFS and OS. Therefore, DNA fragment analysis technology was utilized to quantify the relative level of mutant alleles and to define a cutoff value to distinguish different prognostic subgroups (11).

For AML with FLT3 mutation, small molecule tyrosine kinase inhibitors such as sorafenib, midostaurin and sunitinib have been available for the inhibition of the FLT3 signaling pathway and for the targeted killing of leukemia cells. In recent years, a large number of clinical trials have shown great improvements in the therapeutic effect of multitarget small molecule tyrosine kinase inhibitors on AML patients compared with traditional chemotherapy. However, due to drug resistance, the DORs of such drugs alone are still not satisfying, and combination use with other chemotherapy drugs has become the preferred strategy for the treatment of this type of AML.

2.3 Tumor protein p53

TP53 is located in the short arm of chromosome 17 and encodes a key transcription factor, which is mainly involved in DNA mismatch repair, base excision repair and nucleotide excision repair at the time of cell cycle arrest. When this tumor suppressor gene is mutated, such as with a deletion mutation, cell proliferation becomes uncontrolled, and tumorigenesis may occur. TP53 mutations exist in a variety of cancers, such as Li-Fraumeni syndrome, ovarian cancer, esophageal cancer, colorectal cancer and lung cancer, and their mutation frequency is associated with cancer type. The IARC TP53 database shows that TP53 mutations are not as common in hematological malignancies as in other types of cancer (approximately 5.89%, compared with 12.77% in colorectal cancer and 10.2% in breast cancer). In AML, most TP53 mutations involve single nucleotide changes, with missense mutations being the most common, followed by frameshift mutations and nonsense mutations. TP53 mutations account for approximately 10% of newly diagnosed AML, 20-37% of therapy-related AML (T-AML) or secondary AML, and up to 70% of complex karyotype AML. They are important markers of poor prognosis in complex karyotype AML and T-AML. TP53 mutations are more common in elderly patients, patients with 17p mutation or chromosome 5 and 7 aberrations, with significantly lower CRR, higher recurrence rate, and shorter EFS and OS. Compared with patients with wild-type TP53, the CRR of TP53-mutant patients was only 28.6%. After chemotherapy with cytarabine or demethylating drugs, the patients' median OS was 6-8 months. Even after HSCT, such patients will still have a high recurrence rate and serious adverse reactions, with a median OS of 8 months, a one-year survival rate of 35%, and a recurrence rate after one year of 53% (12). Recently, a study showed that TP53-mutant patients were possibly more sensitive to the 10-day regimen of decitabine chemotherapy, and the CRR of the mutant TP53 group was significantly better than that of the wild-type TP53 group (13). The ELN guidelines recommend early screening of TP53 mutation to assist in prognostic stratification and making initial treatment plans. At present, the treatment options for patients with TP53 mutations are limited, and the poor prognosis of standard chemotherapy regimens may be related to resistance to chemotherapy drugs. In 2018, the American Society of Hematology proposed that the therapeutic response of the new TP53 regulator APR-246 was significantly better than those of traditional regimens, with a CRR of approximately 82% and a median OS of more than 7 months. The European Medicines Agency approved APR-246 as an orphan drug for the treatment of myelodysplastic syndromes (MDS), AML and ovarian cancer. The Food and Drug Administration (FDA) also approved APR-246 combined with azacitidine for the treatment of Li-Fraumeni syndrome complicated with MDS in January 2020. A recent study showed that APR-246 and azacitidine play a synergistic role in TP53-mutated MDS/AML, which can restore the transcriptional activation function of mutant TP53 and induce apoptosis of human tumor cells (14), and preclinical trials are currently underway.

2.4 CCAAT enhancer binding protein alpha

The CEBPA gene is located on the long arm of chromosome 19. CEBPA protein is a transcription factor with leucine zipper, the structure of which includes the transcriptional active region at the N-terminus, the DNA-binding region, and the leucine rich dimerization functional region at the C-terminus. There are two types of CEBPA mutations: out-of-frame insertions or deletions at the N-terminus and in-frame insertions or deletions at the C-terminus. CEBPA double mutation (biCEBPA) refers to the mutation of CEPBP on both alleles of chromosome 19. CEBPA plays a key role in the differentiation of hematopoietic myeloid cells. Approximately 10% of AML patients and 7-15% of AML patients with normal karyotypes carry CEBPA mutations. Most of them are the M2 type, and their prognosis is generally good. According to the 2016 WHO classification of hematopoietic and lymphoid neoplasms, "AML with biCEBPA" was defined as a clinical subtype of AML with unique molecular biological characteristics. The ELN guidelines also recommend early screening of CEBPA mutations. Multicenter clinical data showed that compared with all AML patients, biCEBPA was significantly correlated with improved EFS and OS when receiving cytarabine-based chemotherapy, with hazard ratios (HR) of 0.41 and 0.37, respectively, but was not correlated with consolidation strategies such as HSCT, indicating that biCEBPA was positively correlated with improved prognosis. Interestingly, through sequencing analysis of normal karyotype AML patients with CEBPA mutations in recent years, researchers have found that Tet methylcytosine dioxygenase 2 (TET2) and GATA2 mutations are more likely to occur in biCEBPA patients (approximately 30%), while CEBPA single mutation (moCEBPA) patients are more likely to have combined NPM1, FLT-ITD/TKD and IDH2 mutations, and the prognosis is relatively poor when combined with TET2 mutations (15, 16). Although CEBPA has not yet been identified as a marker of MRD, the specific immunophenotype associated with biCEBPA might become a favorable tool for disease screening and treatment monitoring. Here, what needs to be specially mentioned was GATA2 mutation. GATA2 may be a novel susceptibility gene for familial AML (17). GATA2 is considered to be a hematopoietic "stem" gene, which is highly expressed in hematopoietic stem cells and is required for megakaryocyte and mast cell generation. GATA2 is down-regulated during myeloid differentiation, forcing over-expression to inhibit this differentiation. The discovery of GATA2 mutant in AML susceptibility family provides a new method to explore the mechanism of GATA2 inducing leukemia, and may clarify its role in maintaining "stem". The prognosis of AML was poor when the patient with GATA2 mutations. Boldly, it may be appropriate to take active strategies to treat the affected individuals in the family with GATA2 mutations before symptoms.

3 Marker source 2: Chromosome position abnormality-related molecules

3.1 PML-RARA

PML-RARA is encoded by a fusion gene generated by the t (14; 16) (q24; q21) translocation. It is a major molecular feature of APL and is present in approximately 98% of APL patients (18). PML-RARA plays a role in causing APL by two primary effects, which is deregulates transcriptional control (19). PML is mainly involved in the regulation of signaling pathways and induction of the transcription of the cell cycle inhibitor p27Kip and the proapoptotic factor Bim. The RARA gene is located on 17q21 and encodes a nuclear receptor that activates transcription in the presence of its ligand retinoic acid, inducing many target genes involved in differentiation. RARA and retinoic acid X receptor α (RXRA) form the heterodimer RAR-RXR, which constitutes a transcriptional activator complex required for promyelocyte differentiation (20). In the absence of retinoic acid, RAR-RXR acts as a transcriptional repressor by recruiting the accessory repressors DNMT1, DNMT3A, histone deacetylase and histone methyltransferase and participates in chromatin remodeling. In the presence of retinoic acid, RAR-RXR undergoes a conformational change, which leads to the dissociation of RAR-RXR and the activation of genes required for primitive cell differentiation. Fusion of the PML and RARA proteins can disrupt this coactivator recruitment to prevent transcription of retinoic acid response elements (21). APL accounts for approximately 10-15% of all AML cases. Low-risk APL patients can achieve a CRR of 100% and a 2-year EFS of 97% after receiving ATRA combined with ATO. In APL patients, the presence of PML-RARA rearrangement suggests a good response to ATRA and other retinoids, and the combination of ATRA and chemotherapy significantly improved the survival rate of patients (22–24). Therefore, PML-RARA screening for patients with suspected APL is of great value for the optimization of patient management and for etiological research. PML-RARA mutations can be detected by fluorescence *in situ* hybridization (FISH) or real-time quantitative polymerase chain reaction (RT−qPCR), which can not only assist in diagnosis and treatment and evaluate therapy efficacy but also monitor the changes in MRD, which is of great significance in monitoring recurrence, estimating prognosis and determining the time of drug withdrawal. However, to date, more than ten fusion genes with different counterparts of RARA have been found in roughly 1% to 2% of APL patient, contains ZBTB16-RARA(PLZF-RARA), which is the most frequent APL molecular variant (25, 26), and other translocations led to the rearrangement of RARA gene with NPM1, NUMA1, STAT5B, PRKAR1A, FIP1L1, BCOR, NABP1, TBL1XR1, GTF2I, IRF2BP2, and FNDC3B, etc, most of them were non-sensitive to ATRA and ATO (27). So if such fusion genes were detected in APL patients, which indicated that they will not have a good treatment effective to ATRA and ATO.

3.2 CBF

CBF mutations in AML are cytogenetically characterized by t (8; 21) or inv (16)/t (16; 16), producing RUNX1-RUNX1T1 (AML1-ETO) or CFB β subunit-myosin heavy chain 11 (CBFβ-MYH11) fusion proteins, respectively (28). CBF mutations are one of the most common cytogenetic mutations in AML patients, accounting for approximately 30% of pediatric AML and 15% of adult AML cases. Relevant studies have shown that AML1-ETO and CBFβ-Myh11 alterations on their own are not sufficient to induce leukemia. For the pathogenesis of CBF-AML, the "double hit" model is widely recognized at present, in which the molecular genetic alterations of AML1-ETO, CBFβ- MYH11, CCND1, and CCND2 play important roles (29, 30).

The t (8; 21) (q22; q22) translocation is common in leukemia and generates an AML1-ETO fusion protein. The AML1 (RUNX1) protein family is also known as a CBFα. It consists of a group of heterodimeric transcription factors, which consist of an α subunit (CBFα) encoded by 3 different genes RUNX1/RUNX2/RUNX3 and a β subunit (CBFβ) encoded by CBFβ. At the molecular level, RUNX1 is a key transcription factor during hematopoietic cell differentiation and myeloid development, whereas ETO (RUNX1T1) assists transcriptional repression mainly by recruiting corepressors. AML1-ETO, as a transcriptional repressor, directly blocks the transcription of AML1-dependent tumor suppressors, disrupts normal hematopoietic cell differentiation, and promotes leukemia progression. In addition, it also inhibits the activity of hematopoietic transcription factors such as PU1, GATA1, and CEBPA and thus disrupts the normal hematopoietic process. T (8; 21)-positive AML accounts for 5-10% of all AML cases, including 7-12% of adult AML cases. It is common in the AML-M2 subtype but rare in the M1 and M4 subtypes. The clinical characteristics are generally better prognosis, higher remission rate and longer median OS. The most common gene mutation in AML, c-Kit, which accounts for 20-25% of newly diagnosed cases, is one of the important synergistic factors in the pathogenesis of t(8;21)-positive AML. According to the NCCN guidelines, CBF-AML with c-Kit mutation is classified into the intermediate prognosis group.

Chromosome 16 inversion inv (16) (p13; q22) produces the fusion gene CBFβ-MYH11, which encodes the CBFβ-MYH11 fusion protein. As a transcriptional repressor, CBFβ-MYH11 cooperates with AML1 in the transcriptional inhibition of PTEN, Bcl-2, CEBPA, ARF and PSGL-1. Normally, CBFα and CBFβ form a CBFα/CBFβ complex on DNA at the RUNX binding site and regulate gene expression. When gene rearrangement occurs, the C-terminus of MYH11 fuses with the CBFβ residue. As the CBFβ-MYH11 fusion protein is the isomeric to RUNX1 (CBFα), it interrupts the normal function of the CBFα/CBFβ complex through competitive inhibition. CBFα is a key regulator in hematopoiesis. Abnormal fusion products will damage its normal function and inhibit hematopoietic cell differentiation. At present, RT −qPCR and FISH are sensitive and effective measures to detect these rearrangement mutations (31, 32). AML patients with inv (16) generally have good prognosis and better response to conventional chemotherapy (combination therapy with anthracyclines and cytarabine, the so-called "3+7" regimen). In recent years, with the development in cytogenetics and molecular genetics, researchers have found various gene mutations and chromosomal abnormalities related to CBF-AML; the former includes mutations in FLT3, TET2, JAK2V617F, ASXL1, RAS and CBL, and the latter includes sex chromosome deletion, chromosome, 9q-, +8, +4, and chromosome 7 long arm abnormalities. Among them ASXL1 mutation is worth mentioning (33). ASXL1 mutation in patients with hematologic malignancies was first reported in 2009. After that, researchers gradually found that approximately 6% to 30% of patients with AML had ASXL1 mutations, in particular older patients and

patients with secondary were the two most common victims. Additionally, ASXL1 mutations adversely affected the survival of patients with AML. For example, it could accelerate the conversion of MDS to AML. So, only by continuous in-depth study of the pathogenesis of CBF-AML can accurate and individualized treatment of these patients be achieved.

3.3 Histone lysine methyltransferase 2A (KMT2A)

KMT2A is located in region 2 band 3 of the long arm of human chromosome 11 (11q23). It is a member of the trithorax group (TrxG) family. Rearrangement of KMT2A includes translocation, deletion, insertion, inversion and partial tandem duplication, of which translocation is the most common, which was first reported by Ziemin-van der Poel et al. in 1991 (34). In 2002, Armstrong et al. (35) reported that KMT2A encodes a transcription coenzyme that regulates gene expression during early embryonic development and hematopoietic cell differentiation. It contains an SET region with methyltransferase activity, which methylates the lysine residue at the fourth position of histone H3, thereby activating the transcription of homeotic genes (HOX). KMT2A is widely expressed in hematopoietic cells, including stem cells and progenitor cells. It has leukemogenic effects only after fusing with a variety of partner genes, such as AF4, AF9, ENL, AF10 and ELL (36). When MEN1 and LEDGF bind to the N-terminus of KMT2A, they further activate HOXA9 and HOXA10, which are usually upregulated in leukemia with KMT2A mutation. KMT2A rearrangement accounts for 43-58% of cases in infant AML, 39% in children < 2 years, 8-9% in children > 2 years, and approximately 5% in adult AML (37). In general, the incidence of KMT2A rearrangement decreases with age and is approximately four times higher in children than in adults. Approximately 5-10% of topoisomerase II inhibitor therapy-associated AML cases are accompanied by KMT2A rearrangements. These patients usually have a poor prognosis, with a low remission rate and a high chance of recurrence (38). It has been shown that allo-HSCT could reduce the relapse rate and mortality risk of AML patients with KMT2A rearrangement after remission (39). However, allo-HSCT has disadvantages, such as a lack of donors and harsh transplantation conditions. Recently, scientists have focused on the exploration of drugs targeting transcription mediated by fusion proteins. Grembecka et al. screened two small molecule inhibitors, MI-2 and MI-3, through high-throughput sequencing, which were found to interfere with the binding of MEN1 to KMT2A to release the KMT2A-AF9 fusion protein from binding to the target gene promoter (40). Other drugs targeting the fusion protein have also been developed, which is expected to provide a new strategy for the treatment of AML with KMT2A mutation.

4 Marker source 3: Aberrant DNA methylation and related regulatory molecules

DNA methylation is a type of epigenetic modification that regulates gene expression and plays a key role in hematopoiesis and other processes in human development. DNA methylation is catalyzed by three DNA methyltransferases, DNMT3A, DNMT3B, and DNMT1. DNMT3A and DNMT3B are responsible for initiating DNA methylation on unmodified DNA templates, whereas DNMT1 methylates newly synthesized DNA strands using the partially methylated DNA strand as templates during replication. Mutations in NPM1, CEBPA and RUNX1 can be defined by different DNA methylation levels. These genetic phenotypes are associated with DNA methylation levels. For example, DNMT3A is a required oncogenic transcription factor for PML-RARA in APL. In another study on the specific epigenetic characteristics of DNA methylation, AML patients were divided into 16 subgroups based on DNA methylation levels. These subgroups were associated with cytogenetic or molecular genetic changes, such as inv (16), t (8; 21) and PML-RARA (41). Genome-wide DNA methylation levels can also predict the clinical prognosis of AML patients. The overall DNA methylation level of AML patients at relapse was found to be lower than that at the time of first diagnosis, and a high level of demethylation was associated with improvements in prognostic indicators such as CRR and OS (42). The above studies showed that aberrant DNA methylation is an important event in the pathogenesis of AML and can serve as a powerful epigenetic marker in the early diagnosis, prognosis surveillance and treatment decision-making of AML. Of course, the regulatory molecules involved in DNA methylation aberration in AML also deserve attention.

4.1 TET2

TET2 is located on the long arm of chromosome 4 and encodes methylcytosine dioxygenase, which is associated with DNA demethylation. First, 5-methylcytosine is converted to 5-hydroxymethylcytosine, and then 5-formylcytosine is converted to 5-carboxycytosine. Finally, demethylation is achieved through base excision and repair mediated by DNA glycosylase. TET2 and IDH1/2 mutations are mutually exclusive and play key roles in myeloid cell differentiation, leading to abnormal hematopoietic differentiation and inducing abnormal proliferation of hematopoietic stem cells/progenitor cells. A recent study showed that TET2 mutations occur in leukemia hematopoietic stem cell precursors and are early events in leukemogenesis (43). Epigenetic studies have identified the correlation between TET2 mutations and hypermethylation in AML. The specific mechanism is that TET2 mutations lead to decreased levels of 5-hydroxymethylcytosine and induce DNA hypermethylation mainly in the enhancer regions, which are well-known key regulatory sites of tumor suppressor genes, thereby inducing DNA methylation in nearby regions and affecting gene expression. Approximately 10-20% of AML patients carry TET2 mutations (including deletion, nonsense and missense mutations), which often coexist with NPM1, FLT3, and DNMT3A mutations. At present, there is no definitive conclusion on the prognostic value of TET2 in AML patients. Some studies believe that TET2 mutations are associated with poor prognosis of AML, but others suggest that TET2 mutations have no significant impact on the prognosis of AML patients. This controversy remains to be further explored.

4.2 DNMT3A

DNMT3A is located on the short arm of chromosome 2 and plays an important role in DNA *de novo* methylation, catalyzing the addition of new methyl groups to cytosine residues on CpG dinucleotide sequences, thereby regulating gene transcription. DNMT3A mutations have serious impacts on DNA methylation, which leads to global changes in gene expression, accompanied by the blockage of normal differentiation of hematopoietic cells. These mutations mainly interrupt the catalytic domain of DNMT3A and lead to hypomethylation of normally overexpressed hematopoietic stem cell-specific genes (such as RUNX1, ERG, MYC, and SMAD3) in AML, thereby interfering with the normal differentiation of hematopoietic stem cells. Relevant studies have clarified that DNMT3A is required for hematopoietic stem cell self-renewal and bone marrow differentiation and is defined as an early event of AML. DNMT3A mutations induced malignant transformation of myeloid cells *in vivo*, which led to AML (44). The most common mutation of DNMT3A in AML is a missense mutation at R882 that affects the coding of an arginine and leads to the loss of methylation activity of DNMT3A. In addition, there are frameshift mutations and nonsense mutations. DNMT3A mutations are the earliest and recurrent variations in myeloid malignancies, accounting for approximately 20-22% of newly diagnosed AML in adults. DNMT3A mutations are mainly found in the M4 and M5 subtypes, with incidences of 20.5% and 13.6%, respectively. Nearly all AML patients with normal karyotypes have a single site mutation in at least one DNMT3A allele, and 30-37% of patients have loss-of-function mutations in DNMT3A. It has been clear that DNMT3A mutations have important prognostic significance for AML with a normal karyotype. Patients with these mutations generally have a worse prognosis and significantly lower OS than AML patients with wild-type DNMT3A. The hypomethylating drug (HMA) decitabine can improve the response of patients with DNMT3A mutations and achieve a higher clinical remission rate and better OS (75% vs 34% and 15.2 vs 11 months, respectively) than wild-type DNMT3A patients. High levels of mir29b targeting DNMT3A are a good marker to evaluate the therapeutic response to decitabine. Patients with myeloid malignancies harboring DNMT3A and IDH1/2 mutations showed good responses to decitabine, azacitidine, specific DNMT inhibitors, and HMAs.

4.3 IDH1/2

IDH1 and IDH2 are located in the long arm of chromosome 2 and chromosome 15, respectively, encoding the tumor suppressor proteins IDH1/2, which localize in the cytoplasm and peroxisomes. They are involved in intermediate metabolism and energy production in organisms. IDH1/2 promote leukemogenesis by causing DNA and histone hypermethylation, which destroys the normal differentiation of bone marrow. There are three isoforms of isocitrate dehydrogenase, namely, IDH1, IDH2 and IDH3. IDH1 is located in the cytoplasm, and IDH2 and IDH3 are located in mitochondria. Approximately 15-20% of AML cases and 25-30% of AML with normal karyotypes have IDH1/2 mutations. There was no significant difference in mutation frequency between pediatric and adult patients. IDH1/2 mutations are usually accompanied by NPM1 mutations but not FLT3-ITD mutations. Epigenetic alterations caused by IDH1/2 mutations exacerbate the proliferation of hematopoietic progenitor cells. IDH1/2 mutations inhibit histone demethylation, which is closely correlated with DNA hypermethylation, differentiation arrest and clonal expansion of hematopoietic stem cells. AML patients with IDH1/2 mutations have poor prognosis, generally with low white blood cell counts and high platelet counts, especially when accompanied by other mutations, such as NMP1 and FLT3-ITD. However, IDH1/2 mutations rarely coexist with TET2 or WT1 mutations, probably because they all affect DNA methylation (45). However, the results of relevant clinical studies on the prognostic role of IDH mutations in AML are not consistent. In NPM1-mutated AML, the combination of IDH1/2 mutations is negatively correlated with patient prognostic indicators such as relapse-free survival (RFS) and OS (46, 47). In contrast, Patel et al. reported that IDH1/2 mutations are beneficial to the survival of NPM1-mutated AML patients (48). In another study, IDH1/2 mutations were detected in 31 AML patients by second-generation sequencing, and the correlation between IDH1/2 mutations and MRD was explored. The results showed that IDH1/2 mutations were reliable MRD markers, which could predict the recurrence of most patients (49). In recent years, a large number of clinical studies have been carried out on small molecule IDH1/2 inhibitors. The newly reported small molecule inhibitor of IDH1 ivosidenib (AG-120) can inhibit the production of 2-hydroxyglutarate and promote normal cell differentiation. In 2018, the FDA approved ivosidenib for the treatment of relapsed or refractory AML with IDH1 mutations (50). Similar to ivosidenib, enasidenib (AG-221), a small molecule IDH2 inhibitor, was developed to bind IDH2 dimers and block the production of 2-hydroxyglutarate in patients with IDH2 mutations. It was also approved by the FDA in August 2017 for treating relapsed or refractory AML with IDH1/2 mutations (51). Current clinical trials mainly focus on exploring the efficacy of the combined therapy of cytarabine with the above two drugs in AML patients.

5 Marker source 4: Non-coding RNAs represented by miRNAs

MicroRNAs (miRNAs) are small RNA molecules composed of 17-25 nucleotides that are mainly involved in the post-transcriptional regulation of mRNA and play important roles in cell proliferation, differentiation and apoptosis. MiRNAs of different subtypes are abnormally expressed in a variety of malignant tumors with tissue specificity. In blood, miRNAs are very stable and resistant to degradation by RNase. Their expression level in blood is related to the type, stage, grade and prognosis of tumors. Ma et al. (52) showed that cytogenetically normal AML (CN-AML) patients with high miR-362-5p expression had lower OS than the control group, which implied the oncogenic function of miR-362-5p in AML. This study also suggested that miR-362-5p could be an independent poor prognostic factor for CN-AML. Zhang et al. (53) found that mir-216b overexpression was associated with poor chemotherapy efficacy and poor prognosis in AML patients and that the expression of mir-

216b significantly decreased from post-chemotherapy to complete remission and significantly increased after relapse. Mir-3151 is located within the first intron of the BAALC gene (54). In a study that recruited only CN-AML patients older than 60 years, mir-3151 was identified as an independent prognostic factor (55). The study of Díaz-Beyá et al. (56) showed that AML patients with higher mir-3151 expression had shorter OS and a higher cumulative recurrence rate. Another study by this research group reported that the upregulation of mir-196b and mir-644 was associated with lower OS, and the downregulation of mir-135a and mir-409-3p was associated with higher recurrence risk (57). Lin et al. (58) showed that compared with AML patients with downregulated miR-335 expression, AML patients with upregulated miR-335 expression had shorter RFS and OS. Zhao et al. (59) showed that the expression of miR-96 in newly diagnosed AML patients was significantly downregulated and was significantly increased after treatment compared with the normal control group and that CRR was positively correlated with the miR-96 expression level. Aleksandra et al. (60) reported that the expression of miR-204 was significantly downregulated in AML patients regardless of sex and was significantly increased following successful chemotherapy (daunorubicin + cytarabine). After induction chemotherapy, AML patients with upregulated miR-204 had a higher CRR. Therefore, miR-204 is expected to become a biomarker for the prognostic evaluation of AML (61). Hu et al. (62) suggested that high miR-98 expression in AML patients who had received only chemotherapy was indicative of good prognosis. In conclusion, the above results showed that miRNAs are expected to become biomarkers for the initial screening, diagnosis and prognosis evaluation of AML, but many clinical issues still require further exploration.

6 Summary and prospects

As a group of hematologic malignancies with diverse biological characteristics and prognoses, AML is highly heterogenic. In this review, we summarized the promising AML biomarkers from four aspects, which contributing to a better understanding of the molecular mechanism of the disease. Of course, it must be soberly aware that we have not listed all biomarkers of AML. Anyway, the biomarkers we mentioned are representative. For example, mutations in TP53, FLT3, and ASXL1 suggest poor prognosis, low remission rate, short survival period, and often require allogeneic hematopoietic stem cell transplantation. The CEBPA double mutation, NPM1 and CBF mutation suggest that the prognosis is good, the remission rate is high, the survival period is long, and the effect of chemotherapy or autotherapy is good. As for other mutations mentioned in the article, they usually predict a moderate prognosis. As is known to clinicians, whether or not turn negative of MRD after treatment of AML is extremely important for the prognosis of patients. The group with good prognosis has a higher rate of MRD turning negative after chemotherapy, and the rate of mutation gene turning negative is also high. The group with poor prognosis has a lower rate of MRD turning negative after chemotherapy, and the rate of mutation gene turning negative is also low. So, the study of AML biomarker from cytogenetics, molecular biology and pathophysiology is conducive to the correct evaluation of its prognostic factors to achieve the precise implementation of individualized hierarchical treatment. It is believed that with the progress of experimental technology, more meaningful and novel biological indicators for AML diagnosis and treatment will be found in the future to guide personalized medicine and precise medicine to improve the survival rate and quality of life of patients. At the same time, it should be further emphasized that although the data on emerging biomarkers such as epigenetic indicators and non-coding RNAs are encouraging, we cannot conclude which marker(s) is/are the best based on current knowledge. From a clinical perspective, a set of biomarkers seems more appropriate. Therefore, it is urgently required to develop one or several reproducible and effective schemes adopting a combination of multiple biomarkers through multicenter research to achieve real clinical transformation and application.

Author contributions

(I) Conception and design: P-YY and HW. (II) Administrative support: RJ. (III) Provision of study materials: R-WW, RJ and J-HM. (IV) Collection and assembly of data: P-YY, R-WW and K-ML. (V) Data analysis and interpretation: P-YY and HW. (VI) Manuscript writing: all authors. (VII) Final approval of manuscript: all authors. All authors contributed to the article and approved the submitted version.

Funding

This work was supported by Yantai Philosophy and Social Science Planning Project.

Conflict of interest

The authors declare that the research was conducted in the absence of any commercial or financial relationships that could be construed as a potential conflict of interest.

Publisher's note

References

1. Yi M, Li A, Zhou L, Chu Q, Song Y, Wu K. The global burden and attributable risk factor analysis of acute myeloid leukemia in 195 countries and territories from 1990 to 2017: Estimates based on the global burden of disease study 2017. *J Hematol Oncol* (2020) 13(1):72. doi: 10.1186/s13045-020-00908-z

2. Wiatrowski K, Kim TH, Przespolewski A. Cellular and molecular biomarkers predictive of response to immunotherapy in acute myeloid leukemia. *Front Oncol* (2022) 12:826768. doi: 10.3389/fonc.2022.826768

3. Kayser S, Levis MJ. Clinical implications of molecular markers in acute myeloid leukemia. *Eur J Haematol* (2019) 102(1):20–35. doi: 10.1111/ejh.13172

4. Prada-Arismendy J, Arroyave JC, Röthlisberger S. Molecular biomarkers in acute myeloid leukemia. *Blood Rev* (2017) 31(1):63–76. doi: 10.1016/j.blre.2016.08.005

5. Riva L, Luzi L, Pelicci PG. Genomics of acute myeloid leukemia: The next generation. *Front Oncol* (2012) 2:40. doi: 10.3389/fonc.2012.00040

6. Dawson MA, Gudgin EJ, Horton SJ, Giotopoulos G, Meduri E, Robson S, et al. Recurrent mutations, including NPM1c, activate a BRD4-dependent core transcriptional program in acute myeloid leukemia. *Leukemia* (2014) 28(2):311–20. doi: 10.1038/leu.2013.338

7. El Hajj H, Dassouki Z, Berthier C, Raffoux E, Ades L, Legrand O, et al. Retinoic acid and arsenic trioxide trigger degradation of mutated NPM1, resulting in apoptosis of AML cells. *Blood* (2015) 125(22):3447–54. doi: 10.1182/blood-2014-11-612416

8. Bienz M, Ludwig M, Leibundgut EO, Mueller BU, Ratschiller D, Solenthaler M, et al. Risk assessment in patients with acute myeloid leukemia and a normal karyotype. *Clin Cancer Res* (2005) 11(4):1416–24. doi: 10.1158/1078-0432.CCR-04-1552

9. Nitika WJ, Hui AM. Role of biomarkers in FLT3 AML. *Cancers (Basel)* (2022) 14 (5):1164. doi: 10.3390/cancers14051164

10. Santos FP, Jones D, Qiao W, Cortes JE, Ravandi F, Estey EE, et al. Prognostic value of FLT3 mutations among different cytogenetic subgroups in acute myeloid leukemia. *Cancer* (2011) 117(10):2145–55. doi: 10.1002/cncr.25670

11. Zaidi SZ, Owaidah T, Al Sharif F, Ahmed SY, Chaudhri N, Aljurf M. The challenge of risk stratification in acute myeloid leukemia with normal karyotype. *Hematol Oncol Stem Cell Ther* (2008) 1(3):141–58. doi: 10.1016/s1658-3876(08)50023-9

12. Ciurea SO, Chilkulwar A, Saliba RM, Chen J, Rondon G, Patel KP, et al. Prognostic factors influencing survival after allogeneic transplantation for AML/MDS patients with TP53 mutations. *Blood* (2018) 131(26):2989–92. doi: 10.1182/blood-2018-02-832360

13. Welch JS, Petti AA, Miller CA, Fronick CC, O'Laughlin M, Fulton RS, et al. TP53 and decitabine in acute myeloid leukemia and myelodysplastic syndromes. *N Engl J Med* (2016) 375(21):2023–36. doi: 10.1056/NEJMoa1605949

14. Maslah N, Salomao N, Drevon L, Verger E, Partouche N, Ly P, et al. Synergistic effects of PRIMA-1Met (APR-246) and 5-azacitidine in TP53-mutated myelodysplastic syndromes and acute myeloid leukemia. *Haematologica* (2020) 105(6):1539–51. doi: 10.3324/haematol.2019.218453

15. Li HY, Deng DH, Huang Y, Ye FH, Huang LL, Xiao Q, et al. Favorable prognosis of biallelic CEBPA gene mutations in acute myeloid leukemia patients: a meta-analysis. *Eur J Haematol* (2015) 94(5):439–48. doi: 10.1111/ejh.12450

16. Greif PA, Dufour A, Konstandin NP, Ksienzyk B, Zellmeier E, Tizazu B, et al. GATA2 zinc finger 1 mutations associated with biallelic CEBPA mutations define a unique genetic entity of acute myeloid leukemia. *Blood* (2012) 120(2):395–403. doi: 10.1182/blood-2012-01-403220

17. Hahn CN, Chong CE, Carmichael CL, Wilkins EJ, Brautigan PJ, Li XC, et al. Heritable GATA2 mutations associated with familial myelodysplastic syndrome and acute myeloid leukemia. *Nat Genet* (2011) 43(10):1012–7. doi: 10.1038/ng.913

18. De Braekeleer E, Douet-Guilbert N, De Braekeleer M. RARA fusion genes in acute promyelocytic leukemia: A review. *Expert Rev Hematol* (2014) 7(3):347–57. doi: 10.1586/17474086.2014.903794

19. Noguera NI, Catalano G, Banella C, Divona M, Faraoni I, Ottone T, et al. Acute promyelocytic leukemia: Update on the mechanisms of leukemogenesis, resistance and on innovative treatment strategies. *Cancers (Basel)* (2019) 11(10):1591. doi: 10.3390/cancers11101591

20. Nagpal S, Friant S, Nakshatri H, Chambon P. RARs and RXRs: evidence for two autonomous transactivation functions (AF-1 and AF-2) and heterodimerization *in vivo*. *EMBO J* (1993) 12(6):2349–60. doi: 10.1002/j.1460-2075.1993.tb05889.x

21. Jimenez JJ, Chale RS, Abad AC, Schally AV. Acute promyelocytic leukemia (APL): a review of the literature. *Oncotarget* (2020) 11(11):992–1003. doi: 10.18632/oncotarget.27513

22. Ma H, Yang J. Insights into the all-trans-Retinoic acid and arsenic trioxide combination treatment for acute promyelocytic leukemia: A meta-analysis. *Acta Haematol* (2015) 134(2):101–8. doi: 10.1159/000369242

23. Xin L, Wan-jun S, Zeng-jun L, Yao-zhong Z, Yun-tao L, Yan L, et al. A survival study and prognostic factors analysis on acute promyelocytic leukemia at a single center. *Leuk Res* (2007) 31(6):765–71. doi: 10.1016/j.leukres.2006.07.028

24. Creutzig U, Kutny MA, Barr R, Schlenk RF, Ribeiro RC. Acute myelogenous leukemia in adolescents and young adults. *Pediatr Blood Cancer* (2018) 65(9):e27089. doi: 10.1002/pbc.27089

25. Sanz MA, Fenaux P, Tallman MS, Estey EH, Löwenberg B, Naoe T, et al. Management of acute promyelocytic leukemia: Updated recommendations from an expert panel of the European LeukemiaNet. *Blood* (2019) 133:1630–43. doi: 10.1182/blood-2019-01-894980

26. Baba SM, Pandith AA, Shah ZA, Baba RA. Pathogenetic implication of fusion genes in acute promyelocytic leukemia and their diagnostic utility. *Clin Genet* (2019) 95:41–52. doi: 10.1111/cge.13372

27. Liquori A, Ibañez M, Sargas C, Sanz MÁ, Barragán E, Cervera J. Acute promyelocytic leukemia: A constellation of molecular events around a single PML-RARA fusion gene. *Cancers (Basel)* (2020) 12(3):624. doi: 10.3390/cancers12030624

28. Mosna F, Gottardi M. Stem cell modeling of core binding factor acute myeloid leukemia. *Stem Cells Int* (2016) 2016:7625827. doi: 10.1155/2016/7625827

29. Gilliland DG. Molecular genetics of human leukemias: new insights into therapy. *Semin Hematol* (2002) 39(4 Suppl 3):6–11. doi: 10.1053/shem.2002.36921

30. Rau RE. Beyond KIT in CBF-AML: chromatin and cohesin. *Blood* (2016) 127 (20):2370–1. doi: 10.1182/blood-2016-03-707083

31. Gulley ML, Shea TC, Fedoriw Y. Genetic tests to evaluate prognosis and predict therapeutic response in acute myeloid leukemia. *J Mol Diagn* (2010) 12(1):3–16. doi: 10.2353/jmoldx.2010.090054

32. Lagunas-Rangel FA, Chávez-Valencia V, Gómez-Guijosa MÁ, Cortes-Penagos C. Acute myeloid leukemia-genetic alterations and their clinical prognosis. *Int J Hematol Oncol Stem Cell Res* (2017) 11(4):328–39.

33. Seiter K, Htun K, Baskind P, Liu Z. Acute myeloid leukemia in a father and son with a germline mutation of ASXL1. *Biomark Res* (2018) 6:7. doi: 10.1186/s40364-018-0121-3

34. Ziemin-van der Poel S, McCabe NR, Gill HJ, Espinosa R3rd, Patel Y, Harden A, et al. Identification of a gene, MLL, that spans the breakpoint in 11q23 translocations associated with human leukemias. *Proc Natl Acad Sci USA* (1991) 88(23):10735–9. doi: 10.1073/pnas.88.23.10735

35. Armstrong SA, Staunton JE, Silverman LB, Pieters R, den Boer ML, Minden MD, et al. MLL translocations specify a distinct gene expression profile that distinguishes a unique leukemia. *Nat Genet* (2002) 30(1):41–7. doi: 10.1038/ng765

36. Menghrajani K, Gomez-Arteaga A, Madero-Marroquin R, Zhang MJ, Bo-Subait K, Sanchez J, et al. Risk classification at diagnosis predicts post-HCT outcomes in intermediate-, adverse-risk, and KMT2A-rearranged AML. *Blood Adv* (2022) 6(3):828–47. doi: 10.1182/bloodadvances.2021004881

37. Mann G, Attarbaschi A, Schrappe M, De Lorenzo P, Peters C, Hann I, et al. Interfant-99 study group. improved outcome with hematopoietic stem cell transplantation in a poor prognostic subgroup of infants with mixed-lineage-leukemia (MLL)-rearranged acute lymphoblastic leukemia: Results from the interfant-99 study. *Blood* (2010) 116(15):2644–50. doi: 10.1182/blood-2010-03-273532

38. Schoch C, Schnittger S, Klaus M, Kern W, Hiddemann W, Haferlach T. AML with 11q23/MLL abnormalities as defined by the WHO classification: incidence, partner chromosomes, FAB subtype, age distribution, and prognostic impact in an unselected series of 1897 cytogenetically analyzed AML cases. *Blood* (2003) 102(7):2395–402. doi: 10.1182/blood-2003-02-0434

39. Pigneux A, Labopin M, Maertens J, Cordonnier C, Volin L, Socié G, et al. Acute leukemia working party EBMT. outcome of allogeneic hematopoietic stem-cell transplantation for adult patients with AML and 11q23/MLL rearrangement (MLL-r AML). *Leukemia* (2015) 29(12):2375–81. doi: 10.1038/leu.2015.143

40. Shi A, Murai MJ, He S, Lund G, Hartley T, Purohit T, et al. Structural insights into inhibition of the bivalent menin-MLL interaction by small molecules in leukemia. *Blood* (2012) 120(23):4461–9. doi: 10.1182/blood-2012-05-429274

41. Figueroa ME, Lugthart S, Li Y, Erpelinck-Verschueren C, Deng X, Christos PJ, et al. DNA Methylation signatures identify biologically distinct subtypes in acute myeloid leukemia. *Cancer Cell* (2010) 17(1):13–27. doi: 10.1016/j.ccr.2009.11.020

42. Yang X, Wong MPM, Ng RK. Aberrant DNA methylation in acute myeloid leukemia and its clinical implications. *Int J Mol Sci* (2019) 20(18):4576. doi: 10.3390/ijms20184576

43. Majeti R. Clonal evolution of pre-leukemic hematopoietic stem cells precedes human acute myeloid leukemia. *Best Pract Res Clin Haematol* (2014) 27(3-4):229–34. doi: 10.1016/j.beha.2014.10.003

44. Shlush LI, Zandi S, Mitchell A, Chen WC, Brandwein JM, Gupta V, et al. Identification of pre-leukaemic haematopoietic stem cells in acute leukaemia. *Nature* (2014) 506(7488):328–33. doi: 10.1038/nature13038

45. Rampal R, Alkalin A, Madzo J, Vasanthakumar A, Pronier E, Patel J, et al. DNA Hydroxymethylation profiling reveals that WT1 mutations result in loss of TET2 function in acute myeloid leukemia. *Cell Rep* (2014) 9(5):1841–55. doi: 10.1016/j.celrep.2014.11.004

46. Paschka P, Schlenk RF, Gaidzik VI, Habdank M, Krönke J, Bullinger L, et al. IDH1 and IDH2 mutations are frequent genetic alterations in acute myeloid leukemia and confer adverse prognosis in cytogenetically normal acute myeloid leukemia with NPM1 mutation without FLT3 internal tandem duplication. *J Clin Oncol* (2010) 28(22):3636–43. doi: 10.1200/JCO.2010.28.3762

47. Marcucci G, Maharry K, Wu YZ, Radmacher MD, Mrózek K, Margeson D, et al. IDH1 and IDH2 gene mutations identify novel molecular subsets within *de novo* cytogenetically normal acute myeloid leukemia: A cancer and leukemia group b study. *J Clin Oncol* (2010) 28(14):2348–55. doi: 10.1200/JCO.2009.27.3730

48. Patel JP, Gönen M, Figueroa ME, Fernandez H, Sun Z, Racevskis J, et al. Prognostic relevance of integrated genetic profiling in acute myeloid leukemia. *N Engl J Med* (2012) 366(12):1079–89. doi: 10.1056/NEJMoa1112304

49. Debarri H, Lebon D, Roumier C, Cheok M, Marceau-Renaut A, Nibourel O, et al. IDH1/2 but not DNMT3A mutations are suitable targets for minimal residual disease monitoring in acute myeloid leukemia patients: a study by the acute leukemia French association. *Oncotarget* (2015) 6(39):42345–53. doi: 10.18632/oncotarget.5645

50. Prakash C, Fan B, Altaf S, Agresta S, Liu H, Yang H. Pharmacokinetics, absorption, metabolism, and excretion of [14C]ivosidenib (AG-120) in healthy male subjects. *Cancer Chemother Pharmacol* (2019) 83(5):837–48. doi: 10.1007/s00280-019-03793-7

51. Dutta R, Zhang TY, Köhnke T, Thomas D, Linde M, Gars E, et al. Enasidenib drives human erythroid differentiation independently of isocitrate dehydrogenase 2. *J Clin Invest* (2020) 130(4):1843–9. doi: 10.1172/JCI133344

52. Ma QL, Wang JH, Yang M, Wang HP, Jin J. MiR-362-5p as a novel prognostic predictor of cytogenetically normal acute myeloid leukemia. *J Transl Med* (2018) 16(1):68. doi: 10.1186/s12967-018-1445-3

53. Zhang TJ, Wu DH, Zhou JD, Li XX, Zhang W, Guo H, et al. Overexpression of miR-216b: Prognostic and predictive value in acute myeloid leukemia. *J Cell Physiol* (2018) 233(4):3274–81. doi: 10.1002/jcp.26171

54. Stark MS, Tyagi S, Nancarrow DJ, Boyle GM, Cook AL, Whiteman DC, et al. Characterization of the melanoma miRNAome by deep sequencing. *PloS One* (2010) 5(3): e9685. doi: 10.1371/journal.pone.0009685

55. Eisfeld AK, Marcucci G, Maharry K, Schwind S, Radmacher MD, Nicolet D, et al. miR-3151 interplays with its host gene BAALC and independently affects outcome of patients with cytogenetically normal acute myeloid leukemia. *Blood* (2012) 120(2):249–58. doi: 10.1182/blood-2012-02-408492

56. Díaz-Beyá M, Brunet S, Nomdedéu J, Cordeiro A, Tormo M, Escoda L, et al. The expression level of BAALC-associated microRNA miR-3151 is an independent prognostic factor in younger patients with cytogenetic intermediate-risk acute myeloid leukemia. *Blood Cancer J* (2015) 5(10):e352. doi: 10.1038/bcj.2015.76

57. Díaz-Beyá M, Brunet S, Nomdedéu J, Tejero R, Díaz T, Pratcorona M, et al. MicroRNA expression at diagnosis adds relevant prognostic information to molecular categorization in patients with intermediate-risk cytogenetic acute myeloid leukemia. *Leukemia* (2014) 28(4):804–12. doi: 10.1038/leu.2013.281

58. Lin X, Wang Z, Zhang R, Feng W. High serum microRNA-335 level predicts aggressive tumor progression and unfavorable prognosis in pediatric acute myeloid leukemia. *Clin Transl Oncol* (2015) 17(5):358–64. doi: 10.1007/s12094-014-1237-z

59. Zhao J, Lu Q, Zhu J, Fu J, Chen YX. Prognostic value of miR-96 in patients with acute myeloid leukemia. *Diagn Pathol* (2014) 9:76. doi: 10.1186/1746-1596-9-76

60. Butrym A, Rybka J, Baczyńska D, Tukiendorf A, Kuliczkowski K, Mazur G. Low expression of microRNA-204 (miR-204) is associated with poor clinical outcome of acute myeloid leukemia (AML) patients. *J Exp Clin Cancer Res* (2015) 34(1):68. doi: 10.1186/s13046-015-0184-z

61. Abdelhafiz AS, Elsayed GM, Saber MM, Gameel A, Hamdy N. Low expression of miR-204 is associated with expression of CD34 and poor performance status in denovo AML. *Int J Lab Hematol* (2020) 42(3):263–9. doi: 10.1111/ijlh.13161

62. Hu N, Cheng Z, Pang Y, Zhao H, Chen L, Wang C, et al. High expression of MiR-98 is a good prognostic factor in acute myeloid leukemia patients treated with chemotherapy alone. *J Cancer* (2019) 10(1):178–85. doi: 10.7150/jca.26391

frontiers | Frontiers in Oncology

TYPE Case Report
PUBLISHED 14 March 2023
DOI 10.3389/fonc.2023.1066083

OPEN ACCESS

EDITED BY
Spiros Vlahopoulos,
University of Athens, Greece

REVIEWED BY
Sudha Sharma,
Howard University, United States
Maria S. Pombo-de-Oliveira,
National Cancer Institute (INCA), Brazil

*CORRESPONDENCE
Yi Yang
yangyi@tjh.tjmu.edu.cn

†These authors have contributed equally to this work and share first authorship

SPECIALTY SECTION
This article was submitted to Hematologic Malignancies, a section of the journal Frontiers in Oncology

RECEIVED 10 October 2022
ACCEPTED 02 March 2023
PUBLISHED 14 March 2023

CITATION
Yuan W, Shang Z, Shen K, Yu Q, Lv Q, Cao Y, Wang J and Yang Y (2023) Case report: Germline RECQL mutation potentially involved in hereditary predisposition to acute leukemia. *Front. Oncol.* 13:1066083. doi: 10.3389/fonc.2023.1066083

Case report: Germline RECQL mutation potentially involved in hereditary predisposition to acute leukemia

Wei Yuan[1†], Zhen Shang[2,3†], Kefeng Shen[2,3], Qiuxia Yu[2,3], Qiuxia Lv[2,3], Yang Cao[2,3], Jue Wang[2,3] and Yi Yang[4*]

[1]Department and Institute of Infectious Disease, Tongji Hospital of Tongji Medical College, Huazhong University of Science and Technology, Wuhan, China, [2]Department of Hematology, Tongji Hospital of Tongji Medical College, Huazhong University of Science and Technology, Wuhan, China, [3]Immunotherapy Research Center for Hematologic Diseases of Hubei Province, Tongji Hospital of Tongji Medical College, Huazhong University of Science and Technology, Wuhan, China, [4]Department of geriatrics, Tongji Hospital, Tongji Medical College, Huazhong University of Science and Technology, Wuhan, China

The pathogenesis of acute leukemia is still complex and vague. Most types of acute leukemia are related to somatic gene mutations, and familial incidence is rare. Here we report a case of familial leukemia. The proband presented to our hospital with vaginal bleeding and disseminated intravascular coagulation at the age of 42 and was diagnosed with acute promyelocytic leukemia with typical *PML-RARα* fusion gene caused by t(15;17)(q24;q21) translocation. By taking the history, we found that the patient's second daughter had been diagnosed with B-cell acute leukemia with *ETV6-RUNX1* fusion gene at age 6. Then we performed whole exome sequencing in peripheral blood mononuclear cells from these two patients at remission status and identified 8 shared germline gene mutations. Using functional annotation and Sanger sequencing validation, we finally focused on a single nucleotide variant in RecQ like helicase (*RECQL*), rs146924988, which was negative in the proband's healthy eldest daughter. This gene variant potentially led to a relative lack of RECQL protein, disordered DNA repair and chromatin rearrangement, which may mediate the occurrence of fusion genes, as driving factors for leukemia. This study identified a novel possible leukemia-related germline gene variant and provided a new understanding for the screening and pathogenesis of hereditary predisposition syndromes.

KEYWORDS

case report, acute leukemia, germline mutation, hereditary predisposition, fusion gene

Introduction

In addition to the somatic changes related to diagnosis and prognosis in leukemia cells, many germline mutations have been discovered in hematopoietic malignancies in recent years, namely hereditary predisposition (1, 2). The 'Myeloid Neoplasms with Germline

Predisposition' category has been included in the revised fourth edition of the World Health Organization (WHO) classification of tumors of the hematopoietic and lymphoid tissues (3), which further emphasizes the importance of constitutional mutation in the occurrence and development of hematological neoplasms. Fusion genes are hybrid genes formed by the fusion of two previously separated genes, which are resulting from chromosomal rearrangement, including translocation, inversion, deletion, or tandem duplication (4). Fusion genes are molecular biological characteristics of many leukemia types and have been successfully used as diagnostic markers and therapeutic targets (5). However, its relationship with hereditary predisposition is still unclear.

Here, we report a case of familial acute leukemia with fusion genes and germline RecQ Like Helicase (*RECQL*) mutation. The proband was a 42-year-old female patient with acute promyelocytic leukemia (APL) and *PML-RARα* fusion gene. She has two daughters, and the younger one developed B-cell precursor acute lymphoblastic leukemia (BCP-ALL) with *ETV6-RUNX1* fusion gene at age 6. As of the date of submission, the eldest daughter is still in good health. Comprehensive genetic testing showed that a single nucleotide variant (SNV) in *RECQL*, rs146924988, was potentially involved in this familial case with acute leukemia.

Case presentation

Case 1 (mother)

A previously healthy 42-year-old woman presented to the emergency room due to massive vaginal bleeding in November 2021. Blood routine test showed an abnormal increase of white blood cells (WBC) of 32.83×10^9/L and monocytes of 20.19×10^9/L, with hemoglobin of 100.0g/L and decreased platelet count of 43.0×10^9/L. Coagulation function test indicated a prolonged prothrombin time of 26.8s, decreased fibrinogen level of 0.93g/L and elevated fibrinogen degradation products of 89.7μg/mL and D-Dimer greater than 21μg/mL FEU, suggesting a disseminated intravascular coagulation. An intramural uterine fibroid (approximately 1.8cm*1.3cm) on the anterior wall was found by transabdominal pelvic ultrasonography. Peripheral blood cells smear showed that granulocytes and promyelocytes accounted for 92.00% and 88.00% of the total number of nucleated cells, respectively.

The patient was then admitted to the hematology department for further diagnosis and treatment. Morphological examination of bone marrow (BM) aspirates revealed an abnormal myeloid development with an increased percentage of promyelocytes (approximately 92.00%). BM biopsy analysis revealed marked hyperactive hyperplasia and promyelocytic dysplasia and cytosis (about 90%), and the immunohistochemistry stains for MPO and CD117 were both positive. Flow cytometric immunotyping of BM aspirates showed that abnormal myeloblasts expressed CD117, CD45, cMPO, CD64, CD9, CD33bri, CD13 and CD38, accounting for 83.3% of the total nucleated cells. A few abnormal myeloblasts expressed CD34 (approximately 9.9%), CD11c and CD11b. These abnormal cells were large and had side scatter (SSC) values similar to those of granulocytes. Cytogenetic analysis showed an abnormal karyotype of 46, XX, t(15;17)(q24;q21), del (6)(q22;q32). Molecular genetic analysis detected a typical S-type *PML-RARα* fusion gene transcript caused by t(15;17)(q24;q21) translocation (approximately 60.30%). Based on these results, this patient was diagnosed as APL (7). After being classified as high-risk group, this patient received all-trans retinoic acid (ATRA, 25 $mg{\cdot}m^{-2}{\cdot}d^{-1}$, d1-d3) combined with arsenic trioxide (0.16 $mg{\cdot}kg^{-1}{\cdot}d^{-1}$, d1-d3) induction chemotherapy, and continued with three courses of IA (idarubicin 8 $mg{\cdot}m^{-2}{\cdot}d^{-1}$, d1-d3; cytarabine 100 $mg{\cdot}m^{-2}{\cdot}d^{-1}$, d1-d5) consolidation regimen (6). Six times of prophylactic intrathecal chemotherapy were administered during this process to prevent central nervous system relapse. And then ATRA combined with compound Huangdai tablet (CHDT) was used as maintenance chemotherapy. To this date, the patient was still undergoing maintenance therapy and staying in complete remission at the cytological and molecular levels both in bone marrow and cerebrospinal fluid, with no signs or symptoms of APL recurrence.

Case 2 (daughter)

During medical history collection of case 1 (mother), it was found that a 6-year-old girl, the younger one of the patient's two daughters, was diagnosed with BCP-ALL (low-risk group) in March 2019, just two years before the occurrence of her mother's APL (Figure 1A). At the diagnosis, the blast cells in bone marrow were CD10, CD19 and terminal deoxynucleotidyl transferase (TdT) positive detected by fluorescence activated cell sorting (FACS), and with *ETV6-RUNX1* fusion gene detected by RT-PCR and t(12;21)(p13;q22) translocation by florescence *in situ* hybridization (FISH). After receiving a high-dose chemotherapy regimen according to the CCCG-ALL-2015 protocol (8), the daughter achieved complete remission. Up to this date, the daughter still underwent oral maintenance therapy with mercaptopurine (6-MP) and methotrexate (MTX) and remained in minimum residual disease (MRD) negative remission at cellular and molecular (*ETV6-RUNX1*) levels.

To explore the possible hereditary predisposition in this case, we performed whole exome sequencing (WES) in peripheral blood mononuclear cells (PBMCs) from these two patients at remission status with informed consents. The genomic DNA of each sample was sheared with Biorupter (Diagenode, Belgium) and 150 ~ 200bp fragments were obtained. AIExomeV1 Enrichment Kit (iGeneTech, Beijing, China) and Illumina platform (Illumina, San Diego, CA) were applied to capture and sequence the whole exons. Then clean reads were mapped to the reference genome GRCh37 by using Burrow-Wheeler Aligner. After removing low quality reads and duplications, SNV and insertion-deletion (InDel) were called and annotated by using Genome Analysis Toolkit (GATK). Finally, a total of 8 germline gene mutations shared by both patients were identified (Table 1), including 2 InDel and 6 SNV, in which an SNV in *RECQL* (rs146924988) was noticed by functional annotation. Sanger sequencing of nasopharyngeal swab specimens was used to verify WES results, and to screen the other healthy child of the

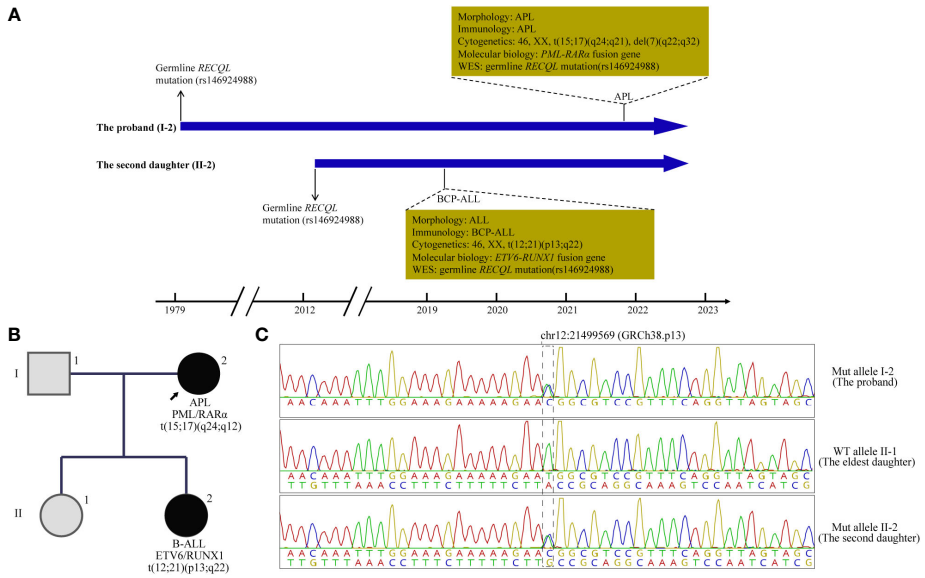

FIGURE 1
A brief summary of medical history and pedigree for the *RECQL* mutation carriers. **(A)** Timeline of clinical events in 2 patients with acute leukemia. **(B)** The Pedigree and germline and tumor chromatopherogram confirmed the presence of single nucleotide variation in *RECQL* (rs146924988) in 2 patients with acute leukemia in this family, while it was negative in healthy members. **(C)** Sanger sequencing of nasopharyngeal swab specimens was used to verify *RECQL* mutation (rs146924988) in the proband and her two daughters. APL, acute promyelocytic leukemia; WES, whole exome sequencing; BCP-ALL, B-cell precursor acute lymphoblastic leukemia; Mut, mutant; WT, wide type.

proband without *RECQL* mutation detected. The pedigree for rs146924988 and leukemia was shown in Figures 1B, C.

Patient perspective

I have an entire family, including a husband and two daughters. I led a busy and happy life, struggling to make ends meet, until my little daughter and I were diagnosed with leukemia in turn. Before I came to Tongji Hospital, I thought my life was coming to an end. Fortunately, after receiving systematic treatment, my daughter and I were cured and there is no sign of recurrence. Our life and work are gradually returning to normal.

Discussion

With the development of genomic sequencing methods, many germline mutations have been found in cancer patients and their immediate relatives. Germline mutations associated with the hereditary predisposition to cancers were highlighted for their clinical relevance and diagnostic values, which were also known as hereditary predisposition syndromes (HPS) (9). For hematological malignancies, hereditary predisposition was first identified in chronic lymphocytic leukemia (CLL) and acute myeloid leukemia (AML), which has led to the identification of several germline mutations, such as *RUNX1, CEBPA, GATA2, ANKRD26, DDX41* and *ETV6* mutations. Furthermore, genetic susceptibility was indicated in ALL and

TABLE 1 Summary of shared germline gene mutations at remission status.

Gene	Vcf_mut	AAChange.HGVS	FRE (case1/case2)	Mut_type	avsnp150
RECQL	chr12:21652503:A/G	c.2T>C:p.0?	45.1%/42.9%	SNP	rs146924988
AK2	chr1:33478892:G/A	c.586C>T:p.(Arg196Trp)	50.5%/49.6%	SNP	rs370429097
C7	chr5:40972681:C/T	c.2059C>T:p.(Arg687Cys)	47.8%/45.9%	SNP	rs117487879
CCDC40	chr17:78069197:G/A	c.2968G>A:p.(Asp990Asn)	50%/50.5%	SNP	rs200958035
NCF4	chr22:37273779:G/T	c.934G>T:p.(Gly312Cys)	46.9%/39.0%	SNP	rs199618052
KCNQ4	chr1:41284190:C/G	c.546C>G:p.(Phe182Leu)	52.7%/41.7%	SNP	rs80358273
GJB2	chr13:20763485:AG/A	c.235del:p.(Leu79Cysfs*3)	47.4%/54.9%	InDel	rs80338943
USH2A	chr1:216595579:G/GA	c.99_100insT:p.(Arg34Serfs*41)	49.0%/41.1%	InDel	rs141672841

Mut, mutation; FRE, frequency; InDel, insertion-deletion; SNP, single nucleotide polymorphism.

multiple myeloma, with constitutional mutations in genes such as *IKZF1, SH2B3, PAX5* (ALL) and *KDM1A/LSD1* (multiple myeloma). Monogenic genomic alterations have also been found to be involved in inborn errors of the immune system and confer a predisposition to hematological malignancies such as ataxia telangiectasia, Nijmegen breakage syndrome, Bloom's syndrome, xeroderma pigmentosum, constitutional mismatch repair deficiency, Fanconi anemia, and telomere syndromes (2, 10–12). Interestingly, previously identified inherited cancer susceptibility syndromes also increase the possibility to develop hematological malignancies. For example, patients with Diamond-Blackfan anemia, severe congenital neutropenia, or familial thrombocytopenia have a significantly increased incidence of myeloid neoplasms (10). Up to 62% of children with lymphoproliferative diseases have primary immune deficiency disease (PID) (13). Compared with the general population, people with PID have a 1.5 times higher risk of developing cancer (14). At present, HPS-related genes or pathways involve transcription factors, RNA function, DNA methylation, ribosome assembly, histone modification, DNA unwinding and DNA repair (9). Other germline mutations in key transcription and translation processes and signal transduction pathways, such as the RAS pathway, cell proliferation, apoptosis, and tumor suppressor genes (e.g., *TP53*) were also considered as possible underlying predispositions.

In this case, the proband and her second daughter both suffered from acute leukemia at different times in their lives. Considering the incidence of acute leukemia, we speculated that there might be HPS in this case. Through WES sequencing and bioinformatics analysis, we finally focused on rs146924988, an SNV in *RECQL*, and the mutation frequencies in the proband and her second daughter were 45.1% and 42.9%, respectively. Further Sanger sequencing showed no such mutation of *RECQL* in the healthy child of the proband, which indicated that rs146924988 might play a role in this case of familial leukemia. The proband of this case was an APL patient, carrying a typical *PML-RARα* fusion gene. The second daughter of the proband was a BCP-ALL patient, carrying the classical *ETV6-RUNX1* fusion gene. Considering the driving role of these two different fusion genes in the occurrences and development of corresponding leukemias (15, 16), it can be inferred that this *RECQL* gene variant (rs146924988) is potentially associated with the generation of acute leukemia. We evaluated the alteration frequency and expression levels of *RECQL* in acute leukemia from publicly available datasets using the cBioPortal database (17), including AML datasets from The Cancer Genome Atlas (TCGA) (18) and B-ALL datasets generated by the Therapeutically Applicable Research to Generate Effective Treatments (TARGET, https://ocg.cancer.gov/programs/target) initiative, phs000464. Samples with complete data of gene mutations, copy-number alterations (CNA) and mRNA expressions were retained after screening. The CNA frequency of *RECQL* was more than 5% both in ALL and AML patients, and the main variants types are deep deletion and shallow deletion that related to low gene expression (Figures 2A, B). Interestingly, the expression of *RECQL* in AML-M3 patients mostly having *PML-RARα* fusion gene, was significantly lower than that in other types of AML patients (Figure 2C). These findings highlighted the potential role of *RECQL* in leukemia.

RECQL gene, as a member of the RecQ helicase family located on chromosome 12p12, encodes a DNA helicase with 649 residues. RECQL protein is a highly conserved protein and plays an important role in DNA repair, replication, recombination and transcription (19). The SNV (rs146924988) detected in this case is an initiator codon variant of *RECQL*, which may lead to start-lost loss-of-function of RECQL (20, 21) (Figures 3A, B). Prior to this report, the *RECQL* germline mutation has been found to be associated with hereditary breast cancer and hereditary ovarian cancer syndrome (22, 23), but its role in hematological malignancies has not been reported. RECQL protein is an ATPase and helicase that can bind and unlock the structural intermediate of DNA replication and repair. RECQL unlocks double-stranded DNA and catalyzes the migration of ATP-dependent branches on Holliday junctions and removable D-loop substrates. In addition to cleavage of DNA, RECQL promotes annealing of complementary single-stranded DNA in an ATP-independent manner (24). Moreover, RECQL can also interact with proteins that are involved in DNA replication, repair and mismatch repair, such as FEN1, RPA, PARP1, and MLH1 (25–27). Deletion of RECQL

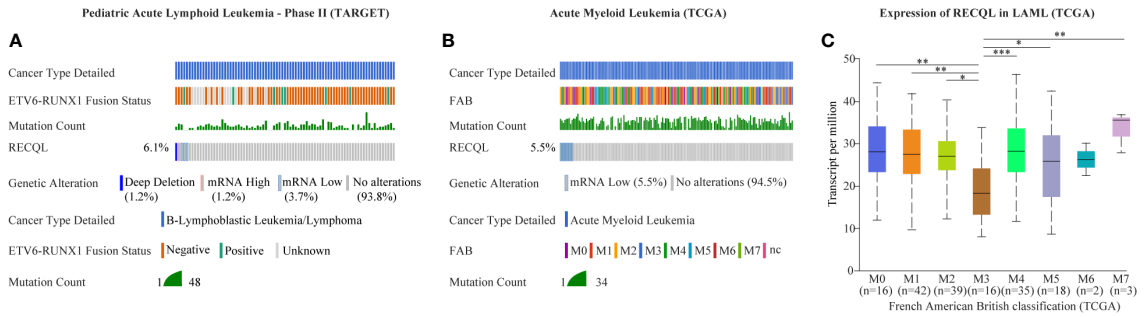

FIGURE 2
Mutation and expression of *RECQL* potentially involved in acute leukemia. The alteration frequency in *RECQL* in acute leukemia was analyzed by using the cBioPortal database, including data of AML from TCGA database and data of BCP-ALL from TARGET database. Samples with complete data of gene mutation, CNA and mRNA expression (log RNA Seq V2 RSEM) were retained after screening. **(A)** The alteration frequency in *RECQL* in B-ALL patients (Pediatric Acute Lymphoid Leukemia - Phase II, TARGET). **(B)** The alteration frequency in *RECQL* in AML patients (TCGA-LAML). **(C)** Comparison of *RECQL* gene expression in AML patients with different French American British classification. AML, Acute Myeloid Leukemia; TCGA, The Cancer Genome Atlas; B-ALL, acute B lymphoblastic leukemia; CNA, copy-number alterations; RSEM, RNA-Seq by Expectation Maximization; TARGET, therapeutically applicable research to generate effective treatments. Statistically significant differences are indicated as follows: *p < 0.05, **p < 0.01, ***p < 0.001.

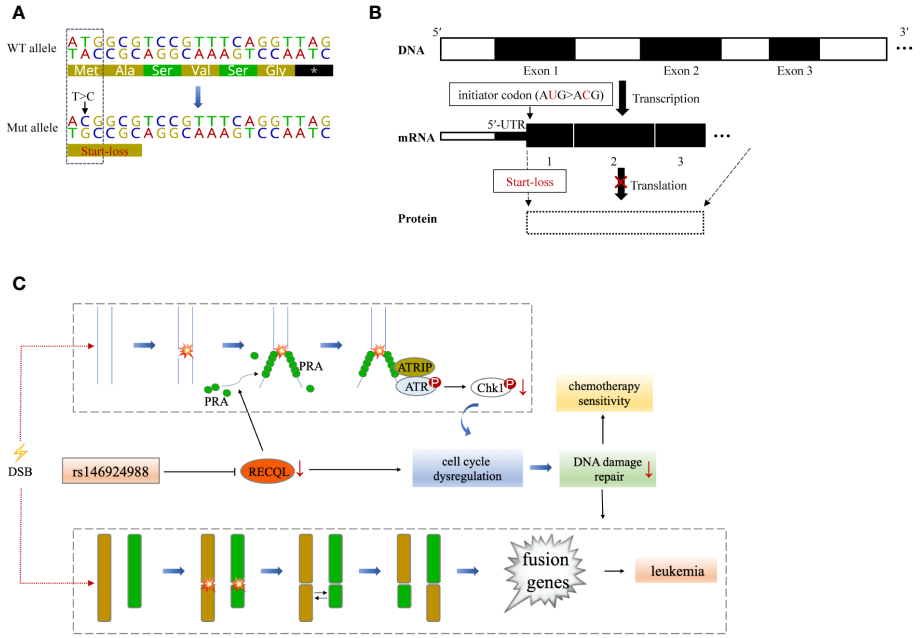

FIGURE 3
A theoretical model that *RECQL* mutation (rs146924988) acts as a potential mediator of hereditary leukemia. **(A)** Variant details of single nucleotide variation in *RECQL* (rs146924988). Dotted box indicates the corresponding DNA sequence of the initiator codon. **(B)** Hypothetical mechanism that *RECQL* mutation (rs146924988) affecting transcription and translation. The rs146924988 mutation is an initiator codon variant of *RECQL*, which may lead to a start-lost loss-of-function of RECQL. **(C)** A theoretical model that rs146924988 acts as a mediator of hereditary leukemia. The germline mutation (rs146924988) was proposed to mediate the occurrence of chromosome rearrangement and fusion genes, as well as affect chemotherapy sensitivity. WT, wide type; Mut, mutant; DSB, DNA double-strand break.

resulted in increased DNA damage accumulation, which indicated that RECQL was involved in the solution of replication fork stagnation. RECQL-deficient mice and cells exhibited frequent spontaneous chromosomal breakage and chromatid translocation (28). In a recent *in-vitro* experiment based on MDA-MB-231 cells, RECQL was considered to be involved in regulating cell stress response (29). It has been found to mediate the recruitment of replication protein A (RPA) in DNA damage sites and to promote the activation of the ATR-Chk1 pathway in response to the DNA damage caused by gemcitabine (29). ATR-Chk1 is a classic pathway of DNA damage response (DDR) induced by DNA double-strand breaks (DSBs), involving cell cycle checkpoint regulation and DNA repair (30). It can promote ubiquitination and proteasome degradation by phosphorylating CDC25 phosphatases (CDC25A, B, C), and induce cell cycle G1-S transition and G2-M transition (31–33). ATR-Chk1 dysfunction is associated with a large number of DNA damage and chromosomal rearrangements in Ataxia-telangiectasia (A-T) patients, especially in lymphocytes, which often leads to the production of fusion genes (34, 35).

Based on these previous findings, we hypothesize that the constitutional mutation in *RECQL* gene (rs146924988) may inhibit the translation of *RECQL* mRNA and lead to a relative lack of RECQL protein, which may further impair the ATR-Chk1 pathway and resulting in functional disorders in DNA replication and DSBs repair. It is conceivable that these functional disorders could ultimately mediate the occurrence of chromosome rearrangement and fusion genes, as driving factors for leukemia (Figure 3C). Admittedly, we have not obtained direct evidence that *RECQL* gene mutation (rs146924988) will lead to decreased *RECQL* expression level because this study is a case report in nature, and the biological process of such mutation potentially affecting DSBs repair and mediating the production of fusion genes needs to be verified in *in-vitro* experiments and larger clinical cohorts in the future. Moreover, there were 7 other shared germline mutations in this case of familial leukemia, which were related to genes *AK2*, *C7*, *CCDC40*, *NCF4*, *KCNQ4*, *GJB2* and *USH2A*. These genes were reported to be involved in ADP biosynthesis, complement activation, oxidation-reduction and other biological processes, and their functional annotations were shown in Table S1. By checking the literature and public data repository, there is no direct evidence that these mutations are associated with genomic instability or genetic predisposition to cancer, but their contributions to the onset of leukemia cannot be completely excluded and needs further evaluation. The loss of RECQL function may increase the probability of the somatic events, such as the occurrence of chromosome rearrangements, in positions given by chance and modulated by other factors, resulting in different genetic fusions genes. This partly explained how germline genetic variants in *RECQL* lead to different types of fusions gene in these 2 cases.

Early recognition of the hereditary predisposition of hematological malignancies is critical for timely diagnosis and individualized treatment. In this study, a potential HPS-related gene mutation was identified by WES sequencing, which highlights the clinical application of WES, especially in patients with early-onset leukemia or familial leukemia. In addition to diagnostic value, screening of the HPS-related gene mutations may provide prognosis evaluation reference for an optimal intervention approach. For

example, previous studies have shown that *RECQL* gene defects not only cause genomic instability and chromatin recombination, but also make cells more sensitive to toxic genomic stress and cytotoxic therapy (29). Particularly, polymorphic variants in *RECQL* was found to be related to the overall survival rate of pancreatic cancer patients treated with gemcitabine (36). RECQL helicase has also been found to protect multiple myeloma cells from melphalan and bortezomib cytotoxicity (37). Therefore, the significance of *RECQL* mutation in the treatment of acute leukemia needs to be evaluated in future studies.

In this study, we performed WES sequencing in a familial leukemia case, and for the first time to our knowledge, found a germline *RECQL* mutation potentially involved in hereditary predisposition to acute leukemia. The hypothetical biological process in which *RECQL* gene mutation (rs146924988) affect DSBs repair and mediate the generation of fusion genes provides a new understanding of the pathogenesis of leukemia, and highlights the necessity for next-generation sequencing-based screening of genes involved in this process in potential HPS patients.

Data availability statement

The datasets presented in this article are not readily available because of ethical/privacy restrictions. Requests to access the datasets should be directed to the corresponding author.

Ethics statement

This study was approved by the Medical Ethics Committee of the Department of Hematology, Tongji Hospital, Tongji Medical College, Huazhong University of Science and Technology. Written informed consent to participate in this study was provided by the participants' legal guardian/next of kin.

Author contributions

All authors designed the study, interpreted the findings and revised the manuscript. WY, ZS, KS, QY, and QL carried out data management and statistical analysis and drafted the manuscript. YC and JW helped with English language editing and data management. YY performed project administration. All authors contributed to the article and approved the submitted version.

Funding

This work was supported by the National Natural Science Foundation of China No.82171575 and the National Key Research and Development Program of China 2021YFA1101504.

Acknowledgments

The authors would like to thank the patients and their families for agreeing to report this case, and all the faculty and staff in our clinical and laboratory unit for clinical and technical support.

Conflict of interest

The authors declare that the research was conducted in the absence of any commercial or financial relationships that could be construed as a potential conflict of interest.

Publisher's note

Supplementary material

The Supplementary Material for this article can be found online at: https://www.frontiersin.org/articles/10.3389/fonc.2023.1066083/full#supplementary-material

References

1. Pui CH, Nichols KE, Yang JJ. Somatic and germline genomics in paediatric acute lymphoblastic leukaemia. *Nat Rev Clin Oncol* (2019) 16(4):227–40. doi: 10.1038/s41571-018-0136-6

2. Bochtler T, Haag GM, Schott S, Kloor M, Krämer A, Müller-Tidow C. Hematological malignancies in adults with a family predisposition. *Dtsch Arztebl Int* (2018) 115(50):848–54. doi: 10.3238/arztebl.2018.0848

3. Arber DA, Orazi A, Hasserjian R, Thiele J, Borowitz MJ, Le Beau MM, et al. The 2016 revision to the world health organization classification of myeloid neoplasms and acute leukemia. *Blood* (2016) 127(20):2391–405. doi: 10.1182/blood-2016-03-643544

4. Mertens F, Johansson B, Fioretos T, Mitelman F. The emerging complexity of gene fusions in cancer. *Nat Rev Cancer*. (2015) 15(6):371–81. doi: 10.1038/nrc3947

5. Papaemmanuil E, Gerstung M, Bullinger L, Gaidzik VI, Paschka P, Roberts ND, et al. Genomic classification and prognosis in acute myeloid leukemia. *N Engl J Med* (2016) 374(23):2209–21. doi: 10.1056/NEJMoa1516192

6. Chinese Society of Hematology, Chinese Medical Doctor Association, Chinese Medical Association and Chinese Medical Doctor Association. Chinese Guidelines for diagnosis and treatment of acute promyelocytic leukemia. *Zhonghua Xue Ye Xue Za Zhi* (2018) 39(3):179–83. doi: 10.3760/cma.j.issn.0253-2727.2018.03.002

7. Sanz MA, Fenaux P, Tallman MS, Estey EH, Löwenberg B, Naoe T, et al. Management of acute promyelocytic leukemia: updated recommendations from an expert panel of the European LeukemiaNet. *Blood* (2019) 133(15):1630–43. doi: 10.1182/blood-2019-01-894980

8. Yang W, Cai J, Shen S, Gao J, Yu J, Hu S, et al. Pulse therapy with vincristine and dexamethasone for childhood acute lymphoblastic leukaemia (CCCG-ALL-2015): an open-label, multicentre, randomised, phase 3, non-inferiority trial. *Lancet Oncol* (2021) 22(9):1322–32. doi: 10.1016/S1470-2045(21)00328-4

9. Garber JE, Offit K. Hereditary cancer predisposition syndromes. *J Clin Oncol* (2005) 23(2):276–92. doi: 10.1200/JCO.2005.10.042

10. Mangaonkar AA, Patnaik MM. Hereditary predisposition to hematopoietic neoplasms: When bloodline matters for blood cancers. *Mayo Clin Proc* (2020) 95 (7):1482–98. doi: 10.1016/j.mayocp.2019.12.013

11. Bakry D, Aronson M, Durno C, Rimawi H, Farah R, Alharbi QK, et al. Genetic and clinical determinants of constitutional mismatch repair deficiency syndrome: report from the constitutional mismatch repair deficiency consortium. *Eur J Cancer.* (2014) 50(5):987–96. doi: 10.1016/j.ejca.2013.12.005

12. Oetjen KA, Levoska MA, Tamura D, Ito S, Douglas D, Khan SG, et al. Predisposition to hematologic malignancies in patients with xeroderma pigmentosum. *Haematologica* (2020) 105(4):e144–6. doi: 10.3324/haematol.2019.223370

13. Forbes LR, Eckstein OS, Gulati N, Peckham-Gregory EC, Ozuah NW, Lubega J, et al. Genetic errors of immunity distinguish pediatric nonmalignant lymphoproliferative disorders. *J Allergy Clin Immunol* (2022) 149(2):758–66. doi: 10.1016/j.jaci.2021.07.015

14. Ballow M, Sánchez-Ramón S, Walter JE. Secondary immune deficiency and primary immune deficiency crossovers: Hematological malignancies and autoimmune diseases. *Front Immunol* (2022) 13:928062. doi: 10.3389/fimmu.2022.928062

15. Tan Y, Wang X, Song H, Zhang Y, Zhang R, Li S, et al. A PML/RARα direct target atlas redefines transcriptional deregulation in acute promyelocytic leukemia. *Blood* (2021) 137(11):1503–16. doi: 10.1182/blood.2020005698

16. Nishii R, Baskin-Doerfler R, Yang W, Oak N, Zhao X, Yang W, et al. Molecular basis of ETV6-mediated predisposition to childhood acute lymphoblastic leukemia. *Blood* (2021) 137(3):364–73. doi: 10.1182/blood.2020006164

17. Gao J, Aksoy BA, Dogrusoz U, Dresdner G, Gross B, Sumer SO, et al. Integrative analysis of complex cancer genomics and clinical profiles using the cBioPortal. *Sci Signal* (2013) 6(269):l1. doi: 10.1126/scisignal.2004088

18. Cancer Genome Atlas Research Network, Ley TJ, Miller C, Ding L, Raphael BJ, Mungall AJ, et al. Genomic and epigenomic landscapes of adult *de novo* acute myeloid leukemia. *N Engl J Med* (2013) 368(22):2059–74. doi: 10.1056/NEJMoa1301689

19. Veith S, Mangerich A. RecQ helicases and PARP1 team up in maintaining genome integrity. *Ageing Res Rev* (2015) 23(Pt A):12–28. doi: 10.1016/j.arr.2014.12.006

20. Wang X, Liu Z, Li G, Dang L, Huang S, He L, et al. Efficient gene silencing by adenine base Editor-mediated start codon mutation. *Mol Ther* (2020) 28(2):431–40. doi: 10.1016/j.ymthe.2019.11.022

21. Mengel D, Traschütz A, Reich S, Leyva-Gutiérrez A, Bender F, Hauser S, et al. A *de novo* STUB1 variant associated with an early adult-onset multisystemic ataxia phenotype. *J Neurol* (2021) 268(10):3845–51. doi: 10.1007/s00415-021-10524-7

22. Cybulski C, Carrot-Zhang J, Kluźniak W, Rivera B, Kashyap A, Wokołorczyk D, et al. Germline RECQL mutations are associated with breast cancer susceptibility. *Nat Genet* (2015) 47(6):643–6. doi: 10.1038/ng.3284

23. Kaneyasu T, Mori S, Yamauchi H, Ohsumi S, Ohno S, Aoki D, et al. Prevalence of disease-causing genes in Japanese patients with BRCA1/2-wildtype hereditary breast and ovarian cancer syndrome. *NPJ Breast Cancer* (2020) 6:25. doi: 10.1038/s41523-020-0163-1

24. Sharma S, Sommers JA, Choudhary S, Faulkner JK, Cui S, Andreoli L, et al. Biochemical analysis of the DNA unwinding and strand annealing activities catalyzed by human RECQ1. *J Biol Chem* (2005) 280(30):28072–84. doi: 10.1074/jbc.M500264200

25. Sami F, Lu X, Parvathaneni S, Roy R, Gary RK, Sharma S. RECQ1 interacts with FEN-1 and promotes binding of FEN-1 to telomeric chromatin. *Biochem J* (2015) 468 (2):227–44. doi: 10.1042/BJ20141021

26. Doherty KM, Sharma S, Uzdilla LA, Wilson TM, Cui S, Vindigni A, et al. RECQ1 helicase interacts with human mismatch repair factors that regulate genetic recombination. *J Biol Chem* (2005) 280(30):28085–94. doi: 10.1074/jbc.M500265200

27. Sharma S, Phatak P, Stortchevoi A, Jasin M, Larocque JR. RECQ1 plays a distinct role in cellular response to oxidative DNA damage. *DNA Repair (Amst)* (2012) 11 (6):537–49. doi: 10.1016/j.dnarep.2012.04.003

28. Sharma S, Stumpo DJ, Balajee AS, Bock CB, Lansdorp PM, Brosh RM, et al. RECQL, a member of the RecQ family of DNA helicases, suppresses chromosomal instability. *Mol Cell Biol* (2007) 27(5):1784–94. doi: 10.1128/MCB.01620-06

29. Parvathaneni S, Sharma S. The DNA repair helicase RECQ1 has a checkpoint-dependent role in mediating DNA damage responses induced by gemcitabine. *J Biol Chem* (2019) 294(42):15330–45. doi: 10.1074/jbc.RA119.008420

30. Sørensen CS, Syljuåsen RG. Safeguarding genome integrity: the checkpoint kinases ATR, CHK1 and WEE1 restrain CDK activity during normal DNA replication. *Nucleic Acids Res* (2012) 40(2):477–86. doi: 10.1093/nar/gkr697

31. Kastan MB, Bartek J. Cell-cycle checkpoints and cancer. *Nature* (2004) 432 (7015):316–23. doi: 10.1038/nature03097

32. Matthews HK, Bertoli C, de Bruin RAM. Cell cycle control in cancer. *Nat Rev Mol Cell Biol* (2022) 23(1):74–88. doi: 10.1038/s41580-021-00404-3

33. Karlsson-Rosenthal C, Millar JBA. Cdc25: mechanisms of checkpoint inhibition and recovery. *Trends Cell Biol* (2006) 16(6):285–92. doi: 10.1016/j.tcb.2006.04.002

34. Taylor AM, Metcalfe JA, Thick J, Mak YF. Leukemia and lymphoma in ataxia telangiectasia. *Blood* (1996) 87(2):423–38. doi: 10.1182/blood.V87.2.423.bloodjournal872423

35. Yamauchi M. Mechanisms underlying the suppression of chromosome rearrangements by ataxia-telangiectasia mutated. *Genes* (2021) 12(8):1232. doi: 10.3390/genes12081232

36. Li D, Frazier M, Evans DB, Hess KR, Crane CH, Jiao L, et al. Single nucleotide polymorphisms of RecQ1, RAD54L, and ATM genes are associated with reduced survival of pancreatic cancer. *J Clin Oncol* (2006) 24(11):1720–8. doi: 10.1200/JCO.2005.04.4206

37. Viziteu E, Klein B, Basbous J, Lin YL, Hirtz C, Gourzones C, et al. RECQ1 helicase is involved in replication stress survival and drug resistance in multiple myeloma. *Leukemia* (2017) 31(10):2104–13. doi: 10.1038/leu.2017.54

Frontiers in Oncology

Advances knowledge of carcinogenesis and tumor progression for better treatment and management

The third most-cited oncology journal, which highlights research in carcinogenesis and tumor progression, bridging the gap between basic research and applications to imrpove diagnosis, therapeutics and management strategies.

Discover the latest Research Topics

See more →

Frontiers

Avenue du Tribunal-Fédéral 34
1005 Lausanne, Switzerland
frontiersin.org

Contact us

+41 (0)21 510 17 00
frontiersin.org/about/contact